AFOSR-TR-96 97

REPORT DOCUMENTATION PAGE

0035

4-0188

| 1a. REPORT SECURITY CLASSIFICATION | 1b. REST |
| Unclassified | |

2a. SECURITY CLASSIFICATION AUTHORITY	3. DISTRIBUTION / AVAILABILITY OF REPORT
	Unrestricted
2b. DECLASSIFICATION / DOWNGRADING SCHEDULE	

| 4. PERFORMING ORGANIZATION REPORT NUMBER(S) | 5. MONITORING ORGANIZATION REPORT NUMBER(S) |
| Texas A&M Center for Mechanics and Control Report No. AE 941201 | |

| 6a. NAME OF PERFORMING ORGANIZATION | 6b. OFFICE SYMBOL (If applicable) | 7a. NAME OF MONITORING ORGANIZATION |
| Texas Engineering Experiment Station | | same as 8a |

| 6c. ADDRESS (City, State, and ZIP Code) | 7b. ADDRESS (City, State, and ZIP Code) |
| 701 H.R. Bright Building Texas A&M University College Station, Texas 77843-3141 | same as 8c |

| 8a. NAME OF FUNDING / SPONSORING ORGANIZATION | 8b. OFFICE SYMBOL (If applicable) | 9. PROCUREMENT INSTRUMENT IDENTIFICATION NUMBER |
| AFOSR | | F49620-92-J-0496 |

| 8c. ADDRESS (City, State, and ZIP Code) | 10. SOURCE OF FUNDING NUMBERS | | | |
| AFOSR/NA Building 410 Bolling AFB, DC 20332-6448 | NA | | | |

PROGRAM ELEMENT NO.	PROJECT NO.	TASK NO.	WORK UNIT ACCESSION NO.
61102F	2306	BS	

11. TITLE (Include Security Classification)

Mechanics and Control of Nonlinear Structures

12. PERSONAL AUTHOR(S)
John L. Junkins

| 13a. TYPE OF REPORT | 13b. TIME COVERED | 14. DATE OF REPORT (Year, Month, Day) | 15. PAGE COUNT |
| Annual | FROM 8/31/93 to 7/31/96 | 1996 November 22 | 335 |

16. SUPPLEMENTARY NOTATION

17. COSATI CODES			18. SUBJECT TERMS (Continue on reverse if necessary and identify by block number)
FIELD	GROUP	SUB-GROUP	Structural Response, Nonlinear Systems, Dynamics, Control, Vibration, Robotics

19. ABSTRACT (Continue on reverse if necessary and identify by block number)

This report documents results of analytical, computational, and experimental research on nonlinear structural analysis. In particular, a novel inverse dynamics method is presented whereby exact solutions for nonlinear dynamical response can be determined near a given approximate numerical solution. This method is useful for validation and tuning of dynamic response simulations. Also, novel results are reported for parameterization of NxN proper orthogonal matrices and applications in mechanics and control are explored. A novel quasi-coordinate method is developed for nonlinear flexible multi-body structural systems having a configuration variable mass matrix. This approach avoids the necessity of inverting the mass matrix through the derivation of differential equations which generate an instantaneously diagonalizing transformation. Finally, experimental results of maneuvers of the ASTREX Test Article are presented.

19970122 032

| 20. DISTRIBUTION / AVAILABILITY OF ABSTRACT | 21. ABSTRACT SECURITY CLASSIFICATION |
| ☒ UNCLASSIFIED/UNLIMITED ☐ SAME AS RPT. ☐ DTIC USERS | Unclassified |

| 22a. NAME OF RESPONSIBLE INDIVIDUAL | 22b. TELEPHONE (Include Area Code) | 22c. OFFICE SYMBOL |
| Brian Sanders | (202) 767-6963 | AFOSR/NA |

DD Form 1473, JUN 86   Previous editions are obsolete.   SECURITY CLASSIFICATION OF THIS PAGE
unclassified

DTIC QUALITY INSPECTED 1

Mechanics and Control
of Nonlinear Structures

John L. Junkins

Center for Mechanics and Control

Department of Aerospace Engineering

Texas A&M University

College Station, Texas 77843-3141

prepared for

U. S. Air Force Office of Scientific Research

November 1996

SUMMARY

This report summarizes the results of a three year study sponsored by the Air Force Office of Sponsored Research under contract No. F49620-92-J-0496. The enthusiastic technical and administrative effort of Drs. Spencer Wu and Brian Sanders of AFOSR are warmly acknowledged.

This project has involved analytical and experimental research across a family of structural mechanics and control problems. Our effort has been mainly addressed to four sets of research issues:

1. **Solution and Validation Methodology for Simulation of Nonlinear Structural Systems**
   See Attachments [2,3,14].

2. **NonlinearMechanics and Control of Flexible Structural and Robotic Systems**
   See Attachments [4-8,14-18].

3. **Representation of Finite Rotations in 3 and N-Dimensions: Applications in Mechanics**
   See Attachments [9-11,13].

4. **Radial Basis Approximation Methods and Associated Optimization Algorithms**
   See Attachments [12].

In addition to the above four sets of research issues, we have also engaged in significant research on ancillary topics which are documented in the references listed in Attachment 1. The above research spans a broad set of theoretical/conceptual [6,7,9-11,13-18], computational [2-4,12,14], and hardware experimental [8] research topics.

In the text of this report, we present a brief guided tour of the results as a preamble to the nineteen attachments which present the details of the research methodology and results.

CONTENTS

1.0 Introduction

This report presents results achieved during a three year research project at Texas A&M University sponsored by AFOSR under contract F49620-92-J-0496 P0001. The work was carried out by the Principal Investigator (J. L. Junkins) and a team of mainly Ph.D. candidate co-researchers. As is evident from a brief review of the attachments, a substantial volume of research results have emerged from this work. Given the volume of results, we decided to overview only the main features of the results in the text, and make the technically more detailed attachments the heart of our report.

The level of effort required to produce the attached results represents approximately five man-years of total effort. Since only half that level of effort was funded by contract F49620-92-J-0496, it is evident that the matching State of Texas support (Advanced Technology Project Numbers 999903-231 and 999903-232) has resulted in an augmentation of this project which considerably leveraged the AFOSR support.

This report documents our results in four broad categories:
> Solution and Validation Methodology for Simulation of Nonlinear Structural Systems
> Nonlinear Mechanics and Control of Flexible Structural and Robotic Systems
> Representation of Finite Rotations in 3 and N-Dimensions: Applications in Mechanics
> Radial Basis Approximation Methods and Associated Optimization Algorithms

Attachment No. 1 lists 19 refereed publications that have been the result of this work during 1993-1996, and also lists the graduate students that have been supported under this contract. In addition, two additional students and a post-doctoral researcher have been supported under support of State of Texas support (Advanced Technology Project Numbers 999903-231 and 999903-232) performing ancillary research.

The discussion below overviews selected aspects of the contribution in each of the above categories; the details are covered in the attachments.

2.0 Selected of Technical Results

In Attachment [2,3], we present some very significant results from this research project; we have developed methodology for validation of solution accuracy of nonlinear dynamical response. This methodology applies to a wide class of physical systems modeled as systems of ordinary, partial, or integro differential equations and associated boundary condition operators. It permits the analytical construction of *exact* solutions (along with rigorously consistent, small perturbing force functions), which neighbor given approximate numerical solutions. We show that is is possible to construct these special case exact solutions in spite of the fact that the original initial value problem cannot be solved exactly in closed form. The research reported in these papers consist of basic analytical results and a careful proof-of-concept experiments for several example systems described by ordinary and partial differential equation systems. For a wide class of nonlinear dynamical systems described by ordinary differential equations, we have developed an algorithm and software that represent a standardized approach which promises to be of broad utility. For the class of distributed parameter systems, we have worked several examples and established proof of concept, however, we have not found it feasible to construct a general purpose software package for this

case. Shown below in Figure 1 is a slide format result abstracted from Attachment 3; we depict the error surfaces between a family of approximate response solutions compared to an exact solution we constructed using the method of Attachments [1,2].

Figure 1.

Structural Mechanics: Nonlinear Response Methodology

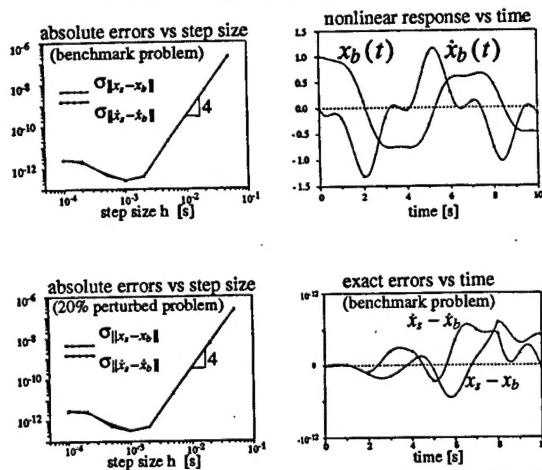## A Rigorous Means for Solution Validation - Junkins (Texas A&M)

- **A method for construction of *exact benchmark solutions* neighboring available aproximate solutions.**
- **Provides capability to determine *exact* special case space-time solution errors of numerical methods.**
- **Permits rigorous validation of numerical methods => assess accuracy limitations of methodology.**
- **Permits optimal tuning of a given numerical method (e.g., select step size, FEM grid, order, etc.).**
- **Permits rigorous tradeoff studies for evaluating merits of competing numerical methods.**

Refs.: Junkins, J. and Lee, S., "Validation of Finite Dimensional Approximation Solutions for Dynamics of Distributed Parameter Systems,"
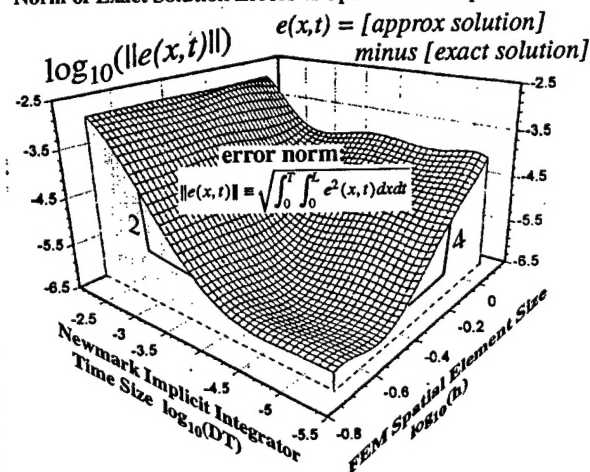*Adv. in the Astron. Sciences*, Vol. 85, pp. 2089-2111 (1994)
Lee, S., and Junkins, J., "Construction of Exact Benchmark Problems for Dynamical Systems," *Shock and Vibration*, Vol. 1, No. 5, pp. 403-414 (1994).

Absolute Error Convergence Study:
Nonlinear Oscillator Example

absolute errors vs step size
(benchmark problem)
$\sigma_{|x_s - x_b|}$
$\sigma_{|\dot{x}_s - \dot{x}_b|}$

nonlinear response vs time
$x_b(t)$ $\dot{x}_b(t)$
time [s]

absolute errors vs step size
(20% perturbed problem)
$\sigma_{\|x_s - x_b\|}$
$\sigma_{\|\dot{x}_s - \dot{x}_b\|}$
step size h [s]

exact errors vs time
(benchmark problem)
$\dot{x}_s - \dot{x}_b$
$x_s - x_b$
time [s]

Multi-Flexible Body Example => Hybrid ODE/PDE System
Norm of Exact Solution Errors vs Space-Time Step Sizes:

$e(x,t) = [approx\ solution]$
$minus\ [exact\ solution]$

$\log_{10}(\|e(x,t)\|)$

error norm:
$$\|e(x,t)\| = \sqrt{\int_0^T \int_0^L e^2(x,t)\,dx\,dt}$$

Newmark Implicit Time Size $\log_{10}(DT)$
Time Size Implicit Integrator

FEM Spatial Element Size $\log_{10}(h)$

In Attachments [4,5,15,18], we present a substantial volume of new material on stability and control of multi-body structural systems and, in particular, explore some of the conceptual, mathematical, and numerical issues in underlying cooperation between two or more autonomously controlled manipulators maneuvering a common paylod or object. For the typical case of redundant actuation, there are an infinity of controls to affect essentially the same dynamical motion, however, each control policy and resulting control forces represent different constraint loading on the structure. A familar example is two or more humans manipulating a heavy object such as a soffa or a pool table; it is apparent that, due to actuator redundancy, the same rigid body trajectory can be acheived by an infinity of actuation forces, but most of these control policies result in the actuators 'fighting' each other and imposing unnecessary constraint loads on the payload (and frustration of the actuators). By defining an appropriate optimization policy, it is possible to minimize the norm of the constraint forces, for example, and thereby cause the manipulators to cooperate in carrying out the maneuver. In Attachments [4,5], we develop a conceptual and mathematical basis for formulating cooperative optimal control strategies and study the efficacy and robustness of this approach through several simulation studies. Recently, Agrawal and his student Gary Yale at the Naval Postgraduate

School have successfully implemented this idea experimentally in collaboration with the Principal Investigator, and have verified that the approach has practical validity as well as theoretical elegance.

In attachments [6], we extend the classical linear quadratic regulator (LQR) to admit inequality constraints on the control variables. This modest extension of the LQR is very significant, because one of the classical shortcomings of the LQR is that there was no apriori guarantee that the opt control derived was in fact physically realizable. A numerical example is given in [6], to illustrate that the algorithm obtained is indeed numerically feasible.

In Attachment [7], we present an analytical result; we introduce a novel theoretical path for asymptotic stability analysis for systems wherein the chosen Lyapunov function is negative semi-definite. We use the new methodololgy to show that a commonly applied output feedback control law (for controlling a symmetric four appendage structure) guarantees asympotic stability of all infinity of the *anti-symmetric- in-unison modes*, however, it does not guarantee the stability of the infinity of *anti-symmetric- in- opposition modes* which are both unobservable and uncontrollable.

Attachment [8] presents analytical, computational, and experimental results for near minimum-fuel and near-minimum-time control of the ASTREX structure at Phillips Laboratory. The results in [8] establish the validity and effectiveness of our overall approach, however some experimental anomalies were revealed due to several constraints imposed by the present sensor/actutor system development.

In attachments [9-11,13], we present another significant result of our research that we expect to have important consequences. We have been able to greatly extend and generalize a fundamental classical result known as the *Cayley Transform*, to establish a revolutionary method for parameterization of NxN proper orthogonal matrices. These results permit one to view the evlolution of an NxN orthogonal matrix in terms of a minimal [N(N-1)/2-dimensional] set of 'orientation parameters' that are closely related to the *quaternions* or *Euler Parameters* famous for the usual 3x3 orthogonal direction cosine matrix case. Thus the evolution of an NxN orthogonal matrix can be qualitatively conceptualized as the motion of a generalized rigid body reference frame. Since the spectral decomposition of all NxN symmetric positive definite matrices (which abound in mechanics!) is a similarity transformation involving the orthogonal NxN matrix of eigenvectors and the N positive scalar eigenvalues, it is apparent that nonsingular minimal parameter descriptions of orthogonal matrices immediately enables minimal parameter descriptions of a general positive definite N*N matrices. Several applications are considered in the references that illustrate the utility and support the conclusion that these results are fundamental in nature and will have a broad impact.

In attachment [12], we present a method for converting a general functional optimization problem into a nonlinear programming problem by prameterizing the unknown control using radial basis functions (RBFs). An adaptive RBF approximation method is introduced wherein an initially small number of basis functions is gradually increased with the center locations being decided based upon the sensitivity of the trajectory to variations of the weights on the currently existing set of RBFs. The method adapts both the center locations and the local sharpness of the RBFs, and uses the converged result from the previous iterations to initiate the subsequent iteration with an

5

accurate starting iterative which satisfies the terminal boundary contions. The convergence and efficacy of the method is studied through two examples (an optimal trajectory problem and an optimal aerodynamic shape problem) fopr which the optimal solution has been previously determined in the literature. The method is also compared to a non-adaptive RBF approach and the results clearly establish the validity and attractiveness of this approach.

In attachment [14], we introduce a potentially revolutionary method for simulating dynamics of nonlinear multi-body systems wherein a configuration-variable mass matrix occurs. In conventional algorithms, computing acceleration requires inversion of this configuration-variable mass matrix which directly limits the speed and precision, and ultimately, the practical dimensionality of multibody simulations. It also means that so-called order N methods are not really order N when considering the dynamics of nonlinear flexible multibody systems. The new method introduced involves a unique coordinate transformation to a new coordinate system which maps the instantaneous mass matrix into an identity matrix. This is not done by solving a local algebraic eigenvalue problem via conventional solvers, but rather new differential equations are derived that inherently generate the instantaneous diagonalizing transformation. The validity and utility of the algorithm is proven conclusively in [14], including a low dimensioned application, and in [19], we apply it to a 14th order dynamical model for the Freewing Scorpion UAV. These analytical and numerical studies prove the validity and show that this formulation has broad applicability in nonlinear multi-body dynamics.

3.0 Conclusions

It is evident that the research progress is excellent on many fronts. We have achieved significant analytical progress and in several important instances have progressed from introduction of a basic concept, to analytical studies, and proof-of-concept conputational and hardware demonstrations, within this three year effort. Of course, this progress has been achieved in large measure due to historical investments of AFOSR resources in support of our effort to develop the analytical and experimental foundation upon which this progress rests. It is also significant that the ancillary financial support obtained from Texas Advanced Research Project grants has greatly accelerated our work and thereby leveraged the AFOSR investment. It is of special significance to note that five exceptional graduate students and a postdoctoral researcher have been supported during this project and three of the four Ph. D. students have successully defended their dissertations. Thus, quite apart from the technical fruits of this research project, the development of outstanding young engineers and scientists has been significant indeed.

Attachments Index

Principal Investigator Annual Data Collection (PIADC) Form

PI Name: **Junkins, John L.**

Institution: **Texas A&M University**

Contract No.: **F49620-92-J-0496**

A. Researchers

Faculty: Junkins, J. L., Eppright Endowed Chair Professor, Aerospace Engr, 1.5 months, US citizen

Students: Hurtado, J.E., Ph.D. completed, Aerospace Engineering, US citizen

Lee, S. L., Ph.D. completed, Aerospace Engineering, non-US citizen

Bell, M., M.S. caompleted, Aerospace Engineering, US citizen

Akella, M.R., Ph.D. candidate, non-US citizen

Verma, A.J., Ph.D. candidate, non-US citizen

B. Publications

Books: Junkins, J., and Kim, Y., **Dynamics and Control Flexible Structures**, 452 pages, *AIAA Education Series*, American Institute of Aeronautics and Astronautics, Washington, D. C., 1993.

Archival Journal Publications (during 1995-96):

1. Junkins, J. L., and Lee, S., "Validation of Finite Dimensional Approximations of the Dynamics of Distributed Parameter Systems," AAS/AIAA Astrodynamics Conference, Vancouver, BC (August, 1993), also, *AIAA Journal of Guidance, Control, and Dynamics*, Vol 18, No. 1, (Jan-Feb, 1995), pp87-95.

2. Junkins, J.L.,"Benchmark Problems for the Solution of Ordinary Differential Equations," *Shock and Vibration Computer Programs*, Vol SVM-13, pp 497-523, Dec 1995.

3. Kim, Y., Lee, S., and Junkins, J. L., "Eigenvector Derivatives for Mechanical Second Order Systems," *AIAA Journal of Guidance, Control and Dynamics*, Vol. 18, No. 4, July-Aug 1995, pp 899-906.

4. Schaub, H. Tsiotras, P., and Junkins, J. L., "Principal Rotation Representations of NxN Orthogonal Matrices," *International Journal of Engineering Sciences.*, Vol 33, No. 15, pp 2277-2295, 1995.

5. Junkins, J.L., and Y. Kim, "Stability and Control of Robotic Manipulators," *Teleoperation and Robotics in Space, AIAA Progress in Astro. and Aero.* Vol. 161, pp. 315-350, 1995.

6. Junkins, J.L.,"Benchmark Problems for the Solution of Ordinary Differential Equations," *Shock and Vibration Computer Programs*, W. Pilkey, Ed., SVM-13, Booz Allen &Hamilton, 1995.

7. Junkins, J., and Y. Kim, "Stability and Control of Nonlinear Mechanical Systems," *Smart Structures, Nonlinear Dynamics and Control*, Vol. I, pp. 108-162, 1995.

8. Schaub, H. and Junkins, J. L., "Stereographic Orientation Parameters for Attitude Dynamics: A Generalization of the Rodrigues Parameters," AAS/AIAA Flight Mechanics Conference, Albuquerque, NM, Feb, 1995, AAS *Journal of the Astronautical Sciences.*, Vol. 44, No. 1, pp. 1-20, 1996.

9. Kim,Y., Suk, T., and Junkins, J. L., "Optimal Slewing and Vibration Control of Smart Structures," in *Smart Structures, Nonlinear Dyanamics and Control*, Vol. II Prentice Hall, to appear, 1996.

10. Junkins, J.L. and Hurtado, J. E., "Optimal Control of Second Order Dynamical Systems," AIAA Structural Dynamics and Materials Conference, April 1995, New Orleans, LA., to appear, *AIAA Journal of Guidance, Control and Dynamics*.

11. Schaub, H. Robinett, R.,and Junkins, J. L.,"Adaptive External Torque Estimation by Means of Tracking a Lyapunov Function," AAS/AIAA Flight Mech. Conf., Austin, TX, Feb, 1996, to appear, AAS *Journal of the Astronautical Sciences*.

12. Tsiotras, P., Junkins, J. L., "Higher Order Cayley Transforms with Applications to Attitude Representations," AIAA/AAS Astrodynamics Conference, San Diego, CA, August 1996, to appear, AAS *Journal of the Astronautical Sciences*.

13. Schaub, H., Junkins, J. L., and Robinett, R. "New Attitude Penalty Functions for Spacecraft Optimal Control Problems," AIAA/AAS Astrodynamics Conference, San Diego, CA, August 1996, to appear, *AIAA Journal of Guidance, Control, and Dynamics*.

14. Junkins, J.L., "Adventures on the Interface of Dynamics and Control," invited *Theodore von Karman Lecture*, AIAA Aerospace Sciences Conference, Reno, NV, January, 1997, to appear *AIAA Journal of Guidance, Control, and Dynamics*.

15. Robinett, R. D. , Parker, G.P., Schaub, H., and Junkins, J., "Lyapunov Optimal Saturated Control for Nonlinear Systems," invited paper, AIAA Aerospace Sciences Conference, Reno, NV, January, 1997, to appear, *AIAA Journal of Guidance, Control, and Dynamics*.

16. Junkins, J.L., and Schaub, H., "An Instantaneous Eigenstructure Quasi-Coordinate Formulation for Nonlinear Dynamics," invited paper, AIAA Aerospace Sciences Conference, Reno, NV, January, 1997, to appear, *AIAA Journal of Guidance, Control, and Dynamics*.

17. Junkins, J.L., and Schaub, H., "A Square Root Quasi-Coordinate Formulation for Constrained Nonlinear Dynamics," AAS Space Flight Mechanics Conference, Reno, NV, Huntsville, AL, Feb 1997, to be submitted to the AAS *Journal of the Astronautical Sciences*.

18. Akella, M.R., and Junkins, J.L., "Some Studies on Linearized Uncertainty Propagation in rigid Body Motion," AAS Space Flight Mechanics Conference, Reno, NV, Huntsville, AL, Feb 1997, to be submitted to the AAS *Journal of the Astronautical Sciences*.

19. Junkins, J.L., Akella, M.R., and Robinett, R.D., III, "Adaptive Control of Near-Minimum-Time Spacecraft Maneuvers," AAS Space Flight Mechanics Conference, Reno, NV, Huntsville, AL, Feb 1997, to be submitted to the AAS *Journal of the Astronautical Sciences*.

C. Honors/Awards (bestowed upon John L. Junkins)

Elected to the National Academy of Engineering (1996).

Elected to the International Academy of Astronautics (1996).

Fellow of the American Institute of Aeronautics and Astronautics (1987).

Fellow of the American Astronautical Society (1984).

THEODORE VON KARMAN LECTURE & VON KARMAN MEDAL presented by the American Institute of Astronautics and Aeronautics(Jan, 1997).

DISTINGUISHED SCIENTIST AWARD, Sigma Xi, 1992.

OUTSTANDING AEROSPACE ENGINEERING ALUMNUS, Auburn University, 1991.

G. EDWARD PENDRAY AEROSPACE LITERATURE AWARD presented by the American Institute of Astronautics and Aeronautics (1990). Citation: *"for his numerous, high quality, and influential contributions of both timely practical value and lasting significance, to the professional literature of spacecraft dynamics and control, ..."*

Appointed *George J. Eppright Endowed Chair Professor* Texas A&M University (1989-)

JOHN LELAND ATWOOD AWARD bestowed jointly by American Institute of Aeronautics and Astronautics and the American Society of Engineering Education (1988). citation: *"for his contributions to research and the literature of modern optimal control theory, especially in spacecraft attitude control and control of large space structures. His innovative style and infectious enthusiasm has inspired his students..."*

DIRK BROUWER AWARD presented by the American Astronautical Society (1987). Citation: *"for his outstanding contributions to space flight mechanics and astrodynamics."*

MECHANICS AND CONTROL OF FLIGHT AWARD presented by the American Institute of Aeronautics and Astronautics (AIAA) (1983). Citation: *"for his significant contributions to analytical dynamics, optimal spacecraft maneuver strategies, modeling of the gravity field, and especially, his ..... optimal spacecraft maneuvers."*

Sangchul Lee
John L. Junkins
Texas A&M University
Aerospace Engineering Department
College Station, TX 77843-3141

Construction of Benchmark Problems for Solution of Ordinary Differential Equations

An inverse method is introduced to construct benchmark problems for the numerical solution of initial value problems. Benchmark problems constructed in this fashion have a known exact solution, even though analytical solutions are generally not obtainable. The process leading to the exact solution makes use of an initially available approximate numerical solution. A smooth interpolation of the approximate solution is forced to exactly satisfy the differential equation by analytically deriving a small forcing function to absorb all of the errors in the interpolated approximate solution. Using this special case exact solution, it is possible to directly investigate the relationship between global errors of a candidate numerical solution process and the associated tuning parameters for a given code and a given problem. Under the assumption that the original differential equation is well-posed with respect to the small perturbations, we thereby obtain valuable information about the optimal choice of the tuning parameters and the achievable accuracy of the numerical solution. Five illustrative examples are presented. © *1994 John Wiley & Sons, Inc.*

INTRODUCTION

We consider the initial value problem for linear or nonlinear ordinary differential equations. In general, we do not know the true solution and any numerical method gives us an approximate solution; the numerical solutions generally contain two sources of error, round-off and truncation (Gear, 1971). We must somehow evaluate the accuracy of a given approximate solution, typically without knowing the true solution. The most common way of assessing the true error of a numerical solution is to reduce some tolerance parameter, integrate again, and compare the results (Hairer et al., 1987; Shampine, 1987). Although more sophisticated error analyses can be conducted, there is no general way to absolutely

guarantee the final accuracy of the solutions. This does not preclude obtaining practical solutions for most applications, but it remains very difficult to answer subtle questions.

Many numerical methods are available for solving initial value problems. Early numerical methods were merely fixed step size implementations and these methods were straightforward to implement, but the results were often inconclusive. In the 1960s, research on numerical methods for highly nonlinear initial value problems led to adaptive methods that could automatically vary the step size and/or the order of the method to match a user-specified local error tolerance at each step. This work led to the current generation of numerical methods. Due the presence of round-off error, it is common to find that accu-

racy improves until step sizes or tolerances are decreased below some critical value; the accuracy then degrades while solution costs increase (Gear, 1971; Shampine, 1974). Shampine (1974, 1980) pointed out that a typical adaptive code will not quit when impossible accuracies are specified. He also reported that the standard ways to assess true errors may lead to wrong conclusions even using the best codes available at that time. Shampine (1974) considered a machine dependent limit on the step size and one on the local error tolerance, and he suggested a way of automatically selecting an initial step size that appears to be reliable and reasonably efficient (Shampine, 1978). Enright (1989) pointed out that the relationship between the accuracy obtained and the specified tolerances is generally extremely sensitive to both the problem and the method. In particular, for Runge–Kutta methods with interpolants, he proposed an error and step size control mechanism based on monitoring and controlling the defect of a continuous approximation rather than the local error of the discrete approximation.

In view of the historical and recent developments, we observe that the theory of differential equation solvers is far from complete, so that the understanding of a given code's performance invariably requires a study of experimental results. Hull, et al. (1972) and Krogh (1973) provided two outstanding collections of test problems for this purpose. These test problems have been used in the development and testing of many codes and can be regarded as standard benchmark problems for initial value problem solvers. Whenever we know the true solutions of a test problem, however, we can investigate the relationship between the true, or global error and the tuning parameters of a given code (e.g., step size, local error tolerance, order, etc.). The relationship between the behavior of an algorithm on a benchmark problem and the behavior of the algorithm on a problem of interest is difficult to establish. Because the problem of interest is almost never exactly solvable, we need a means to establish a customized benchmark problem that is a close neighbor of any given problem of interest. We introduce here a broadly applicable inverse method that constructs a neighbor of a given numerical approximate solution; the neighboring problem does in fact exactly satisfy the original differential equations (with a known, small forcing function) and serves as an excellent benchmark problem. More specifically, we pre-sent a broadly useful approach to construct a benchmark problem near the problem of interest in a particular application. By virtue of the fact that the benchmark problem is a customized near neighbor of the problem of interest, we show that numerical convergence studies on the benchmark problem are directly useful in algorithm selection, tuning, and accuracy validation.

The difficulties mentioned earlier result from not knowing the true solution. What happens if we are able to construct a problem-dependent "exact" benchmark problem? First we can easily investigate the true error/parameter relationship and find the limiting precision and associated values of critical parameters of a given code. Second, the problem of how to assess global error vanishes automatically. Finally, we have an absolute standard to find which method is most suitable for an important member of our particular family of problems. The sensitivity of the accuracy/tolerance relation of a given method is primarily a result of the heuristics used to monitor the local error and control the step size. If we do not know the true solution, then it is very hard to assess which method is the best for a class of problems because of the high sensitivity of accuracy to variations in step size control logic. The remaining and most critical question is: How useful is the convergence and accuracy information obtained for the exactly solved benchmark problem, in regard to drawing conclusions for the (neighboring) original problem? It is important to recall that the benchmark problem includes a regular perturbation to the original problem. If the perturbation is small enough, it is to be expected that all derivatives will be close for the two problems and consequently, the behavior of standard discrete variable methods will be similar both with respect to accuracy and stability. It is certainly true that there are open questions on this issue needing further investigation; however, by constructing a family of neighboring benchmark problems, it is usually possible to judge the size of the neighborhood in which the convergence and accuracy properties are relatively invariant with respect to the perturbation. Several applications presented herein provide strong evidence supporting the practicality of this approach.

In this study we propose a method to construct a benchmark problem that is a close neighbor of a given approximate solution of the original problem. The benchmark problem is constructed so that it satisfies exactly the differ-

ential equation but with a known, usually small, time varying forcing function. We can investigate the global error/parameter relationship of the benchmark problem with the true solution in hand. Under the assumption that the original problem is well-posed with respect to small perturbations, we have valuable information about the optimal parameters and the accuracy of the numerical solution. Actually the stability assumption is not so severe because any numerical method needs it more or less to obtain reliable solutions. Also, by introducing several neighboring approximate solutions with initial condition and parameter variations, then repeating the entire process, it is possible to experimentally establish insight on the size of the region over which the convergence properties are invariant.

Lee and Junkins (1993) presented two computer codes for first order and second order systems of differential equations, when the classical Runge–Kutta fourth order method with a fixed step size was used. An illustrations, we show the utility of these codes for two simple nonstiff problems. When we use the IMSL (1989) subroutines DIVPRK and DIVPBS as solvers, we show the utility of this methodology for two celestial mechanics problems (Krogh, 1973) that have been used as test problems several times in the literature. Subroutine DIVPRK uses the Runge–Kutta formulas of order five and six developed by J. H. Verner. Subroutine DIVPBS uses the Bulirsh–Stoer extrapolation method and will terminate when impossible accuracies are specified. In the fifth example, we consider a typical stiff problem and discuss some limitations and restrictions of this methodology.

CONSTRUCTION OF EXACT BENCHMARK PROBLEMS

We want to construct new differential equations that are slightly perturbed versions of the original differential equations. For these new differential equations, we can establish the true analytical solution using an algebraic inverse idea. Then we can investigate the error/tolerance relationship with an absolute standard. Under local stability assumptions, we have valuable information about the optimal parameters and the accuracy of the particular numerical solution for the given original differential equations. The stability assumption is easily validated by constructing some neighboring benchmark problems.

Here we introduce one way for constructing exact benchmark problems. We take a global approach for the perturbation term instead of a piecewise polynomial perturbation to avoid the lack of smoothness at break points. First we consider the following two distinct initial value problems:

$$\dot{x} = f_1(x, t), \quad x(t_0) = x_0 \quad \text{over } t_0 \leq t \leq t_f \tag{1}$$
$$f_1: R^N \times R - R^N$$

$$\ddot{x} = f_2(x, \dot{x}, t), \quad x(t_0) = x_0, \quad \dot{x}(t_0) = \dot{x}_0$$
$$\text{over } t_0 \leq t \leq t_f \tag{2}$$
$$f_2: R^N \times R^N \times R \to R^N.$$

A candidate discrete approximate solution can be obtained from the original first or second order differential Eqs. (1) and (2) using a numerical method. We distinguish between first and second order systems because there are certain drawbacks if one converts a naturally second order system into a first order system. To establish a continuous, differentiable motion near a given approximate solution, least square approximation using the discrete version of the Chebyshev polynomials can be invoked to obtain the solution from the the already discrete solution (Abramowitz and Stegun, 1972; Junkins, 1978). We first consider the least square approximation process. There are n data points denoted as

$$x_1 = g(t_1), \quad x_2 = g(t_2), \quad \ldots, \quad x_n = g(t_n)$$

where t_i are the values of the equally spaced independent variable ($h_t = (t_{i+1} - t_i) = $ constant).

A linear transformation of independent variables should be made to use discrete orthogonality with weight function $w(t) = 1$,

$$\bar{t}(t) = \frac{t - t_1}{h_t}$$

where h_t is the constant increment of t,

$$x = g(t) = G(\bar{t}). \tag{3}$$

From n data points, the function G can be established as a linear combination of m basis functions that form the discrete version of the Chebyshev polynomials as follows:

$$G(\bar{t}) \equiv \sum_{i=1}^{m} a_i T_i(\bar{t})$$

where $m \leq n$ and $T_i(\bar{t})$ is the ith Chebyshev polynomial.

The Chebyshev polynomials are defined as follows: If $u_m = m(m = 0, 1, 2, \ldots, N)$ and $w(u) = 1$, then

$$T_n(u) = \sum_{m=0}^{n} (-1)^m \binom{n}{m}\binom{n+m}{m} \frac{u!(N-m)!}{(u-m)!N!}.$$

With the recurrence relations:

$$T_0(u) = 1$$

$$T_1(u) = 1 - \frac{2u}{N}$$

$$(n+1)(N-n)T_{n+1}(u) = (2n+1)(N-2u)T_n(u) - n(N+n+1)T_{n-1}(u).$$

Note that the recurrence relations make it easy to evaluate an expansion in Chebyshev polynomials, and a similar recurrence makes it easy to evaluate the derivative of the expansion.

Using discrete orthogonality of the Chebyshev polynomials, the typical coefficient a_j can be obtained as follows:

$$a_j = \frac{\sum_{i=1}^{n} x_i T_j(\bar{t}_i)}{\sum_{i=1}^{n} T_j(\bar{t}_i)T_j(\bar{t}_i)}$$

where $1 \leq j \leq m$.

We can find $g(t)$ from $G(\bar{t})$ because $g(t) = G(\bar{t}(t))$. Using the least square approximation, we can find the continuous, differentiable, analytical solution $x(t)$ of Eq. (3) that interpolates the n discrete numerical solutions obtained from Eqs. (1) and (2). Now this analytical expression $x(t)$ does not satisfy exactly the Eqs. (1) and (2). However, substituting $x(t)$, $\dot{x}(t)$ into Eq. (1) allows us to determine an analytical function for the perturbation term $e_1(t)$ that appears in the following differential equation:

$$\dot{x}(t) = f_1(x(t), t) + e_1(t) \equiv F_1(x, t). \quad (4)$$

Alternatively, if the system is second order, then substituting $x(t)$, $\dot{x}(t)$, $\ddot{x}(t)$ into Eq. (2) allows us to determine the perturbation term $e_2(t)$ that appears in the following differential equation:

$$\ddot{x}(t) = f_2(x(t), \dot{x}(t), t) + e_2(t) \equiv F_2(x, \dot{x}, t). \quad (5)$$

Note that because $x(t)$, $\dot{x}(t)$, $\ddot{x}(t)$ are available functions, $F_1(x, t)$, $F_2(x, \dot{x}, t)$ are also available

functions that satisfy Eqs. (4) and (5) exactly, and $x(t)$ is a neighbor of the original numerical solution $\{x_1, x_2, \ldots, x_n\}$. By construction, the functions $e_1(t) = \dot{x}(t) - f_1(x(t), t)$ and $e_2(t) = \ddot{x}(t) - f_2(x(t), \dot{x}(t), t)$ are known analytically and therefore these small forcing functions can be computed exactly at all t. These functions are programmed and Eqs. (4) and (5) can be solved by numerical methods and the results can be compared to the exact $x(t)$, $\dot{x}(t)$. The above mathematical procedure can be performed in an automated fashion using computer symbol manipulation. The symbol manipulation can also automate the generation of C or FORTRAN Code to compute function e, (t) and/or $e_2(t)$.

Now Eq. (4) is a benchmark problem neighboring Eq. (1) and we have arranged that $x(t)$, $\dot{x}(t)$ satisfy Eq. (4) exactly; and Eq. (5) becomes the benchmark problem neighboring Eq. (2) and we have arranged that $x(t)$, $\dot{x}(t)$, $\ddot{x}(t)$ satisfies Eq. (5) exactly. We obviously want the perturbation function $e(t)$ to be as small as possible, that is, the benchmark problem is not only a near neighbor of the original discrete solution, but it also very nearly satisfies the same differential equations. The previously discussed least square approximation method typically gives the poorest approximation near the ends of the interval. This may result in a relatively large $e(t)$ near the initial and final times. To avoid this problem we can integrate Eqs. (1) and (2) over the enlarged interval $t_{0-} \leq t \leq t_{f+}$ (where $t_{0-} < t_0$, $t_{f-} > t_f$) and use these numerical results as generators for analytical solutions over the original interval ($t_0 \leq t \leq t_f$). Experience indicates that a 20% "enlargement" $\{(t_{f+} - t_{0-}) \geq 1.2(t_f - t_0)\}$ is almost always sufficient to support good interpolation over the original interval ($t_0 \leq t \leq t_f$). If the measure of $e(t)$ is judged too large then we increase the number of Chebyshev polynomials m to reduce $e(t)$ over the whole interval, or "start over" by attempting to find a better approximate numerical solution to initiate the process. Figures 1 and 2 provide logical flow charts showing construction of a benchmark problem and an associated convergence study for second order systems.

ILLUSTRATIVE EXAMPLES

Now we demonstrate the previous ideas using five initial value problems for ordinary differential equations. First we show the utility of the computer codes (Lee and Junkins, 1993) for two simple nonstiff problems. Then, two celestial me-
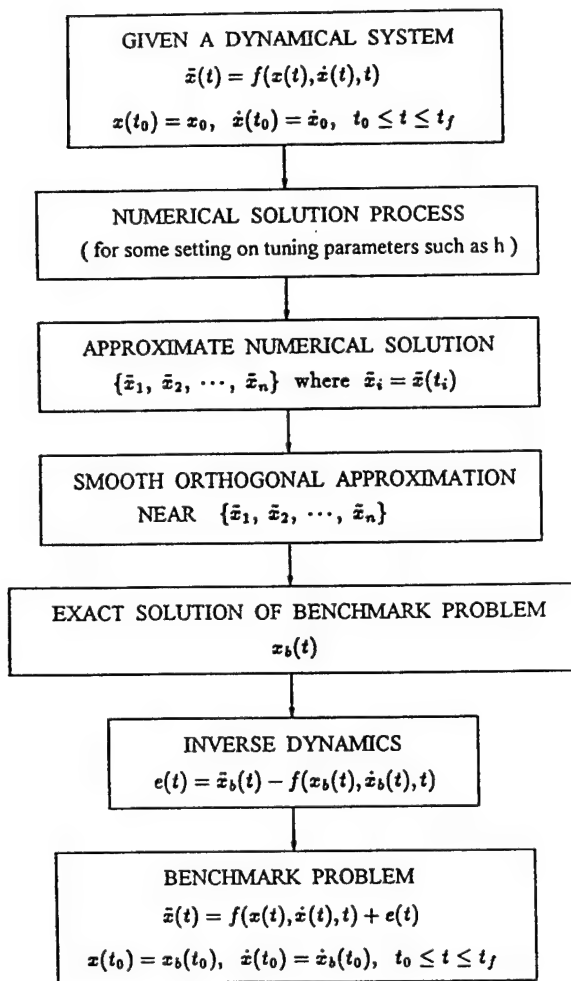
FIGURE 1 Flow chart for construction of a benchmark problem.

chanics problems are introduced to illustrate the utility of this methodology when we use the IMSL (1989) subroutines DIVPRK and DIVPBS. Finally, we consider a stiff problem in the fifth example.

First Order Systems

We consider the following pair of nonlinear differential equations.

$$\dot{x} = 2x_1 - 2x_1 x_2$$
$$\dot{x} = -x_2 + x_1 x_2 \tag{6}$$

where $x_1(0) = 1$ and $x_2(0) = 3$, and we seek the solution over the interval $0 \leq t \leq 10$.

First, we solve Eq. (6) using the Runge–Kutta fourth order method to evaluate the candidate discrete approximate solution. Here we use 121 data points over the 20% enlarged time interval $-1 \leq t \leq 11$. Second, we establish a continuous, differentiable, analytical expression for interpolating $x_1(t)$ and $x_2(t)$ from the discrete approximate solution. We use 51 Chebyshev polynomials for fitting. Finally we substitute $x_1(t)$, $x_2(t)$, $\dot{x}_1(t)$, $\dot{x}(t)$ into Eq. (6) and determine functions for $e_1(t)$ and $e_2(t)$ that satisfy the following equations exactly

$$\dot{x}_1 = 2x_1 - 2x_1 x_2 + e_1$$
$$\dot{x}_2 = -x_2 + x_1 x_2 + e_2. \tag{7}$$

Now, Eq. (7) provides a benchmark problem for Eq. (6), and $x_1(t)$, $x_2(t)$ are the solutions that satisfy Eq. (7) exactly. Upon solving Eq. (7) numerically with various values chosen for h, we establish the relationship between step size and global error. When we use the pointwise error in the root mean square sense, Fig. 3 shows the relationship in log/log scale. The critical value h is about 0.0005 and if h decreased below 0.0005, then the results begin to deteriorate. The rate of convergence is 4 in this problem and this coincides with the fact that an rth order method should have a global error of $O(h^r)$ in the absence of arithmetic errors (Gear, 1971). Figure 4 shows the perturbation terms over the time interval. For the benchmark problem, the numerical results are very reliable when we use 0.0005 as h because the error measures are about 10^{-13} while the solutions for $x_1(t)$, $x_2(t)$ vary from 10^{-2} to 10^0 order. Now we turn our attention to the original problem. Figure 5 shows the relationship between step size and error at $t = 10$ on a log/log scale for the original problem. Because we do not know the true solution, we could follow the common way of assessing the accuracy of a family of approximate solutions using the IMSL (1989) subroutines DIVPRK and DIVPBS. Comparing Figs. 3 and 5, we notice that the shape is roughly similar but, in Fig. 5, the critical value h is 0.0002 instead of 0.0005. The reason for this minor discrepancy is the relatively large perturbation terms in Fig. 4. If we decrease the perturbation terms $e_1(t)$ and $e_2(t)$ by finding a higher order, more accurate interpolation and thereby make the benchmark problem closer to the original Eq. (6), then we can reduce this discrepancy.

Second Order Systems

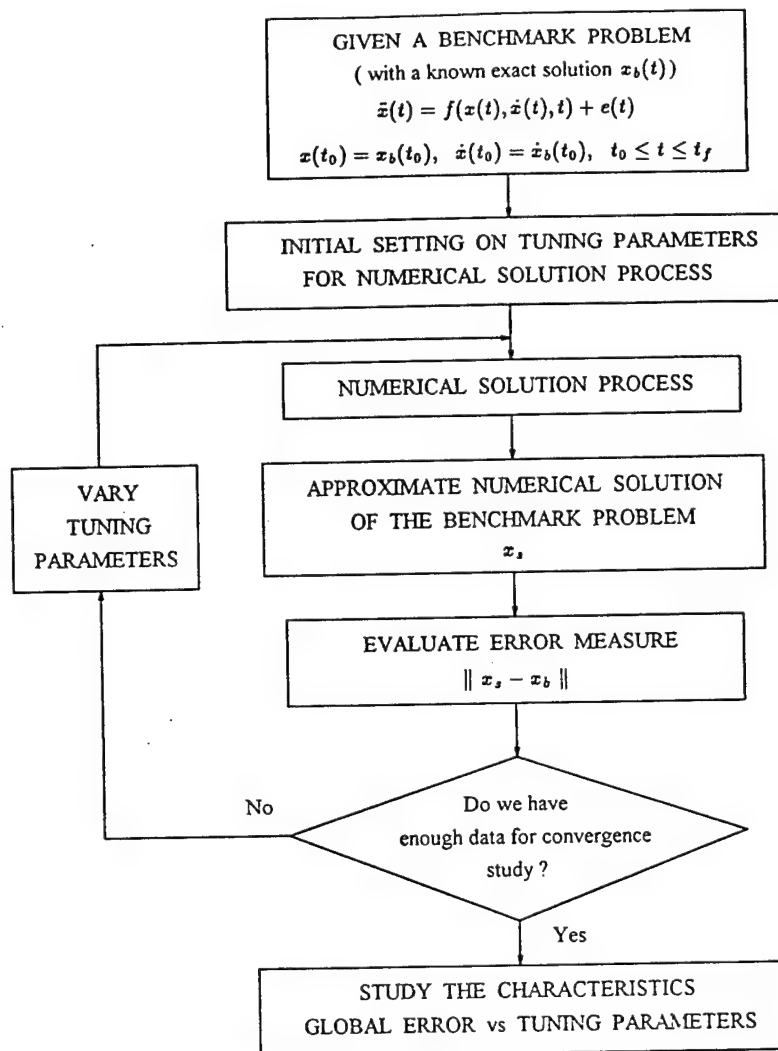We consider the following nonlinear, nonautonomous second order differential equation.

14

GIVEN A BENCHMARK PROBLEM
(with a known exact solution $x_b(t)$)

$$\ddot{x}(t) = f(x(t), \dot{x}(t), t) + e(t)$$

$$x(t_0) = x_b(t_0), \quad \dot{x}(t_0) = \dot{x}_b(t_0), \quad t_0 \leq t \leq t_f$$

INITIAL SETTING ON TUNING PARAMETERS
FOR NUMERICAL SOLUTION PROCESS

NUMERICAL SOLUTION PROCESS

VARY
TUNING
PARAMETERS

APPROXIMATE NUMERICAL SOLUTION
OF THE BENCHMARK PROBLEM
x_s

EVALUATE ERROR MEASURE
$\| x_s - x_b \|$

No

Do we have
enough data for convergence
study ?

Yes

STUDY THE CHARACTERISTICS
GLOBAL ERROR vs TUNING PARAMETERS

FIGURE 2 Flow chart for convergence study.
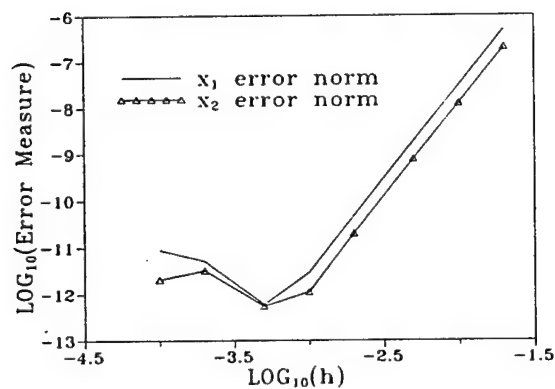
FIGURE 3 Global error vs. step size for the benchmark problem.
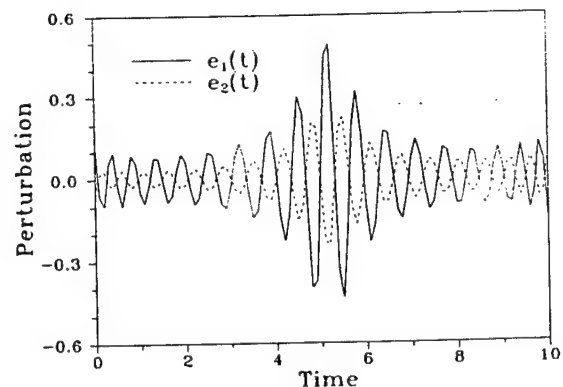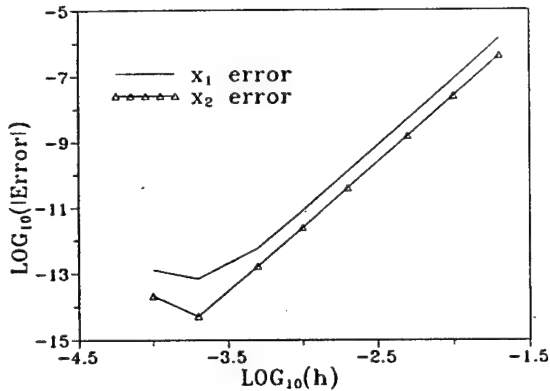

FIGURE 4 Perturbation terms of example 1.

15

FIGURE 5 Error (at $t = 10$) vs. step size for the original problem.

FIGURE 6 Global error vs. step size for the benchmark problem.

$$\ddot{x} = -x - 0.1(1 + x^2)\dot{x} + 0.1x^3 + \sin 3t \quad (8)$$

where $x(0) = 1$ and $\dot{x}(0) = 0$, and we seek the solution over the interval $0 \leq t \leq 10$. We convert Eq. (8) to a first order system as follows:

$$\dot{x}_1 = x_2$$
$$\dot{x}_2 = -x_1 - 0.1(1 + x_1^2)x_2 + 0.1x_1^3 + \sin 3t \quad (9)$$

where $x_1(0) = 1$ and $x_2(0) = 0$.

We solve Eq. (9) using the Runge–Kutta fourth order method to evaluate the candidate discrete approximate solution. Here we construct the interpolated solution using 121 data points over the 20% enlarged time interval $-1 \leq t \leq 11$. An analytical expression for $x_1(t)$ is obtained from the discrete approximate solution. In this problem, a degree 30 Chebyshev polynomial is established by the least square approximation. Substituting $x_1(t)$, $\dot{x}_1(t)$, $\ddot{x}_1(t)$, into Eq. (8) we calculate the function $e(t)$ that satisfies the following equation exactly.

$$\ddot{x} = -x - 0.1(1 + x^2)\dot{x} + 0.1x^3 + \sin 3t + e. \quad (10)$$

To use the Runge–Kutta method, Eq. (10) can be converted to a first order system as follows:

$$\dot{x}_1 = x_2$$
$$\dot{x}_2 = -x_1 - 0.1(1 + x_1^2)x_2 + 0.1x_1^3 + \sin 3t + e. \quad (11)$$

Now, Eq. (10) becomes a benchmark problem for Eq. (8), and $x(t)$ is an algebraic function that satisfies Eq. (10) exactly. When we use the pointwise error in the root mean square sense,
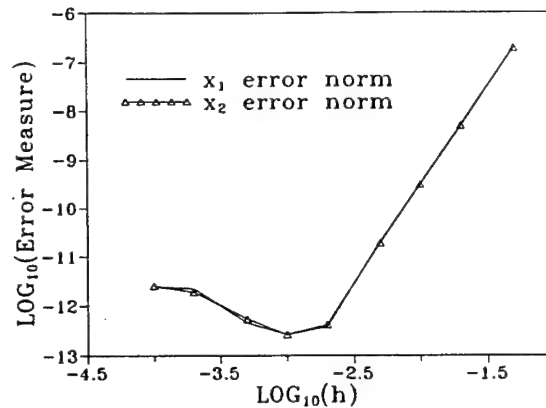
Fig. 6 shows the relationship between global error and step size. The rate of convergence is 4 as expected. Figure 7 shows the perturbation term over the time interval. The critical value for step size is about 0.001. Now we consider the original problem. The relationship between step size and error at $t = 10$ is shown in Fig. 8 when we follow the common way assessing the true solution using the IMSL (1989) subroutines DIVPRK and DIVPBS. Comparing Figs. 6 and 8. we observe that the critical value h and the accuracy are almost the same.

We change the initial conditions slightly and the nonautonomous term in the differential equation as follows:

$$\ddot{x} = -x - 0.1(1 + x^2)\dot{x} + 0.1x^3 + 1.2 \sin 3t \quad (12)$$

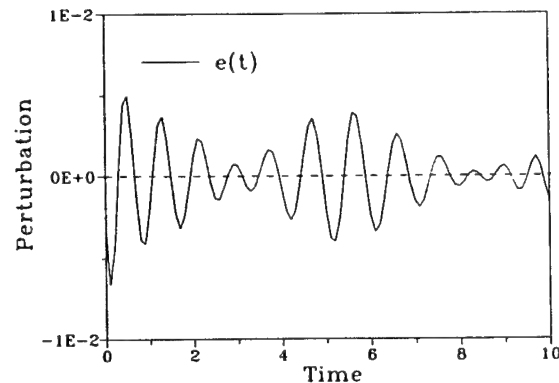where $x(0) = 1.2$ and $\dot{x}(0) = 0.2$ over the interval $0 \leq t \leq 10$.

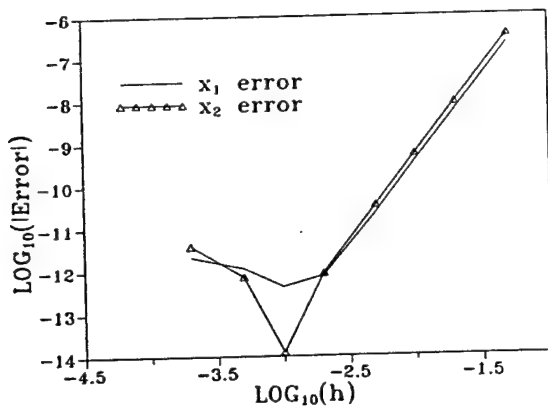**FIGURE 7** Perturbation term of example 2.

16

FIGURE 8 Error (at $t = 10$) vs. step size for the original problem.

FIGURE 10 Absolute error vs. tolerance for the benchmark problem (DIVPRK).

After using the same procedure, we obtain the global error/step size relationship shown in Fig. 9. We notice that Figs. 6 and 9 are almost the same. In other words, the critical value for h and the accuracy are almost identical even though there are 20% perturbations in the initial condition and the forcing term in the differential equation, in this case.

Two Body Problem

We consider the simple two body problem. The exact solution is periodic with period 2π and the solution traces out an ellipse with eccentricity 0.6.

$$\ddot{x} = -x/r^3, \quad x(0) = 0.4, \quad \dot{x}(0) = 0$$
$$\ddot{y} = -y/r^3, \quad y(0) = 0, \quad \dot{y}(0) = 2$$
(13)

where $r = (x^2 + y^2)^{1/2}$.

These equations can be solved exactly (Battin, 1987): the analytical solution is not included here because of space limitations. We reformulate Eq. (13) as a first order system as follows:

$$\dot{x}_1 = x_2$$
$$\dot{x}_2 = -x_1/(x_1^2 + x_3^2)^{3/2}$$
$$\dot{x}_3 = x_4$$
$$\dot{x}_4 = -x_3/(x_1^2 + x_3^2)^{3/2}$$
(14)

where $x_1(0) = 0.4$, $x_2(0) = 0$, $x_3(0) = 0$, $x_4(0) = 2$.

We solve Eq. (14) using DIVPRK to evaluate the candidate discrete approximate solution. Here we use 121 data points over the 20% enlarged time interval and a degree 50 Chebyshev polynomial approximation is used for the least square fitting of $x_1(t)$ and $x_3(t)$. After constructing the benchmark problem, we do an absolute error test on $(0. 2\pi)$. Figures 10 and 11 show the
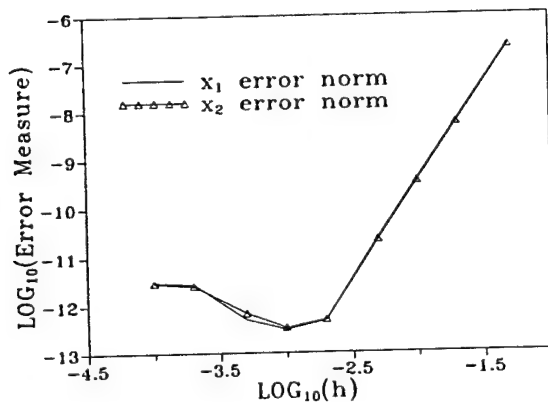

FIGURE 9 Global error vs. step size for the benchmark problem of 20% perturbations.

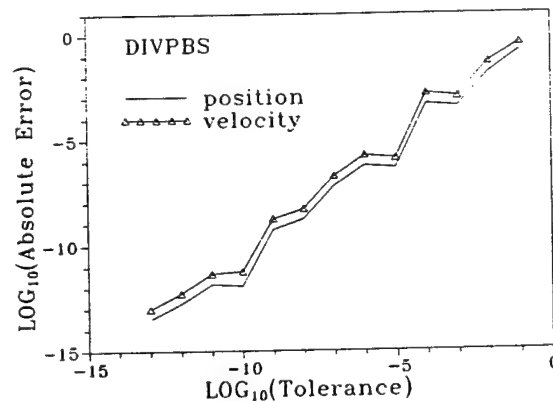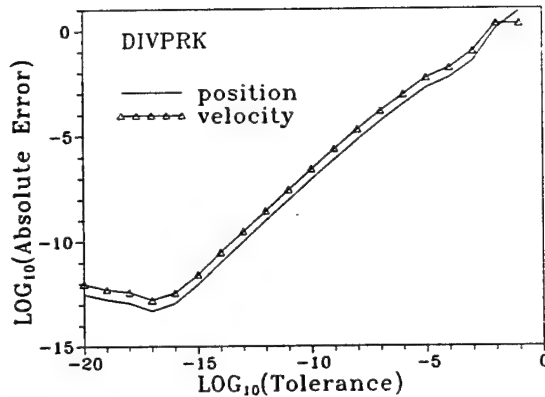**FIGURE 11** Absolute error vs. tolerance for the benchmark problem (DIVPBS).

17

FIGURE 12   Absolute error vs. tolerance for the two body problem (DIVPRK).

FIGURE 14   Perturbation terms of the two body problem.

relationship between absolute error and tolerance in log/log scale when we use DIVPRK and DIVPBS for the benchmark problem. Figures 12 and 13 show the relationship between absolute error and tolerance in log/log scale when we use DIVPRK and DIVPBS for the original two body problem. We notice that Figs. 10 and 11 are almost identical to Figs. 12 and 13, respectively. The perturbation terms are shown in Fig. 14. We plot the relationship between the number of function calls and the absolute error in Fig. 15. Thus the benchmark problem (constructed by the method of this study) essentially gives results that are identical to those obtained by using the exact solution of the original problem.

Euler Equations of Motion

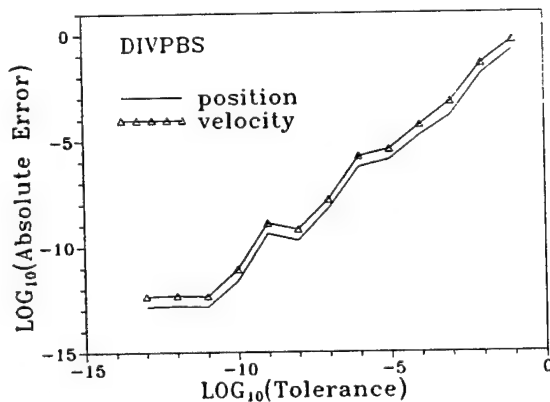We consider the Euler equation of motion for a rigid body without external forces,

$$\dot{x}_1 = x_2 x_3$$
$$\dot{x}_2 = -0.51 x_3 x_1 \qquad (15)$$
$$\dot{x}_3 = -x_1 x_2$$

where $x_1(0) = 0$, $x_2(0) = 1$, $x_3(0) = 1$.

The classical exact solutions of Eq. (15) are the Jacobian elliptic functions (Abramowitz and Stegun, 1972) as follows:

$$x_1 = sn(t \mid 0.51), \quad x_2 = dn(t \mid 0.51),$$
$$x_3 = cn(t \mid 0.51).$$

They are periodic with a quarter period K where $K = 1.86264\ 08023\ 32738\ 55203\ \cdots$ in this case.

We solve Eq. (15) using DIVPRK to evaluate the candidate discrete approximate solution. To

FIGURE 13   Absolute error vs. tolerance for the two body problem (DIVPBS).

FIGURE 15   Number of function calls vs. absolute error.
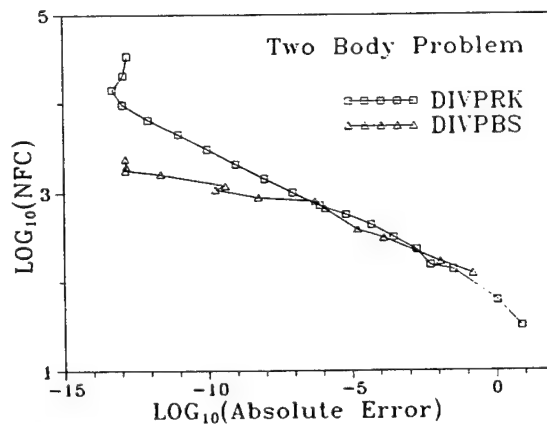
FIGURE 16 Absolute error vs. tolerance for the benchmark problem (DIVPRK).
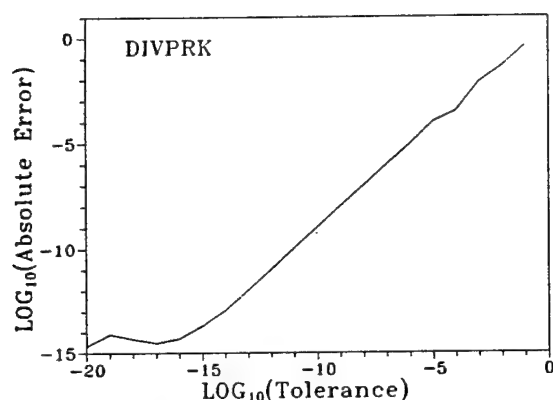

FIGURE 18 Absolute error vs. tolerance for the Euler equations (DIVPRK).

establish a benchmark using our method, we use 121 data points over the 20% enlarged time interval and determine a degree 50 Chebyshev least square polynomial approximation of $x_1(t)$, $x_2(t)$, and $x_3(t)$. After constructing the benchmark problem, we do an absolute error test on $(0, 4K)$. Figures 16 and 17 show the relationship between absolute error and tolerance in log/log scale when we use DIVPRK and DIVPBS for the benchmark problem. Figures 18 and 19 show the relationship between absolute error and tolerance in log/log scale when we use DIVPRK and DIVPBS to solve Eq. (15) and compare to the classical Jacobian elliptic function solution. We notice that Figs. 16 and 17 are almost identical to Figs. 18 and 19, respectively. The perturbation terms are shown in Fig. 20. We plot the relationship between the number of function calls and the absolute error in Fig. 21. Thus, again, this example indicates that our neighboring

benchmark problem leads to essentially identical convergence properties to using the exact solution of the original problem.

A Stiff Problem

We consider the following problem (Shampine and Gordon, 1975) that represents a typical stiff problem.

$$\dot{x}_1 = -29998x_1 - 39996x_2$$
$$\dot{x}_2 = 14998.5x_1 + 19997x_2 \tag{16}$$

where $x_1(0) = 1$, $x_2(0) = 1$.

The exact solutions of Eq. (16) are as follows:

$$x_1(t) = 7\exp(-10^4 t) - 6\exp(-t)$$
$$x_2(t) = -3.5\exp(-10^4 t) + 4.5\exp(-t). \tag{17}$$
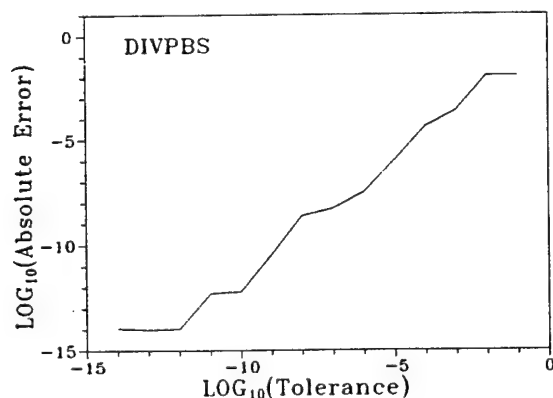

FIGURE 17 Absolute error vs. tolerance for the benchmark problem (DIVPBS).
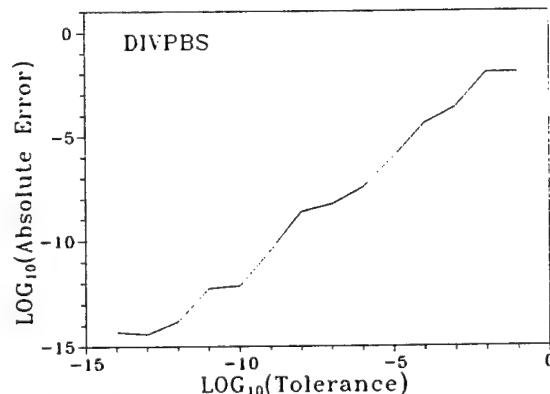
FIGURE 19 Absolute error vs. tolerance for the Euler equations (DIVPBS).

19
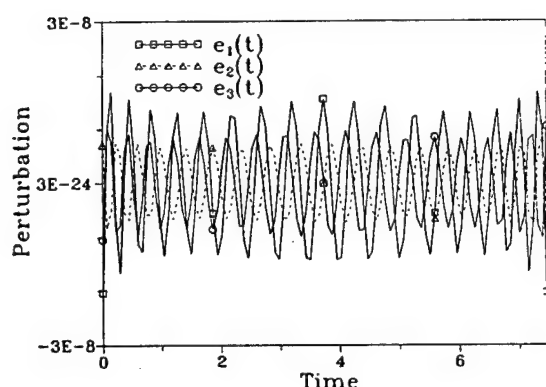
FIGURE 20 Perturbation terms of the Euler equations.

FIGURE 22 Solution of example 5 for the rapid change region.

The eigenvalues of the coefficient matrix are -1 and -10^4. Figures 22 and 23 show the solutions over two different intervals, a region of very rapid change followed by gradual asymptotic behavior. It is almost impossible to obtain a satisfactory orthogonal function benchmark problem that covers both regions with a reasonable number of terms. We conclude that the proposed methodology is not adequate for such stiff problems unless piecewise approximation methods, for example, the type introduced by Junkins et al. (1973) are used. Stiff problems are relatively expensive to solve and the expense depends strongly on the tolerance (Gear, 1971; Shampine and Gordon, 1975; Shampine and Gear, 1979). Enright et al. (1975) provide a good collection of stiff test problems.

SUMMARY AND CONCLUSION

The present article introduces an inverse method for constructing exact benchmark problems for initial value problems. This methodology gives valuable information about the optimal tuning parameters and the accuracy of the numerical solution for a class of ordinary differential equation problems and for a given solution code. Numerical examples indicate that a rigorous error analysis is usually obtained not merely for one nominal solution, but for a substantial neighborhood of the nominal solution. If one wants to use the classical Runge–Kutta method with a fixed step size, then the codes (Lee and Junkins, 1993) provide directly useful information about the optimal step size h and the associated accuracy.

FIGURE 21 Number of function calls vs. absolute error.
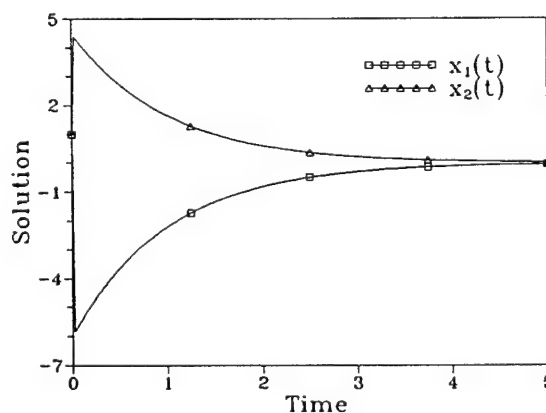
FIGURE 23 Solution of example 5 for the gradual change region.

More sophisticated users who are familiar with adaptive and robust codes can also construct similar benchmark problems; however, the Chebyshev approximation method may have to be replaced or modified to obtain a method not restricted to uniformly spaced data. For stiff systems, special purpose approximations may be required in lieu of the global Chebyshev approximations. The analytical expressions for the benchmark problem and its solution can be established using computer symbol manipulation [e.g., MACSYMA (1988), Mathematica, MAPLE, etc.]. Then the user investigates the global error/parameter relationship and compares various codes with special case absolute standards. In examples 3 and 4, we show the utility of this methodology using the IMSL (1989) subroutines DIVPRK and DIVPBS as solvers. And we investigate the absolute error/tolerance relationship and compare DIVPRK and DIVPBS. We have developed some basic methodologies, but there remains a need for additional numerical experiments to further evaluate the practical utility of this approach.

REFERENCES

Abramowitz, M., and Stegun, I. A., 1972, *Handbook of Mathematical Functions with Formulas, Graphs, and Mathematical Tables*, National Bureau of Standards, Applied Mathematics Series 55, U.S. Department of Commerce.

Battin, R. H., 1987, *An Introduction to the Mathematics and Methods of Astrodynamics*, AIAA Education Series, New York, New York.

Enright, W. H., 1989, "Analysis of Error Control Strategies for Continuous Runge–Kutta Methods," *SIAM Journal of Numerical Analysis*, Vol. 26, pp. 588–599.

Enright, W. H., Hull, T. E., and Lindberg. B., 1975, "Comparing Numerical Methods for Stiff Systems of ODEs," *BIT*, Vol. 15, pp. 10–48.

Gear, C. W., 1971, *Numerical Initial Value Problems in Ordinary Differential Equations*, Prentice–Hall, Englewood Cliffs, NJ.

Hairer, E., Norsett, S. P., and Wanner, G., 1987, *Solving Ordinary Differential Equations I. Nonstiff Problems*, Springer–Verlag, Berlin, pp. 236–241.

Hull, T. E., Enright, W. H., Fellen, B. M., and Sedgwick, A. E., 1972, "Comparing Numerical Methods for Ordinary Differential Equations," *SIAM Journal of Numerical Analysis*, Vol. 9, pp. 603–637.

IMSL Math/Library User's Manual Version 1.1, IMSL Inc., 1989.

Junkins, J. L., 1978, *An Introduction to Optimal Estimation of Dynamical Systems*, Sijhoff & Noordhoff, Alphen aan den Rijn, The Netherlands.

Junkins, J. L., Miller, G. W., and Jancaitis, J. R., 1973, "A Weighting Function Approach to Modeling of Irregular Surfaces," *Journal of Geophysical Research*, Vol. 78, pp. 1794–1803.

Krogh, F. T., 1973, "On Testing a Subroutine for the Numerical Integration of Ordinary Differential Equations," *Journal of the Association for Computing Machinery*, Vol. 20, pp. 545–562.

Lee, S., and Junkins, J. L., 1993, *Construction of Benchmark Problems for Solution of Ordinary Differential Equations*, Dept. of Aerospace Engineering, Texas A&M Univ., Technical Report, AERO 93-0801, College Station, TX.

MACSYMA Reference Manual Version 13, Symbolics Inc., 1988.

Shampine, L. F., 1974, "Limiting Precision in Differential Equation Solvers," *Mathematical Computation*, Vol. 28, pp. 141–144.

Shampine, L. F., 1978, "Limiting Precision in Differential Equation Solvers, II: Sources of Trouble and Starting a Code," *Mathematical Computation*. Vol. 32, pp. 1115–1122.

Shampine, L. F., 1980, "What Everyone Solving Differential Equations Numerically Should Know," in I. Gladwell and D. K. Sayers. *Computational Techniques for Ordinary Differential Equations*, Academic Press. London, pp. 1–18.

Shampine, L. F., 1987, "Tolerance Proportionality in ODE Codes." in A. Bellen. C. W. Gear, and E. Russo, *Numerical Methods for Ordinary Differential Equations*, Proceedings, L'Aquila. Springer–Verlag, New York, pp. 118–135.

Shampine, L. F., and Gear, C. W., 1979. "A User's View of Solving Stiff Ordinary Differential Equations," *SIAM Review*, Vol. 21, pp. 1–17.

Shampine, L. F., and Gordon, M. K., 1975, *Computer Solution of Ordinary Differential Equations*, W. H. Freeman, San Francisco.

VALIDATION OF FINITE DIMENSIONAL APPROXIMATE SOLUTIONS FOR DYNAMICS OF DISTRIBUTED PARAMETER SYSTEMS

John L. Junkins[*] and Sangchul Lee[†]

VALIDATION OF FINITE DIMENSIONAL APPROXIMATE SOLUTIONS FOR DYNAMICS OF DISTRIBUTED PARAMETER SYSTEMS

John L. Junkins[*] and Sangchul Lee[†]

An inverse dynamics method is introduced for constructing exact special case solutions for hybrid coordinate ordinary/partial systems of differential equations (hybrid ODE/PDE systems), and the utility of this method in validating numerical solution methods is explored.

INTRODUCTION: Construction of Benchmark Problems for Solution of Ordinary Differential Equations

Given a flexible multi-body dynamical system, most rigorously described by a hybrid system of nonlinear ordinary and partial differential equations, we seek to validate simulations of the behavior of the system by numerical methods. With most applications of approximate solution algorithms, we must somehow evaluate the accuracy of a given approximate solution, without knowing the true solution. What happens if we can construct an exact forced response solution for a special case motion near(in a sense to be established) a candidate approximate solution? This gives us an absolute standard and promises the capability of displaying exactly the space/time distribution of solution errors for the special-case solution and therefore suggesting remedies, if needed, to improve the discretization-based solution process.

The idea is easily introduced by first considering the initial value problem for nonlinear ordinary differential equations.[1] In general, we do not know the true solution and the numerical methods give us an approximate solution. The most common way of assessing the true error of a numerical solution is to reduce the tolerance, integrate again, and compare the results.[2,3] While more sophisticated error analyses can be conducted, there is no general way to absolutely guarantee the final accuracy of the solutions. While this does not preclude obtaining practical solutions for most applications, it remains very difficult to answer subtle questions. Actually the theory of differential equation solvers is far from complete, so that the understanding of a given code's performance invariably requires a study of experimental results. Hull, et al[4] and Krogh[5] provided two outstanding collections

[*]   Eppright Chair Professor, Department of Aerospace Engineering, Texas A&M University, College Station, Texas 77843-3141. Fellow AAS; Fellow AIAA.

[†]   Graduate Student, Department of Aerospace Engineering, Texas A&M University, College Station, Texas 77843-3141. Student Member AIAA.

of test problems for this purpose, for the case of ordinary differential equations. These test problems have been used in the development and testing of the codes and can be regarded as standard benchmark problems for initial value problem solvers.

Whenever we know the true solution of a test problem we can investigate the relationship between the true, or global error and parameters of a given code(e.g., step size, local error tolerance, order, etc.). Of course, only for a small minority of interesting problems can the initial value problem be solved analytically. We introduce here an inverse method which algebraicly constructs a continuous neighbor of a given numerical approximate solution; the neighboring continuous motion does in fact exactly satisfy the differential equations(with a known small forcing function) and serves as an excellent benchmark problem. The remaining and most critical question is: *How useful is the convergence and accuracy information obtained for the benchmark problem, as regards drawing conclusions for the original problem?* It is certainly true that there are open questions on this issue, however, by constructing a family of neighboring benchmark problems, it is usually possible to judge the size of the neighborhood in which the convergence and accuracy properties are relatively invariant with respect to the perturbation, and thereby gain the practical insight needed to proceed with confidence in a solution and associated error measures.

Now, we propose a method to construct a benchmark problem which is a closely neighboring trajectory of a given approximate solution of the original problem. As will be evident, the benchmark problem motion is constructed algebraicly so that it satisfies exactly the differential equation but with a known, usually small, time varying forcing function. We can then investigate the global error/parameter relationship of the benchmark problem with the true solution in hand. Under the assumption that the original problem is well-posed with respect to small perturbations, we have valuable information about the optimal parameters and the accuracy of the numerical solution. Through study of a family of neighboring benchmark problems, we can directly establish insight on the "stability" of this error analysis.

Initially, we restrict attention to nonlinear ordinary differential equation(ODE) systems, we subsequently broaden the discussion and examples to consider hybrid differential equation systems. Here we introduce one way for constructing the exact benchmark problem. First we consider the following initial value problem for a second order ODE system:

$$\ddot{x} = f(x, \dot{x}, t), \qquad x(t_0) = x_0, \quad \dot{x}(t_0) = \dot{x}_0 \qquad over\ t_0 \leq t \leq t_f$$

$$f : R^N \times R^N \times R \rightarrow R^N \tag{1}$$

Here we consider the case where x is a scalar(i.e.,$N=1$). The following approach can be easily generalized for the vector case. A candidate discrete approximate solution can be obtained from the original second order differential equation (1)

2090

24

using a numerical method. To establish a continuous, differentiable motion near a given approximate solution, we use a least square approximation based upon the discrete version of the Chebyshev polynomials; this polynomial approximation can be established directly from the discrete approximate solution.[6,7] We first consider the least square process. There are n data points such as $x_1 = g(t_1)$, $x_2 = g(t_2)$, $\cdots$, $x_n = g(t_n)$ where t_i are the equally spaced values of the independent variable($h_t = (t_{i+1} - t_i) = $ constant).

A linear transformation to nondimensionalize the independent variable should be made to use the discrete version of the Chebyshev polynomials.

$$\bar{t}(t) = \frac{t - t_1}{h_t}$$

where h_t is the constant increment of t.

$$x = g(t) = G(\bar{t})$$

From n data points, the least square polynomial approximation function G can be established by a linear combination of m basis functions; we use the discrete version of the Chebyshev polynomials[7] with weight function $w(t) = 1$ as follows:

$$G(\bar{t}) \equiv \sum_{i=1}^{m} a_i T_i(\bar{t})$$

where $m \leq n$ and the $T_i(\bar{t})$ are the discretely orthogonal Chebyshev polynomials.

The Chebyshev polynomials are defined as follows:

If $u_m = m$ $(m = 0, 1, 2, \cdots, N)$ and $w(u) = 1$, then

$$T_n(u) = \sum_{m=0}^{n} (-1)^m \binom{n}{m} \binom{n+m}{m} \frac{u! \, (N - m)!}{(u - m)! \, N!}$$

with the recurrence relationships:

$$T_0(u) = 1$$

$$T_1(u) = 1 - \frac{2u}{N}$$

$$(n + 1)(N - n)T_{n+1}(u) = (2n + 1)(N - 2u)T_n(u) - n(N + n + 1)T_{n-1}(u)$$

Using the discrete orthogonality property of the Chebyshev polynomials[7], coefficient a_j can be obtained as follows:

$$a_j = \frac{\sum_{i=1}^{n} x_i T_j(\bar{t}_i)}{\sum_{i=1}^{n} T_j(\bar{t}_i) T_j(\bar{t}_i)}$$

2091

where $1 \le j \le m$. Since no matrix inverse is required, and owing to the completeness of these polynomials, it is well known that most smooth functions can usually be approximated accurately using a modest degree (n).

We can find $g(t)$ from $G(\bar{t})$, since $g(t) = G(\bar{t}(t))$. Using this least square approximation, we can find a continuous, differentiable, analytical solution $x_b(t)$ which interpolates or lies very near the given n discrete numerical $\tilde{x}_i$ approximate solutions of Eq.(1). Of course this analytical expression $x_b(t)$ does not satisfy exactly the Eq.(1). However, substituting $x_b(t)$, $\dot{x}_b(t)$, $\ddot{x}_b(t)$ into the equation $e(t) = \ddot{x}(t) - f(x(t), \dot{x}(t), t)$ allows us to determine an analytical function for the perturbation term $e(t)$ which appears in the following differential equation:

$$\ddot{x}(t) = f(x(t), \dot{x}(t), t) + e(t) \equiv F(x, \dot{x}, t) \tag{2}$$

Since $f(x(t), \dot{x}(t), t)$ is given and $e(t)$ is an available algebraic function, $F(x, \dot{x}, t)$ is available. Now $x_b(t)$ satisfies Eq.(2) exactly, and finally, this known function $x_b(t)$ is a neighbor of the original numerical solution $\{\tilde{x}_1, \tilde{x}_2, \cdots, \tilde{x}_n\}$. By algebraic construction the function $e(t) = \ddot{x}_b(t) - f(x_b(t), \dot{x}_b(t), t)$ is known analytically and therefore we know this small forcing function at all t, and obviously, we know "how small" $e(t)$ is. This function is programmed and Eq.(2) can then be solved by numerical methods and the results can be compared to the known exact $x_b(t), \dot{x}_b(t)$. The above mathematical procedure can be performed successfully using computer symbol manipulation[8], this is especially important for the generalizations to consider hybrid differential equations. Now Eq.(2) is a benchmark problem of Eq.(1) and $x_b(t)$, $\dot{x}_b(t)$, $\ddot{x}_b(t)$ satisfy Eq.(2) exactly. We obviously want the perturbation function $e(t)$ to be as small as possible, i.e., the benchmark problem is not only a near neighbor of the original discrete solution, but it also very nearly satisfies the given differential equations.

The previous least square approximation method has often been found to give poor results near the ends of the interval. This poor fit may cause a relatively large $e(t)$ near the initial and final times. To avoid this problem we integrate Eq.(1) over the enlarged interval $t_{0-} \le t \le t_{f+}$ (where $t_{0-} < t_0$, $t_{f+} > t_f$) and use these numerical results as generators for analytical solutions over the original interval $(t_0 \le t \le t_f)$. Experience indicates that a 20% "enlargement"$\{(t_{f+} - t_{0-}) \ge 1.2(t_f - t_0)\}$ is almost always sufficient to support good interpolation over the original interval $(t_0 \le t \le t_f)$. If the measure of $e(t)$ is judged too large then we increase the number of Chebyshev polynomials m to reduce $e(t)$ over the whole interval, or "start over" by attempting to find a better approximate numerical solution to initiate the process. Figures 1 and 2 provide logical flow charts showing construction of a benchmark problem and associated convergence study.

Now we demonstrate the idea using a simple nonstiff problem. We use the Runge-Kutta 4th order method with fixed step size, therefore we have the most common case that the integration control parameter is simply the step size h. The

2092

26

relationship between step size h and the global, or true errors gives us the information about the critical value for h and the accuracy of the numerical solution. We consider the following nonlinear, nonautonomous second order differential equation.

$$\ddot{x} = -x - 0.1(1 + x^2)\dot{x} + 0.1x^3 + \sin 3t \qquad (3)$$

where $x(0) = 1$ and $\dot{x}(0) = 0$, and we seek the solution over the interval $0 \le t \le 10$. We convert Eq.(3) to a first order system as follows:

$$\dot{x}_1 = x_2$$
$$\dot{x}_2 = -x_1 - 0.1(1 + x_1^2)x_2 + 0.1x_1^3 + \sin 3t \qquad (4)$$

where $x_1(0) = 1$ and $x_2(0) = 0$.

First, we solve Eqs.(4) using the Runge-Kutta 4th order method to evaluate the candidate discrete approximate solution. Here we use 121 data points over the 20% enlarged time interval $-1 \le t \le 11$. Second, we establish a continuous, differentiable, analytical expression for interpolating $x_{1b}(t)$ from the discrete approximate solution $\bar{x}_1(t)$. We use a degree 30 Chebyshev polynomial approximation for the least square fitting. Finally we substitute $x_{1b}(t)$, $\dot{x}_{1b}(t)$, $\ddot{x}_{1b}(t)$ into Eq.(3) and symbolically determine the function $e(t)$ which appears in the following equation.

$$\ddot{x} = -x - 0.1(1 + x^2)\dot{x} + 0.1x^3 + \sin 3t + e \qquad (5)$$

To use the Runge-Kutta method, Eq.(5) can be converted to a first order system as follows:

$$\dot{x}_1 = x_2$$
$$\dot{x}_2 = -x_1 - 0.1(1 + x_1^2)x_2 + 0.1x_1^3 + \sin 3t + e \qquad (6)$$

Now, Eq.(5) serves as a benchmark problem for Eq.(3), because we know functions $x_b(t)$ and $e(t)$ which satisfy Eq.(5) exactly. Upon solving Eqs.(6) numerically with various values chosen for h, and using the benchmark initial state as initial conditions $\{x_1(0) = x_b(0), \; x_2(0) = \dot{x}_b(0)\}$, we can establish the relationship between step size and global error. When we use the pointwise error in the root mean square sense, we are led to the results in Fig.3 which shows the global error/step size relationship on a log/log scale. The rate of convergence on a log/log scale is 4 in this problem; this coincides with the fact that an rth order method should have a global error of $O(h^r)$ in the absence of arithmetic errors.[9] The critical value for step size is about 0.001; if h decreased below 0.001, then the results deteriorate due to the round-off error. The exact solution of this benchmark problem and simulation errors are shown in Figs.5 and 6. To study the robustness of the convergence characteristics of Fig.3, we introduce relatively large perturbations in the initial conditions and the nonautonomous term in the differential equation as follows:

2093

27

$$\ddot{x} = -x - 0.1(1 + x^2)\dot{x} + 0.1x^3 + 1.2sin3t \qquad (7)$$

where $x(0) = 1.2$ and $\dot{x}(0) = 0.2$ over the interval $0 \leq t \leq 10$.

After using the same procedure to vary the step size and therefrom we obtain the global error/step size relationship shown in Fig.4. Notice that Fig.3 and Fig.4 are almost identical. In other words, both the critical value h and the associated accuracy are essentially unchanged, even though we introduced large(20%) perturbations in the initial conditions and in the forcing term of the differential equation. Obviously these results are problem dependent, but a similar process will provide the needed insight for other problems.

Now we apply this idea to an idealized three-body distributed parameter system. The main difference is that there are two independent variables for space and time. Therefore, the least square approximation method must be generalized to deal with two independent variables. In order to obtain an approximate candidate discrete solution, we use linear quadratic regulator(LQR) to design control forces and we use the finite element approach for space discretization. From this approximate solution, we construct a smooth, differentiable, analytical solution which is physically meaningful. We investigate the exact space/time distribution of errors of the numerical simulation using Newmark method with finite element modeling.

A THREE-BODY DISTRIBUTED PARAMETER SYSTEM

Now we demonstrate the idea on an idealized three-body distributed parameter system. With reference to Fig.7, we consider a rigid hub with a cantilevered flexible appendage which has a finite tip mass. Table 1 summarizes the configuration parameters of this flexible structure.

Table 1 Configuration Parameters of a Three-Body Problem

PARAMETER	SYMBOL	VALUE
Hub radius	r	1 ft
Rotary inertia of hub	J_h	8slug·ft^2
Mass density of beam	ρ	0.0271875 slug/ft
Elastic modulus of beam	E	0.1584×10^{10} lb/ft^2
Beam length	L	4.0 ft
Moment of inertia of beam	I	0.4709502797×10^{-7} ft^4
Tip mass	m_t	0.156941 slug
Rotary inertia of tip mass	J_t	0.0018 slug·ft^2

2094

28

The appendage is considered to be a uniform flexible beam and we make the Euler-Bernoulli assumptions of negligible shear deformation and negligible distributed rotatory inertia. The beam is cantilevered rigidly to the hub. Motion is restricted to the horizontal plane and we neglect the velocity component $-y\dot{\theta}$, that is perpendicular to the y direction. The control system is assumed to generate a torque u acting upon the hub, a torque u_{tip} and a force f_{tip} acting upon the tip mass, and a distributed force density $\hat{f}$ acting upon the appendage. We assume small elastic motions viewed from the hub-fixed rotating reference frame. Overdots denote derivatives with respect to time and primes denote derivatives with respect to the spatial position.

The kinetic and potential energies of this hybrid system are as follows:

$$2T = J_h\dot{\theta}^2 + \int_0^L [\rho\{\dot{y} + (x+r)\dot{\theta}\}^2]\,dx + m_t\{\dot{y}(L) + (r+L)\dot{\theta}\}^2 + J_t\{\dot{\theta} + \dot{y}'(L)\}^2 \quad (8)$$

$$2V = \int_0^L \{EI(y'')^2\}\,dx \quad (9)$$

The nonconservative virtual work of this system is given by

$$\delta W_{nc} = \{u + \int_0^L \hat{f}(x)(x+r)\,dx + (L+r)f_{tip} + u_{tip}\}\delta\theta$$

$$+ \int_0^L \hat{f}(x)\delta y\,dx + f_{tip}\delta y(L) + u_{tip}\delta y'(L) \quad (10)$$

Using an explicit version of the classical Lagrange's equation for hybrid coordinate distributed parameter systems[10], the governing differential equations and the boundary conditions are obtained efficiently.

$$J_h\ddot{\theta} + \int_0^L \rho(x+r)(\ddot{y} + (x+r)\ddot{\theta})\,dx + m_t(L+r)\left((L+r)\ddot{\theta} + \ddot{y}(L)\right) + J_t(\ddot{\theta} + \ddot{y}'(L))$$

$$= u + \int_0^L \hat{f}(x)(x+r)\,dx + (L+r)f_{tip} + u_{tip} \quad (11)$$

$$\rho\{\ddot{y} + (x+r)\ddot{\theta}\} + EI\,y'''' = \hat{f} \quad (12)$$

$$EI\frac{\partial^3 y}{\partial x^3}\bigg|_L - m_t\{(L+r)\ddot{\theta} + \ddot{y}(L)\} + f_{tip} = 0 \quad (13)$$

$$EI\frac{\partial^2 y}{\partial x^2}\bigg|_L + J_t\{\ddot{\theta} + \ddot{y}'(L)\} - u_{tip} = 0 \quad (14)$$

Notice that if we knew an explicit, differentiable solution for the motion variables $\{y(x,t), \theta(t)\}$, then the Eqs.(11-14) can be solved directly and exactly for the four corresponding time and space varying forces and moments

2095

29

$\{u(t), \hat{f}(x,t), u_{tip}(t), f_{tip}(t)\}$ thus yielding the desired inverse solution. Since we are interested in physically meaningful problems, we do not wish to randomly guess the solution $\{y(x,t), \theta(t)\}$. Motivated by the above results for ODEs, we will construct an exact solution which is a near neighbor of a given approximate solution. First we consider a conventional path to construct the approximate solution.

FINITE ELEMENT APPROACH

Using the FEM, the partial differential equations of the motion are transformed into an approximate set of second-order differential equations in terms of the displacements, velocities, and accelerations of the finite element coordinates, and the external forcing functions. Several finite element models for a flexible arm are presented in Refs.[11] and [12]. In this section, we will develop a finite element model for a hub with an appendage and a tip mass by using the extended Hamilton's principle that provides a variational weak form for the finite element model. It is significant to note that we carefully introduce the finite element approximations in such a way that large hub rotations are admitted; the FEM represents small elastic displacements with respect to hub-fixed axis.

The application of the extended Hamilton's principle yields

$$\int_{t_1}^{t_2} (\delta T - \delta V + \delta W_{nc})\, dt = 0, \qquad \delta\theta = \delta y = 0 \quad \text{at} \quad t = t_1, t_2 \qquad (15)$$

Substituting Eqs.(8-10) into Eq.(15) and integrating by parts gives

$$\int_{t_1}^{t_2} \left[\int_0^L \left[\rho(\ddot{y} + (x+r)\ddot{\theta})\delta y + EI\left(\frac{\partial^2 y}{\partial x^2}\right)\delta\left(\frac{\partial^2 y}{\partial x^2}\right) - \hat{f}\delta y \right] dx \right.$$

$$+ \left\{ \int_0^L \rho(x+r)(\ddot{y} + (x+r)\ddot{\theta})\, dx + J_h\ddot{\theta} + m_t(L+r)(\ddot{y}(L) + (L+r)\ddot{\theta}) \right.$$

$$+ J_t\left(\frac{\partial\ddot{y}}{\partial x}\bigg|_L + \ddot{\theta}\right) - \left(u + \int_0^L \hat{f}(x)(x+r)\, dx + (L+r)f_{tip} + u_{tip}\right)\right\}\delta\theta$$

$$+ \left\{ m_t(\ddot{y}(L) + (L+r)\ddot{\theta}) - f_{tip} \right\}\delta y(L)$$

$$\left. + \left\{ J_t\left(\frac{\partial\ddot{y}}{\partial x}\bigg|_L + \ddot{\theta}\right) - u_{tip} \right\}\delta\left(\frac{\partial y}{\partial x}\bigg|_L\right) \right] dt = 0$$

$$(16)$$

The displacement $y(x,t)$ can be discretized using a finite element expansion [13,14]

$$y(x,t) = \sum_{i=1}^4 \psi_i^{(e)}(x)\nu_i^{(e)}(t) \qquad (17)$$

2096

30

where $\nu_1^{(e)}, \nu_2^{(e)}$ $(\nu_3^{(e)}, \nu_4^{(e)})$ are transverse deflection and rotation at the left (right) end of the element, and $\psi_i^{(e)}$ are the Hermite cubic polynomial shape functions which satisfy the conditions for the admissibility and that are defined over the finite element.

The acceleration and curvature are expressed as follows:

$$\ddot{y}(x,t) = \sum_{i=1}^{4} \psi_i^{(e)}(x)\ddot{\nu}_i^{(e)}(t), \qquad \frac{\partial^2 y}{\partial x^2} = \sum_{i=1}^{4} \frac{\partial^2}{\partial x^2}\left(\psi_i^{(e)}(x)\right)\nu_i^{(e)}(t) \qquad (18)$$

The following cubic functions are adopted as the shape functions for i-th finite element[14]

$$\begin{aligned}
\psi_1 &= 1 - 3\bar{x}_i^2 + 2\bar{x}_i^3, \qquad \psi_2 = h\bar{x}_i - 2h\bar{x}_i^2 + h\bar{x}_i^3 \\
\psi_3 &= 3\bar{x}_i^2 - 2\bar{x}_i^3, \qquad \psi_4 = -h\bar{x}_i^2 + h\bar{x}_i^3, \qquad \bar{x}_i \equiv (x - x_i)/h
\end{aligned} \qquad (19)$$

where x_i is the distance from the root of the appendage to the left end of the i-th finite element, and h is the length of the finite element. These are the most commonly used shape functions for one-dimensional beam elements.

Substitution of Eqs.(17-19) into Eq.(16) and carrying out the spatial integrations yield the global mass, stiffness and forcing matrices. After some algebra, the assembled matrix differential equation is as follows:

$$\begin{bmatrix} J_h + M_{\theta\theta} & M_{\theta\nu} \\ M_{\nu\theta} & M_{\nu\nu} \end{bmatrix} \begin{Bmatrix} \ddot{\theta} \\ \underline{\ddot{\nu}} \end{Bmatrix} + \begin{bmatrix} 0 & 0 \\ 0 & K_{\nu\nu} \end{bmatrix} \begin{Bmatrix} \theta \\ \underline{\nu} \end{Bmatrix}$$

$$= \begin{bmatrix} 1 & (r+L) & 1 \\ 0 & 0 & 0 \\ \vdots & \vdots & \vdots \\ 0 & 1 & 0 \\ 0 & 0 & 1 \end{bmatrix} \begin{Bmatrix} u \\ f_{tip} \\ u_{tip} \end{Bmatrix} + \begin{bmatrix} \int_0^L \hat{f}(x)(x+r)\,dx \\ \int_0^h \hat{f}(x)\psi_3^{(1)}(x)dx + \int_h^{2h} \hat{f}(x)\psi_1^{(2)}(x)dx \\ \int_0^h \hat{f}(x)\psi_4^{(1)}(x)dx + \int_h^{2h} \hat{f}(x)\psi_2^{(2)}(x)dx \\ \vdots \\ \int_{(n-2)h}^{(n-1)h} \hat{f}(x)\psi_4^{(n-1)}(x)dx + \int_{(n-1)h}^{nh} \hat{f}(x)\psi_2^{(n)}(x)dx \\ \int_{(n-1)h}^{nh} \hat{f}(x)\psi_3^{(n)}(x)dx \\ \int_{(n-1)h}^{nh} \hat{f}(x)\psi_4^{(n)}(x)dx \end{bmatrix}$$

$$(20)$$

where $\underline{\nu}$ is the coordinate which consists of the transverse deflection and rotation at each node of the appendage, and the matrix elements of Eq.(20) are presented in the Appendix.

2097

CONSTRUCTION OF A CANDIDATE DISCRETE SOLUTION

We can find a physically meaningful approximate solution by using any given approximate forward solution process. For simplicity, we assume that only the hub torque $u(t)$ is non zero. Then Eq.(20) can be written in a linear second order matrix form as follows:

$$M\ddot{\mathbf{x}} + K\mathbf{x} = \begin{bmatrix} 1 \\ \underline{0} \end{bmatrix} u \tag{21}$$

where

$$\mathbf{x} = \begin{Bmatrix} \theta \\ \underline{\nu} \end{Bmatrix}$$

We design a typical control law using the linear quadratic regulator(LQR), and modal coordinates are used to design controller. To perform the modal coordinate transformation, the following open-loop eigenvalue problem should be solved first[15]

$$K\underline{\phi}_i = \lambda_i M\underline{\phi}_i \qquad i = 1, 2, \cdots, n \tag{22}$$

with the normalization equation

$$\underline{\phi}_i^T M\underline{\phi}_i = 1 \qquad i = 1, 2, \cdots, n \tag{23}$$

We introduce the modal matrix

$$\Phi = [\underline{\phi}_1, \underline{\phi}_2, \cdots, \underline{\phi}_n] \tag{24}$$

The general modal coordinate transformation is then

$$\mathbf{x}(t) = \Phi\underline{\eta}(t) \tag{25}$$

where $\underline{\eta}(t)$ is the $n \times 1$ vector of modal coordinates.
The transformed equation of motion becomes

$$\tilde{M}\ddot{\underline{\eta}} + \tilde{K}\underline{\eta} = \tilde{D}u \tag{26}$$

where

$$\tilde{M} = \Phi^T M\Phi = I, \quad \tilde{K} = \Phi^T K\Phi = diag(0, \omega_1^2, \omega_2^2, \cdots, \omega_{n-1}^2), \quad \tilde{D} = \Phi^T \begin{bmatrix} 1 \\ \underline{0} \end{bmatrix}$$

Note that diagonal zero in $\tilde{K}$ corresponds to the rigid body mode. For control applications the system dynamics are usually modeled as first order state space differential equations. We introduce the "2n" dimensional modal state vector

$$\mathbf{z} = \begin{Bmatrix} \eta \\ \dot{\underline{\eta}} \end{Bmatrix} \tag{27}$$

2098

32

Eq.(26) can be written as the first order system

$$\dot{\mathbf{z}} = A\mathbf{z} + Bu \qquad (28)$$

where

$$A = \begin{bmatrix} 0 & I \\ -\bar{K} & 0 \end{bmatrix} , \qquad B = \begin{bmatrix} 0 \\ \bar{D} \end{bmatrix}$$

We adopted the following performance index for the LQR control design:

$$J = \int_0^\infty (\mathbf{z}^T Q \mathbf{z} + u^T R u)\, dt \qquad (29)$$

with

$$Q = \begin{bmatrix} \Omega & 0 \\ 0 & I_n \end{bmatrix} , \qquad R = 1$$

where $\Omega = diag(q, \omega_1^2, \cdots, \omega_{n-1}^2)$.

The above performance index is an energy type, since the first term and second term in the performance index corresponds to the state energy and the control energy respectively.

By solving the Riccati equation[16], the optimal feedback control is obtained

$$u = -g\mathbf{z} \qquad (30)$$

Now we can solve the initial value problem using a time discretization process(e.g. Runge-Kutta) and through Eqs.(17,25,30) we obtain $\tilde{y}(x_i, t_i)$, $\tilde{\theta}(t_i)$ and $\tilde{u}(t_i)$, at discrete points in space and time. The approximate motion $\{\tilde{y}(x_i, t_i), \tilde{\theta}(t_i)\}$ corresponds to the system response to a hub torque designed to maneuver the system and arrest vibration.

CONSTRUCTION OF A BENCHMARK PROBLEM

We want to construct a continuous, differentiable, analytical solution that has physical meaning. A candidate discrete approximate solution for the hybrid system can be obtained using any given approximate forward solution process and a given controller. This approximate solution can be used as a generator for a nearby smooth space/time motion for which we can determine the exact forces(required to be consistent with this prescribed motion and the exact equations of motion). Least square approximation associated with using the discrete version of the Chebyshev polynomials can be invoked to obtain the smooth motion $f(x,y)$ solution from the discrete solution. While we invoke a least square approximation to construct the smooth $f(x,y)$ from an already approximate discrete solution, we subsequently

2099

33

determine the modified forces to be exactly consistent with this motion $f(x,y)$. We first consider the least square process.

There are $n' \times m'$ discrete data points such as

$$z_{11} = f(x_1, y_1), \; z_{12} = f(x_1, y_2), \; \cdots, \; z_{1m'} = f(x_1, y_{m'})$$
$$z_{21} = f(x_2, y_1), \; z_{22} = f(x_2, y_2), \; \cdots, \; z_{2m'} = f(x_2, y_{m'})$$
$$\vdots$$
$$z_{n'1} = f(x_{n'}, y_1), \; z_{n'2} = f(x_{n'}, y_2), \; \cdots, \; z_{n'm'} = f(x_{n'}, y_{m'})$$

where x_i, y_j are equally spaced independent variables.

How can we reliably compute a continuous, differentiable, analytical function f from the data points in the least square sense? Analogous to the ODE case, we elect to make use of discrete orthogonality. We nondimensionalize (x,y) using

$$\bar{x}(x) = \frac{x - x_1}{h_x} \qquad \bar{y}(y) = \frac{y - y_1}{h_y}$$

where h_x, h_y are the increments of x and y respectively.

$$z = f(x,y) = F(\bar{x}, \bar{y})$$

From two-dimensional $n' \times m'$ data points, the function F can be approximated by $p \times q$ two-dimensional basis functions that come from the discrete version of the Chebyshev polynomials [weight function $w(x) = 1$] as follows:

$$F(\bar{x}, \bar{y}) \equiv \sum_{i=1}^{p} \sum_{j=1}^{q} b_{ij} T_i(\bar{x}) T_j(\bar{y})$$

where $p \leq n'$, $q \leq m'$ and $T_*(*)$ is the univariate Chebyshev polynomial in the discrete range.

We use the previous definition of Chebyshev polynomials and the recurrence relation. Using discrete orthogonality properties of Chebyshev polynomials, the typical coefficient b_{rs} can be obtained as follows:

$$b_{rs} = \frac{\sum_{i=1}^{n'} \sum_{j=1}^{m'} z_{ij} \, T_r(\bar{x}_i) \, T_s(\bar{y}_j)}{\sum_{i=1}^{n'} \sum_{j=1}^{m'} T_r(\bar{x}_i) \, T_s(\bar{y}_j) \, T_r(\bar{x}_i) \, T_s(\bar{y}_j)}$$

where $1 \leq r \leq p$, $1 \leq s \leq q$.

We can find $f(x,y)$ from $F(\bar{x}, \bar{y})$, since $f(x,y) = F(\bar{x}(x), \bar{y}(y))$.

Using the previous method associated with the Chebyshev polynomials, we interpolate a smooth differentiable function $y_b(x,t)$ as a two-variable orthogonal function expansion which passes near the $\bar{y}(x_i, t_i)$ points. Similary, we can interpolate a smooth differentiable function $\theta_b(t)$ from $\bar{\theta}(t_i)$ data points. Since $y_b(x,t)$ and

2100

34

$\theta_b(t)$ are smooth, differentiable functions, we can force them to be exact solutions of our dynamical model by simply substituting $y_b(x,t)$, $\theta_b(t)$ and their space/time derivatives into Eqs.(11-14) and solving the four equations analytically for four new forces $\{u(t), \hat{f}(x,t), u_{tip}(t), f_{tip}(t)\}$ which satisfy these equations exactly. Computer symbol manipulation makes this process possible.

SIMULATED RESULTS

First we find a candidate discrete solution for the enlarged time interval $(-1 \leq t \leq 2)$ with initial conditions $\theta(-1) = 0.1$rad and $y(x,-1) = 0$ for all x. We use LQR to design control force $\bar{u}(t)$ and use the finite element approach for space discretization. Here we use 1 for q of Eq.(29) and use the configuration parameters as shown Table 1. Then we construct a benchmark problem for time interval $(0 \leq t \leq 2)$. Figures 8-13 show $y_b(x,t)$, $\theta_b(t)$, $u(t)$, $\hat{f}(x,t)$, $u_{tip}(t)$, and $f_{tip}(t)$ which satisfy Eqs.(11-14) exactly. Note that even though we use the enlarged time interval and have good interpolations for $\theta_b(t)$ and $y_b(x,t)$ near the boundary, there exists relatively large error for control forces, near the boundary, compared to the nonlinear ODE cases. This is due to the fact that we have two independent variables, time and space, and have coupling terms which are time and space derivatives of $y_b(x,t)$ in the evaluation of control forces. In contrast to enlarging the time interval for ODE problems, it is neither physically nor mathematically meaningful to enlarge the spatial domain. As will be evident, this is a minor problem, and does not prevent us from establishing "exact" benchmark problems.

Finite element approach gives us Eq.(20) and for simulation we use step-by-step solution using Newmark integration method. Given initial conditions $\{y(x,0) = y_b(x,0), \theta(0) = \theta_b(0)\}$ and force functions $\{u(t), \hat{f}(x,t), u_{tip}(t), f_{tip}(t)\}$, the approximate simulation of this structure's dynamics $\{y_s(x,t), \theta_s(t)\}$ can proceed. Figure 14 shows the space/time error distribution $e_y(x,t) = y_s(x,t) - y_b(x,t)$ when we use 20 finite elements and 0.002 sec. for step size.

Second we find a candidate solution for the enlarged time interval $(0 \leq t \leq 0.1)$. Initial condition for θ is 0.1rad and the third natural mode of this flexible structure is used for $y(x,0)$. We use LQR to design control force $\bar{u}(t)$ and FEM is used for sapce discretization. Here we use 100 for q of Eq.(29) and use the configuration parameters as shown Table 1 except m_t and J_t (m_t=0.256941, J_t=0.0028). Then we construct a benchmark problem for time interval $(0 \leq t \leq 0.08)$, i.e., we have new set $y_b(x,t)$, $\theta_b(t)$, and $\{u(t), \hat{f}(x,t), u_{tip}(t), f_{tip}(t)\}$ which satisfy Eqs.(11-14) exactly.

Now we can investigate the convergence errors in a family of approximate solutions with special case absolute standards. When we use the Newmark integration method with finite element modeling, the convergence and accuracy behavior is studied as a function of the number of finite elements and the integration step size. Figure 15 shows the error norm $\|e_\theta\|$ and $\|e_y\|$ for various mesh sizes for

2101

a fixed integration step size on a log/log scale. Figure 16 shows the error norm $\|e_\theta\|$ and $\|e_y\|$ for various integration step sizes for a fixed number of finite elements on a log/log scale. The error norm distribution of θ and y is shown in Figs.17, 18 respectively, as a function of DT(time step size) and H(mesh size).

Here we introduce the following definitions for the *supmetric* error.

$$\|e_\theta(t)\|_{L^2(0,T)} \equiv \left\{ \int_0^T e_\theta(t)^2 dt \right\}^{\frac{1}{2}}$$

$$\|e_y(x,t)\|_{L^2(0,T;L^2)} \equiv \left\{ \int_0^T \int_0^L e_y(x,t)^2 dx\, dt \right\}^{\frac{1}{2}}$$

where $e_\theta(t) = \theta_s(t) - \theta_b(t)$.

The relative errors are defined as follows:

$$RE_\theta \equiv \frac{\|e_\theta(t)\|_{L^2(0,T)}}{\|\theta(t)\|_{L^2(0,T)}}, \quad RE_y \equiv \frac{\|e_y(x,t)\|_{L^2(0,T;L^2)}}{\|y(x,t)\|_{L^2(0,T;L^2)}}$$

We observe that the rate of convergence is 2 in Δt(decrease DT to reduce error measure) and 4 in h(decrease H to reduce error measure) from Figs.15 and 16, except for the small$(\Delta t, h)$ region where arithmetic errors dominate and provide computer limitations to accuracy. It is this latter insight that is essentially impossible to obtain by pre-existing methods, but is easily established by the methods of this paper. We should be careful in saying that adjusting h (to achieve accuracy) is less expensive than adjusting Δt, because the rate of convergence of 4 in h and the rate of convergence of 2 in Δt does not guarantee this fact. Each approach to improving accuracy results in different amount of computational load, which depends on the specific program. From Figs.15-18, we can also notice that if H is too crude then Δt reduction does not improve the solution and if DT is too big then h reduction does not improve the solution. The numerical results indicate that the minimum value of RE_θ is 0.7×10^{-7} (when H=0.2 and DT=0.00002) and the minimum value of RE_y is 0.3×10^{-3} (when H=0.4 and DT=0.00005). We know of no method that could give this insight before the introduction of the present method.

We construct a neighboring benchmark problem to investigate the robustness of the convergence characteristics of Figs.15-18. To construct a neighboring benchmark problem, first we find a candidate discrete solution with the following initial condition and forcing function $\tilde{u}(t)$. Comparing to the previous case, we make a 10% increase of the initial condition $y(x,0)$ and arbitrarily add a sinusoidal perturbation term $0.4186 sin(2\pi t/0.08)$ to the previous hub control $\tilde{u}(t)$ for a new perturbed hub control. The error norm distributions of the perturbed case are almost identical to the previous problem. So we can conclude that the convergence and accuracy

2102

36

properties of this approximate solution process are indeed relatively invariant in the presence of these finite perturbations, in this case.

SUMMARY AND CONCLUSION

The present paper introduces an inverse dynamic method for constructing exact special case solutions for hybrid ODE/PDE systems. A multi-variable orthogonal function expansion method and computer symbol manipulation are successfully used for this process. The hybrid ODE/PDE systems with exact solutions can serve as a benchmark problem to validate approximate solution methods. This methodology makes it possible for one to rigorously determine exact solution errors and to study the convergence and accuracy behavior as a function of tuning parameters for a class of ODE/PDE systems for which the initial value problem is not exactly solvable. Numerical examples indicate that a rigorous error analysis is obtained not merely for one nominal solution, but for a substantial neighborhood of the nominal solution. By constructing a family of neighboring benchmark problems, one can obtain valuable information about the convergence and accuracy properties that are relatively invariant with respect to perturbations within a known bound.

REFERENCES

1 Lee, S., and Junkins, J.L., "Construction of Benchmark Problems for Solution of Ordinary Differential Equations," Dept. of Aerospace Engineering, Texas A&M Univ., Technical Rept. AERO 93-0801, College Station, TX, August 1993.

2 Shampine, L.F., "Tolerance Proportionality in ODE Codes," in Bellen, A., Gear, C.W., and Russo, E., eds., *Numerical Methods for Ordinary Differential Equations*, Proceedings, L'Aquila, Springer-Verlag, 1987, pp.118-135.

3 Hairer, E., Norsett, S.P., and Wanner, G., *Solving Ordinary Differential Equations I. Nonstiff Problems*, Springer-Verlag, Berlin, 1987, pp.236-241.

4 Hull, T.E., Enright, W.H., Fellen, B.M., and Sedgwick, A.E., "Comparing Numerical Methods for Ordinary Differential Equations," *SIAM J. Numer. Anal.*, Vol. 9, No. 4, 1972, pp.603-637.

5 Krogh, F.T., "On Testing a Subroutine for the Numerical Integration of Ordinary Differential Equations," *Journal of the Association for Computing Machinery*, Vol. 20, No. 4, 1973, pp.545-562.

6 Junkins, J.L., *An Introduction to Optimal Estimation of Dynamical Systems*, Sijhoff & Noordhoff, Alphen aan den Rijn, The Netherlands, 1978.

7 Abramowitz, M., and Stegun, I.A., *Handbook of Mathematical Functions with Formulas, Graphs, and Mathmatical Tables*, National Bureau of Standards, Applied Mathematics Series 55, U.S. Department of Commerce, 1972.

8 *MACSYMA Reference Manual Version 13*, Symbolics Inc., 1988.

9 Gear, C.W., *Numerical Initial Value Problems in Ordinary Differential Equations*, Prentice-Hall, Englewood Cliffs, NJ, 1971.

10 Lee, S., and Junkins, J.L., "Explicit Generalization of Lagrange's Equations

2103

for Hybrid Coordinate Dynamical Systems," *Journal of Guidance, Control, and Dynamics*, Vol. 15, No. 6, 1992, pp.1443-1452.

[11] Bayo, E., "A Finite-Element Approach to Control the End-Point Motion of a Single-Link Flexible Robot," *Journal of Robotic Systems*, Vol. 4, No. 1, 1987, pp.63-75.

[12] Naganathan, G., and Soni, A.H., "Coupling Effects of Kinematics and Flexibility in Manipulators," *The International Journal of Robotics Research*, Vol. 6, No. 1, 1987, pp.75-84.

[13] Reddy, J.N., *An Introduction to the Finite Element Method*, McGraw-Hill Book Company, New York, NY, 1984.

[14] Craig, R.R.Jr., *Structural Dynamics - an Introduction to Computer Methods*, John Wiley and Sons, New York, NY, 1981.

[15] Meirovitch, L., *Computational Methods in Structural Dynamics*, Sijhoff & Noordhoff, The Netherlands, Rockville, MD, 1980.

[16] Junkins, J.L., and Kim, Y., *An Introduction to Dynamics and Control of Flexible Structures*, American Institute of Aeronautics and Astronautics, Washington, D.C., 1993.

APPENDIX

Submatrix Elements of Finite Element Method

The local mass and stiffness matrices of the i-th element of the appendage is defined as follows:

$$M_e^{(i)} \equiv \begin{bmatrix} M_{11}^i & M_{12}^i & M_{13}^i \\ M_{21}^i & M_{22}^i & M_{23}^i \\ M_{31}^i & M_{32}^i & M_{33}^i \end{bmatrix} , \qquad K_e^{(i)} \equiv \begin{bmatrix} 0 & 0 & 0 \\ 0 & K_{22}^i & K_{23}^i \\ 0 & K_{32}^i & K_{33}^i \end{bmatrix}$$

where

$$M_{11}^i = \frac{\rho h}{3}\{(x_i + r)^2 + (x_i + r + h)(x_i + r) + (x_i + r + h)^2\}$$

$$M_{12}^i = [M_{21}^i]^T = \rho h\left[\tfrac{3}{20}h + \tfrac{1}{2}(x_i + r) \quad \tfrac{1}{30}h^2 + \tfrac{1}{12}h(x_i + r)\right]$$

$$M_{13}^i = [M_{31}^i]^T = \rho h\left[\tfrac{7}{20}h + \tfrac{1}{2}(x_i + r) \quad -\tfrac{1}{20}h^2 - \tfrac{1}{12}h(x_i + r)\right]$$

$$M_{22}^i = \frac{\rho h}{420}\begin{bmatrix} 156 & 22h \\ 22h & 4h^2 \end{bmatrix}, \quad M_{23}^i = [M_{32}^i]^T = \frac{\rho h}{420}\begin{bmatrix} 54 & -13h \\ 13h & -3h^2 \end{bmatrix}$$

$$M_{33}^i = \frac{\rho h}{420}\begin{bmatrix} 156 & -22h \\ -22h & 4h^2 \end{bmatrix}$$

$$K_{22}^i = \frac{EI}{h^3}\begin{bmatrix} 12 & 6h \\ 6h & 4h^2 \end{bmatrix}, \quad K_{23}^i = [K_{32}^i]^T = \frac{EI}{h^3}\begin{bmatrix} -12 & 6h \\ -6h & 2h^2 \end{bmatrix}$$

$$K_{33}^i = \frac{EI}{h^3}\begin{bmatrix} 12 & -6h \\ -6h & 4h^2 \end{bmatrix}$$

2104

where x_i is the distance from the root of the appendage to the left end of the i-th finite element, r is the radius of the hub, and h is the length of the finite element. The matrix due to the tip mass is defined as follows:

$$M_t \equiv \begin{bmatrix} M_{11}^t & M_{12}^t \\ M_{21}^t & M_{22}^t \end{bmatrix}$$

where

$$M_{11}^t = J_t + m_t(r + L)^2$$

$$M_{12}^t = [M_{21}^t]^T = \begin{bmatrix} m_t(r + L) & J_t \end{bmatrix}$$

$$M_{22}^t = \begin{bmatrix} m_t & 0 \\ 0 & J_t \end{bmatrix}$$

Now, the submatrices in Eq.(20) can be defined as follows:

$$M_{\theta\theta} = \sum_{i=1}^{N} M_{11}^i + M_{11}^t$$

$$M_{\theta\nu} = \begin{bmatrix} M_{13}^1 + M_{12}^2 & M_{13}^2 + M_{12}^3 & M_{13}^3 + M_{12}^4 & \cdots & M_{13}^{N-1} + M_{12}^N & M_{13}^N + M_{12}^t \end{bmatrix}$$

$$M_{\nu\nu} = \begin{bmatrix} M_{33}^1 + M_{22}^2 & M_{23}^2 & & & & \\ M_{32}^2 & M_{33}^2 + M_{22}^3 & M_{23}^3 & & & \\ & M_{32}^3 & M_{33}^3 + M_{22}^4 & M_{23}^4 & & \\ & & & \ddots & & \\ & & & M_{32}^{N-1} & M_{33}^{N-1} + M_{22}^N & M_{23}^N \\ & & & & M_{32}^N & M_{33}^N + M_{22}^t \end{bmatrix}$$

$$K_{\nu\nu} = \begin{bmatrix} K_{33}^1 + K_{22}^2 & K_{23}^2 & & & & \\ K_{32}^2 & K_{33}^2 + K_{22}^3 & K_{23}^3 & & & \\ & K_{32}^3 & K_{33}^3 + K_{22}^4 & K_{23}^4 & & \\ & & & \ddots & & \\ & & & K_{32}^{N-1} & K_{33}^{N-1} + K_{22}^N & K_{23}^N \\ & & & & K_{32}^N & K_{33}^N \end{bmatrix}$$
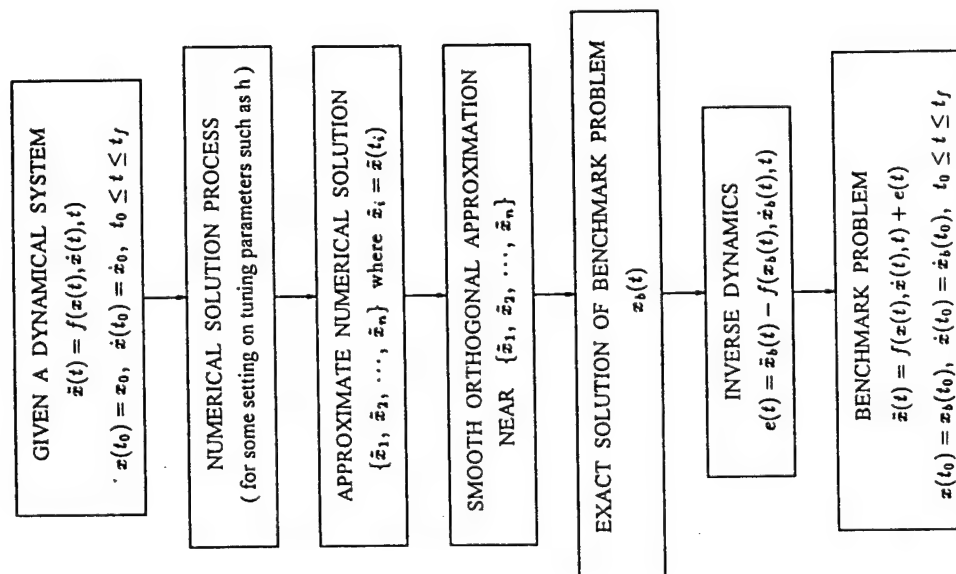
where N is the number of finite elements.

2105

39

Fig. 2 Flow Chart for Convergence Study

GIVEN A BENCHMARK PROBLEM (with a known exact solution $x_b(t)$)
$$\ddot{x}(t) = f(x(t), \dot{x}(t), t) + e(t)$$
$$x(t_0) = x_b(t_0), \quad \dot{x}(t_0) = \dot{x}_b(t_0), \quad t_0 \le t \le t_f$$

INITIAL SETTING ON TUNING PARAMETERS FOR NUMERICAL SOLUTION PROCESS

NUMERICAL SOLUTION PROCESS

APPROXIMATE NUMERICAL SOLUTION OF THE BENCHMARK PROBLEM x_s

EVALUATE ERROR MEASURE $\| x_s - x_b \|$

Do we have enough data for convergence study?

Yes

No

STUDY THE CHARACTERISTICS GLOBAL ERROR vs TUNING PARAMETERS

VARY TUNING PARAMETERS

2106

Fig. 1 Flow Chart for Construction of a Benchmark Problem

GIVEN A DYNAMICAL SYSTEM
$$\ddot{x}(t) = f(x(t), \dot{x}(t), t)$$
$$x(t_0) = x_0, \quad \dot{x}(t_0) = \dot{x}_0, \quad t_0 \le t \le t_f$$

NUMERICAL SOLUTION PROCESS (for some setting on tuning parameters such as h)

APPROXIMATE NUMERICAL SOLUTION $\{\bar{x}_1, \bar{x}_2, \cdots, \bar{x}_n\}$ where $\bar{x}_i = \bar{x}(t_i)$

SMOOTH ORTHOGONAL APPROXIMATION NEAR $\{\bar{x}_1, \bar{x}_2, \cdots, \bar{x}_n\}$

EXACT SOLUTION OF BENCHMARK PROBLEM $x_b(t)$

INVERSE DYNAMICS
$$e(t) = \ddot{x}_b(t) - f(x_b(t), \dot{x}_b(t), t)$$

BENCHMARK PROBLEM
$$\ddot{x}(t) = f(x(t), \dot{x}(t), t) + e(t)$$
$$x(t_0) = x_b(t_0), \quad \dot{x}(t_0) = \dot{x}_b(t_0), \quad t_0 \le t \le t_f$$

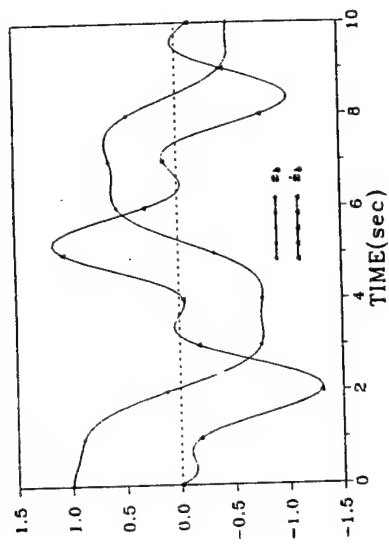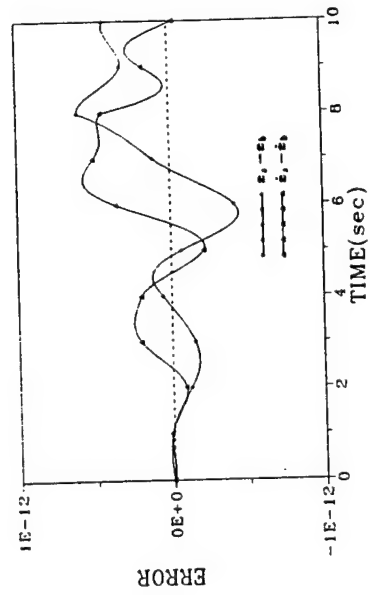Fig. 5 Known Exact Solution (H=0.001, MT=30)

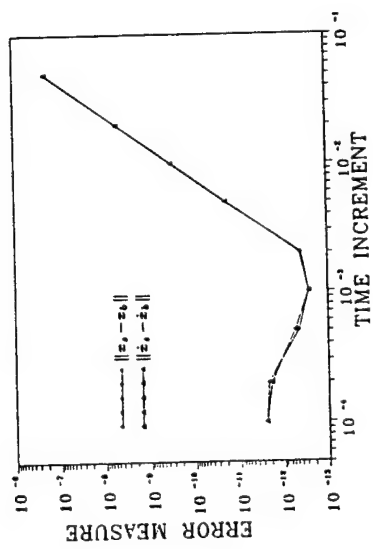Fig. 6 Simulation Error (H=0.001, MT=30)
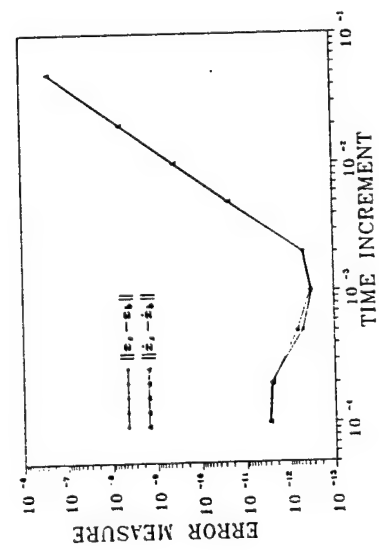

Fig. 3 Error measure vs Time step size

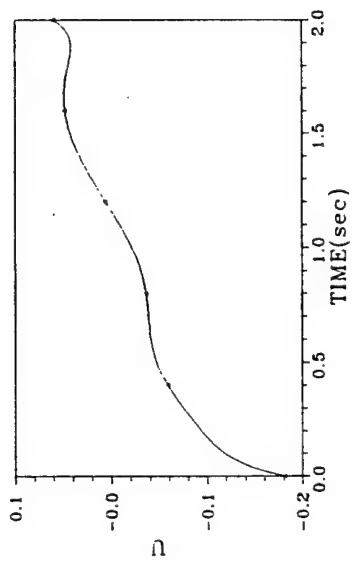Fig. 4 Error measure vs Time step size (Perturbed Case)

2107

41

Fig. 10 Hub control $u(t)$

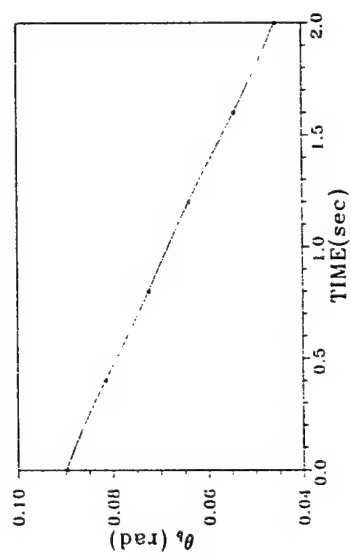

Fig. 11 Distributed force density $\hat{f}(x,t)$

Fig. 8 Hub rotation angle $\theta_b(t)$
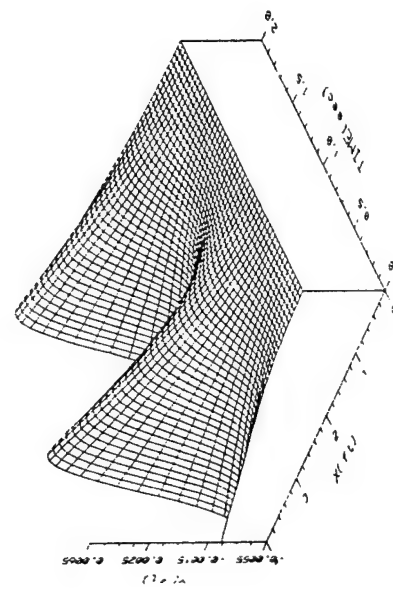
Fig. 9 Elastic displacement $y_b(x,t)$

2108

42
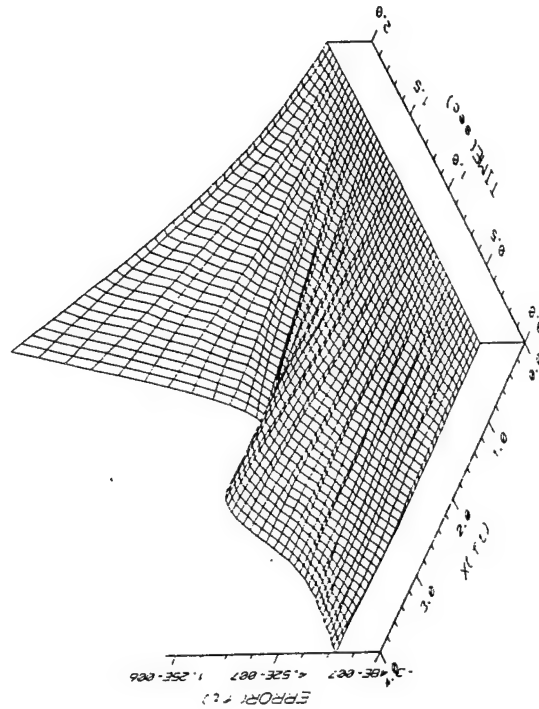
Fig. 12 Torque applied at tip $u_{tip}(t)$
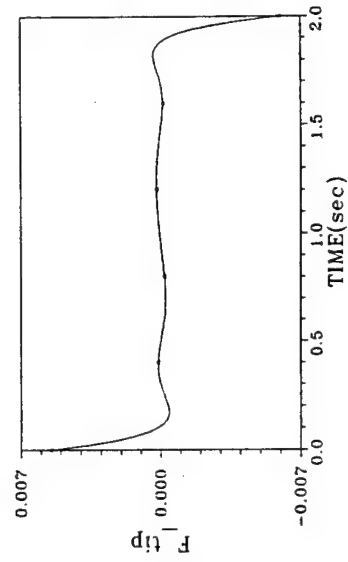
Fig. 13 Force applied at tip $f_{tip}(t)$

Fig. 7 A three-body distributed parameter system

Fig. 14 Error distribution $e_y(x,t) = y_s(x,t) - y_b(x,t)$

2109

43
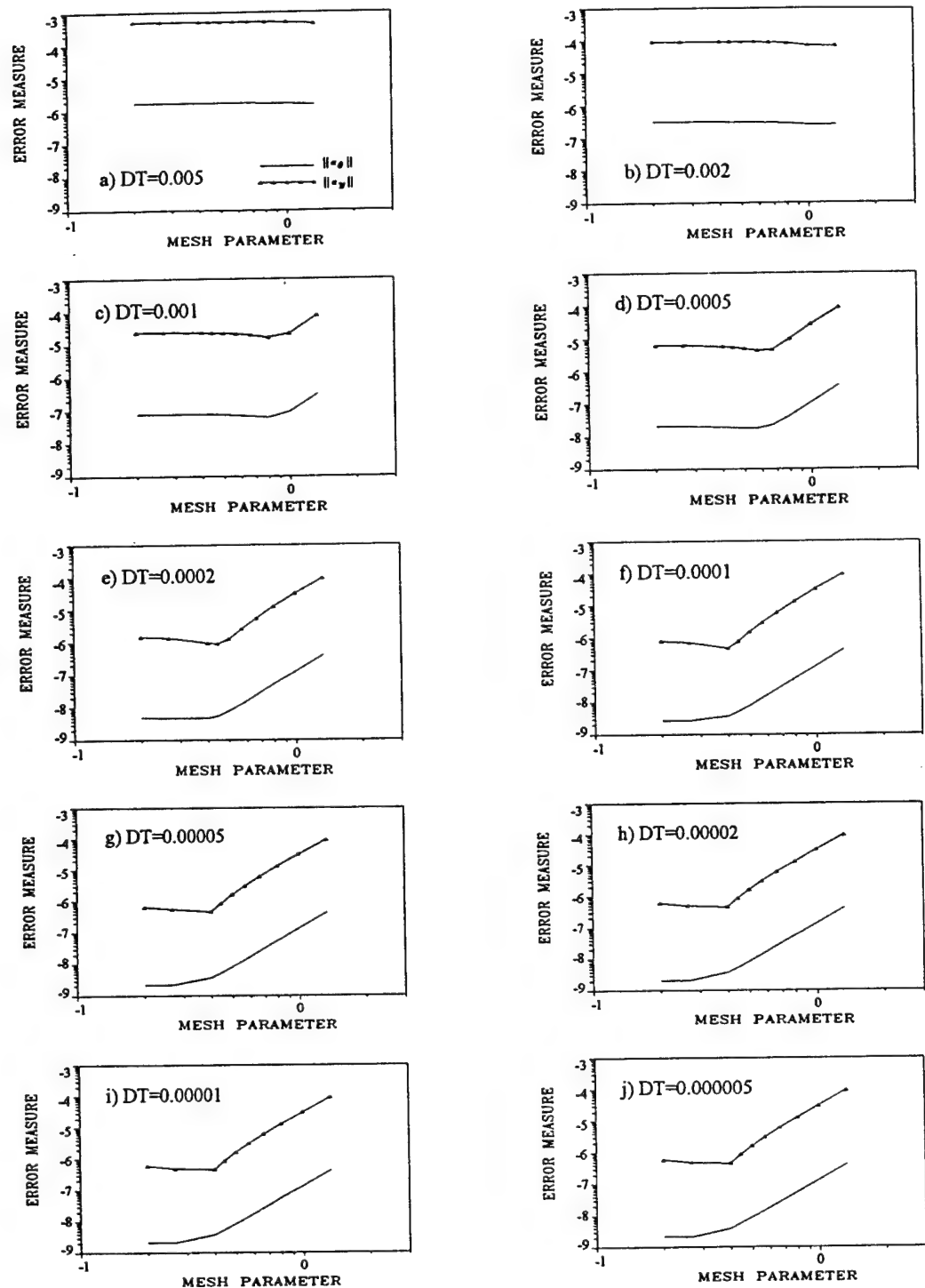
Fig. 15 Error norms for various mesh sizes for a fixed integration step size

2110

44
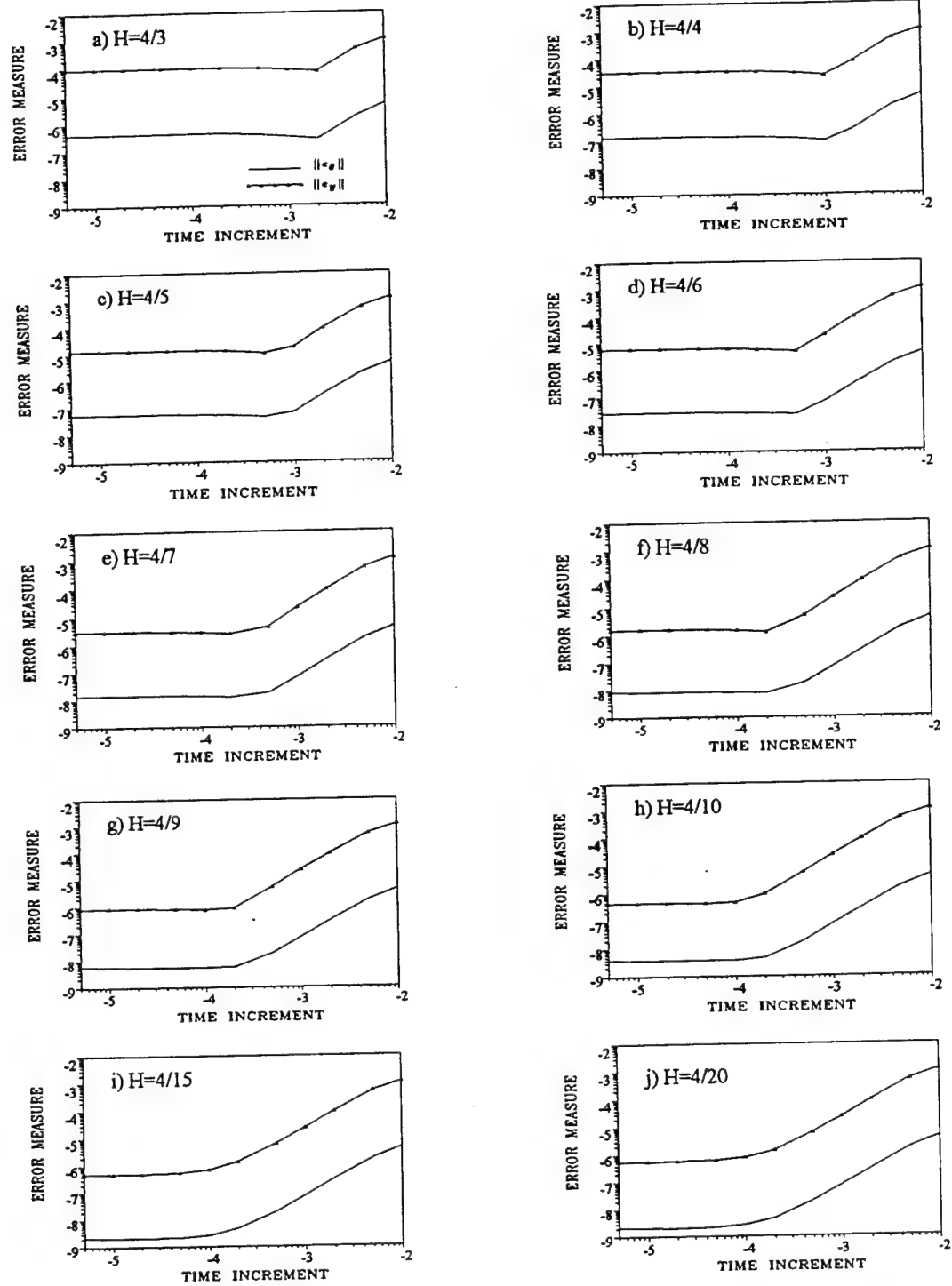
Fig. 16 Error norms for various integration step sizes for a fixed mesh size

2111

45
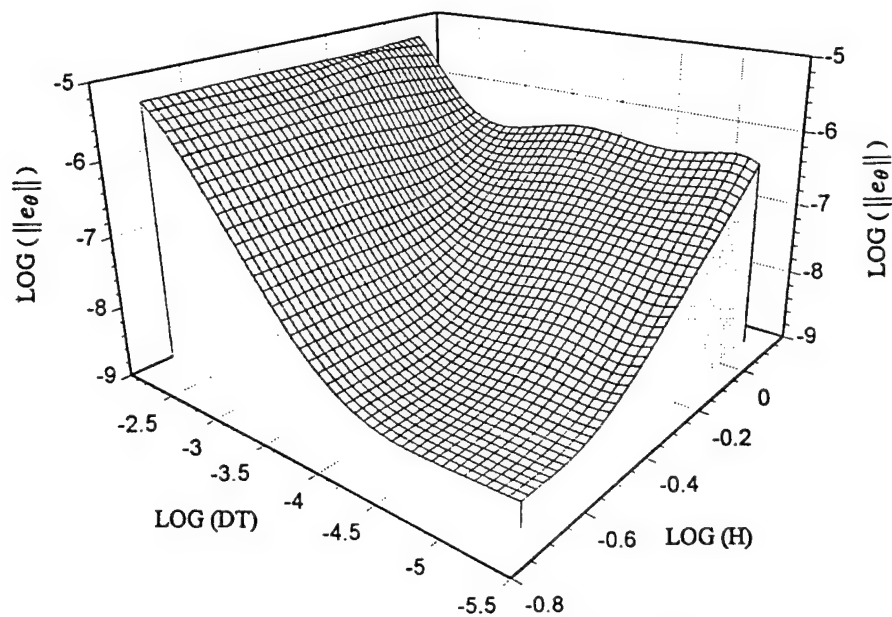
Fig. 17 Error norm distribution of θ
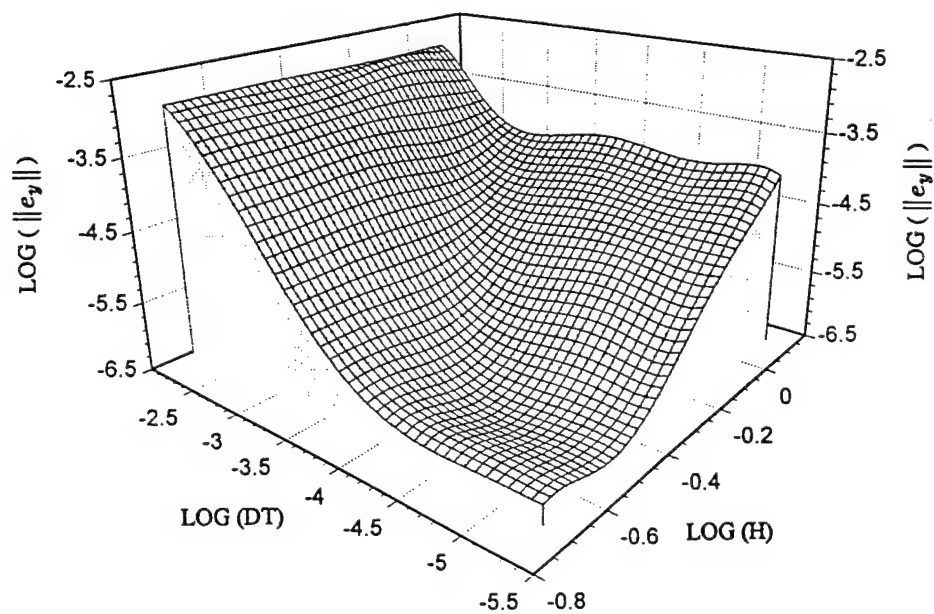
Fig. 18 Error norm distribution of y

2112

46

Stability and Control of Robotic Space Manipulators

John L. Junkins*
Texas A&M University, College Station, Texas 77843
and
Youdan Kim†
Seoul National University, Seoul, Korea

I. Introduction

I N the present chapter, we present some elegant concepts from stability theory, and consider their applicability to the problem of designing control laws for multiple-degree-of-freedom robotic space manipulators. While the spirit of our presentation is classical, we include some novel stability results and a methodology for designing globally stable control laws for nonlinear finite-dimensional and distributed-parameter systems. We find that the Lyapunov approach is attractive not only because it plays an important role in stability and control theory, but also because it provides the only broadly applicable approach to design guaranteed stable control laws for nonlinear, time-varying, and distributed-parameter systems. Especially significant is the fact that the Lyapunov approach leads to a unified stability and control perspective for both linear and nonlinear systems, as well as systems described by ordinary, partial, and hybrid differential equations. The first half of this chapter is an efficient summary of the main features of Lyapunov stability theory, however a few examples are considered to help illustrate this material. The second half of the chapter is addressed to significant studies wherein we apply the analytical developments to formulate stabilizing feedback control laws for idealized manipulator systems undergoing large generally nonlinear motions.

In Sec. II, several important definitions and concepts fundamental to stability analysis are stated. Section III reviews three basic stability and instability theorems stemming from the so-called direct method of Lyapunov. In Sec. IV, a Lyapunov stability analysis for systems described by linear first order systems of differential

equations is presented. In Sec. V, the indirect method of Lyapunov is presented to characterize the local stability of motion of a nonlinear system near an equilibrium state. Section IV presents a method of designing guaranteed stable controllers for two or more multilink robots which are cooperatively manipulating a payload through large nonlinear motions.

II.   Basic Definitions

Consider any member of the family of continuous, finite-dimensional dynamical systems which can be described by a first-order nonlinear vector differential equation of the form

$$\dot{x} = f(x, t), \quad x \in R^n \quad (1)$$

where $x(t)$ is the state vector at time t, and the dot denotes time differentiation.

A.   Definition: Equilibrium State

A vector $x_e \in R^n$ is said to be an equilibrium state of the system described by Eq. (1) at time t_0 if

$$f(x_e, t) = 0 \quad \forall t \geq t_0 \quad (2)$$

If x_e is an equilibrium state of Eq. (1) at time t_0, then x_e is also an equilibrium state of Eq. (1) at all times $t_1 \geq t_0$. In other words, motion initiating at x_e remains there for all time.

B.   Definition: Stability of an Equilibrium State

The equilibrium state x_e, or the equilibrium solution $x(t) = x_e$, is said to be stable, if for any given t_0 and positive ϵ, there exists a positive $\delta(\epsilon, t_0)$ such that every time-varying trajectory (or solution) $x(t)$ initiating (time t_0) at a point x_0 which lies within a δ neighborhood of x_e [$\|x_0 - x_e\| < \delta$, $x_0 \equiv x(t_0)$] remains for all time within an ϵ neighborhood of x_e [$\|x(t) - x_e\| \forall t \geq t_0$]. The equilibrium state is said to be unstable if it is not stable.

C.   Definition: Asymptotic Stability of an Equilibrium State

The equilibrium state x_e is said to be asymptotically stable if 1) it is stable (Sec. II.B) and if, in addition, 2) for any t_0, there exist a $\delta_1(t_0)$, such that

$$\|x_0 - x_e\| < \delta_1 \quad \text{implies that} \quad \lim_{t \to \infty} x(t) \to x_e$$

If δ and δ_1 are not functions of t_0, then the equilibrium state is said to be uniformly stable and uniformly asymptotically stable, respectively. The definition in Secs. II.B and II.C constitute the two basic definitions of stability of an equilibrium state (a fixed point in the state space) for an unforced continuous time system. More generally, we need to consider the stability of a trajectory or a motion. Qualitatively, stability of a trajectory is concerned with whether or not a perturbed motion remains near the unperturbed trajectory, or diverges from it. Stability of a motion is of central interest in many practical feedback control situations whereby a system is designed to execute a large nominal motion, and control inputs must be

developed not only to generate the nominal motion but also closed-loop feedback is required to stabilize neighboring motions, with respect to the nominal motion, so that the actual system will behave in a near-nominal fashion.

D.   Definition: Stability of a Motion

The motion $x(t)$ is said to be stable if for all initial times t_0 and prescribed positive ϵ, there exists a positive $\delta(\epsilon, t_0)$, such that

$$\|x(t) - \bar{x}(t)\| < \epsilon \quad \forall t \geq t_0 \text{ if } \|x_0 - \bar{x}_0\| < \delta$$

where $x(t)$ and $\bar{x}(t)$ are neighboring trajectories with the given initial conditions x_0 and $\bar{x}_0$, respectively, at time t_0.

This bounded motion stability property is sometimes referred to as path stability. Qualitatively, path stability means that if the perturbed initial state $\bar{x}(t_0)$ is near $x(t_0)$, then the ensuing perturbed trajectory $\bar{x}(t)$ will remain near $x(t)$ for all time t.

E.   Definition: Asymptotic Stability of a Motion

The motion $x(t)$ is said to be asymptotically stable if 1) it is stable (see the definition in Sec. II.D), and if, in addition; 2) for any t_0, there exist a positive $\delta_1(t_0)$, such that

$$\|x_0 - \bar{x}_0\| < \delta_1 \quad \text{implies that} \quad \lim_{t \to \infty} \|x(t) - \bar{x}(t)\| = 0 \quad (3)$$

Note that $\bar{x}(t)$ is any member of the set of it all neighboring (perturbed) trajectories satisfying Eq. (3), and all members of this set asymptotically approach $x(t)$.

The preceding definitions are not directly concerned with the global properties of systems, but of the motion in a finite local neighborhood of an equilibrium state or a motion of the system of differential equations. If a system has a globally asymptotically stable equilibrium state, then it is obviously the only equilibrium state, and every motion converges to that unique equilibrium. An analogous global stability property can be defined for the stability of a motion.

The simplest class of Lyapunov stability analysis methods arises in the context of systems described by linear unforced differential equations. We now summarize some of the central ideas.

Consider the linear system

$$\dot{x}(t) = A(t)x(t)$$

which obviously has one equilibrium state at the origin. This linear system can be classified as stable, asymptotically stable, or unstable, depending on the stability of the origin.[1,2]

Now, we introduce two definitions associated with the concept of positive definite functions; these are very important to understand when applying Lyapunov stability theory.

F.   Definition: Positive Definite Function

A single-valued function $U(x)$, which is continuous and has continuous partial derivatives with respect to the components of the vector x, is said to be positive

definite in some region Ω about the origin if it vanishes at the origin and is positive definite in some region Ω about the origin if it vanishes at the origin and is positive elsewhere, i.e.,

$$\text{i) } U(0) = 0$$
$$\text{ii) } U(x) > 0 \quad \text{for all nonzero } x \in \Omega$$

If the positivity condition ii) is relaxed to simply the nonnegative condition $U(x) \geq 0$ for all $x \in \Omega$, then $U(x)$ is said to be positive semidefinite. If the inequality sign in ii) is reversed, then the condition for a negative definite function is obtained. If a function is neither positive nor negative definite, then it is indefinite.

G. Definition: Positive Definite Quadratic Forms

In the analysis of linear dynamical systems, quadratic functions of the state vector arise often in the context of energy, stability, and control analyses. Especially important are symmetric quadratic forms. The quadratic form $U(x) = x^T Q x$ is said to be positive definite if

$$U(x) = x^T Q x > 0 \quad \text{for all nonzero } x \in R^n$$

where Q is a real symmetric matrix.

The definition in Sec. II.G is equivalent to requiring that all the eigenvalues of Q are strictly positive, such a matrix is naturally called a positive definite matrix.

For further discussion of background material, the reader is referred to Vidyasagar[1] and Willems.[2] The following example is useful to illustrate the ideas underlying the preceding discussion.

H. Example

Consider the functions $U_1(x) = x_1^2 + x_2^2$ and $U_2(x) = (x_1 + x_2)^2$. Clearly U_1 satisfies the condition of the definition in Sec. II.C, therefore it is a positive definite function in a two-dimensional space; but U_1 is only positive semidefinite if the underlying space has more than two dimensions. U_2 is only positive semidefinite in two-dimensional space, since it is zero everywhere along the line $x_1 + x_2 = 0$.

III. Lyapunov Stability Theory (Lyapunov's Direct Method)

The central ideas of the Lyapunov stability theorem are now introduced. For a given general dissipative, forced mechanical system, it is often useful to consider a conservative idealized approximation of system without the dissipative or non-conservative external forces acting. For this idealized system, suppose that there exists one equilibrium state x_e of the system at the desired target postion. Also suppose that the total mechanical energy or Hamiltonian of this idealized system is a positive definite function and is an exact integral of the idealized system. For a broad class of practical applications, the total energy or Hamiltonian of an idealized conservative system is a suitable Lyapunov function for studying the stability of the system, including dissipative internal and external forces. More generally, a candidate Lyapunov function must belong to a class of admissible energy functions which have as the most fundamental property the fact that they are zero at the desired equilibrium state and positive everywhere else.

Now suppose that the system is initially perturbed to a state neighboring the desired equilibrium point where the energy level is positive by assumption, and we consider the time evolution of the distance to the desired equilibrium as measured by the energy function. Depending on the nature of the selected energy function (Lyapunov function), the stability of the motion may be described qualitatively as follows:

1) If the system dynamics evolve such that the initial energy of the system is not increasing with time for all starting points in a finite neighborhood, we can conclude that the equilibrium state is stable.

2) If the system dynamics evolve such that the energy of the system is monotonically decreasing with time for all initial conditions in the neighborhood (and thus eventually approaches zero), the equilibrium state is asymptotically stable.

3) If the energy of the system is increasing with time, for any initial condition in the neighborhood, then the equilibrium state is unstable.

4) If the chosen energy measure is indefinite (i.e., it is neither strictly decreasing nor increasing), then no conclusion can be drawn on the stability of the system.

The following theorem, which is a rigorous statement of the preceding remarks, is the basic stability concept underlying Lyapunov's direct (second) method.

A. Theorem: Stability Theorem

The equilibrium state x_e is stable if there exists a continuously differentiable function $U(x)$ such that

$$\text{i) } U(x_e) = 0$$
$$\text{ii) } U(x) > 0 \quad \text{for all } x \neq x_e, x \in \Omega$$
$$\text{iii) } \dot{U}(x) \leq 0 \quad \text{for all } x \neq x_e, x \in \Omega$$

where $\dot{U}(x)$ denotes the time derivative of the function $U(x)$, and Ω is some region containing x_e. Notice that the energy rate $\dot{U}(x)$ is evaluated along a typical trajectory $x(t)$, and the conditions ii) and iii) must hold along all infinity of trajectories of the dynamical system, which ensue from initial states in Ω.

A modest perturbation of the above theorem (making the final inequality strict) results in the following theorem which provides necessary and sufficient conditions for asymptotic stability.

B. Theorem: Asymptotic Stability Theorem

The equilibrium state x_e is asymptotically stable if there exists a continuously differentiable function U such that

$$\text{i) } U(x_e) = 0$$
$$\text{ii) } U(x) > 0 \quad \text{for all } x \notin x_e, x \in \Omega$$
$$\text{iii) } \dot{U}(x) < 0 \quad \text{for all } x \notin x_e, x \in \Omega$$

Both of the previous theorems relate to local stability in the vicinity of the equilibrium state. A system has global asymptotic stability with respect to a unique equilibrium point if the following theorem is satisfied.

C.   Theorem: Global Asymptotic Stability Theorem

The equilibrium state x_e is globally asymptotically stable if there exists a continuously differentiable function U with the following properties:

i) $U(x_e) = 0$
ii) $U(x) > 0$　for all $x \neq x_e$
iii) $\dot{U}(x) < 0$　for all $x \neq x_e$
iv) $U(x) \to 0$　as $\|x\| \to \infty$

Note that the stable region Ω extends to infinity in the theorem in Sec. III.C. The reader is referred to Ref. 1 for further discussion, including the complete proofs of the preceding theorems. Observe that there is no one unique Lyapunov function for a given system; some may be better than others. This is especially important when we seek the least conservative stability information when, for example, we seek to determine the size of the Ω region in which we have stability. If a poor choice of $U(x)$ results in a pessimistic conclusion that the Ω is much smaller than it actually is, then this is an obvious (and very frequently occurring) concern. It should also be noted that if a Lyapunov function cannot be found, nothing can be concluded about the stability of the system, since the Lyapunov stability theorem provides only sufficient conditions for stability. Therefore the conditions required to prove stability, based on an arbitrary choice of Lyapunov function, may be very conservative.

Unfortunately, the Lyapunov theorems are not constructive; these theorems do not reveal a process to find a candidate Lyapunov function. It is often difficult to find a suitable Lyapunov function for a given nonlinear system. The physical and mathematical insights of the analyst has historically played an important role in most successful applications of this approach, however more systematic methods have recently emerged[3-5] for certain classes of control design problems. In particular, when the stability analysis and the control design analysis are merged, one is often able to exploit the additional freedom to simultaneously design control laws and select a Lyapunov function which guarantees stability of the closed-loop (controlled) system.

D.   Example

Consider the system described by the nonlinear ordinary differential equation

$$\ddot{x}(t) - \epsilon x^2(t)\dot{x}(t) + x(t) = 0$$

The objective is to use Lyapunov analysis to investigate the stability of motion near the origin for this system.

Introducing the state variable representation of this system with the definitions $x_1 = x$, $x_2 = \dot{x}$, we write the equivalent first-order system

$$\dot{x}_1 = x_2, \quad \dot{x}_2 = -x_1 + \epsilon x_1^2 \dot{x}_2$$

It is easy to verify that the preceding oscillator with quadratic damping has an equilibrium state at the origin $(x_1, x_2) = (0, 0)$. Our goal is to determine if this

state is stable. For this purpose, let us choose the simplest candidate Lyapunov function

$$U(x_1, x_2) = (x_1^2 + x_2^2)/2$$

We note that a physical motivation for choosing this positive definite function as a candidate Lyapunov function that it is an exact (total mechanical energy) integral of the motion, for $\epsilon = 0$. Clearly $U(0,0) = 0$ and $U(x_1, x_2) > 0$ in any neighborhood of $(0, 0)$, and investigating the energy rate, we find

$$\dot{U}(x_1, x_2) = x_1\dot{x}_1 + x_2\dot{x}_2 = x_1x_2 + x_2(-x_1 + \epsilon x_1^2 x_2) = \epsilon x_1^2 x_2^2$$

Thus U is a positive definite function which is strictly decreasing along all system trajectories if $\epsilon < 0$. Therefore, by the preceding theorems, $(0, 0)$ is a globally stable equilibrium point for $\epsilon = 0$, is globally asymptotically stable for $\epsilon < 0$, and is globally unstable for $\epsilon > 0$. Thus Lyapunov analysis was completely successful in this case of establishing the global stability characteristics of this system.

E.   Example

Investigate the stability of the system of nonlinear differential equations

$$\dot{x}_1 = x_1(x_1^2 + x_2^2 - 1) - x_2, \quad \dot{x}_2 = x_1 + x_2(x_1^2 + x_2^2 - 1)$$

We try the candidate Lyapunov function

$$U(x_1, x_2) = x_1^2 + x_2^2$$

which is an exact integral of the simplified system $\dot{x}_1 = -x_2, \dot{x}_2 = x_1$. This choice for U is obviously a positive definite function having its global minimun at the origin. It is also obvious after inspection that the origin is the only equilibrium point of the nonlinear system. Investigating the energy rate, we find

$$\dot{U}(x_1, x_2) = 2(x_1^2 + x_2^2)(x_1^2 + x_2^2 - 1)$$

It is evident that $\dot{U}$ is negative definite over the finite circular region $[(x_1, x_2) \mid x_1^2 + x_2^2 < 1]$ which includes the equilibrium point at the origin. Hence, the origin $(0, 0)$ is an asymptotically stable equilibrium state of this system. Note that all points within the unit circle are asymptotically attracted to the origin. However, because $\dot{U}$ is not a negative definite function over all of R^2, we cannot conclude global asymptotic stability without more information. Although we are certain we have stability within the unit circle, this conclusion results from a particular choice of $U(x_1, x_2)$, and without further analysis we cannot conclude that the stable region is not actually larger than the unit circle. However, since $\dot{U}$ is positive everywhere outside the unit circle, we can finally conclude, using the following theorem (in Sec. III.F) that we have instability for all trajectories which initiate outside the unit circle and asymptotic stability for all trajectories initiating inside the unit circle. Thus we are able to use both the stability and instability insights simultaneously to establish the complete story vis-a-vis the global stability properties of this system, since the stable and unstable regions have a mutual boundary, and together the stable and unstable regions span all of state space R^2.

The following theorem is sometimes useful in avoiding a fruitless search for Lyapunov functions for systems which can be proven unstable. This theorem is also useful in obtaining theoretical closure of the stability analysis, in the sense that it is sometimes possible to simultaneously apply the instability theorem with the stability theorems to conclusively establish a particular system's global stability properties. For example, in Sec. III.E, we concluded that our simple choice on U gave us all of the stability information (i.e., the system is stable only within the unit circle).

F. Theorem: Instability Theorem

The equilibrium state x_e is unstable in Ω if there exists a continuously differentiable function U such that

i) $U(x_e) = 0$ and $\dot{U}(x_e) = 0$

ii) $\dot{U}(x) > 0$ for all $x \neq x_e, x \in \Omega$

iii) and there exists points x arbitrarily close to x_e such that $U(x_e) > 0$

Some versions of the instability theorem require a function U such that both U and $\dot{U}$ are positive definite, and this unnecessarily more restrictive version is somewhat less efficient[1] than the preceding theorem, which makes no requirement on the definiteness of U. Actually, if one can find any such function U satisfying the preceding conditions, then x_e is a completely unstable equilibrium point in Ω, and the quest for Lyapunov functions can be halted. In the example shown in Sec. III.E, the Ω for the instability theorem is clearly the compliment of the Ω for the asymptotically stable region, and it is apparent that the stable and unstable regions being complimentary is the key to establishing global stability/instability information.

IV. Stability of Linear Systems

A. Lyapunov Theorem for Linear Systems

Lyapunov's method is easily applied to test the stability of a linear system. Consider an autonomous system described by the linear vector differential equation

$$\dot{x}(t) = Ax(t) \qquad (4)$$

The preceding system is said to be stable in the sense of Lyapunov, if the solution of Eq. (4) tends toward zero (which is obviously the only equilibrium state if A is of full rank) as $t \to \infty$ for arbitrary initial condition.

Consider the case of a constant A matrix. If all eigenvalues of A are distinct, the response of system (4), given initial condition x_0, can be written as

$$x(t) = \sum_{i=1}^{n} \underline{\psi}_i^T x_0 e^{\lambda_i t} \underline{\phi}_i \qquad (5)$$

where λ_i are the eigenvalues of A, and $\underline{\phi}_i$ and $\underline{\psi}_i$ are, respectively, the right and left eigenvectors of A associated with λ_i. For the repeated eigenvalue case, the situation is much more complicated (i.e., we should solve for the generalized eigenvectors of A). The generalization of Eq. (5) for the case of generalized eigenvectors has a similar form but will not be discussed here.[8]

From Eq. (5), we can see by inspection that the system will be asymptotically stable if and only if all the eigenvalues of A have negative real parts, i.e.,

$$\Re[\lambda_i(A)] < 0 \qquad (6)$$

Thus, we have the well-known result that the stability of a linear constant-coefficient dynamical system can be completely characterized by the eigenvalues of the system. This approach to stability analysis yields both necessary and sufficient conditions. However, calculating all the eigenvalues of the system matrix is not always desirable. As will be evident later, other stability viewpoints lead to important insights and generalized methods, especially vis-a-vis stability analysis for time-varying, distributed-parameter, and nonlinear systems.

For the linear dynamical system of Eq. (4), we choose a symmetric quadratic form as a candidate Lyapunov function

$$2U(x) = x^T P x \qquad (7)$$

where P is a positive definite, real symmetric matrix. Thus U is positive definite with its global minimum at the origin, which is obviously an equilibrium state. Differentiating Eq. (7) and substituting Eq. (4) into the result gives the energy rate

$$\dot{U}(x) = x^T (A^T P + PA)x \qquad (8)$$

Using the Lyapunov stability theorem in Sec. III.B, we require $\dot{U}(x)$ to be negative definite. We can rewrite the energy rate of Eq. (8) as

$$\dot{U}(x) = -x^T Q x \qquad (9)$$

So we see that, for asymptotic stability, P and Q must be positive definite matrices which satisfy the condition

$$A^T P + PA = -Q \qquad (10)$$

Equation (10) is commonly known as the algebraic Lyapunov equation.

To examine the stability of a linear system via the preceding Lyapunov approach we can proceed as follows: Choose Q to be any positive definite matrix for a given A, and check the eigenvalues of the resulting P which we obtain by solving Eq. (10), if P is positive definite (all positive eigenvalues), the given system is asymptotically stable, whereas if P has any negative eigenvalues, the system is unstable. One of the potential difficulties with selecting Q and solving the Lyapunov equation (which, of course, depends on the system matrix A) is the uniqueness of the resulting solution for P. The following theorem gives the necessary and sufficient conditions for the Lyapunov Eq. (10) to have a unique solution.

B. Theorem

If $\{\lambda_1, \ldots, \lambda_n\}$ are the eigenvalues of the system matrix A, then the Lyapunov equation [Eq. (10)] has a unique solution P if and only if

$$\lambda_i + \lambda_j^H \neq 0, \qquad i, j = 1, \ldots, n$$

where $(\ )^H$ denotes complex conjugate.

The reader is referred to Chen[8] for the proof. One cannot solve the Lyapunov equation for undamped second-order systems having pairs of eigenvalues on the

imaginary axis (including rigid-body modes, whose eigenvalues reside at the origin of the complex plane), and so we see that stability analysis for systems having a neutrally stable subspace cannot be completed via solution of an algebraic Lyapunov equation.

C. Theorem: Lyapunov Stability Theorem for Linear Systems

A linear system is asymptotically stable or, equivalently, all the eigenvalues of A have negative real parts, if and only if for any given positive definite symmetric matrix Q there exists a positive definite (symmetric) matrix P that satisfies the Lyapunov equation

$$A^T P + PA = -Q$$

D. Proof of Theorem in Section IV.C

1. Necessity

The uniqueness condition of the solution (theorem of Sec. IV.B) is automatically met in the theorem Sec. IV.C, since $\Re[\lambda_i(A)] < 0$ for all i, for asymptotically stable systems. The unique solution P of the Lyapunov equation can be expressed as[9]

$$P = \int_0^\infty e^{A^T t} Q e^{At} dt \qquad (11)$$

The integrand is an infinite summation of terms of the form $t^k e^{\lambda t}$, where λ is an eigenvalue of A, and since $\Re[\lambda_i(A)] < 0$, the integrand will exist for all values of t. Next, by direct substitution of Eq. (11) into the left hand side of Eq. (10), we can verify that the combined integrand is a perfect differential, so we see

$$A^T P + PA = \int_0^\infty \frac{d}{dt}(e^{A^T t} Q e^{At}) dt$$
$$= e^{A^T t} Q e^{At}\big|_0^\infty = -Q$$

Note that e^{At} (and $e^{A^T t}$) $\to 0$ as $t \to \infty$, since all eigenvalues of A have negative real parts, and since e^{At} (and $e^{A^T t}$) equal 1 at $t = 0$.

2. Sufficiency

Consider

$$U(x) = x^T P x$$

From Eqs. (7–10), we see that $\dot{U}(x) = -x^T Q x$ along all trajectories of $\dot{x} = Ax$. From the assumptions, P and Q are positive definite matrices, therefore we see that for any $x \neq 0$ that $U(x) > 0$, and $\dot{U}(x) < 0$. We can apply the theorem in Sec. III.C and conclude that the equilibrium state [the state space origin ($x = 0$)] is globally asymptotically stable, and of course, all eigenvalues of A must have negative real parts.   Q.E.D.

Note that the Lyapunov equation is equivalent to a set of $n(n + 1)/2$ linear equations in $n(n + 1)/2$ unknowns for an nth-order system. The Lyapunov equation can be solved by using numerical algorithms utilizing QR factorization, Schur

decomposition, or spectral decomposition, however our experience indicates that the most efficient and robust algorithms utilize the QR factorization.[32]

E. Example

Consider the system matrix

$$A = \begin{bmatrix} -2 & 1 \\ -1 & 1 \end{bmatrix}$$

The simplest choice of Q is the identity matrix or some other diagonal matrix; we take $Q = I$ for this example, and let the three distinct elements in P be denoted

$$P = \begin{bmatrix} p_1 & p_2 \\ p_2 & p_3 \end{bmatrix}$$

Substituting this A and P into the Lyapunov equation [Eq. (10)] yields the following three linear algebraic equations

$$-4p_1 - 2p_2 = -1$$
$$p_1 - p_2 - p_3 = 0$$
$$2p_2 + 2p_3 = -1$$

The solution of these three equations is straightforward, we find

$$p_1 = -\frac{1}{2}, \quad p_2 = \frac{3}{2}, \quad p_3 = -2$$
$$\Rightarrow P = \begin{bmatrix} -1/2 & 3/2 \\ 3/2 & -2 \end{bmatrix}$$

Even though we have a unique solution, the resulting matrix P is not positive definite. Hence, we conclude that the system is unstable, and implicitly, that not all of the eigenvalues of A have negative real parts. We would have to calculate the eigenvalues to make further assessments of eigenvalue placement.

In the case of a linear time varying system $\dot{x}(t) = A(t)x(t)$, the sufficient conditions for the stability of the equilibrium state can be discussed based on the concept of matrix measure,[1] and if the system is asymptotically stable, then a quadratic Lyapunov function exists for this system. Of course, eigenvalue analysis is not applicable to the time-varying case and therefore the more general Lyapunov approach provides one possible avenue to characterize the stability of nonautonomous systems. The reader is referred to Ref. 1 for more information on this generalization of the preceding discussion.

F. Linear Dynamic Systems Subject to Arbitrary Disturbances

To make the Lyapunov stability analysis in this section more complete, we will briefly discuss stability in the presence of disturbances. We consider the class of systems described by the matrix differential equation

$$\dot{x}(t) = Ax(t) + f(t, x(t)) \qquad (12)$$

where the uncertainty and/or perturbations of the system are assumed representable by an arbitrary nonlinear function $f[t, x(t)]$ [except we require $f(t, 0) = 0$, so that the origin of the state space remains an equilibrium state for this class of model errors or disturbances]. Furthermore, we assume that exact expressions for $f[t, x(t)]$ are unknown and only bounds on $f[t, x(t)]$ are known. A central question is the following: Given that A is asymptotically stable, and without using specific knowledge of $f[t, x(t)]$, is it possible to obtain a bound on all $f[t, x(t)]$ such that the system maintains its stability? Put another way, can we determine some measure of how large $f[t, x(t)]$ can be without destabilizing a given stable linear system? Some insight on these issues are embodied in the following theorem.

G.   Theorem[10,37]

Suppose that the system of Eq. (12) is asymptotically stable for $f[t, x(t)] = 0$, then the system remains asymptotically stable for all nonzero perturbations $f[t, x(t)]$ which are sufficiently small that they satisfy the following inequality:

$$\frac{\|f\|}{\|x\|} \leq \frac{\min}{\max} \frac{\lambda(Q)}{\lambda(P)} \equiv \mu_{PT} \qquad (13)$$

where P and Q satisfy the following Lyapunov equation

$$A^T P + P A = -2Q$$

and where the otherwise arbitrary $f[t, x(t)]$ vanishes at the origin $f(t, 0) = 0$.

The Proof of this theorem is given in Refs. 10 and 32. Since P is a positive definite matrix, the maximum eigenvalue of P is same as the largest singular value of P. It has been also shown in Refs. 10 and 32 that when the identity matrix is chosen for Q, μ_{PT} in Eq. (13) is a maximum and for this choice, μ_{PT} can be expressed as

$$\mu_{PT} = \frac{1}{\max \lambda(P)} = \frac{1}{\sigma_{max}(P)} \qquad (14)$$

The preceding bound is often very conservative, since it is only a sufficient condition for the stability of the system, and this stringent bound is not usually necessary.

An important special case is for the class of perturbations having the linear structure

$$f[t, x(t)] = Ex(t) \qquad (15)$$

Clearly this corresponds to an additive error in the A matrix (i.e. $A \rightarrow A + E$). We can apply the theorem Sec. IV.G to arrive at the desired result. That is, the system remains stable if E is bounded by the following modified stability margin:

$$\|E\| \leq \frac{\min[-\Re\{\lambda_i(A)\}]}{\mathcal{K}(\Phi)} \qquad (16)$$

where $\mathcal{K}(\Phi)$ is the condition number of Φ, and Φ is the normalized eigenvector (modal) matrix of A. The condition number can be conveniently computed as the ratio of the largest and least singular values of Φ,

$$\mathcal{K}(\Phi) = \frac{\sigma_{max}(\Phi)}{\sigma_{min}(\Phi)}$$

As is evident in the preceding discussion, the stability margin is closely related to the Patel-Toda[10] robustness margin; the more stable the nominal system is, the larger the bound on the allowable perturbation E becomes. However, the important ingredient evident in Eq. (16) is the fact that a large condition number $\mathcal{K}(\Phi)$ degrades the effective stability margin. The intimate connection of the Patel-Toda robustness measure (for stability of linear dynamical systems in the presence of additive perturbations) to the Bauer-Fike Theorem (original result in Ref. 37; for conditioning of the algebraic eigenvalue problem see Ref. 32) is clear.

Note that the condition number $\mathcal{K}(\Phi)$ approaches its smallest possible value of unity if Φ is any unitary matrix (one for which $\Phi^H\Phi = I$), and the upper bound on the condition number is infinity which occurs if Φ is any singular matrix. Observe that an infinity of unitary matrices exist, some of them are closer to Φ than others. When one has the freedom to modify A (and therefore Φ), a natural question arises: For a given class of A modifications, how can we make Φ as nearly unitary as possible? Of course, one way to modify the A matrix is through design of a feedback controller, and one avenue toward designing gains in linear robust control laws is to maximize the right-hand side of Eq. (16) by minimizing $\mathcal{K}(\Phi)$. It is also of significance that the choice of actuator locations considered simultaneously with the design of control gains can often significantly reduce the condition number $\mathcal{K}(\Phi)$. These ideas provide some of the motivation for the robust eigenstructure algorithms and actuator placement optimization approaches presented in Ref. 32.

V.   Nonlinear and Time Varying Dynamical Systems

In this section, we present stability analysis methods for nonlinear systems. In Sec. V.B, we consider a method known as Lyapunov's indirect (or first) method, whereby we can determine partial stability information for nonlinear systems by examining the behavior of locally linearized systems. In Sec. V.C, we develop an important result which provides easy-to-test sufficient conditions to determine if we have asymptotic stability in spite of the common situation that the energy function's time derivative is only a negative semidefinite function of the state variables. In addition to the classical stability analysis for which the Lyapunov methods were developed, these ideas can be used to motivate design methods which yield control laws for the control of large maneuvers for distributed parameter systems.

This approach is used throughout the remainder of this chapter. In Sec. VI, we consider a nonlinear multibody idealization of two robots cooperatively manipulating a payload. Both open-loop and feedback control designs are studied, and Lyapunov methods are used to ensure stability of the resulting tracking control law.

A.   Local Stability of Linearized Systems

The stability analysis of linear motion arises often in practical analysis of nonlinear systems when one is concerned with motion near an equilibrium state. The linear results presented in Secs. IV.A–IV.E enable us to obtain necessary and sufficient conditions for the stability of linear systems but also provide us with a method

for determining the local stability of a nonlinear system by linearization, which is called Lyapunov's indirect method.

Consider the autonomous system

$$\dot{x}(t) = f[x(t)] \quad \text{with} \quad f(x_e) = 0 \tag{17}$$

Let $z(t)$ be the perturbation (departure motion) from the equilibrium state as

$$x(t) = x_e + z(t) \tag{18}$$

Using Taylor's series expansion of $f(\cdot)$ around the equilibrium state x_e, we can write

$$f[z(t) + x_e] = f(x_e) + \left[\frac{\partial f}{\partial x}\right]_{x=x_e} z(t) + O[z(t)]^2 \tag{19}$$

Using Eq. (19) in Eq. (17) gives the perturbation equation

$$\dot{z}(t) = Az(t) + O[z(t)]^2 \tag{20}$$

where A denotes the Jacobian matrix of f evaluated at $x = x_e$, $A = [\partial f/\partial x]_{x=x_e}$, and so we find the linear, constant coefficient matrix differential equation

$$\dot{z}(t) = Az(t) \tag{21}$$

The following theorem is given here (without proof); this is the main stability result of Lyapunov's indirect method.

B. Theorem: Lyapunov's Indirect Method

If the linearized system [Eq. (21)] is asymptotically stable, then the original nonlinear system [Eq. (17)] is also asymptotically stable if the motion initiates in a sufficiently small neighborhood containing the equilibrium state.

The preceding theorem is useful since we can analyze the local stability of an equilibrium state of a given nonlinear system by examining a linear system. However, the conclusions based on linearizations are local, and therefore to study global stability we should rely on Lyapunov's direct method. On the other hand, if one can find all equilibrium points and investigate their local stability, a fairly complete picture of the overall global stability characteristics can often be derived. Note that one key shortcoming (of the indirect approach) is the absence of information on the size or boundary of the domain of attraction of each locally stable equilibrium point; this is precisely the information which a completely successful application of the direct approach determines. Finally, we note the most important point: If the linear motion is critical (e.g., zero damping, some eigenvalues have zero real parts), then the stability of the locally linearized analysis should be considered inconclusive and nonlinear effects must be included to conclude local stability or instability.

C. What to Do When $\dot{U}$ is Negative Semidefinite

Several subtle possibilities arise if the function derived for $\dot{U}$ is not negative definite. For a significant fraction of the practical occurences of this condition, including several applications considered subsequently in this chapter, we can

prove global asymptotic stability in spite of the fact that the function derived for $\dot{U}$ is negative semidefinite. The main results from the traditional literature for dealing with this problem are embodied in a theorem due to LaSalle and Lefschetz[29]; this theorem sometimes allows us to conclude that we have local asymptotic stability for the case that $U > 0$ and $\dot{U} \leq 0$, provided we can prove that the equilibrium point is contained in a region of state space known as the *maximum invariant subspace* M. It is usually easy to identify the subset Z of points in the state space for which $\dot{U} = 0$, but LaSalle and Lefschetz's maximum invariant subspace M is in general a subset of Z. The main challenge of applying LaSalle and Lefschetz's theorem then reduces to the quest to identify or approximate M; this is difficult when the differential equations are complicated nonlinear functions. While these ideas are elegant, we elect not to discuss this approach in greater detail. Instead we present a recently developed result[30,31,36] which is easier to apply.

D. Theorem

Prior to stating the theorem, we need some notations: Let $x = 0$ be an equilibrium state of the nonlinear system $\dot{x} = f(t, x)$, where f is a smooth, twice differentiable n vector function of t and x. Note that the trajectories of the nonlinear differential equation $\dot{x} = f(t, x)$ generates a smooth vector field in the region Ω which includes $x = 0$. Let $U(t, x)$ be a scalar analytic function in Ω, which is locally positive definite. Suppose $\dot{U}(t, x)$ is only negative semidefinite. Let Z denote the set of points for which $\dot{U}(t, x)$ vanishes. We will be concerned with the first k derivatives $d^k U/dt^k$, evaluated on the set Z. We are now prepared to state the theorem:

A sufficient condition for asymptotic stability, when $U > 0$ and $\dot{U} \leq 0$ for all $x \in \Omega$ is that the first $(k-1)$ derivatives of U vanish on Z, up through some even order $(k-1)$ as

$$\frac{d^j U}{dt^j} = 0, \quad \forall x \in Z, \quad \text{for} \quad j = 1, 2, \ldots, \quad k-1 \tag{22}$$

and the first (the kth) nonzero derivative of U (evaluated on Z) is of odd order and is negative definite for all points on Z:

$$\frac{d^k U}{dt^k} < 0, \quad \forall x \in Z, \quad \text{for } k \text{ odd} \tag{23}$$

In the event that all infinity of U derivatives vanish on Z, sufficient conditions for stability are that U is positive definite and that $x = 0$ is the only equilibrium point.

The proof of this theorem is given in Ref. 30 and further discussed in Ref. 31. This theorem is fairly easy to apply and useful results can often be obtained efficiently, as will be evident in the several nonlinear and distributed parameter applications considered in the remainder of this chapter. As is evident in the following example, this theorem is also useful for determining the stability of time varying systems.

E. Example[20]

Consider the damped Mathieu equation: $\dot{x}_1 = x_2$, $-\dot{x}_2 = -x_2 - (2 + \sin t)x_1$. We select the candidate Lyapunov function: $U(t, x_1, x_2) = x_1^2 + x_2^2(2 + \sin t)$, which we observe is positive definite and analytic for all (t, x_1, x_2). On differentiation of U, and substitution of the equations of motion, we find that

$$\dot{U}(x) = -x_2^2 g(t), \quad \text{where} \quad g(t) = \frac{4 + 2\sin t + \cos t}{(2 + \sin t)^2}$$

Since $\dot{U}(x)$ does not depend on x_1, it is obviously not positive definite and without further analysis, we can only conclude mere stability; however, we'd like to make a stronger statement and conclude asymptotic stability. This can be done by considering the applicability of the Sec. V.D theorem. Note that the set Z of points for which $\dot{U}(x)$ vanishes is the set of all real values for x_1, and zero values for x_2. On taking the second and third derivatives of U, and evaluating them on Z, we find that

$$\frac{d^2 U}{dt^2} = 0, \quad \text{and} \quad \frac{d^3 U}{dt^3} = -2(2 + \sin t)^2 g(t)x_1^2, \quad \forall x \in Z$$

Since the second derivative vanishes on Z and the third derivative is negative on Z, except at the origin, we conclude that all of the conditions of the Sec. V.D theorem are satisfied; indeed this system is globally asymptotically stable.

F. Lyapunov Control Law Design Method

Here, we present a method for generating globally stable feedback control laws for maneuvers of nonlinear systems and distributed parameter systems. A Lyapunov function is selected which is conserved for the uncontrolled system. Then when the control $u(t) \neq 0$ is considered, $\dot{U}(x)$ depends on $u(t)$ through the equations of motion. One strategy is to select the control function $u(t, x)$ (from a set of admissible controls) to make $\dot{U}(x)$ as negative as possible; this Lyapunov optimal control strategy ensures that $U(x)$ will locally approach zero as fast as possible. On the other hand, any control law which makes $U(x)$ negative is asymptotically stabilizing, and in many instances it will be seen that very simple, yet globally stable control laws can be determined which are attractive for applications.

We will use specific dynamical systems to introduce Lyapunov control design methods for nonlinear and distributed-parameter systems using Lyapunov's direct method in this section. The broadest and most productive viewpoint is to simultaneously consider $U(x)$ and $u(t, x)$ to be determined in the design process; as will be seen, the class of problems for which globally stable feedback laws can be obtained is surprisingly large. As will be evident, we place the initial emphasis on using work/energy methods together with stability theory to determine the structure of a stabilizing feedback law and thereby parameterize an infinite family of stable controllers. Conventional nonlinear programming algorithms can then be invoked to optimize a specified closed-loop performance criterion over the linearly stable set. Although we subsequently develop methods for controlling

multibody manipulators, and for distributed parameter systems governed by hybrid coupled sets of ordinary and partial differential equations, we first consider a system described by a sixth-order set of nonlinear, ordinary differential equations.

G. Example: Large Angle Rigid-Body Maneuvers

Some key ideas are easily introduced by considering general three-dimensional nonlinear maneuvers of a single rigid body. The equations governing large motion can be written as[17]

$$I_1\dot{\omega}_1 = (I_2 - I_3)\omega_2\omega_3 + u_1$$
$$I_2\dot{\omega}_2 = (I_3 - I_1)\omega_3\omega_1 + u_2$$
$$I_3\dot{\omega}_3 = (I_1 - I_2)\omega_1\omega_2 + u_3$$
$$2\dot{q}_1 = \omega_1 - \omega_2 q_3 + \omega_3 q_2 + q_1(q_1\omega_1 + q_2\omega_2 + q_3\omega_3)$$
$$2\dot{q}_2 = \omega_2 - \omega_3 q_1 + \omega_1 q_3 + q_2(q_1\omega_1 + q_2\omega_2 + q_3\omega_3)$$
$$2\dot{q}_3 = \omega_3 - \omega_1 q_2 + \omega_2 q_1 + q_3(q_1\omega_1 + q_2\omega_2 + q_3\omega_3)$$

$$(24)$$

where $(\omega_1, \omega_2, \omega_3)$ and (q_1, q_2, q_3) are the principal-axis components of angular velocity and the Euler-Rodriguez parameters ("Gibbs vector"), respectively. Note that (I_1, I_2, I_3) and (u_1, u_2, u_3) are the principal moments of inertia and the principal-axis components of the external control torque, respectively.

For the case of zero control torque, it can be readily verified that total rotational kinetic energy is an exact integral of the motion described by differential Eq. (24), viz., $2T = (I_1\omega_1^2 + I_2\omega_2^2 + I_3\omega_3^2)$. Motivated by total system energy integral, we investigate the trial Lyapunov function

$$U = \frac{1}{2}(I_1\omega_1^2 + I_2\omega_2^2 + I_3\omega_3^2) + k_0(q_1^2 + q_2^2 + q_3^2)$$
$$\equiv \text{kinetic energy} + k_0 \tan^2\left(\frac{\phi}{2}\right)$$

$$(25)$$

where ϕ is the instantaneous principal rotation angle (about the instantaneous Eulerian principal rotation axis, from the current angular position to the desired final angular position of the body[17]). It is apparent that the additive term $k_0(q_1^2 + q_2^2 + q_3^2)$ can be viewed as the potential energy stored in a conservative spring. We can therefore anticipate that the system dynamics will evolve such that U is constant if the only external torque is the associated conservative moment. Of course, we are not interested in preserving U as a constant, but rather we seek to drive it to zero, because it measures the departure of the system from the desired equilibrium state at the origin. We therefore anticipate the necessity of determining an additional judicious control moment to guarantee that U is a decreasing function of time. It is obvious by inspection that U is positive definite and vanishes only at the desired state $q_i = \omega_i = 0$. Differentiation of Eq. (25) and substitution of Eq. (24) lead directly to the following (power) expression for U:

$$\dot{U} = \sum_{i=1}^{3} \omega_i[u_i + k_0 q_i(1 + q_1^2 + q_2^2 + q_3^2)]$$

$$(26)$$

Of all of the infinity of possible control laws, we can see that any control u_i that reduces the bracketed terms to a function whose sign is opposite to ω_i will

guarantee that $\dot{U}$ is globally negative semi definite. The simplest choice consists of the following: Select u_I so that the ith bracketed term becomes $-k_I\omega_I$. This gives the control law

$$u_I = -[k_I\omega_I + k_0q_I(1 + q_1^2 + q_2^2 + q_3^2)], \qquad i = 1, 2, 3 \qquad (27)$$

The closed-loop equations of motion are obtained by substitution of the control law of Eq. (27) into Eq. (24) to establish

$$I_1\dot{\omega}_1 = (I_2 - I_3)\omega_2\omega_3 - [k_1\omega_1 + k_0q_1(1 + q_1^2 + q_2^2 + q_3^2)]$$
$$I_2\dot{\omega}_2 = (I_3 - I_1)\omega_3\omega_1 - [k_2\omega_2 + k_0q_2(1 + q_1^2 + q_2^2 + q_3^2)] \qquad (28)$$
$$I_3\dot{\omega}_3 = (I_1 - I_2)\omega_1\omega_2 - [k_3\omega_3 + k_0q_3(1 + q_1^2 + q_2^2 + q_3^2)]$$

Since $\dot{U} = -(k_1\omega_1^2 + k_2\omega_2^2 + k_3\omega_3^2)$ does not depend on the qs, it is only a negative semidefinite function, and while we have stability; if we choose all $k_I > 0$, we cannot immediately conclude that we have asymptotic stability. We can prove that we do indeed have asymptotic stability; for illumination we establish this truth by two logical paths.

1. Path 1

This analysis is physically motivated. We try to see if there is some equilibrium point or trajectory other than the target state where the system can get stuck with $\dot{U}(x) = 0$. We directly investigate the preceding three closed-loop equations of motion [Eq. (28)] for the existence of equilibrium points in these nonlinear closed-loop equations of motion. It can be verified that $(q_1, q_2, q_3, \omega_1, \omega_2, \omega_3) = (0, 0, 0, 0, 0, 0)$ is the only equilibrium state where all velocity and acceleration coordinates vanish. In fact, imposing the conditions $(\dot{\omega}_1, \dot{\omega}_2, \dot{\omega}_3) = (0, 0, 0)$ and $(\omega_1, \omega_2, \omega_3) = (0, 0, 0)$ on the preceding closed-loop equations of motion immediately gives the requirement that the qs satisfy the three equations

$$0 = -[k_0q_I(1 + q_1^2 + q_2^2 + q_3^2)], \qquad \text{for} \quad i = 1, 2, 3$$

and it is obvious by inspection that these three nonlinear equations are simultaneously satisfied only at the origin.

Since we have shown that with the body at rest, $(\dot{\omega}_1 \neq 0, \dot{\omega}_2 \neq 0, \dot{\omega}_3 \neq 0)$, for $(q_1 \neq 0, q_2 \neq 0, q_3 \neq 0)$, everywhere except the origin $x = (q_1, q_2, q_3, \omega_1, \omega_2, \omega_3)^T = (0, 0, 0, 0, 0, 0)^T$, we conclude that $\dot{U}(x) = 0$ can only be encountered for $(q_1 \neq 0, q_2 \neq 0, q_3 \neq 0)$ at (possibly) apogee-like points in the behavior of U [$\dot{U}$ instantaneously vanishes but these points cannot be equilibrium states because $(\dot{\omega}_1 \neq 0, \dot{\omega}_2 \neq 0, \dot{\omega}_3 \neq 0)$]. Therefore we are guaranteed that $\dot{U}(x) < 0$ almost everywhere (thus, we have the ideal situation that the largest invariant subspace is all of state space). We asymptotically approach the origin from all finite initial states and therefore have global asymptotic stability.

2. Path 2

This analysis is more formal (exactly analogous to Sec. V.E); we simply apply the Sec. V.D theorem. First notice that the set Z where $\dot{U}(x)$ vanishes is the set

of arbitrary real values for the qs and zero values for the ωs. It can be verified by direct differentiation of U that for general motion

$$\frac{d^2U}{dt^2} = -2\sum_{I=1}^{3} k_I\omega_I\dot{\omega}_I, \quad \text{and} \quad \frac{d^3U}{dt^3} = -2\sum_{I=1}^{3} k_I(\dot{\omega}_I^2 + \omega_I\ddot{\omega}_I) \qquad (29)$$

On evaluation of these derivatives for motion on Z where angular velocity vanishes $(\omega_1, \omega_2, \omega_3) = (0, 0, 0)$; but from the closed-loop equations of motion, the nonzero acceleration components are $\dot{\omega}_I = -k_0(1 + q_1^2 + q_2^2 + q_3^2)(q_I/I_I)$, we find that

$$\frac{d^2U}{dt^2} = 0, \quad \text{and}$$
$$\frac{d^3U}{dt^3} = -2k_0^2(1 + q_1^2 + q_2^2 + q_3^2)^2 \sum_{I=1}^{3} k_I\left(\frac{q_I}{I_I}\right)^2, \qquad \forall x \in Z \qquad (30)$$

Since the second derivative of U vanishes everywhere on Z, the third derivative is negative definite everywhere on Z, the conditions of the theorem Sec. V.D are fully satisfied, and we again conclude that the nonlinear control law of Eq. (27) gives us globally asymptotically stable attitude control.

Since we have shown U to be a positive definite, decreasing function of time along all trajectories, and since it vanishes at the origin, then the necessary and sufficient conditions are satisfied for global Lyapunov stability. We have implicitly excluded the geometric singularity $(q_I \rightarrow \infty)$ associated with this parameterization of rotational motion as $\phi \rightarrow n\pi$; we can use the quaternion or Euler parameter description of motion and avoid all geometric singularities as well. This path has been successfully pursued in Refs. 3 and 20.

The nonlinear feedback control law of Eq. (27) guarantees stability of the nonlinear closed-loop system under the assumption of zero model errors. In practice, of course, guaranteed stability in the presence of zero model error is not a sufficient condition to guarantee stability of the actual plant having arbitrary model errors and disturbances. On the other hand, rigorously defining a region in gain space, guaranteeing global stability for our best model of the nonlinear system is an important step; it is reasonable to restrict the optimization of gains to this stable family of designs. The determination of the particular gain values, selected from the space of globally stabilizing gains, is usually based on performance optimization criteria specified in consideration of the disturbance environment, sensitivity to model errors, desired system time constants, actuator saturation, and sensor/actuator bandwidth limitations.

Before generalizing the methodology to consider multibody and partial differential equation systems, it is important to reflect on the selection of the Lyapunov function previously given. Notice that, if a system has no inherent stiffness with respect to rigid-body displacement, it is necessary to augment the open-loop energy integral by a pseudopotential energy term [such as $k_0(q_1^2 + q_2^2 + q_3^2)$ in the preceding example]; generally speaking, the pseudoenergy term should be defined, if possible, such that the resulting candidate Lyapunov function (U) is a positive definite measure of departure motion that has its global minimum at the desired target state. Then the still-to-be-determined controls are usually selected as simply as possible (from an implementation point of view) to force pervasive dissipation

($\dot{U} < 0$) of the modified energy (Lyapunov) function along all trajectories of the closed-loop system, and thereby guarantee closed-loop stability.

Although the preceding insights are useful, the Lyapunov function is generally not unique. However, these ideas lead to an attractive strategy that defines the Lyapunov function with relative weights on the portions of total mechanical energy associated with structural subsystems,[5] and leads to a systematic work/energy method to bypass much of the algebra and calculus leading to the power equations, analogous to Eq. (26), for each particular physical system.[5] The lack of uniqueness of the Lyapunov function is not necessarily a disadvantage in practice because it is a source of user flexibility providing control design freedom that is qualitatively comparable to the freedom one has in selecting performance indices when applying optimal control theory. Indeed, formulating the Lyapunov function as a weighted error energy to be dissipated by the controller is qualitatively attractive for both linear and nonlinear systems, since this gives intuitive and physical meaning to the Lyapunov function and the control gains. Other stability analysis approaches, e.g., Refs. 7 and 11–18, as illustrated in the application studies (Refs. 19 and 21–28), remain useful alternatives and supplement the present discussion.

VI. Cooperative Control of Multibody Manipulators

A. Mechanics

Consider the class of dynamical systems whose behavior is governed by the discrete coordinate version of Lagrange's equations

$$\frac{d}{dt}\left(\frac{\partial \mathcal{L}}{\partial \dot{q}_i}\right) - \frac{\partial \mathcal{L}}{\partial q_i} = Q_i, \quad i = 1, 2, \ldots, N \quad (31)$$

or, in matrix form

$$\frac{d}{dt}\left(\frac{\partial \mathcal{L}}{\partial \dot{q}}\right) - \frac{\partial \mathcal{L}}{\partial q} = Q \quad (32)$$

where the Lagrangian $\mathcal{L}$ is defined in the classical form $\mathcal{L} = T - V$. Restrictions imposed in deriving Eq. (32) are such that the coordinates q_i are independent functions of time only and that the potential and kinetic energies have the functional forms $T = T(q, \dot{q}, t)$, $V = V(q)$, and the nonconservative virtual work has the form $\delta W_{nc} = \Sigma_{i=1}^{n} Q_i \delta q_i = Q^T \delta q$. Thus, Eq. (32) are valid for nonlinear, nonconservative systems as well as linear, conservative systems.

A modest generalization allows Eq. (32) to be applied to a significant class of redundant coordinate or constrained systems (i.e., the coordinates q_i are not independent). To accommodate kinematic constraints which depend on the qs and their time derivatives, Lagrange multipliers can be introduced to generate additive generalized constraint forces on the right-hand side of Eq. (32).[17] In particular, for m Pfaffian (linear in the generalized velocities) constraints of the matrix form

$$A\dot{q} + a_o = 0 \quad (33)$$

The generalized constraint force that needs to be added to the right-hand side of Eq. (32) is the vector $A^T \lambda$, where q is an $N \times 1$ vector containing the generalized coordinates, $A = A(q)$ is an $m \times n$ continuous, differentiable matrix function,

$a_o(q)$ is a smooth, $m \times 1$ vector function, and λ is an $m \times 1$ vector of Lagrange multipliers. One standard solution process is to differentiate the kinematic constraint of Eq. (33) to obtain

$$A\ddot{q} + \dot{A}\dot{q} + \dot{a}_o = 0 \quad (34)$$

Note that the N differential equations of Eqs. (32) must be solved simultaneously with the m kinematic equations [Eq. (34)] to determine the $N + m$ unknowns in the vectors $q(t)$ and $\lambda(t)$. During recent years, significant methodology has evolved for effecting numerical solutions for differential/algebraic systems of equations; see Refs. 33 and 34 for discussion of the recent literature.

For a significant class of systems, the algebra and calculus required in a straightforward application of Lagrange's equations can be dramatically reduced. For the most common case of natural systems in which kinetic energy is a symmetric quadratic form in the generalized-coordinate time derivatives, one finds:

$$T = \frac{1}{2}\sum_{i=1}^{N}\sum_{j=1}^{N} m_{ij}(q)\dot{q}_i \dot{q}_j = \frac{1}{2}\dot{q}^T M \dot{q} \quad (35)$$

Note that q is an $N \times 1$ configuration vector of generalized coordinates. It is convenient to collect the mass matrix $M = M(q)$ before the differentiations implied by Lagrange's equations are carried out. Including the possibility of Pfaffian nonholonomic constraints, the equations of motion follow from Eq. (32) as the following $N + m$ system of differential and algebraic equations:

$$M\ddot{q} + G + \frac{\partial V}{\partial q} = Q + A^T \lambda, \quad A\dot{q} + a_o = 0 \quad (36)$$

where $\partial V/\partial q$ is the $N \times 1$ vector gradient of the potential energy function, and $G = G(q, \dot{q})$ is the $N \times 1$ vector:

$$G = [\dot{q}^T C^1 \dot{q} \cdots \dot{q}^T C^N \dot{q}]^T, \quad c_{jk}^{(i)} = \frac{1}{2}\left(\frac{\partial m_{ij}}{\partial q_k} + \frac{\partial m_{ik}}{\partial q_j} - \frac{\partial m_{jk}}{\partial q_i}\right) \quad (37)$$

and where the last equation that generates the typical element $C_{jk}^{(i)}$ of the $N \times N$ symmetric matrix $C^{(i)} = C^{(i)}(q)$ is the Christoffel operator. It is apparent that deriving the equations of motion, for natural systems subject to Pfaffian nonholonomic constraints, has been reduced to formation of the kinetic energy to identify the mass matrix, then carrying out the indicated gradient operations on the mass matrix elements m_{ik} and the potential energy to form the vectors $G = G(q, \dot{q})$ and $\partial V/\partial q$.

For the case wherein the nonconservative forces are generated by an $m_c \times 1$ vector u of control inputs, we have $Q = Bu$ and Eq. (36) assume the form

$$M(q)\ddot{q} + \frac{\partial V}{\partial q} + G(q, \dot{q}) = Bu + [A(q)]^T \lambda \quad (38)$$
$$A(q)\dot{q} + a_o(q) = 0$$

To appreciate some of the issues of cooperation associated with control design for redundantly actuated robotic systems, we consider a specific example in the following discussion.

B. Prototype Cooperative Manipulation Example

1. Equations of Motion

Consider the pair of robot arms shown in Fig. 1. We assume that there are four active joints, namely, the shoulder and elbow joints on the left and right robots, for simplicity; the wrist torques are neglected. The objective is to design a feedback controller to command the four torques so as to stabilize the payload with respect to a prescribed trajectory of the payload moving from an arbitrary, reachable state A to an arbitrary, reachable state B. It is desired that the control law have the following attributes: 1) accommodate an arbitrary feasible reference trajectory, 2) be of a simple feedforward/output output error feedback form, 3) guarantee global asymptotic stability, including nonlinear kinematics, and 4) handoff smoothly between large trajectory-tracking motion and terminal error suppression, without gain scheduling.

We present a control strategy possessing these four desirable attributes.

Under the assumption that each manipulator is composed of two rigid links, that the payload is a rigid body, and that the entire system undergoes only planar motion, but retaining all nonlinear kinematic effects, the kinetic energy of the system has the natural form

$$T = \frac{1}{2}\dot{q}^T[M(q)]\dot{q}$$
$$= \frac{1}{2}\dot{q}_L^T[M_L(q_L)]\dot{q}_L + \frac{1}{2}\dot{q}_R^T[M_R(q_R)]\dot{q}_R + \frac{1}{2}\dot{q}_P^T[M_P(q_P)]\dot{q}_P \quad (39)$$

where the configuration coordinate vector naturally partitions into left (L), right (R), and payload (P) configuration coordinate subsets as

$$q_L = \begin{Bmatrix} \theta_1 \\ \theta_2 \end{Bmatrix}, \quad q_R = \begin{Bmatrix} \theta_6 \\ \theta_5 \end{Bmatrix}, \quad q_P = \begin{Bmatrix} \theta_3 \\ x_{c_3} \\ y_{c_3} \end{Bmatrix}$$

$$q = \begin{Bmatrix} q_L \\ q_R \\ q_P \end{Bmatrix} = \{\theta_1 \quad \theta_2 \quad : \quad \theta_6 \quad \theta_5 \quad : \quad \theta_3 \quad x_{c_3} \quad y_{c_3}\}^T$$

The 7×7 system mass matrix has the block diagonal structure

$$M(q) = \begin{bmatrix} M_L & & \\ & M_R & \\ & & M_P \end{bmatrix} \quad (40)$$

where, introducing the elbow angles $\theta_{ij} = \theta_j - \theta_i$, the substructure mass matrices are compactly written as

$$M_L = \begin{bmatrix} I_1 + \frac{1}{4}m_1 l_1^2 + m_2 l_1^2 & \frac{1}{2}m_2 l_1 l_2 \cos\theta_{12} \\ \frac{1}{2}m_2 l_1 l_2 \cos\theta_{12} & I_2 + \frac{1}{4}m_2 l_2^2 \end{bmatrix} \quad (41)$$

$$M_R = \begin{bmatrix} I_5 + \frac{1}{4}m_5 l_5^2 + m_4 l_5^2 & \frac{1}{2}m_4 l_5 l_4 \cos\theta_{65} \\ \frac{1}{2}m_4 l_5 l_4 \cos\theta_{65} & I_4 + \frac{1}{4}m_4 l_4^2 \end{bmatrix} \quad (42)$$
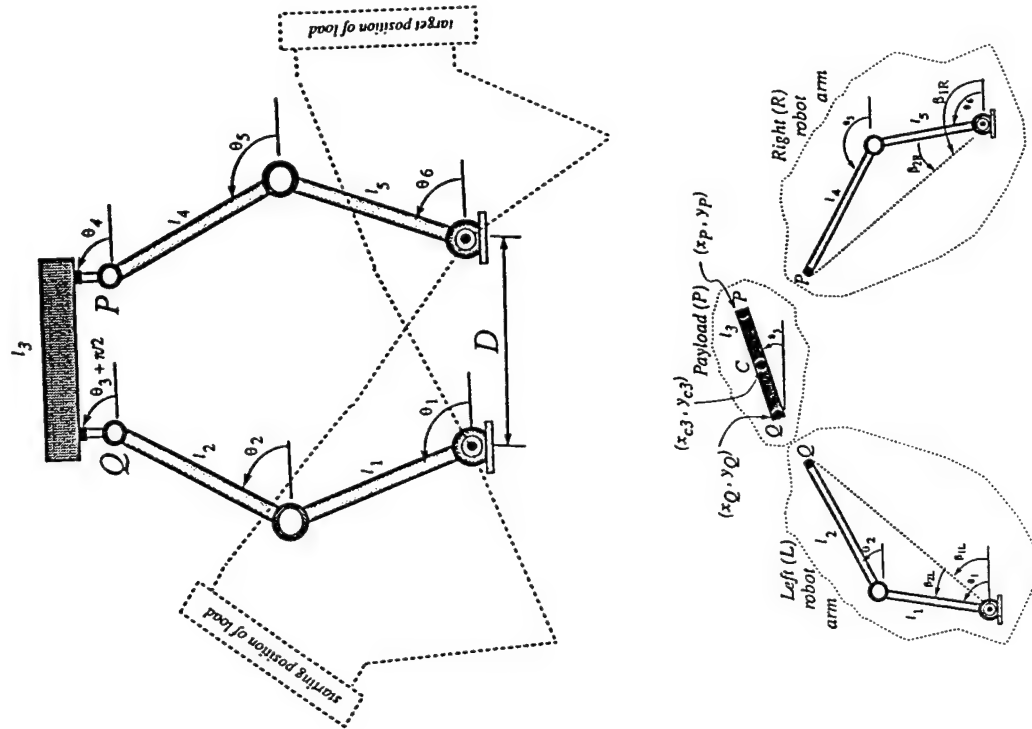
starting position of load

target position of load

Fig. 1 Dual robot cooperative manipulation example.

and

$$M_P = \begin{bmatrix} l_3 & & \\ & m_3 & \\ & & m_3 \end{bmatrix}$$ (43)

The equations of motion follow in the form of Eq. (38), where, using Eq. (37), the nonlinear vector $G(q,\dot q)$ has the following specific form

$$G(q,\dot q) = \left\{ \begin{matrix} G_L \\ G_R \\ 0 \end{matrix} \right\}, \quad \left\{ \begin{matrix} G_L \\ G_R \end{matrix} \right\} = \frac{1}{2} \left\{ \begin{matrix} -m_2\dot\theta_2^2 l_1 l_2 \sin\theta_{12} \\ m_2\dot\theta_1^2 l_1 l_2 \sin\theta_{12} \\ \cdots\cdots\cdots \\ -m_4\dot\theta_5^2 l_4 l_5 \sin\theta_{65} \\ m_4\dot\theta_6^2 l_4 l_5 \sin\theta_{65} \end{matrix} \right\}$$ (44)

The control vector (containing the four shoulder and elbow torques) is

$$u = (u_1 \ u_2 \ u_6 \ u_5)^T$$ (45)

and, using the virtual work principle, we can establish that the control influence matrices are

$$B = \begin{bmatrix} B_L & O \\ O & B_R \\ O & O \end{bmatrix}, \quad B_L = B_R = \begin{bmatrix} 1 & -1 \\ 0 & 1 \end{bmatrix}$$ (46)

Taking the origin for a nonrotating (x, y) coordinate system in the joint at the base of the left arm, the geometric constraint arising from the pinning of the left and right robot wrists to the payload at points Q and P are captured by the four holonomic constraints:

$$l_1\cos\theta_1 + l_2\cos\theta_2 + \tfrac{1}{2}l_3\cos\theta_3 - x_{c_3} = 0$$
$$l_1\sin\theta_1 + l_2\sin\theta_2 + \tfrac{1}{2}l_3\sin\theta_3 - y_{c_3} = 0$$
$$l_5\cos\theta_6 + l_4\cos\theta_5 - \tfrac{1}{2}l_3\cos\theta_3 - x_{c_3} + D = 0$$
$$l_5\sin\theta_6 + l_4\sin\theta_5 - \tfrac{1}{2}l_3\sin\theta_3 - y_{c_3} = 0$$ (47)

On differentiation with respect to time, Eqs. (47) yield a kinematic constraint of the Pffafian form [the second equation of Eqs. (38)], with $a_o = 0$ and with

$$A(q) = \begin{bmatrix} -l_1\sin\theta_1 & -l_2\sin\theta_2 & 0 & 0 & -\tfrac{1}{2}l_3\sin\theta_3 & -1 & 0 \\ l_1\cos\theta_1 & l_2\cos\theta_2 & 0 & 0 & \tfrac{1}{2}l_3\cos\theta_3 & 0 & -1 \\ 0 & 0 & -l_5\sin\theta_6 & -l_4\sin\theta_5 & \tfrac{1}{2}l_3\sin\theta_3 & -1 & 0 \\ 0 & 0 & l_5\cos\theta_6 & l_4\cos\theta_5 & -\tfrac{1}{2}l_3\cos\theta_3 & 0 & -1 \end{bmatrix}$$ (48)

and also, for subsequent use, we record the time derivative of A as

$$\dot A(q,\dot q) = \begin{bmatrix} -l_1\dot\theta_1\cos\theta_1 & -l_2\dot\theta_2\cos\theta_2 & 0 & 0 & -\tfrac{1}{2}l_3\dot\theta_3\cos\theta_3 & 0 & 0 \\ -l_1\dot\theta_1\sin\theta_1 & -l_2\dot\theta_2\sin\theta_2 & 0 & 0 & -\tfrac{1}{2}l_3\dot\theta_3\sin\theta_3 & 0 & 0 \\ 0 & 0 & -l_5\dot\theta_6\cos\theta_6 & -l_4\dot\theta_5\cos\theta_5 & \tfrac{1}{2}l_3\dot\theta_3\cos\theta_3 & 0 & 0 \\ 0 & 0 & -l_5\dot\theta_6\sin\theta_6 & -l_4\dot\theta_5\sin\theta_5 & \tfrac{1}{2}l_3\dot\theta_3\sin\theta_3 & 0 & 0 \end{bmatrix}$$ (49)

Now, solving the first of Eqs. (38) and Eq. (34) simultaneously for the generalized constraint force $Q_c = A^T\lambda$ and $M\ddot q$, we obtain

$$Q_c = A^T\lambda = F_1 + F_2 u$$
$$F_1 = A^T(AM^{-1}A^T)^{-1}(AM^{-1}G - \dot A\dot q)$$
$$F_2 = -A^T(AM^{-1}A^T)^{-1}AM^{-1}B$$ (50)

and

$$M\ddot q + \bar G = \bar B u$$
$$\bar G = G - A^T(AM^{-1}A^T)^{-1}(AM^{-1}G - \dot A\dot q)$$
$$\bar B = [I - A^T(AM^{-1}A^T)^{-1}AM^{-1}]B$$ (51)

It is natural to introduce the consistent partitions

$$M = \begin{bmatrix} M_L & & \\ & M_R & \\ & & M_P \end{bmatrix}, \quad \bar G = \left\{ \begin{matrix} \bar G_L \\ \bar G_R \\ \bar G_P \end{matrix} \right\}, \quad \bar B = \begin{bmatrix} \bar B_L \\ \bar B_R \\ \bar B_P \end{bmatrix}$$ (52)

and rewrite the first of Eqs. (51) as three equations

$$M_L\ddot q_L + \bar G_L(q,\dot q) = \bar B_L(q,\dot q)u$$
$$M_R\ddot q_R + \bar G_R(q,\dot q) = \bar B_R(q,\dot q)u$$
$$M_P\ddot q_P + \bar G_P(q,\dot q) = \bar B_P(q,\dot q)u$$ (53)

This constraint-free form of the equations of motion implicitly reflects the constraints; the third of Eqs. (53) is sufficient to describe the dynamics of the system, since all other coordinates can be determined as a function of $(q_P, \dot q_P)$ through use of the constraint equations.

Prior to a discussion of control law design approaches, it is useful to consider the inverse kinematics problem: Given a smooth desired (prescribed) payload motion $q_P(t)$, determine feasible/desirable corresponding control inputs. Inverse kinematics for the case of redundant coordinates involves some subtle issues which are captured in the following sections.

2. Inverse Kinematics

Notice that the four holonomic constraints of Eqs. (47) reduce the number of degrees of freedom from seven to three. Thus, in principle, we could derive all coordinates and their time derivatives history from a given trajectory of the payload coordinates $q_P(t) = [\theta_3(t)x_{c_3}(t)y_{c_3}(t)]^T$. Obviously, if we know all of the coordinates and their first two time derivatives, then the differential equations of motion [Eqs. (51) or (53)] can be considered algebraic equations for determination of the corresponding control torques. Since there are only three degrees of freedom and four control torques, there is obviously an issue of uniqueness, and it is through the exploitation of the lack of uniqueness that we can seek an optimal control by which the robot arms may cooperate in carrying out the manipulation. It is also important to anticipate geometric singularities on the boundary of the reachable region (the maximum feasible workspace). First let us consider some geometric issues.

With reference to Fig. 1, observe that a given motion $q_P(t)$ of the payload dictates the motion of points P and Q through the four geometric formulas:

$$x_Q = x_{c_3} - \left(\frac{l_3}{2}\right)\cos\theta_3$$
$$y_Q = y_{c_3} - \left(\frac{l_3}{2}\right)\sin\theta_3$$
$$x_P = x_{c_3} + \left(\frac{l_3}{2}\right)\cos\theta_3$$
$$y_P = y_{c_3} + \left(\frac{l_3}{2}\right)\sin\theta_3$$

(54)

and obviously, the companion equations can be obtained to determine the first two time derivatives of the grapple point coordinates (x_P, y_P, x_Q, y_Q) as a function of the payload motion

$$(\theta_3, x_{c_3}, y_{c_3}, \dot\theta_3, \dot x_{c_3}, \dot y_{c_3}, \ddot\theta_3, \ddot x_{c_3}, \ddot y_{c_3})$$

These straightforward equations are not recorded for the sake of brevity. However, given the payload motion, we can obviously determine the grapple point's velocity and acceleration coordinates

$$(\dot x_P, \dot y_P, \dot x_Q, \dot y_Q, \ddot x_P, \ddot y_P, \ddot x_Q, \ddot y_Q)$$

from the time derivatives of Eqs. (54). We consider how to determine the motion of the left and right robot arms. Considering the geometry of the left robot arm, from Fig. 1, it is evident that the left shoulder and elbow angles θ_1 and θ_2 are related to the instantaneous position of the grapple point (x_Q, y_Q) by

$$\theta_1 = \beta_{1L} + \beta_{2L}$$
$$\beta_{1L} = \tan^{-1}(y_Q/x_Q)$$
$$\beta_{2L} = \cos^{-1}\left(\frac{l_1^2 - l_2^2 + (x_Q^2 + y_Q^2)}{2l_1(x_Q^2 + y_Q^2)^{1/2}}\right), \quad \text{two roots, take } \beta_{2L} > 0$$
$$\theta_2 = \tan^{-1}\left(\frac{y_Q - l_1\sin\theta_1}{x_Q - l_1\cos\theta_1}\right)$$

(55)

Similarly, considering the right robot, it is evident that the right robot angles θ_6 and θ_5 are related to (x_P, y_P) by

$$\theta_6 = \beta_{1R} - \beta_{2R}$$
$$\beta_{1R} = \tan^{-1}(y_P/x_P)$$
$$\beta_{2R} = \cos^{-1}\left[\frac{l_5^2 - l_4^2 + (x_P^2 + y_P^2)}{2l_5\left[\left(D - x_P\right)^2 + y_P^2\right]^{1/2}}\right], \quad \text{two roots, take } \beta_{2R} > 0$$
$$\theta_5 = \tan^{-1}\left(\frac{y_P - l_5\sin\theta_6}{D - x_P - l_5\cos\theta_6}\right)$$

(56)

It can be verified that taking β_{2L} and β_{2R} as positive corresponds to the elbows out configuration shown in Fig. 1. Obviously, the elbows in configuration results from choosing the negative signs for β_{2L} and β_{2R}, and two other asymmetric configurations are possible if opposite signs are selected. The lack of uniqueness is a consequence of redundancy and the choice of manipulation modes is dictated by practical configurations. Except near certain singular configurations discussed later, it is possible to manipulate smoothly through an infinite family of neighboring configurations for any one of the four choices of signs for $\beta_{2L}(t)$ and $\beta_{2R}(t)$. Straightforward differentiation yields the following kinematic equations which determine the first two time derivatives of the left and right shoulder and elbow angles:

$$\begin{Bmatrix}\dot\theta_1 \\ \dot\theta_2\end{Bmatrix} = A_L^{-1}\begin{Bmatrix}\dot x_Q \\ \dot y_Q\end{Bmatrix}, \quad \begin{Bmatrix}\ddot\theta_1 \\ \ddot\theta_2\end{Bmatrix} = A_L^{-1}\left[\begin{Bmatrix}\ddot x_Q \\ \ddot y_Q\end{Bmatrix} - \dot A_L\begin{Bmatrix}\dot\theta_1 \\ \dot\theta_2\end{Bmatrix}\right]$$
$$\begin{Bmatrix}\dot\theta_6 \\ \dot\theta_5\end{Bmatrix} = A_R^{-1}\begin{Bmatrix}\dot x_P \\ \dot y_P\end{Bmatrix}, \quad \begin{Bmatrix}\ddot\theta_6 \\ \ddot\theta_5\end{Bmatrix} = A_R^{-1}\left[\begin{Bmatrix}\ddot x_P \\ \ddot y_P\end{Bmatrix} - \dot A_R\begin{Bmatrix}\dot\theta_6 \\ \dot\theta_5\end{Bmatrix}\right]$$

(57)

where we have introduced the matrices

$$A_L = \begin{bmatrix}-l_1\sin\theta_1 & -l_2\sin\theta_2 \\ l_1\cos\theta_1 & l_2\cos\theta_2\end{bmatrix}, \quad A_R = \begin{bmatrix}-l_5\sin\theta_6 & -l_4\sin\theta_5 \\ l_5\cos\theta_6 & l_4\cos\theta_5\end{bmatrix}$$

(58)

It is easy to verify that the preceding matrices are singular if $\theta_1 = \theta_2$, and $\theta_6 = \theta_5$, respectively. It is obvious that these singularities corresponded to the left and right arms being fully extended, and it is clear that these boundaries of the workspace are to be avoided [the reachable set of points interior to the workspace must be taken into account in the trajectory planning for the payload, leading to the nominal trajectory $q_P(t)$ of the payload].

3. Cooperative Actuation

Given the inverse kinematic solution for all system coordinates and time derivatives, as a function of a prescribed payload trajectory $q_P(t)$, the corresponding control torque vector $u(t)$ is not unique for the case of more actuators and degrees of freedom. In our particular example, since we have four actuators and three degrees of freedom, we expect an infinity of torque vectors for the nominal maneuver. As in the case of human beings jointly manipulating a heavy object, we desire to exploit the redundancy of actuation to cooperate in the sense that large, nonworking constraint forces are avoided.

To capture these considerations as a control strategy, we introduce the following cooperation criterion to be minimized

$$J = \frac{1}{2}u^T W_u u + \frac{1}{2}Q_c^T W_c Q_c$$

(59)

subject to satisfying the third of Eqs. (53). Notice that the weight matrix selection permits us the flexibility of emphasizing small torques (u), or small constraint forces ($Q_c = A^T\lambda$), or a compromise between these two competing objectives.

Using the Lagrange multiplier rule, we introduce the $m \times 1$ Lagrange multiplier vector γ and the augmented function $\bar{J}$, and use Eqs. (50) and (53) to write

$$\bar{J} = \frac{1}{2} u^T W_u u + \frac{1}{2} (F_1 + F_2 u)^T W_c (F_1 + F_2 u) + \gamma^T (M_P \ddot{q}_P + \bar{G}_P - \bar{B}_P u) \tag{60}$$

Requiring that the gradients $\nabla_u \bar{J}$ and $\nabla_\gamma \bar{J}$ both vanish as a necessary condition for minimizing J leads to the solution

$$u = H(\bar{B}_P^T \gamma - F_2^T W_c F_1)$$

$$\gamma = (\bar{B}_P H \bar{B}_P^T)^{-1} (M_P \ddot{q}_P + \bar{G}_P + \bar{B}_P H F_2^T W_c F_1) \tag{61}$$

$$H = (W_u + F_2^T W_c F_2)^{-1}$$

Some simple calculations with example payload motions reveal the utility of this formulation of the inverse kinematics and cooperative actuation strategy.

4. Example Nominal Payload Trajectory

Perhaps the simplest and easiest to motivate scheme for prescribing a nominal motion $q_P(t)$ for the payload is to adopt a smooth polynomial spline from the initial state $q_P(t_0)$ to the target final state $q_P(t_f)$ of the form

$$q_P(t) = f(\tau)[q_P(t_f) - q_P(t_0)] + q_P(t_0), \quad \tau = \frac{(t - t_0)}{(t_f - t_0)}$$

$$\dot{q}_P(t) = \dot{f}(\tau)[q_P(t_f) - q_P(t_0)], \quad \dot{f}(\tau) = \frac{1}{(t_f - t_0)} \frac{df}{d\tau} \tag{62}$$

$$\ddot{q}_P(t) = \ddot{f}(\tau)[q_P(t_f) - q_P(t_0)], \quad \ddot{f}(\tau) = \frac{1}{(t_f - t_0)^2} \frac{d^2 f}{d\tau^2}$$

where we choose the particular shape function

$$f(\tau) = \tau^3 (10 - 15\tau + 6\tau^2)$$

$$\frac{df}{d\tau} = \tau^2 (30 - 60\tau + 30\tau^2) \tag{63}$$

$$\frac{d^2 f}{d\tau^2} = \tau(60 - 180\tau + 120\tau^2)$$

This trajectory can be shown to be optimal for the idealized case where we consider only the payload trajectory and the vector sums (F, M) of the forces and moments applied to the payload, without regard to how these are generated. Equations (62) and (63) can be shown[17] to simultaneously minimize the translational and rotational jerk integrals

$$J_1 = \int_{t_0}^{t_f} F^T F dt, \quad \text{and} \quad J_2 = \int_{t_0}^{t_f} \dot{M}^T \dot{M} dt$$

subject to satisfaction of the third of Eqs. (53), and the boundary conditions:

$q_P(t_0) = $ specified initial position $\quad q_P(t_f) = $ specified final position

$$\dot{q}_P(t_0) = 0 \qquad\qquad \dot{q}_P(t_f) = 0$$

$$\ddot{q}_P(t_0) = 0 \qquad\qquad \ddot{q}_P(t_f) = 0 \tag{64}$$

Since the idealized optimal trajectory [Eqs. (62) and (63)] does not explicitly consider workspace constraints, this nominal motion must be checked to make sure it remains feasible throughout the motion, and of course, optimality with respect to the entire system's dynamics and minimization of other performance measures cannot be claimed. These smooth, easy-to-compute, motions usually represent excellent starting solutions, however, and we elect to use this family of solutions to generate the nominal trajectories throughout the remainder of this chapter. A typical example motion of the system is shown in Fig. 2.

5. Lyapunov Stable Tracking Control Law

A smooth nominal (reference) trajectory for the entire system can be computed using Eqs. (62) and (63), and via inverse kinematics; the left and right robot joint coordinates are determined from Eqs. (54–57), while the nominal (cooperative) shoulder and elbow torques are determined from Eqs. (61). This is a possible way to determine the reference trajectory, and can be replaced by a more appropriate path-planning method in particular applications. However the reference trajectory satisfying the boundary conditions of Eqs. (64) is determined, we denote all state and control variables along the reference trajectory with a subscript reference. Of course, in actual applications, we can expect that the system will not follow the reference trajectory $q_{ref}(t)$ exactly when we command the control $u_{ref}(t)$, because of model errors, external disturbances, and nonideal actuation. We seek a control law $\delta u = \text{function}[\delta q(t), \delta\dot{q}(t)]$ which will guarantee that an initially disturbed motion will asymptotically return to the reference trajectory in the absence of model or implementation errors. Actually, it is preferable that the control perturbation δu is in output feedback form where it depends only on a measurable subset of the coordinates and their time derivatives.

In view of the four kinematic constraints, we know that a minimal coordinate description requires only three generalized coordinates. By considering $(q, \dot{q})$ to be functions of $(q_P, \dot{q}_P)$, in the third of Eqs. (53), we are motivated to investigate the kinetic energy

$$T_P = \frac{1}{2} \dot{q}_P^T M_P \dot{q}_P \tag{65}$$

and observe that

$$\dot{T}_P = \dot{q}_P^T \bar{B}_P u \tag{66}$$

This motivates the Lyapunov function

$$U = \frac{1}{2} \delta\dot{q}_P^T M_P \delta\dot{q}_P + \frac{1}{2} \delta q_P^T K_1 \delta q_P \tag{67}$$

where $\delta q_P = q_P - q_{P\,\text{ref}}(t)$. For the simplest case where $q_{P\,\text{ref}}(t)$ is a constant

vector, then it is easy to verify that the Lyapunov function derivative is

$$\dot{U} = \delta \dot{q}_P^T[\bar{B}_P u + K_1 \delta q_P]$$ (68)

and selecting the bracketed term to equal $-K_2 \delta \dot{q}_P$ (so that $\dot{U}$ is never positive), we are led to the global stability condition

$$\bar{B}_P u = -[K_1 \delta q_P + K_2 \delta \dot{q}_P]$$ (69)

Since $\bar{B}_P$ is a 3×4 matrix, it is evident that u is underdetermined and we are free to introduce an optimization criterion to select a particular control satisfying Eq. (69). One attractive possibility is to minimize $u^T u$; this gives the minimum actuator torque controller

$$u = -\bar{B}_P^T(\bar{B}_P \bar{B}_P^T)^{-1}[K_1 \delta q_P + K_2 \delta \dot{q}_P]$$ (70)

For the trajectory tracking case, in which we desire to stabilize the motion with respect to a prescribed reference motion, the situation is more complicated. Suppose that the reference trajectory $q_{P\,ref}(t)$ and an associated control $u_{ref}(t)$ are determined consistent with the system dynamics [for example, using Eqs. (54–64)]. Then it follows that the payload dynamics at every instant on the actual and reference trajectories satisfy

$$M_P \ddot{q}_P = \bar{G}_P + \bar{B}_P u$$ (71)
$$M_{P\,ref} \ddot{q}_{P\,ref} = \bar{G}_{P\,ref} + \bar{B}_{P\,ref} u_{ref}$$

and it also follows that the Lyapunov function [Eq. (67)] has the time derivative

$$\dot{U} = \delta \dot{q}_P^T \left[\bar{B}_P u - \bar{B}_{ref} u_{ref} + K_1 \delta q_P - \delta \bar{G}_P - \delta M_P \ddot{q}_{P\,ref} + \frac{1}{2} \dot{M}_P \delta q_P \right]$$ (72)

Setting the bracketed term to $-K_2 \delta \dot{q}_P$ gives the stabilizing control condition

$$\bar{B}_P u = \bar{B}_{P\,ref} u_{ref} - [K_1 \delta q_P + K_2 \delta \dot{q}_P] + \left[\delta \bar{G}_P + \delta M_P \ddot{q}_{P\,ref} - \frac{1}{2} \dot{M}_P \delta q_P \right]$$ (73)

and for the case of minimum control torque, a particular solution of Eq. (73) gives the nonlinear feedback law

$$u = \bar{B}_P^T \left(\bar{B}_P \bar{B}_P^T \right)^{-1} \left\{ \bar{B}_{P\,ref} u_{ref} - [K_1 \delta q_P + K_2 \delta \dot{q}_P] \right.$$
$$\left. + \left[\delta \bar{G}_P + \delta M_P \ddot{q}_{P\,ref} - \frac{1}{2} \dot{M}_P \delta q_P \right] \right\}$$ (74)

This law, while guaranteeing stability (neglecting model errors), is cumbersome to implement because of the detailed computation required to produce all of the nonlinear terms. Note that the payload coordinates $q_P = [\theta_3 \quad x_{c3} \quad y_{c3}]^T$ may not be directly measurable. For example, assume that the measurable quantities are $q_L = [\theta_1 \quad \theta_2]^T$ and $q_R = [\theta_6 \quad \theta_5]^T$, and the time derivatives thereof; then it

is easy to verify from geometry that the payload coordinates are computable as follows

$$\theta_3 = \tan^{-1}\left[\frac{y_Q - y_P}{x_Q - x_P}\right]$$

$$= \tan^{-1}\left[\frac{(l_5 \sin\theta_6 + l_4 \sin\theta_5) - (l_1 \sin\theta_1 + l_2 \sin\theta_2)}{(D + l_5 \cos\theta_6 + l_4 \cos\theta_5) - (l_1 \cos\theta_1 + l_2 \cos\theta_2)}\right]$$ (75)

$$x_{c3} = \frac{1}{2}(x_Q + x_P) = \frac{1}{2}[(D + l_5 \cos\theta_6 + l_4 \cos\theta_5) + (l_1 \cos\theta_1 + l_2 \cos\theta_2)]$$

$$y_{c3} = \frac{1}{2}(y_Q + y_P) = \frac{1}{2}[(l_5 \sin\theta_6 + l_4 \sin\theta_5) + (l_1 \sin\theta_1 + l_2 \sin\theta_2)]$$

and the time derivative $\dot{q}_P = [\dot{\theta}_3 \quad \dot{x}_{c3} \quad \dot{y}_{c3}]^T$ follows from differentiation of Eq. (75).

As an alternative to the preceding developments, and to obtain a direct output error feedback form for the control law, we can observe the following kinematic form for the work rate of the control torques

$$\dot{T} = u_1\dot{\theta}_1 + u_2\dot{\theta}_2 + u_6\dot{\theta}_6 + u_5\dot{\theta}_5 = \begin{Bmatrix} \dot{q}_L \\ \dot{q}_R \end{Bmatrix}^T u = \dot{q}_L^T u_L + \dot{q}_R^T u_R$$ (76)

and it is obvious by inspection that setting $u_L = -K_{2L}\dot{q}_L$, $u_R = -K_{2R}\dot{q}_R$ will decrease T for all nonzero motion of the system. This energy dissipative control suggests the following output error feedback law for controlling the departure motion relative to the reference trajectory

$$u = u_{ref}(t) - \left\{K_1\begin{pmatrix} \delta q_L \\ \delta q_R \end{pmatrix} + K_2\begin{pmatrix} \delta \dot{q}_L \\ \delta \dot{q}_R \end{pmatrix}\right\}$$ (77)

where the 4×4 positive definite gain matrices have the structure $K_i = \begin{bmatrix} K_{iL} & 0 \\ 0 & K_{iR} \end{bmatrix}$.

It can be verified that the control law of Eq. (77) is globally stabilizing only for the case that q_{ref} = constant. Although global asymptotic stability is not guaranteed during the time interval [$t_0 < t < t_f$], it is guaranteed during the interval ($t > t_f$), for all reference maneuvers satisfying the boundary conditions of Eq. (64). These developments can be better appreciated in the light of some illustrative numerical examples, as provided in the next section.

6. Cooperative Robotic Manipulation: A Numerical Example

To illustrate the preceding discussion, we consider each link of the robots to be 1 m long and to have a mass of 1 kg. The distance D between the shoulder joints is taken as 0.75 m, and the nominal initial and desired target values of five angles are listed in Table 1. The inverse kinematic process of Eqs. (54–64) was used to compute the solution shown in Fig. 2. All the initial conditions were then perturbed by moderately large angles (order of 10 deg), and the feedback control law of Eq. (77) was used. A typical controlled response from large initial disturbances is shown in Fig. 3. Notice that the order of 10-deg initial errors are less than 0.5 deg by the nominal final time of 10 s, however a few more seconds of terminal control are required to effectively null the errors. The weight
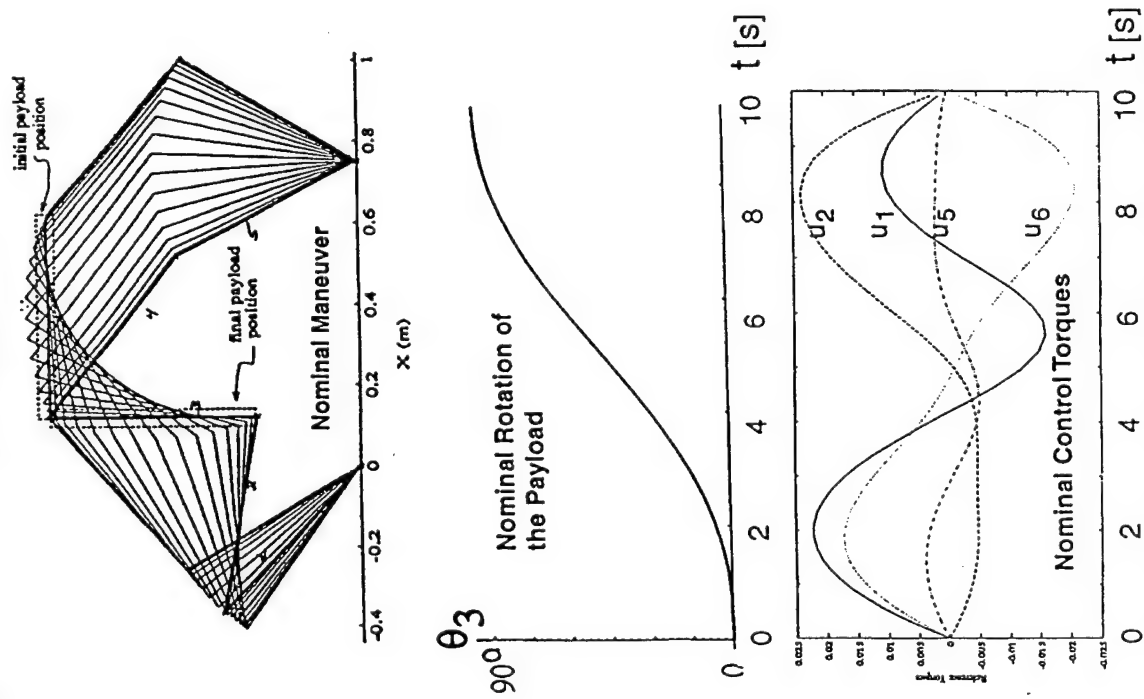
J. L. JUNKINS AND Y. KIM

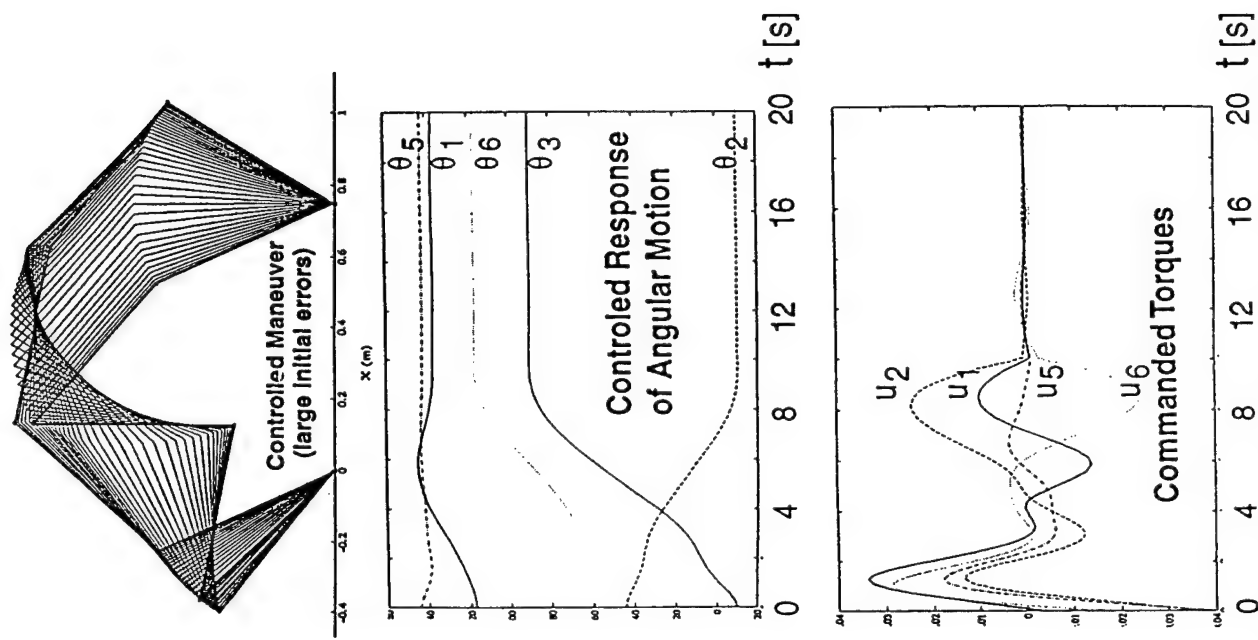Fig. 2 Cooperative manipulation example: open-loop reference motion.

Fig. 3 Cooperative manipulation example: closed-loop tracking controller.

Table 1   Initial and final angles for the nominal maneuver

	θ_1, deg	θ_2, deg	θ_3	θ_6, deg	θ_9, deg	Time, s
Initial	121.0430	40.0323	00.0000	58.9570	139.9677	0
Target	137.2041	−10.3342	90.0000	117.3017	142.3095	10

matrices [in Eq. (59)] were $W_u = I$, $W_c = 0$, and the control gains [in Eq. (77)] were $K_1 = 0.5I$, $K_2 = 0.2I$; these affect the controlled response, however, we found a large family of feasible values. From evaluating the response using several other initial conditions and variations in the selections of the control gains and weight matrices, we confirmed that a wide range of choices give excellent tracking stability over a large domain of initital condition errors. Thus the control law of Eq. (77) seems to be an attractive candidate for practical applications.

The preceding results have been extended, including a successful experimental study in Ref. 35.

VII.   Concluding Remarks

In this chapter, we have summarized the central aspects of Lyapunov stability theory with particular emphasis on the role that it can play in designing stable controllers for nonlinear multibody robotic manipulation. Several elementary analytical and numerical examples are provided to illustrate the ideas and to provide some basis for extrapolating the practical implications of the methods presented. A more extensive example is offered to introduce some ideas on cooperative robotic manipulation, in which two or more manipulators are manipulating a payload while cooperating with each other to minimize a measure of the associated control and constraint forces and moments. The chapter concludes with a numerical example which supports the practical value of these developments.

Acknowledgments

References

[1]Vidyasagar, M., *Nonlinear System Analysis*, Prentice-Hall, Englewood Cliffs, NJ, 1978.

[2]Willems, J. L., *Stability Theory of Dynamical Systems*, John Wiley and Sons, New York, 1970.

[3]Oh, H. S., Vadali, S. R., and Junkins, J. L., "On the Use of the Work-Energy Rate Principle for Designing Feedback Control Laws," *Journal of Guidance, Control, and Dynamics*, Vol. 15, No. 1, 1992, pp. 275–277.

[4]Junkins, J. L., Rahman, Z. H., and Bang, H., "Near-Minimum-Time Control of Distributed Parameter Systems: Analytical and Experimental Results," *Journal of Guidance, Control, and Dynamics*, Vol. 14, No. 2, 1991, pp. 406–415.

[5]Junkins, J. L., Rahman, Z. H., and Bang, H., "Near-Minimum Time Maneuvers of Flexible Vehicles: A Lyapunov Control Law Design Method," *Mechanics and Control of Large Flexible Structures*, edited by J. L. Junkins, Vol. 129, Progress in Astronautics and Aeronautics, AIAA, Washington, DC, 1990, Chap. 22.

[6]Kalman, R. E., "Lyapunov Function for the problems of Lure in Automatic Control," *Proceedings of the National Academy Science*, Vol. 49, 1963, pp. 201–205.

[7]Popov, V. M., "Hyperstability and Optimality of Automatic Systems with Several Control Functions," *Review of Romanian Science and Technology*, Vol. 9, 1964, pp. 629–690.

[8]Chen, C. T., *Linear System Theory and Design*, Holt, Rinehart, and Winston, New York, 1984.

[9]Kalman, R. E., and Bertram, J. E., "Control System Analysis and Design via the Second Method of Lyapunov," *Transactions of the ASME, Journal of Basic Engineering*, Vol. 82, 1960, pp. 371–392.

[10]Patel, R. V., and Toda, M., "Quantitative Measures of Robustness for Multivariable Systems," Proceedings of the JACC, TP-8A, San Francisco, CA, 1980.

[11]Inman, D. J., *Vibration with Control, Measurement, and Stability*, Prentice-Hall, Englewood Cliffs, NJ, 1989.

[12]Creamer, N. G., and Junkins, J. L., "A Pole Placement Technique for Vibration Suppression of Flexible Structures," AIAA/AAS Astrodynamics Conference, Minneapolis, MN, Aug. 15–17, 1988.

[13]Junkins, J. L., and Kim, Y., "A Minimum Sensitivity Design Method for Output Feedback Controllers," *Mechanics and Control of Large Flexible Structures*, edited by J. L. Junkins, Vol. 129, Progress in Astronautics and Aeronautics, AIAA, Washington, DC, 1990, Chap. 25.

[14]Canavin, J. R., "The Control of Spacecraft Vibrations Using Multivariable Output Feedback," AIAA/AAS Astrodynamics Conference, Palo Alto, CA, Aug. 7–9, 1978.

[15]Goh, C. J., and Caughey, T. K., "On the Stability Problem Caused by Finite Actuator Dynamics in the Collocated Control of Large Space Structures," *International Journal of Control*, Vol. 41, No. 3, 1985, pp. 787–802.

[16]Joshi, S. M., *Control of Large Flexible Space Structures*, Lecture Notes in Control and Information Sciences, Vol. 131, Springer-Verlag, New York, 1989.

[17]Junkins, J. L., and Turner, J. D., *Optimal Spacecraft Rotational Maneuvers*, Elsevier, Amsterdam, The Netherlands, 1986.

[18]Juang, J. N., Horta, L. G., and Robertshaw, N. H., "A Slewing Control Experiment for Flexible Structures," *Proceedings of the 5th VPI and SU Symposium on Dynamics and Control of Large Structures*, Virginia Polytechnic Inst. and State Univ., Blacksburg, VA, 1985, pp. 547–551.

[19]Fujii, H., Ohtsuka, T., and Udou, S., "Mission Function Control for Slew Maneuver Experiment," *Journal of Guidance, Control, and Dynamics*, Vol. 12, No. 6, 1989, pp. 858–865.

[20]Wie, B., Weiss, H., and Araposthathis, A., "Quaternion Feedback for Spacecraft Eigenaxis Rotations," *Journal of Guidance, Control, and Dynamics*, Vol. 12, No. 3, 1989, pp. 375–380.

[21]Thompson, R. C., Junkins, J. L., and Vadali, S. R., "Near-Minimum-Time Open-Loop Slewing of Flexible Vehicles," *Journal of Guidance, Control, and Dynamics*, Vol. 12, No. 1, 1989, pp. 82–88.

[22]Vadali, S. R., "Feedback Control of Space Structures: A Lyapunov Approach," *Mechanics and Control of Large Flexible Structures*, edited by J. L. Junkins, Vol. 129, Progress in Astronautics and Aeronautics, AIAA, Washington, DC, 1990, Chap. 24.

[23]Meirovitch, L., and Quinn, R., "Maneuvering and Vibration Control of Flexible Spacecraft," *Journal of Astronautical Sciences*, Vol. 35, No. 3, 1987, pp. 301–328.

[24]Singh, G., Kabamba, P., and McClamroch, N., "Planar Time Optimal Slewing Maneuvers of Flexible Spacecraft," *Journal of Guidance, Control, and Dynamics*, Vol. 12, No. 1, 1989, pp. 71–81.

[25]Breakwell, J. A., "Optimal Feedback Control for Flexible Spacecraft," *Journal of Guidance, Control, and Dynamics*, Vol. 4, No. 5, 1981, pp. 427–479.

[26]Slotine, J.E., and Weiping, L., *Applied Nonlinear Control*, Prentice-Hall, Englewood Cliffs, NJ, 1991.

[27]VanderVelde, W., and He, J., "Design of Space Structure Control Systems Using On-Off Thrusters," *Journal of Guidance, Control, and Dynamics*, Vol. 6, No. 1, 1983, pp. 759–775.

[28]Byers, R. M., Vadali, S. R., and Junkins, J. L., "Near-Minimum-Time Closed-Loop Slewing of Flexible Spacecraft," *Journal of Guidance, Control, and Dynamics*, Vol. 13, No. 1, 1990, pp. 57–65.

[29]LaSalle, J., and Lefschetz, S., *Stability by Lyapunov's Direct Method with Applications*, Academic Press, New York, 1961.

[30]Mukherjee, R., and Chen, D., "Stabilization of Free-Flying Under-Actuated Mechanisms in Space," Proceedings of the 1992 American Control Conference, 1992.

[31]Mukherjee, R., and Chen, D., "An Asymptotic Stability Theorem for Nonautonomous Systems," *Journal of Guidance, Control, and Dynamics*, Vol. 16, No. 6, Nov.–Dec. 1993, pp. 1191–1194.

[32]Junkins, J. L., and Kim, Y., *An Introduction to Dynamics and Control of Flexible Structures*, AIAA Education Series, AIAA, Washington, DC, 1993.

[33]Ahmad, S., and Zribi, M., "Lyapunov Based Control Design for Multiple Robots Handling a Common Object," *Lecture Notes in Control and Information Sciences*, edited by J. M. Skowronski, H. Flashner, and R. S. Guttalu, Vol. 170, Springer-Verlag, New York, 1991, Chap. 1.

[34]Krishnan, H., "Control of Nonlinear Systems with Applications to Constrained Robots and Spacecraft Attitude Stabilization," Ph.D. Dissertation, Univ. of Michigan, Ann Arbor, MI, 1992.

[35]Yale, G., "Cooperative Control of Multiple Space Manipulators," Naval Postgraduate School, Ph.D. Dissertation, Montercy, CA, Sept. 1993.

[36]Mukherjee, R., and Junkins, J. L., "An Invariant Set Analysis of the Hub-Appendage Problem," *Journal of Guidance, Control, and Dynamics*, Vol. 16, No. 6, 1993, pp. 1191–1193.

[37]Bauer, F. L., and Fike, C. T., "Norms and Exclusion Theorems," *Numerische Mathematique*, Vol. 2, 1960, pp. 137–141.

COOPERATIVE CONTROL OF MULTI-ROBOT MANIPULATOR SYSTEMS

Johnny E. Hurtado§ and John L. Junkins¶

Center for Mechanics and Control

Department of Aerospace Engineering

Texas A&M University, College Station, TX 77843

§ Graduate Student

¶ George Eppright Professor

Overview

I. Natural Systems Subject to Holonomic Constraints

   a. Governing Equations

   b. Solution Methods

II. Cooperative Open Loop Control

   a. Reference Trajectories

   b. Reference Controls

III. Closed Loop Tracking Control

   a. Minimum State Feedback

   b. Output Feedback

67

1a. Governing Equations

For natural systems, the discrete coordinate version of Lagrangian Mechanics leads to

$$M(q)\ddot{q} + H(q,\dot{q}) = Bu.$$

When the coordinates q are related thru a set of nonlinear scleronomic constraint equations, the constrained dynamical system is described by

$$M(q)\ddot{q} + H(q,\dot{q}) = Bu + C(q)^T\lambda,$$

$$\text{subject to}\quad \varphi(q) = 0.$$

Note,

$$C(q)^T\lambda = \frac{\partial\varphi}{\partial q}^T\lambda,$$

are the associated constraint forces which restrict the time/space evolution of the system.

△ We emphasize that this set of differential-algebraic equations must be solved simultaneously for the unknown vectors $q(t)$ and $\lambda(t)$.

68

1b. Solution Methods

There are many solution strategies for solving sets of DAE's (e.g. augmented Lagrangian methods, Projection methods, ...).

Range Space Method:

1. differentiate the constraint equations

$$\ddot{\varphi} = C\ddot{q} + \dot{C}\dot{q} = 0$$

2. solve the dynamic equations for $\ddot{q}$

$$\ddot{q} = M^{-1}\left[Bu + C^T\lambda - H\right]$$

3. substitute to obtain

$$\lambda = \Lambda_1(q,\dot{q}) - \Lambda_2(q)\,u$$
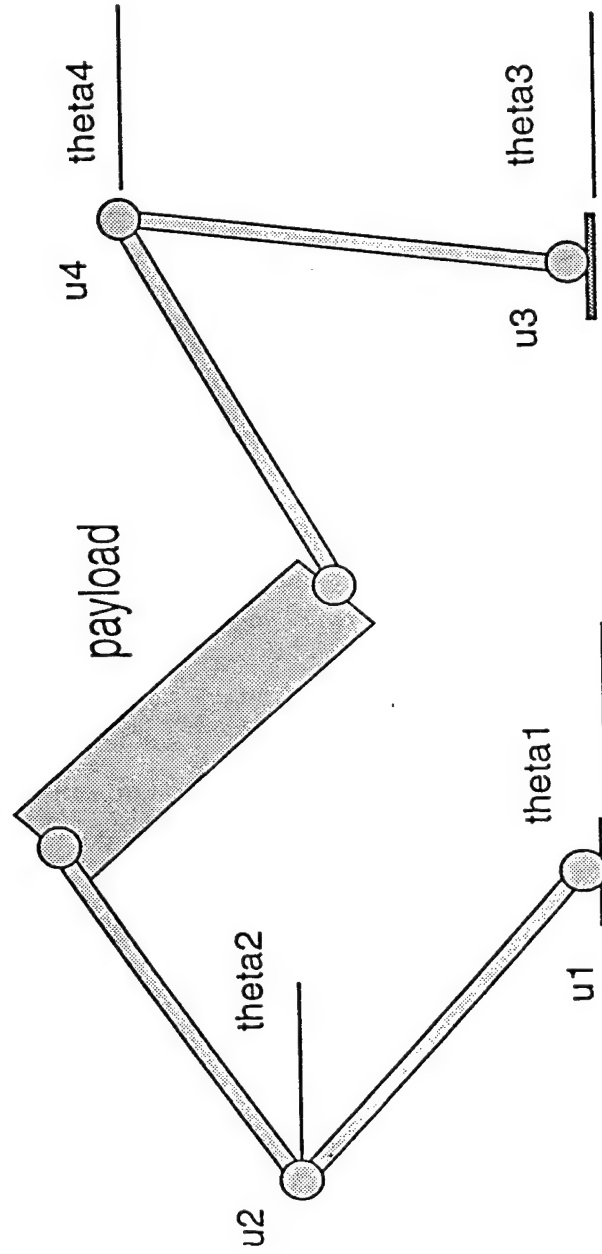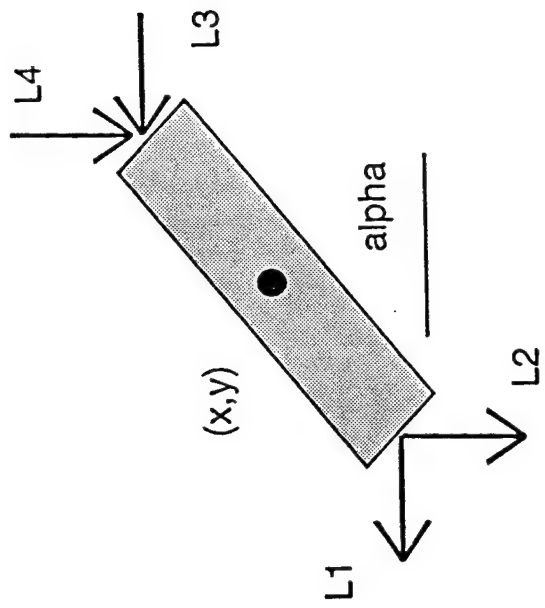
4. the *unconstrained* system equations read

$$M(q)\,\ddot{q} + \hat{H}(q,\dot{q}) = \hat{B}(q)\,u$$

generalized coordinates: 7
controls: 4
constraints: 4
degrees of freedom: 3

For many system representations, the equations partition nicely into a block diagonal form

$$M_d(q)\,\ddot{q}_d + \widehat{H}_d(q,\dot{q}) = \widehat{B}_d(q)\,u,$$

$$M_p(q)\,\ddot{q}_p + \widehat{H}_p(q,\dot{q}) = \widehat{B}_p(q)\,u.$$

2a. Reference Trajectories

Because the constraints are scleronomic $\qquad \rightarrow \qquad q_d = q_d\,(q_p)$.

That is, the coordinates q_p are sufficient to describe the system configuration.

Spse q_p is prescribed via,

▷ cubic polynomial

▷ quintic polynomial

▷ any other sufficiently smooth function

subject to initial and final value conditions. Then q_d and its derivatives are known.

The above choices minimize

$$J = \int_{t_0}^{t_f} u^T W_1 u + \dot{u}^T W_2 \dot{u}\, dt$$

71

subject to the payload equations and the prescribed end conditions for a rest-to-rest manuever.

2b. Reference Controls

▷ Knowing $q_p, \dot{q}_p$ and $\ddot{q}_p$, the payload equations of motions become a set of algebraic equations in the unknown controls u.

▷ Since the system is *over actuated*, we exploit this redundancy to allow cooperation such that large (nonworking) constraint forces are avoided.
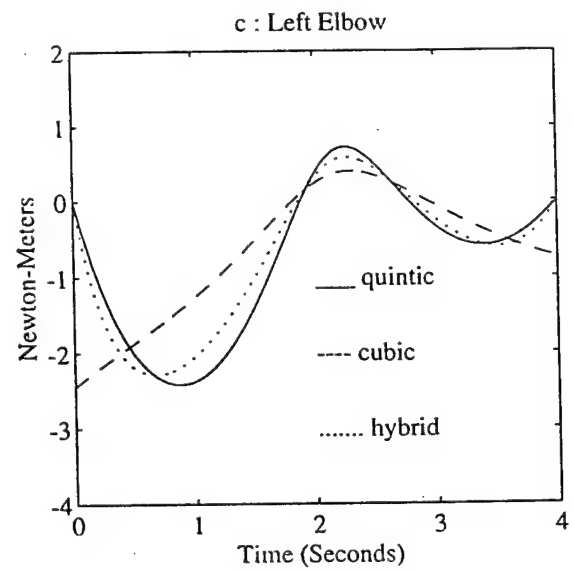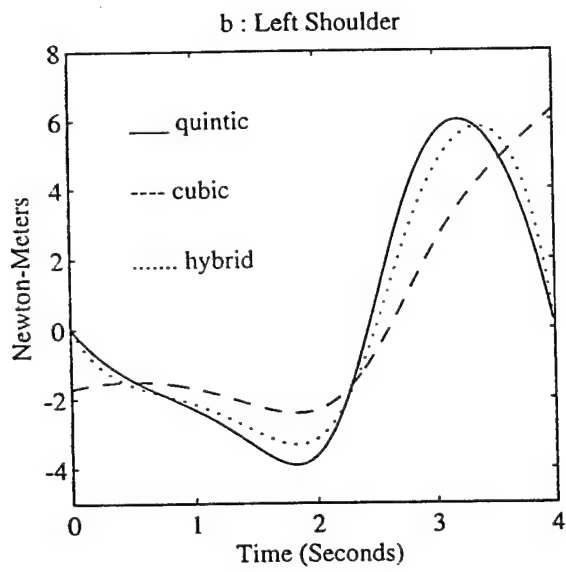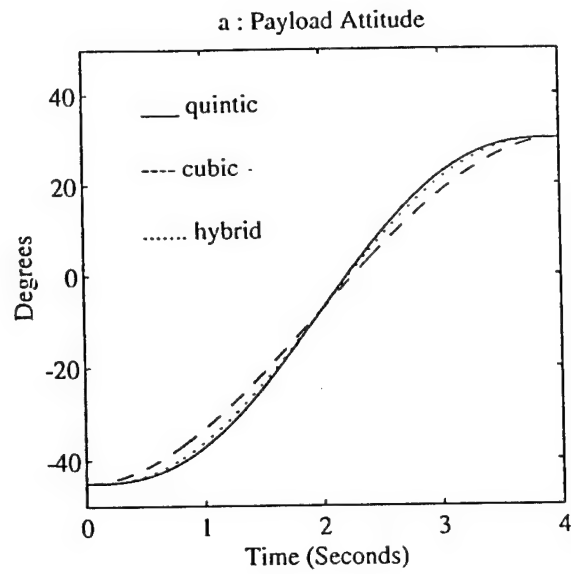
Minimize the cooperation functional

$$J = \frac{1}{2} u^T W_u u + \frac{1}{2} \lambda^T W_\lambda \lambda$$

subject to

$$M_p(q)\, \ddot{q}_p + \widehat{H}_p(q, \dot{q}) = \widehat{B}_p(q)\, u.$$

Using that $\lambda = \Lambda_1(q, \dot{q}) - \Lambda_2(q)\, u$, and the lagrange multiplier rule leads to the necessary

a : Payload Attitude

b : Left Shoulder

c : Left Elbow

73

conditions

$$u = P \left[\widehat{B}_p^T \gamma + \Lambda_2{}^T W_\lambda \Lambda_1 \right]$$

$$\gamma = \left[\widehat{B}_p P \widehat{B}_p^T \right]^{-1} \left\{ M_p \ddot{q}_p + \widehat{H}_p - \widehat{B}_p P \Lambda_2{}^T W_\lambda \Lambda_1 \right\}$$

$$P = \left[W_u + \Lambda_2{}^T W_\lambda \Lambda_2 \right]^{-1}$$

3a. Reference Tracking—Minimum State Feedback

Consider the (tracking) Lyapunov function and its time derivative

$$U = \frac{1}{2} \delta \dot{q}_p^T M_p \delta \dot{q}_p + \frac{1}{2} \delta q_p{}^T K_2 \delta q_p,$$

$$\dot{U} = \delta \dot{q}_p^T M_p \delta \ddot{q}_p + \delta \dot{q}_p^T K_2 \delta q_p,$$

where $\delta q_p = q_p - q_{pr}$, etc.

A choice of u which results in $\dot{U} < 0$ is

$$u = \widehat{B}_p^* \left[\widehat{B}_{pr} u_r - K_1 \delta \dot{q}_p - K_2 \delta q_p + \delta \widehat{H}_p \right]$$

74

△ globally asymptotically stable

△ cumbersome to implement

△ q_p probably not directly measurable

3b. Reference Tracking—Output Error Feedback

Let's note,

1. The system kinetic energy reads

$$T = \frac{1}{2}\dot{q}_d^T M_d \dot{q}_d + \frac{1}{2}\dot{q}_p^T M_p \dot{q}_p$$

2. The Work-Energy Rate principle reveals

$$\dot{T} = (\dot{q}_d, \dot{q}_p)^T B u = \dot{q}_d^T B_d u$$

3. This suggests the output error control

$$B_d u = B_d u_r - G_1 \delta \dot{q}_d - G_2 \delta q_d$$

▷ the control provides for stable tracking.

▷ this control law allows attractors other than the origin.

4. Future Studies

1. further investigation of the output feedback controller.

2. other path parameterizations.

3. develop an experimental testbed involving novel sensing techniques.

Robot Maneuver

alpha: -45
x: -.2
y: .5
theta1: 137.0
theta2: 36.9
theta3: 84.6
theta4: 196.2

alpha: 30
x: .2
y: .25
theta1: 85.1
theta2: -44.1
theta3: 20.1
theta4: 159.8

initial configuration

final configuration
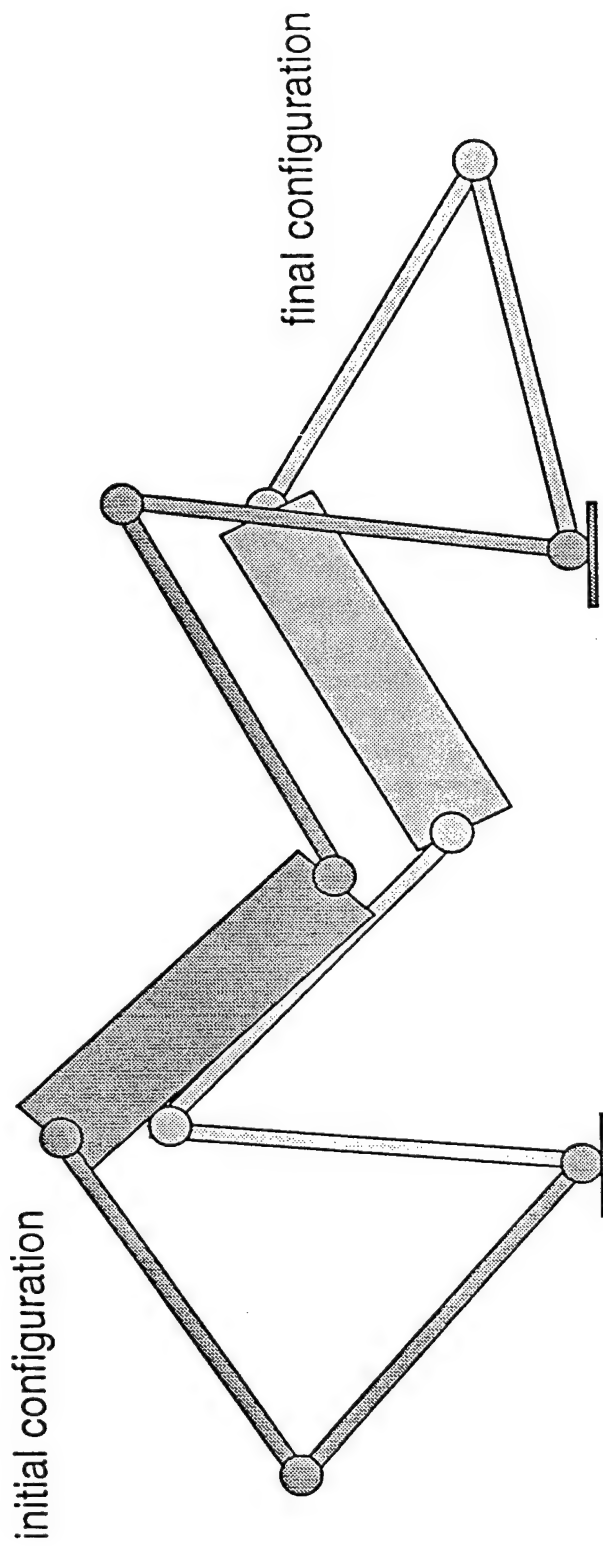
a : Theta1 Profile
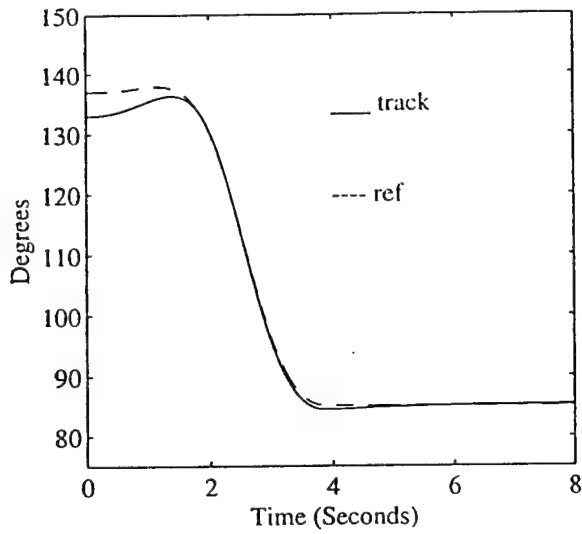
b : Theta2 Profile
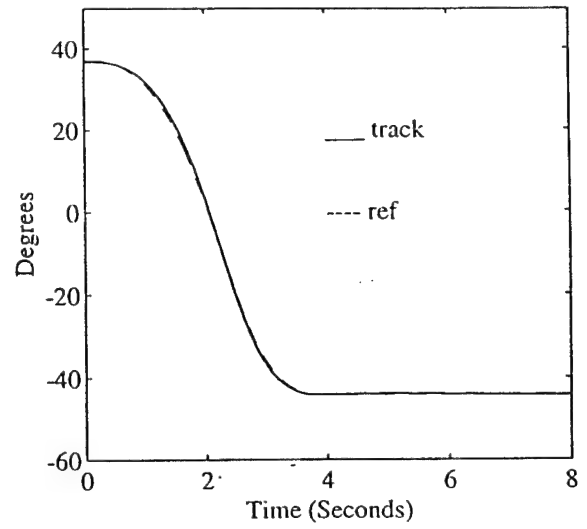
c : Theta3 Profile
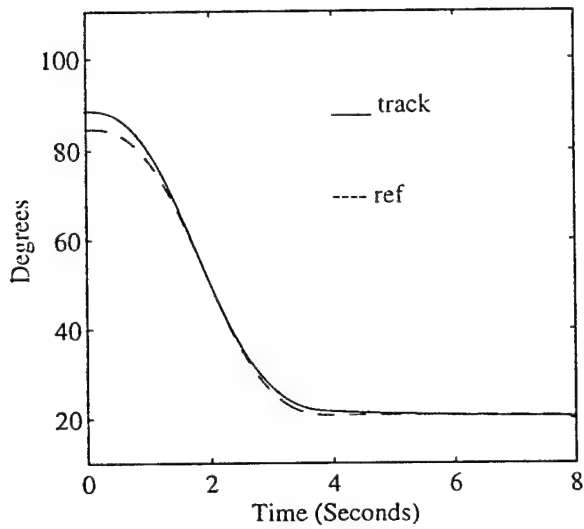
d : Theta4 Profile
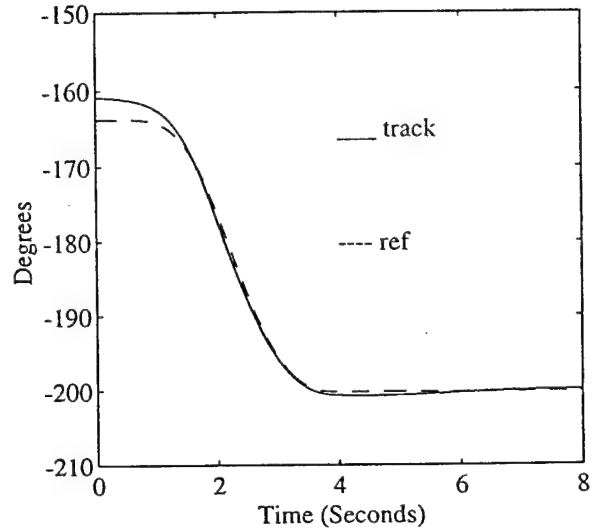
e : Payload Profile

f : Payload Profile

78

a : Left Arm Controls

b : Right Arm Controls

c : Left Constraint Forces

d : Right Constraint Forces

e : Left Arm Controls

f : Right Arm Controls

79
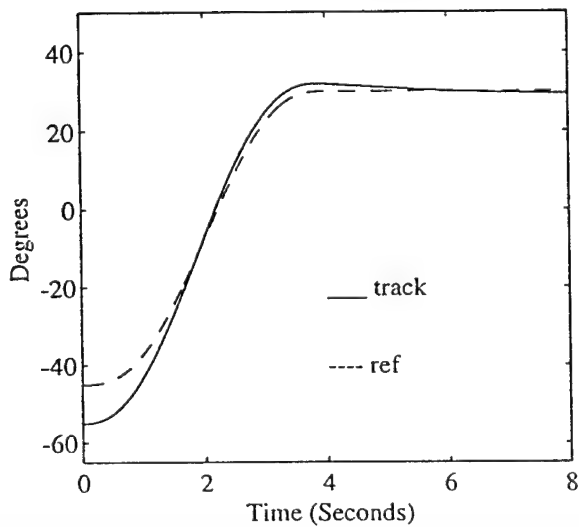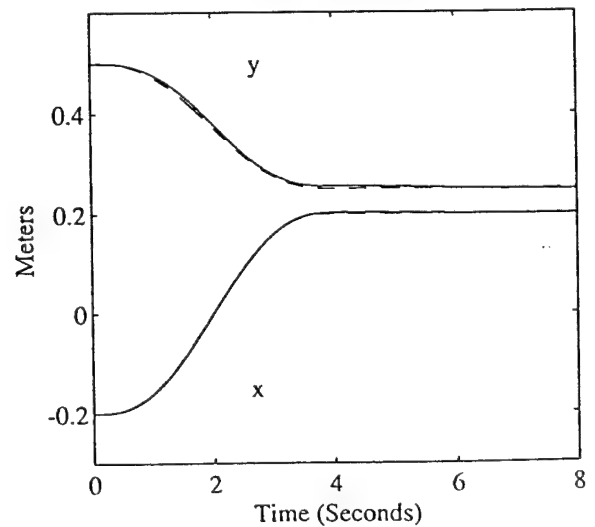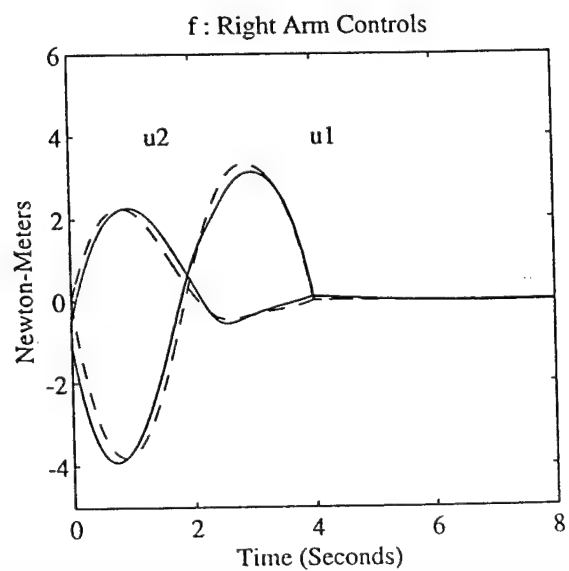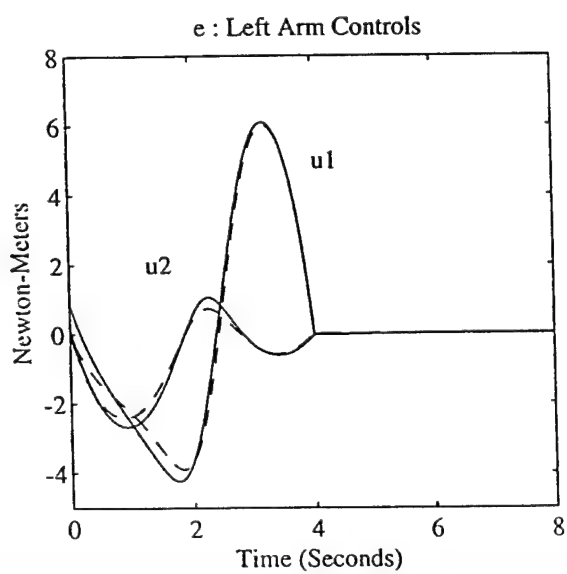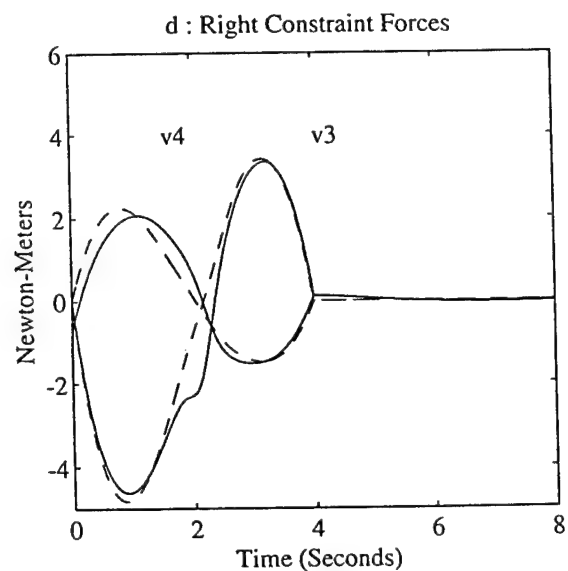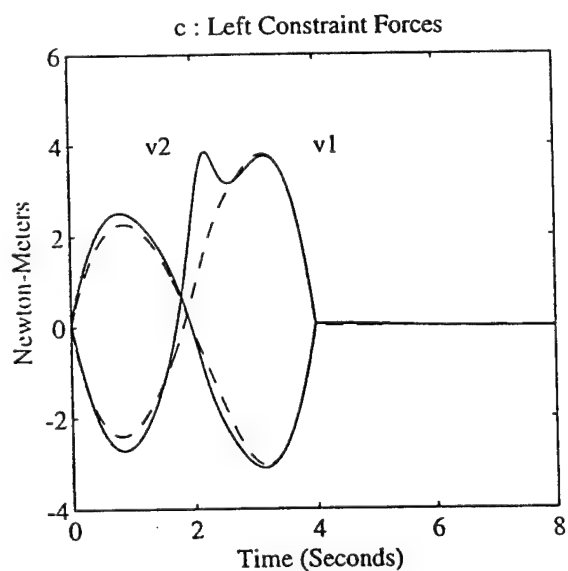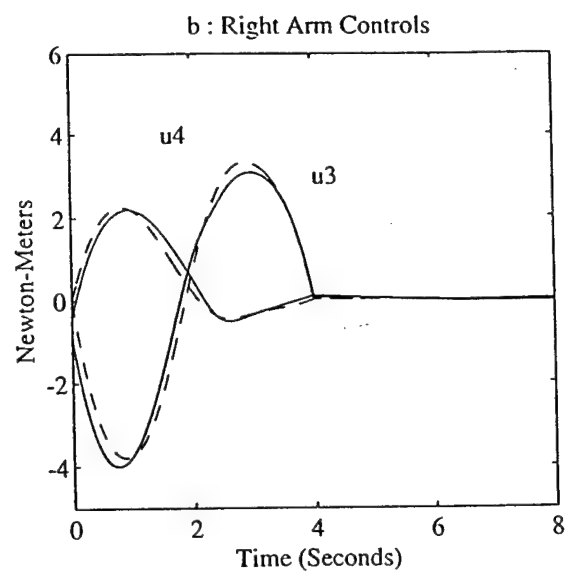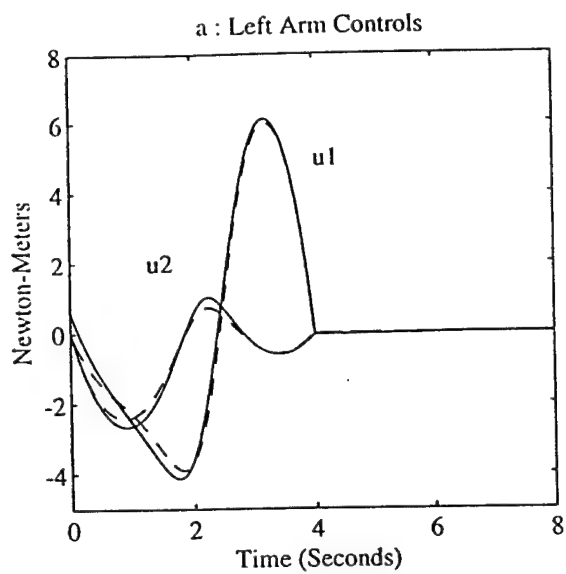
AIAA-94-3754

Linear Quadratic Regulator Problem With Inequality Control Constraints for Flexible Space Structures

S. Lee and J. Junkins
Texas A&M University
College Station, Texas

AIAA/AAS Astrodynamics Conference
August 1-3, 1994 / Scottsdale, AZ

LINEAR QUADRATIC REGULATOR PROBLEM
WITH INEQUALITY CONTROL CONSTRAINTS
FOR FLEXIBLE SPACE STRUCTURES

Sangchul Lee* and John L. Junkins[†]

Texas A&M University, College Station, TX 77843

Abstract

We consider the simultaneous slewing and vibration suppression control problem of an idealized structural model which has a rigid hub with two cantilevered flexible appendages and finite tip masses. The finite element method(FEM) is used to obtain linear finite dimensional equations of motion for the model. In the linear quadratic regulator(LQR) problem, a simple method is introduced to provide a physically meaningful performance index for space structure models. This method gives us a mathematically minor but physically important modification of the usual energy type performance index. A numerical procedure to solve a time-variant LQR problem with inequality control constraints is presented using the method of particular solutions.

Introduction

The problem of simultaneous slewing and vibration suppression of large flexible space structures has been the focus of intense research[1-4]. Since Large Space Structures(LSS) are mechanically flexible systems, they are most generally described as hybrid coordinate dynamical systems. Their motion is described by a coupled system of ordinary and partial differential equations. The corresponding nonlinear integro-differential equation of motion are usually linearized, discretized in space, and truncated to a finite number of modes. The assumed mode method and the FEM are widely used for obtaining discretized linear equation of motion for large flexible structures.

Several approaches to associated control of LSS have been investigated. The linear quadratic regulator and associated tracking problems have been treated successfully and represent an important class of optimal control application[5]. In the LQR problem, the choice of performance index is very important and problem de-

---

* Graduate Student, Department of Aerospace Engineering. Student Member AIAA.

† Eppright Chair Professor, Department of Aerospace Engineering. Fellow AIAA and AAS.

pendent task. Usually LQR problems are considered without any bounds for states and controls. If there are inequality constraints on the controls, however, then Pontryagin's minimum principle could be applied to find the necessary conditions for optimality. Unfortunately, the resulting equations from the optimality conditions give us nonlinear differential equations even though the original system of equations is linear[6]. For this reason, we can not determine controls analytically. Rather, we must attempt to find the solutions by an iterative numerical procedure.

In this paper, we consider the simultaneous slewing and vibration suppression control problem of a rigid hub with two cantilevered flexible appendages which have finite tip masses. The FEM is used to obtain linear finite dimensional equations of motion for the flexible space structure model. We introduce a simple method which provides a physically meaningful performance index for space structure models. This method gives us a mathematically minor but physically important modification of the usual energy type performance index. A numerical procedure to solve a time-variant LQR problem with inequality control constraints is presented using the method of particular solutions[7,8]. We also present simulated results to explore the utility of this method.

Finite Element Modeling

Using the FEM, the partial differential equations of the motion are transformed into an approximate set of second-order differential equations in terms of the displacements, velocities, and accelerations of the finite element coordinates, and the external forcing functions. With reference to Fig.1, we consider a rigid hub with two cantilevered flexible appendages which have finite tip masses. Table 1 summarizes the configuration parameters of this flexible structure. The appendage is considered to be a uniform flexible beam and we make the Euler-Bernoulli assumptions of negligible shear deformation and negligible distributed rotatory inertia. The beam is cantilevered rigidly to the hub. Motion is restricted to the horizontal plane and we neglect the velocity component $-y\dot{\theta}$, that is perpendicular to the y direction. Several finite element models for a flexible arm are presented in Refs.[9] and [10]. In this section, we present a finite element

model for the model by using the extended Hamilton's principle that provides a variational weak form for the finite element model. It is significant to note that we introduce the finite element approximations in such a way (co-rotational coordinates) that large hub rotations are admitted; the FEM represents small elastic displacements with respect to hub-fixed axis.
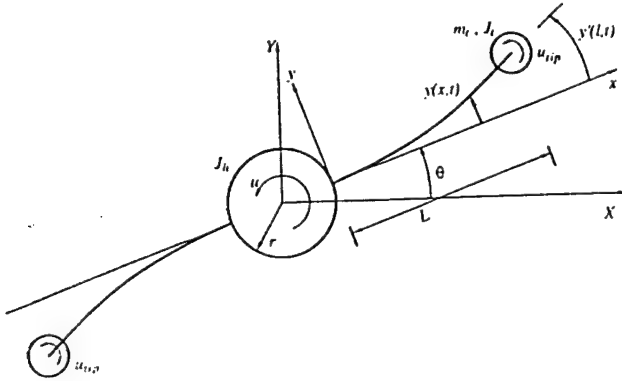

Fig.1 A five-body hybrid coordinate system

Table 1 Configuration Parameters

PARAMETER	SYMBOL	VALUE
Hub radius	r	1 ft
Rotary inertia of hub	J_h	8 slug·ft^2
Mass density of beam	ρ	0.0271875 slug/ft
Elastic modulus of beam	E	0.1584×10^{10} lb/ft^2
Beam length	L	4.0 ft
Moment of inertia of beam	I	0.4709503×10^{-7} ft^4
Tip mass	m_t	0.156941 slug
Rotary inertia of tip mass	J_t	0.0018 slug·ft^2

The application of the extended Hamilton's principle yields

$$\int_{t_1}^{t_2} (\delta T - \delta V + \delta W_{nc})\, dt = 0 \tag{1}$$
$$\delta\theta = \delta y = 0 \quad \text{at} \quad t = t_1, t_2$$

The displacement $y(x,t)$ can be discretized using a finite element expansion[11,12]

$$y(x,t) = \sum_{i=1}^{4} \psi_i^{(e)}(x)\nu_i^{(e)}(t) \tag{2}$$

where $\nu_1^{(e)}, \nu_2^{(e)}$ ($\nu_3^{(e)}, \nu_4^{(e)}$) are transverse deflection and rotation at the left (right) end of the element, and $\psi_i^{(e)}(x)$ are the Hermite cubic polynomial shape functions, defined over the local element, which satisfy the conditions for admissibility.

Specifically, the following cubic functions are adopted as the shape functions for the i-th finite element[12]

$$\psi_1 = 1 - 3\bar{x}_i^2 + 2\bar{x}_i^3, \qquad \psi_2 = h\bar{x}_i - 2h\bar{x}_i^2 + h\bar{x}_i^3$$
$$\psi_3 = 3\bar{x}_i^2 - 2\bar{x}_i^3, \qquad \psi_4 = -h\bar{x}_i^2 + h\bar{x}_i^3 \tag{3}$$
$$\bar{x}_i \equiv (x - x_i)/h$$

where x_i is the distance from the root of the appendage to the left end of the i-th finite element, and h is the length of the finite element. These are the most commonly used shape functions for one-dimensional beam elements.

As a consequence of the space/time separation implicit in Eq.(2), the acceleration and curvature are expressed as follows:

$$\ddot{y}(x,t) = \sum_{i=1}^{4} \psi_i^{(e)}(x)\ddot{\nu}_i^{(e)}(t)$$
$$\frac{\partial^2 y}{\partial x^2} = \sum_{i=1}^{4} \frac{\partial^2}{\partial x^2}\left(\psi_i^{(e)}(x)\right)\nu_i^{(e)}(t) \tag{4}$$

After some algebra, the assembled matrix differential equation is as follows:

$$\begin{bmatrix} J_h + 2M_{\theta\theta} & 2M_{\theta\nu} \\ 2M_{\nu\theta} & 2M_{\nu\nu} \end{bmatrix} \left\{ \begin{matrix} \ddot{\theta} \\ \ddot{\underline{\nu}} \end{matrix} \right\} + \begin{bmatrix} 0 & 0 \\ 0 & 2K_{\nu\nu} \end{bmatrix} \left\{ \begin{matrix} \theta \\ \underline{\nu} \end{matrix} \right\}$$
$$= \begin{bmatrix} 1 & 2 \\ 0 & 0 \\ \vdots & \vdots \\ 0 & 2 \end{bmatrix} \left\{ \begin{matrix} u \\ u_{tip} \end{matrix} \right\} \tag{5}$$

where $\underline{\nu}$ is the coordinate which consists of the transverse deflections and rotations at each node of the appendage, and we assume symmetric deformations of the appendages. The matrix elements of Eq.(5) are presented in Ref.[13]. The control system is assumed to generate a torque u acting upon the hub and a torque u_{tip} acting upon the tip mass.

LQR with Inequality Control Constraints

We introduce a method to find a physically meaningful performance index. First Eq.(5) can be written in a linear second order matrix form as follows:

$$M\ddot{\mathbf{x}} + K\mathbf{x} = \begin{bmatrix} 1 & 2 \\ 0 & 0 \\ \vdots & \vdots \\ 0 & 2 \end{bmatrix} \left\{ \begin{matrix} u \\ u_{tip} \end{matrix} \right\} \quad \text{where} \quad \mathbf{x} = \left\{ \begin{matrix} \theta \\ \underline{\nu} \end{matrix} \right\} \tag{6}$$

Modal coordinates are used to design the controller. To perform the modal coordinate transformation[14],

82

the following open-loop eigenvalue problem should be solved first

$$K\underline{\phi}_i = \lambda_i M\underline{\phi}_i \qquad i = 1, 2, \cdots, n \qquad (7)$$

with the normalization equation

$$\underline{\phi}_i^T M\underline{\phi}_i = 1 \qquad i = 1, 2, \cdots, n \qquad (8)$$

We introduce the modal matrix

$$\Phi = [\underline{\phi}_1, \underline{\phi}_2, \cdots, \underline{\phi}_n] \qquad (9)$$

The general modal coordinate transformation is then

$$\mathbf{x}(t) = \Phi\underline{\eta}(t) \qquad (10)$$

where $\underline{\eta}(t)$ is the $n \times 1$ vector of modal coordinates. The transformed equation of motion becomes

$$\bar{M}\underline{\ddot{\eta}} + \bar{K}\underline{\eta} = \bar{D}\mathbf{u} \qquad (11)$$

where

$$\bar{M} = \Phi^T M \Phi = I_n$$
$$\bar{K} = \Phi^T K \Phi = diag(0, \omega_1^2, \omega_2^2, \cdots, \omega_{n-1}^2)$$
$$\bar{D} = \Phi^T \begin{bmatrix} 1 & 2 \\ 0 & 0 \\ \vdots & \vdots \\ 0 & 2 \end{bmatrix}$$

Note that diagonal zero in $\bar{K}$ corresponds to the rigid body mode. For control applications the system dynamics are usually modeled as first order state space differential equations. We introduce the "2n" dimensional modal state vector $z = \{\eta \ \dot{\eta}\}^T$, then Eq.(11) can be written as the first order system

$$\dot{z} = Az + B\mathbf{u} \qquad (12)$$

where

$$A = \begin{bmatrix} 0 & I_n \\ -\bar{K} & 0 \end{bmatrix}, \qquad B = \begin{bmatrix} 0 \\ \bar{D} \end{bmatrix}$$

Now the kinetic energy and potential energy are as follows:

$$T = \frac{1}{2}\dot{\mathbf{x}}^T M \dot{\mathbf{x}}, \quad V = \frac{1}{2}\mathbf{x}^T K \mathbf{x} \qquad (13)$$

Usually we include the position feedback control-induced potential energy term $\frac{1}{2}k_\theta\theta^2$ since we expect the control to drive θ to zero. We introduce a new weighting matrix Q in the performance index J as follows:

$$J = \frac{1}{2}\int_0^{t_f} (a_1\dot{\mathbf{x}}^T M\dot{\mathbf{x}} + a_2\mathbf{x}^T K\mathbf{x} + k_\theta\theta^2 + \mathbf{u}^T R\mathbf{u})\,dt$$
$$= \frac{1}{2}\int_0^{t_f} (z^T Q z + \mathbf{u}^T R\mathbf{u})\,dt$$
$$(14)$$

where

$$Q = \begin{bmatrix} a_2\Phi^T \hat{K}\Phi & 0 \\ 0 & a_1 I_n \end{bmatrix}, \qquad \hat{K} = \begin{bmatrix} k_\theta & 0 \\ 0 & 2K_{\nu\nu} \end{bmatrix}$$

Note that the usual energy type performance index adopts $diag(q, \omega_1^2, \omega_2^2, \ldots, \omega_{n-1}^2)$ instead of $\Phi^T \hat{K}\Phi$ as the upper left submatrix of Q.

We assume that the control is constrained in magnitude by the relation

$$|u_j(t)| \le 1 \qquad j = 1, 2, \cdots, m \qquad (15)$$

Note that the B matrix of Eq.(12) and the R matrix of Eq.(14) can be defined to obsorb the normalization $u_{j_{max}}$ to allow the normalized magnitude of $u_j(t)$ to have a unity saturation limit, without restriction.

The Pontryagin's minimum principle consists of the state and costate equations and the optimality condition as follows:

$$\dot{z}^* = Az^* + B\mathbf{u}^*$$
$$\dot{\mathbf{p}}^* = -Qz^* - A^T\mathbf{p}^*$$
$$H(z^*, \mathbf{u}^*, \mathbf{p}^*, t) \le H(z^*, \mathbf{u}, \mathbf{p}^*, t) \text{ for all admissible } \mathbf{u}$$
$$(16)$$

where H is the Hamiltonian function.

The solution of the open-loop problem which represented by Eqs.(12,14,15) must satisfy the following nonlinear two point boundary value problem(TPBVP) derived from Pontryagin's minimum principle[6]. The detail proof of Eq.(17) is in the Appendix.

$$\dot{z}^* = Az^* - B\,\mathrm{SAT}(R^{-1}B^T\mathbf{p}^*)$$
$$\dot{\mathbf{p}}^* = -Qz^* - A^T\mathbf{p}^* \qquad (17)$$

where $\mathbf{p}$ is the costate vector and $sat(y_i)$ is defined that $sat(y_i) = y_i$ if $|y_i| \le 1$ and $sat(y_i) = sgn(y_i)$ if $|y_i| > 1$, and $\mathrm{SAT}()$ is a similar vector valued function.

When the initial condition of $z^*(t)$ and the terminal condition of $\mathbf{p}^*(t)$ are assigned as $z^*(0) = z_0$ and $\mathbf{p}^*(t_f) = hz^*(t_f)$, the method of particular solutions associated with a quasi-linearization method gives us the open loop optimal solution.

Method of Particular Solutions

A general technique for solving nonlinear TPBVPs was presented in [7,8]. The method of particular solutions and an associated quasi-linearization method are summarized and then applied to LQR problems with inequality control constraints.

First consider the linear differential system

$$\dot{\mathbf{v}} = F(t)\mathbf{v} + D(t) \qquad 0 \le t \le t_f \qquad (18)$$

83

with the boundary conditions

$$v_i(0) = \alpha_i \qquad i = 1, 2, \cdots, n \qquad (19)$$

$$Cv(t_f) = \beta \qquad (20)$$

where C is a known $n \times 2n$ matrix and β is a known constant vector.

Let $v^j(t)$ $(j = 1, 2, \cdots, n+1)$ denote $n+1$ particular solutions obtained by forward numerical solution of Eq.(18) with the following $n+1$ sets of initial conditions;

$$v_i^j(0) = \alpha_i \qquad i = 1, 2, \cdots, n \quad j = 1, 2, \cdots, n+1$$

$$v_{n+k}^j(0) = \delta_{jk} \qquad k = 1, 2, \cdots, n \quad j = 1, 2, \cdots, n+1 \qquad (21)$$

where δ_{jk} is the kronecker delta.

Due to the linear property of Eq.(18), we can combine the $n+1$ particular solutions to obtain another solution

$$v(t) = \sum_{j=1}^{n+1} k_j \, v^j(t) \qquad (22)$$

The unknown coefficients k_j's are determined in such a fashion that the solution $v(t)$ satisfies the boundary conditions of Eq.(21). From the initial and terminal conditions, we obtain the following equations.

$$\sum_{j=1}^{n+1} k_j = 1$$

$$C \sum_{j=1}^{n+1} k_j v^j(t_f) = \beta \qquad (23)$$

Equation (23) constitutes $n+1$ equations which can be solved to determine the $n+1$ k_j's. The solution is then obtained by recombining the individual particular solutions according to Eq.(22).

Second, consider the nonlinear differential system

$$\dot{v} = f(v, t) \qquad 0 \le t \le t_f \qquad (24)$$

with the boundary conditions

$$v_i(0) = \alpha_i \qquad i = 1, 2, \cdots, n \qquad (25)$$

$$\Psi(v(t_f)) = 0 \qquad (26)$$

Equation (24) is linearized about a nominal solution $v_n(t)$. The linearized equations are given by

$$\dot{v}_n + \triangle\dot{v} = f(v_n, t) + \left[\frac{\partial f}{\partial v}\bigg|_{v_n(t)}\right]\triangle v \qquad (27)$$

where $\triangle v$ are corrections to the nominal solutions. Eq.(27) is rewritten as follows

$$\triangle\dot{v} = \left[\frac{\partial f}{\partial v}\bigg|_{v_n(t)}\right]\triangle v + \{f(v_n, t) - \dot{v}_n\} \qquad (28)$$

If $v_n(t)$ is selected such that the initial conditions of Eq.(25) are satisfied exactly but the terminal conditions

of Eq.(26) are satisfied only approximately, then the boundary conditions are as follows:

$$\triangle v_i(0) = 0 \qquad i = 1, 2. \cdots, n$$

$$\left[\frac{\partial \Psi}{\partial v}\bigg|_{v_n(t_f)}\right]\triangle v(t_f) = -\Psi(v_n(t_f)) \qquad (29)$$

Then, Eqs.(28) and (29) constitute a linear differential system and can be solved by the method of particular solutions. In order to avoid numerical differentiation $\dot{v}_n$ in Eq.(28), we can rewrite Eqs.(28) and (29) using $\tilde{v} = v_n + \triangle v$ as follows:

$$\dot{\tilde{v}} = \left[\frac{\partial f}{\partial v}\bigg|_{v_n(t)}\right]\tilde{v} + \left\{f(v_n, t) - \left[\frac{\partial f}{\partial v}\bigg|_{v_n(t)}\right]v_n\right\} \qquad (30)$$

with boundary conditions

$$\tilde{v}_i(0) = \alpha_i \qquad i = 1, 2. \cdots, n$$

$$\left[\frac{\partial \Psi}{\partial v}\bigg|_{v_n(t_f)}\right]\tilde{v}(t_f) = \left[\frac{\partial \Psi}{\partial v}\bigg|_{v_n(t_f)}\right]v_n(t_f) - \Psi(v_n(t_f)) \qquad (31)$$

The solution $\tilde{v}(t)$ becomes a new nominal solution $v_n(t)$.

Now, we consider the nonlinear TPBVP of Eq.(17) with boundary conditions. Let

$$v = \left\{\begin{array}{c} z^* \\ p^* \end{array}\right\}$$

Then

$$\tilde{v}_i(0) = z_{0i} \qquad i = 1, 2, \cdots, n$$

$$[-h \quad I_n]\tilde{v}(t_f) = 0 \qquad (32)$$

To obtain the linearized differential equation, we need $\left[\frac{\partial f}{\partial v}\big|_{v_n(t)}\right]$ of Eq.(30). For the case of the LQR problem with inequality control constraints, $\left[\frac{\partial f}{\partial v}\big|_{v_n(t)}\right]$ can be obtained easily by the following procedure.

By the presence of SAT function in Eq.(17), first we evaluate the $m \times 1$ vector $R^{-1}B^T p^*$. If $|(R^{-1}B^T p^*)_j| \le 1$ for all $j = 1, 2, \cdots, m$, then the nonlinearity of Eq.(17) disappears, so obviously

$$\left[\frac{\partial f}{\partial v}\bigg|_{v_n(t)}\right] = \left[\begin{array}{cc} A & -BR^{-1}B^T \\ -Q & -A^T \end{array}\right]$$

If there are j's such that $|(R^{-1}B^T p^*)_j| > 1$, then we define a $m \times n$ matrix Y. This matrix is basically $R^{-1}B^T$ but each j-th row is replaced by a zero row vector when j is the index such that $|(R^{-1}B^T p^*)_j| > 1$. Then,

$$\left[\frac{\partial f}{\partial v}\bigg|_{v_n(t)}\right] = \left[\begin{array}{cc} A & -BY \\ -Q & -A^T \end{array}\right] \qquad (33)$$

Substituting Eq.(33) into Eq.(30) gives us a linearized differential equation.

Simulated Results

We consider the previous flexible structure with reference to Fig.1 and use the configuration parameters as shown Table 1. The discretized equations of motion are presented in Eq.(5). Here we use 3 finite elements and time interval $(0 \leq t \leq 1)$ with initial conditions $\theta(0) = 0.2$ rad and $y(x, 0) = 0$ for all x. We use 1 for a_1 and a_2, 100 for k_θ, $diag(5, 50)$ for R of Eq.(14). We assume that the controls are constrained in magnitude as follows:

$$|u(t)| \leq 0.4 \quad \text{and} \quad |u_{tip}(t)| \leq 0.015$$

Figures 2-5 show $\theta(t)$, $y_{tip}(t)$, $u(t)$, and $u_{tip}(t)$ for both cases (constrained control case and unconstrained control case). The first four state and costate histories of the constrained control case are shown in Figs.6 and 7 respectively. Figure 7 shows that the costates satisfy the terminal condition $p^*(t_f) = 0$.
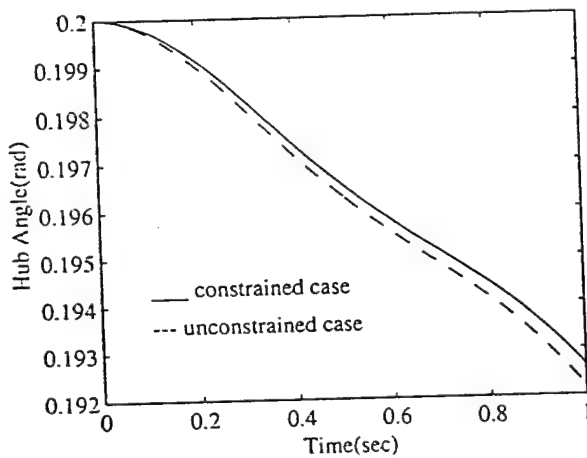
Fig.2 Hub angle $\theta(t)$
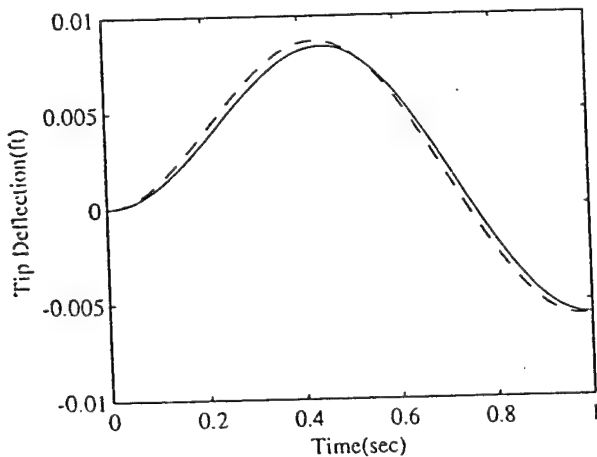
Fig.3 Tip deflection $y_{tip}(t)$
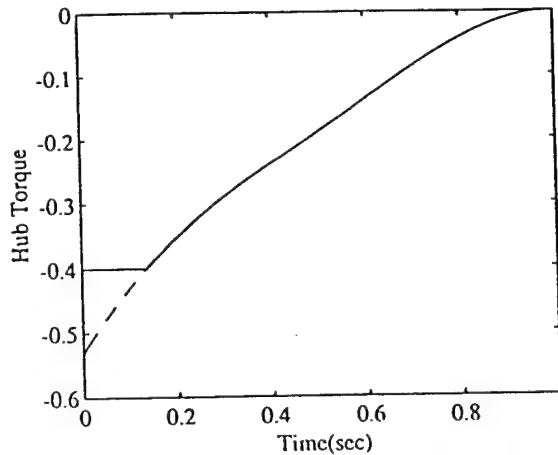
Fig.4 Torque acting on hub $u(t)$
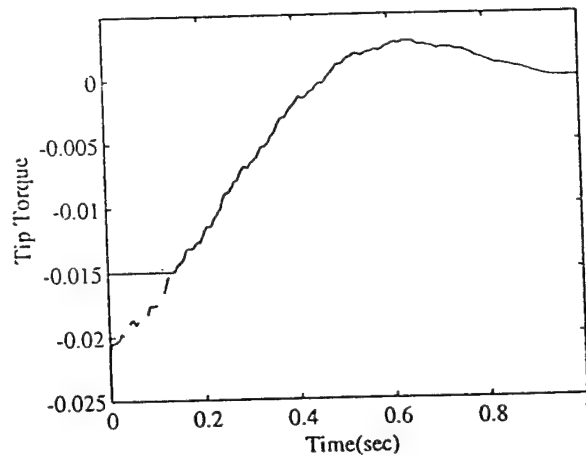
Fig.5 Torque applied at tip mass $u_{tip}(t)$

Summary and Conclusion

The present paper introduces a simple method which provides a physically meaningful performance index for space structure models in the LQR problem. This method gives us a reasonable modification of the usual energy type performance index. A numerical procedure is presented to obtain open loop solution of the time-variant LQR problem with inequality control constraints, using the method of particular solutions incorporated with a quasi-linearization technique. This approach does explicitly consider control saturation constraints and therefore represents a generalization of the standard(unbounded) control assumptions for LQR problems. Numerical results are presented which shows the utility of the method, using the idealized structural model which has a rigid hub with two flexible appendages and finite tip masses.
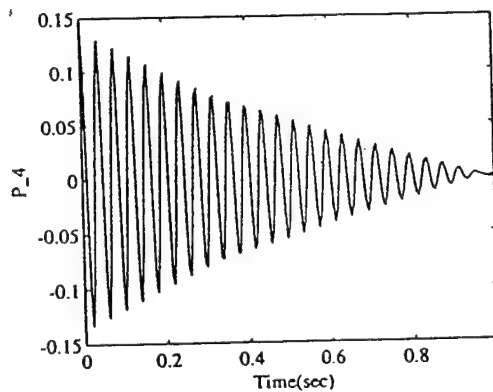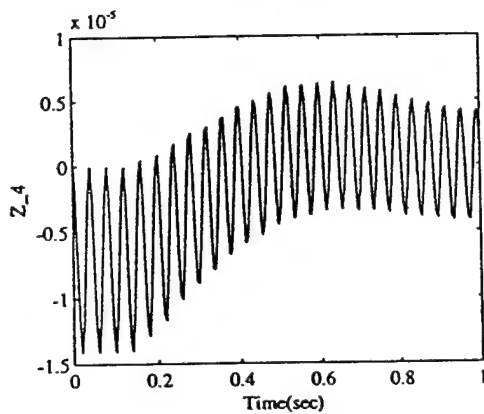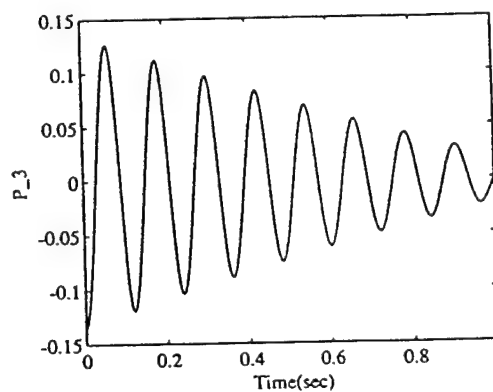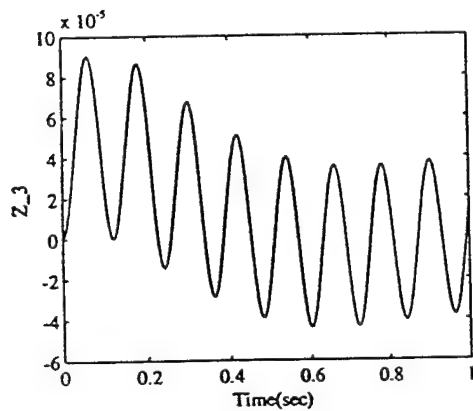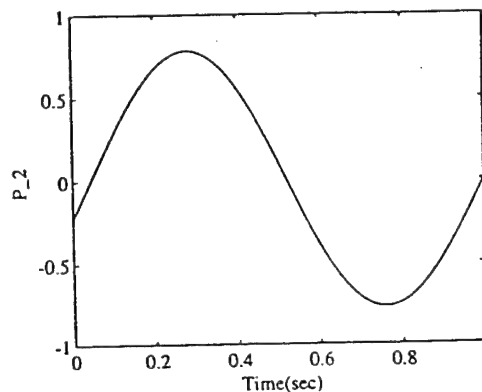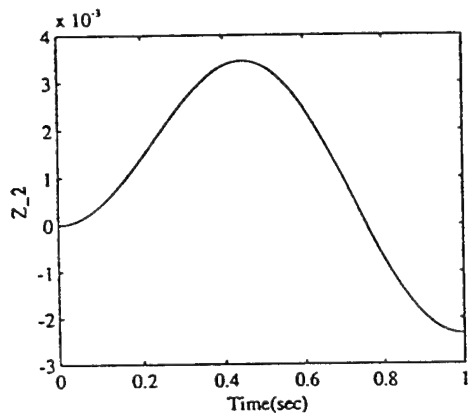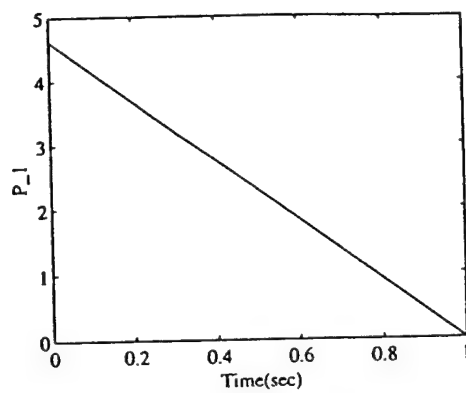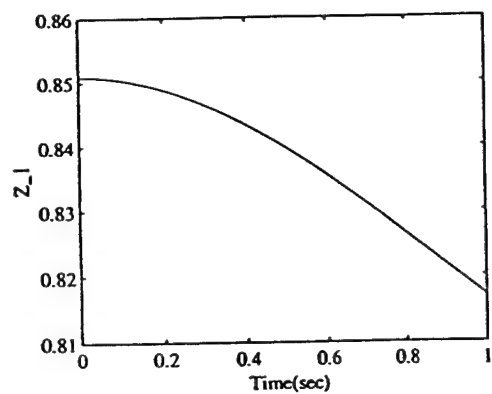
Fig.6 Evolution of system states

Fig.7 Evolution of system costates

References

[1] Modi, V.J., "Attitude Dynamics of Satellites with Flexible Appendages - A Brief Review," *Journal of Spacecraft*, Vol. 11, No. 11, 1974.

[2] Balas, M.J., "Trends in Large Space Structures Control Theory : Fondest Hopes, Wildest Dreams," *IEEE Transactions on Automatic Control*, Vol. AC-27, No. 3, 1982.

[3] Likins, P., "Spacecraft Attitude Dynamics and Control - A Personal Perspective on Early Developments," *AIAA Journal of Guidance, Control, and Dynamics*, Vol. 9, No. 2, 1986, pp.129-134.

[4] Junkins, J.L., and Turner, J.D., *Optimal Spacecraft Rotational Maneuvers*, Elsevier, Amsterdam, The Netherlands, 1986.

[5] Kirk, D.E., *Optimal Control Theory*, Prentice-Hall, Englewood Cliffs, NJ, 1970.

[6] Athans, M., and Falb, P.L., *Optimal Control*, McGraw-Hill, New York, NY, 1966.

[7] Miele, A., and Iyer, R.R., "General Technique for Solving Nonlinear, Two-Point Boundary-Value Problems via the Method of Particular Solutions," *Journal of Optimization Theory and Applications*, Vol. 5, No. 5, 1970, pp.382-403.

[8] Vadali, S.R., "Solution of the Two-Point Boundary Value Problems of Optimal Spacecraft Rotational Maneuvers," Ph.D. Dissertation, Virginia Polytechnic Institute and State University, Blacksburg, VA, 1982.

[9] Bayo, E., "A Finite-Element Approach to Control the End-Point Motion of a Single-Link Flexible Robot," *Journal of Robotic Systems*, Vol. 4, No. 1, 1987, pp.63-75.

[10] Naganathan, G., and Soni, A.H., "Coupling Effects of Kinematics and Flexibility in Manipulators," *The International Journal of Robotics Research*, Vol. 6, No. 1, 1987, pp.75-84.

[11] Reddy, J.N., *An Introduction to the Finite Element Method*, McGraw-Hill Book Company, New York, NY, 1984.

[12] Craig, R.R.Jr., *Structural Dynamics - an Introduction to Computer Methods*, John Wiley and Sons, New York, NY, 1981.

[13] Junkins, J.L., and Lee, S., "Validation of Finite Dimensional Approximate Solutions for Dynamics of Distributed Parameter Systems," to appear, *Advances in the Astronautical Sciences*, Vol. 85, see also..., AAS/AIAA Astrodynamics Specialist Conference, Paper AAS 93-641, Victoria, B.C., Canada, Aug., 1993.

[14] Meirovitch, L., *Computational Methods in Structural Dynamics*, Sijhoff & Noordhoff, The Netherlands, Rockville, MD, 1980.

Appendix

The LQR problem of Eqs.(12,14,15) can be written as the nonlinear TPBVP of Eq.(17) using the Pontryagin's minimum principle.

Pontryagin's minimum principle:

$$\dot{z}^* = Az^* + B\,u^* \qquad (A1)$$

$$\dot{p}^* = -Qz^* - A^T p^* \qquad (A2)$$

$$H(z^*, u^*, p^*, t) \leq H(z^*, u, p^*, t) \text{ for all admissible } u$$
$$(A3)$$

where H is the Hamiltonian function.

From Eq.(A3) $\frac{1}{2}\langle u^*, Ru^* \rangle + \langle Bu^*, p^* \rangle \leq \frac{1}{2}\langle u, Ru \rangle + \langle Bu, p^* \rangle$ hold for all u such that $|u_j(t)| \leq 1$ $j = 1, 2, \cdots, m$.

Let us define w^* as $w^* = R^{-1}B^T p^*$, then

$$\frac{1}{2}\langle u^*, Ru^* \rangle + \langle u^*, Rw^* \rangle \leq \frac{1}{2}\langle u, Ru \rangle + \langle u, Rw^* \rangle$$

Now we add $\frac{1}{2}\langle w^*, Rw^* \rangle$ to both sides,

$$\frac{1}{2}\langle u^*, Ru^* \rangle + \langle u^*, Rw^* \rangle + \frac{1}{2}\langle w^*, Rw^* \rangle$$
$$\leq \frac{1}{2}\langle u, Ru \rangle + \langle u, Rw^* \rangle + \frac{1}{2}\langle w^*, Rw^* \rangle$$

$$\langle (u^* + w^*), R(u^* + w^*) \rangle \leq \langle (u + w^*), R(u + w^*) \rangle \quad (A4)$$

for all u such that $|u_j| \leq 1$ where $j = 1, 2, \cdots, m$.
Equation (A4) implies that $u_j^* = -w_j^*$ if $|w_j^*| \leq 1$ and $u_j^* = -sgn\{w_j^*\}$ if $|w_j^*| > 1$.

To prove above statement, we proceed as follows:

$$a \equiv u + w^*$$

Equation (A4) implies that the function $\psi(u) = \langle a, Ra \rangle$ attains its minimum at $a^* = u^* + w^*$.

Since R is positive definite, the eigenvalues of R are positive for all t.

Let D be the diagonal matrix of the eigenvalues. $D = P^T RP$ where P is an orthogonal matrix.

$$\psi(u) = \langle a, Ra \rangle = \langle a, PDP^T a \rangle$$
$$= \langle P^T a, DP^T a \rangle = \langle b, Db \rangle$$
$$= \sum_{j=1}^{m} d_j\, b_j^2$$

where $b = P^T a$.

Since P and P^T are both orthogonal, $\langle b, b \rangle = \langle a, a \rangle$ equivalently

$$\sum_{j=1}^{m} b_j^2 = \sum_{j=1}^{m} a_j^2 \qquad (A5)$$

Now we establish the relations

$$\min_{u} \psi(u) = \min_{a} \langle a, Ra \rangle$$

$$= \min_{b=P^T a} \sum_{j=1}^{m} d_j \, b_j^2 = \sum_{j=1}^{m} d_j \, \min_{b_j} b_j^2 \qquad (A6)$$

Equation (A6) implies that if a^* minimizes $\langle a, Ra \rangle$, then the components $b_1^*, b_2^*, \cdots, b_m^*$ also minimize the scalar product $\langle b, b \rangle$ where $b = P^T a$.

In view of Eq.(A5), we may conclude that the vector $PP^T a^* = a^*$ minimizes the scalar product $\langle a, a \rangle$.

Therefore, if $\langle a^*, Ra^* \rangle \leq \langle a, Ra \rangle$ then $\langle a^*, a^* \rangle \leq \langle a, a \rangle$.

We can reverse our reasoning as follows:
 If $\langle a^*, a^* \rangle \leq \langle a, a \rangle$ then $\langle a^*, Ra^* \rangle \leq \langle a, Ra \rangle$.

We know that

$$\langle a, a \rangle = \langle (u + w^*), (u + w^*) \rangle = \sum_{j=1}^{m} (u_j + w_j^*)^2.$$

We can deduce that $\quad \min_{u} \langle a, a \rangle = \sum_{j=1}^{m} \min_{|u_j| \leq 1} (u_j + w_j^*)^2.$

To minimize the positive quantity $(u_j + w_j^*)^2$, one must set

$$u_j = -w_j^* \qquad \text{whenever } |w_j^*| \leq 1$$
$$u_j = +1 \qquad \text{whenever } w_j^* < -1$$
$$u_j = -1 \qquad \text{whenever } w_j^* > 1 \qquad \blacksquare$$

Invariant Set Analysis of the
Hub-Appendage Problem
R. Mukherjee and J. L. Junkins

Invariant Set Analysis of the Hub-Appendage Problem

Ranjan Mukherjee*
*Naval Postgraduate School,
Monterey, California 93943*
and
John L. Junkins†
Texas A&M University, College Station, Texas 77843

Introduction

IN the recent literature, an asymptotic stability theorem[1] for autonomous and periodic nonautonomous systems was used to prove the global asymptotic stability of the mass-spring-damper system and the damped Mathieu system. For such systems, the application of LaSalle's invariant set theorem[3] has been the conventional approach adopted to prove the global asymptotic stability. When the derivative of the Lyapunov function[2] vanishes, LaSalle's theorem[3] requires us to show that the maximum invariant set of the system consists only of the equilibrium point at its entry. Although it is always simple to identify the set of points Q where the derivative of the Lyapunov function vanishes, the maximum invariant set $I \subset Q$ is not always easy to identify. The main challenge of

LaSalle's theorem[3] is therefore to sort out the maximum invariant set. For a distributed parameter system the dynamics are described by a hybrid set of ordinary and partial differential equations. For such a system, the sorting out of the maximum invariant set is not a trivial task. In such a situation it is useful to apply the theorem in Ref. 1 so as to comment on the asymptotic stability of the system.

The distributed parameter system consisting of a rigid hub with one or more cantilevered flexible appendages has appeared in the technical literature quite frequently (see Refs. 4, 5, 6, and 7). The system described in Fig. 1 consists of four appendages that are identical uniform beams conforming to the Euler-Bernoulli assumptions. Each beam cantilevered rigidly to the hub is assumed to have a tip mass. The motion of the system is confined to the horizontal plane and the control torque is generated by a single-reaction wheel actuator. Under the assumption that the system undergoes antisymmetric motion with deformation in unison (see Fig. 2), a class of rest-to-rest maneuvers was considered in Ref. 4. For the particular Lyapunov function considered, the best choice of the control input only guaranteed the negative semidefiniteness of the derivative of the Lyapunov function. To conclude the global asymptotic stability using LaSalle's theorem, it would be necessary to formally prove that the maximum invariant set consists only of the equilibrium point. The global asymptotic stability of the system was claimed in Ref. 4 in the absence of this proof.

In this Note we consider the hub-appendage problem[4] with modifications. The modeling and successful control of such a system is expected to provide us with insight into the modeling and control of a general class of distributed parameter systems. Using a Lyapunov function approach and the asymptotic stability theorem in Ref. 1, we prove that global asymptotic stability of the system is guaranteed provided the system undergoes antisymmetric motion with deformation in unison.

In other situations, such as symmetric motion with deformation in opposition (see Fig. 2), such a conclusion cannot be drawn.

Theorem on Asymptotic Stability

Consider the nonautonomous system

$$\dot{x} = f\Big((t, x(t)\Big) \tag{1}$$

where $f : R_+ \times D \to R^n$ is a smooth vector field on $R_+ \times D$, $D \subset R^n$ in the neighborhood of the origin $x = 0$. Let $x = 0$ be an equilibrium point for the system described by Eq. (1). We now state the theorem on asymptotic stability.[1]

Theorem. 1) A necessary condition for stable nonautonomous systems: Let $V(t, x) : R_+ \times D \to R_+$ be locally positive definite and analytic on $R_+ \times D$, such that

$$\dot{V}(t, x) \triangleq \frac{\partial V}{\partial t} + \left(\frac{\partial V}{\partial x}\right) f(t, x)$$

is locally negative semidefinite. Then whenever an odd derivative of V vanishes, the next derivative necessarily vanishes and the second next derivative is necessarily negative semidefinite. 2) A sufficient condition for asymptotically stable autonomous systems: Let $V(x) : D \to R_-$ be locally positive definite and analytic on D, such that $\dot{V} \leq 0$. If there exists a positive integer k such that

$$\begin{cases} V^{(2k-1)}(x) < 0 & \forall x \neq 0 : \dot{V}(x) = 0 \\ V^{(i)}(x) = 0 & \text{for } i = 2, 3, \ldots, 2k \end{cases} \tag{2}$$

where $V^{(*)}(x)$ denotes the $(*)$th time derivative of V with respect to time, then the system is asymptotically stable. However, if $V^{(j)}(x) = 0$, $\forall j = 1, 2, \ldots, \infty$, then the sufficient condition for the autonomous system to be asymptotically stable is that the set

$$S = \Big\{ x : V^{(j)}(x) = 0, \quad \forall j = 1, 2, \ldots, \infty \Big\}$$

contains only the trivial trajectory $x = 0$.

Hub-Appendage Problem

This example is taken from Ref. 4 with some modifications. The hybrid system of ordinary and partial differential equations governing the dynamics of the system, which has already been described in the introduction, is

$$I_{\text{hub}} \frac{d^2\theta}{dt^2} = u + \sum_{i=1}^{4} (M_{i0} - r S_{i0}) \tag{3}$$

$$-(M_{i0} - r S_{i0}) = \int_r^l \rho x \left(\frac{\partial^2 y_i}{\partial t^2} + x \frac{d^2\theta}{dt^2}\right) dx + ml\left(l \frac{d^2\theta}{dt^2} + \frac{\partial^2 y_i}{\partial t^2}\Big|_l\right) \cdot$$
$$i = 1, 2, 3, 4 \tag{4}$$

$$\rho\left(\frac{\partial^2 y_i}{\partial t^2} + x \frac{d^2\theta}{dt^2}\right) + EI \frac{\partial^4 y_i}{\partial x^4} = 0, \qquad i = 1, 2, 3, 4 \tag{5}$$

The boundary conditions on Eqs. (3–5) are

$$y_i(t, r) = \frac{\partial y_i}{\partial x}\Big|_r = 0, \qquad i = 1, 2, 3, 4 \tag{6}$$

$$\frac{\partial^2 y_i}{\partial x^2}\Big|_l = 0, \qquad i = 1, 2, 3, 4 \tag{7}$$

$$\frac{\partial^3 y_i}{\partial x^3}\Big|_l = \frac{m}{EI}\left(l \frac{d^2\theta}{dt^2} + \frac{\partial^2 y_i}{\partial t^2}\Big|_l\right), \qquad i = 1, 2, 3, 4 \tag{8}$$
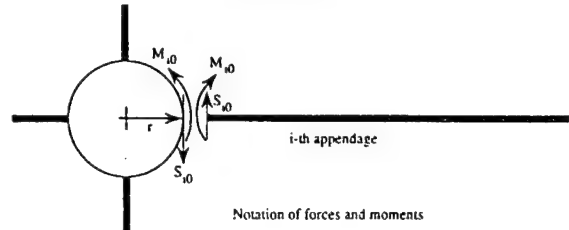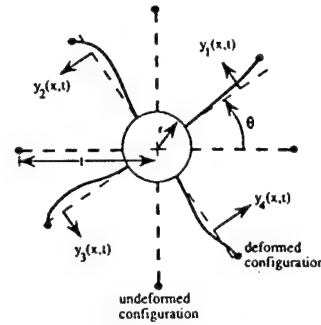
Fig. 1 Distributed parameter autonomous system consisting of a rigid hub with four cantilevered flexible appendages.
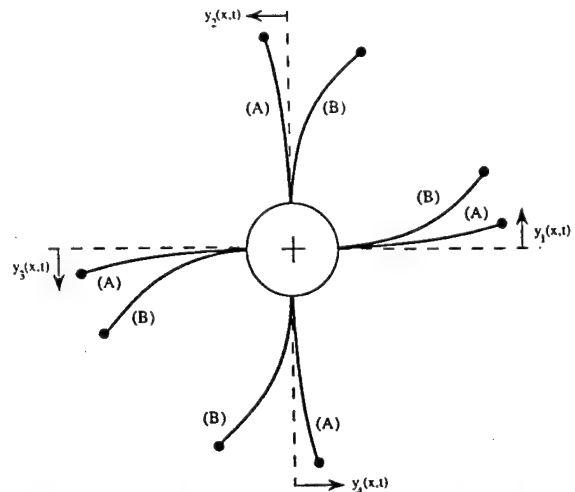
Fig. 2 Antisymmetric and symmetric motion of the system consisting of a rigid hub and four flexible appendages: A is the antisymmetric motion (deformation in unison), $y_1(x, t) = y_2(x, t) = y_3(x, t) = y_4(x, t)$ and B is the symmetric motion (deformation in opposition), $y_1(x, t) = -y_2(x, t)$, $y_3(x, t) = -y_4(x, t)$.

The state of the system is described by a hybrid set of discrete and continuous variables:

$$Z = \left[\theta, \dot{\theta}, y_1(x, t), \ldots, y_4(x, t), \frac{\partial y_1(x, t)}{\partial t}, \ldots, \frac{\partial y_4(x, t)}{\partial t}\right] \tag{9}$$

We choose the Lyapunov function V as

$$V = \frac{a_1}{2} I_{\text{hub}} \dot{\theta}^2 + \frac{a_2}{2}(\theta - \theta_f)^2 + \frac{a_3}{2} \sum_{i=1}^{4} \left[\left[\int_r^l \rho\left(\frac{\partial y_i}{\partial t} + x\dot{\theta}\right)^2 dx\right.\right.$$
$$\left.\left. + \int_r^l EI\left(\frac{\partial^2 y_i}{\partial x^2}\right)^2 dx + m\left(l\dot{\theta} + \frac{\partial y_i}{\partial t}\Big|_l\right)^2\right] \tag{10}$$

to derive control laws that will drive the system to its desired state $Z_{\text{desired}} = (\theta_f, 0, 0, \ldots, 0, 0, \ldots, 0)$. In Eq. (10), a_1, a_2, and

a_3 are positive constants. It can be shown[4] that the choice of $u(t)$ as

$$u = -(1/a_1)\left[a_2(\theta - \theta_f) + a_4\theta + (a_3 - a_1)\sum_{i=1}^{4}(rS_{i0} - M_{i0})\right]$$
$$a_4 > 0 \quad (11)$$

in Eq. (3), leads to $\dot{V} = -a_4\dot{\theta}^2$. Clearly, $\dot{V}$ is negative semidefinite and is equal to zero if $\dot{\theta} = 0$. To check for the asymptotic stability of the system using the theorem in Ref. 1, we first compute the higher-order derivatives of V. We find that when $\dot{V} = 0$, the following always holds

$$V^{(2k+1)} = -2^k a_4[\theta^{(k+1)}]^2, \quad V^{(i)} = 0, \quad i = 1, 2, \ldots, 2k \quad (12)$$

for some positive integer k. In Eq. (12), $V^{(*)}$ denotes the (*)th time derivative of V, and $\theta^{(*)}$ denotes the (*)th time derivative of θ. Using Eq. (12) and the sufficient conditions of the asymptotic stability theorem,[1] we conclude that the system is globally asymptotically stable if $\theta^{(k)} \neq 0$ for any positive integer k. In other words, if $\dot{V} = 0$ at some time $t = T$, then the system will be globally asymptotically stable if θ is not a constant for all $t \geq T$, and is a constant only at the equilibrium point.

We now investigate the case where θ is a constant at a point other than at the equilibrium point where $Z \neq Z_d$. Let this constant be θ_C. Then Eqs. (3–5) simplify to

$$u - \sum_{i=1}^{4}(rS_{i0} - M_{i0}) = 0 \quad (13)$$

$$-(M_{i0} - rS_{i0}) = \int_r^l \rho x \frac{\partial^2 y_i}{\partial t^2}\, dx + ml\frac{\partial^2 y_i}{\partial t^2}\bigg|_l, \quad i = 1, 2, 3, 4 \quad (14)$$

$$\rho \frac{\partial^2 y_i}{\partial t^2} + EI\frac{\partial^4 y_i}{\partial x^4} = 0, \quad i = 1, 2, 3, 4 \quad (15)$$

The boundary conditions given by Eqs. (6) and (7) remain unchanged, but the boundary condition given by Eq. (8) simplifies to

$$\frac{\partial^3 y_i}{\partial x^3}\bigg|_l = \frac{m}{EI}\frac{\partial^2 y_i}{\partial t^2}\bigg|_l, \quad i = 1, 2, 3, 4 \quad (16)$$

Also, the input to the system $u(t)$ defined by Eq. (11) can be simplified, using Eq. (13), to

$$u = \sum_{i=1}^{4}(rS_{i0} - M_{i0}) = \frac{a_2}{a_3}(\theta_f - \theta_C) \triangleq C = \text{const} \quad (17)$$

If we define $Y = \sum_{i=1}^{4} y_i$, then Eq. (17) implies

$$\left[r\frac{\partial^3 Y}{\partial x^3} - \frac{\partial^2 Y}{\partial x^2}\right]_{x=r} = \frac{C}{EI} = \text{const} \quad (18)$$

If we make the reasonable assumption that $Y(x, t)$ is of the form $Y(x, t) = F(x)G(t)$, then Eq. (18) leads to

$$G(t)\left[r\frac{\partial^3 F}{\partial x^3} - \frac{\partial^2 F}{\partial x^2}\right]_{x=r} = \text{const} \quad (19)$$

Equation (19) implies that $G(t)$ is a constant. Summing Eqs. (15) and (16) over $i = 1$ to $i = 4$, we have

$$\rho \frac{\partial^2 Y}{\partial t^2} + EI\frac{\partial^4 Y}{\partial x^4} = 0 \quad (20)$$

$$\frac{\partial^3 Y}{\partial x^3}\bigg|_l = \frac{m}{EI}\frac{\partial^2 Y}{\partial t^2}\bigg|_l \quad (21)$$

Because $Y(x, t) = F(x)G(t)$, and $G(t)$ is a constant, Eqs. (20) and (21) imply

$$\frac{\partial^4 Y}{\partial x^4} = 0 \Rightarrow \frac{\partial^3 Y}{\partial x^3} = \text{const} \quad (22)$$

$$\frac{\partial^3 Y}{\partial x^3}\bigg|_l = 0 \quad (23)$$

From Eqs. (22) and (23) it follows that $(\partial^3 Y/\partial x^3) = 0$, which implies that $(\partial^2 Y/\partial x^2)$ is a constant. Additionally, the value of this constant can be shown to be zero from the boundary condition in Eq. (7). Proceeding in the same way and using the boundary conditions in Eq. (6), it is trivial to show that $(\partial Y/\partial x) = Y(x, t) = 0$. This implies from Eqs. (18) and (17) that $u = 0$ and $\theta_C = \theta_f$. Clearly, the maximum invariant set for the system comprises the set of points where $\theta = \theta_f$, $\dot{\theta} = 0$, and $\Sigma_{i=1}^{4} y_i(x, t) = 0$. If there exist functions $y_i(x, t) \neq 0$, $i = 1, 2, 3, 4$ such that $Y = \Sigma_{i=1}^{4} y_i = 0$ holds, then the set $S = \{Z : V^{(j)}(Z) = 0, \forall j = 1, 2, \ldots, \infty\}$ contains entries other than the trivial solution $Z = Z_{\text{desired}}$. In such a situation we cannot claim global asymptotic stability of the equilibrium point. Such a situation may arise in the case of symmetric deformation in opposition, shown in Fig. 2, where $y_1(x, t) = -y_2(x, t)$ and $y_3(x, t) = -y_4(x, t)$. In such a situation, the residual energy of the system remains trapped within the beams. There exists no net interacting moment between the hub and the beams, and the hub remains motionless at its desired configuration $\theta = \theta_f$.

The case of antisymmetric deformation in unison, shown in Fig. 2, was considered in Ref. 4. In this case, it is assumed that $y_1(x, t) = y_2(x, t) = y_3(x, t) = y_4(x, t)$. When $Y(x, t) = 0$, this implies that $y_i(x, t) = 0$ for $i = 1, 2, 3, 4$. Therefore, for antisymmetric deformation in unison, it is quite simple to show that the set $S = \{Z : V^{(j)}(Z) = 0, \forall j = 1, 2, \ldots, \infty\}$ contains only the equilibrium point $Z = Z_{\text{desired}}$. Consequently, we can establish the asymptotic stability property of the hub with the flexible appendages undergoing antisymmetric deformation in unison under the input defined by Eq. (11). The control law given in Eq. (11) was used to stabilize the system to the equilibrium point in Ref. 4, but no formal proof for the asymptotic stability was provided.

Conclusion

The rest-to-rest maneuver of the distributed parameter system consisting of a rigid hub with four cantilevered flexible appendages was studied. The best choice of the control input resulted in the negative semidefiniteness of the derivative of the Lyapunov function. An invariant set analysis of the system was subsequently carried out using an asymptotic stability theorem.[1] The analysis establishes the fact that the hub-appendage system is globally asymptotically stable when the system undergoes antisymmetric motion with deformation in unison.

References

[1]Mukherjee, R., and Chen, D., "An Asymptotic Stability Theorem for Autonomous Systems," *Journal of Guidance, Control, and Dynamics*, Vol. 16, No. 5, 1993, pp. 960–962.

[2]Lyapunov, A. M., "On the General Problem of Stability of Motion," Kharkov Mathematical Society, Russia (in Russian), 1892.

[3]LaSalle, J., and Lefschetz, S., *Stability by Lyapunov's Direct Method with Applications*, Academic, New York, 1961.

[4]Junkins, J. L., Rahman, Z. H., and Bang, H., "Near-Minimum Time Control of Distributed Parameter Systems: Analytical and Experimental Results," *Journal of Guidance, Control, and Dynamics*, Vol. 14, No. 2, 1991, pp. 406–415.

[5]Junkins, J. L., and Turner, J. D., *Optimal Spacecraft Rotational Maneuvers*, Elsevier, Amsterdam, The Netherlands, 1986, Chap. 5.

[6]Fujii, H., Ohtsuka, T., and Odou, S., "Mission Function Control for Slew Maneuver Experiment," *Journal of Guidance, Control, and Dynamics*, Vol. 12, No. 6, 1989, pp. 858–865.

[7]Singh, G., Kabamba, P., and McClamroch, N., "Planar Time Optimal Slewing Maneuvers of Flexible Spacecraft," *Journal of Guidance, Control, and Dynamics*, Vol. 12, No. 1, 1989, pp. 71–81.

AMERICAN **ASTRONAUTICAL** SOCIETY

AIAA

Near-Minimum-Time Three-Dimensional Maneuvers of Rigid and Flexible Spacecraft

Mark J. Bell and John L. Junkins

Texas A&M University
College Station, Texas

AAS/AIAA Astrodynamics Specialist Conference

NEAR-MINIMUM-TIME THREE-DIMENSIONAL MANEUVERS OF RIGID AND FLEXIBLE SPACECRAFT

Mark J. Bell[1] and John L. Junkins[2]

An approach is presented to accomplish large angle, nonlinear, three dimensional attitude maneuvers in either near-minimum-time or near-minimum-fuel. The method permits the specification of a torque shaped reference maneuver of the near-minimum-time (bang-bang) or near-minimum-fuel (bang-off-bang) type; the instantaneous switches are replaced by controllably sharp spline switches to reduce excitation of flexible degrees of freedom. A Lyapunov method is used to design tracking-type control perturbations to suppress errors due to disturbances and model errors. The method is illustrated by numerical simulations and some experimental results using the ASTREX test article.

INTRODUCTION

Primarily due to mass considerations, future spacecraft will most likely have large flexible appendages and exhibit significant coupling between overall rigid body motion and vibratory motion. Many of these spacecraft will be required to perform a variety of maneuvers in three-dimensions in near-minimum-time, or near-minimum-fuel, with limited computational abilities, while suppressing flexible modes of vibration. A torque-shaped reference maneuver design, augmented by a Lyapunov stable tracing law can achieve these stated requirements with robustness in the presence of uncertainty.

The main goal of this paper is to demonstrate one effective approach to control a flexible spacecraft in near-minimum-time in three dimensions while actively and passively suppressing flexible modes of vibration. Secondarily, an analogous development for the the near-minimum-fuel case are presented. Feasibility of this approach is discussed based upon analysis, computer simulation using both a rigid-body and a flexible-body simulator, and through results from laboratory experimentation. The experimental portion of this research was performed on the Advanced Space Structure Technology Research Experiment (ASTREX) test article

---

[1] Student Member AIAA, Graduate Research Assistant

[2] George J. Eppwright Professor, Fellow AAS, Fellow AIAA

located in the Phillips Laboratory, Edwards Air Force Base, California. This study was undertaken as a part of the NASA/DOD Guest Investigator program.

The basic concepts underlying modern spacecraft dynamics and control have been treated by many authors, including Junkins and Turner.[1] Single-axis control of flexible spacecraft has been studied[2-6] and the optimal control problem in three-dimensions has been addressed by Vadali, Singh, and Carter.[7,8] Near-minimum-time control of dynamic systems, which include single-axis maneuvers of flexible spacecraft and flexible manipulators, have also been studied.[9-12] The purpose of this paper is to present a general three-dimensional approach, leading to maneuver laws for the ASTREX structure. General model information, as well as a rigid body model and a flexible body model for the ASTREX test article, are available.[13,2,14] A near-minimum-time approach is formulated to control the ASTREX orientation while vibration is attenuated using input smoothing[11]. Additionally, effects of model errors and disturbances are compensated using an asymptotically stable feedback controller based on the work by Junkins et al[11], Wie et al[15], Vadali[16], and Junkins and Kim[17].

EQUATIONS OF MOTION

The rigid body dynamics are modeled using Euler's equations for a rigid body. The matrix $[I]$ is the inertia matrix, $\underline{\omega}$ is the angular velocity vector, $[\widetilde{\omega}]$ is the matrix representation of the standard cross-product, and $[B]$ is the control influence matrix, each of which has dimension 3×3.

$$[I]\underline{\dot{\omega}} + [\widetilde{\omega}][I]\underline{\omega} = [B]\underline{u} \tag{1}$$

The control input to this equation consists of a reference control, $\underline{u}_{ref}$, and a tracking control or terminal control, $\delta\underline{u}$, as shown below.

$$\underline{u} = \underline{u}_{ref} + \delta\underline{u} \tag{2}$$

The kinematic equations used in the spacecraft model, equations (3) and (4), are the set of 1-2-3 Euler angles which were used to determine the body's position in space relative to a fixed coordinate system.

$$\left\{\underline{\dot{\theta}}\right\} = \frac{1}{Cos(\theta_2)} \begin{bmatrix} Cos(\theta_3) & -Sin(\theta_3) & 0 \\ Cos(\theta_2)Sin(\theta_3) & Cos(\theta_2)Cos(\theta_3) & 0 \\ -Sin(\theta_2)Cos(\theta_3) & Sin(\theta_2)Sin(\theta_3) & Cos(\theta_2) \end{bmatrix} \left\{\underline{\omega}\right\} \tag{3}$$

$$\left\{\underline{\omega}\right\} = \begin{bmatrix} Cos(\theta_2)Cos(\theta_3) & Sin(\theta_3) & 0 \\ -Cos(\theta_2)Sin(\theta_3) & Cos(\theta_3) & 0 \\ Sin(\theta_2) & 0 & 1 \end{bmatrix} \left\{\underline{\dot{\theta}}\right\} = [C(\theta)]\left\{\underline{\dot{\theta}}\right\} \tag{4}$$

These equations are used to orient the rigid body relative to a fixed inertial frame.

THE CONTROL LAWS
Near-Minimum-Time Maneuvers

The simplest minimum-time maneuver for a near-rigid vehicle undergoing a single-axis maneuver is a single switch "bang-bang" control law. However, the sharp switching will excite some flexible modes of vibration. The near-minimum-time maneuver proposed rounds off the sharp switches by replacing the sharp discontinuities with a controllably sharp cubic polynomial and introducing a shaping parameter $\alpha : 0 \leq \alpha \leq 0.25$, where at $\alpha = 0$, the torque profile is a square wave and at $\alpha = 0.25$, the torque profile is a smooth sine-shaped profile satisfying zero initial and final slope conditions. It should be noted that as α increases, the maneuver time (t_f) increases, and the vibrational energy is expected to decrease due to the greatly increased rolloff in the spectral content of the control input. The cubic polynomial, defined as the shaping function $f(t, \alpha, t_f)$ is defined[11] as follows.

$$f(t, \alpha, t_f) = \begin{cases} \left(\frac{t}{\Delta t}\right)^2 \left[3 - 2\left(\frac{t}{\Delta t}\right)\right] & \text{for } 0 \leq t \leq \Delta t \equiv \alpha t_f \\ 1 & \text{for } \Delta t \leq t \leq t_f/2 - \Delta t \equiv t_1 \\ 1 - 2\left(\frac{t-t_1}{2\Delta t}\right)^2 \left[3 - 2\left(\frac{t-t_1}{2\Delta t}\right)\right] & \text{for } t_1 \leq t \leq t_f/2 + \Delta t \equiv t_2 \\ -1 & \text{for } t_2 \leq t \leq t_f - \Delta t \equiv t_3 \\ -1 + \left(\frac{t-t_3}{\Delta t}\right)^2 \left[3 - 2\left(\frac{t-t_3}{\Delta t}\right)\right] & \text{for } t_3 \leq t \leq t_f \end{cases} \quad (11)$$

The basic idea underlying this torque-shaping approach is to establish a smooth rigid body reference maneuver, $\underline{\theta}_{ref}(t)$, then calculate the corresponding open loop control law by inverse dynamics. This reference torque, when applied to the body, will make $\underline{\theta}(t)$ approximate $\underline{\theta}_{ref}(t)$. The Lyapunov tracking law, which is discussed in the next section, seeks to cause $\underline{\theta}(t)$ to track $\underline{\theta}_{ref}(t)$ in the presence of disturbances and other non-ideal effects while also suppressing structural vibrations. As will be evident, it is possible to develop the tracking law to guarantee asymptotic stability in the absence of model errors. The development of the open loop control law is shown below, beginning with the standard linear second order equation of motion for a rigid body:

$$[I]\ddot{\underline{\theta}} = [B]\underline{u} \tag{6}$$

$$= [B]\underline{u}_{max} f(t, \alpha, t_f) \tag{7}$$

This equation can be applied to the reference maneuver, manipulated, and then integrated twice, yielding $\ddot{\theta}_{ref}$, $\dot{\theta}_{ref}$, and θ_{ref} as shown.

$$\ddot{\underline{\theta}}_{ref}(t) = [I]^{-1}[B]\underline{u}_{max} f(t, \alpha, t_f) \tag{8}$$

$$\dot{\underline{\theta}}_{ref}(t) = \dot{\underline{\theta}}_o + [I]^{-1}[B]\underline{u}_{max} \int_0^t f(\tau, \alpha, t_f)\, d\tau \tag{9}$$

$$\underline{\theta}_{ref}(t) = \underline{\theta}_o + \dot{\underline{\theta}}_o t + [I]^{-1}[B]\underline{u}_{max} \int_0^t \int_0^\tau f(\eta, \alpha, t_f)\, d\eta\, d\tau \tag{10}$$

However, the shaping function, $f(t, \alpha, t_f)$, can be integrated twice, piecewise, with the elegant generalization of the bang-bang ($\alpha = 0$)result:

$$\int_0^{t_f} \int_0^\tau f(\eta, \alpha, t_f)\, d\eta\, d\tau = \left(\frac{1}{4} - \frac{1}{2}\alpha + \frac{1}{10}\alpha^2 \right) t_f^2 \tag{11}$$

Substituting this result into the previous equation and considering a rest-to-rest maneuver $\left(\dot{\underline{\theta}}(t_o) = \dot{\underline{\theta}}(t_f) = 0 \right)$ yields the following expression for $\underline{\theta}_f - \underline{\theta}_o$:

$$\underline{\theta}_f - \underline{\theta}_o = [I]^{-1}[B]\left\{\underline{u}_{max}\, t_f^2\right\} \left(\frac{1}{4} - \frac{1}{2}\alpha + \frac{1}{10}\alpha^2 \right) \tag{12}$$

This equation can then be inverted to solve for the required maneuver time on each axis, as a function of the maneuver angle change, shaping parameter, and maximum torques as:

$$\left\{ \begin{matrix} t_{f_1}^2\, u_{max_1} \\ t_{f_2}^2\, u_{max_2} \\ t_{f_3}^2\, u_{max_3} \end{matrix} \right\} = \left| \frac{[B]^{-1}[I]\,(\underline{\theta}_f - \underline{\theta}_o)}{\left(\frac{1}{4} - \frac{1}{2}\alpha + \frac{1}{10}\alpha^2 \right)} \right| \tag{13}$$

The total maneuver time, t_f, is then simply:

$$t_f = max\left(t_{f_1} t_{f_2} t_{f_3} \right) \tag{14}$$

The effect of increasing alpha on a normalized maneuver time and the resulting profiles are shown below as Figure 1. As expected, the maneuver time increases as α increases, as illustrated in the figure.
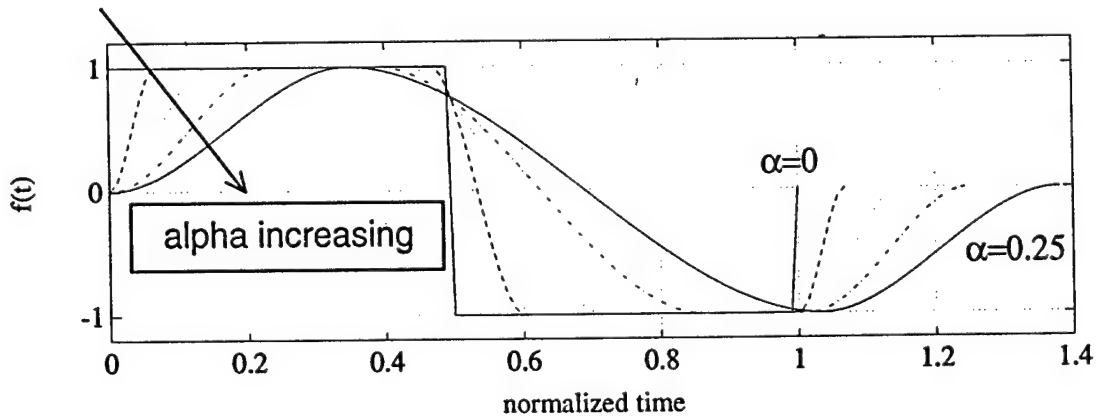
Figure 1. - Bang-Bang Shaping Function vs. Normalized
Time for Increasing α.

The total maneuver time, t_f, can be substituted into the previous equation and a vector of constants containing the maximum torques, which will be applied on each axis, $\underline{u}_R$, can be determined.

$$\underline{u}_R = \frac{[B]^{-1}\,[I]\,(\underline{\theta}_f - \underline{\theta}_o)}{\left(\frac{1}{4} - \frac{1}{2}\,\alpha + \frac{1}{10}\,\alpha^2\right)}\,\frac{1}{t_f^2} \tag{15}$$

The values of $\underline{u}_R$, t_f, and a selected value of α, can then be inserted into equations (8)-(10), yielding:

$$\underline{\ddot{\theta}}_{ref}(t) = [I]^{-1}\,[B]\,\underline{u}_R\,f(t,\alpha,t_f) \tag{16}$$

$$\underline{\dot{\theta}}_{ref}(t) = \underline{\dot{\theta}}_o + [I]^{-1}\,[B]\,\underline{u}_R \int_0^t f(\tau,\alpha,t_f)\,d\tau \tag{17}$$

$$\underline{\theta}_{ref}(t) = \underline{\theta}_o + \underline{\dot{\theta}}_o\,t + [I]^{-1}\,[B]\,\underline{u}_R \int_0^t \int_0^\tau f(\eta,\alpha,t_f)\,d\eta\,d\tau \tag{18}$$

Now, using the exact rigid body dynamics, we can solve for a control $u_{ref}(t)$ which would cause the rigid body vehicle to execute the maneuver $\theta_{ref}(t)$. First, the kinematic equations for the set of 1-2-3 Euler angles, shown in matrix form as equation (4), can be used and then differentiated to determine $\underline{\omega}_{ref}(t)$ and $\underline{\dot{\omega}}(t)$.

$$\underline{\omega}_{ref}(t) = \left[C\left(\underline{\theta}_{ref}\right)\right]\underline{\dot{\theta}}_{ref} \tag{19}$$

$$\underline{\dot{\omega}}(t) = \frac{d}{dt}\left[C\left(\underline{\theta}_{ref}\right)\right]\underline{\dot{\theta}}_{ref} + \left[C\left(\underline{\theta}_{ref}\right)\right]\underline{\ddot{\theta}}_{ref} \tag{20}$$

The reference torque, $\underline{u}_{ref}(t)$, can then be found by inverse dynamics, using Euler's equation.

$$\underline{u}_{ref}(t) = [B]^{-1}\left([I]\,\underline{\dot{\omega}}_{ref} + [\widetilde{w}_{ref}]\,[I]\,\underline{\omega}_{ref}\right) \tag{21}$$

Hence, the near-minimum-time torque-shaped maneuver has been extended to the three dimensional case.

Motivated by the need to consider a wider class of reference maneuvers, such as near-minimum-fuel, it was noted that any function which is twice integrable may in principle be used as the shaping function. Seeking to establish a torque-shaped family of near-minimum-fuel maneuvers, we consider the bang-off-bang control parameterization shown below as equation (22), where t_3 denotes the time at the end of the first pulse, β corresponds to the coast time, and α parameterizes the

sharpness of the of the control on/off profile.

$$g(t, \alpha, \beta, t_3) = \begin{cases} \left(\frac{t}{\Delta t}\right)^2 \left[3 - 2\left(\frac{t}{\Delta t}\right)\right] & \text{for } 0 \leq t \leq t_1 \equiv \alpha 2\alpha t_3 \\ 1 & \text{for } t_1 \leq t \leq t_2 \equiv (1 - 2\alpha)t_3 \\ 1 - \left(\frac{t-t_2}{2\Delta t}\right)^2 \left[3 - 2\left(\frac{t-t_2}{2\Delta t}\right)\right] & \text{for } t_2 \leq t \leq t_3 \equiv t_3 \\ 0 & \text{for } t_3 \leq t \leq t_4 \equiv t_3 + \beta \\ -\left(\frac{t-t_4}{\Delta t}\right)^2 \left[3 - 2\left(\frac{t-t_4}{\Delta t}\right)\right] & \text{for } t_4 \leq t \leq t_5 \equiv t_1 + t_3 + \beta \\ -1 & \text{for } t_5 \leq t \leq t_6 \equiv t_2 + t_3 + \beta \\ -1 + \left(\frac{t-t_6}{\Delta t}\right)^2 \left[3 - 2\left(\frac{t-t_6}{\Delta t}\right)\right] & \text{for } t_6 \leq t \leq t_f \equiv 2t_3 + \beta \end{cases} \quad (22)$$

Following the same procedure yields an alternative torque shaped control law. Figure 2 shows the effect of increasing alpha from 0 to 0.25 on the normalized maneuver time while holding β constant at 1. This figure shows that the maneuver time increases as the control profile becomes smoother.
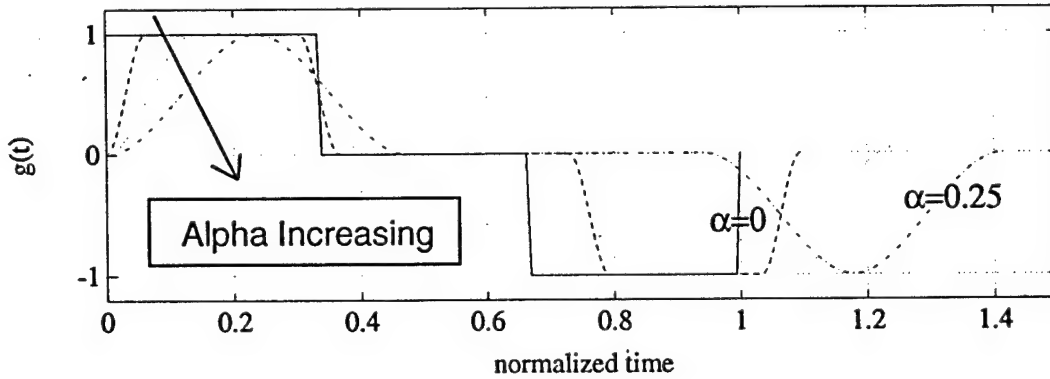
Figure 2. - Bang-Off-Bang Shaping Function vs. Normalized Time for Increasing α.

The effect of decreasing beta, while maintaining a constant value for α of 0.25 on the maneuver time, is shown in Figure 3. Again, the maneuver time increases as the coast time is increased, as seen in the figure.
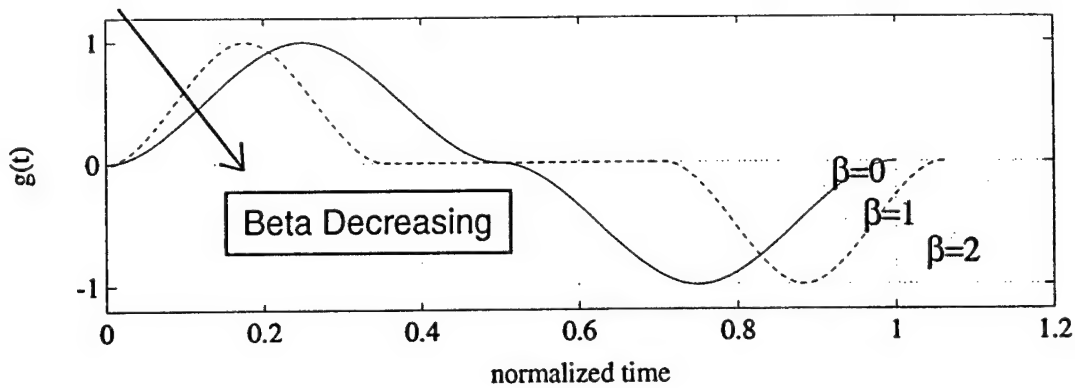
Figure 3. - **Bang-Off-Bang Shaping Function vs. Normalized Time for Decreasing** β.

Two open-loop control laws have been developed in this section; computational and laboratory experimental results are discussed below. These open-loop control laws are established for a general rigid body that moves in three-dimensional space, although it is recognized that these reference maneuvers may be significantly sub-optimal for the case when the gyroscopic coupling effects are large. Application of this torque-shaping scheme to any rigid body requires a priori knowledge of the inertia matrix and the control influence matrix, both of which are required to be invertible. As is evident in the robustness studies, however, including a well designed tracking law to compensate for larger-than-expected errors.

The open-loop control laws presented in this section are exact solutions based on an inverse dynamics approach. Although the control laws are expected to perform well, a closed-loop feedback control law will almost always be needed to compensate for approximation errors as well as disturbances and identification errors.

A Lyapunov Tracking Controller

The tracking controller is a Lyapunov tracking controller which uses a different parameterization of the positional error energy term. The Euler parameters, ζ, are used to relate the actual frame to the reference frame of the body; note $\underline{\zeta}$ is often known as the "error quaternion". Hence, when these two frames coincide, the Euler parameters will be identically $\underline{\zeta} = [1\,0\,0\,0]^T$. The Lyapunov function and its first derivative is shown below.

$$2V = \delta\underline{\omega}^T [I]\, \delta\underline{\omega} + \underline{\zeta}^T [W]\, \underline{\zeta} \tag{23}$$

$$\dot{V} = \delta\underline{\omega}^T [I]\, \delta\underline{\dot{\omega}} + \dot{\underline{\zeta}}^T [W]\, \underline{\zeta} \tag{24}$$

Through manipulations to follow, the time derivative of V in Equation (24) can be re-arranged to form $\dot{V} = \delta\underline{\omega}\{\text{fnct}(\delta\underline{u}, \zeta, \underline{\omega})\}$, and this structure can be exploited

to determine a control law for $\delta\underline{u}$ which guarantees $\dot{V} \leq 0$. Calculating the Euler parameters from the 1-2-3 set of Euler angles of the actual frame and the reference frame is a straightforward process. The orthonormal rotation matrix from the inertially fixed frame to the actual frame is shown below. It should be noted that s_i and c_i stand for $sin(\theta_i)$ and $cos(\theta_i)$, respectively.

$$[T(\underline{\theta})] = \begin{bmatrix} c_2 c_3 & s_3 c_1 + c_3 s_2 s_1 & s_1 s_3 - c_3 s_2 c_1 \\ -c_2 s_3 & c_3 c_1 - s_3 s_2 s_1 & s_1 c_3 - s_3 s_2 c_1 \\ s_2 & -c_2 s_1 & c_2 c_1 \end{bmatrix} \tag{25}$$

Additionally, the rotation from the fixed frame to the reference frame is identical in format with the exception that S_i and C_i stand for $sin(\theta_{ref_i})$ and $cos(\theta_{ref_i})$, respectively. The rotation matrix between these two frames can be found easily using linear algebra, noting the fact that the inverse of an orthonormal matrix is its transpose. The rotation from the fixed frame, whose orthogonal unit vectors are denoted by $\hat{\underline{n}}$, to the body reference frame, $\hat{\underline{b}}_{ref}$, and to the actual frame, $\hat{\underline{b}}$, are shown below.

$$\hat{\underline{b}} = [T(\underline{\theta})]\,\hat{\underline{n}} \tag{26}$$

$$\hat{\underline{b}}_{ref} = [T(\underline{\theta}_{ref})]\,\hat{\underline{n}} \tag{27}$$

The second of these equations can then be inverted yielding an expression for projecting the fixed frame unit vectors onto the reference frame.

$$\hat{\underline{n}} = [T(\underline{\theta}_{ref})]^T\,\hat{\underline{b}}_{ref} \tag{28}$$

This equation can then be substituted into equation (26), yielding the desired relationship between the actual frame and the reference frame.

$$\hat{\underline{b}} = [T(\underline{\theta})]\,[T(\underline{\theta}_{ref})]^T\,\hat{\underline{b}}_{ref} \tag{29}$$

The error rotation matrix between the two frames is then defined as $[R]$.

$$[R] = [T(\underline{\theta})]\,[T(\underline{\theta}_{ref})]^T \tag{30}$$

We note that $[R]$ is typically a near-identity matrix because it represents the tracking error angular displacement of $\hat{\underline{b}}$ from $\hat{\underline{b}}_{ref}$. Once $[R]$ has been computed, the set of Euler parameters between these two frames can be computed as follows:

$$trace(R) = R_{11} + R_{22} + R_{33} \tag{31}$$

$$\zeta_0 = \sqrt{|\frac{1}{4}(1 + trace(R))|} \tag{32}$$

$$\zeta_1 = \frac{1}{4\zeta_0}(R_{23} - R_{32}) \tag{33}$$

$$\zeta_2 = \frac{1}{4\zeta_0}(R_{31} - R_{13}) \tag{34}$$

$$\zeta_3 = \frac{1}{4\zeta_0}(R_{12} - R_{21}) \tag{35}$$

This set of Euler parameters is governed by the following matrix differential equation:

$$\dot{\zeta} = \begin{bmatrix} -\zeta_1 & -\zeta_2 & -\zeta_3 \\ \zeta_0 & -\zeta_3 & \zeta_2 \\ \zeta_3 & \zeta_0 & -\zeta_1 \\ -\zeta_2 & \zeta_1 & \zeta_0 \end{bmatrix} \delta\omega \tag{36}$$

$$\underline{\dot{\zeta}} = [G(\zeta)]\,\delta\underline{\omega} \tag{37}$$

Taking the transpose of this equation yields:

$$\underline{\dot{\zeta}}^T = \delta\underline{\omega}^T[G(\zeta)]^T \tag{38}$$

By utilizing this result and Euler's equation (1) to eliminate $[I]\delta\underline{\dot{\omega}}$, equation (24), the derivative of the Lyapunov function can be arranged in the desired form. This will permit construction of a stabilizing feedback control law.

$$\dot{V} = \delta\underline{\omega}\left(-[\widetilde{\omega}][I]\underline{\omega} + [\widetilde{\omega}_{ref}][I]\underline{\omega}_{ref} + [B]\delta\underline{u} + [G(\zeta)]^T[W]\underline{\zeta}\right) \tag{39}$$

$$= -\delta\underline{\omega}^T[K]\delta\underline{\omega} \tag{40}$$

The second step, Equation (40), is motivated by the desire that $\delta\underline{u}$ be chosen such that $\dot{V} \le 0$. Equating the right hand sides of the previous two equations yields an intermediate algebraic equation:

$$-[K]\delta\underline{\omega} = -[\widetilde{\omega}][I]\underline{\omega} + [\widetilde{\omega}_{ref}][I]\underline{\omega}_{ref} + [B]\delta\underline{u} + [G(\zeta)]^T[W]\underline{\zeta} \tag{41}$$

Solving for the feedback control $\delta\underline{u}$ from equation (41) yields the asymptotically stable feedback control law:

$$\delta\underline{u} = [B]^{-1}\left(-[K]\delta\underline{\omega} + [\widetilde{\omega}][I]\underline{\omega} - [\widetilde{\omega}_{ref}][I]\underline{\omega}_{ref} - [C(\zeta)]^T[W]\underline{\zeta}\right) \tag{42}$$

This perturbation is superimposed on the reference control in the sense $\underline{u}(t) = \underline{u}_{ref}(t) + \delta\underline{u}(t)$. The gains [K] and [W] were selected subject to the eigenvalue placement constraint that they produce critical damping on the linearized second

order linear model for rigid body motion. In addition, a scaled inertia matrix was used as the gain matrix [K], since this provides a one-parameter family of symmetric and positive-definite gain matrices. It should be noted that the matrix [W], as shown below, is not positive-definite. However, if the last three terms in the relative Euler parameter set ζ are zero, then perfect tracking is accomplished (i.e. the set of Euler parameters is redundant). Hence, the fact that [W] is semi-positive definite is not a problem due to the redundancy of the Euler parameters. The gains used throughout this paper are shown below. More generally, the gain matrices would be subject to optimization over the set of stable gains to extremize a performance measure, along the lines of Junkins and Bang[18].

$$[K] = c_1[I]; \quad c_1 = 2.5298 \quad \text{and} \quad [W] = c_2 \begin{bmatrix} 0 & 0^T \\ 0 & [I] \end{bmatrix}; \quad c_2 = 1.6$$

EXPERIMENTAL RESULTS

Bang-Bang Experimental Results

The Advanced Space Structure Technology Research Experiment (ASTREX) test article is a large experimental structure that resembles a spaced-based laser beam expander as shown in Figure 4. The 5000 kilogram structure is mounted on a spherical air bearing and is maneuvered using a specified set of cold gas thrusters. A set of six 8-pound thrusters or a set of four 200-pound thrusters plus two 8-pound thrusters are available for controlling the structure. For each set, two thrusters fire in unison to produce torque. Hence, three sets of two thrusters firing in unison are needed to control the test article in three dimensions. All thrusters are powered by compressed air which is stored in two pressurized tanks. These pressure tanks have a limited supply of compressed gas which results in a fuel constraint. To avoid difficulties with the fuel constraint, only the bang-off-bang control law is used in conjunction with the 200-pound thruster set.

The first set of experimental results was tested using the set of 8-pound thrusters operating at a maximum thrust of 3 pounds in conjunction with the open-loop bang-bang control profile. The inertia matrix and the control influence matrix for the structure were given in reference 14 and were found by using a system identification technique. Due to the fuel constraint and to a nonlinear valve problem associated with low tank pressure, the maximum thrust from each thruster was limited to three pounds . The open-loop reference profile used on the first test is a fifty-degree yaw maneuver.

02-MAR-93
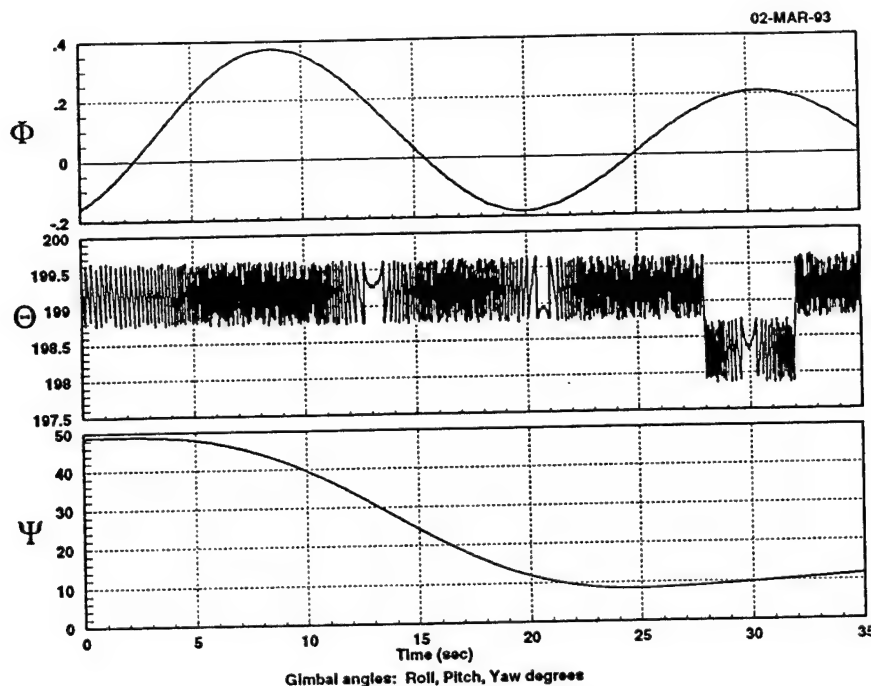
Figure 5 - Bang-Bang Open-Loop Experimental Angle Profile on the ASTREX Test Article

During experimentation, the thruster commands were given in volts, which were measured and stored as input, and a pressure feedback on each individual thruster was used to determine the output force at each thruster. Additionally, three gimbal angles and tank pressure were also sensed and stored as output. Figure 5 shows the gimbal angles in the body frame with respect to time in the form of three strip plots.

This figure shows that the test article moved approximately forty-two degrees in the yaw direction. This is eight degrees short of the specified maneuver. The rotation in the roll direction is oscillatory, but small. This small discrepancy could have been caused by any unmodeled, unsymmetric mass in the model or by a thruster pair generating slightly different forces, or due to unmodeled suspension system dynamics. The pitch angle encoder appears to have a sensor or grey code problem which causes the noisy output signal. However, the actual and measured motion in the pitch direction are small. It should be noted that these tests were performed open-loop and thus no on-line feedback corrections were made to compensate for modeling or hardware errors. It is anticipated that the closed-loop control capability for the ASTREX structure will exist in the calendar year 1994 time frame.

The motion in the yaw direction is approximately 16% short of the specified 50 degree maneuver; this could have been caused by a number of factors. If the inertia used in the design model was smaller than the actual inertia of the structure, a smaller angle change would be expected. The hardware cables are suspended from the structure; this produces cable drag, a rotational spring-like force in the yaw direction, as the cables are pulled away from their equilibrium position. A cable-

follower mechanism attempts to compensate for this problem; while the magnitude of the cable-follower induced disturbances are reduced, the cable-follower dynamics adds additional complexity in modeling the disturbances acting on the structure. This uncompensated cable drag phenomena would also produce smaller motion in the yaw direction in addition to a small angular velocity which would remain about the yaw axis as the structure returned to its equilibrium position. A final cause of the under-rotation problem is known to be due to low tank pressure near the end of the maneuver. Figure 6 shows the thrust commanded to each individual thruster in volts, this graph is identical to the output from the control law design except for the conversion of thrust to volts.

Figure 6 - Bang-Bang Open-Loop Experimental 8 Lb. Commanded Thruster Profile on the ASTREX Test Article

Figure 7 shows the output thrust at the nozzle of each thruster. The degradation of the thrust on the first two sets of thrusters can be seen beginning around 18 seconds, where the output profile becomes piecewise linear and decreases in comparison with the smooth commanded thrust. Although the degradation is not severe, it is definitely present. At low pressures, the solenoid valves behave in a poorly-modeled nonlinear fashion, especially evident when the valves are being closed. Notice the lack of left-right symmetry on all six final "braking" pulses of Figure 7.

02-MAR-93

8 lb thrusters PFB(volts)

Figure 7 - Bang-Bang Open-Loop Experimental 8 Lb. Actual Thruster Profile on the ASTREX Test Article

02-MAR-93

Tank pressure in voltage(CDAC) and psi(calibrated)
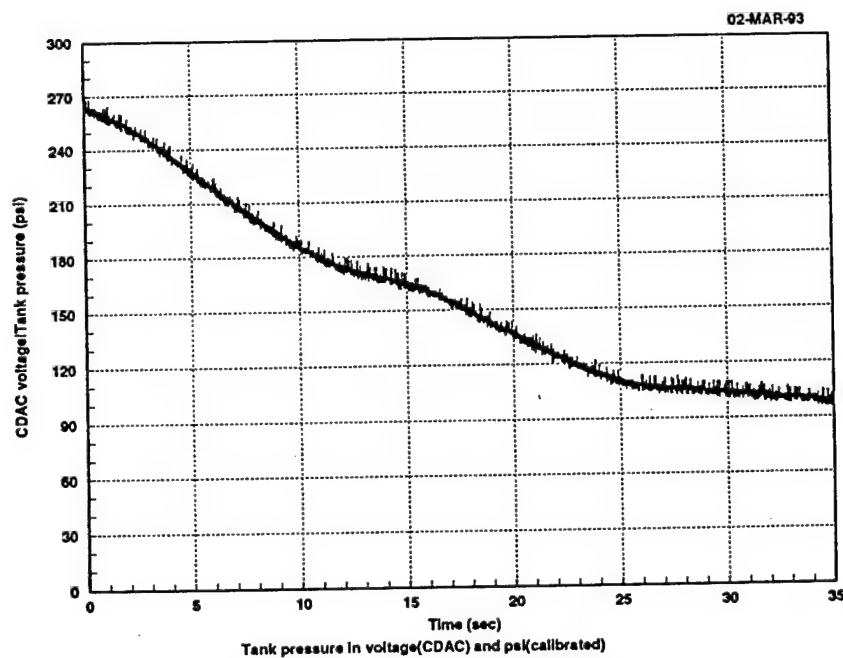
Figure 8 - Bang-Bang Open-Loop Experimental Tank Pressure Profile on the ASTREX Test Article

Figure 8 shows the tank pressure profile in pounds per square inch. It is noted

that thrust deterioration for the 8-pound thrusters occurs as the tank pressure falls below 150 psi at 18 seconds. Notice, comparing Figures 7 and 8, that the relatively most significant thruster anomalies occurred at tank pressures well below 150 psi (i.e. the final 15 seconds of the maneuver).

Bang-Off-Bang Experimental Results

The second set of experimental results was performed using the bang-off-bang open-loop control law in conjunction with the set of four 200-pound thrusters and two 8-pound thrusters. The specified maneuver was a 150 degree yaw maneuver, with the 8-pound thrusters limited to three pounds each and the 200-pound thrusters limited to 50 pounds each for fuel and safety reasons. Figure 9 shows the gimbal angles verses time for the second set of experimental results.
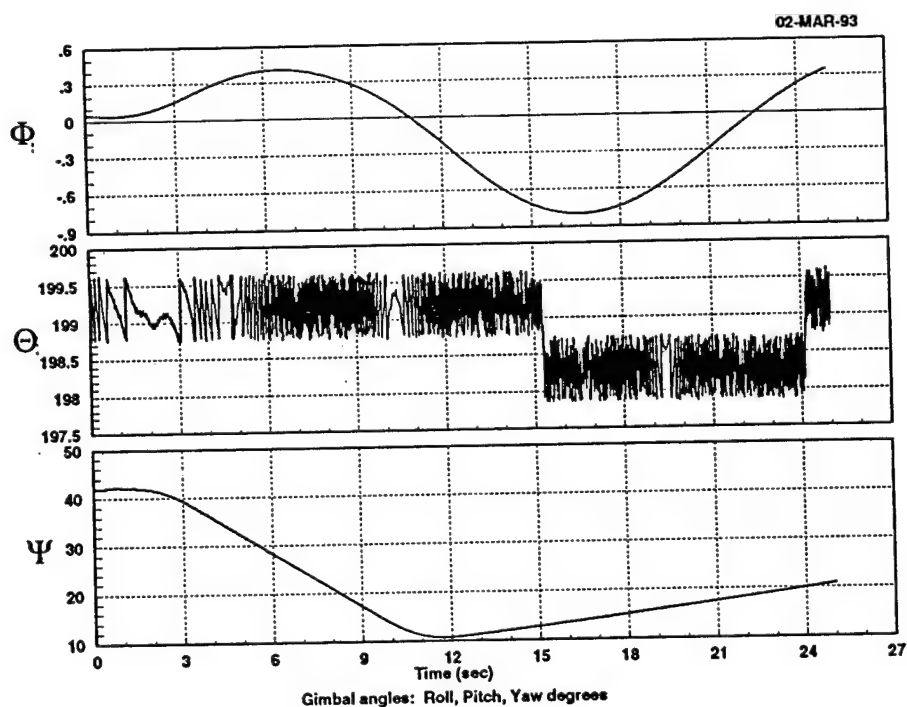
Figure 9 - Bang-Off-Bang Open-Loop Experimental Angle Profile on the ASTREX Test Article

This figure shows that a yaw angular rotation of only 32 degrees was accomplished from a required 50 degrees. The yaw angular velocity at the end of the maneuver was in the direction opposite of the maneuver; this appears to be the result of cable drag. The roll angle was again oscillatory but small and the pitch sensor exhibits the same noise characteristics.

Figure 10 shows the commanded voltage to the set of 200-pound thrusters. Each 200-pound thruster consists of two components which fire in opposite directions and are measured and controlled separately.

Figure 10 - Bang-Off-Bang Open-Loop Experimental 200 Lb. Commanded Thruster Profile on the ASTREX Test Article
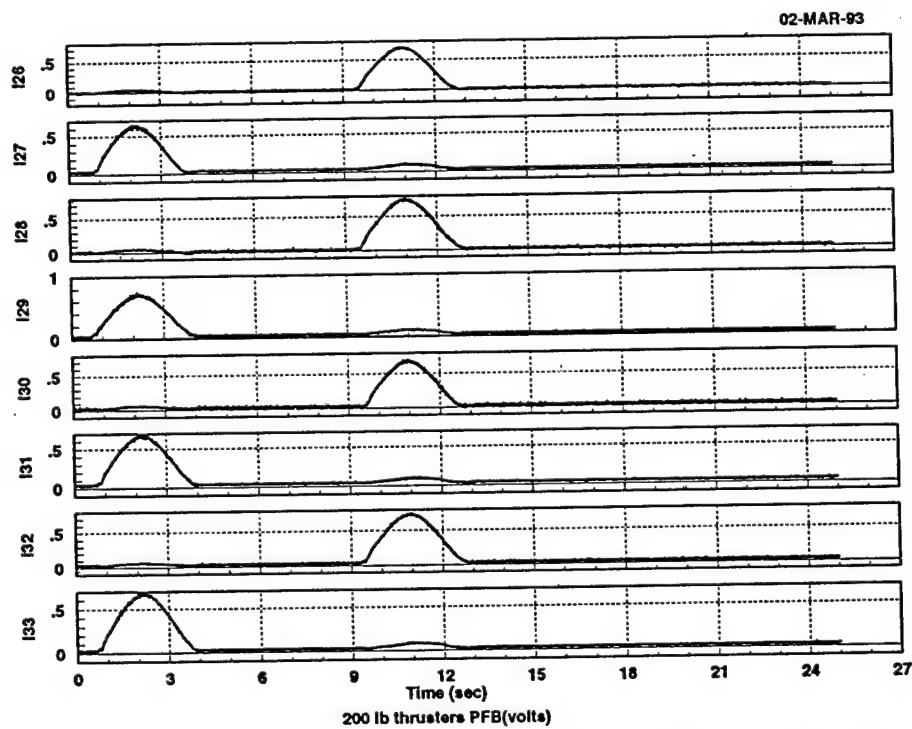
Figure 11 - Bang-Off-Bang Open-Loop Experimental 200 Lb. Actual Thruster Profile on the ASTREX Test Article

The output pressure measured at the nozzle of the 200-pound thrusters is shown as Figure 11. This figure illustrates how the two components of each thruster work in unison to produce the positive and negative components of the input signal. Although the reproduction of the input signal does not deteriorate near the end of the maneuver, some anomalous pressure leakage is evident.

Figure 12 shows the commanded voltage levels to the 8-pound thruster set which is used in conjunction with the 200-pound thrusters to provide controllability. This figure shows that the first two sets of 8-pound thrusters are zero since they have been replaced by the 200-pound thrusters. The third set of 8-pound thruster commands are shown as the two lower plots.
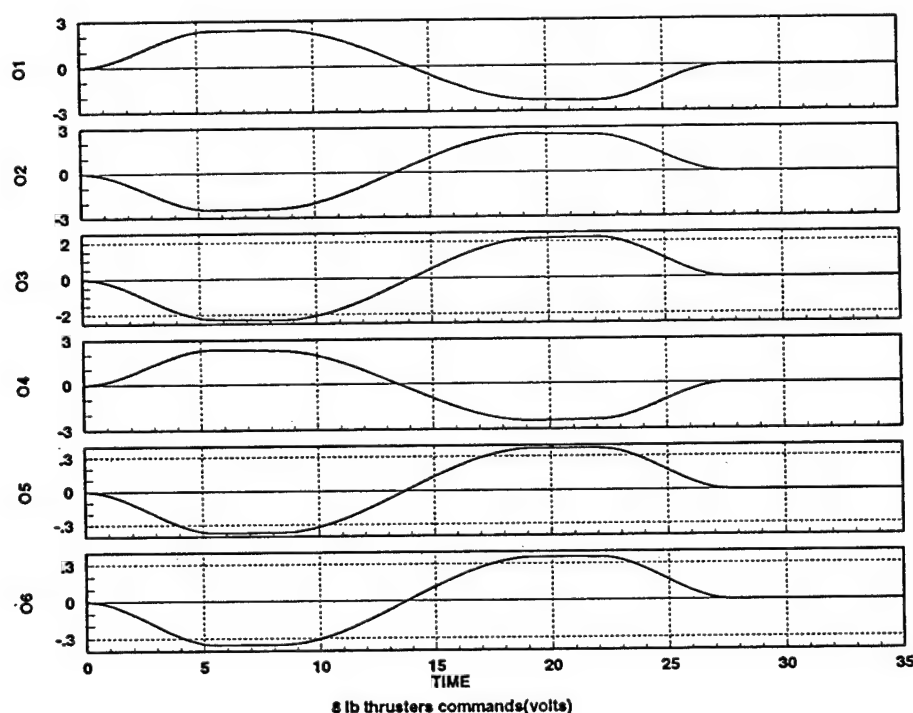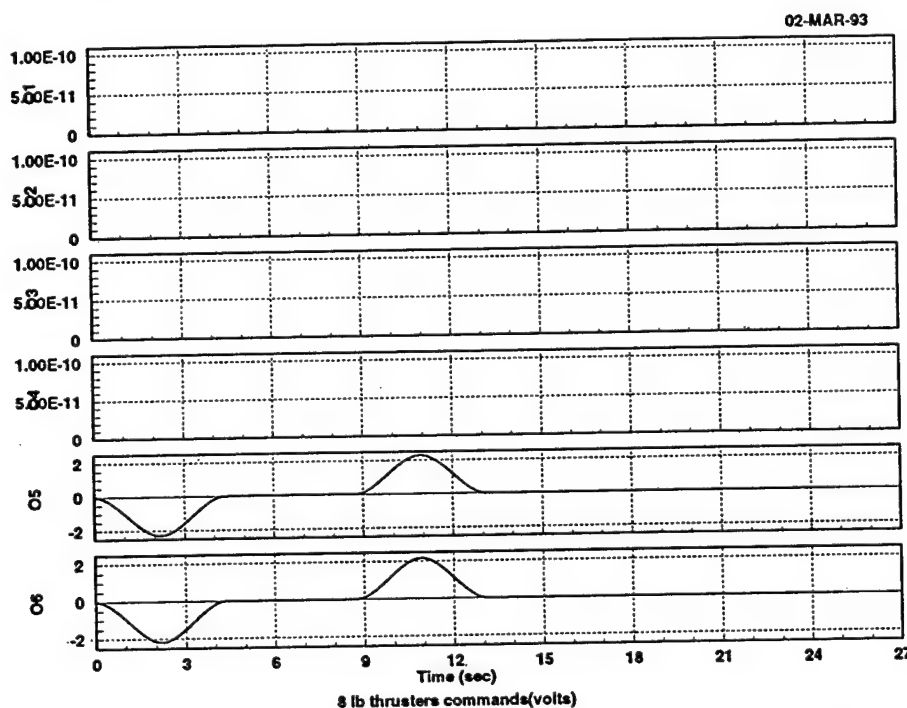

Figure 12 - Bang-Off-Bang Open-Loop Experimental 8 Lb. Commanded Thruster Profile on the ASTREX Test Article

The pressure sensor at the nozzle of the 8-pound thrusters is shown as figure 13. The first two sets of readings show that these thrusters are firing although they have been commanded to be off. This phenomena may be the result of electrical feedback within the hardware. Again, the third set of 8-pound thrusters have output deterioration near the end of the maneuver beginning at 10 seconds.

The final experimental figure (Figure 14) shows the tank pressure verses time. It is noted that at 10 seconds, where the 8-pound thruster degradation begins, the tank pressure has fallen below 150 psi. Figure 14 shows the tank pressure verses time for the bang-off-bang control law. It should be noted that during the coast period, the rate of pressure loss is approximately zero. This is the characteristic of the bang-off-bang control law which, of course, that saves fuel. The fact that there is a measurable negative slope, however, indicates that significant leakage is

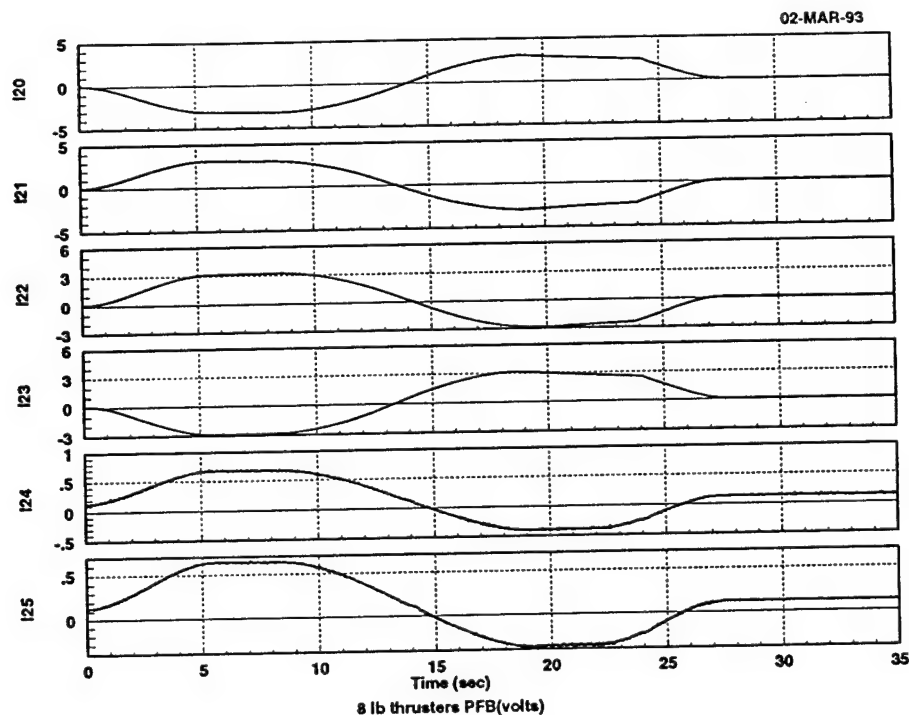occurring somewhere in the complicated plumbing system.
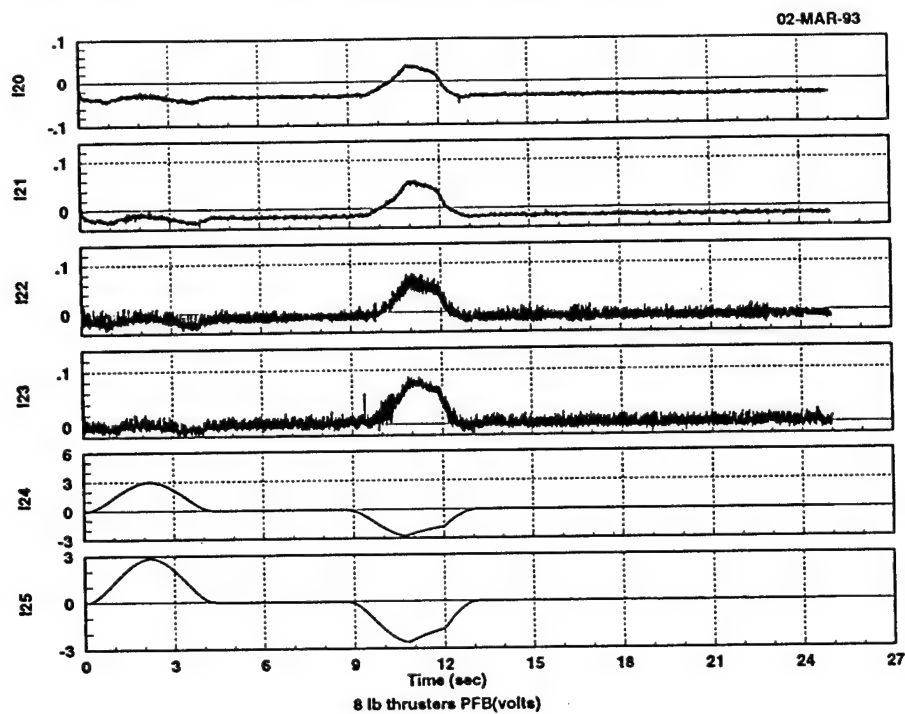
Figure 13 - Bang-Off-Bang Open-Loop Experimental 8 Lb. Actual
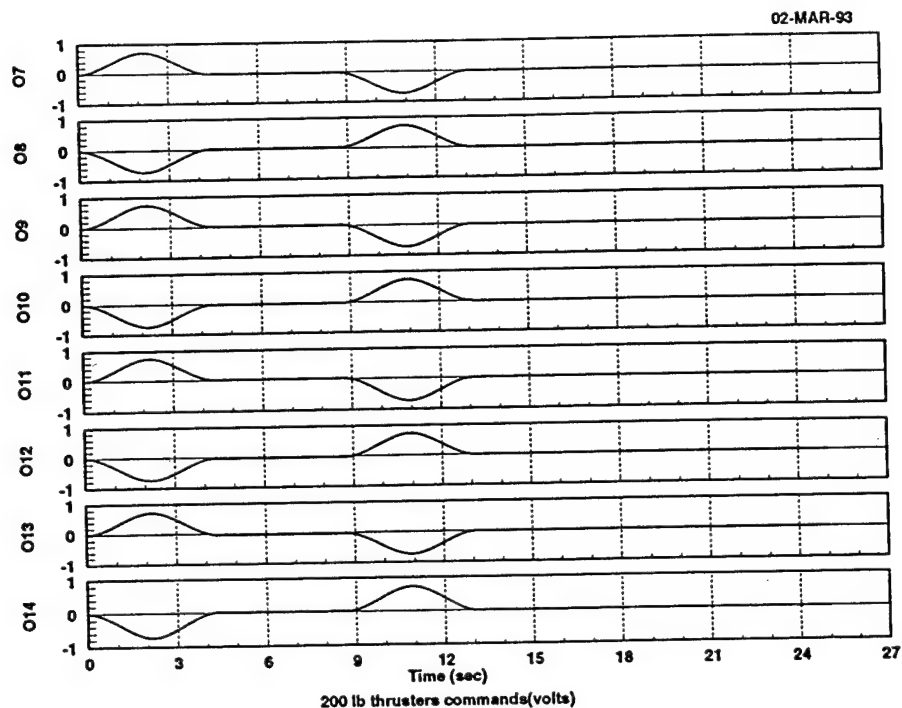Thruster Profile on the ASTREX Test Article
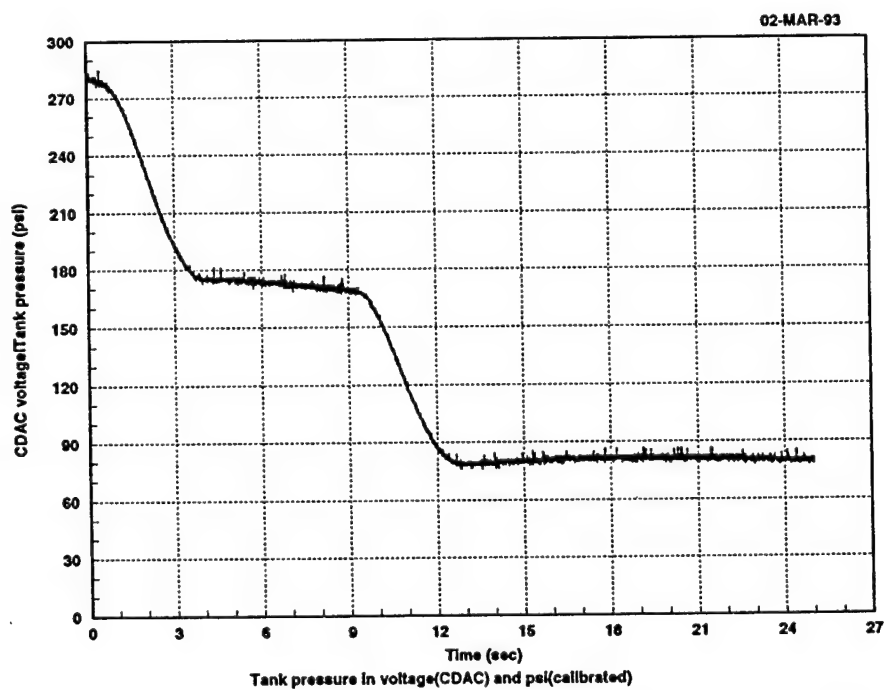
Figure 14 - Bang-Off-Bang Open-Loop Experimental Tank
Pressure Profile on the ASTREX Test Article

CONCLUSIONS

A torque-shaped maneuver approach for a spacecraft in three-dimensions has been developed and demonstrated to work extremely well using open-loop and closed-loop simulations for the bang-bang and the bang-off-bang maneuvers. In each case tested, the open-loop tracking error was essentially zero; the only errors introduced in the simulation were due to integration and interpolation errors. The closed-loop Lyapunov tracking control law drove large initial tracking errors to essentially zero within a few seconds and kept errors negligible until the final time using simulations where only initial condition errors were introduced. Additionally, only modest degradation of this performance resulted when significant model errors were introduced into the simulation, the Lyapunov tracking control law compensated for the model errors and initial condition errors, and again regulated the tracking error to essentially zero by the final time. Hence, the Lyapunov tracking controllers were shown to be robust with respect to modeling errors and initial condition errors.

The experimental portion of this research showed some positive results, however, also revealed are several hardware problems likely to be resolved with future evolution of this experimental facility. The experimental open-loop maneuvers showed the same general trends as the simulated data although they differed in magnitude. This discrepancy appears to have been caused by an underestimation of the mass of the structure and some unmodeled effects due to solenoid valve nonlinearities. Secondary problems are apparent in modeling the gimbal and cable-follower dynamics. Simulated maneuvers using an increase in mass of 10% on the open and closed-loop simulations were performed. The experimental data exhibits similar open-loop characteristics to the simulated data with a mass error. This problem was easily compensated for in simulation by closing the control loop. Closed-loop experimental results are not yet available due to current system hardware limitations, mainly, the angular rate measurements. Also, a significant number of unexplained anomalies were encountered in the experimental results; however, these may be considered typical of the early experimental "shakedown" of such a complicated electromechanical system.

The ASTREX test results also revealed some actuator problems generating the commanded thrust profiles using the 8-pound thrusters near the end of the maneuver when the tank pressure dropped below 150 psi. This problem stems from the fact that the cold gas thrusters' solenoid valves were designed assuming a constant back pressure of 500 psi. Our results suggest that the design specification of 500 psi is quite conservative; the thrusters operate reliably down to 175 psi using low thrust commands. With the present pressurized gas supply system, very low tank pressures (¡ 150 psi) routinely occurred because the tanks can only be pressurized between maneuvers. The thrust generation problem could be handled by performing maneuvers that only require only a very small amount of fuel and thus maintain a tank pressure above 150 psi, however, these small angle maneuver are less interesting and remove many of the nonlinear issues of intent from the system dynamics. Another problem was the support system in the yaw direction which was caused by to the natural equilibrium position of the structure and a

disturbance torque due to cable drag and cable-follower dynamics. These two phenomena could also cause the open-loop experimental maneuver to fall short of the required final yaw angle as well as causing the yaw angle to drift back towards its starting orientation upon completion of the open-loop torque profile. Each of these problems can be handled with rigorous modeling before deriving the open-loop control law or by using feedback compensation with appropriate sensing system enhancements.

The goal of this paper, to extend the near-minimum-time maneuver design technique to three-dimensions, was accomplished. The simulated results, both open-loop and closed-loop, were excellent and the preliminary experimental tests showed promising results.

ACKNOWLEDGEMENTS

REFERENCES

1 Junkins, J.L. and Turner, J.D., *Optimal Spacecraft Rotational Maneuvers*, Elsevier Scientific, Amsterdam, Holland, 1985.

2 Byers, R.M., Vadali, S.R., and Pollock, T.C., "Feedforward\Feedback Control Law for Near-Time Optimal Spacecraft Reorientation," AAS Paper 91-406, presented at the AAS\AIAA Astrodynamics Specialist Conference, Durango, Colorado, August 1991.

3 Singh, G., Kabamba, P.T., and McClamroch, N.H., "Planar, Time-Optimal, Rest-to-Rest Slewing Maneuvers of Flexible Spacecraft," *Journal of Guidance, Control, and Dynamics*, Vol. 12, No. 1, 1989, pp. 71-81.

4 Skaar, S.B., Tang, L., and Yalda-Mooshaabad, "On-Off Attitude Control of Flexible Satellites," *Journal of Guidance, Control, and Dynamics*, Vol. 9, No. 4, 1986, pp. 507-510.

5 Ben-Asher, J., Burns, J.A., and Cliff, E.M., "Time-Optimal Slewing of Flexible Spacecraft," *Journal of Guidance, Control, and Dynamics*, Vol. 15, No. 2, 1992, pp. 360-367.

6 Scrivener, S. and Thompson, R.C., "Survey of Time-Optimal Attitude Maneuvers," AAS Paper 92-168, presented at the AAS\AIAA Spaceflight Mechanics Meeting, Colorado Springs, Colorado, February 1992.

7 Vadali, S.R., Singh, T., and Carter, T., "Computation of Near-Minimum-Time Maneuvers of Flexible Structures by Parameter Optimization," AIAA Paper 92-4459, presented at the 1992 Guidance, Navigation, and Control Conference, Hilton Head, South Carolina, August 1992.

8 Singh, T. and Vadali, S.R., "Input Shaped Control of 3-Dimensional Maneuvers of Flexible Spacecraft," AIAA Paper 92-4459, presented at the 1992 Guidance, Navigation, and Control Conference, Hilton Head, South Carolina, August 1992.

9 Thompson, R.C., Junkins, J.L., and Vadali, S.R., "Near-Minimum-Time Open-Loop Slewing of Flexible Vehicles," *Journal of Guidance, Control, and Dynamics*, Vol. 12, No. 1, 1989, pp. 82-88.

10 Byers, R.M., Vadali, S.R., and Junkins, J.L., "Near-Minimum-Time Closed-Loop Slewing of Flexible Spacecraft,' ' *Journal of Guidance, Control, and Dynamics*, Vol. 13, No. 1, 1990, pp. 57-65.

11 Junkins, J.L., Rahman, Z.H., and Bang, H., "Near-Minimum-Time Control of Distributed Parameter Systems: Analytical and Experimental Results," *Journal of Guidance, Control, and Dynamics*, Vol. 14, No. 2, 1991, pp. 406-415.

12 Hecht, N.K. and Junkins, J.L., "Near-Minimum-Time Control of a Flexible Manipulator," *Journal of Guidance, Control, and Dynamics*, Vol. 15, No. 2, 1992, pp. 477-481.

13 Das, A., "Large-Angle Maneuver Experiments in Ground Based Laboratories," *Mechanics and Control of Large Flexible Structures*, Junkins, J.L., editor, AIAA, Washington, D.C., 1990.

14 Abhyankar, N.S. and Berg, J.L., "ASTREX Model Information: Supplement to astabcd.mat File," Phillips Laboratory, Edwards Air Force Base, California, August 15, 1991.

15 Wie, B., Weiss, H., and Araposthathis, A., "Quaternion Feedback for Spacecraft Eigenaxis Rotations," *Journal of Guidance, Control, and Dynamics*, Vol. 12, No. 3, 1989, pp. 375-380.

16 Vadali, S.R., "Feedback Control of Flexible Spacecraft Large-Angle Maneuvers Using Lyapunov Theory," *Proceedings of the American Control Conference*, Vol. 3, 1984, pp. 1674-1678.

17 Junkins, J.L. and Kim, Y., *Dynamics and Control of Flexible Structures*, AIAA Educational Series, Washington, D.C., 1993.

18 Junkins, J.L., Bang, H., and Fleming, P., "Lyapunov Optimal Control Laws for Flexible Structure Maneuver and Vibration Control," *Journal of the Astronautical Sciences*, Vol. 41, No. 1, Jan.-March 1993, pp. 91-118.

Stereographic Orientation Parameters for Attitude Dynamics: A Generalization of the Rodrigues Parameters

Hanspeter Schaub and John L. Junkins

Stereographic Orientation Parameters for Attitude Dynamics: A Generalization of the Rodrigues Parameters[1]

Hanspeter Schaub[2] and John L. Junkins[3]

Abstract

A new family of orientation parameters derived from the Euler parameters is presented. They are found by a general stereographic projection of the Euler parameter constraint surface, a four-dimensional unit sphere, onto a three-dimensional hyperplane. The resulting set of three stereographic parameters have a low degree polynomial non-linearity in the corresponding kinematic equations and direction cosine matrix parameterization. The stereographic parameters are not unique, but have a set of "shadow" parameters. These "shadow" parameters are generally numerically different, yet represent the same physical orientation. Using the original stereographic parameters combined with their shadow set it is possible to establish a set of three parameters which can describe any rotation without a singularity, yet with one discontinuity. The symmetric stereographic parameters are ideal to describe departure motions, since they can be chosen such that they are nonsingular for up to a principal rotation of ±360°. The asymmetric stereographic parameters are well suited for describing the kinematics of spinning bodies, since they only go singular when oriented at a specific angle about a specific axis. A globally regular and stable control law using symmetric stereographic parameters is presented which can bring a spinning body to rest in any desired orientation without backtracking the motion.

Introduction

While the Euler parameters (quaternions) describe an arbitrary orientation without a singularity, they form a once-redundant set. The following development studies a method to stereographically project the Euler parameters onto a three-dimensional hyperplane and form a family of sets of three parameters called the *stereographic parameters*. This study is motivated by

---

earlier work done by Marandi and Modi [1], Tsiotras [2] and Shuster [3]. In particular, Marandi and Modi introduce a set of three parameters similar to the Rodrigues parameters (singular at a principal rotation of $\Phi = \pm180°$), which move the singularity out to a principal rotation Φ of $\pm360°$! Marandi, Modi and Tsiotras describe this modified set of Rodrigues parameters as the result of a stereographic projection of a four-dimensional unit sphere onto a three-dimensional hyperplane. This paper will explore the stereographic projection idea further and in a more generalized way, and show that both the classical Rodrigues parameters and the Modi/Tsiotras modified Rodrigues parameters can be considered a special case of the general symmetric stereographic parameters. Indeed, the method presented can be used to construct a set of three symmetric stereographic parameters which have their singular point anywhere between a principal rotation of 0° and 360°, or to construct a set of three asymmetric stereographic parameters which have their singular point determined by both a principal angle and an axis of rotation. Analogous to the Euler parameters, the stereographic parameters are generally not unique. The Euler parameters time variation, for any physical motion, generate a trajectory on the surface of the unit sphere constraint surface. The reflection of the Euler parameters (reversing all parameters signs) generates a second trajectory on the opposite of the sphere which corresponds to the same physical rotation. Each set of stereographic parameters has a set of "shadow parameters" which correspond to the reflection set of Euler parameters. These "shadow" stereographic parameters are generally numerically different from the original parameters, yet physically parameterize the same rotation. The developments presented herein are of significant academic importance; using stereographic projections it is easy to visualize the singularities of this infinite family of three parameter sets which include the classical and modified Rodrigues parameters.

The modified Rodrigues parameters, as introduced by Marandi and Modi, are studied in further detail, since they present the largest range of non-singular rotations for the symmetric stereographic parameters. In combination with the corresponding set of "shadow parameters", a globally regular and non-singular Lyapunov attitude control is established in feedback form.

The Euler Parameter Unit Sphere

The four Euler parameters are well known and well studied in the literature. They can be developed directly from Euler's principal rotation theorem [3,4]. The angle Φ is the principal

rotation angle and the unit vector e is the principal line of rotation.

$$\beta_0 = \cos\frac{\Phi}{2} \qquad \beta_i = e_i \cdot \sin\frac{\Phi}{2} \qquad i = 1, 2, 3 \tag{1}$$

$$\underline{\beta}^T\underline{\beta} = \beta_0^2 + \beta_1^2 + \beta_2^2 + \beta_3^2 = 1 \tag{2}$$

The four Euler parameters β_i abide by the holonomic constraint given in equation (2). This equation describes a four-dimensional unit sphere. The Euler parameter trajectories on this sphere completely describe any possible rotational motion without any singularities or discontinuities.

Note that the Euler parameters are not unique. The mirror image trajectory $-\underline{\beta}(t)$ describes the identical rotational motion as $\underline{\beta}(t)$. The negative sign means the rotation is accomplished about a principal axis of the opposite direction through the negative principal angle. Usually this non-uniqueness does not pose any difficulties since both sets have identical properties, correspond to the same physical orientation, and can be solved uniquely once initial conditions are prescribed.

Because the Euler parameters satisfy one holonomic constraint, they form a once redundant set of equations. Three parameters are sufficient to describe a general rotation. However, the problem with any set of three parameters is that, as is well known, singularities will occur at certain orientations. Different three-parameter sets distinguish themselves by having different geometric interpretations and, especially, having their singular behavior at different orientations. Also of significance, most three-parameter sets introduce transcendental nonlinearities into the parameterization of the direction cosine matrix and related kinematical relationships. However, the classical Rodrigues parameters and other sets discussed herein involve low degree polynomial nonlinearities in both the direction cosine matrix and associated kinematical differential equation, without approximation. The Euler parameter description represents an attractive regularization which has no singularity, at the cost of having one extra variable.

Stereographic Projection of the 4D unit Sphere

If a minimum parameter representation is desired, the four Euler parameters can be reduced to any parameter set of three by an appropriate transformation. For example, the 3-1-3 Euler angles

or the Rodrigues parameters are very commonly used sets that are easily transformed from the Euler parameters [3,4]. Marandi, Modi and Tsiotras found a set of modified Rodrigues parameters by means of a stereographic projection of the four-dimensional unit sphere onto a three-dimensional hyperplane. To describe the stereographic projection, imagine a three-dimensional sphere being projected onto a two-dimensional plane (analogous to the Earth map projection problem). A certain point is chosen in the 3D space called a projection point. Next a 2D mapping plane is chosen. Every point on the unit sphere is then projected onto the mapping plane by drawing a line from the projection point through the point on the unit sphere and intersected with the mapping plane.
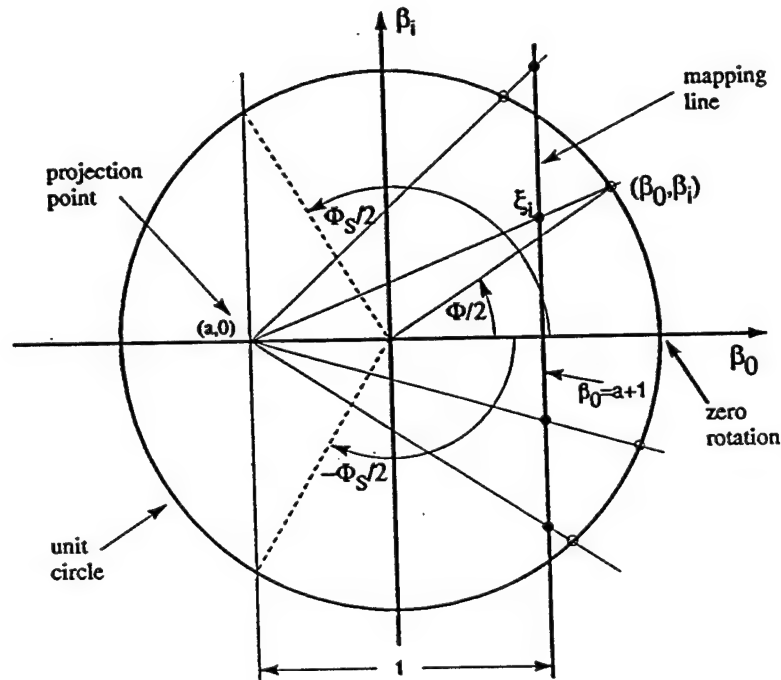
Fig. 1. Illustration of a Symmetric Stereographic Projection onto Hyperplane
Orthogonal to β_0 axis.

Figure 1 shows only a 2D to 1D stereographic projection to keep the illustration simple. The results though can easily be expanded to a four-dimensional sphere since the axes are orthogonal to each other. Figure 1 shows a 2D unit circle getting projected onto a mapping line. With all these projections the Euler parameter β_0 is eliminated, since the mapping hyperplane normal is the β_0 axis. They are called symmetric projections since the principal angle range is symmetric about the zero rotation angle. Asymmetric stereographic projections are projections onto a hyperplane with

a normal other than the β_0 axis, which do not have a symmetric principal angle range. The case where the Euler parameter β_1, β_2 or β_3 is eliminated is discussed later in this paper.

Placing the projection point on the β_0 axis yields an even principal angle range about the zero rotation point. The mapping line is placed a distance of +1 from the projection point. The parameters are scaled by this arbitrary distance, so having a distance of 2 between the projection point and the mapping plane would simply scale all the parameters by a factor of 2.

Keep in mind that the Euler parameters are defined in terms of *half* of the principal rotation angle Φ. The point (1,0) on the circle corresponds to a zero rotation. The point (0,1) corresponds to a +180° rotation. Studying Fig. 1 it becomes evident that the reduced parameters go off to infinity when a point on the circle is projected which lies directly in the plane perpendicular to the β_0 axis through the projection point. The two lines that need to be intersected are parallel to each other, causing the intersection point to move to infinity. The corresponding principal rotation obviously yields the angle at which the reduced set of parameters will go singular! By placing the projection point at different locations on the β_0 axis, the maximum principal rotation angle is varied. If the projection point is outside the unit circle, no singularity will occur, but the projection is no longer one-to-one. Some areas of the mapping will start to overlap in the projection plane. Clearly this is not a desirable feature because of the ambiguity this lack of uniqueness would introduce (given the projected coordinates, we cannot uniquely orient the reference frame).

The angle Φ_S is the principal angle of rotation where the stereographic parameter vector ζ encounters a singularity. This angle Φ_S determines the placement of the projection point a.

$$a = \cos\frac{\Phi_S}{2} \qquad (3)$$

The transformation from the Euler parameters to a general set of three symmetric stereographic parameters ζ is defined as:

$$\zeta_i = \frac{\beta_i}{\beta_0 - a} \qquad i = 1, 2, 3 \qquad (4)$$

The condition for a symmetric stereographic parameter singularity, evident in equation (4), is shown below.

$$a = \beta_0 = \cos\frac{\Phi}{2} \tag{5}$$

If $a < 1$ this condition is satisfied at an infinite set of orientations. If the projection point is on the unit sphere surface, then $a = -1$ and a singularity is only achieved at $\Phi = \pm 360°$.

$$\beta_0 = \frac{a\zeta^T\zeta + \sqrt{1 + \zeta^T\zeta(1 - a^2)}}{1 + \zeta^T\zeta}$$

$$\beta_i = \zeta_i \left[\frac{-a + \sqrt{1 + \zeta^T\zeta(1 - a^2)}}{1 + \zeta^T\zeta} \right] \qquad i = 1, 2, 3 \tag{6}$$

The inverse transformation from the general stereographic parameters ζ to the Euler parameters β_i is given in equation (6). This equation holds for both the symmetric and asymmetric stereographic projections.

Since the Euler parameters are not unique, it is valid to rewrite equation (4) in terms of $-\beta_i$. For the general case these new stereographic parameters ζ^S correspond to the mirror image of the Euler parameters and are generally not numerically equal to ζ of equation (4). However, the resulting vector ζ^S will describe the same orientation as the original parameters and are herein referred to as the "shadow points" of ζ and are denoted with a superscript S:

$$\zeta_i^S = \frac{-\beta_i}{-\beta_0 - a} = \frac{\beta_i}{\beta_0 + a} \tag{7}$$

Using equation (6) the shadow point ζ^S can be expressed directly as a transformation of the original parameters ζ and the projection point a as:

$$\zeta_i^S = \zeta_i \left[\frac{-a + \sqrt{1 + \zeta^T\zeta(1 - a^2)}}{a + 2a\zeta^T\zeta + \sqrt{1 + \zeta^T\zeta(1 - a^2)}} \right] \tag{8}$$

The fact that the shadow point vector ζ^S generally has a different behavior than the original ζ will be useful when describing a rotation. The family of stereographic parameters generally has two distinct sets of parameters, corresponding to $\beta(t)$ and $-\beta(t)$, which describe the identical

rotation and are related to one another by equation (8).

The differential kinematic equations for ζ are found by differentiating equation (4).

$$\dot{\zeta} = \frac{\dot{\beta}_i}{\beta_0 - a} - \frac{\beta_i \dot{\beta}_0}{(\beta_0 - a)^2} \tag{9}$$

By making use of the differential kinematic equations of the Euler parameters [4] given as:

$$\begin{bmatrix} \dot{\beta}_0 \\ \dot{\beta}_1 \\ \dot{\beta}_2 \\ \dot{\beta}_3 \end{bmatrix} = \frac{1}{2} \begin{bmatrix} \beta_0 & -\beta_1 & -\beta_2 & -\beta_3 \\ \beta_1 & \beta_0 & -\beta_3 & \beta_2 \\ \beta_2 & \beta_3 & \beta_0 & -\beta_1 \\ \beta_3 & -\beta_2 & \beta_1 & \beta_0 \end{bmatrix} \begin{bmatrix} 0 \\ \omega_1 \\ \omega_2 \\ \omega_3 \end{bmatrix} \tag{10}$$

and the basic definition of the stereographic parameters given in equation (4), the differential kinematic equations for the stereographic parameters can be found. Their general form is very lengthy and not shown here due to space limitations. The most important special cases are discussed below.

Viewing Fig. 1, it becomes evident that a set of three symmetric stereographic parameters cannot have the singularity point moved beyond a principal rotation of $\pm 360°$. Going beyond $\pm 360°$ would mean finding a projection point that would map the entire unit sphere more than once, i.e. not a one-to-one map onto the projection plane. Therefore the symmetric parameters are better suited for regulator or "moderately large" departure motion problems, than for spinning body or large angle maneuver cases.

Note that for the zero principal rotation, the asymmetric stereographic parameters are not equal to zero. The projection of the β_0 parameter onto $\beta_i = a + 1$ is not zero because β_0 is one at the zero principal rotation.

Asymmetric stereographic parameters have a qualitatively different singular behavior from the symmetric stereographic parameters. The Euler parameter β_0 contains information about the principal rotation angle only (i.e., the direction of $\underline{e}$ does not affect β_0). Eliminating β_0 during a symmetric projection causes the singularity to appear at a certain principal rotation angle,

independent from the principal axis of rotation e. Since for the symmetric projections, the zero rotation point $(1,0,0,0)$ lies on the β_0 axis and the singularity occurs at $\pm\Phi_S$, we have a symmetric range of nonsingular principal rotations $\{-\Phi_S < \Phi < +\Phi_S\}$ about the zero rotation, regardless of the direction of e.
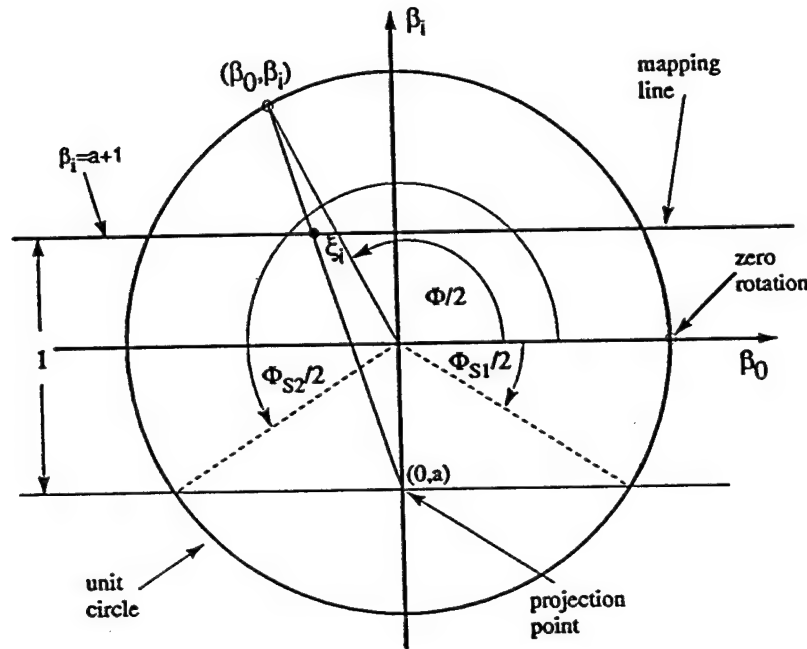
Fig. 2. Illustration of a Asymmetric Stereographic Projection onto Hyperplane Orthogonal to β_i axis.

For an asymmetric projection, one of the Euler parameters β_1, β_2, or β_3 is eliminated. Each one of these parameters contains information about both the principal rotation angle and the direction of e. Therefore singularities will only occur at certain angles about the i-th axis (corresponding to β_i). Figure 2 illustrates an asymmetric stereographic projection where β_i is eliminated. All possible projections points a now lie on the β_i axis, and the mapping hyperplane perpendicular to β_i is defined at $\beta_i = a+1$. Since the zero rotation is no longer in the center of the nonsingular principal angle range, the valid range of principal angles is non-symmetric. A singularity will occur at Φ_{S1} or Φ_{S2}, where these two principal angles are unequal in magnitude. Given a singular principal rotation angle Φ_{S1} which lies between $\pm180°$, the corresponding projection point a is defined as:

$$a = \cos\frac{\Phi_{S1}}{2} \qquad (11)$$

The second singular principal rotation angle Φ_{S2} is then found as:

$$\Phi_{S2} = 2\pi - \Phi_{S1} \qquad (12)$$

The transformation from Euler parameters to the corresponding asymmetric stereographic parameters is the same as given in equation (4), with β_0 and β_i switched. A singularity now occurs when β_i equals a. If the projection point a lies inside the four-dimensional unit sphere, this may occur at several orientations.

$$e_i \cdot \sin\frac{\Phi}{2} = a \qquad (13)$$

Using equation (1), the condition for a singularity becomes equation (13), where the index i stands for the β_i parameter which was eliminated. Since the sine function is bounded between ± 1, a singularity will *never* occur if $|e_i| < a$. If the projection point a is moved to the sphere surface, namely to ± 1, then a singularity may occur with a rotation about the *i-th* body axis only! The reason for this is evident in equation (12). Since a is ± 1 and the sine function is bounded within ± 1, the only way equation (13) is satisfied is if $|e_i| = 1$. Because e is a unit vector, the other two direction components must be zero if $|e_i| = 1$. Thus if the body is spinning about an axis other than the i-th body axis, a singularity will never occur. Therefore these asymmetric stereographic parameters are attractive for spinning body problems, where an object is rotating mainly about a certain axis. The principal rotation angle is now *not bounded* as with the symmetric stereographic parameters, but can grow beyond $\pm 360°$. Simply choose the normal of the projection hyperplane to be far removed from the rotation axis and place the projection point a on the four-dimensional unit sphere surface and the probability of encountering a singularity is virtually nil.

For both the symmetric and asymmetric stereographic parameters, having the projection point on the sphere surface means the singularity can only occur at two distinct orientations. If the projection point lies inside the sphere, there generally exists an infinite set of possible singular orientations.

The inverse transformation from asymmetric stereographic parameters to Euler parameters is the same as given in equation (6). These asymmetric parameters also exhibit the same shadow point behavior as the symmetric parameters do with the same transformation given in equation (8). Therefore, if a singular orientation is approached with the asymmetric stereographic parameters, one can switch to the shadow point to avoid the singularity.

Classical Rodrigues Parameters

The Rodrigues parameters q have a singularity at $\Phi = \pm 180°$. This corresponds to a point on the two-dimensional unit circle in Fig. 1 of $(0, \pm 1)$. The corresponding symmetric stereographic projection has the projection point a at the origin and the mapping line at $\beta_0 = 1$. It becomes evident why the classical Rodrigues parameters must go singular at $\Phi = \pm 180°$ when describing them as a special case of the symmetric stereographic parameters. The transformation from the Euler parameters to the Rodrigues parameters q is found by setting $\Phi_S = \pm 180°$ in equation (3-4). The well known result is shown in equation (14) below.

$$q_i = \frac{\beta_i}{\beta_0} \qquad i = 1, 2, 3 \tag{14}$$

The inverse transformation from the Rodrigues to the Euler parameters is found by using the same Φ_S in equation (6) and is given as:

$$\beta_0 = \frac{1}{\sqrt{1 + \underline{q}^T \underline{q}}} \qquad \beta_i = \frac{q_i}{\sqrt{1 + \underline{q}^T \underline{q}}} \qquad i = 1, 2, 3 \tag{15}$$

The differential kinematic equation in terms of the classical Rodrigues parameters is given in vector form as:

$$\dot{q} = \frac{1}{2} (\omega - [\bar{\omega}] q + q \omega^T q) \tag{16}$$

An explicit matrix form of equation (16) is given below [4].

$$\dot{q} = \frac{1}{2} \begin{bmatrix} 1+q_1^2 & q_1q_2-q_3 & q_1q_3+q_2 \\ q_2q_1+q_3 & 1+q_2^2 & q_2q_3-q_1 \\ q_3q_1-q_2 & q_3q_2+q_1 & 1+q_3^2 \end{bmatrix} \begin{bmatrix} \omega_1 \\ \omega_2 \\ \omega_3 \end{bmatrix} \tag{17}$$

Using the definitions of the Euler parameters in equation (1), the Rodrigues parameters can also be expressed directly in terms of the principal rotation angle Φ and the principal line of rotation φ.

$$q = \varphi \tan\frac{\Phi}{2} \tag{18}$$

From equation (18), it is obvious why the classical Rodrigues parameters go singular at $\pm 180°$. For completeness the direction cosine matrix C is given in explicit matrix form [4]:

$$C(q_1, q_2, q_3) = \frac{1}{1+q_1^2+q_2^2+q_3^2} \begin{bmatrix} 1+q_1^2-q_2^2-q_3^2 & 2(q_1q_2+q_3) & 2(q_3q_1-q_2) \\ 2(q_1q_2-q_3) & 1-q_1^2+q_2^2-q_3^2 & 2(q_2q_3+q_1) \\ 2(q_3q_1+q_2) & 2(q_2q_3-q_1) & 1-q_1^2-q_2^2+q_3^2 \end{bmatrix} \tag{19}$$

and in vector form [3]:

$$C(q) = \frac{1}{1+q^T q} ((1-q^T q)I + 2qq^T - 2[\bar{q}]) \tag{20}$$

Equation (20) and its inverse can also be written as the Cayley Transform [3,4,6]:

$$C(q) = (I - [\bar{q}])(I + [\bar{q}])^{-1} \tag{21a}$$

$$[\bar{q}] = (I - C)(I + C)^{-1} \tag{21b}$$

and the kinematic differential equation shown in equations (16-17) has the "Cayley" form [4]:

$$\frac{d}{dt}[\bar{q}] = \frac{1}{2}(I - [\bar{q}])[\bar{\omega}](1 - [\bar{q}]) \tag{22}$$

The tilde matrix $[\bar{q}]$ is defined by $-[q \times \ldots]$ as given in equation (23).

$$[\bar{q}] = \begin{bmatrix} 0 & -q_3 & q_2 \\ q_3 & 0 & -q_1 \\ -q_2 & q_1 & 0 \end{bmatrix} \tag{23}$$

Let the vector q^S (defined with $-\underline{\beta}$) denote the shadow point of the classical Rodrigues parameters. Solving equation (6), or starting with equation (14), the following definition for the q^S is found.

$$q_i^S = \frac{-\beta_i}{-\beta_0} = \frac{\beta_i}{\beta_0} = q_i \qquad i = 1, 2, 3 \tag{24}$$

Equation (24) shows that for the Rodrigues parameters, the shadow point vector components are identical to the original Rodrigues parameters, with identical values and properties. Therefore the shadow point concept is of no practical consequence in this case; the classical Rodrigues parameters are unique!
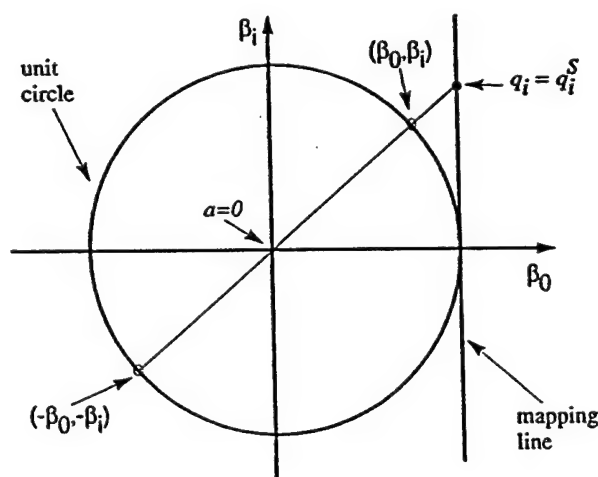
Fig. 3. Original and "Shadow Point" Projection of the Classical Rodrigues Parameters.

Having the projection point a at the origin causes this elegant, degenerate phenomenon. Figure 3 illustrates why both sets of Rodrigues parameters are identical. The classical Rodrigues parameters are the only symmetric stereographic parameters which exhibit this lack of distinction

between the original parameters and their shadow point counterparts, as is evident below. This proves simultaneously to be an advantage and a disadvantage.

Modified Rodrigues Parameters

The modified Rodrigues parameters presented by Modi and Tsiotras move the projection point to the far left of the unit sphere at (-1,0,0,0) and project the Euler parameters onto the hyperplane at $\beta_0 = 0$. This pushes the singularity as far away from the zero-rotation as possible. The parameters will now go singular at $\Phi = \pm 360°$. As Tsiotras points out, this new set of parameters is able to describe any type of rotation except a complete revolution back to its original orientation. Carrying out the stereographic projection with $\Phi_S = \pm 360°$, the transformation from Euler parameters to the modified Rodrigues parameter vector σ and the inverse transformation are given as:

$$\sigma_i = \frac{\beta_i}{1+\beta_0} \qquad i = 1, 2, 3 \tag{25}$$

$$\beta_0 = \frac{1-\sigma^T\sigma}{1+\sigma^T\sigma} \qquad \beta_i = \frac{2\sigma_i}{1+\sigma^T\sigma} \qquad i = 1, 2, 3 \tag{26}$$

Using equation (1) again, the modified Rodrigues parameters can be written as [2]:

$$\sigma = \varepsilon \tan\frac{\Phi}{4} \tag{27}$$

This formula immediately reveals the singularity at a principal rotation of $\pm 360°$, double the range of the classical Rodrigues parameters. It is interesting that $\Phi = 0°$ and $\Phi = \pm 360°$ correspond physically to the same body orientation. This fact has both theoretical and practical consequences in "avoiding" the singularity.

$$\dot{\sigma} = \frac{1}{2}\left[\omega\left(\frac{1-\sigma^T\sigma}{2}\right) - [\tilde{\omega}]\sigma + \sigma\omega^T\sigma\right] \tag{28}$$

The kinematic differential equations in terms of σ are given in equation (28). They are very

similar to equation (16) except for one extra term. This terms makes the equations only slightly more complicated, but not any more non-linear.

The explicit matrix form for the elements of equation (28) is given as [2]:

$$\dot{\underline{\sigma}} = \frac{1}{4}\begin{bmatrix} (1+\sigma_1^2-\sigma_2^2-\sigma_3^2) & 2(\sigma_1\sigma_2-\sigma_3) & 2(\sigma_1\sigma_3+\sigma_2) \\ 2(\sigma_2\sigma_1+\sigma_3) & (1-\sigma_1^2+\sigma_2^2-\sigma_3^2) & 2(\sigma_2\sigma_3-\sigma_1) \\ 2(\sigma_3\sigma_1-\sigma_2) & 2(\sigma_3\sigma_2+\sigma_1) & (1-\sigma_1^2-\sigma_2^2+\sigma_3^2) \end{bmatrix}\begin{bmatrix} \omega_1 \\ \omega_2 \\ \omega_3 \end{bmatrix} \tag{29}$$

The direction cosine matrix in terms of the modified Rodrigues parameters [2] can be shown to be:

$$C(\underline{\sigma}) = \frac{1}{(1+\underline{\sigma}^T\underline{\sigma})^2}\begin{bmatrix} 4(\sigma_1^2-\sigma_2^2-\sigma_3^2)+\Sigma^2 & 8\sigma_1\sigma_2+4\sigma_3\Sigma & 8\sigma_1\sigma_3-4\sigma_2\Sigma \\ 8\sigma_1\sigma_2-4\sigma_3\Sigma & 4(-\sigma_1^2+\sigma_2^2-\sigma_3^2)+\Sigma^2 & 8\sigma_2\sigma_3+4\sigma_1\Sigma \\ 8\sigma_1\sigma_3+4\sigma_2\Sigma & 8\sigma_2\sigma_3-4\sigma_1\Sigma & 4(-\sigma_1^2-\sigma_2^2+\sigma_3^2)+\Sigma^2 \end{bmatrix} \tag{30}$$
$$\Sigma = 1-\underline{\sigma}^T\underline{\sigma}$$

or more compactly in vector form as [3]:

$$C(\underline{\sigma}) = I - \frac{4(1-\underline{\sigma}^T\underline{\sigma})}{(1+\underline{\sigma}^T\underline{\sigma})^2}[\tilde{\sigma}] + \frac{8}{(1+\underline{\sigma}^T\underline{\sigma})^2}[\tilde{\sigma}]^2 \tag{31}$$

The modified Rodrigues parameter vector $\underline{\sigma}$ is transformed into classical Rodrigues parameters as:

$$\underline{q} = \left(\frac{2}{1-\underline{\sigma}^T\underline{\sigma}}\right)\underline{\sigma} \tag{32}$$

Naturally, this transformation goes singular at a principal rotation of $\pm 180°$, because $\|\underline{\sigma}\| \to 1$ and $\|\underline{q}\| \to \infty$ as $\Phi \to \pm 180°$.

Comparing equation (27) and equation (18) it is immediately evident that both the classical and the modified Rodrigues parameter vectors have the direction of the principal rotation vector $\underline{e}$, but a different magnitude. The transformation from modified to classical Rodrigues parameters

shown in equation (32) can be rewritten in terms of the principal angle of rotation Φ.

$$g = \frac{\tan\dfrac{\Phi}{2}}{\tan\dfrac{\Phi}{4}}\sigma \qquad (33)$$

Using the image set $-\beta(t)$ of Euler parameters, the shadow point of the modified Rodrigues parameter vector σ is found.

$$\sigma_i^S = \frac{-\beta_i}{1-\beta_0} = \frac{-\sigma_i}{\sigma^T\sigma} \qquad (34)$$

Contrary to the classical Rodrigues parameters, these modified Rodrigues parameter shadow points are not numerically equal to the original parameters. While they generate exactly the same direction cosine matrix, they are not generally a mirror image of one another. While generally $\sigma^S \neq -\sigma$, note that everywhere on the unit sphere $\sigma^T\sigma = 1$ that, in fact, $\sigma^S = -\sigma = -\beta_i$. This simple observation has significant practical consequences.

Fig. 4. Original and "Shadow Point" Projection of the Modified Rodrigues Parameters.

The shadow points σ^S have some interesting properties. They go singular at the zero rotation

and go to zero at a ±360° principal rotation! This is the exact opposite of the qualitative behavior of σ. The reason for this behavior becomes evident in Fig. 4. At a zero rotation, the shadow point will intersect the mapping line at infinity. At a rotation of ±180° the shadow points will be the negative of their original values. We note that σ^S is distinguished from σ merely for book-keeping purposes. Transforming initial conditions (from [C] or $\underline{\beta}$) for any given case, could initiate motion on either $\underline{\sigma}(t)$ or $\underline{\sigma}^S(t)$.

Using $\underline{\sigma}$ together with the shadow vector $\underline{\sigma}^S$, it is possible to describe *any* rotation without singularities and with only three parameters, but with one discontinuity at the switching point. If the original $\underline{\sigma}(t)$ trajectory approaches the singularity at $\Phi = \pm 360°$, the vector $\underline{\sigma}(t)$ can be switched to the shadow trajectory $\underline{\sigma}^S(t)$. This transformation is very simple as is seen in equation (34). Rather than waiting until $|\underline{\sigma}(t)| \to \infty$ or $|\underline{\sigma}^S(t)| \to \infty$ to switch, however, the most convenient switching surface is the $\underline{\sigma}^T\underline{\sigma} = 1$ sphere; the unit sphere which corresponds to a principal rotation of ±180°. The Euler parameter β_0 is zero everywhere on this sphere. This causes the shadow point to have the same unit magnitude as the original with the transformation being $\underline{\sigma}^S = -\underline{\sigma}$. Thus whenever $\underline{\sigma}(t)$ exits (enters) the unit sphere, $\underline{\sigma}^S(t)$ enters (exits) at the opposite side of the sphere.
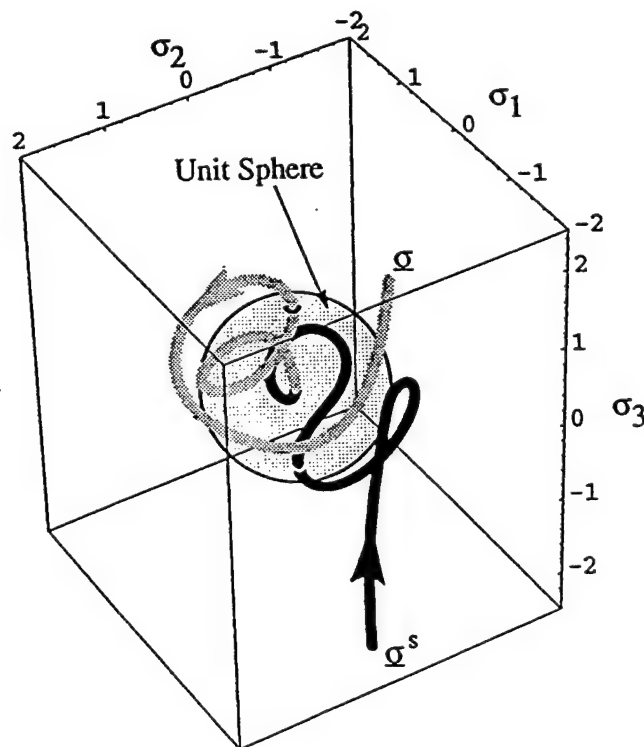
Fig. 5. Illustration of the Original and Shadow Modified Rodrigues Parameter.

Switching at the $\sigma^T \sigma = 1$ surface can be very elegantly accomplished when finding σ by extracting the Euler parameters from the direction cosine matrix. Simply keep $\beta_0 \geq 0$ and the resulting set of parameters will always have $\sigma^T \sigma \leq 1$ [1]. Switching on the $\beta_0 = 0$ sphere (where $\sigma^T \sigma = \sigma^{S^T} \sigma^S = 1$) keeps the combined set of original and shadow points bounded within the unit sphere.

This bounded behavior of the combined set is illustrated in Fig. 5 above. The grey line represents the $\sigma(t)$ trajectory and the black line the corresponding shadow trajectory of $\sigma^S(t)$. The motion starts out at a zero rotation with the grey line at the origin and the black line at infinity. After a while the principal angle of the object grows beyond 180° and the grey line exits the unit sphere. At the same time the shadow parameters (black line) enter the sphere at the opposite position. If the body rotates back to the original orientation, the shadow parameters approach zero as the original parameters go off to infinity. Any tumbling motion would give rise to a qualitatively identical discussion of $\sigma(t)$ and $\sigma^S(t)$.

Example of Asymmetric Stereographic Parameters

A sample set of asymmetric stereographic parameter vector $\underline{\eta}$ is constructed by eliminating the Euler parameter β_1 and setting a equal to -1. Adjusting equation (4), the vector $\underline{\eta}$ is defined as:

$$\eta_1 = \frac{\beta_0}{\beta_1 + 1} \qquad \eta_2 = \frac{\beta_2}{\beta_1 + 1} \qquad \eta_3 = \frac{\beta_3}{\beta_1 + 1} \tag{35}$$

Using equation (11,12) the singular principal rotations about the positive β_1 axis become $\Phi_{S1} = -180°$ and $\Phi_{S1} = +540°$. As mentioned earlier, the direction at which a singular orientation is approached is important with asymmetric stereographic parameters. Here a negative principal rotation of 180° about the first body axis causes a singularity. A positive principal rotation of 180° would yield an identical physical position, yet causes no singularity. Only after a +540° does this representation go singular, even though this position is the same as +180°. This non-symmetric principal angle range is due to the fact that the zero rotation point ($\pm 1,0,0,0$) does not lie on the β_1 axis.

Differentiating equation (35) and using equation (10), the differential kinematic equation for vector $\underline{\eta}$ is found to be:

$$\dot{\underline{\eta}} = \frac{1}{4} \begin{bmatrix} (-1-\eta_1^2+\eta_2^2+\eta_3^2) & 2(\eta_1\eta_3-\eta_2) & -2(\eta_1\eta_2+\eta_3) \\ 2(\eta_3-\eta_1\eta_2) & 2(\eta_2\eta_3+\eta_1) & (-1+\eta_1^2-\eta_2^2+\eta_3^2) \\ -2(\eta_1\eta_3+\eta_2) & (1-\eta_1^2-\eta_2^2+\eta_3^2) & 2(\eta_1-\eta_2\eta_3) \end{bmatrix} \begin{bmatrix} \omega_1 \\ \omega_2 \\ \omega_3 \end{bmatrix} \qquad (36)$$

Note that equation (36) contains no transcendental functions in it and is similar qualitatively to equation (29). Because $\underline{\eta}$ is an asymmetric stereographic parameter vector, however, there is less symmetry in the matrix. This lack of symmetry is linked with the absence of a symmetric principal rotation angle range. Therefore, equation (36) cannot be written in a more compact vector as was the case with the symmetric stereographic parameters.

The direction cosine matrix in terms of $\underline{\eta}$ can be found to be:

$$C(\underline{\eta}) = \frac{1}{(1+\underline{\eta}^T\underline{\eta})^2} \begin{bmatrix} 4(\eta_1^2-\eta_2^2-\eta_3^2)+\Sigma^2 & 8\eta_1\eta_3+4\eta_2\Sigma & -8\eta_1\eta_2+4\eta_3\Sigma \\ -8\eta_1\eta_3+4\eta_2\Sigma & 4(\eta_1^2+\eta_2^2-\eta_3^2)-\Sigma^2 & 8\eta_2\eta_3+4\eta_1\Sigma \\ 8\eta_1\eta_2+4\eta_3\Sigma & 8\eta_2\eta_3-4\eta_1\Sigma & 4(\eta_1^2-\eta_2^2+\eta_3^2)-\Sigma^2 \end{bmatrix} \qquad (37)$$

$$\Sigma = 1-\underline{\eta}^T\underline{\eta}$$

Analogously, asymmetric stereographic parameters could be derived by projecting onto a hyperplane orthogonal to the β_2 or β_3 axis, or actually any non-β_0 axis. All these parameters would have a similar singular behavior.

To illustrate the use of the asymmetric stereographic parameters $\underline{\eta}$ for describing a spinning body, a sample motion was generated. The motion was achieved by forcing the following 3-1-3 Euler angle time history upon the body.

$$\theta_1(t) = t \qquad \theta_2(t) = (1-\cos 2t)\frac{\pi}{2} \qquad \theta_3(t) = (\sin 2t)\frac{\pi}{4} \qquad (38)$$

The body is mainly spinning about the third body axis while oscillating about the other two. Therefore the stereographic parameter vector $\underline{\eta}$ will never go singular, since a singularity can only occur with a pure rotation about the first body axis.
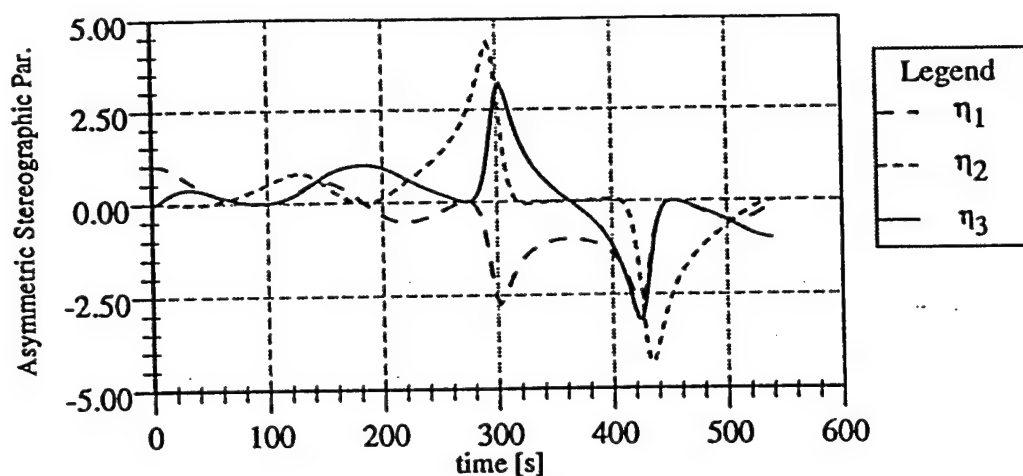
Fig. 6. Spinning Body Description with Asymmetric Stereographic Parameters.

As Fig. 6 shows, the asymmetric stereographic parameters $\underline{\eta}$ are smooth and continuous at all time. The sample motion shown performs one and a half revolutions without encountering any singularity.
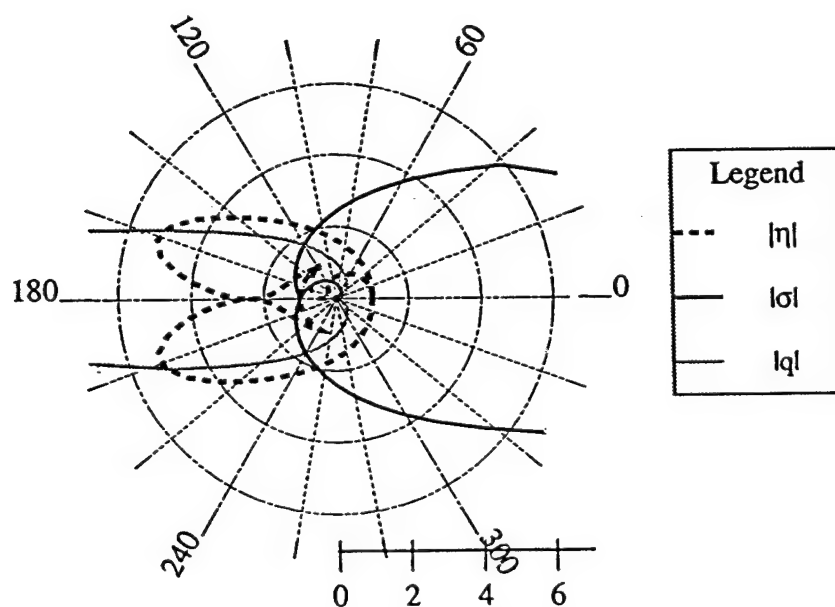
Fig. 7. Comparison of Symmetric and Asymmetric Stereographic Parameters.

To compare the asymmetric with the symmetric stereographic parameter description for this spinning body, the polar plot in Fig. 7 was generated. The magnitude of each parameter vector is

plotted versus the principal rotation angle ϕ. As expected, the symmetric stereographic parameters go singular at certain ϕ, while the vector η is bounded at all times.

Figure 8 shows the time history of the principal rotation angle ϕ for this spinning body maneuver. Because of the oscillations about the first and second body axis, ϕ gets reduced during some portions of the maneuver. Because the magnitude of the symmetric stereographic parameters depends only on the principal rotation angle, these "backing up" phases are not visible on the polar plot in Fig. 7. However, the magnitude of the asymmetric stereographic parameters depends on both the principal rotation angle and the direction of the principal rotation axis. This explains the more irregular features of the $|\eta|$ plot in Fig. 7.
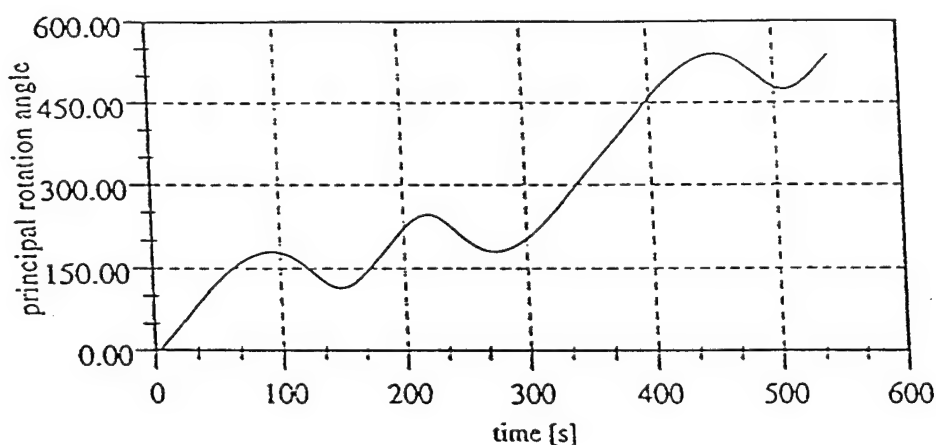
Fig. 8. Principal Rotation Angle Time History of Spinning Body Maneuver

While some loss in symmetry and elegance of the equations results, asymmetric sets of stereographic parameters are able to represent the motion of a spinning body without switching between the shadow and the original parameters, like the modified Rodrigues parameters would require. In [7] Tsiotras develops a set of orientation parameters which are also well suited for the spinning body problem and have a low polynomial degree nonlinearity in their kinematic equations. They differ in form to the asymmetric stereographic parameters, but are similar in behavior.

Globally Stable Control using Modified Rodrigues Parameters

The combined set of modified Rodrigues parameters and their shadow counterparts lend themselves very well for regulator type control design. Adopting the switching surface $\sigma^T\sigma = 1$ has a surprising benefit in designing control laws. Consider the dynamics of a generally tumbling rigid body. The Lyapunov function

$$V(\omega, \sigma) = \frac{1}{2}\omega^T J\omega + 2K\log(1 + \sigma^T\sigma) \tag{39}$$

will not have any discontinuities at the switching surface, since both the original σ and its shadow σ^S point have unit magnitude there! $V(\omega, \sigma)$ is by inspection only zero if both ω and σ are zero. As a consequence, it is easy to establish a globally stable Lyapunov controller with a three rotation parameter set which never encounters a singularity! J in equation (39) denotes the 3x3 inertia matrix in body axis. The scalar K is a positive feedback gain. For this nonlinear regulator type problem, the external control torque u is found by setting the time derivative of equation (39) equal to

$$\dot{V} = -\omega^T P\omega \tag{40}$$

with P being a positive definite matrix, and using equation (28) and Euler's equation of motion:

$$J\dot{\omega} = -[\tilde{\omega}]J\omega + u \tag{41}$$

to solve for the torque u. Using the logarithm of $\sigma^T\sigma$ in equation (39) results in a globally nonlinear control law u which is *linear* in σ [2].

$$u = -P\omega - K\sigma + [\tilde{\omega}]J\omega \tag{42}$$

The control law in equation (42) is valid for any arbitrary departure motion σ. Conventional sets of three parameters would encounter singular orientations. Another problem with conventional parameter sets is that they have no inherent mechanism to accommodate tumbling situations when the object has performed a principal rotation beyond $\pm180°$ away from the desired

state. When this happens, it would probably be desirable to "help" the object complete the revolution, rather than to attempt to force it back the way it came. The only set of parameters that can "almost" handle this scenario is the classical set of Rodrigues parameters. They fail because they go singular near the "up-side-down" orientation at $\Phi=\pm180°$. The combined set of σ and σ^S, however, are well behaved up to and well beyond $\Phi = \pm180°$. Switching at $\sigma^T\sigma = 1$ makes it possible for the control law to let the object go past the "up-side-down" orientation and then let it rotate back to the origin the short way, as we illustrate in an example below.

The angular velocity ω feedback is required for global stability, and the P matrix should be chosen to achieve satisfactory damping of the nonlinear oscillations.

The results of a single-axis spin maneuver using the control law in equation (43) are presented. The inertia J used was 12000 kgm^2; the feedback gains were chosen as $K=300$ and $P=1800$. Initial angular velocity was +60°/s. Figure 9 below shows the time history of the principal angle of rotation. The object clearly spins beyond the "up-side-down" point of $\Phi=+180°$ and then returns back to the origin by continuing the motion and completing the revolution. The ω feedback sufficiently dampens the system to prevent excessive oscillations about the origin.
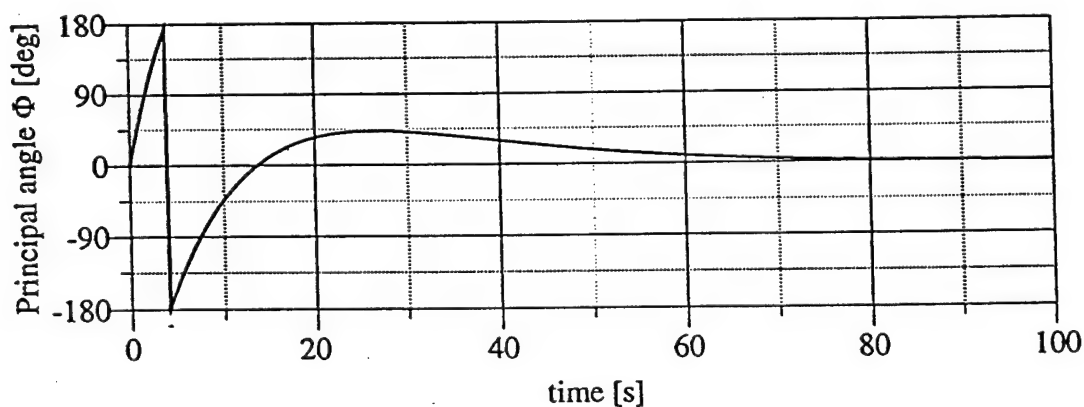
Fig. 9. Principal Angle of Rotation of Spin Maneuver.

The angular velocity, shown in Fig. 10, decreases steadily from +60°/s and converges to zero. Where the Φ goes beyond 180° there is a discontinuity in the slope of ω.
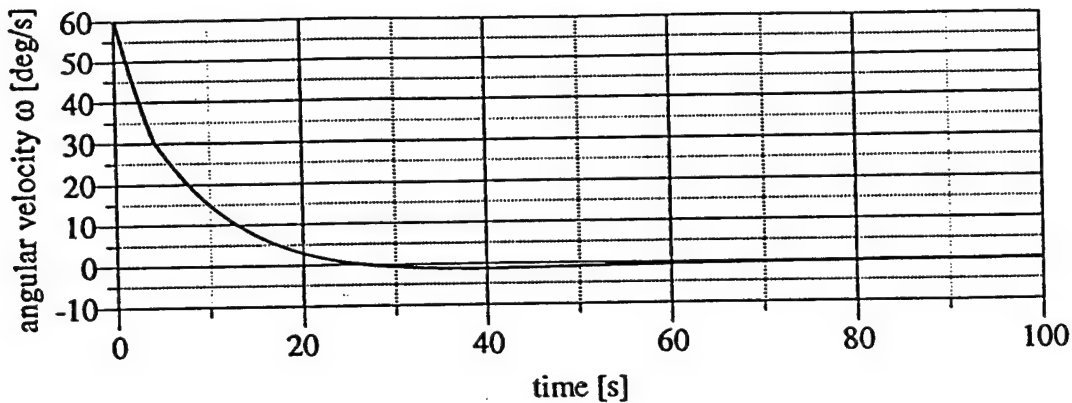
Fig. 10. Angular Velocity of Spin Maneuver.

The corresponding external control torque is presented in Fig. 11. A large torque is demanded initially because of the large initial angular velocity $\underline{\omega}$. As $\underline{\omega}$ decreases, so does the torque. There is a discontinuity where the modified Rodrigues parameter switch from the original to the shadow point trajectory. This is because the position error σ reversed its sign, driving the object towards the origin about the other way. However, the control torque does not jump to a negative value because of the $\underline{\omega}$ feedback. It keeps the torque positive; i.e. the controller is still slowing down the spin, even during the switching.
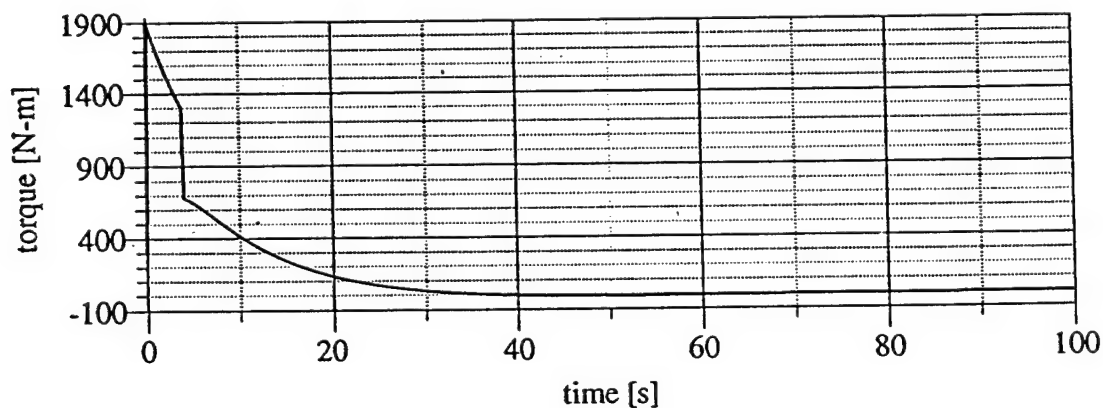
Fig. 11. External Control Torque of Spin Maneuver.

The position error and the associated torque discontinuity due to switching to the shadow trajectory may be troublesome for highly flexible bodies. However, this is easily addressed in practice by replacing the instantaneous switch by a smooth one. Also, introducing a simple digital

filter will effectively smooth out such jump discontinuities.

It is conceptually easy to introduce a reference trajectory and design analogous tracking-type feedback control with, using the methods of [4], global stability guaranteed. This is useful in achieving global control shaping, and also to permit selection of feedback gains sufficiently large to reject disturbances.

Conclusion

A new family of stereographic parameters has been presented, including the general transformation from and to the Euler parameters. The general stereographic parameters are not unique and have a corresponding set of shadow point parameters whose singular behavior is different from the original parameters.

The classical Rodrigues parameters are a special set of the symmetric stereographic parameters where the original parameters and their shadow points coincide. The modified Rodrigues parameters are also a special case of the symmetric stereographic parameters. They have the largest non-singular principal angle range of $\pm 360°$. Their associated shadow points are singular at the zero rotation and zero and $\Phi = \pm 360°$. This combined set of stereographic parameters and their shadow point parameters are able to describe any rotation without encountering a singularity, but with one discontinuity.

The asymmetric stereographic parameters have their singular orientations defined both by an axis and a principal rotation angle. The two singular angles do not have equal magnitude as with the symmetric stereographic parameter. Asymmetric parameters do allow rotations beyond $\pm 360°$ and are therefore attractive to spinning body type problems.

The globally stable control law presented implicitly "knows" when an object has rotated beyond $\pm 180°$ from the target state, and to let it complete the revolution back to the desired state. This control implicitly seeks out the smallest principal rotation angle to the target state. This control law was developed by making use of the modified Rodrigues parameter and their shadow points.

Acknowledgments

and Malcolm Shuster regarding this topic.

References

[1] MARANDI, S.R., and MODI, V.J., "A Preferred Coordinate System and the Associated Orientation Representation in Attitude Dynamics," *Acta Astronautica*, Vol. 15, 1987, pp.833-843.

[2] TSIOTRAS, PANAGIOTIS, "On New Parameterizations of the Rotation Group in Attitude Kinematics," *IFAC Symposium on Automatic Control in Aerospace*, Palo Alto, California, Sept. 12-16, 1994.

[3] SHUSTER, M.D., "A Survey of Attitude Representations," *Journal of the Astronautical Sciences*, Vol. 41, No. 4, 1993, pp. 439-517.

[4] JUNKINS, J.L., and KIM, Y., *Introduction to Dynamics and Control of Flexible Structures*, AIAA Education Series, Washington D.C., 1993.

[5] JUNKINS, J.L., and TURNER, J.D., *Optimal Spacecraft Rotational Maneuvers*, Elsevier Science Publishers, Netherlands, 1986.

[6] CAYLEY, A., "On the Motion of Rotation of a Solid Body," *Cambridge Mathematics Journal*, Vol 3, 1843, pp. 224-232.

[7] TSIOTRAS, P., "On New Parameterizations of the Rotation Group in Attitude Kinematics," submitted to IFAC 94 Symposium on Aerospace Control, 1994.

Orthogonal Projections Revisited: Concepts from Classical Mechanics and Modern Dynamical Systems Analysis

John L. Junkins

Department of Aerospace Engineering

Texas A&M University

Society of Engineering Science

31st Annual Technical Meeting

October 10-12, 1994

Texas A&M University

College Station, Texas

Acknowledgements

I am pleased to acknowledge productive collaborations with

My excellent Ph.D. Student:
Hanspeter Schaub

My Insightful Colleague:
Prof. P. (Takis) Tsiotras
the Univ of Virginia

Question: Which of the two 'dynamically equivalent' sets of differential equations would you prefer to solve?

Set I: The Classical 3-1-3 Euler Angles:

$$\ddot{\psi} = -\frac{\cos\theta\sin\psi}{\sin\theta}\left[r_1\dot{\phi}^2\sin\theta\cos\theta\cos\psi - (1+r_1)\dot{\phi}\dot{\theta}\cos\theta\sin\psi - (1-r_1)\dot{\phi}\dot{\psi}\sin\theta\cos\psi + (1-r_1)\dot{\theta}\dot{\psi}\sin\psi + u_1/I_1\right]$$

$$-\frac{\cos\theta\cos\psi}{\sin\theta}\left[r_2\dot{\phi}^2\sin\theta\cos\theta\sin\psi - (1-r_2)\dot{\phi}\dot{\theta}\cos\theta\cos\psi + (1+r_2)\dot{\phi}\dot{\psi}\sin\theta\sin\psi + (1-r_2)\dot{\theta}\dot{\psi}\cos\psi + u_2/I_2\right]$$

$$+\sin\theta\left[r_3\dot{\phi}^2\sin^2\theta\cos\psi\sin\psi - r_3\dot{\theta}^2\cos\psi\sin\psi + (1-r_3)\dot{\phi}\dot{\theta}\sin\theta + u_3/I_3\right]$$

$$\ddot{\theta} = analogous\ expression \qquad where\ the\ inertia\ ratios\ are:\quad r_1 \equiv (I_2-I_3)/I_1,\quad r_2 \equiv (I_3-I_1)/I_2,\quad r_3 \equiv (I_1-I_2)/I_3$$

$$\ddot{\phi} = analogous\ expression$$

Set II: The Euler ('quaternion') Parameters & Orthog. Components of Angular Velocity:

$$\dot{\beta}_0 = (-\omega_1\beta_1 - \omega_2\beta_2 - \omega_3\beta_3)/2$$
$$\dot{\beta}_1 = (-\omega_1\beta_0 - \omega_2\beta_3 + \omega_3\beta_2)/2$$
$$\dot{\beta}_2 = (+\omega_1\beta_3 + \omega_2\beta_0 - \omega_3\beta_1)/2$$
$$\dot{\beta}_3 = (-\omega_1\beta_2 + \omega_2\beta_1 - \omega_3\beta_0)/2$$

$$\dot{\omega}_1 = r_1\omega_2\omega_3 + u_1/I_1$$
$$\dot{\omega}_2 = r_2\omega_3\omega_1 + u_2/I_2$$
$$\dot{\omega}_3 = r_3\omega_1\omega_2 + u_3/I_3$$

Remark: If you chose Set I, I have no further questions!

Moral: It is difficult to overemphasize the choice of coordinates, especially for describing Nonlinear Rotational Motion.

Question: To what extent does these results extend to other large classes of problems in mechanics and applied analysis?

143

SESJ

Euler's Principal Rotation Theorem

A rigid body (ref. frame) can be brought from an arbitrary initial orientation to an arbitrary final orientation by a single rotation (Φ) about a principal line ($\hat{e}$).
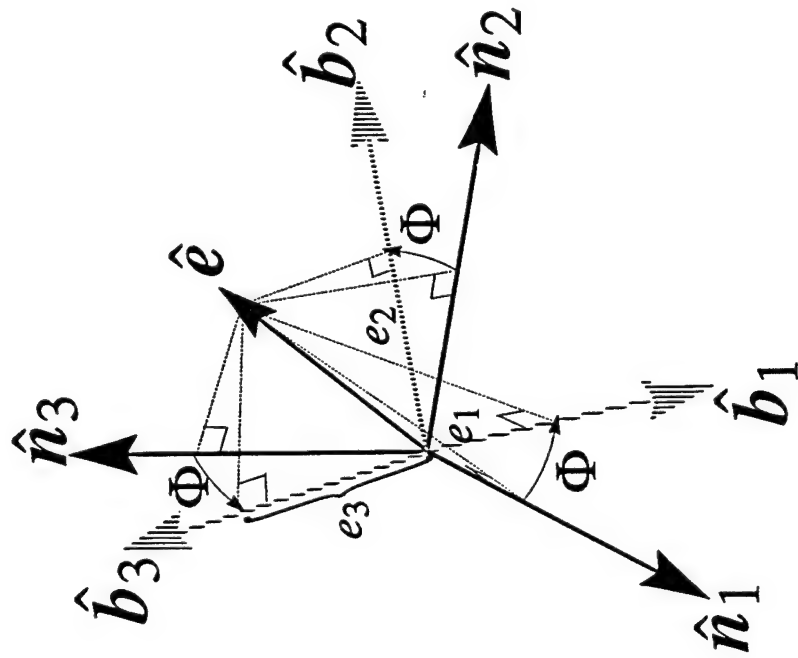
Orthog. compon. of unit vector $\hat{e}$:

$$\hat{e} = e_{b1}\hat{b}_1 + e_{b2}\hat{b}_2 + e_{b3}\hat{b}_3$$

$$\hat{e} = e_{n1}\hat{n}_1 + e_{n2}\hat{n}_2 + e_{n3}\hat{n}_3$$

$$\begin{Bmatrix} e_{b1} \\ e_{b2} \\ e_{b3} \end{Bmatrix} = [C] \begin{Bmatrix} e_{n1} \\ e_{n2} \\ e_{n3} \end{Bmatrix}$$

But, according to Euler's Prin. Rot. Thm:

$$e_{bi} = e_{ni} \equiv e_i$$

so, we conclude that

$$\begin{Bmatrix} e_1 \\ e_2 \\ e_3 \end{Bmatrix} = [C] \begin{Bmatrix} e_1 \\ e_2 \\ e_3 \end{Bmatrix}$$

$\Leftrightarrow \hat{e}$ *must be an eigenvector of* $[C]$ *corresponding to the eigenvalue of* $+1$

$$\{\hat{b}\} = [C]\{\hat{n}\}$$

144

Macroscopic Properties of Classical 'Rigid Body' Parameterizations of Orthogonal 3x3 Matrices

	#	coordinates	direction cosines	kinematic differential equation	singularities
Direction Cosines	9	c_{ij}	$C = [c_{ij}]$	$\dot{C} = -\tilde{\omega}C, \quad C^TC = I, \quad \tilde{\omega} \equiv \begin{bmatrix} 0 & -\omega_3 & \omega_2 \\ \omega_3 & 0 & -\omega_1 \\ -\omega_2 & \omega_1 & 0 \end{bmatrix}$	*none*
Euler Angles	3	$\{\phi, \theta, \psi\}$	$C = \begin{bmatrix} transcend. \\ functions \\ of\ \phi, \theta, \psi \end{bmatrix}$	$\begin{Bmatrix} \dot{\phi} \\ \dot{\theta} \\ \dot{\psi} \end{Bmatrix} = \frac{1}{\cos\theta} \begin{bmatrix} 0 & \sin\psi & \cos\psi \\ 0 & \cos\psi\cos\theta & -\sin\psi\cos\theta \\ \cos\theta & \sin\psi\sin\theta & \cos\psi\sin\theta \end{bmatrix} \begin{Bmatrix} \omega_1 \\ \omega_2 \\ \omega_3 \end{Bmatrix}$	$\theta = \pm\pi/2$
Euler Parameters	4	$\beta_i = e_i\sin\dfrac{\Phi}{2}$ $\beta_0 = \cos\dfrac{\Phi}{2}$	$C = \begin{bmatrix} quadratic \\ function \\ of\ \beta_i\text{'s} \end{bmatrix}$	$\begin{Bmatrix} \dot{\beta}_0 \\ \dot{\beta}_1 \\ \dot{\beta}_2 \\ \dot{\beta}_3 \end{Bmatrix} = \frac{1}{2} \begin{bmatrix} \beta_0 & -\beta_1 & -\beta_2 & -\beta_3 \\ \beta_1 & \beta_0 & -\beta_3 & \beta_2 \\ \beta_2 & \beta_3 & \beta_0 & -\beta_1 \\ \beta_3 & -\beta_2 & \beta_1 & \beta_0 \end{bmatrix} \begin{Bmatrix} 0 \\ \omega_1 \\ \omega_2 \\ \omega_3 \end{Bmatrix}, \quad \beta^T\beta = 1$	*none*
Rodrigues Parameters	3	$r_i = \beta_i/\beta_0$ $= e_i\tan\dfrac{\Phi}{2}$	$C = \begin{bmatrix} ratio\ of \\ quadratic \\ fcts\ of\ r_i \end{bmatrix}$	$\begin{Bmatrix} \dot{r}_1 \\ \dot{r}_2 \\ \dot{r}_3 \end{Bmatrix} = \frac{1}{2} \begin{bmatrix} 1+r_1^2 & r_1r_2 - r_3 & r_1r_3 + r_2 \\ r_1r_2 + r_3 & 1+r_2^2 & r_2r_3 - r_1 \\ r_1r_3 - r_2 & r_2r_3 + r_1 & 1+r_3^2 \end{bmatrix} \begin{Bmatrix} \omega_1 \\ \omega_2 \\ \omega_3 \end{Bmatrix}$	$\Phi = \pm\pi$
Mod. Rod. Parameters	3	$\sigma_i = \dfrac{\beta_i}{1+\beta_0}$ $= e_i\tan\dfrac{\Phi}{4}$	$C = \begin{bmatrix} ratio\ of \\ quartic \\ fcts\ of\ s_i \end{bmatrix}$	$\begin{Bmatrix} \dot{\sigma}_1 \\ \dot{\sigma}_2 \\ \dot{\sigma}_3 \end{Bmatrix} = \frac{1}{4} \begin{bmatrix} 1+\sigma_1^2-\sigma_2^2-\sigma_3^2 & 2(\sigma_1\sigma_2-\sigma_3) & 2(\sigma_1\sigma_3+\sigma_2) \\ 2(\sigma_1\sigma_2+\sigma_3) & 1-\sigma_1^2+\sigma_2^2-\sigma_3^2 & 2(\sigma_2\sigma_3-\sigma_1) \\ 2(\sigma_1\sigma_3-\sigma_2) & 2(\sigma_2\sigma_3+\sigma_1) & 1-\sigma_1^2-\sigma_2^2+\sigma_3^2 \end{bmatrix} \begin{Bmatrix} \omega_1 \\ \omega_2 \\ \omega_3 \end{Bmatrix}$	$\Phi = \pm 2\pi$

SES_2

145

Euler (Quaternion) Parameters

Introducing Euler's (1776) definitions

$$\beta_0 = \cos\frac{\Phi}{2}, \quad \beta_i = e_i \sin\frac{\Phi}{2}, \quad i = 1, 2, 3 \implies \beta^T\beta = \sum_{i=0}^{3}\beta_i^2 = 1$$

we can show* that the direction cosine matrix is given by

$$[C] = \begin{bmatrix} \beta_0^2 + \beta_1^2 - \beta_2^2 - \beta_3^2 & 2(\beta_1\beta_2 + \beta_0\beta_3) & 2(\beta_1\beta_3 - \beta_0\beta_2) \\ 2(\beta_1\beta_2 - \beta_0\beta_3) & \beta_0^2 - \beta_1^2 + \beta_2^2 - \beta_3^2 & 2(\beta_2\beta_3 + \beta_0\beta_1) \\ 2(\beta_1\beta_3 + \beta_0\beta_2) & 2(\beta_2\beta_3 - \beta_0\beta_1) & \beta_0^2 - \beta_1^2 - \beta_2^2 + \beta_3^2 \end{bmatrix}, \implies$$

$$\beta_i^2 = \frac{1}{4}(1 + 2c_{ii} - tr[C])$$

$$\beta_0\beta_1 = \frac{1}{4}(c_{23} - c_{32}), \quad \beta_2\beta_3 = \frac{1}{4}(c_{23} + c_{32})$$
$$\beta_0\beta_2 = \frac{1}{4}(c_{31} - c_{13}), \quad \beta_1\beta_3 = \frac{1}{4}(c_{31} + c_{13})$$
$$\beta_0\beta_3 = \frac{1}{4}(c_{12} - c_{21}), \quad \beta_1\beta_2 = \frac{1}{4}(c_{12} + c_{21})$$

and the kinematic differential equations can be written as

$$\begin{Bmatrix} \dot\beta_0 \\ \dot\beta_1 \\ \dot\beta_2 \\ \dot\beta_3 \end{Bmatrix} = \frac{1}{2}\begin{bmatrix} 0 & -\omega_1 & -\omega_2 & -\omega_3 \\ \omega_1 & 0 & \omega_3 & -\omega_2 \\ \omega_2 & -\omega_3 & 0 & \omega_1 \\ \omega_3 & \omega_2 & -\omega_1 & 0 \end{bmatrix}\begin{Bmatrix} \beta_0 \\ \beta_1 \\ \beta_2 \\ \beta_3 \end{Bmatrix}, \iff \begin{Bmatrix} \dot\beta_0 \\ \dot\beta_1 \\ \dot\beta_2 \\ \dot\beta_3 \end{Bmatrix} = \frac{1}{2}\begin{bmatrix} \beta_0 & -\beta_1 & -\beta_2 & -\beta_3 \\ \beta_1 & \beta_0 & -\beta_3 & \beta_2 \\ \beta_2 & \beta_3 & \beta_0 & -\beta_1 \\ \beta_3 & -\beta_2 & \beta_1 & \beta_0 \end{bmatrix}\begin{Bmatrix} 0 \\ \omega_1 \\ \omega_2 \\ \omega_3 \end{Bmatrix}$$

There are many other useful properties, such as the transformation from the 3-1-3 Euler angles:

$$\beta_0 = \cos\frac{\theta}{2}\cos\frac{\phi+\psi}{2}, \quad \beta_2 = \sin\frac{\theta}{2}\sin\frac{\phi-\psi}{2}$$
$$\beta_1 = \sin\frac{\theta}{2}\cos\frac{\phi-\psi}{2}, \quad \beta_3 = \cos\frac{\theta}{2}\cos\frac{\phi+\psi}{2}$$

* Junkins, J. and Turner, J., Optimal Spacecraft Rotational Maneuvers, Ch 2., Elsevier, 1986.

Rodrigues (Gibbs' Vector) Parameters

Introduce Rodrigues' definitions

$$r_i = \frac{\beta_i}{\beta_0} \equiv e_i \tan\frac{\Phi}{2}, \text{ or } \mathbf{r} = \hat{e}\tan\frac{\Phi}{2}, \Rightarrow \text{ note } |\mathbf{r}| \to \infty \text{ as } \Phi \to \pm\pi$$

we can show* that the direction cosine matrix is given by

$$[C] = \frac{1}{1 + r_1^2 + r_2^2 + r_3^2}\begin{bmatrix} 1 + r_1^2 - r_2^2 - r_3^2 & 2(r_1 r_2 + r_3) & 2(r_1 r_3 - r_2) \\ 2(r_1 r_2 - r_3) & 1 - r_1^2 + r_2^2 - r_3^2 & 2(r_2 r_3 + r_1) \\ 2(r_1 r_3 + r_2) & 2(r_2 r_3 - r_1) & 1 - r_1^2 - r_2^2 + r_3^2 \end{bmatrix}$$

and the kinematic differential equations can be written as

$$\begin{Bmatrix} \dot{r}_1 \\ \dot{r}_2 \\ \dot{r}_3 \end{Bmatrix} = \frac{1}{2}\begin{bmatrix} 1 + r_1^2 & r_1 r_2 - r_3 & r_1 r_3 + r_2 \\ r_1 r_2 + r_3 & 1 + r_2^2 & r_2 r_3 - r_1 \\ r_1 r_3 - r_2 & r_2 r_3 + r_1 & 1 + r_3^2 \end{bmatrix}\begin{Bmatrix} \omega_1 \\ \omega_2 \\ \omega_3 \end{Bmatrix}$$

---

* *Junkins, J. and Kim, Y., Dynamics and control of Flexible Structures, Ch 2., AIAA, 1993.*

147

Modified Rodrigues Parameters

Following Modi and Tsiotras, introduce the parameters

$$\sigma_i = \frac{\beta_i}{1+\beta_0} \equiv e_i tan\frac{\Phi}{4}, \quad or \quad \underline{\sigma} = \hat{e}\,tan\frac{\Phi}{4}, \quad \Rightarrow \quad note\,|\underline{\sigma}| \to \infty \; as \; \Phi \to \pm 2\pi$$

Notice that there are two sets of $\underline{\sigma}$ vectors, corresponding to the fact that $\underline{\beta}$ and $-\underline{\beta}$ parameterize the same physical orientation.

We can show that the direction cosine matrix is given by

$$[C] = \frac{1}{(1+\underline{\sigma}^T\underline{\sigma})^2}\begin{bmatrix} (1-\underline{\sigma}^T\underline{\sigma})^2+4(\sigma_1^2-\sigma_2^2-\sigma_3^2) & 4\sigma_3(1-\underline{\sigma}^T\underline{\sigma})+8\sigma_1\sigma_2 & -4\sigma_2(1-\underline{\sigma}^T\underline{\sigma})+8\sigma_1\sigma_3 \\ -4\sigma_3(1-\underline{\sigma}^T\underline{\sigma})+8\sigma_1\sigma_2 & (1-\underline{\sigma}^T\underline{\sigma})^2+4(-\sigma_1^2+\sigma_2^2-\sigma_3^2) & 4\sigma_1(1-\underline{\sigma}^T\underline{\sigma})+8\sigma_2\sigma_3 \\ 4\sigma_2(1-\underline{\sigma}^T\underline{\sigma})+8\sigma_1\sigma_3 & -4\sigma_1(1-\underline{\sigma}^T\underline{\sigma})+8\sigma_2\sigma_3 & (1-\underline{\sigma}^T\underline{\sigma})^2+4(-\sigma_1^2-\sigma_2^2+\sigma_3^2) \end{bmatrix}$$

and the kinematic differential equations can be written as

$$\begin{Bmatrix} \dot{\sigma}_1 \\ \dot{\sigma}_2 \\ \dot{\sigma}_3 \end{Bmatrix} = \frac{1}{4}\begin{bmatrix} 1+\sigma_1^2-\sigma_2^2-\sigma_3^2 & 2(\sigma_1\sigma_2-\sigma_3) & 2(\sigma_1\sigma_3+\sigma_2) \\ 2(\sigma_1\sigma_2+\sigma_3) & 1-\sigma_1^2+\sigma_2^2-\sigma_3^2 & 2(\sigma_2\sigma_3-\sigma_1) \\ 2(\sigma_1\sigma_3-\sigma_2) & 2(\sigma_2\sigma_3+\sigma_1) & 1-\sigma_1^2-\sigma_2^2+\sigma_3^2 \end{bmatrix}\begin{Bmatrix} \omega_1 \\ \omega_2 \\ \omega_3 \end{Bmatrix}$$

Well, so what? How does all of this generalize to something other than rigid body dynamics?

Consider the following theorem* due to Cayley (Cayley Transform):

Let C denote an nxn orthogonal matrix and let $Q = -Q^T$ name a related nxn skew symmetric matrix, then the following relationship holds:

Forward Transformation:

$$C = (I - Q)(I + Q)^{-1} \quad (1)$$

$$C = (I + Q)^{-1}(I - Q) \quad (2)$$

Inverse Transformation:

$$Q = (I - C)(I + C)^{-1} \quad (3)$$

$$Q = (I + C)^{-1}(I - C) \quad (4)$$

These are beautiful equations! It is easy to verify, for the 3x3 case, that taking

$$Q = \tilde{r} = \begin{bmatrix} 0 & -r_3 & r_2 \\ r_3 & 0 & -r_1 \\ -r_2 & r_1 & 0 \end{bmatrix}$$

immediately generates the classical Rodrigues parameters equation for the direction cosine matrix and the inverse thereof. Hmmmm!

---

* *Junkins, J. and Kim, Y., Dynamics and control of Flexible Structures, Ch 2., AIAA, 1993.*

Kinematics of nxn Rotations

We can show* that nxn orthogonal matrices evolve according to

$$\dot{C} = -\tilde{\omega}C, \quad C^T C = I$$

where the 'generalized angular velocity' matrix $\tilde{\omega}$ can be related to the skew-symmetric parameter matrix Q and its time derivative by

$$\tilde{\omega} = 2(I+Q)^{-1}\dot{Q}(I-Q)^{-1}$$

$$\dot{Q} = \frac{1}{2}(I+Q)\tilde{\omega}(I-Q)$$

and where

$$C = (I-Q)(I+Q)^{-1} = (I+Q)^{-1}(I-Q)$$

$$Q = (I-C)(I+C)^{-1} = (I+C)^{-1}(I-C)$$

It is easy to verify* that these same equations hold for the 3x3 special case, & are in fact, identical to the eqns. for the Rodrigues parameters. Well, very nice, but what are these higher dimensional equations good for?

---

* Junkins, J. and Kim, Y., Dynamics and control of Flexible Structures, Ch 2., AIAA, 1993.

Spectral Parameterization of nxn Symmetric Matrices

An arbitrary symmetric positive matrix P has the spectral decomposition

$$P = C\Lambda C^T, \quad \Lambda = diag\{\lambda_1, ..., \lambda_n\}, \quad C^T C = I$$

Notice that the 'shape' of P is uniquely captured by the eigenvalues Λ, and the orientation of the principal axes is captured (redundantly) by the columns C, which are the corresponding eigenvectors of P.

Further notice that a minimal parameter representation of directions of the eigenvectors is available. We can parameterize the eigenvector matrix using the Cayley transform.

$$C = (I - Q)(I + Q)^{-1} = (I + Q)^{-1}(I - Q)$$

$$Q = (I - C)(I + C)^{-1} = (I + C)^{-1}(I - C)$$

Notice, if $P = P(t)$ is time varying, then a very attractive 'minimal' coordinate set is $\Lambda(t)$ and $Q(t)$.

In particular, if P(t) satisfies a differential equation, then, we can transform the differential eqn. for P(t) into new eqns. for $\Lambda(t)$ and $Q(t)$. This 'time varying spectral decomposition' seems elegant and attractive. An example ...

Example: Transformation of Matrix Riccati Equation

A frequently occuring diff. eqn. in optimal control and optimal estimation is the Matrix Riccati Equation:

$$\dot{P} + A^T P + PA - PW_1 P + W_2 = 0, \quad W_i = W_i^T > 0$$

The solution for $P(t)$, a sym. pos. def. matrix, is not-trivial, this eqn. is often stiff. Notice that there are n^2 diff. eqns, even though $P = P^T$. Introducing a coordinate transformation: $P(t) = C\Lambda C^T$, we can seek $C(t)$ and $\Lambda(t)$. Since we can use the Cayley transform to express C as a fct of $Q = -Q^T$, then we can reduce the # of variables from n^2 to $n(n+1)/2$, the n elements of Λ, plus the $n(n-1)/2$ distinct elements of Q.

The transformed differential equations are tedious to derive but have the form:

$$\dot{Q} = \frac{1}{2}(I + Q)\tilde{\omega}(I - Q), \quad \dot{\Lambda} = C^T \dot{P} C, \quad P = C\Lambda C^T$$

$$C = [\underline{C}_1 \, \underline{C}_2 \cdots \underline{C}_n], \quad C = (I - Q)(I + Q)^{-1} \quad \Leftrightarrow \quad Q = (I - C)(I + C)^{-1}$$

$$\tilde{\omega}_{ii} = 0, \quad \tilde{\omega}_{ij} = \left(\frac{1}{\lambda_j - \lambda_i}\right)\underline{C}_j^T \dot{P} \underline{C}_i, \quad for \, j > i$$

These eqns may look messy, and they are! They also behave poorly near repeated eigenvalues of P, but they are attractive conceptually!

SES.

152

Macroscopic Properties of n-Dimensional Parameterizations of Orthogonal Matrices

R^3 interpretation	R^n generalizations
Direction Cosines c_{ij} direction cosines	$\dot{C} = -\tilde{\omega}C, \quad C^T C = I, \quad \tilde{\omega} = -\tilde{\omega}^T$
Rodrigues Parameters $r_i = \beta_i/\beta_0$ $= e_i \tan\dfrac{\Phi}{2}$	$C = (I-Q)(I+Q)^{-1} = (I+Q)^{-1}(I-Q), \quad Q = -Q^T$ $Q = (I-C)(I+C)^{-1} = (I+C)^{-1}(I-C), \quad C^T C = I$
Mod. Rod. Parameters $\sigma_i = \dfrac{\beta_i}{1+\beta_0}$ $= e_i \tan\dfrac{\Phi}{4}$	$C = (I-S)^2(I+S)^{-2} = (I+S)^{-2}(I-S)^2, \quad S = -S^T$ $S = (I-M)(I+M)^{-1} = (I+M)^{-1}(I-M), \quad M^2 = C$
Euler Parameters $\beta_i = e_i \sin\dfrac{\Phi}{2}$ $\beta_0 = \cos\dfrac{\Phi}{2}$	$C = (\beta_0 I - B)(\beta_0 I + B)^{-1} = (\beta_0 I + B)^{-1}(\beta_0 I - B), B = -B^T, B = \beta_0 R$ $\displaystyle\sum_{j=0}^m \beta_j^2 = 1, \; \{\beta_1,...,\beta_m\}$ are the $m = n\dfrac{(n-1)}{2}$ distinct elements of B.

Concluding Remarks

Parameterizations of 3x3 orthogonal projection matrices

Classical Rigid Body *Principal Rotation Coordinates*
Euler Parameters, Rodrigues Parameters, Modified Rod. Parameters

Advantages of Principal Rotation Coordinates:

less intensive computationally   `<=>`   *more nearly linear equations*
regularized differential equations   `<=>`   *elimination of singularities*
derivation of globally stable control laws feasible, ...

Generalizations to nxn orthogonal matrices

Cayley's Transform   `<=>`   *Generalizes Rodrigues Parameters*
Two new results
Generalization of the Modified Rodrigues Parameters for nxn matrices
Generalization of 'Euler Parameters' for nxn matrices

Approach for Parameterization of nxn Positive Definite Matrix

Covariance Matrices, Weight Matrices, Solutions of Riccati Eqns, ...

Thank you Cayley et al, for leaving me a few fun things to do!!

Principal Rotation Representations of Proper $N \times N$ Orthogonal Matrices

Hanspeter Schaub
Panagiotis Tsiotras
John L. Junkins

Principal Rotation Representations of Proper NxN Orthogonal Matrices

Hanspeter Schaub
Panagiotis Tsiotras
John L. Junkins

Abstract

Three and four parameter representations of 3x3 orthogonal matrices are extended to the general case of proper NxN orthogonal matrices. These developments generalize the classical Rodrigues parameters, the Euler parameters, and the recently introduced modified Rodrigues parameters to higher dimensional spaces. The developments presented are motivated by, and significantly generalize and extend the classical result known as the Cayley transformation.

Introduction

It is well known in rigid body dynamics, and many other areas of Euclidean analysis, that the rotational coordinates associated with Euler's Principal Rotation Theorem [1,2,3] lead to especially attractive descriptions of rotational motion. These parameterizations of proper orthogonal 3x3 matrices include the four-parameter set known widely as the *Euler (quaternion) parameters* [1,2,3], as well as the classical three-parameter set known as the *Rodrigues parameters* or *Gibbs vector* [1,2,3,4]. Also included is a recently introduced three parameter description known as the *modified Rodrigues parameters* [4,5,6]. As we review briefly below, these parameterizations are of fundamental significance in the geometry and kinematics of three-dimensional motion. Briefly, their advantages are as follows:

Euler Parameters: This once redundant four-parameter description of three-dimensional rotational motion maps all possible motions into arcs on a four-dimensional unit sphere. This accomplishes a regularization and the representation is universally nonsingular. The kinematic differential equations contain no transcendental functions and are bi-linear without approximation.

Classical Rodrigues Parameters: This three parameter set, also referred to as the *Gibbs vector*, is proportional to Euler's principal rotation vector. The magnitude is $tan(\phi/2)$, with ϕ being the principal rotation angle. These parameters are singular at $\phi = \pm\pi$ and have elegant, quadrati-

cally nonlinear differential kinematic equations.

Modified Rodrigues Parameters: This three parameter set is also proportional to Euler's principal rotation vector, but with a magnitude of $tan(\phi/4)$. The singular orientation is at $\phi = \pm 2\pi$, doubling the principal rotation range over the classical Rodrigues parameters. They also have a quadratic nonlinearity in their differential kinematic equations.

The question naturally arises; can these elegant principal rotation parameterizations be extended to orthogonal projections in higher dimensional spaces? Cayley partially answered this question in the affirmative; his "Cayley Transform" fully extends the classical Rodrigues parameters to higher dimensional spaces [1,2,7]. A proper NxN orthogonal matrix can be generally parameterized by a vector with dimension $M = \frac{1}{2}N(N-1)$. Only for the 3x3 case is N equal to M. Any proper orthogonal matrix has a determinant of +1 and can be interpreted as analogous to a rigid body rotation representation. This paper extends the classical Cayley transform to parameterize a proper NxN orthogonal matrix into a set of M-dimensional modified Rodrigues parameters. Further, a method is shown to parameterize the NxN matrix into a once-redundant set of (M+1)-dimensional Euler parameters.

The first section will review the Euler, Rodrigues and the modified Rodrigues parameters for the 3x3 case, generalized later in this paper to parameterize the proper NxN orthogonal matrices. The second section will review the classical Cayley transform resulting with the representation of a proper orthogonal matrix using the Rodrigues parameters, followed by the new representation of the NxN orthogonal matrices using an M-dimensional set of modified Rodrigues parameters, and finally, a new representation of the NxN orthogonal matrices using an (M+1)-dimensional Euler parameters.

Review of Three-Dimensional Rigid Body Rotation Parameterizations

The Direction Cosine Matrix

The 3x3 direction cosine matrix C completely describes any three-dimensional rigid body rotation. The matrix elements are bounded between ±1 and possess no singularities. The famous Poisson kinematic differential equation for the direction cosine matrix is:

$$\dot{C} = -[\tilde{\omega}]C \tag{1}$$

where the tilde matrix is defined as

$$[\tilde{\omega}] = \begin{bmatrix} 0 & -\omega_3 & \omega_2 \\ \omega_3 & 0 & -\omega_1 \\ -\omega_2 & \omega_1 & 0 \end{bmatrix} \tag{2}$$

The direction cosine matrix C is orthogonal, therefore it satisfies the following constraint.

$$C^T C = CC^T = I \tag{3}$$

This constraint causes the direction cosine matrix representation to be highly redundant. Instead of considering all nine matrix elements, it usually suffices to parameterize the matrix into a set of three or four parameters. However, any minimal set of three parameters will contain singular orientations.

The constraint in equation (3) shows that besides being orthogonal, the direction cosine matrix is also normal [8]. Consequently it has the spectral decomposition

$$C = U\Lambda U^* \tag{4}$$

where U is a unitary matrix containing the orthonormal eigenvectors of C, and Λ is a diagonal matrix whose entries are the eigenvalues of C. The * symbol stands for the adjoint operator, which takes the complex conjugate transpose of a matrix. Since C represents a rigid body rotation, it always has a determinant of +1.

The Principal Rotation Vector

Euler's principal rotation theorem states that in a three-dimensional space, a rigid body (reference frame) can be brought from an arbitrary initial orientation to an arbitrary final orientation by a single principal rotation (ϕ) about a principal line $\hat{e}$ [3].
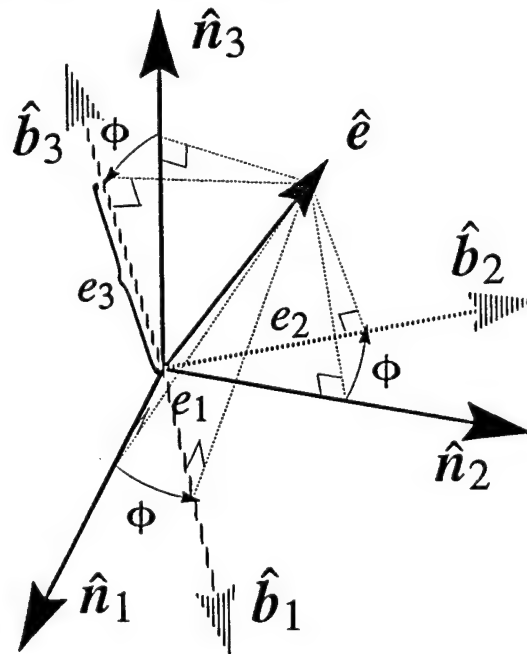
Fig. 1: Euler's Principal Rotation Theorem.

With reference to Fig. 1, the body axis $\hat{b}_i$ components of the principal line $\hat{e}$ are identical to the spatial components projected onto $\hat{n}_i$.

$$\begin{Bmatrix} e_1 \\ e_2 \\ e_3 \end{Bmatrix} = \hat{e} = C \cdot \hat{e} \tag{5}$$

Therefore $\hat{e}$ must be an eigenvector of the 3x3 C matrix with a corresponding eigenvalue of +1. If the 3x3 C matrix has an eigenvalue of -1, the matrix represents a reflection, not a proper rotation and the principal rotation theorem does not hold. In this case the $det(C)$ would be +1. The *principal rotation vector* $\bar{\gamma}$ is defined as:

$$\bar{\gamma} = \phi\hat{e} \tag{6}$$

Let us now consider the case where a rigid body performs a pure single-axis rotation about the fixed $\hat{e}$. This rotation axis is identical to Euler's principal line of rotation $\hat{e}$. Let the rotation angle be ϕ. The angular velocity vector for this case becomes:

$$\bar{\omega} = \dot{\phi}\hat{e} \tag{7}$$

or in matrix form:

$$[\tilde{\omega}] = \dot{\phi}[\tilde{e}] \tag{8}$$

Substituting equation (8) into (1), one obtains the following development.

$$\frac{dC}{dt} = -\frac{d\phi}{dt}[\tilde{e}]C$$

$$\frac{dC}{d\phi} = -[\tilde{e}]C$$

$$C = e^{-\phi[\tilde{e}]} \tag{9}$$

The last step follows since the $[\tilde{e}]$ matrix is constant during this single axis maneuver. Due to Euler's principal rotation theorem, however, any arbitrary rotation can always be described instantaneously by the equivalent single-axis principal rotation. Hence equation (9) will hold at any instant for an arbitrary time-varying direction cosine matrix C. However, ϕ and $\hat{e}$ must be considered time-varying functions. Using the following substitution

$$[\bar{\gamma}] = \phi[\tilde{e}] \tag{10}$$

equation (9) can be rewritten as [2]

$$C = e^{-[\tilde{\gamma}]} = \sum_{n=0}^{\infty} \frac{1}{n!} (-[\tilde{\gamma}])^n \tag{11}$$

Instead of using an infinite matrix power series expansion of equation (11) to find C, the elegant finite transformation shown below can be used [2]. That is, the evaluation of $e^{-[\tilde{\gamma}]}$ does not require the spectral decomposition of $[\tilde{\gamma}]$, but can be written directly in term of $\bar{\gamma}$ itself. Unfortunately, this transformation only holds for the 3x3 case. A general transformation for the NxN case is unknown at this point, at least as far as the authors know.

$$e^{-[\tilde{\gamma}]} = I\cos\phi - [\bar{e}]\sin\phi - \hat{e}\hat{e}^T(\cos\phi - 1) \tag{12}$$
$$\phi = \|\bar{\gamma}\|, \quad \hat{e} = \bar{\gamma}/\phi$$

To find the inverse transformation from the direction cosine matrix C to $[\tilde{\gamma}]$, the matrix logarithm can be taken of equation (11) to obtain

$$[\tilde{\gamma}] = -\log C = \sum_{n=1}^{\infty} \frac{1}{n} (I - C)^n \tag{13}$$

Using the spectral decomposition of C given in equation (4), the above equation can be rewritten as

$$[\tilde{\gamma}] = -\log(U\Lambda U^*) = -U(\log\Lambda)U^* \tag{14}$$

where calculating the matrix logarithm of a diagonal matrix becomes trivial. Since all eigenvalues of an orthogonal matrix have unit norm, the matrix logarithm in equation (14) is defined everywhere except when an eigenvalue is -1. Generally, equation (14) will return a $[\tilde{\gamma}]$ which corresponds to a principal rotation angle ϕ in (-180°,+180°). Note however, that when C has eigenvalues of -1, equation (14) does not return a skew-symmetric matrix. The transformation breaks down here for this singular event. The geometric interpretation is that a 180° rotation has been performed about one axis (leading to one positive and two negative eigenvalues of C), which is the only rotation not covered by the domain of equation (14).

The principal vector representation of C is not unique. Adding or subtracting 2π from the principal rotation angle ϕ describes the same rotation. As expected, equation (11) will always yield the same C matrix for the different principal rotation angles, since all angles correspond to the same physical orientation. However, the inverse transformation given in equation (14) yields only the principal rotation angle which lies between -180° and +180°.

As do all minimal parameter sets, the principal rotation vector parameterization has a singular orientation. The vector is not uniquely defined for a zero rotation from the reference frame. The

principal rotation vector parameterization will be found convenient, however, to derive useful relationships.

The Euler (Quaternion) Parameters

The Euler parameters are a once-redundant set of rotation parameters. They are defined in terms of the principal rotation angle ϕ and the principal line components e_i as follows:

$$\beta_0 = \cos\frac{\phi}{2}, \quad \beta_i = e_i\sin\frac{\phi}{2} \quad i = 1, 2, 3 \tag{15}$$

They satisfy the holonomic constraint:

$$\beta_0^2 + \beta_1^2 + \beta_2^2 + \beta_3^2 = 1 \tag{16}$$

Equation (16) states that all possible Euler parameter trajectories generate arcs on the surface of a four-dimensional unit hypersphere. This behavior bounds the parameters to values between ± 1. However, the Euler parameters are not unique. The mirror image trajectories $\beta(t)$ and $-\beta(t)$ both describe the identical physical orientation histories. Given a 3x3 orthogonal matrix, there will be two corresponding sets of Euler parameters which differ by a sign. The Euler parameters are the only set of rotation parameters which have a bi-linear system of kinematic differential equations [1], other than the direction cosine matrix itself, as follows

$$\begin{Bmatrix} \dot{\beta}_0 \\ \dot{\beta}_1 \\ \dot{\beta}_2 \\ \dot{\beta}_3 \end{Bmatrix} = \frac{1}{2}\begin{bmatrix} \beta_0 & -\beta_1 & -\beta_2 & -\beta_3 \\ \beta_1 & \beta_0 & -\beta_3 & \beta_2 \\ \beta_2 & \beta_3 & \beta_0 & -\beta_1 \\ \beta_3 & -\beta_2 & \beta_1 & \beta_0 \end{bmatrix}\begin{Bmatrix} 0 \\ \omega_1 \\ \omega_2 \\ \omega_3 \end{Bmatrix} \tag{17}$$

It is also of significance that the above 4x4 matrix is orthogonal, so "transportation" between ω_i's and $\dot{\beta}_i$'s is "painless". The direction cosine matrix in term of the Euler parameters is [1,3]

$$[C] = \begin{bmatrix} \beta_0^2 + \beta_1^2 - \beta_2^2 - \beta_3^2 & 2(\beta_1\beta_2 + \beta_0\beta_3) & 2(\beta_1\beta_3 - \beta_0\beta_2) \\ 2(\beta_1\beta_2 - \beta_0\beta_3) & \beta_0^2 - \beta_1^2 + \beta_2^2 - \beta_3^2 & 2(\beta_2\beta_3 + \beta_0\beta_1) \\ 2(\beta_1\beta_3 + \beta_0\beta_2) & 2(\beta_2\beta_3 - \beta_0\beta_1) & \beta_0^2 - \beta_1^2 - \beta_2^2 + \beta_3^2 \end{bmatrix} \tag{18}$$

The Euler parameters have several advantages over all minimal sets of rotation parameters. Namely, they are bounded between ± 1, never encounter a singularity, and have linear kinematic differential equations if the $\omega_i(t)$ are considered known. All of these advantages are slightly offset by the cost of having one extra parameter.

The Classical Rodrigues Parameters

The classical Rodrigues parameter vector $\bar{q}$ can be interpreted as the coordinates resulting from a stereographic projection of the four-dimensional Euler parameter hypersphere onto a three-dimensional hyperplane [6], with the projection point at the origin and the stereographic mapping hyperplane at $\beta_0 = +1$. As discussed in [6], it follows that they have their singular orientation at a principal rotation angle of $\phi = \pm 180°$ from the reference. Their transformation from the Euler parameters is

$$q_i = \frac{\beta_i}{\beta_0} \qquad i = 1, 2, 3 \tag{19}$$

Unlike the Euler parameters, the Rodrigues parameters are unique. The q_i uniquely define a rotation on the open range of $(-180°, +180°)$ [6]; as is evident in equation (19), reversing the sign of the Euler parameters has no effect on the q_i. Using equation (15), the classical Rodrigues parameters can also be defined directly in terms of the principal rotation angle and the principal axis components as

$$q_i = e_i \tan \frac{\phi}{2} \qquad i = 1, 2, 3 \tag{20}$$

It is apparent that $\bar{q}$ has the same direction as the principal rotation and the magnitude is $tan(\phi/2)$. The singular condition of $\phi = \pm 180°$ is evident by inspection of equation (20). The kinematic differential equation for the Rodrigues parameters contain a quadratic nonlinear dependence on the q_i. They can be verified from equations (17,20) to be [1-4]

$$\begin{Bmatrix} \dot{q}_1 \\ \dot{q}_2 \\ \dot{q}_3 \end{Bmatrix} = \frac{1}{2} \begin{bmatrix} 1 + q_1^2 & q_1 q_2 - q_3 & q_1 q_3 + q_2 \\ q_2 q_1 + q_3 & 1 + q_2^2 & q_2 q_3 - q_1 \\ q_3 q_1 - q_2 & q_3 q_2 + q_1 & 1 + q_3^2 \end{bmatrix} \begin{Bmatrix} \omega_1 \\ \omega_2 \\ \omega_3 \end{Bmatrix} \tag{21}$$

Notice that the above coefficient matrix is not orthogonal, although the inverse is well behaved everywhere except at $\phi = \pm 180°$ where $|\bar{q}| \to \infty$. The direction cosine matrix in terms of the Rodrigues parameters is [1-4]:

$$C(\bar{q}) = \frac{1}{1 + q_1^2 + q_2^2 + q_3^2} \begin{bmatrix} 1 + q_1^2 - q_2^2 - q_3^2 & 2(q_1 q_2 + q_3) & 2(q_1 q_3 - q_2) \\ 2(q_2 q_1 - q_3) & 1 - q_1^2 + q_2^2 - q_3^2 & 2(q_2 q_3 + q_1) \\ 2(q_3 q_1 + q_2) & 2(q_3 q_2 - q_1) & 1 - q_1^2 - q_2^2 + q_3^2 \end{bmatrix} \tag{22}$$

The Modified Rodrigues Parameters

The modified Rodrigues parameter vector $\bar{\sigma}$ is also a set of stereographic parameters, closely related to the classical Rodrigues parameters [2,4-6]. The modified Rodrigues parameters have

the projection point at (-1,0,0,0) and the stereographic mapping hyperplane at $\beta_0 = 0$. This projection results in a set of parameters which do not encounter a singularity until a principal rotation from the reference frame of $\pm 360°$ has been performed. Therefore they are able to describe any rotation except a complete revolution $\pm 360°$. Their transformation from the Euler parameters is

$$\sigma_i = \frac{\beta_i}{1 + \beta_0} \qquad i = 1, 2, 3 \qquad (23)$$

While the classical Rodrigues parameters have a singularity at $\beta_0=0$ ($\phi = \pm 180°$), the modified Rodrigues parameters have moved the singularity out to a *single point* at $\beta_0=-1$ ($\phi = \pm 360°$). Figure 2 below illustrates these two singular conditions. Since the classical Rodrigues parameters are only defined for $-180° < \phi < +180°$, they can only describe rotations on the upper hemisphere of the four-dimensional unit hyper-sphere where $\beta_0 > 0$. However, the modified Rodrigues parameters can describe any rotation on this hypersphere except the point $\beta_0=-1$. Therefore the modified Rodrigues parameters have twice the nonsingular range as the classical Rodrigues parameters.

4D Unit Hyper-Sphere
with $\beta_0^2+\beta_1^2+\beta_2^2+\beta_3^2=1$
$\beta_0 = +1$
β_0-axis
origin
$\beta_0 = -1$
(Modified Rodrigues
Parameter singularity point)
$\beta_0 = 0$
(Rodrigues Parameter
singularity surface)
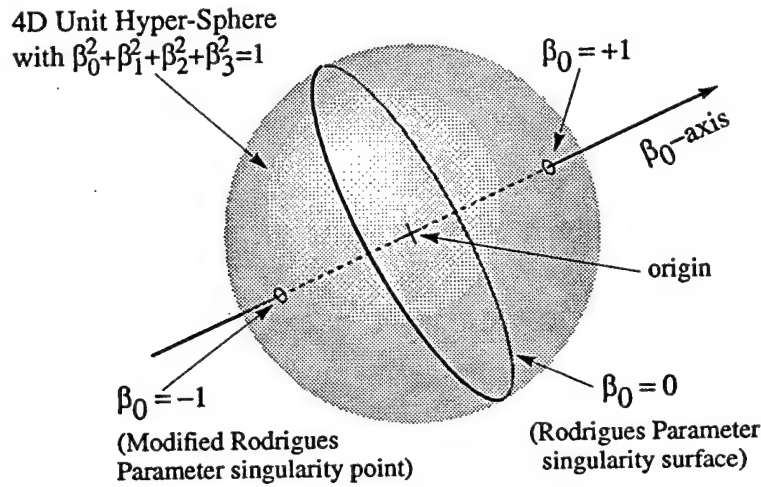
Fig. 2.: Illustration of the Singular Conditions of the Classical and
the Modified Rodrigues Parameters.

Like the Euler parameters, the modified Rodrigues parameters are not unique. They have an associated "shadow" set found by using $-\beta(t)$ instead of $\beta(t)$ in equation (23) [5,6]. The transformation from the original set to the "shadow" set is [2,5,6]

$$\sigma_i^S = \frac{-\sigma_i}{\vec{\sigma}^T \vec{\sigma}} \qquad i = 1, 2, 3 \qquad (24)$$

The "shadow" points are denoted with a superscript S merely to differentiate them from σ_i. Keep in mind that both $\vec{\sigma}$ and $\vec{\sigma}^S$ describe the same physical orientation, similar and related to the case of the two possible sets of Euler parameter and the principal rotation vector. It turns out that

the modified Rodrigues "shadow" vector $\bar{\sigma}^S(t)$ has the opposite singular behavior to the original vector $\bar{\sigma}(t)$. The original parameters have differential kinematic equations which are very linear near a zero rotation and are singular at a $\pm360°$ rotation. On the other hand, the "shadow" parameters have differential kinematic equations which are linear near the $\pm360°$ rotation and singular at the zero rotation. [6] Using equation (15), the definition for the modified Rodrigues parameters in equation (23) can be rewritten as [4]

$$\sigma_i = e_i \tan\frac{\Phi}{4} \qquad (25)$$

Equation (25) is very similar to equation (20), except for the scaling factor of the principal rotation angle. The singularity at $\pm360°$ is evident in equation (25), and small rotations behave like quarter angles. All three parameter representations must possess a singularity. This set maximizes the nonsingular principal rotation range to $\pm360°$. The following differential kinematic equations display a similar degree of quadratic nonlinearity as do the corresponding equations in terms of the classical Rodrigues parameters [4-6]

$$\dot{\bar{\sigma}} = \frac{1}{4}\begin{bmatrix} 1+\sigma_1^2-\sigma_2^2-\sigma_3^2 & 2(\sigma_1\sigma_2-\sigma_3) & 2(\sigma_1\sigma_3+\sigma_2) \\ 2(\sigma_2\sigma_1+\sigma_3) & 1-\sigma_1^2+\sigma_2^2-\sigma_3^2 & 2(\sigma_2\sigma_3-\sigma_1) \\ 2(\sigma_3\sigma_1-\sigma_2) & 2(\sigma_3\sigma_2+\sigma_1) & 1-\sigma_1^2-\sigma_2^2+\sigma_3^2 \end{bmatrix}\begin{Bmatrix} \omega_1 \\ \omega_2 \\ \omega_3 \end{Bmatrix} \qquad (26)$$

Note that the coefficient matrix of the differential kinematic equation is not orthogonal, but almost. Multiplying it with its transpose yields a *scalar* $\left(1+\bar{\sigma}^T\bar{\sigma}\right)^2$ times the identity matrix. As far as we know, this is the *only* three parameter representation possessing this elegant property; further attesting to the uniqueness and importance of the modified Rodrigues parameterization. This almost orthogonal behavior allows for a simple transformation between the ω_i and the $\dot{\sigma}_i$

$$C(\bar{\sigma}) = \frac{1}{\left(1+\bar{\sigma}^T\bar{\sigma}\right)^2}\begin{bmatrix} 4\left(\sigma_1^2-\sigma_2^2-\sigma_3^2\right)+\Sigma^2 & 8\sigma_1\sigma_2+4\sigma_3\Sigma & 8\sigma_1\sigma_3-4\sigma_2\Sigma \\ 8\sigma_2\sigma_1-4\sigma_3\Sigma & 4\left(-\sigma_1^2+\sigma_2^2-\sigma_3^2\right)+\Sigma^2 & 8\sigma_2\sigma_3+4\sigma_1\Sigma \\ 8\sigma_3\sigma_1+4\sigma_2\Sigma & 8\sigma_3\sigma_2-4\sigma_1\Sigma & 4\left(-\sigma_1^2-\sigma_2^2+\sigma_3^2\right)+\Sigma^2 \end{bmatrix} \qquad (27)$$
$$\Sigma = 1-\bar{\sigma}^T\bar{\sigma}$$

The direction cosine matrix is shown above [6,9]. It has a slightly higher degree of nonlinearity than the corresponding direction cosine matrix in terms of the classical Rodrigues parameters.

Parameterization of Proper NxN Orthogonal Matrices

A proper orthogonal matrix is an orthogonal matrix whose determinant is +1. Some aspects of parameterizing proper NxN orthogonal matrices into M-dimensional Rodrigues parameters have been studied recently by Junkins and Kim [1] and Shuster [2]. Keep in mind that M =

½N(N-1). These classical developments, generalizing the Rodrigues parameters to NxN proper rotation matrices, date from the work of Cayley [7] and are included below for comparative purposes with the new representations.

Any NxN orthogonal matrix abides by the constraint given in equation (3). This equation is an exact integral of equation (1), as can be verified by differentiation of equation (3) to obtain

$$\dot{C}^T C + C^T \dot{C} = 0 \tag{28}$$

The $\dot{C}$ matrix defined in equation (1) can be shown to satisfy this condition exactly. Substitute equation (1) into (27) and expand as follows

$$(-[\tilde{\omega}]C)^T C + C^T (-[\tilde{\omega}]C) = 0$$

$$(-C^T[\tilde{\omega}]^T)C - C^T[\tilde{\omega}]C = 0$$

$$C^T(-[\tilde{\omega}]^T - [\tilde{\omega}])C = 0$$

The above statement is obviously satisfied if $[\tilde{\omega}]$ is a skew-symmetric matrix, e.g. $[\tilde{\omega}] = -[\tilde{\omega}]^T$. Consequently equation (1) will generate an NxN orthogonal matrix, as long as $[\tilde{\omega}]$ is skew-symmetric and the initial condition $C(t=0)$ is orthogonal. This observation allows for the evolution of NxN orthogonal matrices to be viewed as higher dimensional direction cosine matrices, somewhat analogous to the motion generated by a "higher dimensional rigid body rotation," and also suggests parameterization of of higher dimensional rigid body-motivated rotation parameters.

Higher Dimensional Classical Rodrigues Parameters

Cayley's transformation [7] parameterizes a proper orthogonal matrix C as a function of a skew-symmetric matrix Q; these elegant transformations are

$$C = (I-Q)(I+Q)^{-1} = (I+Q)^{-1}(I-Q) \tag{29a}$$

$$Q = (I-C)(I+C)^{-1} = (I+C)^{-1}(I-C) \tag{29b}$$

The Cayley's transformation is one-to-one and onto from the set of skew-symmetric matrices to the set of proper orthogonal matrices with no eigenvalues at -1. Notice the remarkable truth that the forward and inverse transformations are identical. The transformation in equation (29b) fails if any of the eigenvalues of C are -1, because the $I+C$ matrix becomes singular and is thus not invertible. The Cayley transformation in equation (29a) produces only proper orthogonal matrices C with $det(C)=+1$. This can be verified by examining the determinant of C as shown below. Using equation (29a), $det(C)$ can be expressed as

$$\det(C) = \det(I-Q)\det\left((I+Q)^{-1}\right) = \frac{\det(I-Q)}{\det(I+Q)}$$

Since the Q matrix is skew-symmetric, it has purely imaginary complex conjugate pairs of eigenvalues of the form $\pm i\lambda_j$. Let R be the corresponding eigenvector matrix to Q. Multiplying and dividing the above equation by $\det(R)$ yields

$$\det(C) = \frac{\det(R)\det(I-Q)/\det(R)}{\det(R)\det(I+Q)/\det(R)} = \frac{\det(R)\det(I-Q)\det(R^{-1})}{\det(R)\det(I+Q)\det(R^{-1})}$$

$$\det(C) = \frac{\det(R(I-Q)R^{-1})}{\det(R(I+Q)R^{-1})} = \frac{\det(I-RQR^{-1})}{\det(I+RQR^{-1})}$$

where the RQR^{-1} term is a diagonal matrix containing the eigenvalues of the Q matrix. Since the determinant of a matrix is the product of all the eigenvalues, the above can be written as

$$\det(C) = \frac{\prod_{j=1}^{p}(1-i\lambda_j)(1+i\lambda_j)}{\prod_{j=1}^{p}(1+i\lambda_j)(1-i\lambda_j)} = \frac{\prod_{j=1}^{p}(1+\lambda_j^2)}{\prod_{j=1}^{p}(1+\lambda_j^2)} = +1 \quad q.e.d$$

where p is the number of nonzero (imaginary) eigenvalues of Q. The above statement proves that all C matrices formed with equation (29a) are indeed proper matrices. For the 3x3 case, let the Q matrix be defined as the following skew-symmetric matrix:

$$Q = [\tilde{q}] = \begin{bmatrix} 0 & -q_3 & q_2 \\ q_3 & 0 & -q_1 \\ -q_2 & q_1 & 0 \end{bmatrix} \tag{30}$$

After substituting equation (30) into (29a), it can be verified that resulting C matrix is indeed equal to equation (22). Cayley's transformation (29) is a generalization of the classical Rodrigues parameter representation for NxN proper orthogonal matrices [1,2], while the Q matrix generalizes the Gibbs vector in higher dimensions [2,10].

Using the $[\tilde{\gamma}]$ matrix defined in equation (14) the Q matrix can be expressed as follows [2]:

$$Q = -\tanh\left(\frac{[\tilde{\gamma}]}{2}\right) = -\left(e^{\frac{[\tilde{\gamma}]}{2}} - e^{-\frac{[\tilde{\gamma}]}{2}}\right)\left(e^{\frac{[\tilde{\gamma}]}{2}} + e^{-\frac{[\tilde{\gamma}]}{2}}\right)^{-1} \tag{31}$$

The above transformation can be verified by performing a matrix power series expansion of equation (31) and substituting it into a matrix power series expansion of equation (29a). The result is a matrix power series expansion for the matrix exponential function as expected from equation (11). However, equation (12) cannot be used to calculate the matrix exponentials, since this equations only holds for the 3x3 case. Note the similarity between equation (31) and (20). Both

calculate the Rodrigues parameters in terms of half the principal rotation angle!

The differential kinematic equations of the C matrix were shown in equation (1), where the skew-symmetric matrix $[\tilde{\omega}]$ is related to Q and $\dot{Q}$ via the kinematic relationship [1]

$$[\tilde{\omega}] = 2(I+Q)^{-1}\dot{Q}(I-Q)^{-1} \tag{32}$$

or conversely, $\dot{Q}$ can be written as

$$\dot{Q} = \frac{1}{2}(I+Q)[\tilde{\omega}](I-Q) \tag{33}$$

The equations (32-33) are proven to hold for the higher dimensional case in reference 1. For NxN orthogonal matrices, $[\tilde{\omega}] = -[\tilde{\omega}]^T$ represents an analogous "angular velocity" matrix.

Higher Dimensional Modified Rodrigues Parameters

As is evident above, the modified Rodrigues parameters have twice the principal rotation range as the classical Rodrigues parameters. It can be shown that the higher dimensional modified Rodrigues parameters also have twice the nonsingular domain as the higher dimensional classical Rodrigues parameters.

To find a transformation from the NxN proper orthogonal matrix C to the modified Rodrigues parameters, let us first examine what happens when taking the matrix square root of C. Let the square root matrix W be defined by the necessary, but not sufficient condition

$$WW = C \tag{34}$$

Obviously, for the general NxN case, there will be many W matrices that satisfy equation (34). Using the spectral decomposition of C given in equation (4), the spectral decomposition of W can be written as

$$W = U\sqrt{\Lambda}\,U^* \tag{35}$$

Since the C matrix is orthogonal, all the eigenvalues in Λ must have unit magnitude. Keep in mind that the Λ matrix in equation (35) is diagonal and that the matrix square root is trivial to calculate. Since taking the square root of an eigenvalue with unit magnitude results in another expression with unit magnitude, the W matrix itself is unitary, or orthogonal if all entries are real. It turns out that W is always real and orthogonal, as long as no eigenvalue of C is -1. If an eigenvalue of C is -1, then W has complex values and is a unitary matrix. The product of all eigenvalues of C is the determinant of C and must be +1 since C is proper. For even dimensions of C, the eigenvalues must all be complex conjugate pairs for the $det(C)$ to be +1. For odd dimensions, the

extra eigenvalue must be real and +1 in order for the matrix to be proper.

Each time a square root is calculated, there are two possible solutions. If the eigenvalue in question is one of the complex conjugate pairs, then the sign does not matter for W to be a proper matrix. If the matrix dimension is odd, then the root of the extra eigenvalue must be +1 for W to be proper. In the 3x3 case there is only one complex conjugate pair of eigenvalues. Hence only two W matrices satisfy the above conditions. This is to be expected, since any three-dimensional rotation can be described by two principal rotation angles which differ by 2π, one of which is positive and the other is negative. To make the choice of W unique, let us select all the roots of the complex conjugate pairs to have a positive real part.

Since the W matrix is orthogonal, with one exception, it has a principal line and angle associated with it. If the C matrix had an eigenvalue of -1, the same numerical problems arise as we encountered with finding the principal rotation vector. Multiplying W with itself in equation (34) simply doubles the principal angle, but leaves the principal line unchanged. Therefore W represents a rotation about the same principal line as C, but with half the principal angle. This provides conceptually elegant interpretations of the square root of C as defined above..

For three-dimensional rotations, the simple restriction on the square roots of the eigenvalues can be shown to restrict the principal rotation angle to satisfy $-180° < \phi < +180°$. This choice is consistent with many numerical matrix manipulation packages and their computation of a square root of a matrix. Let the j-th complex conjugate eigenvalue of C be denoted as $e^{\pm i\theta_j}$, where the the phase is $-180° \le \theta_j \le +180°$. If the dimension N is an odd number, W has the structure

$$W = U \cdot \begin{bmatrix} e^{+i\frac{\theta_1}{2}} & 0 & \cdots & 0 & 0 & 0 \\ 0 & e^{-i\frac{\theta_1}{2}} & \cdots & 0 & 0 & 0 \\ \vdots & \vdots & \ddots & 0 & 0 & 0 \\ 0 & 0 & 0 & e^{+i\frac{\theta_{N-1}}{2}} & 0 & 0 \\ 0 & 0 & 0 & 0 & e^{-i\frac{\theta_{N-1}}{2}} & 0 \\ 0 & 0 & 0 & 0 & 0 & +1 \end{bmatrix} \cdot U^* \tag{36}$$

If the dimension N is even, then W is

$$W = U \cdot \begin{bmatrix} e^{+i\frac{\theta_1}{2}} & 0 & \cdots & 0 & 0 \\ 0 & e^{-i\frac{\theta_1}{2}} & \cdots & 0 & 0 \\ \vdots & \vdots & \ddots & 0 & 0 \\ 0 & 0 & 0 & e^{+i\frac{\theta_N}{2}} & 0 \\ 0 & 0 & 0 & 0 & e^{-i\frac{\theta_N}{2}} \end{bmatrix} \cdot U^* \tag{37}$$

Using the parameterization given in equation (11), the matrix W can also be written directly in

terms of the principal rotation matrix $[\tilde{\gamma}]$ as follows

$$W = e^{\frac{-[\tilde{\gamma}]}{2}} \tag{38}$$

This solution for W can be verified by substituting it into equation (34). Comparing equation (38) with equation (11) it becomes obvious that the W matrix has indeed the same principle rotation direction as C, with half the principle angle. Since, for three-dimensional rotations, there are two possible principal angles for a given attitude, there are two possible solutions for equation (38). Again, by keeping $|\phi| < 180°$, the same W matrix is obtained as with the matrix square root method discussed above.

Remember that the modified Rodrigues parameters have a nonsingular range corresponding to $|\phi| < 360°$. Since W is the direction cosine matrix corresponding to half of the principal rotation angle of C, the resulting nonsingular range of the W matrix has been reduced to $|\phi| < 180°$. This is the same nonsingular range as the classical Rodrigues parameters. Therefore the Cayley transformations, defined in equations (29a,b), can be applied to W. Let S be the skew-symmetric matrix composed of the modified Rodrigues parameters, similar to the construction of the Q matrix in equation (30). Then the transformation from W to S and its inverse are given as:

$$W = (I - S)(I + S)^{-1} = (I + S)^{-1}(I - S) \tag{39a}$$

$$S = (I - W)(I + W)^{-1} = (I + W)^{-1}(I - W) \tag{39b}$$

Using equation (39a) and (34), a direct transformation from S to C is found.

$$C = (I - S)^2(I + S)^{-2} = (I + S)^{-2}(I - S)^2 \tag{40}$$

This direct transformation is very similar to the classical Cayley transform, but no elegant direct inverse exists (i.e. we lose the elegance of equation (29b); no analogous equation can be written for S as a function of C). This is due to the overlapping principal rotation angle range of $\pm360°$ causing the transformation in equation (40) not to be injective (one-to-one). Since the classical Rodrigues parameters are for principal rotations between $(-180°,+180°)$, they have a unique representation and the Cayley transform has the well known elegant inverse.

However, an alternate way to obtain the S matrix from the C matrix is available through the skew-symmetric matrix $[\tilde{\gamma}]$ defined in equation (14).

$$S = -\tanh\left(\frac{[\tilde{\gamma}]}{4}\right) = -\left(e^{\frac{[\tilde{\gamma}]}{4}} - e^{-\frac{[\tilde{\gamma}]}{4}}\right)\left(e^{\frac{[\tilde{\gamma}]}{4}} + e^{-\frac{[\tilde{\gamma}]}{4}}\right)^{-1} \tag{41}$$

The transformations given in equation (41) can be verified by performing a matrix power se-

ries expansion and back-substituting it into equation (40). Note again the similarity between equation (41) and equation (25). The principal rotation angle is divided by four in both cases.

Either the W or the $[\tilde{\gamma}]$ matrix can be solved from the proper NxN orthogonal C matrix to obtain the corresponding S matrix. Neither method is as elegant, however, as equation (29b) of the Cayley transformation. The method using the $[\tilde{\gamma}]$ matrix has the advantage that $[\tilde{\gamma}]$ is found by taking the matrix logarithm of the eigenvalues of the C matrix as shown in equation (14). The uniqueness questions do not arise here as in the matrix square root method because solutions are implicitly restricted to proper rotations with $|\phi| < 180°$. Both methods produce the same results using, for example, the matrix exponential and matrix square root algorithms available as MATLAB or MATHEMATICA operators. Note that both the classical and the "updated" Cayley transform have numerical problems when transforming a proper orthogonal matrix C into a skew-symmetric matrix if C has eigenvalues of -1.

Since each set of modified Rodrigues parameters has its associated "shadow" set [6], it is usually not important which S parameterization one obtains, as long as at least one valid S matrix is found. Once a parameter set is found, either the original ones or the "shadow" set, it is trivial to remain with this set during the forward integration of the differential equations governing the evolution of S.

The differential kinematic equations for S are not written directly from C as they were with the classical Cayley transform. Instead W is used to describe the kinematics of the NxN system. The relationship between W and S is the same as between C and Q. Therefore the same equations can be used. The differential kinematic equation for W is:

$$\dot{W} = -[\tilde{\Omega}]W \tag{42}$$

where the skew-symmetric matrix $[\tilde{\omega}]$ is:

$$[\tilde{\Omega}] = 2(I+S)^{-1}\dot{S}(I-S)^{-1} \tag{43}$$

or conversely $\dot{S}$ could be defined as:

$$\dot{S} = \frac{1}{2}(I+S)[\tilde{\Omega}](I-S) \tag{44}$$

Equation (34) can be used during the forward integration to obtain $C(t)$. The time evolution of C in terms of W and $[\tilde{\Omega}]$ is:

$$\dot{C} = -[\tilde{\Omega}]WW - W[\tilde{\Omega}]W = -[\tilde{\Omega}]C - W[\tilde{\Omega}]W \tag{45}$$

Equating equation (45) and (1), the direct transformation from $[\tilde{\Omega}]$ to $[\tilde{\omega}]$ is:

$$[\tilde{\omega}] = [\tilde{\Omega}] + W[\tilde{\Omega}]W^T \qquad (46)$$

To verify that equation (46) yields a skew-symmetric matrix $[\tilde{\omega}]$, the definition of a skew-symmetric matrix is used:

$$[\tilde{\omega}] = -[\tilde{\omega}]^T = -\left([\tilde{\Omega}] + W[\tilde{\Omega}]W^T\right)^T$$

$$[\tilde{\omega}] = -[\tilde{\Omega}]^T - \left(W^T\right)^T[\tilde{\Omega}]^T W^T$$

$$[\tilde{\omega}] = [\tilde{\Omega}] + W[\tilde{\Omega}]W^T \quad q.e.d.$$

Although this new parameterization is somewhat more complicated than the classical parameterization into M-dimensional Rodrigues parameters, the complications arise only when setting up the parameterization in terms of S. Once an S matrix and a corresponding W matrix have been found, this method is no different from the classical method. The important improvement is that the range of possible principle rotations has been doubled over the classical M-dimensional Rodrigues parameters.

A Preliminary Investigation of Higher Dimensional Euler Parameters

The classical Euler parameters stood apart from the other parameterizations, because they were bounded, universally nonsingular and had an easy-to-solve bi-linear differential kinematic equations. All of these attractive features were only slightly affected by the cost of increasing the dimension of the parameter vector by one. These classical Euler parameters are extended below to higher dimensions, where they will retain some, but not all, of the above desirable features.

The Rodrigues parameters and the Euler parameters are very closely related as seen in equation (19). They are identical except for the scaling term of β_0. The classical Rodrigues parameters have been shown to expand to the higher dimensional case where they parameterize a NxN orthogonal matrix C [1]. Analogous to equation (19), they can always be described as the ratio of a once-redundant set of parameters.

$$q_i = \frac{\beta_i}{\beta_0} \qquad i = 1, 2, 3, ..., M = \frac{N(N-1)}{2} \qquad (47)$$

The skew-symmetric matrix Q in equation (29a) can be written as:

$$Q = \frac{1}{\beta_0}B \qquad (48)$$

where B is a NxN skew-symmetric matrix containing the numerators β_i of Q. For the three dimensional case, this matrix is the "vector" part of the classical Euler parameters β_1, β_2, β_3, and

has the familiar structure

$$B = \begin{bmatrix} 0 & -\beta_3 & \beta_2 \\ \beta_3 & 0 & -\beta_1 \\ -\beta_2 & \beta_1 & 0 \end{bmatrix} \tag{49}$$

Substituting the transformation relating Q to $\{\beta_0, \beta_1, ..., \beta_M\}$, as given in equation (48) the Cayley transform of equation (29a) results in the following

$$C = (\beta_0 I - B)(\beta_0 I + B)^{-1}$$

$$C(\beta_0 I + B) = (\beta_0 I - B)$$

$$(I - C)\beta_0 - (I + C)B = 0 \tag{50}$$

Equation (50) represents an NxN system of linear equations in $\{\beta_0, \beta_1, ..., \beta_M\}$. Let the $[N^2 \times (M+1)]$ matrix A represent the linear relationship between the β_i.

$$A \cdot \begin{bmatrix} \beta_0 \\ \beta_1 \\ \vdots \\ \beta_M \end{bmatrix} = 0 \tag{51}$$

Clearly the set of all possible higher dimensional Euler parameters spans the kernel of A. We know that the M Rodrigues parameters are a minimal set to parameterize the orthogonal NxN matrix C. By adding the scaling factor β_0, a once redundant set of parameters has been generated. Even though there are N^2 linear equations in equation (50), the dimension of the range of A is only M. The problem is still under determined. The dimension of the kernel of A must be one, since only one additional term was added to a minimal set of rotation parameters. The solution space is a multi-dimensional line through the origin.
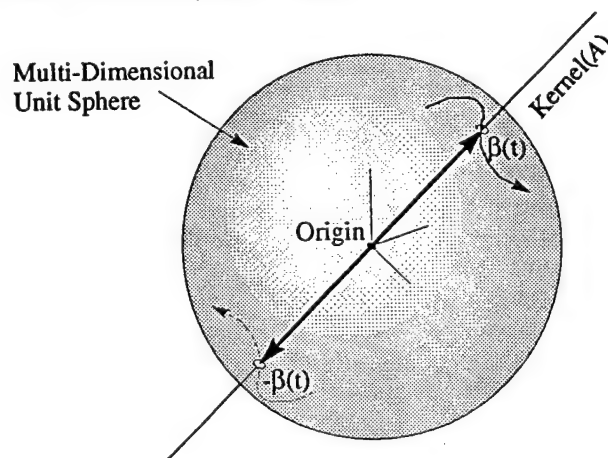
Fig. 3: Solution of the Higher Dimensional Euler Parameters.

After finding the kernel base vector, an infinite number of solutions still exist. Another constraint is needed. Let us set the norm of the higher dimensional Euler parameter vector to be unity. This concept is illustrated in Fig. 3 above.

$$\beta_0^2 + \beta_1^2 + \cdots + \beta_M^2 = 1 \tag{52}$$

Equation (52) is the higher dimensional equivalent of the holonomic constraint of the classical Euler parameters introduced in equation (16).

Two solutions are found scaling the base vector of the kernel of A to unit length. Just as with the classical Euler parameters, any point on the multi-dimensional Euler parameter unit sphere describes the same physical orientation as its antipodal pole. Therefore the higher order Euler parameters are not unique, but contain a duality. This is exactly analogous to the classical case. This duality does not pose any practical problems, except under one circumstance discussed below.

$$C = (\beta_0 I - B)(\beta_0 I + B)^{-1} = (\beta_0 I + B)^{-1}(\beta_0 I - B) \tag{53}$$

The inverse transformation from higher order Euler parameters to the orthogonal matrix C is found by using Q from equation (48) in the classical Cayley transform. The result is shown in equation (53). Using a B, as shown in equation (49) for the three-dimensional case, in equation (53) results in the same transformation as given in equation (18). Observe that the inverse transformation has a singularity when β_0 is zero. This singularity is a mathematical singularity only. Contrary to the Rodrigues parameters, the higher order Euler parameters are well defined at this orientation. After an appropriate skew-symmetric matrix B is constructed and carrying out the algebra in equation (53), a closed form algebraic transformation is found

For the 2x2 case, the B matrix is given by

$$B = \begin{bmatrix} 0 & -\beta_1 \\ \beta_1 & 0 \end{bmatrix} \tag{54}$$

Using the B defined above in equation (53), the 2x2 direction cosine matrix C is:

$$C_{2x2} = \begin{bmatrix} \beta_0^2 - \beta_1^2 & 2\beta_0\beta_0 \\ -2\beta_0\beta_0 & \beta_0^2 - \beta_1^2 \end{bmatrix} \tag{55}$$

The 2x2 C matrix contains no polynomial fractions and is easy to calculate. To find the direction cosine matrix for the 3x3 case, use the B matrix defined in equation (51) in equation (53).

$$C_{3x3} = \frac{1}{\beta_0(\beta_0^2 + \beta_1^2 + \beta_2^2 + \beta_3^2)} \begin{bmatrix} \beta_0(\beta_0^2 + \beta_1^2 - \beta_2^2 - \beta_3^2) & 2\beta_0(\beta_1\beta_2 + \beta_0\beta_3) & 2\beta_0(\beta_1\beta_3 - \beta_0\beta_2) \\ 2\beta_0(\beta_1\beta_2 - \beta_0\beta_3) & \beta_0(\beta_0^2 - \beta_1^2 + \beta_2^2 - \beta_3^2) & 2\beta_0(\beta_2\beta_3 + \beta_0\beta_1) \\ 2\beta_0(\beta_1\beta_3 + \beta_0\beta_2) & 2\beta_0(\beta_2\beta_3 - \beta_0\beta_1) & \beta_0(\beta_0^2 - \beta_1^2 - \beta_2^2 + \beta_3^2) \end{bmatrix}$$

After making the obvious cancellations and enforcing the holonomic constraint equation, the well known result is found which represents the 3x3 direction cosine matrix as a function of the classical Euler parameters as given in equation (18). This classical representation contains no polynomial fractions and no singularities, just as was the case with the 2x2 system.

For dimensions greater than 3x3's, however, the algebraic transformation contains polynomial fractions. The nice cancelations that occur with a 2x2 and a 3x3 orthogonal matrices *do not* occur with the higher dimensions. This might have been anticipated, because [2] it is well-known that quaternion algebra does not generalize fully to arbitrary higher-dimensional spaces, and the elegant classical Euler parameter results are essentially manifestations of quaternion algebra. To find C_{4x4} in terms of the higher dimensional Euler parameters, we define the 4x4 B matrix as:

$$B_{4x4} = \begin{bmatrix} 0 & -\beta_6 & \beta_5 & -\beta_4 \\ \beta_6 & 0 & -\beta_3 & \beta_2 \\ -\beta_5 & \beta_3 & 0 & -\beta_1 \\ \beta_4 & -\beta_2 & \beta_1 & 0 \end{bmatrix} \tag{56}$$

and substitute it into equation (53), this leads to

$$C_{4x4} = \frac{1}{\Delta} \begin{bmatrix} \beta_0^2(\beta_0^2 + \beta_1^2 + \beta_2^2 + \beta_3^2 - \beta_4^2 - \beta_5^2 - \beta_6^2) - \delta^2 & 2\beta_0(\beta_0(\beta_2\beta_4 + \beta_3\beta_5 + \beta_0\beta_6) + \beta_1\delta) \\ 2\beta_0(\beta_0(\beta_2\beta_4 + \beta_3\beta_5 - \beta_0\beta_6) - \beta_1\delta) & \beta_0^2(\beta_0^2 + \beta_1^2 - \beta_2^2 - \beta_3^2 + \beta_4^2 + \beta_5^2 - \beta_6^2) - \delta^2 \\ 2\beta_0(\beta_0(\beta_0\beta_5 + \beta_3\beta_6 - \beta_1\beta_4) - \beta_2\delta) & 2\beta_0(\beta_0(\beta_1\beta_2 - \beta_0\beta_3 + \beta_5\beta_6) - \beta_4\delta) \\ 2\beta_0(\beta_0(-\beta_0\beta_4 - \beta_1\beta_5 - \beta_2\beta_6) - \beta_3\delta) & 2\beta_0(\beta_0(\beta_1\beta_3 + \beta_0\beta_2 - \beta_4\beta_6) - \beta_5\delta) \end{bmatrix} \cdots$$

$$\cdots \begin{bmatrix} 2\beta_0(\beta_0(-\beta_0\beta_5 + \beta_3\beta_6 - \beta_1\beta_4) + \beta_2\delta) & 2\beta_0(\beta_0(\beta_0\beta_4 - \beta_1\beta_5 - \beta_2\beta_6) + \beta_3\delta) \\ 2\beta_0(\beta_0(\beta_1\beta_2 + \beta_0\beta_3 + \beta_5\beta_6) + \beta_4\delta) & 2\beta_0(\beta_0(\beta_1\beta_3 - \beta_0\beta_2 - \beta_4\beta_6) + \beta_5\delta) \\ \beta_0^2(\beta_0^2 - \beta_1^2 + \beta_2^2 - \beta_3^2 + \beta_4^2 - \beta_5^2 + \beta_6^2) - \delta^2 & 2\beta_0(\beta_0(\beta_0\beta_1 + \beta_4\beta_5 + \beta_2\beta_3) + \beta_6\delta) \\ 2\beta_0(\beta_0(-\beta_0\beta_1 + \beta_4\beta_5 + \beta_2\beta_3) - \beta_6\delta) & \beta_0^2(\beta_0^2 - \beta_1^2 - \beta_2^2 + \beta_3^2 - \beta_4^2 + \beta_5^2 + \beta_6^2) - \delta^2 \end{bmatrix} \tag{57}$$

with $\quad \delta = \beta_3\beta_4 + \beta_1\beta_6 - \beta_2\beta_5$
$\qquad \Delta = \beta_0^2 + \delta^2$

This denominator Δ can vanish for several β_i configurations. Observe, however, that whenever Δ is zero, so is the numerator. For each singular case we can confirm that a finite limit exists, as was to be expected, since the original orthogonal C matrix was finite. In all cases $\beta_0 = 0$ is a prerequisite for a (0/0) condition to occur. Finding the transformations for matrices with dimensions greater than 4x4 would show the same behavior. $\beta_0 = 0$ is always a indicator that a mathematical singularity *may* occur. In none of these cases are the higher dimensional Euler parameters themselves actually singular. It is always a mathematical singularity of the transforma-

tion itself. To circumvent this problem for particular applications, the limit of the fraction can be found as $\beta_0 \rightarrow 0$. After substituting $\beta_0 = 0$ into equation (57), for example, most fractions become trivial and the matrix is reduced to

$$C_{4x4} = \begin{bmatrix} -1 & 0 & 0 & 0 \\ 0 & -1 & 0 & 0 \\ 0 & 0 & -1 & 0 \\ 0 & 0 & 0 & -1 \end{bmatrix} = -I_{4x4} \tag{58}$$

Substituting $\beta_0 = 0$ into equation (55) yields the same result. Actually, as long as C is of *even* dimension the matrix will be $-I$ if $\beta_0 = 0$. If the dimension is *odd*, as it is for the 3x3 case, the C matrix will be fully populated. With this observation it is easy to circumvent the singular situations if the dimension is even. If the dimension is odd a numerical limit must be found. In either case the transformation will be well behaved everywhere except the $\beta_0 = 0$ surface. The fact that the 0/0 condition can be resolved analytically to obtain finite limits should not obscure the frustrating fact that these 0/0 conditions would pose numerical difficulties in general numerical algorithms.

Let us examine the uniqueness of the transformation given in equation (53). Assuming that the transformation is not unique, two possible higher dimensional Euler parameter sets $\acute{\beta}$ and $\tilde{\beta}$ are chosen, these parameterize C as

$$C = (\acute{\beta}_0 I - \acute{B})(\acute{\beta}_0 I + \acute{B})^{-1}$$
$$C = (\tilde{\beta}_0 I + \tilde{B})^{-1}(\tilde{\beta}_0 I - \tilde{B})$$

Subtracting one equation from the other the following condition is obtained:

$$0 = (\acute{\beta}_0 I - \acute{B})(\acute{\beta}_0 I + \acute{B})^{-1} - (\tilde{\beta}_0 I + \tilde{B})^{-1}(\tilde{\beta}_0 I - \tilde{B})$$

$$0 = (\tilde{\beta}_0 I + \tilde{B})(\acute{\beta}_0 I - \acute{B}) - (\tilde{\beta}_0 I - \tilde{B})(\acute{\beta}_0 I + \acute{B})$$

$$0 = \acute{\beta}_0 \tilde{B} - \tilde{\beta}_0 \acute{B}$$

or

$$\frac{\acute{B}}{\acute{\beta}_0} = \frac{\tilde{B}}{\tilde{\beta}_0} \tag{59}$$

Equation (59) is the necessary condition for two higher order Euler parameter sets to yield the same direction cosine matrix C. Obviously, for $\beta_0 \neq 0$ this can only occur when

$$\tilde{B} = k \cdot \acute{B}$$
$$\tilde{\beta}_0 = k \cdot \acute{\beta}_0 \tag{60}$$

where k is a scalar. This condition apparently yields an infinite number of solutions. But since the higher dimensional Euler parameters must satisfy the holonomic constraint given in equation (52), only unit scaling values of k are permissible. Therefore k must be either ± 1. The above uniqueness study results in exactly the same duality as is observed with the classical Euler parameters, except the restriction on $\beta_0 \neq 0$. There are always *two* possible sets of classical Euler parameters which describe an orthogonal 3x3 matrix C. It is evident that this truth extends to the more general case of NxN orthogonal matrices . This duality was seen earlier when applying the holonomic constraint to the kernel of A.

$$C_{NxN}[\beta(t)] = C_{NxN}[-\beta(t)] \tag{61}$$

Based on the above, if $\beta_0 = 0$ nothing can be said about the transformation uniqueness. As was seen with the 4x4 C matrix, the $\beta_0 = 0$ condition permits any point on the unit sphere $\sum_{i=1}^{6} \beta_i^2 = 1$.

Having established the forward and backward transformations between the NxN orthogonal matrices and the higher order Euler parameters, their kinematic equations are also of interest. To describe the orthogonal matrix C as a generalized rigid body rotation, C must satisfy a differential equation of the form given in equation (1). After substituting equation (48) into equation (33), $\dot{Q}$ is

$$\dot{Q} = \frac{1}{2}\left(I + \frac{B}{\beta_0}\right)[\tilde{\omega}]\left(I - \frac{B}{\beta_0}\right) \tag{62}$$

After differentiating equation (48) directly, $\dot{Q}$ is found to be

$$\dot{Q} = \frac{\beta_0 \dot{B} - \dot{\beta}_0 B}{\beta_0^2} \tag{63}$$

Upon substituting equation (62) into equation (63) and after making some simplifications, the following kinematic relationship is found.

$$\beta_0 \dot{B} - \dot{\beta}_0 B = \frac{1}{2}(\beta_0 I + B)[\tilde{\omega}](\beta_0 I - B) \tag{64}$$

This equation can be solved for the skew-symmetric angular velocity matrix $[\tilde{\omega}]$.

$$[\tilde{\omega}] = 2(\beta_0 I + B)^{-1}(\beta_0 \dot{B} - \dot{\beta}_0 B)(\beta_0 I - B)^{-1} \tag{65}$$

Note that this equation contains the same *mathematical* singularity at $\beta_0 = 0$ as did equation

(53). Carrying out the algebra a closed form algebraic equation is found for the higher order angular velocities.

Let us verify that equation (65) for the angular velocities does indeed generate a skew-symmetric matrix. This is easily accomplished using the definition of a skew-symmetric matrix as follows

$$[\tilde{\omega}] = -[\tilde{\omega}]^T = -2\left((\beta_0 I + B)^{-1}(\beta_0 \dot{B} - \dot{\beta}_0 B)(\beta_0 I - B)^{-1}\right)^T$$

$$[\tilde{\omega}] = -2(\beta_0 I - B)^{-1^T}(\beta_0 \dot{B} - \dot{\beta}_0 B)^T(\beta_0 I + B)^{-1^T}$$

$$[\tilde{\omega}] = -2(\beta_0 I^T - B^T)^{-1}(\beta_0 \dot{B}^T - \dot{\beta}_0 B^T)(\beta_0 I^T + B^T)^{-1}$$

Since the matrix B and its derivative are skew-symmetric matrices by definition, further simplifications are possible to obtain the following result

$$[\tilde{\omega}] = -2(\beta_0 I + B)^{-1}(-\beta_0 \dot{B} + \dot{\beta}_0 B)(\beta_0 I - B)^{-1}$$

$$[\tilde{\omega}] = 2(\beta_0 I + B)^{-1}(\beta_0 \dot{B} - \dot{\beta}_0 B)(\beta_0 I - B)^{-1} \quad q.e.d.$$

All higher order Euler parameter differentials must abide by the derivative of the constraint equation (52).

$$2\dot{\beta}_0 \beta_0 + 2\dot{\beta}_1 \beta_1 + \ldots + 2\dot{\beta}_M \beta_M = 0 \tag{66}$$

After using the B from equation (49) the linear differential kinematic equations of the classical Euler parameters are found. To verify that equation (65) generalizes correctly, known classical results let us verify two special cases. For the 2x2 case, a scalar differential kinematic equation results from equation (65) as

$$\omega_1 = 2[-\beta_1 \quad \beta_0]\begin{bmatrix} \dot{\beta}_0 \\ \dot{\beta}_1 \end{bmatrix} \tag{67}$$

Adding the constraint in equation (66), equation (67) can be padded to make it full rank.

$$\begin{bmatrix} 0 \\ \omega_1 \end{bmatrix} = 2\begin{bmatrix} \beta_0 & \beta_1 \\ -\beta_1 & \beta_0 \end{bmatrix}\begin{bmatrix} \dot{\beta}_0 \\ \dot{\beta}_1 \end{bmatrix} \tag{68}$$

Note that as with the 3x3 case, the matrix transforming $\dot{\beta}$ to ω is orthogonal for the 2x2 case. Therefore the inverse transformation can be written as:

$$\begin{bmatrix} \dot{\beta}_0 \\ \dot{\beta}_1 \end{bmatrix} = \frac{1}{2}\begin{bmatrix} \beta_0 & -\beta_1 \\ \beta_1 & \beta_0 \end{bmatrix}\begin{bmatrix} 0 \\ \omega_1 \end{bmatrix} \tag{69}$$

It is straight forward to show that equations (65) and (66) give equation (17) for the 3x3 case. Analogous to the 3x3 case, the above differential kinematic equation for the 2x2 case is also bi-linear. As with the 4x4 and greater direction cosine matrices, for proper orthogonal matrices having dimensions greater than 3x3 the higher dimensional differential kinematic equations also contain polynomial fractions. Using the B matrix from equation (56) in equation (65) and collecting all the angular velocity term, we find the differential kinematic equations for the 4x4 case

$$
\left\{\begin{array}{c} 0 \\ \omega_1 \\ \omega_2 \\ \omega_3 \\ \omega_4 \\ \omega_5 \\ \omega_6 \end{array}\right\} = \frac{2}{\Delta}
$$

$$
\begin{array}{ccc}
\Delta\beta_0 & \Delta\beta_1 & \Delta\beta_2 \\
\beta_6(\beta_2\beta_5 - \beta_3\beta_4) - \beta_1(\beta_0^2 + \beta_6^2) & \beta_0(\beta_0^2 + \beta_6^2) & \beta_0(\beta_0\beta_3 - \beta_5\beta_6) \\
\beta_5(\beta_1\beta_6 + \beta_3\beta_4) - \beta_2(\beta_0^2 + \beta_5^2) & -\beta_0(\beta_0\beta_3 + \beta_5\beta_6) & \beta_0(\beta_0^2 + \beta_5^2) \\
\beta_4(\beta_2\beta_5 - \beta_1\beta_6) - \beta_3(\beta_0^2 + \beta_4^2) & \beta_0(\beta_4\beta_6 + \beta_0\beta_2) & -\beta_0(\beta_0\beta_1 + \beta_4\beta_5) \\
\beta_3(\beta_2\beta_5 - \beta_1\beta_6) - \beta_4(\beta_0^2 + \beta_3^2) & \beta_0(-\beta_0\beta_5 + \beta_3\beta_6) & -\beta_0(\beta_0\beta_6 + \beta_5\beta_3) \\
\beta_2(\beta_1\beta_6 + \beta_3\beta_4) - \beta_5(\beta_0^2 + \beta_2^2) & \beta_0(\beta_0\beta_4 - \beta_2\beta_6) & \beta_0(\beta_3\beta_4 + \beta_1\beta_6) \\
\beta_1(\beta_2\beta_5 - \beta_3\beta_4) - \beta_6(\beta_0^2 + \beta_1^2) & \beta_0(\beta_2\beta_5 - \beta_3\beta_4) & \beta_0(\beta_0\beta_4 - \beta_1\beta_5)
\end{array} \cdots
$$

$$
\begin{array}{cccc}
\Delta\beta_3 & \Delta\beta_4 & \Delta\beta_5 & \Delta\beta_6 \\
\beta_0(\beta_4\beta_6 - \beta_0\beta_2) & \beta_0(\beta_0\beta_5 + \beta_3\beta_6) & -\beta_0(\beta_0\beta_4 + \beta_2\beta_6) & \beta_0(\beta_2\beta_5 - \beta_3\beta_4) \\
\beta_0(\beta_0\beta_1 - \beta_4\beta_5) & \beta_0(\beta_0\beta_6 - \beta_5\beta_3) & \beta_0(\beta_3\beta_4 + \beta_1\beta_6) & -\beta_0(\beta_0\beta_4 + \beta_1\beta_5) \\
\beta_0(\beta_0^2 + \beta_4^2) & \beta_0(\beta_2\beta_5 - \beta_1\beta_6) & \beta_0(\beta_0\beta_6 - \beta_2\beta_4) & \beta_0(\beta_1\beta_4 - \beta_0\beta_5) \\
\beta_0(\beta_2\beta_5 - \beta_1\beta_6) & \beta_0(\beta_0^2 + \beta_3^2) & \beta_0(\beta_0\beta_1 - \beta_2\beta_3) & \beta_0(\beta_0\beta_2 + \beta_1\beta_3) \\
-\beta_0(\beta_0\beta_6 + \beta_2\beta_4) & -\beta_0(\beta_0\beta_1 + \beta_2\beta_3) & \beta_0(\beta_0^2 + \beta_2^2) & \beta_0(\beta_0\beta_3 - \beta_1\beta_2) \\
\beta_0(\beta_1\beta_4 + \beta_0\beta_5) & \beta_0(-\beta_0\beta_2 + \beta_1\beta_3) & -\beta_0(\beta_0\beta_3 + \beta_1\beta_2) & \beta_0(\beta_0^2 + \beta_1^2)
\end{array}
\left\{\begin{array}{c} \dot\beta_0 \\ \dot\beta_1 \\ \dot\beta_2 \\ \dot\beta_3 \\ \dot\beta_4 \\ \dot\beta_5 \\ \dot\beta_6 \end{array}\right\} \quad (70)
$$

$$
with \quad \Delta = \beta_0^2 + (\beta_3\beta_4 - \beta_2\beta_5 + \beta_1\beta_6)^2
$$

Note that this transformation matrix is no longer orthogonal as were the corresponding matrices for both the 2x2 and 3x3 cases. The bi-linearity found for 2x2 and 3x3 cases is also lost for the higher dimensional cases. Equation (70) has the same denominator as the 4x4 direction cosine matrix. Hence it contains the identical singular situations. However, if $\beta_0 = 0$, the above transformation matrix is singular and cannot be inverted!

Thus the higher dimensional Euler parameters lose some key properties as they are generalized to parameterize higher dimensioned proper orthogonal matrices. They retain the properties of being bounded and mapping all rotations onto arcs on a unit hypersphere. However, the kinematic transformations and orthogonal matrix representations loose the elegance of their classical 3x3 counterparts. In particular, $\beta_0 = 0$ poses several unresolved issues for all dimensions higher than 3x3.

Conclusion

The principal rotation parameterizations presented show great promise as an elegant means for describing the evolution of NxN orthogonal matrices. The modified Rodrigues parameters are

only slightly more complicated than their classical counterparts, but double the nonsingular rotation domain The (M+1)-dimensional Euler parameters retain some of the desirable features of their classical counterparts. However, for orthogonal matrices greater than 3x3 though, the orthogonal matrix representation formulas and the corresponding differential kinematic equations contain some mathematical singularities which require taking the limits of polynomial fractions. The computational effort for calculating the higher dimensional Euler parameters grows rapidly when increasing the dimension of the C matrix. For higher dimensional rotations, the modified Rodrigues parameters show the greatest promise. The gain (increased nonsingular domain in comparison to the classical Cayley transformation), significantly outweighs the extra computation.

Acknowledgments

References

[1] JUNKINS, J.L., and KIM, Y., *Introduction to Dynamics and Control of Flexible Structures*, AIAA Education Series, Washington D.C., 1993.

[2] SHUSTER, M.D., "A Survey of Attitude Representations," *Journal of the Astronautical Sciences*, Vol. 41, No. 4, 1993, pp. 439-517.

[3] JUNKINS, J.L., and TURNER, J.D., *Optimal Spacecraft Rotational Maneuvers*, Elsevier Science Publishers, Netherlands, 1986.

[4] TSIOTRAS, P., "New Control Laws for the Attitude Stabilization of Rigid Bodies," Proceedings, *IFAC Symposium on Automatic Control in Aerospace*, Palo Alto, California, Sept. 12-16, 1994, pp. 316-321.

[5] MARANDI, S.R., and MODI, V.J., "A Preferred Coordinate System and the Associated Orientation Representation in Attitude Dynamics," *Acta Astronautica*, Vol. 15, 1987, pp. 833-843.

[6] SCHAUB, H., and JUNKINS, J.L., "Stereographic Orientation Parameters for Attitude Dynamics: A Generalization of the Rodrigues Parameters," submitted to the *Journal of the Astronautical Sciences*, October 25, 1994.

[7] CAYLEY, A., "On the Motion of Rotation of a Solid Body," Cambridge Mathematics Journal, Vol 3, 1843, pp. 224-232.

[8] PARKER, W. V., EAVES, J. C., *Matrices*, Ronald Press Co., New York, 1960.

[9] TSIOTRAS, P., "On New Parameterizations of the Rotation Group in Attitude Kinematics," Technical Report, School of Aeronautics and Astronautics, Purdue University, West Lafayette, IN, January 1994.

[10] BAR-ITZHACK, I.Y., MARKLEY, F.L., "Minimal Parameter Solution of the Orthogonal Matrix Differential Equation," IEEE Transactions on Automatic Control, AC-25, 1990, pp. 314-317.

Radial Basis Function Approximation Methods

for Optimal Control of Nonlinear Systems

with Terminal Constraints

by

Hyeon C. Gong and John L. Junkins

Department of Aerospace Engineering
Texas A & M University

OUTLINE

- Introduction / Motivation

- RBF Approximation Algorithms

- Example : Interplanetary Orbit Transfer Problem

- Concluding Remarks

Introduction/Motivation

Consider the Optimal Control Problem:
Find $u(t)$ such that the solution of

$$\dot{x} = f(t, x, u) \quad , x(t_0) \text{ specified}$$

extremizes

$$J = \phi + \int_{t_1}^{t_2} F(t, x, u) dt$$

subject to

$$\Psi(t_f, x(t_f)) = 0$$

Two Approaches to Solution :

. Function Space Approach
   Take Variation
      $\Rightarrow$ Pontryagin's Principle & TPBVP

. Parameterize $u(t) = f(t, w_1, w_2, \cdots, w_m)$
   Optimize $(w_1, w_2, \cdots, w_m)$
         via Nonlinear Programming

1

RBF Approximation Algorithm

Consider the System of

$$\dot{x} = f(t, x, u)$$

with radial basis function approximation

$$u = \sum_{i=1}^{N} w_i e^{-\frac{1}{2}\left(\frac{t-\tau_i}{\sigma_i}\right)^2}$$

Then the system becomes

$$\dot{x} = f(t, x, w)$$

Let's consider the matrix of partial derivative.

$$\Psi(t, t_0) = \left[\frac{\partial x(t)}{\partial w}\right]$$

which satisfies

$$\frac{d}{dt}\left[\Psi(t, t_0)\right] = \left[A(t)\right]\left[\Psi(t, t_0)\right] + \left[\frac{\partial f(t, x, w)}{\partial w}\right], \left[\Psi(t_0, t_0)\right] = \left[0\right]$$

where

$$\left[A(t)\right] = \left[\frac{\partial f(t, x, w)}{\partial x(t)}\right]$$

2

Thus, the original system can be represented by augmented system

$$\dot{z} = \Gamma(t, x, w)$$

where

$$\dot{z} = \begin{bmatrix} \dot{x} \\ \dot{\Psi} \end{bmatrix},$$

$$\Gamma(t, x, w) = \begin{bmatrix} f(t,x,w) \\ \left[\dfrac{\partial f}{\partial x}\right]\Psi + \left[\dfrac{\partial f}{\partial w}\right] \end{bmatrix}$$

The solution to this dynamical system ;

$$\Delta y = A \, \Delta w$$

We use minimum norm correction algorithm.

$$\Delta w = A^{T}\left(A \, A^{T}\right)^{-1}\Delta y$$

where

$$A = \left[\frac{\partial y}{\partial w}\right] = \left[\frac{\partial y}{\partial x(t_f)}\right]\left[\frac{\partial x(t_f)}{\partial w}\right] = \left[\frac{\partial y}{\partial x(t_f)}\right]\Psi(t_f, 0)$$

and

$$\Delta y = \begin{bmatrix} \psi_1(t_f) \\ \vdots \\ \psi_q(t_f) \end{bmatrix}$$

3

A Step size limitation filter according to the value of Δw is used as follows;

$$w^{new} = w^{old} + \Delta w$$

where

$$|\Delta w| = \sqrt{\Delta w^T \Delta w}$$

If $\Delta w \leq \varepsilon$ for acceptably small ε, then

$$\Delta w = A^T \left(A\, A^T \right)^{-1} \Delta y$$

else if $\Delta w \geq \varepsilon$ for acceptably small ε, then

$$\Delta w = \left[\frac{\varepsilon}{\Delta w} \right] A^T \left(A\, A^T \right)^{-1} \Delta y$$

4

Even after the terminal constraints are met
we generally do not know whether how near
the performance is to optimal.
To drive the performance value toward the
optimal, we introduce a homotopy concept.

$$J_o = \lambda\, J^* + (1-\lambda)\, J_{current}$$

Since the homotopy concept is used to treat
the performance index (J_o) as an additional
equality constraint, we modify Δy as follows;

$$\Delta y = \begin{bmatrix} \psi_1(t_f) \\ \vdots \\ \psi_2(t_f) \\ J_o - J_{current} \end{bmatrix}$$

For adaptively spaced RBF algorithm
we check the sensitivity of the terminal
constraints and the performance index
w.r.t. parameters as follows;
we form the augmented Jacobian

5

$$A = \begin{bmatrix} \dfrac{\partial \psi_1}{\partial w_1} & \dfrac{\partial \psi_1}{\partial w_2} & \cdots & \dfrac{\partial \psi_1}{\partial w_N} \\ \dfrac{\partial \psi_2}{\partial w_1} & \dfrac{\partial \psi_2}{\partial w_2} & \cdots & \dfrac{\partial \psi_2}{\partial w_N} \\ \vdots & \vdots & \vdots & \vdots \\ \dfrac{\partial \psi_q}{\partial w_1} & \dfrac{\partial \psi_q}{\partial w_2} & \cdots & \dfrac{\partial \psi_q}{\partial w_N} \end{bmatrix} = [A_1, A_2, \cdots, A_N]$$

The A_i vector is the gradient of the constraint and performance index w.r.t. w_i.

Adopting the positive measure of the sensitivity w.r.t. ith parameter as

$$S_i = A_i^T A_i$$

we introduce a new RBF according to S_i. With the newly added RBF we increment λ to obtain a new J_o and follow the same procedure until a small increase$(\Delta \lambda_{min})$ cannot be achieved, while satisfying all constraints within a tolerance.

6

```
                          START

                     Initial  w, τ, σ
```

$$\dot{x} = f(t, x, w)$$

$$\dot{\Psi} = \left[\frac{\partial f}{\partial x}\right]\Psi + \left[\frac{\partial f}{\partial w}\right]$$

$$A = \left[\frac{\partial Y}{\partial w}\right] = \left[\frac{\partial Y}{\partial x(t_f)}\right]\left[\frac{\partial x(t_f)}{\partial w}\right] = \left[\frac{\partial Y}{\partial x(t_f)}\right]\Psi(t_f), \quad Y = \begin{bmatrix} \psi_1 \\ \vdots \\ \psi_q \end{bmatrix}$$

$$w^{new} = w^{old} + A^T(A A^T)^{-1}\Delta Y$$

$$\dot{x} = f(t, x, w)$$

$$\dot{\Psi} = \left[\frac{\partial f}{\partial x}\right]\Psi + \left[\frac{\partial f}{\partial w}\right]$$

$$A = \left[\frac{\partial Y}{\partial w}\right] = \left[\frac{\partial Y}{\partial x(t_f)}\right]\left[\frac{\partial x(t_f)}{\partial w}\right] = \left[\frac{\partial Y}{\partial x(t_f)}\right]\Psi(t_f), \quad Y = \begin{bmatrix} \psi_1 \\ \vdots \\ \psi_q \\ J_o - J_{current} \end{bmatrix}$$

$$w^{new} = w^{old} + A^T(A A^T)^{-1}\Delta Y$$

$$\|\Delta Y\| \langle \text{ tolerance} \qquad \text{No}$$

Yes

$$\lambda \leq \varepsilon ? \qquad \text{No}$$

Yes

```
                         STOP
```
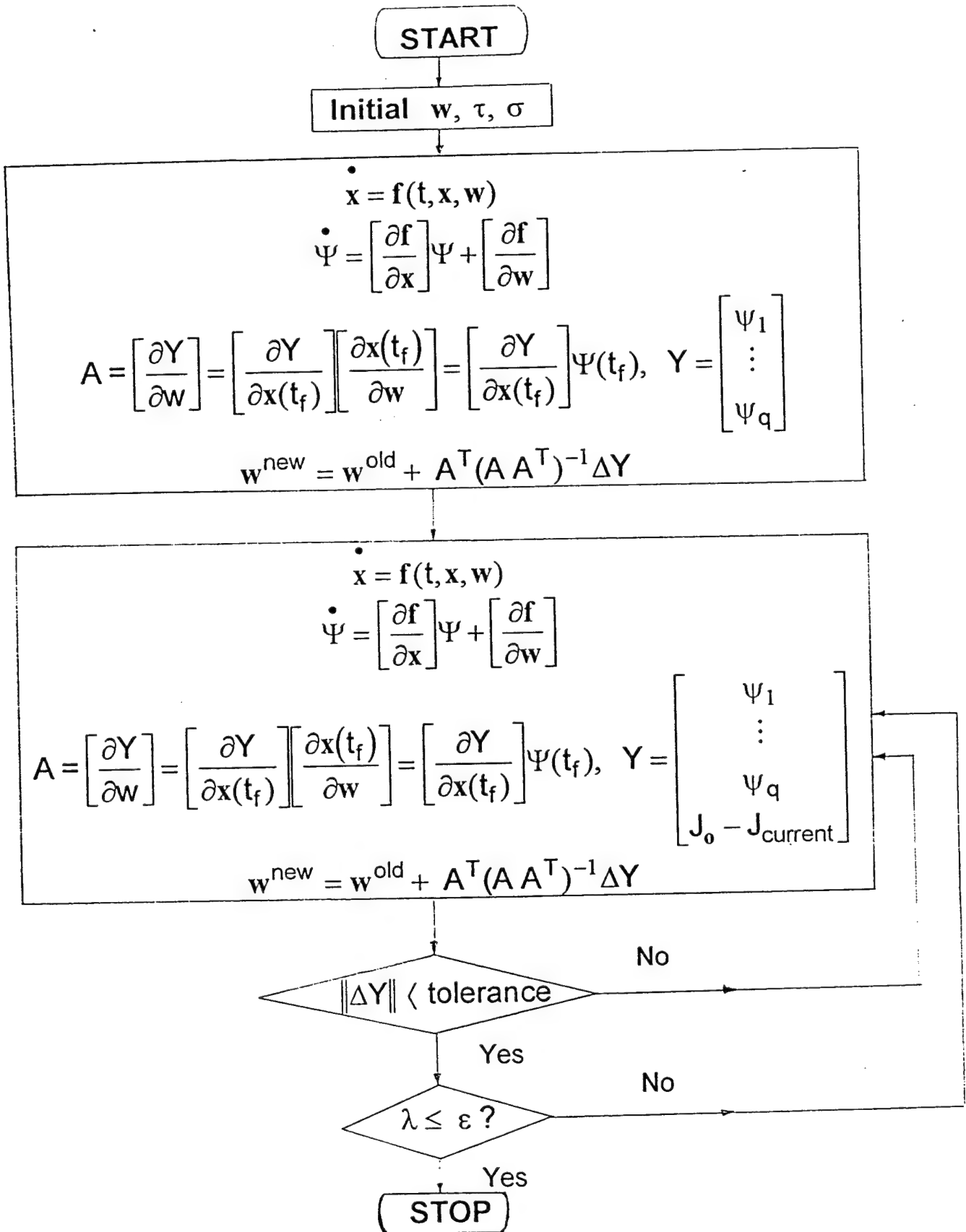
EXAMPLE
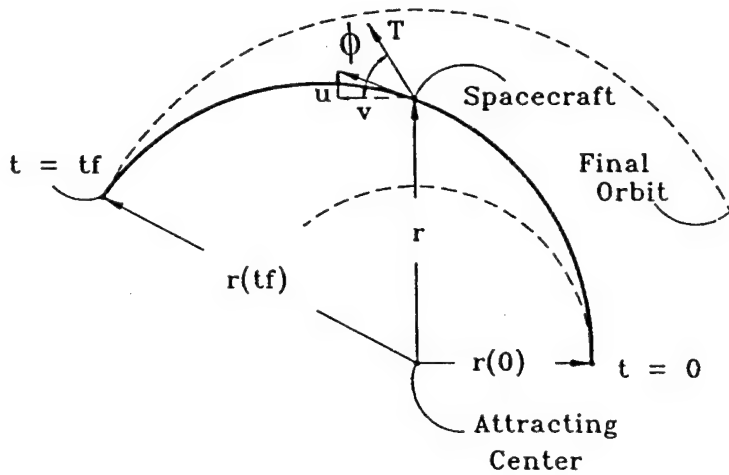
Fig. 1 Maximum Radius Orbit Transfer in a Given Time

The differential equations of the system :

$$\dot{r} = u, \ r(0) = r_0$$

$$\dot{u} = \frac{v^2}{r} - \frac{\mu}{r^2} + \frac{T\sin\phi}{m_0 - |\dot{m}|t}, u(0) = u_0$$

$$\dot{v} = -\frac{u\,v}{r} + \frac{T\cos\phi}{m_0 - |\dot{m}|t}, \ v(0) = \frac{\mu}{r_0}$$

The terminal constraints :

$$\psi_1 = u(t_f) = 0$$

$$\psi_2 = v(t_f) - \frac{\mu}{r(t_f)} = 0$$

Evenly Spaced Radial Basis Function Algorithm
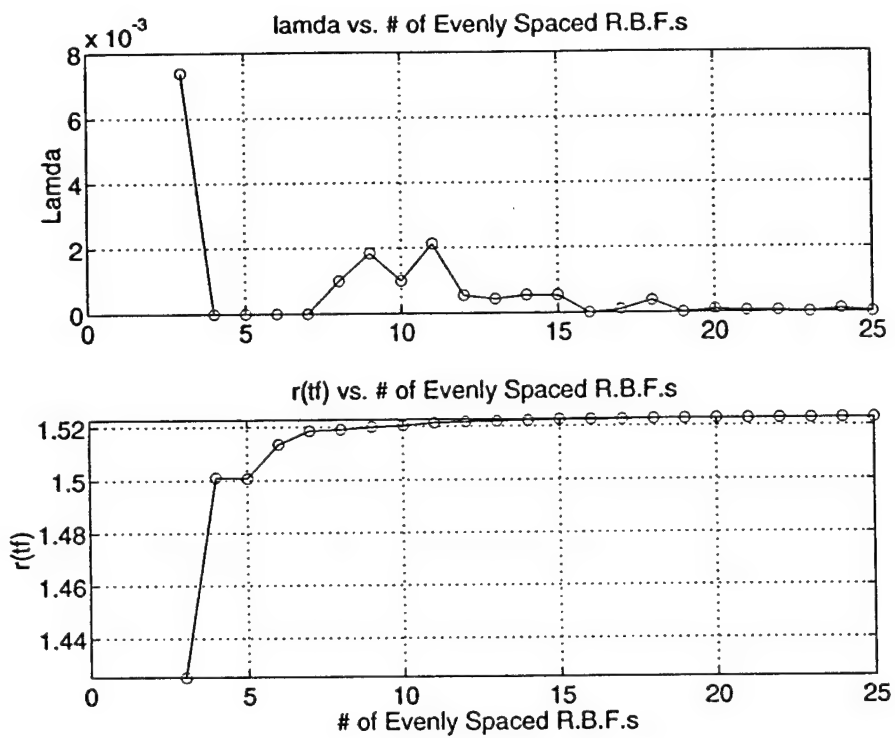
Fig. 2 λ and $r(t_f)$ vs. time for Evenly Spaced R.B.F. Algorithm
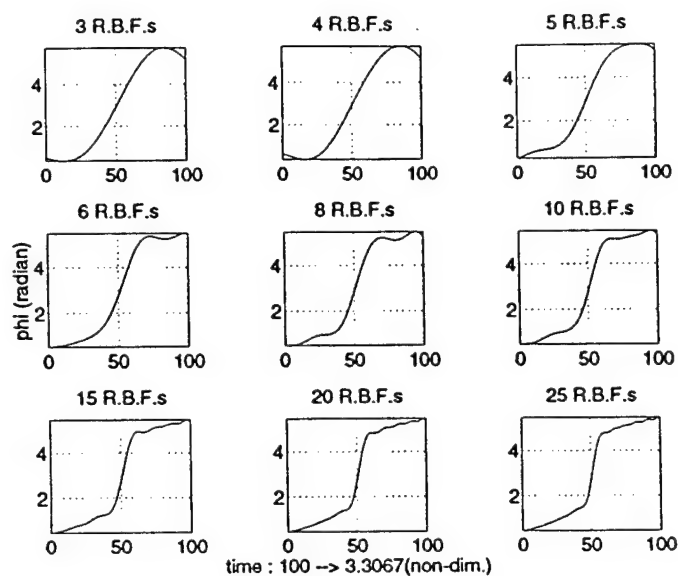
Fig. 3 ϕ vs. time for Evenly Spaced R.B.F. Algorithm
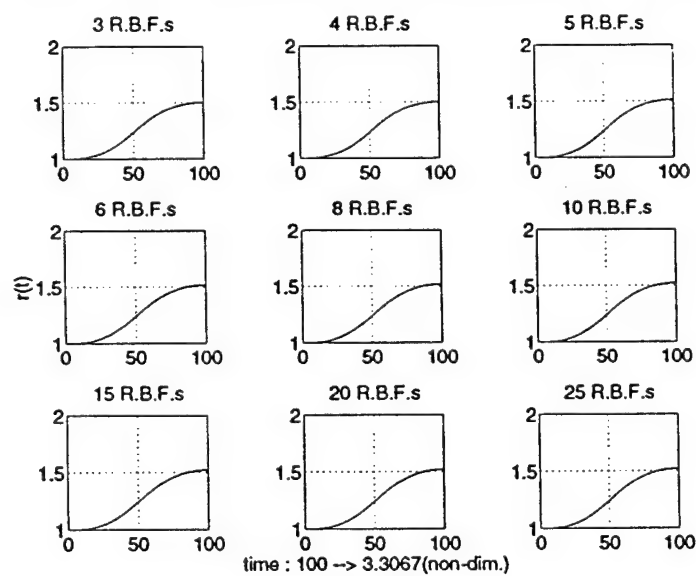
Fig. 4 $r(t_f)$ vs. time for Evenlt Spaced R.B.F. Algorithm

Adaptively Spaced Radial Basis Function Algorithm
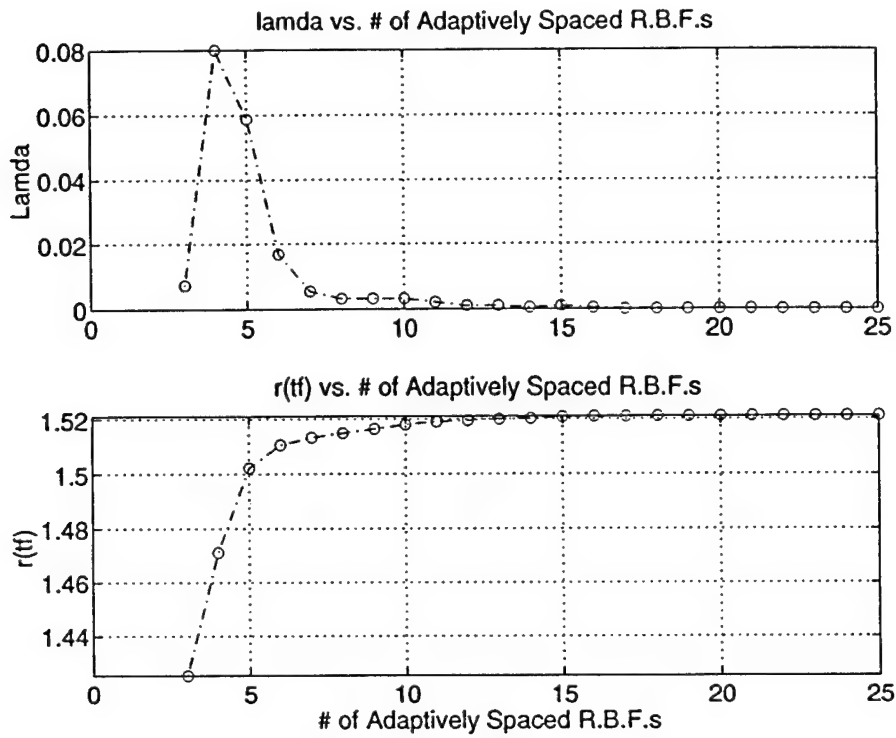
Fig. 5 λ and $r(t_f)$ vs. for # of Adaptively Spaced R.B.F.s
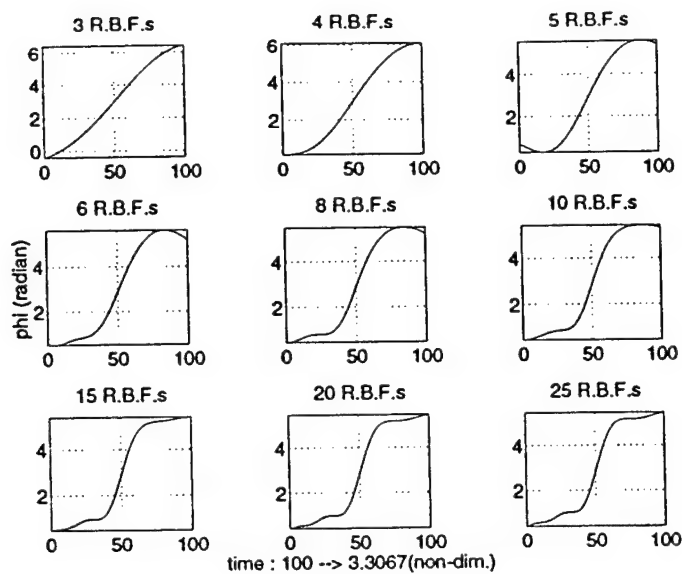
Fig. 6 ϕ vs. time for Adaptively Spaced R.B.F. Algorithm
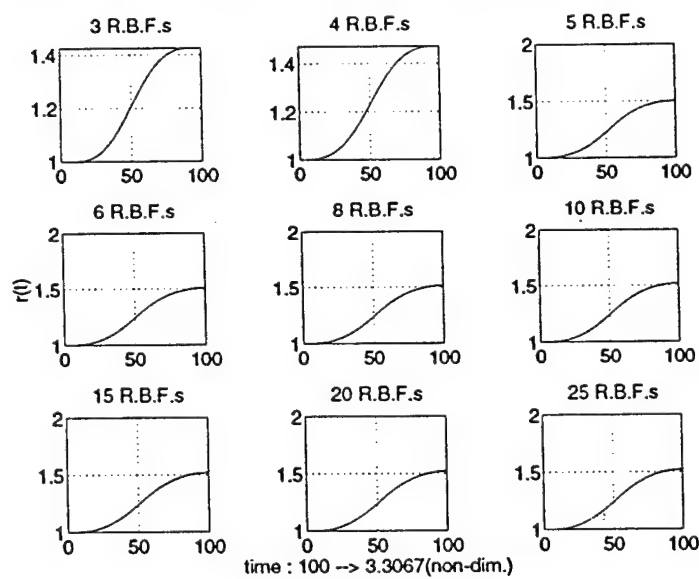
Fig. 7 $r(t_f)$ vs. time for Adaptively Spaced R.B.F. Algorithm

194

Comparison of Two Algorithms
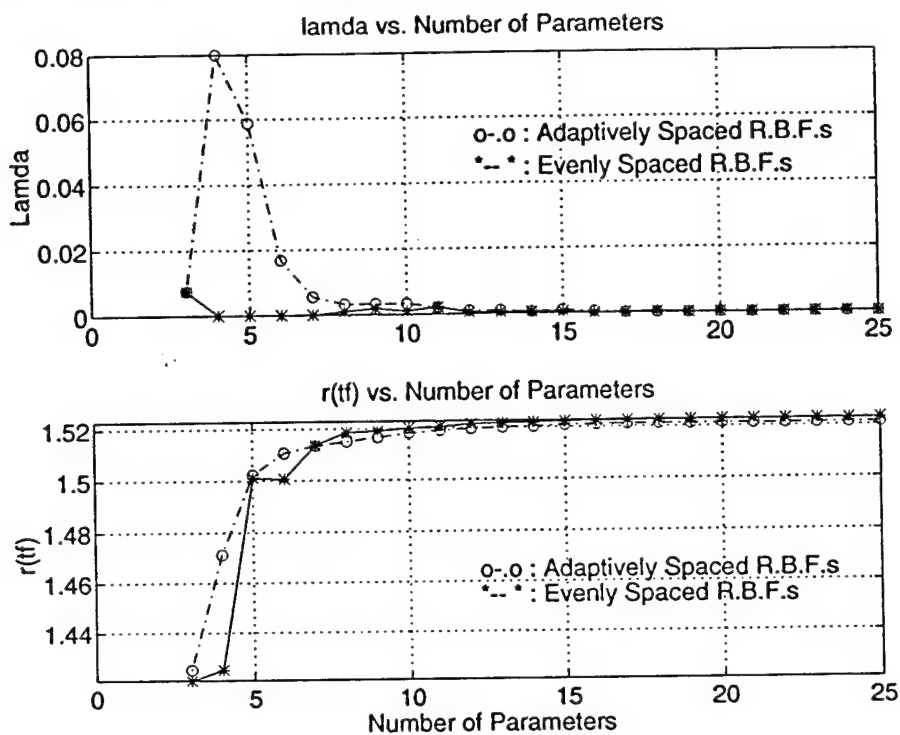
Fig. 8 λ and $r(t_f)$ vs. time for Two Algorithm

CONCLUDING REMARKS

- Radial Basis Function (RBF) Methods Investigated To Parameterize Function Space Optimal Control Problem

- Two Variations Studied
    - Evenly Spaced Centers
    - Adaptive Centers

- Minimum Norm Nonlinear Programming Algorithm Used To Iteratively Adjust RBF Weights

- Applied These Ideas to Low - Thrust Interplanetary Trajectory Optimization Problem

- Our Algorithms Have Been Fully Validated !

HIGHER ORDER CAYLEY TRANSFORMS WITH
APPLICATIONS TO ATTITUDE REPRESENTATIONS

Panagiotis Tsiotras [*]

University of Virginia
Charlottesville, VA 22903-2442

John L. Junkins [†] and Hanspeter Schaub [‡]

Texas A&M University
College Station, TX 77843-3141

Abstract

In this paper we generalize some previous results on attitude representations using Cayley transforms. First, we show that proper orthogonal matrices, that naturally represent rotations, can be generated by a form of "conformal" analytic mappings in the space of matrices. Using a natural parallelism between the elements of the complex plane and the real matrices, we generate higher order Cayley transforms and we discuss some of their properties. These higher order Cayley transforms are shown to parameterize proper orthogonal matrices into higher order "Rodrigues" parameters.

1. Introduction

The question of the proper choice of coordinates for describing rotations has a very long and exciting history. Starting with the work of Euler and Hamilton a series of different parameterizations were introduced by several researchers during the past hundred years. We will not delve into these results here since they can be found in any good textbook on attitude representations[1,2]. We just mention the recent survey article by Shuster[3] in the special issue in Ref. [4].

In this paper we take a slightly more abstract point of view than the previous references. Our main objective is to "unify" some of the existing results in the area of attitude representations. It is hoped that this global view will add to the current understanding of attitude representations. Our motivation stems mainly from the recent results on second order Rodrigues parameters[5,6,7]. In particular, in Ref. [7] it was shown that these (Modified) Rodrigues parameters can be generated by a second

order Cayley transform, the same way the classical Cayley-Rodrigues parameters are generated by the Cayley transform[8]. Viewing the Cayley transform as a bilinear transformation which maps the space of skew-symmetric matrices onto the space of proper orthogonal matrices (and vice versa) one is naturally led to the notion of conformal mappings (a generalization of the bilinear transformation) from the imaginary axis onto the unit circle (and vice versa). We seek to generalize these conformal mappings to matrix spaces. Drawing on the insightful statements by Halmos[9] we show that such an intuitive generalization is indeed possible. We are therefore able to generate the Euler parameters, the Rodrigues parameters and the Modified Rodrigues parameters as special cases of such conformal mappings. Higher order Rodrigues parameters can be easily constructed using this approach, although their relevance to applications is still to be determined. We explicitly develop the third and fourth order "Rodrigues parameters" in order to illustrate potential advantages as well as difficulties. The question of kinematics of these higher order "Rodrigues parameters" is much more subtle and is briefly discussed at the last section of the paper. A more in-depth discussion of the kinematics is left for future investigation.

The first part of the paper reviews the standard Cayley transform and it generalizes this transform to higher orders. There is no restriction on the dimension of the matrices involved, i.e., the results hold for $n \times n$ matrices. In the second part of the paper we apply these results to the case of interest to attitude dynamicists, i.e., the case $n = 3$.

Some notation and terminology is necessary in order to keep the discussion clear and terse. We use the standard mathematical notation $SO(n)$ to denote the space of proper orthogonal matrices of dimension $n \times n$. Invertible $n \times n$ matrices form the space $Gl(n)$, the general linear group. The space of orthogonal matrices is denoted by $O(n)$ and it is the set of all (invertible) matrices $A \in Gl(n)$ such that $A^T A = A A^T = I$. Clearly, if $A \in O(n)$ then

[*]Assistant Professor, Department of Mechanical, Aerospace and Nuclear Engineering. Member AIAA.

[†]Eppright Professor, Department of Aerospace Engineering. Fellow AIAA.

[‡]Graduate Student, Department of Aerospace Engineering. Student member AIAA.

1

$det(A) = \pm 1$. The qualifier "proper" then refers to those orthogonal matrices with positive determinant, that is,

$$SO(n) = \{A \in Gl(n) : AA^T = I, \ det(A) = +1\}$$

These matrices represent rotations, while the orthogonal matrices with determinant -1 represent reflections[10]. The space $SO(n)$ (as well as $Gl(n)$ and $O(n)$) forms a *group*. We will see later on that one can define a differential equation for elements of $SO(n)$. The solutions of this differential equation form trajectories (one-parameter subgroups) on $SO(n)$ and this differentiable structure makes $SO(n)$ actually a *Lie group* (i.e. a group with a differentiable manifold structure).

The space of $n \times n$ skew-symmetric matrices will be denoted by $so(n)$ That is,

$$so(n) = \{A \in \mathbb{R}^{n \times n} : A = -A^T\}$$

The space $so(n)$ is actually the tangent vector space to $SO(n)$ at the identity. This property can be easily verified by differentiating $A \in SO(n)$. Since $AA^T = I$ one has that

$$\frac{d}{dt}\left(AA^T\right) = 0 \Leftrightarrow \dot{A}A^T = -A\dot{A}^T$$

Evaluating the previous expression at $A = I$ one obtains that

$$\dot{A}\Big|_{A=I} = -\dot{A}^T\Big|_{A=I}$$

and so $\dot{A}\Big|_{A=I}$ is skew symmetric.

2. The Cayley Transform

Cayley's transformation parameterizes a proper orthogonal matrix C as a function of a skew-symmetric matrix Q. It is, therefore, a map

$$\psi : so(n) \to SO(n) \tag{1}$$

The classical Cayley transform[8] is given by

$$\begin{aligned} C = \psi(Q) &= (I-Q)(I+Q)^{-1} \\ &= (I+Q)^{-1}(I-Q) \end{aligned} \tag{2}$$

Since Q is skew-symmetric all its eigenvalues are pure imaginary. Thus, all the eigenvalues of the matrix $I+Q$ are nonzero and the inverse in Eq. (2) exists. The Cayley transform is therefore well-defined for all skew-symmetric matrices. The inverse transformation is identical and is given by

$$\begin{aligned} Q = \psi^{-1}(C) = \psi(C) &= (I-C)(I+C)^{-1} \\ &= (I+C)^{-1}(I-C) \end{aligned} \tag{3}$$

The inverse transformation is not defined when C has an eigenvalue at -1, because in this case $det(I+C) = 0$. Since C is orthogonal, all its eigenvalues lie on the unit circle

$$S^1 = \{(x_1, x_2) \in \mathbb{R}^2 : x_1^2 + x_2^2 = 1\} \tag{4}$$

Therefore $sp(C) \subset S^1$, where $sp(\cdot)$ denotes the spectrum of a matrix, and the transformation (3) requires that $-1 \notin sp(C)$. The same result is also shown in Ref. [7].

It is an easy exercise to show that C is orthogonal if Q is skew-symmetric. In order to show that the transformation (2) produces only proper orthogonal matrices, let us examine the determinant of C. Using Eq. (2) the determinant of C can be expressed as

$$\begin{aligned} det(C) &= det(I-Q)det\left((I+Q)^{-1}\right) \\ &= \frac{det(I-Q)}{det(I+Q)} \end{aligned} \tag{5}$$

Since all the eigenvalues of Q are imaginary ($sp(Q) \subset \Im$) they are of the form $\pm i\lambda_j$. The spectral decomposition of the matrix Q then yields

$$Q = R^{-1}\Lambda R$$

where $\Lambda = diag(\pm i\lambda_j)$. (The matrix Q is normal and normal matrices are always diagonalizable[11].) Noting that $I \pm Q = R^{-1}(I \pm \Lambda)R$ we rewrite Eq. (5) as

$$\begin{aligned} det(C) &= \frac{det(R^{-1})det(I-\Lambda)det(R)}{det(R^{-1})det(I+\Lambda)det(R)} = \frac{det(I-\Lambda)}{det(I+\Lambda)} \\ &= \frac{\prod_{j=1}^{p}(1-i\lambda_j)(1+i\lambda_j)}{\prod_{j=1}^{p}(1+i\lambda_j)(1-i\lambda_j)} \\ &= \frac{\prod_{j=1}^{p}(1+\lambda_j^2)}{\prod_{j=1}^{p}(1+\lambda_j^2)} = +1 \end{aligned}$$

where $2p$ is the number of nonzero (imaginary) eigenvalues of Q. Therefore $C \in SO(n)$ if $Q \in so(n)$ and thus, the Cayley transformation is injective (one-to-one) and surjective (onto) from the set of skew-symmetric matrices to the set of *proper* orthogonal matrices with no eigenvalue at -1.

3. Cayley Transforms as Conformal Mappings

The three most important subsets of the complex numbers are the real numbers, the imaginary numbers, and the numbers with absolute value one (i.e., the numbers on the unit circle). Following the standard mathematical language, we use the symbols $\mathbb{R}$,

2

$\Im = i\mathbb{R}$ and S^1 to denote these three sets, respectively. Trivially, these sets are subsets of the complex plane, denoted by $\mathbb{C}$. There is a very elegant analog between these three subsets of the complex plane and the $n \times n$ matrices[9], i.e., the elements of $\mathbb{R}^{n \times n}$. This analog can be easily understood and appreciated as follows: An elementary result in matrix algebra states that every $n \times n$ matrix with real elements can be decomposed into the sum of a symmetric and a skew-symmetric matrix. For example, any $A \in \mathbb{R}^{n \times n}$ can be written as

$$A = \frac{A + A^T}{2} + \frac{A - A^T}{2} \qquad (6)$$

It is easy to verify that the first matrix in Eq. (6) is symmetric and the second matrix is skew-symmetric. Symmetric matrices always have real eigenvalues and skew-symmetric matrices have always imaginary eigenvalues. Recall now that a complex number can always be decomposed into the sum of a real and an imaginary part. This parallelism between complex numbers and matrices allows one to treat the symmetric matrices as the "real numbers" and the skew-symmetric matrices as the "imaginary numbers" in the set of $\mathbb{R}^{n \times n}$ matrices[9]. In addition, recall that an orthogonal matrix in $\mathbb{R}^{n \times n}$ has all its eigenvalues on the unit circle. Drawing the previous parallelism even further we can therefore treat the orthogonal matrices as the "elements on the unit circle" in the space $\mathbb{R}^{n \times n}$. Similar statements can be made for the case of $n \times n$ matrices with complex entries (elements of $\mathbb{C}^{n \times n}$), where now hermitian, skew-hermitian and unitary matrices have to be used instead of symmetric, skew-symmetric and orthogonal matrices, respectively.

We intend to use this heuristic correspondence between complex numbers and $n \times n$ matrices in order to motivate and generalize the Cayley transform to higher order. Before we proceed, we briefly review some elements from complex function theory[12,13]. First, recall that a (complex) function is analytic in an open set if it has a derivative at each point in that set. In particular, f is analytic at a point z_0 if it is analytic in a neighborhood of z_0. Moreover, analytic functions have (uniformly) convergent power series expansions[12].

Definition 3.1 A transformation $w = f(z)$ where $w, z \in \mathbb{C}$ is said to be *conformal* at a point z_0 if f is analytic there and $f'(z_0) \neq 0$.

A conformal mapping is actually conformal at each point in a neighborhood of z_0, since the analyticity of f at z_0 implies analyticity in a neighborhood of z_0. Moreover, since f' is continuous at z_0, it

follows that there is also a neighborhood of z_0 with $f'(z) \neq 0$ for all z in this neighborhood[12]. It is a trivial consequence of the above definition that the composition of conformal mappings is also a conformal mapping.

A significant special class of conformal mappings in the complex plane is the class of *linear fractional transformations* (also called *bilinear transformations*) defined by

$$w = \frac{az + b}{cz + d}, \qquad (ad - bc \neq 0) \qquad (7)$$

An important property of the linear fractional transformations is that they always transform circles and lines into circles and lines[12]. In this paper we are interested – in particular – in conformal transformations of the form (7) which map the unit circle on the imaginary axis and vice versa. One such transformation is given by $w = f(z)$ where

$$f(z) = \frac{1 - z}{1 + z} \qquad (8)$$

It is an easy exercise to show that if $z \in \Im$ then $|w| = 1$, that is, $w \in S^1$ and thus, w is on the unit circle. Conversely, if $w \in S^1$ then the inverse transformation $z = f^{-1}(w)$ given by

$$f^{-1}(w) = \frac{1 - w}{1 + w} \qquad (9)$$

implies that the real part of z is zero and thus, $z \in \Im$.

The inverse transformation (9) is defined everywhere except at $w = -1$. The point $w = -1$ is mapped to infinity (see Fig. 1). In fact, the map (8) introduces a one-to-one transformation $f : \Im \to S^1 \backslash \{-1\}$.
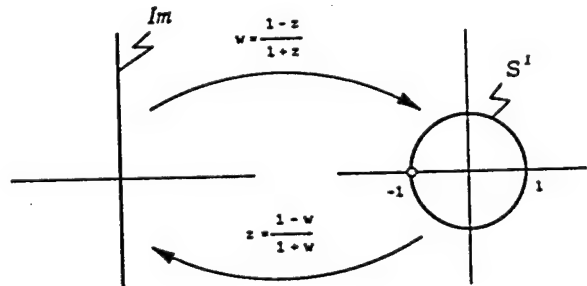

Figure 1: Bilinear transformation.

Let us now introduce the conformal mapping $g_n : S^1 \to S^1$ defined by

$$g_n(w) = w^n, \qquad n = 2, 3, \ldots \qquad (10)$$

The function g_n is a mapping from the unit circle onto the unit circle. This transformation is only

3

locally injective. Therefore the inverse of g_n exists only locally. Given $\chi = e^{i\theta} \in S^1$ the solution of the equation

$$\chi = w^n, \qquad n = 2, 3, \ldots$$

yields that

$$w = e^{i\left(\frac{\theta + 2k\pi}{n}\right)}, \qquad k = 0, 1, 2, \ldots, n-1 \qquad (11)$$

Equation (11) shows that, in general, the equation $\chi = w^n$ has more than one solution. This result will turn out to be beneficial in section 5 when we discuss the application of higher order Cayley-transforms to attitude representations, because these roots can be used to avoid the inherent singularities of three-dimensional parameterizations of $SO(3)$. For $k = 0$ in Eq. (11) we get that $w = e^{i\frac{\theta}{n}}$. We will call this the *principal* nth root of χ.

The composition of the maps f and g_n is the function $h_n : \mathfrak{F} \to S^1$ defined by $h_n = g_n \circ f$, that is

$$h_n(z) = \left(\frac{1-z}{1+z}\right)^n \qquad (12)$$

which maps the imaginary axis onto the unit circle. Similarly to g_n, this map is only locally invertible. A local inverse is obtained, for example, by setting $k = 0$ in Eq. (11), in which case we have that ($\chi = e^{i\theta}$)

$$z = e^{i\frac{\theta}{n}}$$

where

$$\theta = \arctan\left(i\frac{\bar{\chi} - \chi}{\bar{\chi} + \chi}\right)$$

and where bar denotes complex conjugate.

4. Higher Order Cayley Transforms

One of the most celebrated results in matrix algebra is the Cayley-Hamilton theorem. This theorem states that a matrix satisfies its own characteristic polynomial. An important consequence of this theorem is that, given any matrix $A \in \mathbb{R}^{n \times n}$ and an analytic function $F(z)$ inside a disk of radius r in the complex plane, one can unambiguously define the matrix-valued function $F(A)$ if the eigenvalues of A lie inside the disk of radius r. In other words, if F is given by

$$F(z) = \sum_{i=0}^{\infty} \alpha_i z^i, \qquad |z| \leq r$$

then

$$F(A) = \sum_{i=0}^{\infty} \alpha_i A^i$$

and the previous series converges assuming that $|\lambda_j| \leq r$ where $\lambda_j \in sp(A)$ for $j = 1, 2, \ldots, n$. Therefore, the matrix $F(A)$ is well-defined. Moreover, the eigenvalues of the matrix $F(A)$ are $F(\lambda_j)$ ($j = 1, 2, \ldots, n$) (Ref. [11]).

Consider now the conformal mapping f from Eq. (8) which maps the imaginary axis on the unit circle. This function is analytic everywhere. According to the previous discussion, the matrix

$$f(Q) = (I - Q)(I + Q)^{-1} = (I + Q)^{-1}(I - Q) \qquad (13)$$

is well-defined for $Q \in so(n)$ and, actually, $C = f(Q) \in SO(n)$. Comparison between the previous equation and Eq. (2) reveals that the Cayley transform can be viewed as a special case of a conformal mapping in the space of matrices.

We have seen that there is a natural correspondence between $\mathfrak{F}$ and $so(n)$, as well as between S^1 and $SO(n)$. (We caution the the mathematically inclined reader to take these statements in the context of the discussion in section 3. We do not claim that this correspondence carries any more weight than providing one qualitative motivation for the generalization of certain complex analytic results to analogous results in the space of matrices). Following Eq. (12) we can also define a series of transformations $h_n : so(n) \to SO(n)$ by

$$h_n(Q) = (I - Q)^n (I + Q)^{-n} = (I + Q)^{-n}(I - Q)^n \qquad (14)$$

where Q is a skew-symmetric matrix. It should be clear by now that $C = h_n(Q)$ is a proper orthogonal matrix, i.e., $C \in SO(n)$. We shall refer to the family of maps $h_n(Q)$ in Eq. (14) as *Higher Order Cayley Transforms*. The consequences of such a generalization in attitude representations will become apparent in the next section.

For now, let us concentrate on the inverse map $h_n^{-1} : SO(n) \to so(n)$. Since $h_n = g_n \circ f$ one obtains $h_n^{-1} = f^{-1} \circ g_n^{-1}$. The function f^{-1} is given by Eq. (9) which, when applied to a proper orthogonal matrix Q with no eigenvalue at -1, gives the inverse of the classical (or first order) Cayley transform as in Eq. (3). The map $g_n^{-1} : SO(n) \to SO(n)$ on the other hand requires the nth root of an orthogonal matrix. First, we show that g_n^{-1} is well-defined in the sense that the nth root of a (proper) orthogonal matrix with no eigenvalue at -1 is also a (proper) orthogonal matrix with no eigenvalue at -1. This will also prove that the composition of maps g_n^{-1} and f^{-1} is well-defined since the range of g_n^{-1} is in the domain of f^{-1}.

To this end, consider an orthogonal matrix $C \in SO(n)$ such that $\lambda \neq -1$ for all $\lambda \in sp(C)$. The

4

matrix C can be decomposed as follows

$$C = U\Theta U^*$$ (15)

for some unitary matrix U, where

$$\Theta = blockdiag(\Theta_1, \Theta_2, \ldots, \Theta_{n-1}, +1)$$ (16)

if n is odd and

$$\Theta = blockdiag(\Theta_1, \Theta_2, \ldots, \Theta_n)$$ (17)

if n is even, and

$$\Theta_j = \begin{bmatrix} e^{i\theta_j} & 0 \\ 0 & e^{-i\theta_j} \end{bmatrix}, \quad j = 1, \ldots, n$$ (18)

The diagonal elements of the matrix Θ in Eq. (15) are the eigenvalues of C. The principal kth root of the matrix C is then given by

$$W = U\Theta_k U^*$$ (19)

where $W^k = C$ and

$$\Theta_k = blockdiag(\Theta_1^k, \Theta_2^k, \ldots, \Theta_{n-1}^k, +1)$$ (20)

if n is odd and

$$\Theta_k = blockdiag(\Theta_1^k, \Theta_2^k, \ldots, \Theta_n^k)$$ (21)

if n is even, and

$$\Theta_j^k = \begin{bmatrix} e^{i\frac{\theta_j}{k}} & 0 \\ 0 & e^{-i\frac{\theta_j}{k}} \end{bmatrix}, \quad j = 1, \ldots, n$$ (22)

Since $e^{i\theta_j} \neq -1$ for all $j = 1, \ldots, n$ $(n-1)$ the angles $\theta_j \neq \pm 180$ deg and thus also $\frac{\theta_j}{k} \neq \pm 180$ deg for $k = 2, 3, \ldots$ and thus $e^{i\frac{\theta_j}{k}} \neq -1$. Notice that in order to keep W proper we always choose the positive root of the eigenvalue $+1$.

5. Attitude Representations

In this section we concentrate on the ramifications of the previously developed results to attitude representations. Our motivation for investigating Cayley transforms in the first place, stems from the fact that proper orthogonal matrices represent rotations. In particular, $SO(3)$ is the configuration space of all three-dimensional rotations. In other words, every element of $SO(3)$ represents a physical rotation between two reference frames in $\mathbb{R}^3$ and conversely, every rotation can be represented by an element in $SO(3)$.

As a reference frame, viz. a body, rotates freely in the three-dimensional space, the corresponding

rotation matrix C traces a curve in $SO(3)$ such that $C(t) \in SO(3)$ for all $t \geq 0$. The differential equation characterizing this trajectory on $SO(3)$ is given by

$$\dot{C} = [\omega]C$$ (23)

where, given a vector $\omega = (\omega_1, \omega_2, \omega_3) \in \mathbb{R}^3$, the matrix $[\omega]$ is defined by

$$[\omega] = \begin{bmatrix} 0 & \omega_3 & -\omega_2 \\ -\omega_3 & 0 & \omega_1 \\ \omega_2 & -\omega_1 & 0 \end{bmatrix}$$ (24)

In the sequel we apply the results of the previous section in order to parameterize the rotation group. In particular, the series of conformal mappings from Eq. (14) provide a family of coordinates on $SO(3)$. Before undertaking this task we investigate another important conformal mapping.

5.1. The Exponential Map and the Euler Parameters

Linear fractional transformations are not the only class of conformal mappings from the imaginary axis onto the unit circle. The exponential map, defined by

$$w = exp(z) = e^z$$ (25)

also maps $\Im$ onto S^1. Clearly, if $z = i\theta$ then $|z| = 1$. The inverse transformation is

$$z = \log w = i(\theta + 2n\pi), \quad n = 0, \pm 1, \pm 2, \ldots$$

and is defined only locally.

We can therefore define the exponential map from the space of skew-symmetric matrices to the space of proper orthogonal matrices. This exponential map is defined, as usual, by

$$C = e^Q = \sum_{n=0}^{\infty} \frac{1}{n!} Q^n$$ (26)

and the series converges for every Q. For the three-dimensional case, the matrix $Q \in so(3)$ can be parameterized by

$$Q = \begin{bmatrix} 0 & \beta_3 & -\beta_2 \\ -\beta_3 & 0 & \beta_1 \\ \beta_2 & -\beta_1 & 0 \end{bmatrix}$$ (27)

As before, given a vector $\beta = (\beta_1, \beta_2, \beta_3) \in \mathbb{R}^3$ we will also use the notation $[\beta]$ to denote the skew-symmetric matrix in Eq. (27). Noticing that

$$[\beta]^2 = \beta\beta^T - \|\beta\|^2 I$$

5

one obtains that

$$[\beta]^{2k+1} = (-1)^k \|\beta\|^{2k} [\beta], \qquad k = 0, 1, 2, \ldots$$

and

$$[\beta]^{2k} = (-1)^k \|\beta\|^{2k} I - (-1)^k \|\beta\|^{2(k-1)} \beta\beta^T$$

Substituting the previous expressions in Eq. (26) we get Euler's formula[3]

$$C(\beta) = e^{[\beta]} = \cos\phi\, I + \sin\phi\, \frac{[\beta]}{\phi} + (1 - \cos\phi)\frac{\beta\beta^T}{\phi^2}$$

where $\phi = \|\beta\|$. Equivalently,

$$e^{[\beta]} = I + \sin\phi\, \frac{[\beta]}{\phi} + (1 - \cos\phi)\frac{[\beta]^2}{\phi^2} \qquad (28)$$

Normalizing the vector β we get a unit vector

$$\hat{e} = \frac{\beta}{\|\beta\|}$$

or

$$\beta = \phi\hat{e} \qquad (29)$$

Euler's theorem[1] states that any rotation can be represented by a finite rotation (principal rotation) about a single axis (principal axis). That is, the principal axis and the principal angle suffice to determine the rotation matrix. From a mathematical perspective this amounts to parameterizing every element in $SO(3)$ by the principal axis and the principal angle.

By letting the principal axis be along the direction of the unit vector $\hat{e}$ and by letting the principal angle be ϕ as above, Eq. (28) shows how this parameterization is achieved. Clearly,

$$C(\phi, \hat{e}) = e^{\phi[\hat{e}]} \qquad (30)$$

Moreover, introducing the *Euler parameter vector* $q = (q_0, q_1, q_2, q_3)$

$$q_0 = \cos\frac{\phi}{2}, \quad q_i = \hat{e}_i \sin\frac{\phi}{2}, \qquad i = 1, 2, 3 \quad (31)$$

and substituting in Eq. (28) one obtains the well-known formula for the rotation matrix in terms of the Euler parameters

$$C(q) = \begin{bmatrix} q_0^2 + q_1^2 - q_2^2 - q_3^2 & 2(q_1q_2 + q_0q_3) \\ 2(q_1q_2 - q_0q_3) & q_0^2 - q_1^2 + q_2^2 - q_3^2 \\ 2(q_1q_3 + q_0q_2) & 2(q_2q_3 - q_0q_1) \end{bmatrix}$$
$$\begin{matrix} 2(q_1q_3 - q_0q_2) \\ 2(q_2q_3 + q_0q_1) \\ q_0^2 - q_1^2 - q_2^2 + q_3^2 \end{matrix} \qquad (32)$$

Therefore, the Euler parameter representation is obtained by generalizing the conformal mapping in Eq. (25) to the space of matrices. Notice from Eq. (32) that $C(q) = C(-q)$ and both q and $-q$ can be used to describe the same physical orientation. This fact can be used to construct alternative, or "shadow", sets of kinematic parameters obtained via the Cayley transforms.

5.2. Rodrigues Parameters

Since the Euler parameters satisfy the additional constraint $q_0^2 + q_1^2 + q_2^2 + q_3^2 = 1$, one is naturally led to consider the elimination of this constraint, thus reducing the number of coordinates from four to three. The Rodrigues parameters achieve this by defining

$$\rho_j = \frac{q_j}{q_0}, \qquad j = 1, 2, 3 \qquad (33)$$

The three parameters ρ_1, ρ_2, ρ_3 then provide a three-dimensional parameterization of $SO(3)$. The inverse transformation of Eq. (33) is given by

$$q_0 = \frac{1}{(1 + \hat{\rho}^2)^{\frac{1}{2}}}, \quad q_j = \frac{\rho_j}{(1 + \hat{\rho}^2)^{\frac{1}{2}}}, \qquad j = 1, 2, 3 \qquad (34)$$

where $\hat{\rho}^2 = \rho_1^2 + \rho_2^2 + \rho_3^2$. The Rodrigues parameters are related to the principal axis and angle through the equation

$$\rho = \tan\frac{\phi}{2}\,\hat{e}$$

The rotation matrix in terms of the Rodrigues parameters can be easily computed using Eq. (32) and Eq. (34).

$$C(\rho) = \frac{1}{1 + \hat{\rho}^2} \begin{bmatrix} 1 - \hat{\rho}^2 + 2\rho_1^2 & 2(\rho_1\rho_2 + \rho_3) \\ 2(\rho_1\rho_2 - \rho_3) & 1 - \hat{\rho}^2 + 2\rho_2^2 \\ 2(\rho_3\rho_1 + \rho_2) & 2(\rho_2\rho_3 - \rho_1) \end{bmatrix}$$
$$\begin{matrix} 2(\rho_3\rho_1 - \rho_2) \\ 2(\rho_2\rho_3 + \rho_1) \\ 1 - \hat{\rho}^2 + 2\rho_3^2 \end{matrix} \qquad (35)$$

It is remarkable the fact that the previous parameterization of $SO(3)$ can also be achieved by means of the Cayley transformation in Eq. (2). Indeed, if we introduce the skew-symmetric matrix

$$R = -[\rho] = \begin{bmatrix} 0 & -\rho_3 & \rho_2 \\ \rho_3 & 0 & -\rho_1 \\ -\rho_2 & \rho_1 & 0 \end{bmatrix}$$

the transformation

$$C = (I - R)(I + R)^{-1} = (I + R)^{-1}(I - R) \qquad (36)$$

6

produces exactly the matrix in Eq. (35). Therefore the classical Cayley-Rodrigues parameters representation is obtained by generalizing the conformal mapping in Eq. (8) to the space of matrices.

5.3. Modified Rodrigues Parameters

The normalization in Eq. (33) is not the only possible one. A more judicious normalization for eliminating the Euler parameter constraint is through stereographic projection[12,13,14]. Using this approach, the new variables

$$\sigma_j := \frac{q_j}{1 + q_0}, \qquad j = 1, 2, 3 \qquad (37)$$

provide coordinates on $SO(3)$. These parameters are referred to in the literature as the Modified Rodrigues parameters[3] and have distinct advantages over the classical Rodrigues parameters. In particular, while the Rodrigues parameters do not allow eigenaxis rotations of more than 180 deg, the Modified Rodrigues parameters allow for eigenaxis rotations of upto 360 deg[6,7,14,15,16]. This can be immediately deduced by the corresponding relationship between σ and the principal axis and angle

$$\sigma = \tan\frac{\phi}{4}\, \hat{e}$$

which is well-behaved for $0 \le \phi < 2\pi$. Since both q and $-q$ describe the same physical orientation (recall the discussion at the end of section 5.1), a second set of parameters defined by

$$\sigma_j^s := -\frac{q_j}{1 - q_0}, \qquad j = 1, 2, 3$$

referred to as the "shadow" set[15], can be used to describe the same physical orientation. These parameters are also given by

$$\sigma^s = -\frac{1}{\tan\frac{\phi}{4}}\, \hat{e}$$

The transformation between σ and σ^s is given by[15]

$$\sigma^s = -\frac{\sigma}{\hat{\sigma}^2} \qquad (38)$$

where $\hat{\sigma}^2 = \sigma^T \sigma = \sigma_1^2 + \sigma_2^2 + \sigma_3^2 = \tan^2\frac{\phi}{4}$.

The rotation matrix associated with the Modified Rodrigues Parameters is given by

$$C(\sigma) = \frac{1}{1 + \hat{\sigma}^2}
\begin{bmatrix}
4\Sigma_1 + \tilde{\Sigma}^2 & 8\sigma_1\sigma_2 + 4\sigma_3\tilde{\Sigma} \\
8\sigma_1\sigma_2 - 4\sigma_3\tilde{\Sigma} & 4\Sigma_2 + \tilde{\Sigma}^2 \\
8\sigma_1\sigma_3 + 4\sigma_2\tilde{\Sigma} & 8\sigma_2\sigma_3 - 4\sigma_1\tilde{\Sigma}
\end{bmatrix}$$

$$\begin{bmatrix}
8\sigma_1\sigma_3 - 4\sigma_2\tilde{\Sigma} \\
8\sigma_2\sigma_3 + 4\sigma_1\tilde{\Sigma} \\
4\Sigma_3 + \tilde{\Sigma}^2
\end{bmatrix} \qquad (39)$$

where $\tilde{\Sigma} = 1 - \hat{\sigma}^2$ and $\Sigma_j = -\hat{\sigma}^2 + 2\sigma_j^2$, $j = 1, 2, 3$.

In Ref. [7] it was shown that these parameters are defined by a Cayley transformation of second order. That is, if

$$S = -[\sigma] =
\begin{bmatrix}
0 & -\sigma_3 & \sigma_2 \\
\sigma_3 & 0 & -\sigma_1 \\
-\sigma_2 & \sigma_1 & 0
\end{bmatrix} \qquad (40)$$

then the transformation

$$C = (I - S)^2(I + S)^{-2} = (I + S)^{-2}(I - S)^2 \quad (41)$$

produces exactly the matrix in Eq. (39). Notice that the inverse of the transformation (41) is not unique and it requires the square root of an orthogonal matrix. Given $C \in SO(3)$ we find a matrix W such that

$$C = W^2 \qquad (42)$$

Once a matrix W is calculated, the skew-symmetric matrix S containing the Modified Rodrigues parameters is computed from

$$S = (I - W)(I + W)^{-1} = (I + W)^{-1}(I - W) \quad (43)$$

Reference [7] outlines this approach. To every orthogonal matrix corresponds a principal angle and a principal direction according to Eq. (30). From Eqs. (30) and (42) one therefore has that

$$W = e^{\frac{\phi}{2}[\hat{e}]} \qquad (44)$$

and W has half the principal angle of C. It should be apparent now how the Modified Rodrigues parameters double the domain of validity of the parameterization by taking the square of the classical Cayley transform.

This observation motivates the search of higher dimensional Cayley transforms for attitude representations. Such transformations are expected to increase the domain of validity even further. This is the topic of the next section.

5.4. Higher Order Rodrigues Parameters

According to the discussion in the previous section one expects that higher order Cayley transformations will increase the domain of validity of the corresponding parameters. The main task of this section is to derive these higher order parameters and find their connections to the Rodrigues parameters, the Modified parameters and the Euler parameters. To this end, consider first the fourth order Cayley transform defined by

$$C = (I - T)^4(I + T)^{-4} \qquad (45)$$

7

for some skew-symmetric matrix

$$T = -[\tau] = \begin{bmatrix} 0 & -\tau_3 & \tau_2 \\ \tau_3 & 0 & -\tau_1 \\ -\tau_2 & \tau_1 & 0 \end{bmatrix} \quad (46)$$

We know that the matrix C is (proper) orthogonal.

Recall from the results of section 3 that if F is analytic function, then the eigenvalues of the matrix $F(A)$ are given by $F(\lambda_j)$ where λ_j are the eigenvalues of A. It is an easy exercise to show that the eigenvalues of the skew-symmetric matrix in Eq. (46) are given by

$$0, \quad \pm i(\tau_1^2 + \tau_2^2 + \tau_3^2)^{\frac{1}{2}} \quad (47)$$

Similarly, the eigenvalues of the matrix S in Eq. (40) are given by

$$0, \quad \pm i(\sigma_1^2 + \sigma_2^2 + \sigma_3^2)^{\frac{1}{2}} \quad (48)$$

Let λ_τ denote an eigenvalue of T and λ_σ an eigenvalue of S. Comparing Eqs. (41) and (45) one sees that the matrices S and T are related by

$$(I - S)(I + S)^{-1} = (I - T)^2(I + T)^{-2} \quad (49)$$

This suggests that λ_σ and λ_τ are related by

$$\frac{1 - \lambda_\sigma}{1 + \lambda_\sigma} = \left(\frac{1 - \lambda_\tau}{1 + \lambda_\tau}\right)^2 \quad (50)$$

or

$$1 + \lambda_\sigma = \frac{(1 + \lambda_\tau)^2}{1 + \lambda_\tau^2}$$

Solving for λ_σ one obtains that

$$\lambda_\sigma = \frac{2\lambda_\tau}{1 + \lambda_\tau^2}$$

Substituting the expressions for λ_σ and λ_τ from Eqs. (47) and (48) in the previous equation one obtains that

$$\pm i(\sigma_1^2 + \sigma_2^2 + \sigma_3^2)^{\frac{1}{2}} = 2\frac{\pm i(\tau_1^2 + \tau_2^2 + \tau_3^2)^{\frac{1}{2}}}{1 - \tau_1^2 - \tau_2^2 - \tau_3^2}$$

Upon squaring this expression one obtains

$$\sigma_1^2 + \sigma_2^2 + \sigma_3^2 = 4\frac{\tau_1^2 + \tau_2^2 + \tau_3^2}{(1 - \tau_1^2 - \tau_2^2 - \tau_3^2)^2}$$

This equation suggests that σ and τ are related by

$$\sigma_j = \pm\frac{2\tau_j}{1 - \tau_1^2 - \tau_2^2 - \tau_3^2}, \quad j = 1, 2, 3 \quad (51)$$

Arbitrarily, and without loss of generality, we choose the solution with the plus sign. Substitution in S

and computing C from Eq. (41) verifies the expression in Eq. (51).

The relation between τ and q is obtained by observing that

$$\frac{2\tau_j}{1 - \tau_1^2 - \tau_2^2 - \tau_3^2} = \frac{q_j}{1 + q_0}, \quad j = 1, 2, 3 \quad (52)$$

Using the shorthand notation $\hat{\tau}^2 = \tau_1^2 + \tau_2^2 + \tau_3^2$ the previous expression can be written as

$$\frac{2\tau_j}{1 - \hat{\tau}^2} = \frac{q_j}{1 + q_0}, \quad j = 1, 2, 3$$

Therefore,

$$4\frac{\hat{\tau}^2}{(1 - \hat{\tau}^2)^2} = \frac{q_1^2 + q_2^2 + q_3^2}{(1 + q_0)^2}$$

or

$$\begin{aligned} \left(\frac{1 + \hat{\tau}^2}{1 - \hat{\tau}^2}\right)^2 &= \frac{q_1^2 + q_2^2 + q_3^2 + (1 + q_0)^2}{(1 + q_0)^2} \\ &= \frac{2(1 + q_0)}{(1 + q_0)^2} = \frac{2}{1 + q_0} \end{aligned} \quad (53)$$

or that

$$\frac{1 + \hat{\tau}^2}{1 - \hat{\tau}^2} = \pm\frac{\sqrt{2}}{\sqrt{1 + q_0}}$$

and thus,

$$\frac{2}{1 - \hat{\tau}^2} = \frac{\pm\sqrt{2} + \sqrt{1 + q_0}}{\sqrt{1 + q_0}}$$

Using now Eq. (52) one finally obtains that

$$\tau_j = \frac{q_j}{1 + q_0 \pm \sqrt{2(1 + q_0)}}, \quad j = 1, 2, 3 \quad (54)$$

Conversely, from Eq. (53) one obtains that

$$1 + q_0 = 2\left(\frac{1 - \hat{\tau}^2}{1 + \hat{\tau}^2}\right)^2 \quad (55)$$

and using Eq. (52) that

$$q_j = \frac{4\tau_j(1 - \hat{\tau}^2)}{(1 + \hat{\tau}^2)^2}, \quad j = 1, 2, 3$$

From Eq. (55) we also have that

$$q_0 = 2\left(\frac{1 - \hat{\tau}^2}{1 + \hat{\tau}^2}\right)^2 - 1 = \frac{(1 - 6\hat{\tau}^2 + \hat{\tau}^4)}{(1 + \hat{\tau}^2)^2}$$

where $\hat{\tau}^4 = (\hat{\tau}^2)^2$. Letting $W = (I - T)(I + T)^{-1}$ and since $C = W^4$ one obtains that

$$W = e^{\frac{\phi}{4}[\hat{e}]}$$

8

where ϕ is the principal angle of C. Moreover, using the definition of the Euler parameters from Eq. (31) one obtains the following result for the τ parameters

$$\tau = \frac{\sin \frac{\phi}{2}}{1 + \cos \frac{\phi}{2} \pm \sqrt{2(1 + \cos \frac{\phi}{2})}} \hat{e} \qquad (56)$$

where $\hat{e}$ is the unit vector along the principal axis. Using the trigonometric identity $\cos \frac{\phi}{2} = 2\cos^2 \frac{\phi}{4} - 1$, the previous equation reduces to

$$\tau = \frac{\sin \frac{\phi}{2}}{1 + \cos \frac{\phi}{2} \pm 2\cos \frac{\phi}{4}} \hat{e} \qquad (57)$$

Keeping the plus sign, Eq. (57) can be further reduced to the simple formula

$$\tau_+ = \tan \frac{\phi}{8} \hat{e}, \qquad (-4\pi < \phi < 4\pi) \qquad (58)$$

From Eq. (58) it is apparent that τ is proportional to the principal rotation axis, like the classical and the Modified Rodrigues parameters, where now the proportionality factor is $f(\phi) = \tan \frac{\phi}{8}$. A plot of $f(\phi)$ is shown in Fig. 2.
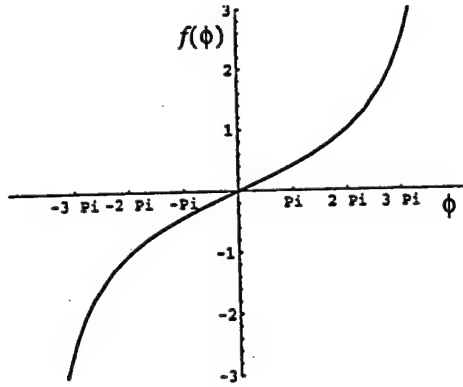

Figure 2: Plot of $f(\phi)$.

Equation (58) is reassuring, since it proves that the τ parameters indeed behave as "higher order" Rodrigues parameters which can be used to "linearize" the domain of validity of the kinematic parameterization. By this, we mean that Eq. (58) behaves almost linearly as a function of the principal angle ϕ (especially in the region $-\pi/8 \le \phi \le \pi/8$); see also Fig. 3.

If we choose the minus sign in Eq. (56) we obtain that

$$\tau_- = -\frac{1}{\tan \frac{\phi}{8}} \hat{e}, \qquad (0 < \phi < 8\pi) \qquad (59)$$

Moreover, reversing the signs of the Euler parameters in Eq. (54), one obtains that the τ parameters

have a unique set of "shadow" parameters like the Modified Rodrigues parameters[15]. These parameters are obtained by setting

$$\tau^s = \frac{-\sin \frac{\phi}{2}}{1 - \cos \frac{\phi}{2} \pm 2\sin \frac{\phi}{4}} \hat{e} \qquad (60)$$

In can be easily verified that the corresponding "shadow" parameters reduce to

$$\tau_+^s = \frac{\tan \frac{\phi}{8} - 1}{\tan \frac{\phi}{8} + 1} \hat{e} \qquad (-2\pi < \phi < 6\pi) \qquad (61)$$

and

$$\tau_-^s = \frac{1 + \tan \frac{\phi}{8}}{1 - \tan \frac{\phi}{8}} \hat{e} \qquad (-6\pi < \phi < 2\pi) \qquad (62)$$

As the original τ parameters approach $+1$, the associated "shadow" parameters τ^s approach zero and vice versa. The general transformation between the original and the "shadow" set is given by

$$\tau^s = -\tau \left(\frac{1 - \hat{\tau}^2}{2\hat{\tau}^2 + (1 + \hat{\tau}^2)\hat{\tau}} \right) \qquad (63)$$

where $\hat{\tau} = (\hat{\tau}^2)^{\frac{1}{2}}$. Equations (58),(59),(61) and (62) can be used in order to compute the four distinct roots of Eq. (45). Note also that Eqs. (58),(61),(59) and (62) can be also written in the form

$$\tau = \tan \left(\frac{\phi}{8} - k\frac{\pi}{4} \right) \hat{e}, \qquad k = 0, 1, 2, 3$$

respectively.

The "shadow" parameter set τ^s is shown side-by-side with the original τ parameters in Fig. 3. The shadow set is plotted in grey color. Figure 3 also shows that τ parameters are indeed very linear for small rotations within ± 180 deg.

As with the Modified Rodrigues parameters (and other stereographic parameters[15]), these "shadow" parameters represent the same physical orientation as the original set and abide by the same differential kinematic equation. They could be used to avoid the problems of approaching the ± 720 deg principal rotation. By switching to the shadow trajectory, all numerical problems would be avoided. Having, however, a principal rotation range of ± 720 deg is really more than needed. Limiting the principal rotations to be within ± 180 deg would suffice and be much more attractive. As the magnitude of τ approaches $\tan \frac{\pi}{8}$ then one would simply switch the τ to their "shadow" set. Having $|\tau| = \tan \frac{\pi}{8}$ corresponds to $q_0 = 0$. From Eq. (54) one can then see
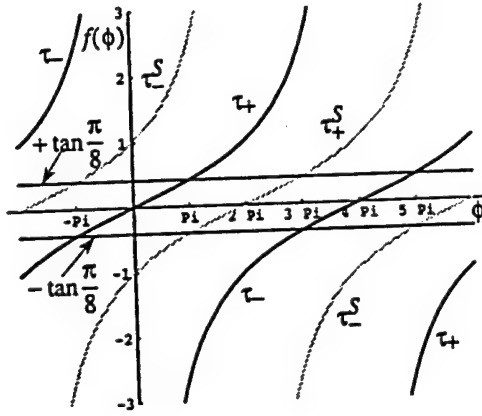
9

Figure 3: Comparison of original and "shadow" τ parameters.

that at this point, the two sets of parameters are related by $\tau = -\tau^s$. The combined set of original and "shadow" τ parameters would provide a set of attitude coordinates which are "very linear" with respect to the principal rotation angle, more so even than the Modified Rodrigues parameters. We note in passing that the previous approach can be easily extended to any Cayley transform of order 2^k, since Eqs. (49) and (50) can be used iteratively.

For the third order Cayley transform we have that

$$C = (I - P)^3(I + P)^{-3} = (I + P)^{-3}(I - P)^3 \quad (64)$$

where $P = -[p]$ and $p = (p_1, p_2, p_3)$ the corresponding parameters. If λ_ρ and λ_p denote the respective eigenvalues of the skew-symmetric matrices R and P then, using Eqs. (36) and (64), they must be related by

$$\frac{1 - \lambda_\rho}{1 + \lambda_\rho} = \left(\frac{1 - \lambda_p}{1 + \lambda_p}\right)^3$$

or, upon expanding the previous equality

$$\frac{1 - \lambda_\rho}{1 + \lambda_\rho} = \frac{1 - \lambda_p^3 + 3\lambda_p^2 - 3\lambda_p}{1 + \lambda_p^3 + 3\lambda_p^2 + 3\lambda_p}$$

thus

$$1 + \lambda_\rho = \frac{(1 + \lambda_p)^3}{1 + 3\lambda_p^2}$$

Solving for λ_ρ we obtain

$$\lambda_\rho = \frac{\lambda_p(3 + \lambda_p^2)}{1 + 3\lambda_p^2}$$

The previous equation suggests that ρ_j and p_j are related by

$$\rho_j = \pm\frac{p_j(3 - p_1^2 - p_2^2 - p_3^2)}{1 - 3(p_1^2 + p_2^2 + p_3^2)}, \quad j = 1, 2, 3$$

In order to get the relation of p to the Euler parameter vector one can set

$$\frac{p_j(3 - p_1^2 - p_2^2 - p_3^2)}{1 - 3(p_1^2 + p_2^2 + p_3^2)} = \frac{q_j}{q_0} \quad (65)$$

and solve for $\hat{p}^2 = p_1^2 + p_2^2 + p_3^2$. After some algebraic calculations, it is not difficult to show that, in fact,

$$\frac{(\hat{p}^2 + 1)^3}{(1 - 3\hat{p}^2)^2} = \frac{1}{q_0^2} \quad (66)$$

Solution of the previous equation for $\hat{p}^2$ requires the solution of a cubic equation. Once $\hat{p}^2$ is known however, it can be substituted into Eq. (65) to get the desired result. Actually, from Eqs. (65) and (66) we have that

$$q_0 = \frac{1 - 3\hat{p}^2}{(1 + \hat{p}^2)^{\frac{3}{2}}}, \quad q_j = \pm\frac{p_j(3 - \hat{p}^2)}{(1 + \hat{p}^2)^{\frac{3}{2}}}, \quad j = 1, 2, 3$$

Letting $W = (I - P)(I + P)^{-1}$ then since $C = W^3$ one obtains that

$$W = e^{\frac{\phi}{3}[\hat{e}]}$$

where ϕ is the principal angle of C.

6. Kinematics

The kinematic equations in terms of the τ parameters can be computed as follows. From Eqs. (23) and (45) we have that

$$\dot{C} = \frac{d}{dt}[(I - T)^4](I + T)^{-4} + (I - T)^4\frac{d}{dt}[(I + T)^{-4}]$$
$$= S(\omega)(I - T)^4(I + T)^{-4}$$

or that

$$\frac{d}{dt}[(I - T)^4] - C(T)\frac{d}{dt}[(I + T)^4] = S(\omega)(I - T)^4 \quad (67)$$

where we have used the fact that

$$\frac{d}{dt}A^{-1} = -A^{-1}\left(\frac{d}{dt}A\right)A^{-1}$$

for any square matrix A. Using also the fact that

$$\frac{d}{dt}A^n = \sum_{j=0}^{n-1} A^j\left(\frac{d}{dt}A\right)A^{n-j-1}$$

and performing the differentiations in the left-hand-side of Eq. (67), one obtains a set of nine linear equations in terms of $\dot{\tau}_1, \dot{\tau}_2$. and $\dot{\tau}_3$. Similarly, the right-hand-side of Eq. (67) is linear in terms of $\omega_1, \omega_2, \omega_3$.

10

Choosing three (independent) equations out of these nine, we get a linear system of the form

$$V(\tau)\dot{\tau} = U(\tau)\omega$$

Solving for $\dot{\tau}$ we finally get that the kinematic equations for the τ orientation parameters are given by

$$\frac{d\tau}{dt} = V^{-1}(\tau)U(\tau)\omega = G(\tau)\omega$$

where the matrix $G(\tau)$ is given by

$$G(\tau) = \frac{1}{1-\hat{\tau}^2}\begin{bmatrix} T_1 + \tau_3^2\tau_2^2 - 3(\tau_2^2 + \tau_3^2) \\ 2\tau_3(1-\hat{\tau}^2) + \tau_1\tau_2(3-\hat{\tau}^2) \\ -2\tau_2(1-\hat{\tau}^2) + \tau_1\tau_3(3-\hat{\tau}^2) \\ \\ -2\tau_3(1-\hat{\tau}^2) + \tau_1\tau_2(3-\hat{\tau}^2) \\ T_2 + \tau_1^2\tau_3^2 - 3(\tau_3^2 + \tau_1^2) \\ 2\tau_1(1-\hat{\tau}^2) + \tau_2\tau_3(3-\hat{\tau}^2) \\ \\ 2\tau(1-\hat{\tau}^2) + \tau_1\tau_3(3-\hat{\tau}^2) \\ -2\tau_1(1-\hat{\tau}^2) + \tau_2\tau_3(3-\hat{\tau}^2) \\ T_3 + \tau_1^2\tau_2^2 - 3(\tau_1^2 + \tau_2^2) \end{bmatrix} \quad (68)$$

and $T_j = \frac{1}{2}(1 + \tau_1^4 + \tau_2^4 + \tau_3^4 - 2\tau_j^4)$, $j = 1, 2, 3$. This equation can be written more compactly in a vector form as follows

$$\begin{aligned} \frac{d\tau}{dt} &= \frac{1}{8(1-\hat{\tau}^2)}\left[2(3-\hat{\tau}^2)\tau\tau^T \right. \\ &- \left. 4(1-\hat{\tau}^2)[\tau] + (1 - 6\hat{\tau}^2 + \hat{\tau}^4)I\right]\omega \quad (69) \end{aligned}$$

These kinematic equations are not as simple as the corresponding kinematic equations for the Rodrigues or the Modified Rodrigues parameters[7,14]. Moreover, there is an apparent singularity at $\hat{\tau} = \pm 1$, equivalently at $\phi = \pm 2\pi$. The limiting behavior of these equations as $\hat{\tau} \to \pm 1$ will be determined through further analytical and numerical studies. At any rate, because of the near-linear behavior between ϕ and the magnitude of τ as seen in Fig. 2, for small principal angles, Eq. (69) is expected to behave in a more "linear-like" fashion than either the Cayley-Rodrigues or the Modified Rodrigues parameters.

Similarly, for the third order Cayley parameters, one can derive the following kinematic equations

$$\begin{aligned} \frac{dp}{dt} &= \frac{1}{6(3-\hat{p}^2)}\left[(11 - \hat{p}^2)pp^T \right. \\ &- \left. 3(3-\hat{p}^2)[p] + 3(1 - 3\hat{p}^2)I\right]\omega \quad (70) \end{aligned}$$

These equations can be derived starting from Eqs. (23) and (64) and using similar arguments as before. Singularities for the p parameters are encountered at $\hat{p} = \pm\sqrt{3}$. As before, further analysis is required to determine the limiting behavior of this system as $\hat{p} \to \pm\sqrt{3}$.

7. Numerical Example

In order to demonstrate the potential benefits or drawbacks of the previous kinematic parameters the following simulation was performed. We integrated Eqs. (69) as well as the corresponding kinematic equations in terms of the Cayley-Rodrigues (ρ) and the Modified Rodrigues parameters (σ) starting from the zero orientation and subject to the constant angular velocity vector $\omega = (0.25, 0.4, -0.1)\,(rad/sec)$. This corresponds to a linearly increasing value of the principal angle ϕ. The results of the simulations are shown in Fig. 4. This figure actually shows only the first components of the kinematic parameter vectors, as the other two components exhibit similar behavior.
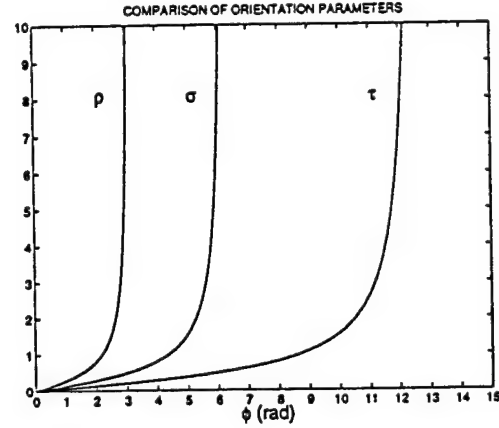
Figure 4: Orientation parameter comparison.

As it is evident from this figure, the classical and the Modified Rodrigues parameters encounter the singularity earlier that the τ parameters. We note, however, that since discontinuities in the parameter description are typically acceptable in applications, the Modified Rodrigues parameters can be made to avoid the singularity altogether by simply switching to their "shadow" set[15]. The same also holds for the τ parameters via Eq. (63). Figure 5 shows the simulation where the parameters σ and τ are allowed to switch to their respective "shadow" sets. Although the points of switching are arbitrary and can be chosen according to the particular application, a reasonable choice is to switch when the parameters and the corresponding "shadow" set have opposite signs. This will ensures continuity of the magnitude. From Eqs. (38) and (63) this occurs when $\phi = k\,\pi$, $k = \pm 1, \pm 2, \dots$. This is the situation depicted in Fig. 5. The τ parameters are shown in solid line, and the σ parameters are shown in dashed line.

11

Figure 5: Orientation parameter and their "shadow" sets.

Since the classical Rodrigues parameters do not have an associated "shadow" set (better, the shadow set coincides with the original parameters), only the the σ and τ parameters are plotted in Fig. 5.

8. Conclusions

We have extended the classical Cayley transform which maps skew-symmetric matrices to proper orthogonal matrices to higher orders. The approach is based on the observation that Cayley transforms can be viewed as generalized conformal (bilinear) mappings in the space of matric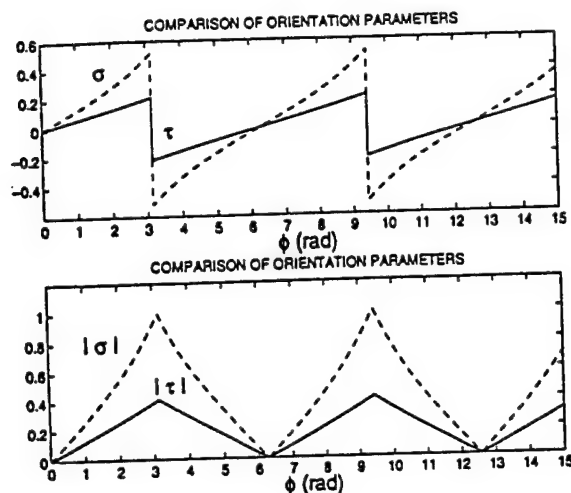es. The Euler parameters, the Rodrigues parameters and the Modified Rodrigues parameters follow as special cases of this approach. In addition, we generate a family of higher order "Rodrigues parameters" which could be used as coordinates for the rotation group. It still remains, however, to determine the applicability of these higher order parameters in realistic attitude problems.

9. References

[1] Hughes, P. C., *Spacecraft Attitude Dynamics*. New York, John Wiley & Sons, 1986.

[2] Wertz, J. R., *Spacecraft Attitude Determination and Control*. Dordrecht, Holland, D. Reidel Publishing Company, 1980.

[3] Shuster, M. D., "A Survey of Attitude Representations," *Journal of the Astronautical Sciences*, Vol. 41, No. 4, 1993, pp. 439–517.

[4] Special Issue on Attitude Representations, *Journal of the Astronautical Sciences*, Vol. 41, No. 4, 1993.

[5] Wiener, T. F., *Theoretical Analysis of Gimballess Inertial Reference Equipment Using Delta-Modulated Instruments*. PhD thesis, Massachusetts Institute of Technology, Cambridge, Massachusetts, March 1962.

[6] Marandi, S. R. and Modi, V., "A Preferred Coordinate System and the Associated Orientation Representation in Attitude Dynamics," *Acta Astronautica*, Vol. 15, No. 11, 1987, pp. 833–843.

[7] Schaub, H., Tsiotras, P., and Junkins, J. L., "Principal Rotation Representations of Proper $N \times N$ Orthogonal Matrices," *International Journal of Engineering Science*, Vol. 33, No. 15, 1995, pp. 2277–2295.

[8] Junkins, J. L. and Kim, Y., *Dynamics and Control of Flexible Structures*. New York, AIAA, 1993.

[9] Halmos, P. R., *Finite Dimensional Vector Spaces*, Vol. 7 of *Annals of Mathematics Studies*. Princeton, NJ, Princeton University Press, 1953.

[10] Curtis, M. L., *Matrix Groups*. New York, Springer-Verlag, 1979.

[11] Horn, R. and Johnson, C. R., *Matrix Analysis*. Cambridge, United Kingdom, Cambridge University Press, 1985.

[12] Churchill, R. V. and Brown, J. W., *Complex Variables and Applications*. New York, McGraw Hill, 1990.

[13] Conway, J. B., *Functions of One Complex Variable*. New York, Springer Verlag, 1978.

[14] Tsiotras, P., "On New Parameterizations of the Rotation Group in Attitude Kinematics," Technical Report, Dept. of Aeronautics & Astronautics, Purdue University, West Lafayette, IN, January 1994.

[15] Schaub, H. and Junkins, J. L., "Stereographic Orientation Parameters for Attitude Dynamics: A Generalization of the Rodrigues Parameters," in *AAS/AIAA Space Flight Mechanics Conference*, Feb. 13-15, 1995. Albuquerque, NM.

[16] Tsiotras, P., "New Control Laws for the Attitude Stabilization of Rigid Bodies," in *13th IFAC Symposium on Automatic Control in Aerospace*, pp. 316–321, Sept. 14-17, 1994. Palo Alto, CA.

AN EIGENFACTOR SQUARE ROOT ALGORITHM FORMULATION FOR NONLINEAR DYNAMICS

John L. Junkins[*] and Hanspeter Schaub[†]

A novel method is presented to solve the equations of motion for a large class of constrained and unconstrained dynamical systems. Given an analytic expression for the system mass matrix, quasi-coordinate equations of motion are derived in a manner that generates equations analogous to the dynamics/kinematics partitioning in Eulerian rigid body dynamics. This separation is accomplished by introducing a new quasi velocity coordinate η which yields a dynamical system with an identity mass matrix. The problem of inverting a complex mass matrix is replaced by the problem of solving two first order differential equations for the mass matrix eigenfactors. A new method is introduced whereby dynamical constraint equations are solved using a related eigenfactor formulation, forgoing any need to solve the algebraic constraint equations simultaneously with the differential equations of motion.

INTRODUCTION

The equations of motion of complex dynamical systems are usually second order nonlinear differential equations which require taking the inverse of a time-varying, configuration variable mass matrix. Such dynamical systems could be a large nonlinear deformation model for an arbitrary body, a multi-body system or a multi-link robot arm. One reason why the resulting dynamics are complicated is that they are usually written in a way that combines coordinates natural to the momentum or energy description with those natural to the displacement description. The result is a split between momentum differential equations and kinematic differential equations. This natural splitting is typically destroyed when the generalized methods of mechanics are employed and result in a more complicated mass matrix. This occurs when the classical Lagrange equations of motion are written in terms of a generalized coordinate and their time derivatives. By using Newton-Eulerian mechanics or the Boltzmann-Hamel version of Lagrange's equations, it is possible to introduce quasi-coordinates which separate the decision of choosing displacement coordinates and velocity (momentum) coordinates. As is well-known, (e.g. Eulerian rigid body dynamics), this process often leads to much more attractive equations than those that result from "brute force" application of Lagrange's equations. It is possible to bring the equations of motion to their most convenient form with a constant mass matrix.[1,2] For general configuration-variable mass matrices, there has not been a generally applicable method to accomplish an analogous transformation.

Several methods have been proposed to carry out the mass matrix inverse[2,3] ranging from taking an algebraic inverse, to using traditional numerical inverse methods (such as a Cholesky decomposition) to the elegant method of using the innovations factorization.[2] Naturally each method has its

[*]George Eppright Chair Professor of Aerospace Engineering, Aerospace Engineering Department, Texas A&M University, College Station TX 77843, Fellow AAS.

[†]Graduate Research Assistant, Aerospace Engineering Department, Texas A&M University, College Station TX 77843.

1

advantages and disadvantages. The algebraic inverse in only feasible for relatively small systems, even with symbol manipulation programs such as Mathematica and Maple. Taking a numerical inverse at each integration step is computationally costly and difficult. The method proposed by Ref. 2 uses the innovations factorizations technique to parameterize the mass matrix and recursively approximate its inverse. The mass matrix factors involved are obtained from a recursive filter. However, this recursive filter is conveniently applicable only to a linked body chain and other kinematically recursive topologies.

This paper presents a method to solve a very general class of constrained and unconstrained dynamical systems and avoids the necessity of inverting a configuration variable mass matrix to obtain instantaneous accelerations. The equations of motion will be separated into dynamical and kinematic differential equations somewhat analogous to classical developments in rigid body dynamics. The mass matrix will be initially parameterized by a numerical eigenfactor decomposition. After establishing this initial condition, only the eigenvectors and the eigenvalues of the mass matrix will be forward integrated from differential equations derived herein. The resulting method will require no matrix inverse to be taken. The eigenfactor differential equations are solved by extending an elegant square root algorithm proposed by Oshman and Bar-Itzhack[4] to solve the matrix Riccati equation. The formulation also allows any Pfaffian constraints to easily be incorporated into the equations of motion, thus avoiding having coupled algebraic constraint equations to be solved simultaneously with the original equations of motion. The implications of these developments for both efficiency and accuracy are enormous.

PROBLEM FORMULATION

The equations of motion for a dynamical system are usually derived by first formulating the kinematic energy T and the potential energy V. Let the system Lagrangian $\mathcal{L}$ be defined as

$$\mathcal{L} = T - V \tag{1}$$

Let x be the system state vector, then the potential energy is given by

$$V = V(x) \tag{2}$$

The kinetic energy can be written in terms of the generalized configuration coordinate vector derivative $\dot{x}$ or in terms of a quasi-velocity vector y defined as

$$y = P(x)\dot{x} \tag{3}$$

A field where quasi-velocities are often preferred over configuration coordinate derivatives is in rigid body dynamics. For example, it is much simpler to write the system kinetic energy in terms of the body angular velocity ω then in terms of the Euler attitude angle derivatives $\dot{\theta}$. Let $\bar{M}(x,t)$ be the mass matrix for a system described with y, then the kinetic energy is given by

$$T = T_2 + T_1 + T_0 = \frac{1}{2}y^T \bar{M}(x,t)y + \bar{G}^T(x,t)y + T_0(x,t) \tag{4}$$

where the T_1 and T_0 terms only appear in unnatural systems. However, to find the traditional version of Lagrange's equations of motion the kinetic energy needs to be written in terms of generalized coordinate derivatives, not quasi-velocities. Using Eq. (3), the kinetic energy can be rewritten in terms of $\dot{x}$.

$$T_2 = \frac{1}{2}\dot{x}^T P(x)^T \bar{M}(x,t)P(x)\dot{x} = \frac{1}{2}\dot{x}^T M(x,t)\dot{x} \tag{5}$$

$$T_1 = \bar{G}^T(x,t)P(x)\dot{x} = G^T(x,t)\dot{x} \tag{6}$$

where $M(x,t) = P(x)^T \bar{M}(x,t)P(x)$ is the system mass matrix for the state vector $(x,\dot{x})$ and $G(x,t) = P^T(x)\bar{G}(x,t)$. For mechanical systems $M(x,t)$ will always by symmetric positive definite. Let Q be

2

a non-conservative forcing term and let $A^T\lambda$ be the constraint force, then the Lagrange equations of motion are defined as

$$\frac{d}{dt}\left(\frac{\partial \mathcal{L}}{\partial \dot{x}}\right) - \frac{\partial \mathcal{L}}{\partial x} = Q - A^T\lambda \tag{7}$$

with the Pfaffian non-holonomic constraint

$$A(x)\dot{x} + b(t) = 0 \tag{8}$$

The partial derivatives of the system Lagrangian $\mathcal{L}$ are

$$\frac{\partial \mathcal{L}}{\partial \dot{x}} = M(x,t)\dot{x} + G(x,t) \tag{9}$$

and

$$\frac{\partial \mathcal{L}}{\partial x} = \frac{1}{2}\dot{x}^T\frac{\partial M(x,t)}{\partial x}\dot{x} + \frac{\partial G^T(x,t)}{\partial x}\dot{x} + \frac{\partial T_0(x,t)}{\partial x} - \frac{\partial V}{\partial x} \tag{10}$$

The resulting standard Lagrange equations of motion are

$$M(x,t)\ddot{x} + \left(\dot{M} - \frac{1}{2}\dot{x}^T\frac{\partial M(x,t)}{\partial x} - \frac{\partial G^T(x,t)}{\partial x}\right)\dot{x} + \dot{G}(x,t) - \frac{\partial T_0(x,t)}{\partial x} + \frac{\partial V}{\partial x} = Q - A^T\lambda \tag{11}$$

or more compactly

$$M(x,t)\ddot{x} + H(x,\dot{x},t) + \frac{\partial V}{\partial x} = Q - A^T\lambda \tag{12}$$

The above equations of motion are a second order nonlinear differential equation, obviously not generally a simple task to solve. In particular, the time and state dependence of the mass matrix poses a particular difficulty. These standard equations of motion, when coupled to the constraint equations in Eq. (8), pose a more significant challenge, especially for high dimensioned systems. The necessity of solving systems of order $n+m$ to obtain $(\ddot{x}, \lambda)$ for each $(x,\dot{x},t)$ lies at the heart of the difficulty.

THE BOLTZMANN-HAMEL EQUATIONS OF MOTION

We motivate this development using rigid body dynamics wherein it is common practice to separate the momentum dynamics and kinematics. Euler's equation of motion are usually written in terms of the body angular velocity ω, not in terms of the time derivative of the attitude coordinate vector θ.

$$\begin{aligned}\Im\dot{\omega} &= -[\tilde{\omega}]\Im\omega + u\\ \dot{\theta} &= f(\theta)\omega\end{aligned} \tag{13}$$

The first equation of Eqs. (13) describes the system momentum time rate of change, the second describes the kinematic relationship between the body angular velocity and the attitude coordinate derivative. Only using θ and its inertial derivatives would yield a much more complex second order differential equation.

This separation of dynamics and kinematics in the equations of motion cannot be accomplished in more general dynamical systems. However, we show a way to accomplish an analogous structure in the system equations, at the expense of increasing the number of differential equations to be solved. This involves projecting the configuration coordinate derivative into a moving reference frame[1,2] by introducing a quasi-velocity vector which diagonalizes the mass matrix. Since the mass matrix M is always symmetric and positive definite, it can be spectrally decomposed using the orthogonal real eigenvector matrix E and the diagonal positive real eigenvalue matrix D. Instead of using E, let us use $C = E^T$.

$$M = C^TDC \qquad CC^T = I \qquad D = diag(\lambda_i) \tag{14}$$

Let the diagonal S matrix be defined as the positive square root of the eigenvalue matrix D.

$$S = \sqrt{D} = diag\left(+\sqrt{\lambda_i}\right) \qquad D = S^T S \tag{15}$$

Substituting Eqs, (14) and (15) into Eq. (5) yields the following kinetic energy expression.

$$T_2 = \frac{1}{2}\dot{x}^T C^T S^T S C \dot{x} \tag{16}$$

By introducing the same velocity coordinate vector η as in Ref. 2

$$\eta = SC\dot{x} \qquad \eta = \eta(\lambda_i(x), c_i(x), \dot{x}) \tag{17}$$

we obtain a new simplified expression for the kinetic energy. The mass matrix associated with η is the identity matrix, so

$$T^* = T_2^* + T_1^* + T_0^* = \frac{1}{2}\eta^T\eta + G^T(x,t)C^T S^{-1}\eta + T_0(x,t) \tag{18}$$

Note that T_2^* depends explicitly on η. However, if we choose $(x, \dot{x})$ as the independent set for taking partial derivatives, we must recall that η depends on $(x, \dot{x})$. The x dependence is implicit in Eq. (14), (15), (17) because $S(x)$, $C(x)$ parameterize $M(x) = C^T S^T S C$. Also note that T^* is equal to T (both represent the same physical kinetic energy quantity), they differ only in their algebraic formulations. The inverse mapping of Eq. (17) describes the kinematic relationship between $\dot{x}$ and η similar to the relationship of $\dot{\theta}$ and ω in Eq. (13), except for the orthogonality of C and the diagonal nature of S make the inverse near-trivial.

$$\dot{x} = C^T S^{-1}\eta \tag{19}$$

The partial derivatives of the system Lagrangian $\mathcal{L}$ are now rewritten in terms of the new generalized velocity vector η using the chain rule.[1]

$$\frac{\partial\mathcal{L}}{\partial\dot{x}} = \frac{\partial T^*}{\partial\dot{x}} + \frac{\partial\eta}{\partial\dot{x}}^T\frac{\partial T^*}{\partial\eta} = C^T S\frac{\partial T^*}{\partial\eta} \tag{20}$$

and

$$\frac{\partial\mathcal{L}}{\partial x} = \frac{\partial T^*}{\partial x} + J^T\frac{\partial T^*}{\partial\eta} - \frac{\partial V}{\partial x} \tag{21}$$

where J is the sensitivity matrix of η with respect to the state vector x. This matrix is non-zero since the C and S both indirectly depend on x.

$$J \equiv \frac{\partial\eta}{\partial x} = \left[\frac{\partial\eta}{\partial x_1}, \cdots, \frac{\partial\eta}{\partial x_n}\right] \tag{22}$$

Using the chain rule $\partial\eta/\partial x_k$ is expressed as

$$\frac{\partial\eta}{\partial x_k} = \left(\frac{\partial S}{\partial x_k} + S\frac{\partial C}{\partial x_k}C^T\right)S^{-1}\eta \tag{23}$$

The partial derivatives of T^* with respect to η and x are

$$\frac{\partial T^*}{\partial\eta} = \eta + S^{-1}CG(x,t) \tag{24}$$

$$\frac{\partial T^*}{\partial x} = \frac{\partial G^T(x,t)}{\partial x}C^T S^{-1}\eta + \frac{\partial T_0(x,t)}{\partial x} \tag{25}$$

With all these substitutions the Lagrange equations of motion in Eq. (7) become

$$\frac{d}{dt}\left(C^T S\eta + G\right) - \frac{\partial G^T}{\partial x}C^T S^{-1}\eta - \frac{\partial T_0}{\partial x} - J^T(\eta + S^{-1}CG) + \frac{\partial V}{\partial x} = Q - A^T\lambda \tag{26}$$

4

After carrying out the time derivative and using the orthogonality of the C matrix, the following first order differential equation is obtained.

$$\dot{\eta} + S^{-1}\left(C\dot{C}^T S + \dot{S} - CJ^T - C\frac{\partial G^T}{\partial x}C^T S^{-1}\right)\eta = S^{-1}CF - B^T\lambda \qquad (27)$$

where

$$B = AC^T S^{-1} \qquad (28)$$

and

$$F = Q - \frac{\partial V}{\partial x} - \dot{G} + \frac{\partial T_0}{\partial x} + J^T S^{-1}CG \qquad (29)$$

The two first order equations (19) and (27) replace the classical second order Eq. (12). Eq. (27) is an interesting new form of the well-known the Boltzmann-Hamel equation[1,5] for our choice of quasi-coordinates η. This diagonalized equation of motion is very similar to the one introduced in Ref. 2 except for the parameterization of the eigenvector matrix and the formulation of the Coriolis term. Note that no matrix inverse needs to be taken thanks to the orthogonality of the C matrix. Inverting the S matrix is trivial since it is a positive diagonal matrix. At this stage the expensive matrix inverse problem has been traded for another problem involving finding the eigenfactor derivatives and the sensitivity matrix J.

MASS MATRIX EIGENFACTOR DERIVATIVES

To solve the Boltzmann-Hamel equation, we seek auxiliary differential equations to yield the eigenfactor derivatives with respect to time and the state vector x, since by solving these we can establish the instantaneous C, S and J matrices. A very elegant square root algorithm[4] developed by Oshman and Bar-Itzhack to solve the matrix Riccati differential equation is extended here to solve for the mass matrix eigenfactor derivatives.

This square root algorithm works very well, even with repeated eigenvalues and clusters of near-equal eigenvalues. Assume that the mass matrix M has k distinct eigenvalues, each with an algebraic multiplicity of m_i, then let the eigenvalues of M be ordered as

$$^1\lambda_1,\ldots,^{m_1}\lambda_1,\ldots,^1\lambda_k,\ldots,^{m_k}\lambda_k \qquad (30)$$

and equate this series to the series $\lambda_1,\ldots,\lambda_n$. The ordered eigenvalue matrix D is then given by

$$D = diag(\lambda_1,\ldots,\lambda_n) \qquad (31)$$

Let c_i be the i-th row of the C matrix. Since C is the transpose of E, c_i is simply an eigenvector written as a row vector. Let $^i c_j$ be the i-th eigenvector corresponding to the j-th eigenvalue. All n eigenvectors are ordered according to their respective eigenvalues in the following manner.

$$C = \begin{bmatrix} ^1c_1 \\ \vdots \\ ^{m_i}c_1 \\ \vdots \\ ^1c_k \\ \vdots \\ ^{m_k}c_k \end{bmatrix} = \begin{bmatrix} c_1 \\ \vdots \\ c_n \end{bmatrix} \qquad (32)$$

Every proper orthogonal matrix satisfies a differential equation of the form[6]

$$\dot{C} = -\Omega C \qquad (33)$$

5

where Ω is a skew-symmetric matrix. All eigenfactor derivatives of M are expressed by a projection onto $c_1, \ldots, c_n$ in terms of μ_{ij} as[4,7]

$$\mu_{ij} = c_j \dot{M}(x,t) c_i^T \tag{34}$$

The distinct elements of the Ω matrix elements are[4,7]

$$[\Omega_{ij}] = \begin{cases} \frac{\mu_{ij}}{s_j^2 - s_i^2} & \text{for } \left| \frac{\mu_{ij}}{s_j^2 - s_i^2} \right| < \Omega_{max} \\ 0 & \text{for } s_i = s_j \\ \Omega_{max} sign \left(\frac{\mu_{ij}}{s_j^2 - s_i^2} \right) & \text{for } \left| \frac{\mu_{ij}}{s_j^2 - s_i^2} \right| \geq \Omega_{max} \end{cases} \tag{35}$$

where Ω_{max} is a maximum bound for the Ω matrix entries depending on the accuracy of the software used. This term is included to smoothly handle the case where λ_i is almost equal to λ_j. Ref. 4 shows that this slight modification has minimal impact on the accuracy of the solution. This is because the eigenvector variations corresponding to the clustered eigenvalues have negligible influence on the diagonalization of M.

The time derivative of the eigenvalues λ_i are[4,7]

$$\dot{\lambda}_i = \mu_{ii} \tag{36}$$

However, the time derivatives of the eigenvalues are not required, but the derivative of the square root of the eigenvalues. Let s_i be the i-th entry of the S matrix. Using the chain rule, the derivative of s_i is

$$\dot{s}_i = \frac{1}{2s_i} \dot{\lambda}_i \tag{37}$$

This is written in a more compact form using the diagonal matrix Γ

$$\Gamma = diag(\mu_{ii}) \tag{38}$$

as[4]

$$\dot{S} = \frac{1}{2} \Gamma S^{-1} \tag{39}$$

Substituting the above eigenfactor time derivatives into Eq. (27), the Boltzmann-Hamel equations are reduced to

$$\dot{\eta} + S^{-1} \left(\Omega S + \frac{1}{2} \Gamma S^{-1} - C J^T - C \frac{\partial G^T}{\partial x} C^T S^{-1} \right) \eta = S^{-1} C F - B^T \lambda \tag{40}$$

At first glance, Eq. (40) may seem more complicated than than the original equations of motion. Keep in mind, however, that S and Γ are diagonal matrices which greatly reduces the computational burden.

To be able to calculate the sensitivity matrix J, we still need an expression for $\partial S / \partial x_k$ and $\partial C / \partial x_k$. Note that in the previous development of $\dot{S}$ and $\dot{C}$ it did not matter with respect to what variable the derivative was taken. This allows $\partial S / \partial x_k$ and $\partial C / \partial x_k$ to be expressed in a very similar manner as were $\dot{S}$ and $\dot{C}$. Let $^k \bar{\mu}_{ij}$ be defined as

$$^k \bar{\mu}_{ij} = c_j \frac{\partial M(x,t)}{\partial x_k} c_i^T \tag{41}$$

and the diagonal matrix $^k \bar{\Gamma}$ be

$$^k \bar{\Gamma} = diag \left(^k \bar{\mu}_{ii} \right) \tag{42}$$

The partial derivative of S with respect to x_k has the same form as the time derivative of S in Eq. /eqrefdS1 as

$$\frac{\partial S}{\partial x_k} = \frac{1}{2} {}^k \bar{\Gamma} S^{-1} \tag{43}$$

6

To find $\partial C/\partial x_k$, let the skew-symmetric matrix ${}^k\bar{\Omega}$ be defined as

$$
{}^k\left[\bar{\Omega}_{ij}\right] = \begin{cases} \frac{{}^k\bar{\mu}_{ij}}{s_j^2 - s_i^2} & \text{for } \left|\frac{{}^k\bar{\mu}_{ij}}{s_j^2 - s_i^2}\right| < \Omega_{max} \\ 0 & \text{for } s_i = s_j \\ \Omega_{max} sign\left(\frac{{}^k\bar{\mu}_{ij}}{s_j^2 - s_i^2}\right) & \text{for } \left|\frac{{}^k\bar{\mu}_{ij}}{s_j^2 - s_i^2}\right| \geq \Omega_{max} \end{cases} \tag{44}
$$

$\partial C/\partial x_k$ is then defined analogously to the time derivative of Eq. (33) as

$$
\frac{\partial C}{\partial x_k} = -{}^k\bar{\Omega}C \tag{45}
$$

Using Eqs. (43) and (45) $\partial\eta/\partial x_k$ can be written as

$$
\frac{\partial\eta}{\partial x_k} = \left(\frac{1}{2}S^{-1}{}^k\bar{\Gamma}S^{-1} - S^k\bar{\Omega}S^{-1}\right)\eta \tag{46}
$$

PFAFFIAN NON-HOLONOMIC CONSTRAINTS

If the dynamical system is unconstrained, then the Pfaffian constraint matrix B will be zero and Eq. (40) is fully defined. However, if the dynamics are constrained through the Pfaffian constraint surface given in Eq. (8), then Eq. (40) will need to be solved simultaneously with the constraint equation. Using Eq. (19) we rewrite the Pfaffian constraint in terms of the new velocity vector η.

$$
AC^TS^{-1}\eta + b = 0 \tag{47}
$$

which can be simplified using Eq. (28) to

$$
B\eta + b = 0 \tag{48}
$$

The dynamic constraint equations is obtained by taking the first time derivative of Eq. (48).

$$
B\dot{\eta} + \dot{B}\eta + \dot{b} = 0 \tag{49}
$$

Using Eqs. (39), (33) and (28) $\dot{B}$ can be expressed as

$$
\dot{B} = (\dot{A}C^T + A\dot{C}^T - AC^TS^{-1}\dot{S})S^{-1} = \left(\dot{A}C^T + AC^T(\Omega - \frac{1}{2}S^{-1}\Gamma S^{-1})\right)S^{-1} \tag{50}
$$

To determine $(\dot{\eta}, \lambda)$, Eq. (40) will need to be solved simultaneously with Eq. (49), we are led to the differential-algebraic system

$$
\begin{bmatrix} I & B^T \\ B & 0 \end{bmatrix}\begin{pmatrix} \dot{\eta} \\ \lambda \end{pmatrix} = \begin{pmatrix} -S^{-1}\left(\Omega S + \frac{1}{2}\Gamma S^{-1} - CJ^T - C\frac{\partial G^T}{\partial x}C^TS^{-1}\right)\eta + S^{-1}CF \\ -\dot{B}\eta - \dot{b} \end{pmatrix} \tag{51}
$$

which can be written in more compact form as

$$
M_2\begin{pmatrix} \dot{\eta} \\ \lambda \end{pmatrix} = \begin{pmatrix} a_1 \\ a_2 \end{pmatrix} \tag{52}
$$

Since B is a mxn matrix, M_2 is a symmetric $(n+m)$x$(n+m)$ matrix. A partitioned matrix inversion formula[7] is used to find the inverse of M_2. Because of the use of the quasi-coordinates η, the upper left partition of M_2 is a nxn identity matrix which simplifies the partitioned inverse immensely. For this case the mxm Schur complement Δ reduces to[7]

$$
\Delta = BB^T \tag{53}
$$

7

Then the partitioned inverse of M_2 is

$$M_2^{-1} = \begin{bmatrix} I - B^T\Delta^{-1}B & B^T\Delta^{-1} \\ \Delta^{-1}B & -\Delta^{-1} \end{bmatrix} \tag{54}$$

Using M_2^{-1} in Eq. (54) the constrained differential equation of motion for η is

$$\dot{\eta} = (I - B^T\Delta^{-1}B)a_1 + B^T\Delta^{-1}a_2 \tag{55}$$

The Lagrange constraint vector λ is

$$\lambda = \Delta^{-1}Ba_1 - \Delta^{-1}a_2 \tag{56}$$

Note that if zero constraint is imposed on the dynamical system then Eq. (55) collapses back to Eq. (40). If the number of system constraints m is small, then Δ^{-1} could be inverted for each time step. However, as m grows larger taking a numerical inverse quickly becomes computationally very expensive.

Since Δ, for linearly independent constraints, is a positive definite symmetric matrix by Eq. (53), it can be decomposed using the eigenfactor parameterization analogous to the mass matrix parameterization. Let C_Δ be the transpose of the eigenvector matrix of Δ, and let S_Δ be a diagonal matrix whose entries are the positive roots of Δ eigenvalues. Then through a spectral decomposition Δ can be written as

$$\Delta = C_\Delta^T S_\Delta^T S_\Delta C_\Delta \tag{57}$$

Since C_Δ is an orthogonal matrix and the diagonal entries of S_Δ are all positive, the inverse of Δ is

$$\Delta^{-1} = C_\Delta^T S_\Delta^{-2} C_\Delta \tag{58}$$

This direct inverse formulation reduces Eq. (55) to the following matrix inverse free formulation.

$$\dot{\eta} = (I - B^T C_\Delta^T S_\Delta^{-2} C_\Delta B)a_1 + B^T C_\Delta^T S_\Delta^{-2} C_\Delta a2 \tag{59}$$

Keep in mind that S_Δ is a diagonal matrix with positive entries. Therefor finding its inverse involves only scalar inversions.

To update the C_Δ and S_Δ matrices without resolving the eigenvalue, eigenvector problem, their time derivatives are found using the square root eigenfactor algorithm[4] analogously to finding the time derivatives of C and S of the mass matrix M. Assume all eigenvectors and eigenvalues are arranged as described in Eq. (30) and (32). Let c_{Δ_i} be the i-th row vector of the C_Δ matrix, then β_{ij} is defined be

$$\beta_{ij} = c_{\Delta_j}\dot{\Delta}c_{\Delta_i}^T \tag{60}$$

where the time derivative of Δ is

$$\dot{\Delta} = \dot{B}B^T + B\dot{B}^T \tag{61}$$

and $\dot{B}$ was defined in Eq. (50). The diagonal matrix Γ_Δ and the skew-symmetric matrix Ω_Δ are then defined as

$$\Gamma_\Delta = diag(\beta_{ii}) \tag{62}$$

$$[\Omega_{\Delta_{ij}}] = \begin{cases} \frac{\beta_{ij}}{s_{\Delta_j}^2 - s_{\Delta_i}^2} & \text{for } \left|\frac{\beta_{ij}}{s_{\Delta_j}^2 - s_{\Delta_i}^2}\right| < \Omega_{max} \\ 0 & \text{for } s_{\Delta_j} = s_{\Delta_i} \\ \Omega_{max} sign\left(\frac{\beta_{ij}}{s_{\Delta_j}^2 - s_{\Delta_i}^2}\right) & \text{for } \left|\frac{\beta_{ij}}{s_{\Delta_j}^2 - s_{\Delta_i}^2}\right| \geq \Omega_{max} \end{cases} \tag{63}$$

The time derivatives of C_Δ and S_Δ are then written as[4]

$$\dot{S}_\Delta = \frac{1}{2}\Gamma_\Delta S_\Delta^{-1} \tag{64}$$

$$\dot{C}_\Delta = -\Omega_\Delta C_\Delta \tag{65}$$

8

SOLUTION METHOD OUTLINE

A method has been presented that brings a general class of constrained multi-body dynamics to a form which completely avoids the necessity of inverting configuration-variable matrices to obtain instantaneous accelerations. The form of the equations is very analogous to classical "dynamics/kinematics" quasi-coordinate development of rigid body dynamics. The eigenvalue, eigenvector problem is only solved once numerically to find the initial $S(t_0)$, $C(t_0)$, $S_\Delta(t_0)$ and $C_\Delta(t_0)$ matrices as outlined in Figure 1. After initially ordering the eigenvalues and eigenvectors as outlined earlier they will need need to be simply rearranged thanks to the square root algorithm. Instead of using the generalized coordinate derivative $\dot{x}$ as the velocity measure, a new quasi-velocity η is introduced to which corresponds an identity mass matrix.

To evaluate the eigenfactor derivatives it is assumed that $\dot{M}(x,t)$ and $\partial M/\partial x_k(x,t)$ are available algebraically. This is a feasible assumption, especially in view of the several modern software packages like Maple and Mathematica which can derive the mass matrix in an explicit algebraic form and automate the generation of, for example, the C-code to compute $\dot{M}(x,t)$ and $\partial M(x,t)/\partial x_k$.
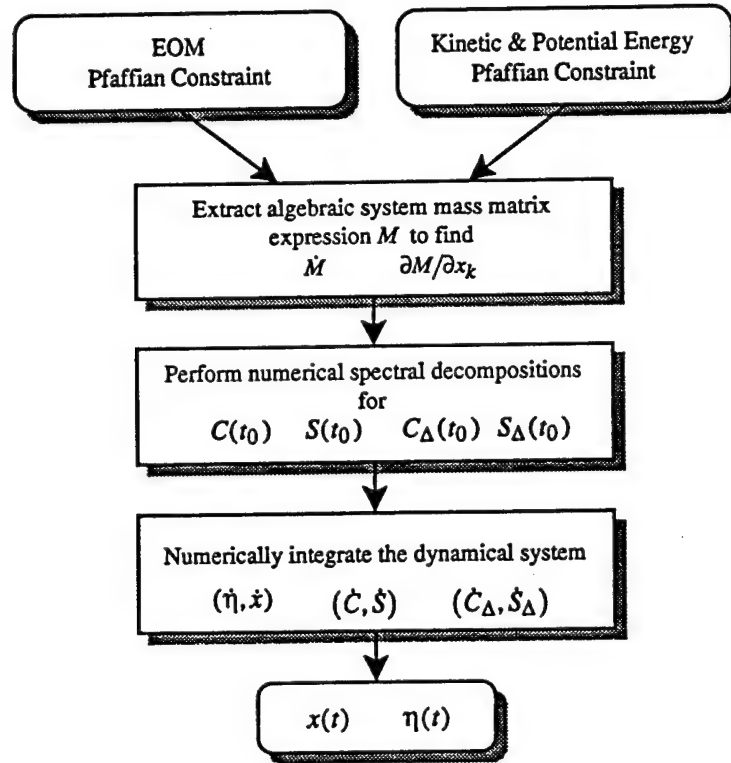

Figure 1 Flow Diagram of Eigenfactor Square Root Algorithm

For a constrained dynamical system, traditional processes lead to the classical Lagrange equations of motion coupled to second order differential constraint equations where a time and configuration varying mass matrix needed to be inverted. In the present development, there are no matrix inverse operations. These equations are mapped into a set of simpler nonlinear first order differential equations. The second order differential equation for $\ddot{x}$ is replaced with two first order differential equations $\dot{\eta}$ and $\dot{x}$. The mass matrix inverse problem is side-stepped by introducing the mass matrix eigenfactor matrices and solving their usually well-behaved differential equations for $\dot{S}$ and $\dot{C}$ instead. This method has no second coupled constraint equation, since the constraint force was already solved for and back-substituted into the equation of motion for η. However, this involved taking the inverse of a symmetric Schur matrix Δ. This inverse can also be avoided very simply by using the eigenfactor

9

matrices of the Schur matrix instead of the Schur matrix itself. Therefor, again a matrix inverse is replaced by solving two first order differential equations $\dot{S}_\Delta$ and $\dot{C}_\Delta$. Evaluation of operation count and error propagation issues shows solving these differential equations to be vastly superior to the conventional approach requiring matrix inversions.

To solve the above first order differential equations many types of integration methods could be used. However, the Runge-Kutta type methods are not attractive since they require the derivatives to be evaluated at discrete point between the time steps. This poses a problem when evaluating J at these intermediate steps since it depends on $\partial S/\partial x$ and $\partial C/\partial x$. It would require resolving the eigenvalue eigenvector problem at these intermediate steps to find the proper J matrix. Clearly not a desirable solution.

In lieu of using Runge-Kutta or analogous single-step methods, it is recommended that a predictor-corrector type method is used. These methods only evaluate the derivatives at the integration steps and not in between them. A very stable and accurate predictor corrector type method is the Hamming's method.[8] Its accuracy is h^5, comparable to the 4-th order Runge Kutta method. One drawback of the predictor corrector method is that they are not self starting. Another method, such as the modified Euler method,[8] can be used to establish the starting table.

DUAL-LINK MANIPULATOR SIMULATION

To demonstrate the eigenfactor square root algorithm, a constrained dual-link manipulator motion is simulated. The shoulder joint is fixed and the elbow joint is free to rotate. The link from the shoulder to the elbow has a length $l_1 = 0.5$ and the link from the elbow to the hand has a length $l_2 = 1/\sqrt{2}$. Both links are assumed to be mass-less. The elbow mass and the hand mass are $m_1 = m_2 = 1$. The hand is connected to a point $(0,4)$ through a spring with a stiffness $K = 1$. The system constraint restricts the hand to move only horizontally as illustrated in Fig. 2. There are no non-conservative forces or torques acting on the system.
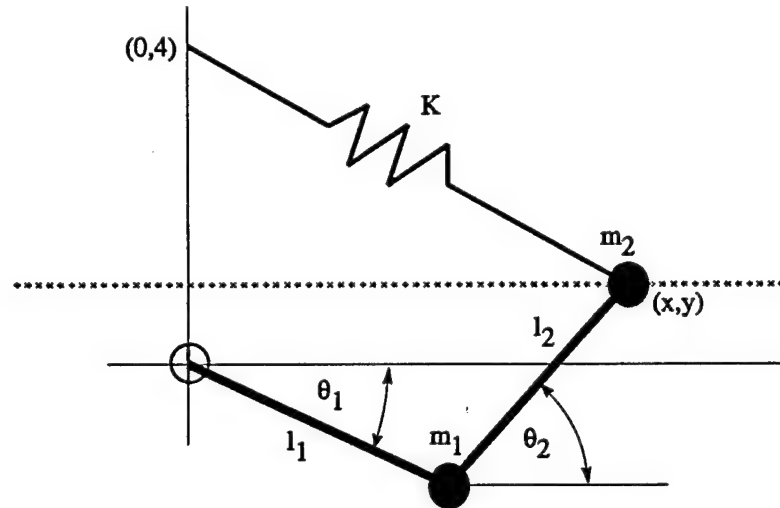

Figure 2 Constrained Dual-Link Manipulator Layout

The hand coordinates (x,y) are given as

$$x = l_1 \cos\theta_1 + l_2 \cos\theta_2 \qquad (66)$$

$$y = l_1 \sin\theta_1 + l_2 \sin\theta_2 \qquad (67)$$

The system potential energy is the total spring energy given as

$$V(\theta) = \frac{1}{2}K\left((4-y)^2 + x^2\right) \qquad (68)$$

10

The system kinetic energy is given as

$$T = \frac{1}{2}m_1 l_1^2 \dot{\theta}_1^2 + \frac{1}{2}m_2 \left(l_1^2 \dot{\theta}_1^2 + 2l_1 l_2 \cos{(\theta_1 - \theta_2)}\dot{\theta}_1 \dot{\theta}_2 + l_2^2 \dot{\theta}_2^2 \right) \tag{69}$$

From the kinetic energy T the system mass matrix can be extracted.

$$M(\theta) = \begin{bmatrix} (m_1 + m_2)l_1^2 & m_2 l_1 l_2 \cos{(\theta_1 - \theta_2)} \\ m_2 l_1 l_2 \cos{(\theta_1 - \theta_2)} & m_2 l_2^2 \end{bmatrix} \tag{70}$$

The eigenfactor square root algorithm requires an algebraic expression for $\dot{M}$ and $\partial M / \partial \theta_k$. They are found directly from the system mass matrix M in Eq. (70).

$$\dot{M}(\theta, \dot{\theta}) = \begin{bmatrix} 0 & m_2 l_1 l_2 \sin{(\theta_1 - theta_2)}(\dot{\theta}_2 - \dot{\theta}_1) \\ m_2 l_1 l_2 \sin{(\theta_1 - theta_2)}(\dot{\theta}_2 - \dot{\theta}_1) & 0 \end{bmatrix} \tag{71}$$

$$\frac{\partial M}{\partial \theta_1} = \begin{bmatrix} 0 & -m_2 l_1 l_2 \sin{(\theta_1 - \theta_2)} \\ -m_2 l_1 l_2 \sin{(\theta_1 - \theta_2)} & 0 \end{bmatrix} \tag{72}$$

$$\frac{\partial M}{\partial \theta_2} = \begin{bmatrix} 0 & m_2 l_1 l_2 \sin{(\theta_1 - \theta_2)} \\ m_2 l_1 l_2 \sin{(\theta_1 - \theta_2)} & 0 \end{bmatrix} \tag{73}$$

The system constraint on m_2 is $\dot{y} = 0$. Using Eq. (67) this can be expressed as $A(\theta)\dot{\theta} = 0$ where

$$A(\theta) = \begin{bmatrix} l_1 \cos{\theta_1} & l_2 \cos{\theta_2} \end{bmatrix} \tag{74}$$

The simulation is started at rest with $\theta_1 = 0°$ and $\theta_2 = 60°$ and let run for 10 seconds. The integration step size is 0.001 seconds. The resulting motion is shown in Fig. 3 below.
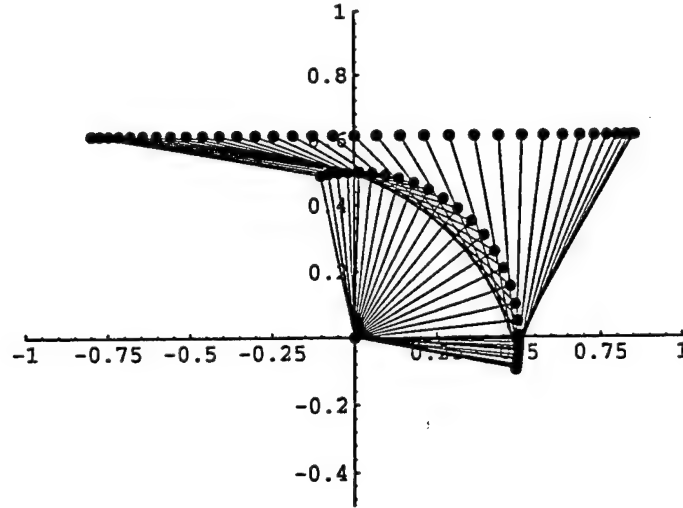

Figure 3 Dual-Link Manipulator Motion

Clearly the Pfaffian constraint was successfully incorporated into the equations of motion. The hand only moved in a horizontal manner. Not having to solve auxiliary constraint equations is of great importance as the number of constraints increases. Since this is a very simple dynamical system, an exact inverse was found of the system mass matrix and used to forward integrate the classical Lagrange equations of motion to verify the new equations of motion. The results were identical to solving the $(\dot{\eta}, \dot{x})$ dynamical system.

One critical case of the eigenfactor square root algorithm is when two or more eigenvalues are clustered very closely around one value. In this case elements of Ω could go to infinity. This case
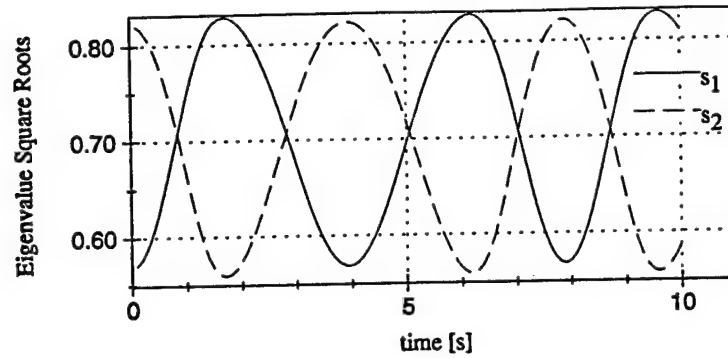
11

Figure 4 Time History of the Eigenvalue Square Roots

was resolving by putting an maximum bound on the magnitude of the eigenvalue square roots. This bound is usually set to machine accuracy (i.e. 10^{15} for this simulation). As can be seen in Fig. (4) the two eigenvalue square roots start out distinct and periodically become equal. The condition $s_1 = s_2$ means geometrically that $|\theta_1 - \theta_2|$ is 90° or that the lower arm is perpendicular to the upper arm. The eigenfactor square root algorithm did not appear to have any difficulty handling this numerical singularity. Not even after repeatably going through this condition. These results seem to confirm some of the robustness predictions made in Ref. 4 about the square root algorithm.
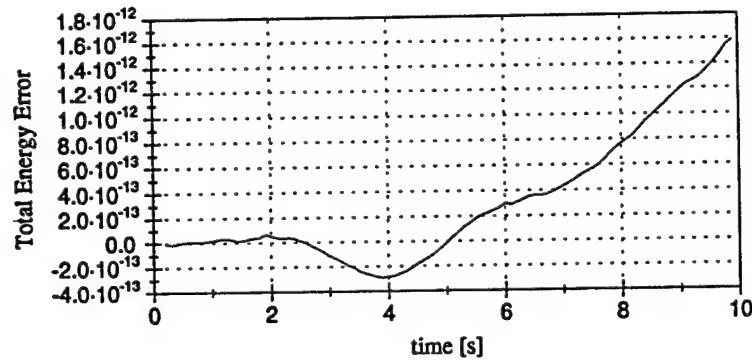

Figure 5 Time History of the Total Energy Integration Error

Since all the forces and torques acting on the dual-link manipulator are conservative, the total system energy should be constant. This makes the total energy a good integration error check and is shown in Fig. 5. Since the motion starts out at rest, the integrations remains very small initially. As the motion gains momentum, the integration error starts to accumulate very slowly. The forward integration was performed with only performing the predictor and corrector process once. For the same step size the error could be further reduced by repeatably applying the P-C method during the forward integration. This is possible since P-C methods allow the integration error to be estimated during the forward integration.

CONCLUSION

The eigenfactor square root algorithm can successfully solve a very large class of nonlinear dynamical systems. The classical second order Lagrange equation of motion is replaced with two first order differential equations by introducing a new quasi-velocity η. Pfaffian constraints can be accounted for directly in the new equations of motion. Constraint equations no longer need to be solved simultaneously with the dynamical equation thus greatly reducing the computational burden. Any inverse of a symmetric positive definite matrix such as the mass matrix is replaced with the

12

problem of solving the respective eigenvalue and eigenvector matrix first order differential equation. Numerical simulations for a dual-link manipulator confirm the validity of the method. Using the square root algorithm for solving the eigenfactor differential equations appears to be very robust even when some eigenvalues are clustered closely together.

REFERENCES

1. M. H. Rheinfurth and H. B. Wilson. "Methods of Applied Dynamics," NASA Reference Publication 1262, NASA, May 1991.

2. A. Jain and G. Rodriguez. "Diagonalized Lagrangian Robot Dynamics," *IEEE Trans. on Robotics and Automation*, Vol. 11, No. 4, Aug. 1995, pp. 571–584.

3. E. Bayo and R. Ledesma. "Augmented Lagranian and Mass-Orthogonal Projection Methods for Constrained Multibody Dynamics," *Journal of Nonlinear Dynamics*, Vol. 9, 1996, pp. 113–130.

4. Y. Oshman and I. Y. Bar-Itzhack. "Eigenfactor Solution of the Matrix Riccati Equation — A Continuous Square Root Algorithm," *IEEE Trans. on Automatic Control*, Vol. AC-30, No. 10, Oct. 1985, pp. 971–978.

5. J. G. Papastavridis. "On the Boltzmann-Hamel Equations of Motion: A Vectorial Treatment," *Journal of Applied Mechanics*, Vol. 61, June 1994, pp. 453–459.

6. J. L. Junkins and J. D. Turner. *Optimal Spacecraft Rotational Maneuvers.* Elsevier Science Publishers, Netherlands, 1986.

7. J. L. Junkins and Y. Kim. *Introduction to Dynamics and Control of Flexible Structures.* AIAA Education Series, Washington D.C., 1993.

8. M. L. James, G. M. Smith, and J. C. Wolford. *Applied Numerical Methods for Digital Computing.* Harper & Row, Publishers Inc., New York, 3rd edition, 1985.

13

GLOBALLY STABLE FEEDBACK LAWS FOR NEAR-MINIMUM-FUEL AND NEAR-MINIMUM-TIME POINTING MANEUVERS FOR A LANDMARK-TRACKING SPACECRAFT

Hanspeter Schaub[*], Rush D. Robinett[†] and John L. Junkins[‡]

Utilizing unique properties of a recently developed set of attitude parameters, the modified Rodrigues parameters, a feedforward/feedback type control laws is developed for a spacecraft undergoing large nonlinear motions using three reaction wheels. The method is suitable for tracking given reference trajectories that spline smoothly into a target state; these reference trajectories may be exact or approximate solutions of the system equations of motion. An associated asymptotically stable nonlinear observer is formulated for state estimation. In particular, we illustrate the ideas using both near-minimum-time and near-minimum fuel rotations about Euler's principal rotation axis, with parameterization of the sharpness of the control switching for each class of reference maneuvers. Lyapunov stability theory is used to prove rigorous global asymptotic stability of the closed-loop motion in the end game and during the tracking of the reference motion. The methodology is illustrated by designing example control laws for a prototype landmark tracking spacecraft; simulations are reported that show this approach to be attractive for practical applications. The inputs to the reference trajectory are designed with user-controlled sharpness of all control switches, to enhance the trackability of the reference maneuvers in the presence of structural flexibility.

INTRODUCTION

Motivated by problems arising in the precision pointing of imaging satellites for non-proliferation and environmental monitoring applications, there is renewed interest in the problem of rapid large angle maneuvers followed by precision pointing/tracking of landmarks from near-earth orbits. Pointing and tracking tolerances for these imaging systems are on the order of microradians. There are many contributors to pointing error, but the vibrational disturbances induced by the effects of rapid maneuvers on flexible solar array structures are one major problem. In previous studies[1,2] it has been shown that, assuming sufficient sensor and actuator bandwidth, reaction wheel actuators can effectively control both the rigid body maneuvers and fine-pointing/vibration arrest; however, the key issue is to perform the large maneuvers in a torque-shaped fashion that minimizes disturbances of the flexural motion. Judicious torque shaping must be coupled with stabilizing feedback control to null tracking and fine pointing errors; this is the approach pursued herein. We seek to extend the developments of Ref. 1,2 to establish a globally asymptotically stable nonlinear control design approach of broad applicability to general three-dimensional pointing and tracking problems.

* Graduate Research Assistant, Aerospace Engineering Department, Texas A&M University, College Station TX 77843.

† Research Engineer at Sandia National Laboratories, Albuquerque, NM 87185.

‡ George Eppright Chair, Professor of Aerospace Engineering, Aerospace Engineering Department, Texas A&M University, College Station TX 77843, Fellow AAS.

1

In recent papers[3-9], the utility of a new set of orientation parameters (the modified Rodrigues parameters, MRPs) has been studied. It has been shown that these parameters have some outstanding properties. They appear to be the canonical three parameter set, owing to the following remarkable truths:

- The nonsingular motion range encompasses ±360 degrees, although the norm of the parameters tend to infinity as ±360 degrees rotations about any axis is approached.
- For rotations within ±180 degrees about any axis, the parameters are bounded by a norm of +1.
- The kinematic differential equations are quadratic nonlinear functions of the MRPs, and have no singular points for rotations less than ±360 degrees.
- The transformation from orthogonal components of angular velocity to the time derivatives of the MRPs involves a coefficient matrix with orthogonal rows and columns, thus the inverse is analytic.
- The MRPs are non unique, there are two trajectories corresponding exactly to a given physical motion. One of the trajectories at any instant of time lies within and the other lies outside a unit sphere. Both trajectories satisfy the same differential equations, only differing in initial conditions.

Regarding the last property, it is easy to establish the transformation between the corresponding points on the two trajectories, and this fact can be utilized to establish, for the first time, a globally nonsingular three parameter description of a generally tumbling rigid body.

These properties, together with recent results from Lyapunov control law design methods[1,2], enable the formulation of a most attractive and effective family of control laws for spacecraft attitude maneuvers and fine pointing. The control law design methodology is important in its own right, as distinct from the use of the MRPs as orientation coordinates. In particular, however, this control law design approach is especially attractive for this coordinate choice. The feedback law is dominated by linear terms for this approach with a judicious choice of a logarithmic Lyapunov function[5]. The analytical results presented herein are illustrated through a simulation study which supports the efficacy and practicality of the concepts introduced.

FORMULATION

The Equations Of Motion For A Rigid Spacecraft

The spacecraft is assumed to have three reaction wheels with distinct inertia aligned with the three body axes to control its attitude. Each reaction wheel inertia about the respective spin axis is given by J_i. Let the inertia matrix $\Im$ contain the spacecraft and the transverse reaction wheel inertia and let the matrix J be defined as

$$J = \begin{bmatrix} J_1 & 0 & 0 \\ 0 & J_2 & 0 \\ 0 & 0 & J_3 \end{bmatrix} \tag{1}$$

Let $\bar{\omega}_{B/N}$ be the spacecraft body angular velocity vector relative to an inertial frame N and let the $\bar{\Omega}$ vector contain the angular velocities of each reaction wheel. The rotational equations of motion can be written as[1]

$$\Im \frac{d\bar{\omega}_{B/N}}{dt} = -[\bar{\omega}_{B/N}]\Im\bar{\omega}_{B/N} - [\bar{\omega}_{B/N}]J(\bar{\Omega} + \bar{\omega}_{B/N}) - \bar{u} + \bar{f} \tag{2}$$

where the control vector $\bar{u}$ also satisfies the reaction axial wheel equation of motion:

$$\bar{u} = J\left(\frac{d\bar{\Omega}}{dt} + \frac{d\bar{\omega}_{B/N}}{dt}\right) \tag{3}$$

The tilde matrix $[\bar{\omega}]$ is defined as

2

$$[\tilde{\omega}] = \begin{bmatrix} 0 & -\omega_3 & \omega_2 \\ \omega_3 & 0 & -\omega_1 \\ -\omega_2 & \omega_1 & 0 \end{bmatrix} \tag{4}$$

and the vector $\bar{f}$ is the sum of all external torques acting on the spacecraft. These torques are in part due to aerodynamic and solar radiation drag and are usually considered to be very small compared to the internal torques being applied. They are assumed to have a known bound $\bar{F}$ which is defined as $|f_i| \leq \bar{F}_i$.

Attitude Coordinates

All spacecraft orientations are described using sets of modified Rodrigues parameters[4-9]. They are a minimal coordinate representation of a rigid body attitude with several useful attributes. They can be defined in terms of the Euler parameters (quaternions) as

$$\sigma_i = \frac{\beta_i}{1 + \beta_0} \qquad i = 1, 2, 3 \tag{5}$$

or in terms of the principal rotation axis $\hat{e}$ and the principal rotation angle ϕ as

$$\bar{\sigma} = \hat{e} \cdot \tan \phi/4 \tag{6}$$

Obviously they go singular at a principal rotation of $\pm 360°$ where $\beta_0 \rightarrow -1$. What makes this set very attractive is that this singularity can be completely avoided by making use of the fact that the modified Rodrigues parameters are not unique. Notice that reversing the sign of the β's in Eq. (5) generates a second set of σ's. The alternate set is called the "shadow set"[4], and goes singular at zero rotations and is very well behaved around the $\pm 360°$ rotations. Hence, if a singularity is approached with the original set, one can switch the attitude description to the "shadow set" and avoid the singularity at the cost of having a discontinuity at the switching point. The transformation between "original" and "shadow" set is[4,6]

$$\sigma_i^S = -\sigma_i / \bar{\sigma}^T \bar{\sigma} \qquad i = 1, 2, 3 \tag{7}$$

Keep in mind that the choice in distinguishing "original" and "shadow" sets is purely arbitrary. Both sets describe the same physical orientation. In this study the switching condition was chosen to be $\bar{\sigma}^T \bar{\sigma} = 1$. This causes the magnitude of the orientation vector to be bounded between $0 \leq |\bar{\sigma}| \leq 1$. In terms of a principal orientation angle this means that the angle is restricted to be within $-180° \leq \phi \leq +180°$. Note that this combined set of "original" and "shadow" parameters implicitly "knows" the shortest way back to the origin[4]. Lengthy principal rotations of more than 180° are avoided. This will be useful when designing a robust attitude feedback control law. Also note from Eq. (6) that for the range $-180° \leq \phi \leq +180°$ the modified Rodrigues parameters behave very linearly. The differential kinematic equation of motion in terms of the modified Rodrigues parameters is given below[4,5]. Note that the equation only contains second order polynomial nonlinearities in $\bar{\sigma}$.

$$\frac{d\bar{\sigma}}{dt} = \frac{1}{2}\left[I\left(\frac{1 - \bar{\sigma}^T\bar{\sigma}}{2}\right) + [\tilde{\sigma}] + \bar{\sigma}\bar{\sigma}^T\right]\bar{\omega} \tag{8}$$

Eq. (8) holds for both the "original" and the "shadow" set. This means that the derivative is well defined even at the switching point. The direction cosine matrix in term of the modified Rodrigues parameters is[4,5]

$$C(\bar{\sigma}) = \frac{1}{\left(1 + \bar{\sigma}^T\bar{\sigma}\right)^2}\begin{bmatrix} 4\left(\sigma_1^2 - \sigma_2^2 - \sigma_3^2\right) + \Sigma^2 & 8\sigma_1\sigma_2 + 4\sigma_3\Sigma & 8\sigma_1\sigma_3 - 4\sigma_2\Sigma \\ 8\sigma_1\sigma_2 - 4\sigma_3\Sigma & 4\left(-\sigma_1^2 + \sigma_2^2 - \sigma_3^2\right) + \Sigma^2 & 8\sigma_2\sigma_3 + 4\sigma_1\Sigma \\ 8\sigma_1\sigma_3 + 4\sigma_2\Sigma & 8\sigma_2\sigma_3 + 4\sigma_1\Sigma & 4\left(-\sigma_1^2 - \sigma_2^2 + \sigma_3^2\right) + \Sigma^2 \end{bmatrix} \tag{9}$$

$$\Sigma = 1 - \bar{\sigma}^T\bar{\sigma}$$

3

OPEN-LOOP DYNAMICS

Rest-to-Rest Principal Rotation Reference Maneuver

Instead of doing a computationally expensive optimal control, all maneuvers performed will be about the *principal axis of rotation*. This will allow real-time pre-computation of the reference maneuvers. This solution is close to the optimal solution and *much* faster to compute. Euler's principal rotation theorem states that any reference frame can be related to another reference frame through a single-axis rotation. This theorem allows any three-dimensional rotation to be viewed as a single-axis rotation about the principal axis, as illustrated by the simple *one-dimensional* equation shown below.

$$\Im \ddot{\theta} = u \tag{10}$$

While certain gyroscopic coupling nonlinearities must be accounted for, since the actual motion will be fully three-dimensional, Eq. (10) provides a simple approach to design a reference trajectory. Let N denote the inertial and R denote the open-loop reference frames. The initial and final reference attitude can be established by the initial and final direction cosine matrices $[RN(t_0)]$ and $[RN(t_f)]$ in the sense

$$\bar{r}(t_f) = [RN(t_f)]\bar{n}(t_f), \qquad \bar{r}(t_0) = [RN(t_0)]\bar{n}(t_0) \tag{11a,b}$$

The rotation from the initial to the final position of the body axes is established by a direction cosine matrix $[RR(t_f, t_0)]$, where

$$\bar{r}(t_f) = [RR(t_f, t_0)]\bar{r}(t_0), \qquad [RR(t_f, t_0)] = [RN(t_f)][RN(t_0)]^T \tag{12a,b}$$

Euler's Principal axis of rotation is determined by finding the eigenvector of $[RR(t_f, t_0)]$ which corresponds to the eigenvalue +1; that is, we find the components $\{l_1, l_2, l_3\}$ of the unit vector satisfying

$$[RR(t_f, t_0)]\begin{Bmatrix} l_1 \\ l_2 \\ l_3 \end{Bmatrix} = \begin{Bmatrix} l_1 \\ l_2 \\ l_3 \end{Bmatrix} = \bar{l} \tag{13}$$

The principal rotation angle θ_f can be found by extracting the diagonal elements from the $[RR(t_f, t_0)]$ matrix[3]. We limit our principal rotation angles to be within $0° \le \theta \le 180°$, which is done automatically when using the inverse cosine function below.

$$\theta_f = \mathrm{acos}\left(\frac{trace([RR(t_f, t_0)]) - 1}{2}\right) \tag{14}$$

The principal axis of rotation can also be found[1], except near the zero and $\pm 180°$ case, from the matrix elements of $[RR(t_f, t_0)]$.

$$\bar{l} = \frac{1}{2\sin\theta_f}\begin{Bmatrix} RR_{23} - RR_{32} \\ RR_{31} - RR_{13} \\ RR_{12} - RR_{21} \end{Bmatrix} \tag{15}$$

Taking the inverse kinematics viewpoint, we can prescribe a *reference trajectory* $\theta_r(t)$ as a rotation about the principal vector of $[RR(t_f, t_0)]$. For the reference trajectory to conform with the desired initial and final attitude, it is necessary that $\theta_r(t)$ satisfy the boundary conditions $\theta_r(0) = 0$ and $\theta_r(t_f) = \theta_f$.

Using the reference principal angle $\theta_r(t)$ and the principal axis of rotation $\bar{l}$, we can define the reference orientation, angular velocity and angular acceleration as

$$\bar{p}(t) = \bar{l} \cdot \tan\frac{\theta_r(t)}{4}, \qquad \bar{\omega}_r(t) = \bar{l}\,\dot{\theta}_r(t), \qquad \frac{d\bar{\omega}_r}{dt}(t) = \bar{l}\,\ddot{\theta}_r(t) \tag{16a,b,c}$$

where $\bar{p}(t)$ is a modified Rodrigues parameter vector which parameterizes the direction co-

4

sine matrix $[RR(t_f, t_0)]$. Given the above reference body angular velocity and acceleration and assuming no external torques, the reference control torque can be found using Eq. (2) with.

$$\bar{u}_r = -\Im \frac{d\bar{\omega}_r}{dt} - [\bar{\omega}_r]\Im \bar{\omega}_r - [\bar{\omega}_r]J(\bar{\Omega}_r + \bar{\omega}_r) \tag{17}$$

Near-Minimum-Time Maneuver

The optimal control for a rigid body minimum time maneuver is a "bang-bang" type control. For a rest-to-rest maneuver through a principal angle θ_f, the "bang-bang" control has the structure:

$$u(t) = u_{max}sign\left(t - \frac{t_f}{2}\right), \quad t_f = \sqrt{\frac{4\Im\theta_f}{u_{max}}} = \sqrt{\frac{4\theta_f}{\ddot{\theta}_{max}}}, \quad \ddot{\theta}_{max} = \frac{u_{max}}{\Im}$$

where $\ddot{\theta}_{max}$ and u_{max} are one-dimensional quantities measured along the principal axis of rotation.

If we anticipate that the "bang-bang" control will excite significant vibration of the flexible degrees of freedom, it is easy to smooth out the control switches using cubic splines and introduce "controllably sharp" torque switches using the smoothed "bang-bang" control shape[3]:

$$\ddot{\theta}_r(t) = \ddot{\theta}_{max} \begin{cases} \left(\frac{t}{\alpha t_f}\right)^2 \left(3 - 2\left(\frac{t}{\alpha t_f}\right)\right), & 0 \leq t \leq \alpha t_f \\ 1, & \alpha t_f \leq t \leq \frac{t_f}{2} - \alpha t_f \equiv t_1 \\ 1 - 2\left(\frac{t - t_1}{\alpha t_f}\right)^2 \left(3 - 2\left(\frac{t - t_1}{\alpha t_f}\right)\right), & t_1 \leq t \leq \frac{t_f}{2} + \alpha t_f \equiv t_2 \\ -1, & t_2 \leq t \leq t_f - \alpha t_f \equiv t_3 \\ -1 + \left(\frac{t - t_3}{\alpha t_f}\right)^2 \left(3 - 2\left(\frac{t - t_3}{\alpha t_f}\right)\right), & t_3 \leq t \leq t_f \end{cases} \tag{18}$$

where α controls the sharpness of the switches. $\alpha = 0$ generates the "bang-bang" instantaneous torque switches and $\alpha = 0.25$ generates the smoothest member of the family. After carrying out the double integration, the final maneuver time is found in terms of the principal angle rotated θ_f, the maximum principal angular acceleration $\ddot{\theta}_{max}$ and the smoothing factor α.

$$t_f = \sqrt{\frac{4\theta_f}{\ddot{\theta}_{max}} \cdot \frac{1}{1 - 2\alpha + \frac{2}{5}\alpha^2}}, \quad \ddot{\theta}_{max} = \frac{u_{max}}{\Im} \tag{19a,b}$$

The resulting principal angles and angular velocities can be seen in Figure 1, where $\alpha = 0.1$ was chosen. Obviously the maximum increase of maneuver time (for $\alpha = 0.25$) is less than 38%, compared to the "bang-bang" ($\alpha = 0$) case. For a flexible spacecraft, due to the decrease in vibrational energy, the actual maneuver time (including vibration settling time) is typically decreased significantly by using the smoothed "bang-bang" control. Even though we are not specifically considering the flexible spacecraft case at this point, we can implicitly consider flexibility by eliminating sharp torque switches which can be anticipated to "ring" the structure. Qualitatively, a sufficiently smooth and low amplitude torque history will make the most flexible structure behave more like a rigid structure and make the corresponding reference trajectory "more trackable." These statements can be made quite rigorously, see for example[1,2]. For well-chosen reference maneuvers and tracking law design, maneuver times for flexible spacecraft can usually be kept within 10 to 20% of the theoretical rigid body minimum maneuver times.
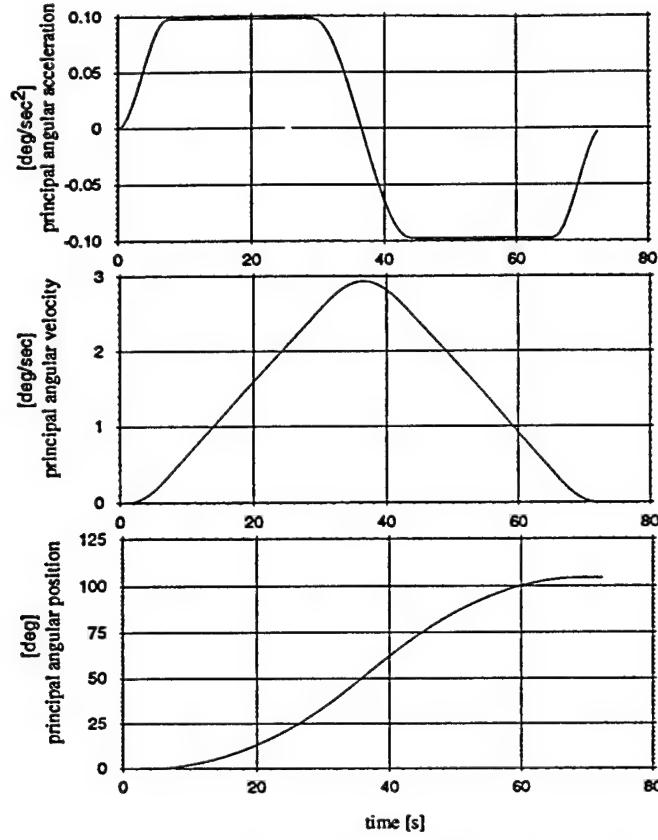
5

Figure 1 A Sample Torque Shaped Family of Near "Bang-Bang" Maneuvers

Near-Minimum-Fuel Maneuver

The torque time history of a optimal rigid body minimum-fuel maneuver consists of a sharp initial impulse to get the spacecraft rotating, a long coasting period, followed by a sharp reverse impulse to arrest the motion. Naturally, these sharp impulses would cause havoc for a highly flexible structure. Therefore a smoothed "bang-off-bang" control is chosen similar to the near-minimum-time maneuver presented previously.

$$
\ddot{\theta}_r(t) = \ddot{\theta}_{max}
\begin{cases}
\left(\dfrac{t}{\alpha_1 t_f}\right)^2\left(3 - 2\left(\dfrac{t}{\alpha_1 t_f}\right)\right), & 0 \le t \le \alpha_1 t_f \\[2ex]
1, & \alpha_1 t_f \le t \le \alpha_1 t_f + \alpha_2 t_f \equiv t_1 \\[2ex]
\left(\dfrac{t_2 - t}{\alpha_1 t_f}\right)^2\left(3 - 2\left(\dfrac{t_2 - t}{\alpha_1 t_f}\right)\right), & t_1 \le t \le 2\alpha_1 t_f + \alpha_2 t_f \equiv t_2 \\[2ex]
0, & t_2 \le t \le t_f - 2\alpha_1 t_f - \alpha_2 t_f \equiv t_3 \\[2ex]
-\left(\dfrac{t - t_3}{\alpha_1 t_f}\right)^2\left(3 - 2\left(\dfrac{t - t_3}{\alpha_1 t_f}\right)\right), & t_3 \le t \le t_f - \alpha_1 t_f - \alpha_2 t_f \equiv t_4 \\[2ex]
-1, & t_4 \le t \le t_f - \alpha_1 t_f \equiv t_5 \\[2ex]
-\left(\dfrac{t_f - t}{\alpha_1 t_f}\right)^2\left(3 - 2\left(\dfrac{t_f - t}{\alpha_1 t_f}\right)\right), & t_5 \le t \le t_f
\end{cases}
\tag{20}
$$

The instantaneous control switches are replaced by cubic splines with the rise and decay shape having controlled sharpness. Hence two torque smoothing factors α_1 and α_2 are used. The fac-

6

tor α_1 determines the rise or fall time from or to the maximum torque to zero torque as a percentage of the total maneuver time. The factor α_2 determines how long maximum torque is applied, also as a fraction of the total maneuver time. The amount of fuel used is chosen implicitly by specifying the two parameters α_1 and α_2.

The total maneuver time for the smoothed "bang-off-bang" control is found again by twice integrating the one dimensional principal rotation equation.

$$t_f = \sqrt{\frac{4\theta_f}{\ddot{\theta}_{max}} \cdot \frac{1}{\alpha_1 + \alpha_2 - 2\alpha_1^2 - 3\alpha_1\alpha_2 - \alpha_2^2}}, \quad \ddot{\theta}_{max} = \frac{u_{max}}{\Im} \qquad (21a,b)$$

The sample time history of principal angular acceleration, velocity and the principal angle for a smoothed "bang-off-bang" control is shown in Figure 2, where $\alpha_1 = \alpha_2 = 0.1$ were chosen.
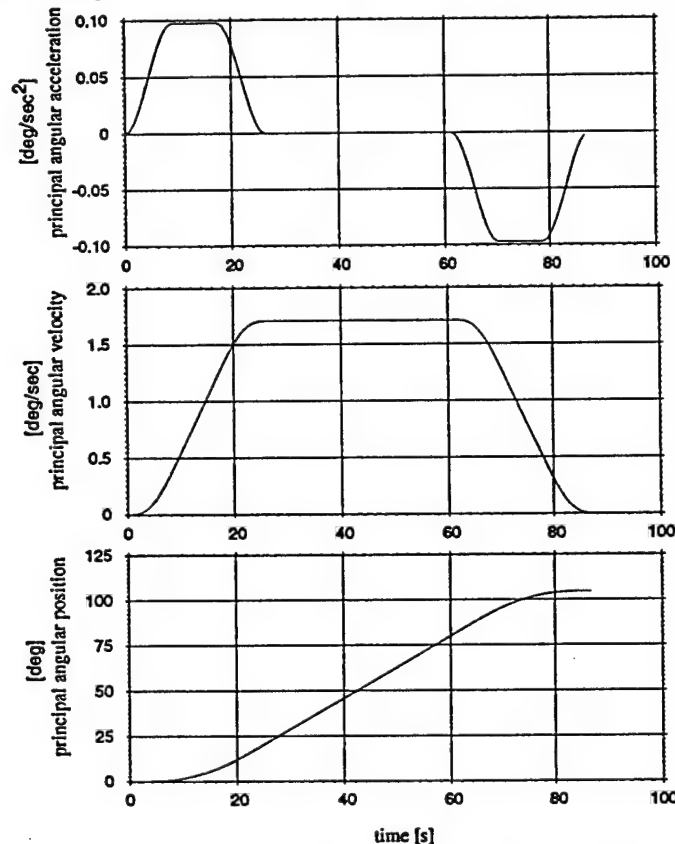

Figure 2 A Sample Torque-Shaped Family of Near "Bang-Off-Bang" Maneuvers

Incorporating Angular Velocity At The Final Maneuver Time

The principal rotation maneuver presented only applies to a rest-to-rest maneuver. To track a landmark, it is desired that the body have a certain angular velocity $\bar{\omega}(t_f)$ at the end of the maneuver. This allows the spacecraft to keep the sensors pointing toward a location on Earth for a finite duration of time and essentially achieve gross "motion compensation" for smear-free imaging. To accomplish this, the reference motion will be described relative to a moving target frame, not the inertial frame. Three coordinate frames are used:

R: open-loop reference coordinate axes (or follows the desired trajectory)

T: target motion coordinate frame

N: inertial coordinate frame

7

Let $\bar{\omega}_{T/N}$ be the body angular velocity vector of the target frame. In order to match up with our desired motion, the target frame T must have the following constraints.

$$\bar{\omega}_{T/N}(0) = 0 \qquad \bar{\omega}_{T/N}(t_f) = \bar{\omega}(t_f) \qquad\qquad (22a,b)$$

$$[TN(t_f)] = [RN(t_f)] \qquad\qquad (23)$$

Since the rest-to-rest principal rotation is described relative to the T frame, these conditions insure that the actual reference motion will have zero inertial angular velocity at $t=0$, and the desired orientation and angular velocity at the maneuver end.

Besides these three conditions any target motion can be chosen. The target motion used in this study was chosen to be a pure spin rotation about the $\bar{\omega}(t_f)$ axis, since an analytic solution exists for this trajectory. The orientation of the T frame at any time t is given as

$$[TN(t)] = [TT(t, t_f)][TN(t_f)] \qquad\qquad (24)$$

where the matrix $[TT(t, t_f)]$ describes the pure spin motion away from the final target position. Let the modified Rodrigues parameter vector $\bar{p}_T$ parameterize the $[TT(t, t_f)]$ matrix with the condition that $\bar{p}_T(t_f) = 0$. The unit vector $\hat{l}_T$ is the principal axis of the target motion and is defined as

$$\hat{l}_T = \frac{\bar{\omega}(t_f)}{|\bar{\omega}(t_f)|} \qquad\qquad (25)$$

and θ_T is the target principal rotation angle. The target motion $\bar{p}_T(t)$ is then defined as

$$\bar{p}_T(t) = \hat{l}_T \cdot \tan\frac{\theta_T}{4} \qquad\qquad (26)$$

where $\theta_T(t_f) = 0$. To match initial and final conditions of the target angular velocity a cubic spline was used. By choice, this will result in the reference motion having no angular acceleration at the maneuver end, but this is not a requirement of the method itself. Any target angular velocity history that matches the conditions in Eqs. (22a,b) could have been used. The target angular velocity and acceleration are defined as:

$$\bar{\omega}_{T/N}(t) = |\bar{\omega}_{T/N}(t_f)|\left(\frac{t}{t_f}\right)^2\left(3 - 2\frac{t}{t_f}\right) \cdot \hat{l}_T \qquad\qquad (27)$$

$$\frac{d\bar{\omega}_{T/N}(t)}{dt} = \frac{|\bar{\omega}_{T/N}(t_f)|}{t_f}\left(6\frac{t}{t_f} - 6\left(\frac{t}{t_f}\right)^2\right) \cdot \hat{l}_T \qquad\qquad (28)$$

After once integrating Eq. (27) the target principal rotation angle is found.

$$\theta_T(t) = \frac{|\bar{\omega}_{T/N}|}{t_f^2}\left(t^3 - \frac{t^4}{2t_f} - \frac{t_f^3}{2}\right) \qquad t_0 \leq t \leq t_f \qquad\qquad (29)$$

The relative position of the reference frame to the target frame is given by the matrix $[RT(t)]$ which is found through

$$[RT(t)] = [RN(t)][TN(t)]^T \qquad\qquad (30)$$

At the times t_0 and t_f the relative orientations are defined as

$$[RT(t_0)] = [RN(t_0)][TN(t_0)]^T \qquad\qquad (31)$$

$$[RT(t_f)] = [RN(t_f)][TN(t_f)]^T = I \qquad\qquad (32)$$

Eq. (12b) is now rewritten as

8

$$[RR(t_f, t_0)] = [RT(t_f)][RT(t_0)]^T = [RT(t_0)]^T \tag{33}$$

The matrix $[RR(t_f, t_0)]$ defined in Eq. (33) is used to define the rest-to-rest principal rotation motion for the case where the reference motion is supposed to have a final angular velocity.

Given the maneuver time t_f, we would be able to accurately describe the complete target motion. To find t_f though, we need to know the $[RR(t_f, t_0)]$ matrix first, which itself depends on the target motion. Since we only know the final, not the initial target position in advance, no closed form solution is available to find t_f. An iterative method was used to find the maneuver time. The initial estimate for t_f was found by assuming complete rest-to-rest motion. Using this t_f a new $[RR(t_f, t_0)]$ matrix was found and with it a new t_f. This method converged very quickly if half of the difference between old and new t_f was added to the old t_f.

The matrix $[RT(t)]$ is given as

$$[RT(t)] = [RR(t, t_0)][RT(t_0)] \tag{34}$$

where the $[RT(t_0)]$ matrix was defined in Eq. (31). The desired reference motion relative to the inertial frame is found from Eq. (30) to be

$$[RN(t)] = [RT(t)][TN(t)] \tag{35}$$

where the target motion $[TN(t)]$ is given in Eq. (24).

The angular velocity and acceleration expressed in Eq. (16b,c) are now expressed relative to the target frame motion. Hence, let us relabel these quantities as expressions relative to the target frame as

$$\bar{\omega}_{R/T}^R(t) = \bar{\omega}_r(t) \ , \quad \frac{d\bar{\omega}_{R/T}^R(t)}{dt} = \frac{d\bar{\omega}_r(t)}{dt} \tag{36}$$

where the superscripts indicate in which coordinate frame the vectors are written. The reference angular velocity expressed relative to the inertial frame is given as

$$\bar{\omega}_{R/N}^R = \bar{\omega}_{R/T}^R + [RT]\bar{\omega}_{T/N}^T \tag{37}$$

To find the reference angular acceleration relative to the inertial frame, the inertial derivative of Eq. (37) is taken.

$$\frac{d}{dt}\left(\bar{\omega}_{R/N}^R\right)^N = \frac{d}{dt}\left(\bar{\omega}_{R/N}^R\right)^R + [\bar{\omega}_{R/N}]\bar{\omega}_{R/N}^R = \frac{d}{dt}\left(\bar{\omega}_{R/N}^R\right)^R$$
$$= \frac{d\bar{\omega}_{R/T}^R}{dt} + [RT]\frac{d\bar{\omega}_{T/N}^T}{dt} - [\bar{\omega}_{R/T}^R][RT]\bar{\omega}_{T/N}^T \tag{38}$$

For the limiting case where the target frame has zero motion, Eqs. (37) and (38) collapse back to the rest-to-rest case given in Eqs. (16b,c).

CLOSED-LOOP DYNAMICS

Lyapunov Method To Design Nonlinear Tracking Control Law

A nonlinear tracking control law is developed to assure that the reference trajectory is asymptotically tracked. One advantage of this nonlinear control law over other control laws is that it is globally, asymptotically stabilizing! The control law has inherently no restrictions on the size of the attitude or the angular velocity error. Secondly, through the choice of the attitude coordinates, this control law will bring a body, which has tumbled beyond ±180° from the reference motion, back to the reference trajectory through the shortest angular distance. The three coordinate frames used are:

B: actual spacecraft coordinate frame

9

R: reference coordinate axes

N: inertial coordinate frame

Let the $[BR]$ matrix define the relative attitude of the spacecraft to the reference frame. It is related to $[BN(t)]$ as

$$[BR] = [BN][RN]^T \qquad (39)$$

Let the modified Rodrigues parameter vector $\bar{\sigma}$ parameterize the direction cosine matrix $[BR]$. This vector defines the orientation error of the spacecraft relative to the reference frame; achieving $\bar{\sigma} \to 0$ assumes asymptotic tracking of the reference motion. The extradition of the $\bar{\sigma}$ vector from the $[BR]$ matrix is easily accomplished by use of the β_0 Euler parameter. The complete transformation is given below.

$$2\beta_0 = +\sqrt{trace([BR]) + 1}$$
$$\sigma_1 = \frac{BR_{23} - BR_{32}}{4\beta_0(1 + \beta_0)}$$
$$\sigma_2 = \frac{BR_{31} - BR_{13}}{4\beta_0(1 + \beta_0)} \qquad (40)$$
$$\sigma_3 = \frac{BR_{12} - BR_{21}}{4\beta_0(1 + \beta_0)}$$

By assuring that $\beta_0 \geq 0$ we are guaranteed to have a modified Rodrigues vector[4] with $|\bar{\sigma}| \leq 1$. By using the modified Rodrigues parameters to describe the error in orientation, the feedback control law will inherently know the "shortest way" back to the reference frame. As an example, if the spacecraft has rotated a principal rotation of $+200°$ off from the reference condition, the control law will know to let the spacecraft complete the rotation. It will perform a $+160°$ principal rotation instead of a $-200°$ maneuver, bringing the spacecraft back to the reference state "the short way round"[4].

Obviously, it is desired to make the body frame track the reference frame, and thus the objective of the tracking control law should be to make any departure motion $\bar{\sigma}$ vanish. Let all the following vectors be written in the body frame B, unless noted otherwise. The error in body angular velocity is given as

$$\delta\bar{\omega} = \bar{\omega}_{B/N} - [BR]\bar{\omega}_{R/N}^R \qquad (41)$$

The reference body angular velocity vector must be transferred into the body frame, since it is only given in the reference frame R. The error in body angular acceleration is found by taking the derivative of Eq. (41).

$$\frac{d}{dt}(\delta\bar{\omega})^N = \frac{d}{dt}(\bar{\omega}_{B/N})^N - [BR]\frac{d}{dt}(\bar{\omega}_{R/N})^N + [\bar{\omega}_{B/N}][BR]\bar{\omega}_{R/N}^R \qquad (42)$$

The Lyapunov function for the feedback control law is defined to be

$$V = \frac{1}{2}\delta\bar{\omega}^T \Im \delta\bar{\omega} + 2K\log(1 + \bar{\sigma}^T\bar{\sigma}) \qquad (43)$$

where K is a scalar gain for the attitude error feedback. Using the logarithm of the departure motion will result in a feedback control law which is linear in $\bar{\sigma}$ [4,5]. As Tsiotras points out in Ref. 5, this remarkable fact occurs because $d/dt\left(2\log\left(1 + \bar{\sigma}^T\bar{\sigma}\right)\right) = \delta\bar{\omega}^T\bar{\sigma}$. To guarantee global asymptotic stability, let us verify that the first time derivative of V is negative definite.

$$\dot{V} = \delta\bar{\omega}^T \Im \frac{d}{dt}(\delta\bar{\omega})^N + K \cdot \delta\bar{\omega}^T\bar{\sigma} \qquad (44)$$

Substituting Eqs. (42) and (2) into Eq. (44) yields

10

$$\dot{V} = \delta\bar{\omega}^T \left(-[\tilde{\omega}_{B/N}]\Im\tilde{\omega}_{B/N} - [\tilde{\omega}_{B/N}]J(\bar{\Omega} + \tilde{\omega}_{B/N}) - \bar{u} + \bar{f} \right.$$
$$\left. - \Im[BR]\frac{d}{dt}(\tilde{\omega}_{R/N})^N + \Im[\tilde{\omega}_{B/N}][BR]\tilde{\omega}_{R/N}^R + K\bar{\sigma} \right) \tag{45}$$

After defining the control torque vector $\bar{u}$ to be

$$\bar{u}^B = -\Im\left([BR]\frac{d}{dt}(\tilde{\omega}_{R/N}^R)^N - [\tilde{\omega}_{B/N}][BR]\tilde{\omega}_{R/N}^R\right)$$
$$- [\tilde{\omega}_{B/N}^B]\Im\tilde{\omega}_{B/N}^B - [\tilde{\omega}_{B/N}^B]J(\bar{\Omega}^B + \tilde{\omega}_{B/N}^B) + K\bar{\sigma}^B + P\delta\bar{\omega}^B + \bar{F} \tag{46}$$

where $\bar{F}$ is defined as[10]

$$\bar{F}_i = F_i \cdot \text{sgn}(\delta\tilde{\omega}_i) \qquad i = 1, 2, 3 \tag{47}$$

and the matrix P is a positive definite angular velocity feedback matrix, and substituting $\bar{u}$ into Eq. (45), $\dot{V}$ is shown to be negative definite.

$$\dot{V} = -\delta\bar{\omega}^T P\delta\bar{\omega} - \delta\bar{\omega}^T(\bar{F} - \bar{f}) < 0 \qquad \forall \delta\bar{\omega}, \bar{\sigma} \neq 0 \tag{48}$$

For clarity, all vectors were labeled with their corresponding coordinate frame in Eq. (46). The control torque given above is dominated by linear terms in the position error $\bar{\sigma}$ and the angular velocity error $\delta\bar{\omega}$. It guarantees global asymptotic stability during both the tracking and the end game phase, assuming, of course, negligible model errors and perfect state measurements. Proper gain selection will result in a good rejection of model and external disturbance errors.

Because of the *sgn* function in $\bar{F}$ this control law could cause some chattering if the angular velocity measurements are noisy. If the magnitude of $\bar{F}$ is small enough though, this should not pose any practical problems. Having the $\bar{F}$ term in the control law does guarantee asymptotic convergence of the states to the target motion, even with unknown external forces present.

Control Feedback Gain Selection

Assuming zero external torques, the closed-loop dynamics are found by substituting Eqs. (2) and (42) into Eq. (46). The resulting differential equation only depends on the attitude error $\bar{\sigma}$ and the body angular velocity error $\delta\bar{\omega}$.

$$\frac{d}{dt}(\delta\bar{\omega})^N = -K \cdot \Im^{-1}\bar{\sigma} - \Im^{-1}P\delta\bar{\omega} \tag{49}$$

Note that the differential equation for $\delta\bar{\omega}$ is *linear* without making any approximations. The nonlinearity of the closed-loop dynamics come in through the coupling with $\bar{\sigma}$. If $\bar{\sigma} = 0$, then the poles of Eq. (49) could be arbitrarily chosen. The differential equation for $\bar{\sigma}$ depends quadratically on $\bar{\sigma}$ and is given by:

$$\frac{d\bar{\sigma}}{dt} = \frac{1}{2}\left[I\left(\frac{1 - \bar{\sigma}^T\bar{\sigma}}{2}\right) + [\tilde{\sigma}] + \bar{\sigma}\bar{\sigma}^T \right]\delta\bar{\omega} \tag{50}$$

After linearizing Eq. (50) about $\bar{\sigma} = 0$, the following approximation is obtained

$$\frac{d\bar{\sigma}}{dt} \approx \frac{\delta\bar{\omega}}{4} \tag{51}$$

Remember that the modified Rodrigues parameters act like angles over four. This fact is visible again in the above approximation. Because of this, the linearization using modified Rodrigues parameters will be valid for twice the rotation range compared to the classical Rodrigues parameters, and four times the range over the most attractive set of Euler angles. After combining Eqs. (49) and (51), the following closed-loop system equations of motion are found:

11

$$\begin{bmatrix} \dfrac{d}{dt}(\bar{\sigma})^N \\ \dfrac{d}{dt}(\delta\bar{\omega})^N \end{bmatrix} = \begin{bmatrix} 0 & \frac{1}{4}I \\ -K \cdot \mathfrak{I}^{-1} & -\mathfrak{I}^{-1}P \end{bmatrix} \begin{bmatrix} \bar{\sigma} \\ \delta\bar{\omega} \end{bmatrix} \tag{52}$$

Given an arbitrary inertia matrix $\mathfrak{I}$, a root-locus method could be used to find the poles of Eq. (52). The roots cannot be placed arbitrarily because K is only a scalar gain. If the inertia matrix $\mathfrak{I}$ and the angular velocity feedback matrix P are chosen to be diagonal matrices, then Eq. (52) can be decoupled into three sets of two equations

$$\begin{bmatrix} \dot{\sigma}_i \\ \delta\dot{\omega}_i \end{bmatrix} = \begin{bmatrix} 0 & \frac{1}{4} \\ -\frac{K}{\mathfrak{I}_i} & -\frac{p_i}{\mathfrak{I}_i} \end{bmatrix} \begin{bmatrix} \sigma_i \\ \delta\omega_i \end{bmatrix} \quad i = 1,2,3 \tag{53}$$

whose roots can be solved explicitly as

$$\lambda = -\frac{1}{2}\left(\frac{p_i}{\mathfrak{I}_i} + \sqrt{-\frac{K}{\mathfrak{I}_i} + \left(\frac{p_i}{\mathfrak{I}_i}\right)^2} \right) \quad and \quad \lambda = -\frac{1}{2}\left(\frac{p_i}{\mathfrak{I}_i} - \sqrt{-\frac{K}{\mathfrak{I}_i} + \left(\frac{p_i}{\mathfrak{I}_i}\right)^2} \right) \tag{54}$$

Note that the only approximations made in the above analysis are the linearization of Eq. (50) and the assumption of a diagonal inertia matrix $\mathfrak{I}$. Since the linearization of the modified Rodrigues parameters are valid for four times the rotational range of the Euler angles, and the off diagonal terms in the inertia matrix are usually very small compared to the diagonal terms, this linearization will typically predict the dynamics of the nonlinear system for moderately large tracking errors.

Figure 3 shows the root-locus plot of Eq. (54). A separate p_i can be chosen for each body axis, but only one attitude error feedback gain K can be chosen.
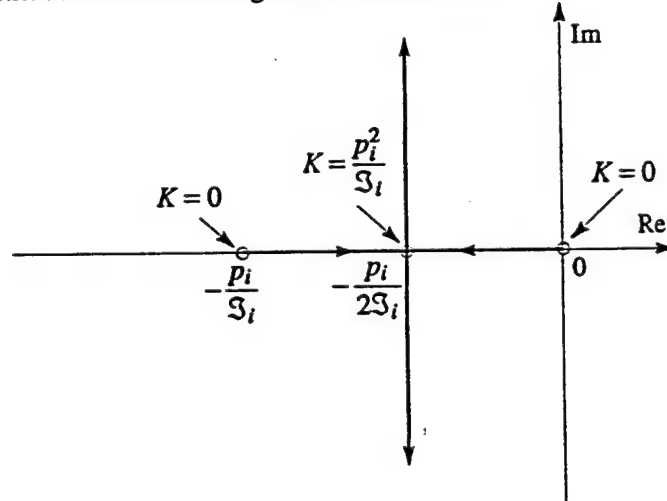

Figure 3 Root-Locus Plot of the Decoupled, Linearized Error Dynamics

Assuming that the closed-loop dynamics will be slightly under-damped, we can write the angular velocity feedback gains p_i in term of the controller decay time constants T_c.

$$p_i = 2\mathfrak{I}_i \frac{\ln 2}{T_c} \quad i = 1,2,3 \tag{55}$$

The scalar attitude feedback gain K is still free to be chosen. For the close-loop dynamics to be under-damped, the condition on K is

$$K > \frac{p_i^2}{\mathfrak{I}_i} \qquad i = 1, 2, 3 \tag{56}$$

Note that both K and p_i determine whether the closed-loop dynamics are over-, critically-, or under-damped. But if the system is under-damped, then only p_i determines how fast a state error will decay. On the other hand, the gain K influences the frequency of the oscillations ω_{c_i}.

$$\omega_{c_i} = \frac{1}{2}\sqrt{\frac{K}{\mathfrak{I}_i} - \left(\frac{p_i}{\mathfrak{I}_i}\right)^2} \qquad K = \mathfrak{I}_i\left(\omega_{c_i}^2 + \left(\frac{p_i}{\mathfrak{I}_i}\right)^2\right) \qquad i = 1, 2, 3 \tag{57a,b}$$

Control Gain Scheduling

To avoid reaction wheel torque saturation, the feedback gains are lowered whenever the system motion error is too large. We suggest a simple heuristic for gain scheduling, which can be sophisticated as necessary. The total system error is calculated as a weighted sum of the attitude and angular velocity error vectors.

$$error = |\delta\bar{\omega}| + \kappa \cdot |\bar{\sigma}| \tag{58}$$

If this measure of tracking error exceeds some nominal value, the gains are lowered to some smaller values. Whenever the error is within the nominal value, the gains are then raised again to their original values. This assumes only two sets of gains, obviously more than two sets could be used.

The body angular velocity feedback gain matrix P can also be permitted to vary with time without any loss of stability of the control law given in Eq. (46). The only requirement is that P remains positive definite. The attitude feedback gain K, however, was considered to be constant during the stability study. Allowing K to vary in time, Eq. (44) is rewritten as

$$\dot{V} = \delta\bar{\omega}^T\left(\mathfrak{I}\frac{d}{dt}(\delta\bar{\omega})^N + K\bar{\sigma}\right) + \dot{K}2\log\left(1 + \bar{\sigma}^T\bar{\sigma}\right) = -\delta\bar{\omega}^T P\delta\bar{\omega} + \dot{K}2\log\left(1 + \bar{\sigma}^T\bar{\sigma}\right) \tag{59}$$

If K is changed from a high gain to a low gain, (i.e. a large system error is present), $\dot{K}$ is negative and stability is still guaranteed during the transition phase. Only if K is changed from a low gain to a high gain, where $\dot{K} > 0$, is stability possibly not guaranteed. If $\dot{K}$ is large enough, $\dot{V}$ could become positive. However, since the transition will occur over a finite period of time, overall stability is not compromised. Also, the maximum positive $\dot{K}$ is computable at any time to satisfy $\dot{V} < tolerance$ as

$$\dot{K}_{max} = \frac{tolerance + \delta\bar{\omega}^T P\delta\bar{\omega}}{2\log\left(1 + \bar{\sigma}^T\bar{\sigma}\right)} \tag{60}$$

Obviously instantaneous jumps in feedback gains should be avoided, because they would cause excessive ringing of the flexible structure. To control the smoothness of the feedback gains time history, a digital low-pass filter is added. Any jumps in feedback gains are thus filtered out to a smooth curve with a controllable rise of $\dot{K}$.

STATE ESTIMATION

The purpose of this nonlinear estimator is to cancel any measurements errors in the body attitude vector $\bar{q}$ (given in modified Rodrigues parameters) and the body angular velocity $\bar{\omega}$, even in the presence of an unmodeled external torque $\bar{f}$ and a gyro rate bias $\bar{b}$. Let the measured states be denoted as $\bar{X}_m$, the estimated states as $\bar{X}_{est}$ and the actual states as $\bar{X}$.

$$\bar{X}_m = \begin{bmatrix} \bar{q}_m \\ \bar{\omega}_m \\ \bar{b}_m \end{bmatrix} \qquad \bar{X}_{est} = \begin{bmatrix} \bar{q}_{est} \\ \bar{\omega}_{est} \\ \bar{b}_{est} \end{bmatrix} \qquad \bar{X} = \begin{bmatrix} \bar{q} \\ \bar{\omega} \\ \bar{b} \end{bmatrix} \tag{61}$$

13

The rate gyro bias $\bar{b}$ is assumed to be constant for small time intervals, thus having the following kinematic equation

$$\frac{d}{dt}(\bar{b}) = 0 \tag{62}$$

Let the estimator error be defined as

$$\bar{e} = \bar{X}_{est} - \bar{X} = \begin{bmatrix} \Delta\bar{q} \\ \Delta\bar{\omega} \\ \Delta\bar{b} \end{bmatrix} \tag{63}$$

From Eqs. (2,8,62), the actual system dynamics can be written as

$$\frac{d}{dt}(\bar{X}) = F(\bar{X}) - \begin{bmatrix} 0 \\ \Im^{-1}\bar{u} \\ 0 \end{bmatrix} + \begin{bmatrix} 0 \\ \bar{d} \\ 0 \end{bmatrix} \tag{64}$$

where the $F()$ function contains the dynamical system. The angular acceleration $\bar{d}$ due to the unmodeled external torques is defined as

$$\bar{d} = \Im^{-1}\bar{f} \tag{65}$$

and is assumed to have a known bound $\bar{D}$ satisfying $\bar{D}_i \geq \bar{d}_i$. If the bounds of the rate gyro bias error $\Delta\bar{b}$ and of the angular acceleration due to external forces $\bar{d}$ are known, then the following dynamics of the estimated state scan be shown to be asymptotically stable for arbitrary large estimated state attitude and angular velocity errors.

$$\frac{d}{dt}(\bar{X}_{est}) = F\left(\bar{X}_m - \begin{bmatrix} 0 \\ \bar{b}_{est} \\ 0 \end{bmatrix}\right) - \begin{bmatrix} 0 \\ \Im^{-1}\bar{u} \\ 0 \end{bmatrix} - \begin{bmatrix} \bar{E}_q \\ \bar{E}_{\omega} \\ 0 \end{bmatrix} - H\left(\bar{X}_{est} - \bar{X}_m + \begin{bmatrix} 0 \\ \bar{b}_{est} \\ 0 \end{bmatrix}\right) \tag{66}$$

The estimator feedback gain matrix H is positive definite and partitioned as

$$J = \begin{bmatrix} H_{11} & H_{12} & H_{13} \\ H_{21} & H_{22} & H_{23} \\ H_{31} & H_{32} & H_{33} \end{bmatrix}$$

Similarly to Eq. (47) of the feedback control law, the vectors $\bar{E}_{\bar{q}}$ and $\bar{E}_{\bar{\omega}}$ are defined as

$$[\bar{E}_q]_i = \max\left(\text{abs}\left([H_{12}\Delta\bar{b}_{max}]_i\right)\right) \cdot \text{sgn}(\Delta\bar{q}_i) \tag{67}$$

$$[\bar{E}_{\omega}]_i = \max\left(\text{abs}\left([H_{22}\Delta\bar{b}_{max}]_i\right) + \bar{D}_i\right) \cdot \text{sgn}(\Delta\bar{\omega}_i) \tag{68}$$

The asymptotic stability of Eq. (66) is proven with the Lyapunov function

$$V = \frac{1}{2}\bar{e}^T\bar{e} \tag{69}$$

Let the measured states be broken up into the true states, the random white noise $\bar{v}$ and the rate bias components.

$$\bar{X}_m = \bar{X} + \bar{v} + \begin{bmatrix} 0 \\ \bar{b} \\ 0 \end{bmatrix} \tag{70}$$

By enforcing the asymptotic stability requirement $\dot{V} < 0$ and by making use of Eqs. (63), (64) and (66), the following asymptotic stability condition is found.

$$\bar{e}^T\left(F\left(\bar{X} + \bar{v} - \begin{bmatrix} 0 \\ \Delta\bar{b} \\ 0 \end{bmatrix}\right) - F(\bar{X}) + H\bar{v}\right) - \Delta\bar{q}^T\left(\bar{E}_q + H_{12}\Delta\bar{b}\right)$$

$$- \Delta\bar{\omega}^T\left(\bar{E}_{\omega} + \bar{d} + H_{22}\Delta\bar{b}\right) - \Delta\bar{b}^T H_{33}\Delta\bar{b} < \bar{e}^T H\bar{e} \tag{71}$$

14

Note that since H is positive definite, the right-hand side (RHS) of Eq. (71) will always be greater than zero for $\bar{e} \neq 0$. Assuming there is no measurement noise, no rate gyro bias and no unmodeled external torques, than the estimator dynamics in Eq. (66) is globally asymptotically stable. We offer the following qualitative observations regarding tuning of the estimator.

If an unmodeled external angular acceleration $\vec{d}$ is present with a known bound $\vec{D}$, then the estimator dynamics are still stable, since the $\Delta \bar{q}^T$ term of the left-hand side (LHS) is guaranteed to be negative definite by the definition of $\bar{E}_{\bar{q}}$. Stability is still guaranteed for any positive definite H and any estimated attitude and angular velocity errors.

If a rate bias $\bar{b}$ is introduced with a bounded error $\Delta \vec{b}$, then H can no longer be arbitrarily small. The first term of the LHS could be positive. The estimator feedback gain matrix H must be chosen large enough such that $\bar{e}^T H \bar{e}$ is always larger than the first term of the LHS. The second, third and fourth term of the LHS are guaranteed to be negative definite by the definition of $\bar{E}_{\bar{q}}$ and $\bar{E}_{\bar{\omega}}$, and because H_{33} is positive definite.

Once white measurement noise is introduced, the estimated states will not converge to the actual states of course, but will oscillate about them. While doing discrete sampling of the states at Δt intervals, the dominant noise term of the estimator dynamics is $H\bar{v}$. The actual jump due to noise from one sample to another is bounded by $H\bar{v}_{max}\Delta t$. To further adjust the filter characteristics, the sampling time interval can be tuned. The measurement noise also has a second degrading effect. It may cause the *sgn* functions in Eqs. (67,68) to return an incorrect sign of $\Delta \bar{q}_i$ and $\Delta \bar{\omega}_i$. This will cause a secondary noise induced effect of the estimated states between samples, of the order of $\bar{E}_{\bar{q}}\Delta t$ and $\bar{E}_{\bar{\omega}}\Delta t$ respectively. Again the filtering errors are controlled by choosing the sampling interval.

Under- and over-damped estimator dynamics were compared. For a given decay time constant, the over-damped system was better able to cancel measurement noise than the under-damped system. To assure that all the attitude and angular velocity measurement errors decay at the same rate, the estimator feedback matrix H was chosen to be of diagonal form.

$$H = \begin{bmatrix} H_{est} \cdot I & 0 & 0 \\ 0 & H_{est} \cdot I & 0 \\ 0 & 0 & H_{\bar{b}} \end{bmatrix} \tag{72}$$

Writing the estimator feedback gain H_{est} in terms of an estimator error decay time constant we get

$$H_{est} = \frac{\ln 2}{T_E} \tag{66}$$

The estimator feedback gain $H_{\bar{b}}$ can have a much larger decay time constant than H_{est}, since the rate gyro bias is assumed to change very slowly. Having a small $H_{\bar{b}}$ helps in reducing the secondary noise effect for the rate gyro bias estimation. In practice, we may use the above estimation algorithm to baseline a Kalman-Filter, or other linear state algorithm, appropriate for real-time on board implementation.

RESULTS

The following figures show the results of rigid body rotation simulation. The body inertia matrix $\mathfrak{I}$ has only diagonal entries of 200 kgm^2, 200 kgm^2 and 118 kgm^2 corresponding to the first, second and third body axis. The spacecraft has three reaction wheels aligned with the body axis whose inertia about the rotation axis are 0.00955 kgm^2, 0.1240 kgm^2 and 0.00955 kgm^2 respectively. The maneuver takes the spacecraft (in 3-2-1 Euler angles) from $(-4°,-55°,4°)$ to $(4°,55°,-4°)$. The rotation is mainly about the pitch axis with some slight yawing and rolling. The craft starts out with zero angular velocity and is required to have a final angular velocity of -1°/s

15

about the pitch axis at the end of the maneuver. The error in initial attitude and angular velocity is (-0.05°,0.8°,0.05°) and (-0.025°/s,0.1°/s,0.025°/s).

The feedback control law was chosen to have a time constant T_c of 4 seconds and an attitude feedback gain K of 44. This results in the feedback response in the pitch and yaw axis having a damped frequency of 9.05 °/s, and the roll axis having damped frequency of 14.4 °/s. The estimator time constant T_E was set to be 0.4 seconds, an order of magnitude faster than T_c. The initial estimated 3-2-1 Euler angles were (-4.1°,-55.5°,3.95°). The attitude noise measurements were subjected to random noise of the magnitude of 4e-5 (given in MRP). The initial estimated body angular velocities were (-0.02°/s,0.15°/s,0.03°/s). The angular velocity measurement noise level was set to 5e-5 °/s.
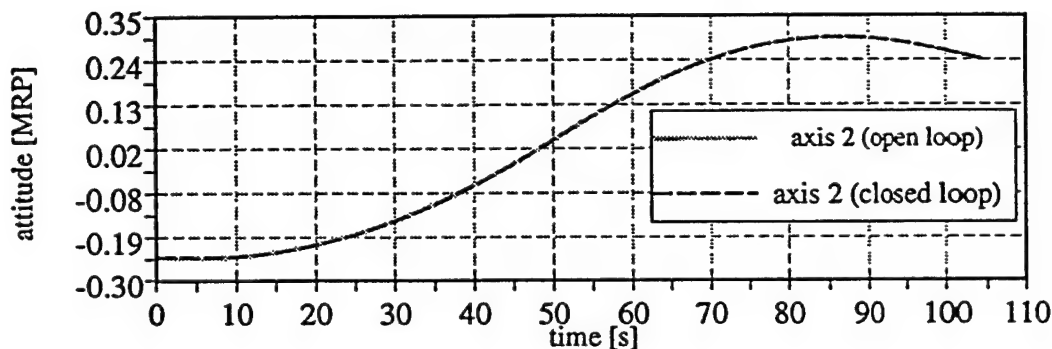

Figure 4 Open- and Closed-Loop Attitude for 2nd Body Axis

The total maneuver time was 104.09 seconds. Figures 4 and 5 show the attitude time history in MRP space. The closed-loop motion accurately tracks the open-loop trajectory. Figure 4 shows the large pitching maneuver. Since a final negative angular velocity is required about the 2nd body axis, the craft has to rotate beyond the target attitude and return to it with the desired angular velocity. The open-loop maneuver designed in this paper performs this task in a very smooth and near-optimum fashion.
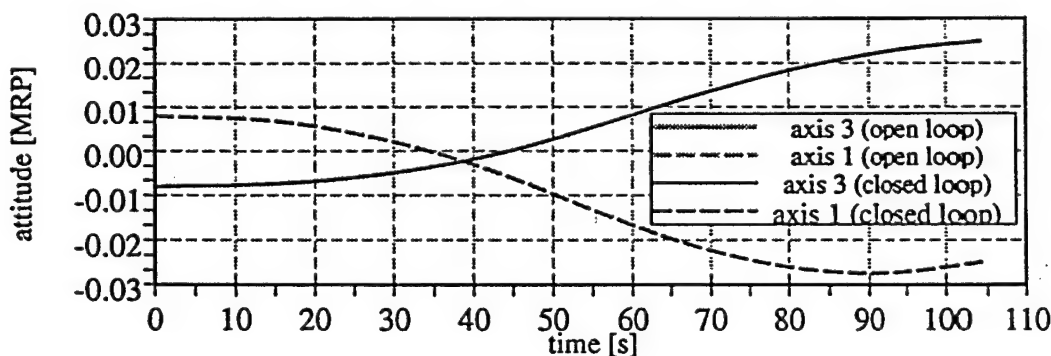

Figure 5 Open- and Closed-Loop Attitude for 1st and 3rd Body Axis

Figures 6 and 7 show the time history of the angular velocities. The open-loop maneuver correctly ends with a zero angular velocity about the 1st and 3rd body axis, and with -1°/s about the second body axis with no angular acceleration. If a final angular acceleration is required, this could easily be incorporated into the target trajectory used to generate the open-loop motion.

16

The initial state errors are canceled by the feedback control law and the open-loop trajectory is tracked accurately.
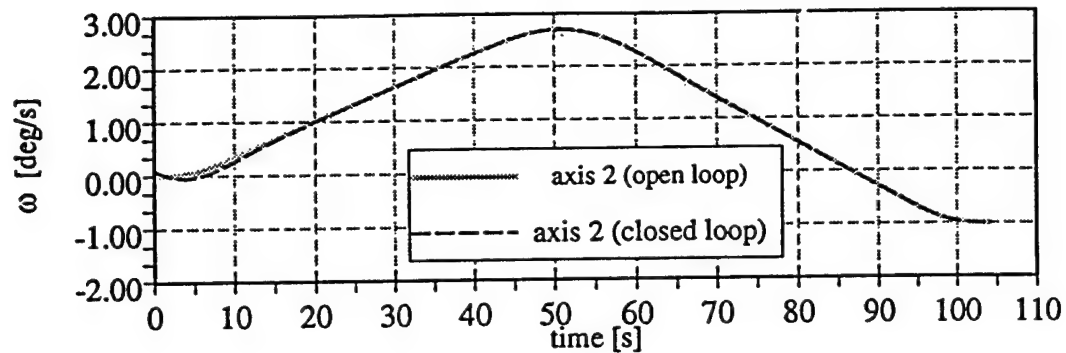

Figure 6 Open- and Closed-Loop Body Angular Velocity for 2nd Body Axis
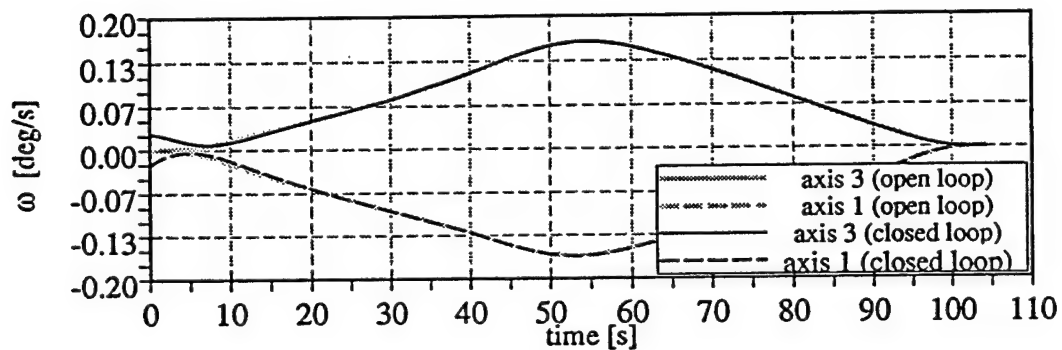

Figure 7 Open- and Closed-Loop Body Angular Velocity for 1st and 3rd Body Axis

Figures 8 and 9 show the time history of the internal control torque exerted onto the three reaction wheels. The maximum torque encountered is 0.3108 Nm by the second reaction wheel. The measurement noise is not visible in Figure 4 because of the relatively high torques. The closed-loop time history appears smooth and asymptotically approaches the open-loop torque time history.
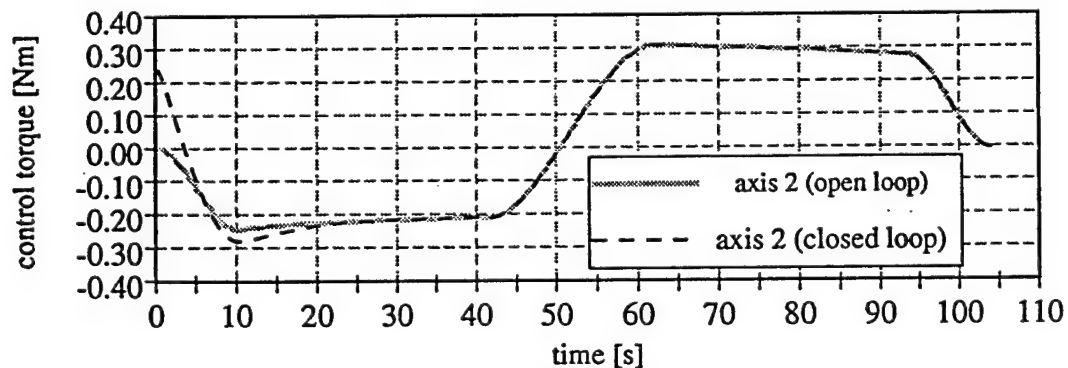

Figure 8 Open- and Closed-LoopControl Torque for 2nd Reaction Wheel

17

The measurement noise is visible in the time histories of the 1st and 3rd reaction wheels, since they are only exerting relatively low torques. But even here the noise is small compared to the torques and does not pose any fine pointing problems. The closed-loop time history still asymptotically approaches the open-loop control torque.
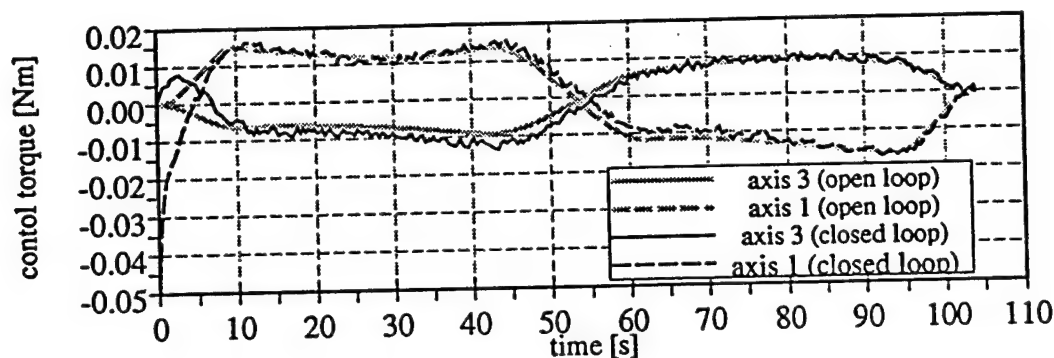

Figure 9 Open- and Closed-Loop Control Torque for 1st and 3rd Reaction Wheels

Figure 10 shows the time history of the attitude tracking error between the estimated states and the open-loop states. The linearization used to find the controller feedback gains very accurately models the actual nonlinear feedback dynamics. The decay time constants and the damped frequencies match with the simulation very well. As predicted, the 1st axis has a higher damped frequency than the 2nd and 3rd axis.
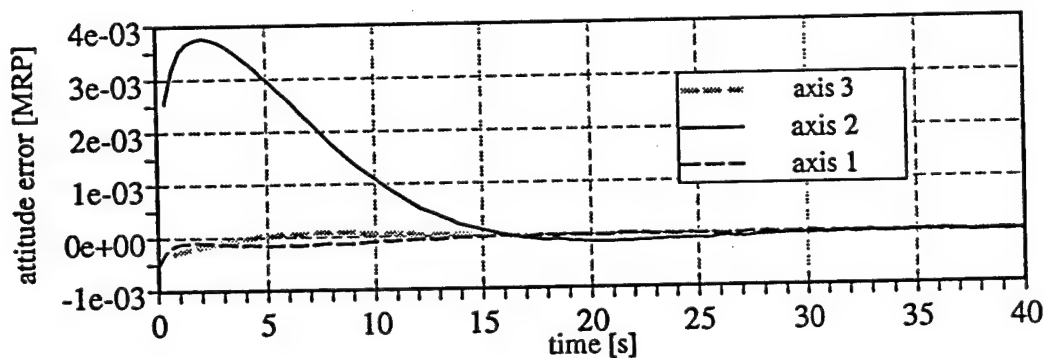

Figure 10 Closed-Loop Attitude Tracking Error

Figure 11 shows the time history of the angular velocity tracking error. Similar observations as with the attitude tracking error can be made. In both cases the initial state error is asymptotically canceled. The error is effectively gone after about 20 seconds. The measurement noise levels are too low to be visible on these figures.

18
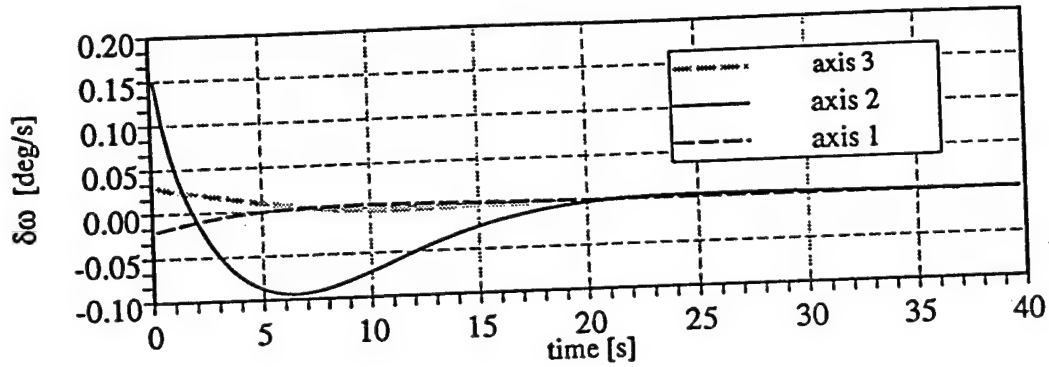
Figure 11 Closed-Loop Body Angular Velocity Tracking Error

Figures 12 and 13 show the time histories of the estimator tracking error between the estimated states and the actual states. Again the predicted estimator responses matches very well with the actual nonlinear response. The estimator dynamics are over-damped and errors decay an order of magnitude faster than the controller dynamics. The errors are effectively gone after about 2 seconds.

Figure 12 Estimator Attitude Tracking Error

Figure 13 Estimator Body Angular Velocity Tracking Error

19

CONCLUSIONS

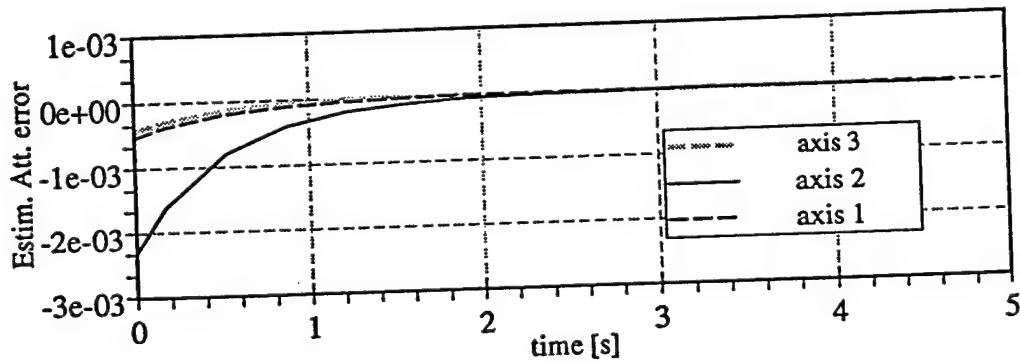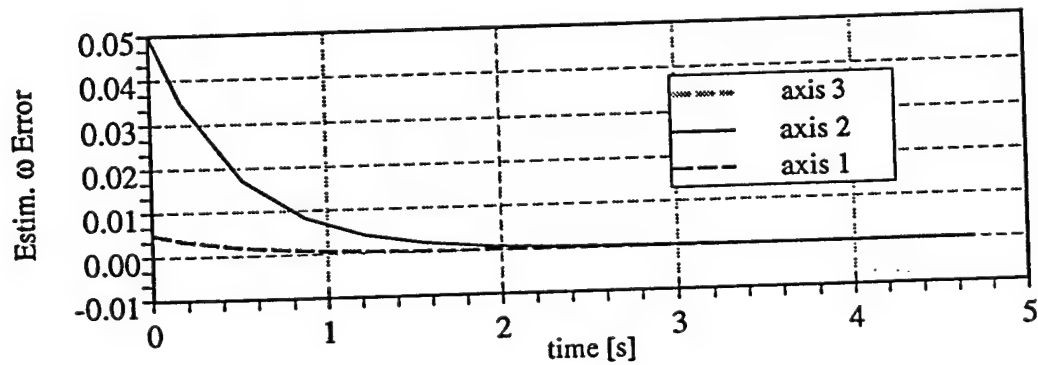A nonlinear feedback control approach has been developed for large three-dimensional rotational maneuvers. A unique coordinate choice and the use of Lyapunov control design methods are the key new ingredients blended to produce these results. To avoid excessive "ringing" of the structure, the near-minimum-time and near-minimum-fuel reference control torques were smoothed with cubic splines.

The feedforward/feedback control law presented is globally asymptotically stable, even under the influence of unmodeled, external torques with a known bound. The nonlinear estimator has proven Lyapunov stability, and asymptotic stability in the absence of measurement noise. It is also able to compensate for unmodeled external torques and rate gyro biases.

The actual closed-loop controller and estimator feedback dynamics matched very well with the dynamics predicted in the feedback gain selection sections, since only the attitude dynamics had to be linearized. Because of the choice of attitude coordinates, the modified Rodrigues parameters, this linearization is valid for a range of attitude errors four times larger than if Euler angles were used, and two times larger than if the classical Rodrigues parameters were used.

The maneuver demonstrated was able to track the open-loop trajectory asymptotically and cancel any initial state or estimator errors.

REFERENCES

[1] Junkins, J. L., and Kim, Y., *Introduction to Dynamics and Control of Flexible Structures*, AIAA Education Series, Washington D.C., 1993.

[2] Junkins, J. L., Rahman, Z. H., and Bang, H., "Near-Minimum-Time Maneuvers of Distributed Parameter Systems: Analytical and Experimental Results," *Journal of Guidance, Control, and Dynamics*, Vol. 14, No. 2 (March-April, 1991), pp. 406-415.

[3] Junkins, J .L, and Turner, J. D., *Optimal Spacecraft Rotational Maneuvers*, Elsevier Science Publishers, Netherlands, 1986.

[4] Schaub, H., and Junkins, J. L., "Stereographic Orientation Parameters for Attitude Dynamics: A Generalization of the Rodrigues Parameters," AAS/AIAA Spaceflight Mechanics Meeting, Albuquerque, New Mexico, Feb. 13-16, 1995, paper AAS 95-137.

[5] Tsiotras, P. "New Control Laws for the Attitude Stabilization of Rigid Bodies," Proceedings, IFAC Symposium on Automatic Control in Aerospace, Palo Alto, CA, Sept. 12-16, 1994, pp. 316-321.

[6] Schaub, H., Tsiotras, P., and Junkins, J. L., "Principal Rotation Representations of Proper NxN Orthogonal Matrices," to appear in International Journal of Engineering Science, 1994.

[7] Marandi, S. R., and Modi, V. J., "A Preferred Coordinate System and the Associated Orientation Representation in Attitude Dynamics," *Acta Astronautica*, Vol. 15, 1987, pp. 833-843.

[8] Wiener, T. F., "Theoretical Analysis of Gimballess Inertial Reference Equipment Using Delta-Modulated Instruments," Diss. Massachusetts Institute of Technology, March 1962.

[9] Shuster, M. D., "A Survey of Attitude Representations," *Journal of the Astronautical Sciences*, Vol. 41, No. 4, 1993, pp. 439-517.

[10] Cristi, R., Burl, J., and Russo, N., "Adaptive Quaternion Feedback Regulation for Eigenaxis Rotations," Department of Electrical and Computer Engineering, Naval Postgraduate School, Monterey, CA, June 1993.

20

Eigenvector Derivatives for Mechanical Second-Order Systems

Youdan Kim* and Seungjae Lee†
Seoul National University, Seoul 151-742, Republic of Korea
and
John L. Junkins‡
Texas A&M University, College Station, Texas 77843-3141

Analytical expressions are developed for computing eigenvector derivatives, specialized for the case of mechanical second-order dynamic systems. Both exact and approximate formulations are developed using a modal expansion approach. The new exact formulations are found to be numerically accurate and to require significantly less computing time than the corresponding generalized formulations. An improved approximate method is also introduced for computing a truncated set of eigenvector derivatives for large structural systems. Numerical examples are included to evaluate the effectiveness of the approximate formulations, and they are found to be very efficient in the cases studied.

I. Introduction

FOR many analysis and design problems in engineering system analysis, including applications such as identification of dynamic systems,[1,2] redesign of vibratory systems,[3-6] and design of control systems by pole placement,[7-12] it is widely known in the engineering literature that eigenvalue and eigenvector derivatives with respect to design parameters are useful.

In the past 20 years, several algebraic methods for computing eigenvector derivatives have been studied by many researchers.[13-17] Nelson[13] has proposed an algebraic method for computing eigenvector derivatives. In this formulation, the eigenvector derivatives can be computed using only the eigenvector of interest together with some algebraic manipulation. Fox and Kapoor[14] present expressions for the rates of change of eigenvalues and eigenvectors with respect to the design parameters of the structure. Recently, Lim et al.[15] re-examined this problem and provided a new formulation for computing eigenvector derivatives and also established important relationships between left and right eigenvector derivatives. Dailey[16] presents an algorithm for computing eigenvector derivatives for real symmetric matrices in the case of repeated eigenvalues. Improved approximate methods for eigenvector derivatives, using only an available subset of mode shapes, are presented[15,17] for extremely large systems. All the above formulations are derived for the general non-self-adjoint systems under the assumption that matrices, eigenvalues, and eigenvectors are differentiable, except at isolated points; most applications reported have been to mechanical dynamic systems.

It is widely known that the dynamics of a large class of mechanical systems can be represented most naturally by second-order systems of differential equations with several special properties. For applying optimization or iterative design ideas to these systems, the second-order differential equations are usually transformed into a higher dimensioned first-order state space. Since the dimension of aerospace structural dynamic systems is usually large, one often encounters uncomfortably high computational burden to compute eigenvector derivatives using any of the available formulations. Note that eigenvector derivatives are central features for many algorithms utilizing iterative methods that modify the eigenstructure, and the computation time per iteration is very important.

There exist several properties of the system matrices describing mechanical systems that we exploit in the present paper to significantly reduce the computational burden. In this paper efficient formulas for computing eigenvector derivatives for a large family of mechanical second-order systems are derived by eliminating some unnecessary steps that are associated with transforming the differential equations into a first-order state space and applying general-purpose algorithms. Note that Fox and Kapoor's formulation[14] reflects structural characteristics instead of treating general eigenvalue problems. Therefore it can be easily applied for optimum design of structures. However, damping characteristics are not considered in their formulation, and therefore it is basically a special case of Lim et al. formulation.[15] In other words, Fox and Kapoor's formulation[14] cannot be applied for both the control law design problem and the structural optimization problem, since, in the general setting, both of these problems include artificial or aerodynamic damping. Since our formulation includes linear damping characteristics, it can be utilized for solving a large class of optimization problems concerned with mechanical second-order systems. A numerical study is included to evaluate the effectiveness of the new formulations. An improved method for approximating a truncated set of eigenvector derivatives for large structural systems is also presented and its utility is evaluated.

II. Eigenvalue Problems and Modal Derivatives

Consider a linear structure (modeled by a finite element or similar discretization scheme) in which the configuration vector x is governed by the system of linear second-order differential equations

$$\mathcal{M}\ddot{x}(t) + \mathcal{C}\dot{x}(t) + \mathcal{K}x(t) = Du(t) \qquad (1)$$

where $\mathcal{M}$ is the $n \times n$ positive-definite symmetric mass matrix, C is the $n \times n$ positive-semidefinite symmetric structural damping matrix that can be diagonalized via modal coordinate transformation, $\mathcal{K}$ is the $n \times n$ positive-semidefinite symmetric stiffness matrix, and D is the $n \times m$ control influence matrix.

The closed-loop system can be written as

$$M\ddot{x}(t) + C\dot{x}(t) + Kx(t) = 0 \qquad (2)$$

In a control design problem, the control law usually feeds back position and velocity information, and mass matrix M maintains its constant, symmetric, positive-definite characteristics, but the damping and stiffness matrices C, K will be changed by feedback such that the open-loop symmetry and definiteness characteristics are not generally guaranteed. In a structural optimization problem, all matrices will most generally be perturbed, but M, C, K will maintain their symmetry and definiteness properties over all admissible designs. In all cases where we consider eigenvector derivatives with respect to system parameters or control gains, the system matrices

M, C, K will be assumed to be analytic functions of the system design parameters or control gains.

Generalized Eigenvalue Problem

In order to solve eigenvalue problems for mechanical second-order systems, Eq. (2) can be transformed to the standard first-order state-space form

$$\begin{bmatrix} L & 0 \\ 0 & M \end{bmatrix} \begin{Bmatrix} \dot{x} \\ \ddot{x} \end{Bmatrix} = \begin{bmatrix} 0 & L \\ -K & -C \end{bmatrix} \begin{Bmatrix} x \\ \dot{x} \end{Bmatrix} \qquad (3)$$

or

$$B\dot{z} = Az \qquad (4)$$

where

$$B = \begin{bmatrix} L & 0 \\ 0 & M \end{bmatrix}, \qquad A = \begin{bmatrix} 0 & L \\ -K & -C \end{bmatrix}, \qquad z = \begin{Bmatrix} x \\ \dot{x} \end{Bmatrix}$$

Equation (4) represents the generalized eigenvalue problem for the given system, and in this paper, only nondefective systems that have a set of n linearly independent eigenvectors will be considered.

We observe that there is an infinity of possibilities implicit in the above transformed equations; the matrix L is at this point unspecified. For selection of the L matrix, we must consider the impact of the selection of L upon numerical accuracy and efficiency in computing eigenvalues and eigenvectors; a symmetric nonsingular matrix is widely used for convenience. In the structural dynamics literature, the most popular choices for L are either the mass matrix M or the stiffness matrix K. If the system includes rigid-body modes, then the K matrix will be singular with the dimension of the null space being the number of rigid-body degrees of freedom, and therefore, the mass matrix M is a better candidate for those systems. Note that for the $L = M$ case, the B matrix is always a constant positive-definite symmetric matrix for the general control design problem (assuming the control law utilizes only position and velocity information for feedback). On the other hand, for the $L = K$ case, the B matrix will be modified during the structural optimization process and the symmetric property is generally lost due to feedback. Note that if B is ill-conditioned, then this can rule out the possibility of computing any generalized eigenvalue accurately (Ref. 18, p. 395). Since the condition number of a matrix provides a useful measure of numerical accuracy in matrix manipulations, it would be useful to discuss the condition of the B matrix for the selected L matrix briefly. Our experience with such studies indicates that the condition number of the B matrix for the $L = M$ choice is typically smaller than that for the $L = K$ case; the common existence of many low-frequency eigenvalues is associated with a nearly rank-deficient stiffness matrix. This practical point of view indicates that constructing the B matrix using $L = M$ will usually lead to better conditioned computations and more accurate numerical results than using $L = K$. For low-dimensioned problems with no rigid-body degrees of freedom, the condition of all system matrices is typically good, and therefore the stiffness matrix can be used in this situation for L with excellent numerical efficiency and also without degrading the numerical accuracy. However, for large structural dynamics problems with rigid-body modes or many low-frequency modes, we recommend choosing L as the mass matrix, as a rule of thumb, for numerical stability and accuracy.

The right and left eigenvalue problems associated with $z = \phi e^{\lambda t}$ solutions of Eq. (4) are, respectively,

$$\lambda_i B \phi_i = A \phi_i \qquad i = 1, 2, \ldots, 2n$$
$$\lambda_i B^T \psi_i = A^T \psi_i \qquad i = 1, 2, \ldots, 2n \qquad (5)$$

where we adopt the conventional normalization of the biorthogonality conditions for the eigenvectors as

$$\phi_i^T B \phi_i = 1 \qquad i = 1, 2, \ldots, 2n$$
$$\psi_j^T B \phi_i = \delta_{ij} \qquad i, j = 1, 2, \ldots, 2n \qquad (6)$$

so that

$$\psi_j^T A \phi_i = \lambda_j \delta_{ij} \qquad i, j = 1, 2, \ldots, n \qquad (7)$$

where $(\cdot)^T$ denotes the transpose of the given vector. It is possible that the above normalization equation cannot be applied in some circumstances, because it occasionally happens that $\phi_i^T B \phi_i$ may generate a zero value. However, the probability of encountering this condition can be reduced to essentially zero for structural dynamics applications when special properties of admissible matrices are taken into account. Also, note that with normalization equation (6) the normalized eigenvectors are unique within a sign; $-\phi_i$ gives the same information as ϕ_i. It is apparent that a consistent and unique eigenvector can be obtained by considering the sign of any one nonzero element of each eigenvector. This property does not generate any problem, if any formulation (for example, eigenvector sensitivity) utilizing eigenvector information also reflects the sign of the corresponding eigenvector, consistently. We will discuss this further in the subsequent section.

Eigenvalue and Eigenvector Derivatives

The usefulness of eigenvalue and eigenvector derivatives in design algorithms for engineering system analysis is well known. Some specific applications include identification of dynamic systems, redesign of vibratory systems, design of control gains by eigenstructure assignment, and sensor/actuator placement optimization. In order to apply gradient-based optimization algorithms, it is useful to compute analytical partial derivatives of eigenvalues and eigenvectors with respect to the system design parameters.

The differentiability of the eigenvectors has been addressed in the recent literature,[13–17] and most of the papers are in the applications-driven engineering optimization literature; some aspects of eigenvector differentiation in a general sense have been addressed in the linear algebra literature[18–22]; however, the circumstances under which eigenvectors are not differentiable does not appear to be adequately treated. Therefore, there may be need for collaboration between engineering community and applied linear algebra researchers to address the problem of eigenvector differentiation, with a special focus upon loss of differentiability (e.g., near the repeated eigenvalues and other singular circumstances). Extensive numerical experience with, for example, the formulations derived by Lim et al.[15] indicate that consistently normalized eigenvectors using Eqs. (6) are differentiable except in isolated events. We avoid the known degenerate situations here, by ruling out the obvious possibilities by enforcing definiteness assumptions on the mass matrix, and we do not treat the case of repeated eigenvalues.

For control design applications, matrix A is typically formed from constant system matrices M, C, K and optimization-process-variable gain matrices, and by taking matrix M for L, matrix B is a constant positive-definite symmetric matrix and the eigenvalues are distinct by assumption. For the structural optimization applications, matrices A and B consist of varying M, C, and K matrices, which are assumed variable as functions of the design parameters such as beam thickness, actuator locations, etc. For dealing with these engineering problems, matrices A and B are assumed to be analytic functions of the design parameters, and we made the heuristically reasonable assumption, consistent with our experience, that eigenvectors are differentiable, but with special care taken in accounting for the normalization conditions in performing the differentiation process. Readers may refer to Refs. 18–20 for discussions related to the sensitivities of perturbation of eigenvectors for the general eigenvalue problem.

Differentiating Eqs. (5) and using Eqs. (6) (utilizing a modal expansion approach) with respect to the design variable ρ, we can obtain the results[15]

$$\frac{\partial \lambda_i}{\partial \rho} = \psi_i^T \left(\frac{\partial A}{\partial \rho} - \lambda_i \frac{\partial B}{\partial \rho} \right) \phi_i \qquad (8)$$

$$\frac{\partial \phi_i}{\partial \rho} = \sum_{j=1}^{2n} a_{ij} \phi_j \qquad i = 1, \ldots, 2n \qquad (9)$$

$$\frac{\partial \psi_i}{\partial \rho} = \sum_{j=1}^{2n} b_{ij} \psi_j \qquad (10)$$

where

$$a_{ij} = \frac{1}{\lambda_i - \lambda_j} \psi_j^T \left(\frac{\partial A}{\partial \rho} - \lambda_i \frac{\partial B}{\partial \rho} \right) \phi_i \qquad i \neq j$$

$$= -\frac{1}{2} \left[\sum_{\substack{k=1 \\ k \neq i}}^{2n} a_{ik} \phi_k^T (B + B^T) \phi_i + \phi_i^T \frac{\partial B}{\partial \rho} \phi_i \right] \quad i = j \tag{11}$$

$$b_{ij} = \frac{1}{\lambda_i - \lambda_j} \psi_i^T \left(\frac{\partial A}{\partial \rho} - \lambda_i \frac{\partial B}{\partial \rho} \right) \phi_j \qquad i \neq j$$

$$= -\psi_i^T \frac{\partial B}{\partial \rho} \phi_i - a_{ii} \qquad i = j$$

Note that the above expressions are valid only for the distinct eigenvalue case. Except for isolated events such as multiple eigenvalues and associated root bifurcations, we assume the eigenvalues and eigenvectors to be smooth differentiable functions of the design parameter. The case of repeated eigenvalues is considered in another recent study.[16]

Modal Derivatives for the Second-Order Systems

The eigenstructure sensitivity formulas introduced in the previous section are useful in control design and structure optimization problems. Since derivative-based iterative routines are often engaged in these applications, it is important to calculate the eigenvector derivatives both accurately and efficiently. In this section, by utilizing well-known properties for linear mechanical second-order systems, efficient formulas for computing eigenvector derivatives are established.

The corresponding right and left eigenvalue problems associated with exponential solutions (i.e., $x = \alpha e^{\lambda t}$) for the mechanical second-order system [Eq. (2)] can be written, respectively, as

$$\left(\lambda_i^2 M + \lambda_i C + K \right) \alpha_i = 0$$
$$\left(\lambda_i^2 M + \lambda_i C + K \right)^T \beta_i = 0 \tag{12}$$

where λ_i, α_i, and β_i are ith eigenvalues and right and left modal vectors, respectively and generally have complex values. The two most popular choices for L in Eq. (3) will be considered in this study.

Case I: $L = M$

The eigenvalue problem using the mass matrix for L can be rewritten as

$$\lambda_i \begin{bmatrix} M & 0 \\ 0 & M \end{bmatrix} \phi_i = \begin{bmatrix} 0 & M \\ -K & -C \end{bmatrix} \phi_i$$

$$\lambda_i \begin{bmatrix} M & 0 \\ 0 & M \end{bmatrix}^T \psi_i = \begin{bmatrix} 0 & M \\ -K & -C \end{bmatrix}^T \psi_i \tag{13}$$

where $\phi_i \in R^{2n}$ and $\psi_i \in R^{2n}$ are eigenvectors normalized using Eq. (6) and can be partitioned as

$$\phi_i = \begin{Bmatrix} \phi_i^{(1)} \\ \phi_i^{(2)} \end{Bmatrix}, \qquad \psi_i = \begin{Bmatrix} \psi_i^{(1)} \\ \psi_i^{(2)} \end{Bmatrix} \tag{14}$$

By substituting Eq. (14) into Eq. (13) and comparing it with Eq. (12), a relationship between the right eigenvectors of the first-order system and the right eigenvectors of the second-order system can be obtained as

$$\phi_i = \begin{Bmatrix} \alpha_i \\ \lambda_i \alpha_i \end{Bmatrix} \tag{15}$$

Also, using Eqs. (13–15) in Eq. (6) yields the normalization equations (biorthogonality conditions)

$$\left(1 + \lambda_i^2 \right) \alpha_i^T M \alpha_i = 1$$

$$\psi_j^{(1)^T} M \alpha_i + \lambda_i \psi_j^{(2)^T} M \alpha_i = \delta_{ij} \tag{16}$$

Considering a positive-definite symmetric M matrix in Eq. (6), whenever a complex eigenvalue pair has purely imaginary parts with an absolute value of unity (i.e., $\lambda_i = \pm i$), the first equation yields zero, and obviously this equation cannot be applied for normalization of the corresponding mode's eigenvector. However, in control design or structure optimization applications, we rarely encounter this condition, since during the optimization procedure our closed-loop eigenvalues are constrained to lie in the stable region due to closed-loop stability constraints, and of course, this singular condition is easy to check. One other condition exists where we may have a problem with normalizing the eigenvector. Suppose that $\alpha_i = x + iy$, where x and y are real vectors, both not zero; then $\alpha_i^T M \alpha_i = 0$ if both $x^T M x = y^T M y$ and $x^T M y = 0$. In response to questions raised during the review process, we have studied this condition and have been unable to formally rule it out. We believe it to be a singular condition rarely encountered but easily tested for. Thus, the normalization is not universally valid because the normalization equation $\phi_i^T B \phi_i = 1$ [Eq. (6)] can fail under a few known circumstances. From an engineering point of view, it is almost always useful (because the singular situations are rarely encountered and furthermore may be easily tested for).

The eigenvalue derivatives for second-order systems can be obtained by using Eqs. (8) and (13–15):

$$\frac{\partial \lambda_i}{\partial \rho} = \psi_i^T \left(\frac{\partial A}{\partial \rho} - \lambda_i \frac{\partial B}{\partial \rho} \right) \phi_i$$

$$= -\psi_i^{(2)^T} \left(\lambda_i^2 \frac{\partial M}{\partial \rho} + \lambda_i \frac{\partial C}{\partial \rho} + \frac{\partial K}{\partial \rho} \right) \alpha_i \tag{17}$$

where

$$\frac{\partial A}{\partial \rho} = \begin{bmatrix} 0 & \frac{\partial M}{\partial \rho} \\ -\frac{\partial K}{\partial \rho} & -\frac{\partial C}{\partial \rho} \end{bmatrix}, \qquad \frac{\partial B}{\partial \rho} = \begin{bmatrix} \frac{\partial M}{\partial \rho} & 0 \\ 0 & \frac{\partial M}{\partial \rho} \end{bmatrix} \tag{18}$$

Following a modal expansion approach, by substituting Eqs. (13–15) into Eqs. (9–11), the eigenvector derivatives for the second-order systems can be represented as

$$\frac{\partial \phi_i}{\partial \rho} = \sum_{j=1}^{2n} a_{ij} \phi_j, \qquad \frac{\partial \psi_i}{\partial \rho} = \sum_{j=1}^{2n} b_{ij} \psi_i \qquad i = 1, \ldots, 2n \tag{19}$$

where

$$a_{ij} = \frac{1}{\lambda_j - \lambda_i} \psi_j^{(2)^T} \left(\lambda_i^2 \frac{\partial M}{\partial \rho} + \lambda_i \frac{\partial C}{\partial \rho} + \frac{\partial K}{\partial \rho} \right) \alpha_i \qquad i \neq j$$

$$= -\frac{1}{2} \sum_{\substack{k=1 \\ k \neq i}}^{2n} a_{ik} (1 + \lambda_k \lambda_i) \alpha_k^T (M + M^T) \alpha_i$$

$$- \frac{1}{2} \left(1 + \lambda_i^2 \right) \alpha_i^T \frac{\partial M}{\partial \rho} \alpha_i \qquad i = j \tag{20}$$

$$b_{ij} = \frac{1}{\lambda_j - \lambda_i} \psi_i^{(2)^T} \left(\lambda_i \lambda_j \frac{\partial M}{\partial \rho} + \lambda_j \frac{\partial C}{\partial \rho} + \frac{\partial K}{\partial \rho} \right) \alpha_j$$

$$- \psi_i^{(1)^T} \frac{\partial M}{\partial \rho} \alpha_j \qquad i \neq j$$

$$= -\left(\psi_i^{(1)^T} + \lambda_i \psi_i^{(2)^T} \right) \frac{\partial M}{\partial \rho} \alpha_i - a_{ii} \qquad i = j$$

Only complex-conjugate pairs of eigenvalues and eigenvectors occur for the case of most interest (underdamped second-order systems without rigid-body degrees of freedom), and the derivatives of the corresponding complex-conjugate eigenvector pairs are also obviously complex-conjugate vector pairs. By making use of this property, the computation time for calculating the eigenvector derivatives for the complex-conjugate pairs can be immediately reduced by half.

Case II: L = K

The eigenvalue problem using the stiffness matrix as L can be rewritten as

$$\phi_i = \left\{ \begin{array}{c} \alpha_i \\ \lambda_i \alpha_i \end{array} \right\}, \qquad \psi_i = \left\{ \begin{array}{c} \beta_i \\ -\lambda_i \beta_i \end{array} \right\} \qquad (21)$$

In this case, the normalization equations (biorthogonality conditions) are obtained as

$$\begin{aligned} \alpha_i^T \left(K + \lambda_i^2 M \right) \alpha_i &= 1 \\ \beta_j^T (K - \lambda_i \lambda_j M) \alpha_i &= \delta_{ij} \end{aligned} \qquad (22)$$

The procedure for deriving eigenvalue and eigenvector derivatives for this case is similar to the previous case, and therefore only the final results are summarized:

$$\frac{\partial \lambda_i}{\partial \rho} = \lambda_i \beta_i^T \left(\lambda_i^2 \frac{\partial M}{\partial \rho} + \lambda_i \frac{\partial C}{\partial \rho} + \frac{\partial K}{\partial \rho} \right) \alpha_i \qquad (23)$$

$$\frac{\partial \phi_i}{\partial \rho} = \sum_{j=1}^{2n} a_{ij} \phi_j, \qquad \frac{\partial \psi_i}{\partial \rho} = \sum_{j=1}^{2n} b_{ij} \psi_j \qquad i = 1, \ldots, 2n \qquad (24)$$

where

$$a_{ij} = \frac{\lambda_j}{\lambda_i - \lambda_j} \beta_j^T \left(\lambda_i^2 \frac{\partial M}{\partial \rho} + \lambda_i \frac{\partial C}{\partial \rho} + \frac{\partial K}{\partial \rho} \right) \alpha_i \qquad i \neq j$$

$$= -\frac{1}{2} \sum_{\substack{k=1 \\ k \neq i}}^{2n} a_{ik} \alpha_k^T \left[(K + K^T) + \lambda_i \lambda_k (M + M^T) \right] \alpha_i$$

$$\qquad -\frac{1}{2} \alpha_i^T \left(\frac{\partial K}{\partial \rho} + \lambda_i^2 \frac{\partial M}{\partial \rho} \right) \alpha_i \qquad i = j \qquad (25)$$

$$b_{ij} = \frac{\lambda_j}{\lambda_i - \lambda_j} \beta_i^T \left(\lambda_i^2 \frac{\partial M}{\partial \rho} + \lambda_i \frac{\partial C}{\partial \rho} + \frac{\partial K}{\partial \rho} \right) \alpha_j \qquad i \neq j$$

$$= \beta_i^T \left(\lambda_i^2 \frac{\partial M}{\partial \rho} - \frac{\partial K}{\partial \rho} \right) \alpha_i - a_{ii} \qquad i = j$$

Note that the eigenvectors ϕ_i and ψ_i of the first-order systems can be simply represented in terms of the eigenvalue and eigenvectors λ_i, α_i, and β_i of the second-order system, as seen in Eq. (21), in the case. Due to this property, the eigenvector sensitivities can be represented in a more compact form than the former case ($L = M$ case). Comparison of Eqs. (20) and (25), especially expressions for b_{ij}, leads to the conclusion that, if an efficient algorithm for solving eigenvalue problems [Eqs. (22)] for the mechanical second-order system is available, then Eq. (25) will be more effective, since these equations do not need full information on the left eigenvectors, including $\psi_i^{(2)}$. It is also possible to utilize this property in Eq. (14) for the $L = M$ case; however, this approach involves a matrix inverse, and therefore both the numerical accuracy and efficiency will be degraded, especially for large mass matrices.

III.   Approximation Methods in Computing Modal Derivatives

Approximation Method for First-Order System

The formulas for eigenvector derivatives derived in the previous section requires knowledge of all $2n$ eigenvectors. For very large structural dynamic systems, it is well-known that only a lowest frequency subset of N_r modes (eigenvalues and eigenvectors) may be computed accurately, where $N_r \ll n$, and in most practical applications, only tens of the lowest frequency modes participate significantly in a typical dynamic response of the system. It is natural to conjecture that the contributions of very high frequency modes to the sensitivity of the lower eigenvectors may also be neglected to some degree of approximation. If we consider the problem that derivatives of only N_r modes are really needed, then a method using all

eigenvectors may lead to inefficiency and a practical difficulty if all of the eigenvectors cannot be accurately computed. For this case, an approximate method for computing eigenvector derivatives has been reported[15,17] by utilizing a modal truncation method, including only a subset of the system modes:

$$\frac{\partial \phi_i}{\partial \rho} \cong \bar{a}_{ii} \phi_i + \bar{z}_i \qquad (26)$$

$$\frac{\partial \psi_i}{\partial \rho} \cong \bar{b}_{ii} \psi_i + \bar{w}_i \qquad (27)$$

where

$$\bar{z}_i = \sum_{\substack{j=1 \\ j \neq i}}^{N_r} \frac{\psi_j^T F_i}{\lambda_i - \lambda_j} \phi_j - A^{-1} F_i + \sum_{j=1}^{N_r} \frac{\psi_j^T F_i}{\lambda_j} \phi_j$$

$$\bar{w}_i = \sum_{\substack{j=1 \\ j \neq i}}^{N_r} \frac{\phi_j^T G_i}{\lambda_i - \lambda_j} \psi_j - A^{-T} G_i + \sum_{j=1}^{N_r} \frac{\phi_j^T G_i}{\lambda_j} \psi_j$$

$$\bar{a}_{ii} = -\frac{1}{2} \left(\phi_i^T \frac{\partial B}{\partial \rho} \phi_i + \phi_i^T B \bar{z}_i + \bar{z}_i^T B \phi_i \right) \qquad (28)$$

$$\bar{b}_{ii} = -\psi_i^T \frac{\partial B}{\partial \rho} \phi_i - \bar{w}_i^T B \phi_i - \psi_i^T B \bar{z}_i - \bar{a}_{ii}$$

$$F_i = \left(\frac{\partial A}{\partial \rho} - \lambda_i \frac{\partial B}{\partial \rho} \right) \phi_i$$

$$G_i^T = \psi_i^T \left(\frac{\partial A}{\partial \rho} - \lambda_i \frac{\partial B}{\partial \rho} \right)$$

The overbar denotes an approximate solution, and it is has been found that the approximation is often very accurate for large structural systems where there exists a large frequency gap between the last included mode (N_r) and the next higher frequency mode. By utilizing the biorthogonality conditions, we introduce a modification of the above results, especially in the terms F_i and G_i^T. Our modification follows.

Eigenvector Derivative Approximation Method for Second-Order Systems

We know from empirical experience that the above approximation method is usually efficient for computing lower mode eigenvector derivatives. In this section, a more efficient method will be derived especially for second-order systems by using results of the previous sections. Again, we develop here approximation expressions only for the special cases that the mass matrix or the stiffness matrix are selected for the L matrix. In the approximation methods, case II (using the stiffness matrix for L matrix) is very efficient, thanks to the elegantly simple expressions for the left eigenvector as seen in Eq. (21), and therefore, this formulation requires much less arithmetic, especially for computing the left eigenvector derivatives.

Case I: L = M

The exact eigenvector derivatives, Eq. (19), can be rewritten as

$$\frac{\partial \phi_i}{\partial \rho} = a_{ii} \phi_i + z_i, \qquad \frac{\partial \psi_i}{\partial \rho} = b_{ii} \psi_i + w_i \qquad (29)$$

where

$$z_i = \sum_{\substack{j=1 \\ j \neq i}}^{2n} a_{ij} \phi_j, \qquad w_i = \sum_{\substack{j=1 \\ j \neq i}}^{2n} b_{ij} \psi_j \qquad (30)$$

The eigenvalues are numbered according to increasing magnitude, and we assume that only the lower N_r modes' derivatives are required for a suitably accurate approximation. Since we use the lower frequency N_r eigenvalues and eigenvectors, the higher mode eigenvectors (higher than the lowest N_r modes) must be approximated. Separating z_i and w_i in Eqs. (30) into two parts, the first term includes the lower N_r mode eigenvectors that may be computed accurately and the second term includes higher mode eigenvectors that will be approximated; this yields

$$z_i = \sum_{\substack{j=1 \\ j \neq i}}^{N_r} a_{ij}\phi_j + \sum_{j=N_r+1}^{2n} a_{ij}\phi_j$$

$$w_i = \sum_{\substack{j=1 \\ j \neq i}}^{N_r} b_{ij}\psi_j + \sum_{j=N_r+1}^{2n} b_{ij}\psi_j \tag{31}$$

Substituting Eqs. (20) into Eq. (30) and using the property for the class of problems with a large frequency gap,

$$\lambda_j - \lambda_i \cong \lambda_j \qquad \text{for} \qquad j > N_r$$

an approximation $\bar{z}_i$ can be written as

$$\bar{z}_i = \sum_{\substack{j=1 \\ j \neq i}}^{N_r} \frac{\psi_j^{(2)^T} F_i}{\lambda_j - \lambda_i}\phi_j + \sum_{j=N_r+1}^{2n} \frac{\psi_j^{(2)^T} F_i}{\lambda_j}\phi_j$$

$$= \sum_{\substack{j=1 \\ j \neq i}}^{N_r} \frac{\psi_j^{(2)^T} F_i}{\lambda_j - \lambda_i}\phi_j + \sum_{j=1}^{2n}\phi_j\frac{\psi_j^{(2)^T} F_i}{\lambda_j} - \sum_{j=1}^{N_r}\frac{\psi_j^{(2)^T} F_i}{\lambda_j}\phi_j \tag{32}$$

where

$$F_i = \left(\lambda_i^2 \frac{\partial M}{\partial \rho} + \lambda_i \frac{\partial C}{\partial \rho} + \frac{\partial K}{\partial \rho}\right)\alpha_i \tag{33}$$

Since $\psi_j^{(2)^T} F_i$ is a scalar, the second summation on the right-hand side of Eq. (32) can be simplified. To do this, we consider the spectral decomposition of the A matrix using Eqs. (5–7):

$$A = \Psi^{-T}\Lambda\Phi^{-1} \tag{34}$$

or

$$A^{-1} = \Phi\Lambda^{-1}\Psi^T = \sum_{j=1}^{2n} \frac{\phi_j\psi_j^T}{\lambda_j} \tag{35}$$

where

$$A = \begin{bmatrix} 0 & M \\ -K & -C \end{bmatrix}, \qquad \Lambda = \text{diag}(\lambda_i)$$

$$\Phi = [\phi_1 \cdots \phi_{2n}], \qquad \Psi = [\psi_1 \cdots \psi_{2n}] \tag{36}$$

Equation (35) can be rewritten using Eqs. (14) and (15) as

$$\sum_{j=1}^{2n} \frac{1}{\lambda_j} \begin{bmatrix} \alpha_j\psi_j^{(1)^T} & \alpha_j\psi_j^{(2)^T} \\ \lambda_j\alpha_j\psi_j^{(1)^T} & \lambda_j\alpha_j\psi_j^{(2)^T} \end{bmatrix} = \begin{bmatrix} -K^{-1}CM^{-1} & -K^{-1} \\ M^{-1} & 0 \end{bmatrix} \tag{37}$$

We obtain the following useful relationship from the above equation:

$$\sum_{j=1}^{2n} \frac{1}{\lambda_j} \begin{bmatrix} \alpha_j\psi_j^{(2)^T} \\ \lambda_j\alpha_j\psi_j^{(2)^T} \end{bmatrix} = \begin{bmatrix} -K^{-1} \\ 0 \end{bmatrix} \tag{38}$$

Utilizing Eq. (38) in Eq. (32), we obtain the final approximation form of $\bar{z}_i$ as

$$\bar{z}_i = \sum_{\substack{j=1 \\ j \neq i}}^{N_r} \frac{\psi_j^{(2)^T} F_i}{\lambda_j - \lambda_i}\phi_j - \begin{bmatrix} K^{-1} \\ 0 \end{bmatrix}F_i - \sum_{j=1}^{N_r}\frac{\psi_j^{(2)^T} F_i}{\lambda_j}\phi_j \tag{39}$$

Now the modal representation of the eigenvector derivative can be approximated as

$$\frac{\partial\phi_i}{\partial\rho} = \bar{a}_{ii}\phi_i + \bar{z}_i \tag{40}$$

where the approximation formula for $\bar{a}_{ii}$ can be obtained by substituting Eqs. (18) and (21) into the formula for $\bar{a}_{ii}$ in Eq. (28),

$$\bar{a}_{ii} = -\frac{1}{2}\left\{(1+\lambda_i^2)\alpha_i^T\frac{\partial M}{\partial\rho}\alpha_i + \bar{z}_i^T\begin{bmatrix} M \\ \lambda_i M \end{bmatrix}\alpha_i \right.$$

$$\left. + \alpha_i^T[M \quad \lambda_i M]\bar{z}_i\right\} \tag{41}$$

For the class of problems that we are dealing with, we have found the above approximate solution is very efficient and is usually sufficiently accurate to be used in a derivative-based design or optimization process. It is straightforward but tedious to validate these equations using finite differences or by retaining all of the eigenvectors in the corresponding "exact" formulas developed above (provided, of course, that it is computationally feasible to solve the full-order eigenvalue problem).

Similarly, the derivatives of the left eigenvectors can be computed using the following modal approximation:

$$\frac{\partial\psi_i}{\partial\rho} = \bar{b}_{ii}\psi_i + \bar{w}_i \tag{42}$$

where

$$\bar{w}_i = -\begin{bmatrix} M^{-T} \\ 0 \end{bmatrix}\frac{\partial M^T}{\partial\rho}\psi_i^{(1)} + \begin{bmatrix} M^{-T} \\ 0 \end{bmatrix}\left(\lambda_i\frac{\partial M^T}{\partial\rho} + \frac{\partial C^T}{\partial\rho}\right)\psi_i^{(2)}$$

$$-\begin{bmatrix} M^{-T}C^T K^{-T} \\ K^T \end{bmatrix}\frac{\partial K^T}{\partial\rho}\psi_i^{(2)} + \sum_{\substack{j=1 \\ j \neq i}}^{N_r}h_{ij} - \sum_{j=1}^{N_r}\bar{h}_{ij}$$

$$h_{ij} = \left\{\frac{1}{\lambda_j - \lambda_i}\psi_i^{(2)^T}\left(\lambda_i\lambda_j\frac{\partial M}{\partial\rho} + \lambda_j\frac{\partial C}{\partial\rho} + \frac{\partial K}{\partial\rho}\right)\right.$$

$$\left. -\psi_i^{(1)^T}\frac{\partial M}{\partial\rho}\right\}\alpha_j\psi_j \tag{43}$$

$$\bar{h}_{ij} = \left\{\frac{1}{\lambda_j}\psi_i^{(2)^T}\left(\lambda_i\lambda_j\frac{\partial M}{\partial\rho} + \lambda_j\frac{\partial C}{\partial\rho} + \frac{\partial K}{\partial\rho}\right) - \psi_i^{(1)^T}\frac{\partial M}{\partial\rho}\right\}\alpha_j\psi_j$$

$$\bar{b}_{ii} = -\bar{w}_i^T\begin{bmatrix} M \\ \lambda_i M \end{bmatrix}\alpha_i - \psi_i^{(1)^T}\frac{\partial M}{\partial\rho}\alpha_i - \lambda_i\psi_i^{(2)^T}\frac{\partial M}{\partial\rho}\alpha_i$$

$$- \bar{a}_{ii} - [\psi_i^{(1)^T}M \quad \psi_i^{(2)^T}M]\bar{z}_i$$

Note that we have made use of the following useful relations for deriving the above equations:

$$\sum_{j=1}^{2n}\frac{1}{\lambda_j}\begin{bmatrix} \psi_j^{(1)}\alpha_j^T \\ \psi_j^{(2)}\alpha_j^T \end{bmatrix} = -\begin{bmatrix} M^{-T}C^T K^{-T} \\ K^{-T} \end{bmatrix}$$

$$\sum_{j=1}^{2n}\begin{bmatrix} \psi_j^{(1)}\alpha_j^T \\ \psi_j^{(2)}\alpha_j^T \end{bmatrix} = \begin{bmatrix} M^{-T} \\ 0 \end{bmatrix} \tag{44}$$

Case II: L = K

As in the previous section, the eigenvector approximation formula

for this case is much simpler than in case I ($L = M$). Since the derivation is quite similar, we only report the final results here:

$$\bar{z}_i = \sum_{\substack{j=1 \\ j \neq i}}^{N_r} \frac{\lambda_j}{\lambda_i - \lambda_j} \beta_j^T F_i \phi_j - \begin{bmatrix} K^{-1} \\ 0 \end{bmatrix} F_i + \sum_{j=1}^{N_r} \beta_j^T F_i \phi_j$$

$$\bar{w}_i = \sum_{\substack{j=1 \\ j \neq i}}^{N_r} \frac{\lambda_j}{\lambda_i - \lambda_j} G_i^T \alpha_j \psi_j - \begin{bmatrix} K^{-T} \\ 0 \end{bmatrix} G_i + \sum_{j=1}^{N_r} G_i^T \alpha_j \psi_j \tag{45}$$

where

$$\bar{a}_{ii} = -\frac{1}{2} \left\{ \alpha_i^T \left(\frac{\partial K}{\partial \rho} + \lambda_i^2 \frac{\partial M}{\partial \rho} \right) \alpha_i + \bar{z}_i^T \begin{bmatrix} K \\ \lambda_i M \end{bmatrix} \alpha_i \right.$$

$$\left. + \alpha_i^T \begin{bmatrix} K^T \\ \lambda_i M^T \end{bmatrix}^T \bar{z}_i \right\}$$

$$\bar{b}_{ii} = -\beta_i^T \left(\frac{\partial K}{\partial \rho} - \lambda_i^2 \frac{\partial M}{\partial \rho} \right) \alpha_i - \bar{a}_{ii} - \bar{w}_i^T \begin{bmatrix} K \\ \lambda_i M \end{bmatrix} \alpha_i$$

$$+ \beta_i^T \begin{bmatrix} -K^T \\ \lambda_i M^T \end{bmatrix}^T \bar{z}_i$$

and

$$F_i = \left(\lambda_i^2 \frac{\partial M}{\partial \rho} + \lambda_i \frac{\partial C}{\partial \rho} + \frac{\partial K}{\partial \rho} \right) \alpha_i$$

$$G_i = \left(\lambda_i^2 \frac{\partial M}{\partial \rho} + \lambda_i \frac{\partial C}{\partial \rho} + \frac{\partial K}{\partial \rho} \right)^T \beta_i$$

We use the following useful relations for deriving the above equations:

$$\sum_{j=1}^{2n} \begin{bmatrix} \alpha_j \beta_j^T \\ \lambda_j \alpha_j \beta_j^T \end{bmatrix} = \begin{bmatrix} K^{-1} \\ 0 \end{bmatrix}$$

$$\sum_{j=1}^{2n} \begin{bmatrix} \beta_j \alpha_j^T \\ -\lambda_j \beta_j \alpha_j^T \end{bmatrix} = \begin{bmatrix} K^{-T} \\ 0 \end{bmatrix} \tag{46}$$

IV. Numerical Example

To demonstrate the efficiency and accuracy of the several eigenvector derivative formulas developed in the previous sections, we consider a moderately dimensioned second-order system. The exact [Eqs. (8–11)] and approximate [Eqs. (26–28)] methods along with the new formulations developed for second-order systems are compared. Eigenvector derivatives in this paper were computed on an IBM PC-486DX (33 MHz) using 386 MATLAB®.

To provide a basis for comparison, we introduce an error measure based on the biorthogonality conditions of Eqs. (6). The partial derivatives of Eq. (6) for the $i = j$ case with respect to the parameter are as follows:

$$\frac{\partial}{\partial \rho} \left(\phi_i^T B \phi_i \right) = 0, \qquad \frac{\partial}{\partial \rho} \left(\psi_i^T B \phi_i \right) = 0 \tag{47}$$

It is obvious that if computed eigenvector derivatives are accurate, then as a necessary condition, the above equation must be satisfied. Therefore, an error measure can be defined as a norm of the differences from zero when computed derivatives are substituted into the above equations. Although this is only a necessary condition test on the validity of the eigenvectors, we have found that it is very useful to identify poorly approximated eigenvector derivatives and can be routinely computed more efficiently than forming a large table of finite difference approximations and comparing them to the corresponding analytic derivatives. We mention, however, that we have done extensive finite difference validations of all of the above eigenvector derivative formulas with typical agreement being four to nine digits, depending upon the smallness of the finite difference steps,

Table 1   Configuration parameters of flexible beam

Parameter	Value	Units
Mass density	0.0271875	slug/ft
Young's modulus	0.1584×10^{10}	lb/ft^2
Beam length	4.0	ft
Moment of inertia	4.7095×10^{-8}	ft^4

and of course, this agreement between finite derivative approximation and analytical formulas is problem dependent. The error measure of Eqs. (47) is convenient; it provides an easy-to-compute measure without requiring a problem-dependent artistic search for "how small" to make a finite difference parameter increment ($\delta\rho$). Generally, the error values computed from Eqs. (47) are complex numbers, and we define an eigenvector derivative error measure by simply using the absolute value of Eqs. (47), i.e.,

$$\mathcal{E}\left(\frac{\partial \phi_i}{\partial \rho} \right) \equiv \left\| \frac{\partial \phi_i^T}{\partial \rho} B \phi_i + \phi_i^T \frac{\partial B}{\partial \rho} \phi_i + \phi_i^T B \frac{\partial \phi_i}{\partial \rho} \right\|$$

$$\mathcal{E}\left(\frac{\partial \psi_i}{\partial \rho} \right) \equiv \left\| \frac{\partial \psi_i^T}{\partial \rho} B \phi_i + \psi_i^T \frac{\partial B}{\partial \rho} \phi_i + \psi_i^T B \frac{\partial \phi_i}{\partial \rho} \right\| \tag{48}$$

We mention the obvious fact that comparing the calculated eigenvector derivatives with computed results using finite difference approximation requires care on two counts. First, since computed results using a finite difference approximation are not exact derivatives, it usually is necessary to explore the size of the appropriate parameter increments, and if the finite difference approximation of the derivative is found to be stable to at least four significant figures (rule of thumb) over an order-of-magnitude variation in the size of the parameter increment, then the derivatives are usually found to be sufficiently accurate for derivative-based optimization processes. However, a patient pursuit of digits in the finite difference tuning can usually result in much higher precision agreement with the analytical partials. Avoiding this finite difference artwork is of course a primary motivation to have analytical partial derivatives and analytical necessary condition tests such as Eq. (48) to test for arithmetic errors. Second, and most importantly, the normalization conditions (in the biorthogonality conditions) that were enforced in deriving the eigenvector derivative formulas must be enforced on the nominal and perturbed eigenvectors used in the finite difference computations. We have concluded that the above error norm represents an attractive necessary condition measure for checking computed eigenvector derivatives and is in many ways more attractive than comparisons to results using the finite difference method. Therefore, in this study, the error measure introduced in Eq. (48) will be used for checking accuracy of computed eigenvector sensitivities.

Consider a transverse vibration of a uniform cantilever beam. A finite element method[23,24] is adopted for modeling, and structural damping (assumed damping ratio of 0.001) is included. The geometric and material parameters of the beam are listed in Table 1. To demonstrate the effectiveness of the new methods for at least moderately high dimensioned problems, 20 elements are considered, and therefore, using the usual cubic spline beam elements (the system configuration coordinates are the deflection and slope at the right end of each element), the dimension of the mass, damping, and stiffness matrices is 40×40. In order to evaluate the eigenvalue/eigenvector derivatives, all elements of the mass, damping, and stiffness matrices are perturbed about 0.1% arbitrarily for this special example, and the errors of the eigenvector sensitivities due to the perturbation are given below. Note that eigenvector derivatives are calculated for the normalized eigenvectors, and for this special example the norm of the eigenvector is of order 1 for all modes, and the norms of the eigenvector's derivatives are of order 1 for the low-frequency modes and of order 2 for the high-frequency modes. Therefore, it is evident that a computed result accurate to better than seven digits in the worst case was obtained using the three alternative formulas developed above for exact eigenvector derivatives.

Table 2 Errors of right eigenvector derivatives

Mode	First-order method	Second-order method	
		Method I[a]	Method II[b]
1	0.1655×10^{-13}	$5\,6456 \times 10^{-9}$	2.6324×10^{-6}
2	0.0083×10^{-13}	$0\,1870 \times 10^{-9}$	0.4660×10^{-6}
3	0.0003×10^{-13}	1.2028×10^{-9}	0.1214×10^{-6}
4	0.0001×10^{-13}	0.4148×10^{-9}	0.0227×10^{-6}
40	0.4805×10^{-18}	1.9319×10^{-8}	3.6814×10^{-11}
Times, s	879.68	310.27	301.04
Percent	100	35.27	34.22

[a]Use $L = M$. [b]Use $L = K$.

Table 3 Errors of left eigenvector derivatives

Mode	First-order method	Second-order method	
		Method I[a]	Method II[b]
1	1.4541×10^{-9}	1.3319×10^{-9}	1.3845×10^{-9}
2	0.0946×10^{-9}	0.1707×10^{-9}	0.0018×10^{-9}
3	0.1575×10^{-9}	0.2062×10^{-9}	0.0023×10^{-9}
4	0.1076×10^{-9}	0.0512×10^{-9}	0.0165×10^{-9}
40	3.5224×10^{-9}	3.4451×10^{-9}	3.2120×10^{-9}
Time, s	1187.11	433.48	393.43
Percent	100	36.52	33.14

[a]Use $L = M$. [b]Use $L = K$.

Table 4 Errors of right eigenvector derivatives: approximation methods

Mode	First-order method	Second-order method	
		Method I[a]	Method II[b]
1	0.0831×10^{-14}	5.3276×10^{-9}	1.3592×10^{-11}
2	0.0018×10^{-14}	0.4207×10^{-9}	0.0122×10^{-11}
3	0.0017×10^{-14}	0.6170×10^{-9}	0.0022×10^{-11}
4	0.0011×10^{-14}	0.1600×10^{-9}	0.0010×10^{-11}
5	0.0002×10^{-14}	0.0402×10^{-9}	0.0004×10^{-12}
Time, s	14.61	2.69	2.80
Percent	100	18.41	19.16

[a]Use $L = M$. [b]Use $L = K$.

Table 5 Errors of left eigenvector derivatives: approximation methods

Mode	First-order method	Second-order method	
		Method I[a]	Method II[b]
1	0.0007×10^{-14}	1.2653×10^{-9}	3.0959×10^{-13}
2	0.0111×10^{-14}	0.0585×10^{-9}	0.0160×10^{-13}
3	0.0014×10^{-14}	0.1310×10^{-9}	0.0015×10^{-13}
4	0.0004×10^{-14}	0.0440×10^{-9}	0.0004×10^{-13}
5	0.0002×10^{-14}	0.0123×10^{-9}	0.0001×10^{-14}
Time, s	27.13	18.07	8.84
Percent	100	66.61	32.58

[a]Use $L = M$. [b]Use $L = K$.

The error of the right and left eigenvector derivatives using the exact formulas are summarized in Tables 2 and 3, respectively, and the error measures of the first four lower modes and the highest (40th) mode are reported. For the first-order method, we use the mass matrix M for the L matrix and apply the exact formula Eqs. (8–11) with Eqs. (3) and (4). Note that for computing the left eigenvector derivatives, we use partial computations (a_{ii}) from the calculation of right eigenvector derivatives, and therefore the errors (of the right eigenvector derivatives) propagate into the computation of the left eigenvector derivatives. It is evident that some of the information needed on the left eigenvector derivative is already known from the right, and this valuable information can be utilized for computing left eigenvector sensitivities. However, left eigenvector sensitivities cannot be computed without former computations of a_{ii}. Therefore computing time for left eigenvector sensitivities includes calculating all a_{ij} coefficients [for computing a_{ii}, we need $a_{ij}(i \neq j)$], and naturally more computing time is needed for computing the left eigenvector derivatives.

There are several formulas for computing the eigenvector sensitivities discussed in this paper. We will refer the exact and approximate methods to the existing exact and approximate formulas for computing eigenvector sensitivities, respectively. For the presented methods for the second-order systems, whether the exact formula or the approximate formula is used, method I refers to the case that mass matrix M is used for matrix L, and method II refers to the case that stiffness matrix M is used for matrix L. As shown in Table 2, the accuracy of method I is lower than that of the first-order method, but both are acceptable. The errors of right eigenvector sensitivities using method II are not uniform and are a little larger than for method I. The computation time for the second-order method is three times less than the computation time required for the exact formula for the first-order system (Tables 2 and 3). In this study, in order to compute eigenvalues and eigenvectors for this second-order system, we use an eigenproblem solver for the first-order system, and the B matrix in Eq. (4) is moderately ill-conditioned [the condition number is $\mathcal{O}(10^7)$]. For method II, the poor conditioning of the B matrix results from the fact that not only the dimension of B matrix is large (i.e., 80), but also the order of magnitude of mass matrix elements is significantly different from that of stiffness matrix elements. For this system, the computed eigenvectors also include errors; this is evident by nonzero residuals if one substitutes the computed eigenvectors into the biorthogonality conditions. Especially for large systems, errors may be propagated from incorrect eigenvector computations into the analytically derived formulas for the eigenvector

derivatives. Thus the validity of the derivative approximation rests not only upon, for example, including all of the important modes in a modal truncation, but also upon the manner in which arithmetic errors in the original eigensolution propagate through the particular derivative equation calculations. From these observations, and other empirical experience, we recommend that method II should be used only for relatively low dimensioned systems, and method I is recommended for high-dimensioned applications.

For the eigenvector derivative approximation methods, only the first five (lowest frequency) modes ($N_r = 10$) are computed. Tables 4 and 5 summarize the results using our (improved) approximation methods. The errors of methods I and II are larger than those for (improved) approximation method for the first-order system but are judged acceptable for most applications. As shown in Tables 4 and 5, when we use approximation method I, the computation time for computing the right eigenvector derivatives is five times faster than the approximation method for the first-order system, and for computing the left eigenvector derivatives, it is approximately twice as fast. Approximation method II is found to be much faster than method I, and the computation errors are also smaller. Another interesting phenomenon is that the results using the approximation methods (Tables 4 and 5) for the lower modes turn out to be more accurate than those of the exact (in theory) methods (Tables 2 and 3). We may explain this phenomenon by noting that numerically inexact computed eigenvectors associated with the higher frequencies are included in evaluating the exact formulas, but not in the approximate solution, and another contributing factor is that the approximate method is much less intense computationally, and therefore the approximate formulas are less susceptible to the accumulation of arithmetic errors. These results provide a basis for optimism as regards the practical utility of the new approximate eigenvector derivative formulas presented herein, but as with any modal truncation method, the issue of which modes to retain is problem dependent and generally impossible to resolve universally.

V. Conclusions

This paper derives some new exact and approximate formulas for computing eigenvector derivatives for second-order mechanical systems. In order to demonstrate the effectiveness and accuracies of the new formulas, a numerical study using a moderately high dimensioned flexible structure is presented. The usefulness of the

new methods has been verified by comparing computation time to the corresponding computation time for the exact formulas for the first-order system, and the accuracy of the new methods has also been found to be excellent in the current example. These formulations are suitable for incorporation into iterative computer-aided design optimization algorithms and should find wide application.

Acknowledgments

References

[1]Collins, J. D., Hart, G. C., Hasselman, T. K., and Kennedy, B., "Statistical Identification of Structures," *AIAA Journal*, Vol. 12, Feb. 1972, pp. 185–190.

[2]Berman, A., and Flannelly, W. G., "Theory of Incomplete Models of Dynamic Structures," *AIAA Journal*, Vol. 9, No. 8, 1971, pp. 1481–1487.

[3]Haftka, R. T., Martinovic, Z. N., Hallauer, W. L., and Schamel, G., "Sensitivity of Optimized Control Systems to Minor Structural Modifications," AIAA Paper 85-0807, April 1985.

[4]Lim, K. B., and Junkins, J. L., "Optimal Redesign of Dynamic Structures via Sequential Linear Programming," *Proceedings of the Fourth International Modal Analysis Conference* (Los Angeles, CA), 1986, pp. 1615–1620.

[5]Chou, Y.-F., and Chen, J.-S., "Structural Dynamics Modification via Sensitivity Analysis," *Proceedings of the Third International Modal Analysis Conference* (Orlando, FL), Vol. 1, 1985, pp. 483–489.

[6]Jin, I. M., and Schmit, L. A., "Control Design Variable Linking for Optimization of Structural/Control Systems," AIAA Paper 91-1157, April 1991.

[7]Bodden, D. S., and Junkins, J. L., "Eigenvalue Optimization Algorithms for Structural/Controller Design Iterations," *Journal of Guidance, Control, and Dynamics*, Vol. 8, No. 6, 1985, pp. 697–706.

[8]Junkins, J. L., Bodden, D. S., and Turner, J. D., "A Unified Approach to Structure and Control System Design Iterations," presented at the Fourth International Conference on Applied Numerical Modeling, Tainan, Taiwan, ROC, Dec. 1984.

[9]Lim, K. B., and Junkins, J. L., "Optimal Design of Dynamic Structures via Sequential Linear Programming," presented at the Fourth International Modal Analysis Conference, Los Angeles, CA, Feb. 1986.

[10]Junkins, J. L., and Kim, Y., "First and Second Order Sensitivity of the Singular Value Decomposition," *Journal of the Astronautical Sciences*, Vol. 38, No. 1, 1990, pp. 69–86.

[11]Junkins, J. L., and Kim, Y., "A Minimum Sensitivity Design Method for Output Feedback Controllers," *Mechanics and Control of Large Space Structures*, Progress in Astronautics and Aeronautics Series, Vol. 129, AIAA, Washington, DC, 1990, Chap. 15.

[12]Sobel, K. M., Yu, W., and Lallman, F. J., "Eigenstructure Assignment with Gain Suppression Using Eigenvalue and Eigenvector Derivatives," *Journal of Guidance, Control, and Dynamics*, Vol. 13, No. 6, 1990, pp. 1008–1013.

[13]Nelson, R. B., "Simplified Calculation of Eigenvector Derivatives," *AIAA Journal*, Vol. 8, No. 9, 1976, pp. 1201–1205.

[14]Fox, R. L., and Kapoor, M. P., "Rates of Change of Eigenvalues and Eigenvectors," *AIAA Journal*, Vol. 6, No. 12, 1968, pp. 2426–2429.

[15]Lim, K. B., Junkins, J. L., and Wang, B. P., "Re-examination of Eigenvector Derivatives," *Journal of Guidance, Control, and Dynamics*, Vol. 10, No. 6, 1987, pp. 581–587.

[16]Dailey, R. L., "Eigenvector Derivatives with Repeated Eigenvalues," *AIAA Journal*, Vol. 27, No. 4, 1989, pp. 486–491.

[17]Wang, B. P., "Improved Approximate Methods for Computing Eigenvector Derivatives in Structural Dynamics," *AIAA Journal*, Vol. 29, No. 6, 1991, pp. 1018–1020.

[18]Golub, G. H., and Van Loan, C. F., *Matrix Computations*, 2nd ed., Johns Hopkins Univ. Press, Baltimore, MD, 1989, Sec. 7.2.

[19]Wilkinson, J. H., *The Algebraic Eigenvalue Problem*, Oxford Univ. Press, New York, 1965, Chap. 2.

[20]Stewart, G. W., *Introduction to Matrix Computations*, Academic, New York, 1965, Sec. 6.4.

[21]Kato, T., *Perturbation Theory for Linear Operators*, 2nd ed., Springer–Verlag, New York, 1976.

[22]Sun, J., "Eigenvalues and Eigenvectors of a Matrix Dependent on Several Parameters," *Journal of Computational Mathematics*, Vol. 3, No. 4, 1985, pp. 351–364.

[23]Craig, R., Jr., *Structural Dynamics: An Introduction to Computer Methods*, Wiley, New York, 1991.

[24]Meirovitch, L., *Computational Methods in Structural Dynamics*, Sijthoff and Noordhoff, The Netherlands, 1980.

Optimal Control of Second Order Dynamical Systems

John L. Junkins and John E. Hurtado
Texas A&M University

AIAA Structures, Structural Dynamics, and
Materials Conference

April 1995
New Orleans, LA

OPTIMAL CONTROL OF NATURAL SECOND ORDER SYSTEMS

Johnny E. Hurtado[*] and John L. Junkins[†]

Texas A&M University, College Station, TX 77843

Abstract

This modest note presents the necessary conditions related to the optimal control of natural second order systems. The development includes systems subject to holonomic constraints. For natural systems, the second order form of the governing differential equations are augmented to the performance index, and as a consequence, the resulting adjoint system defining the necessary conditions of optimality is also second order in form. For natural systems subject to holonomic constraints, the second order differential equations of motion and the algebraic equations of constraint are augmented to the performance index. Following the usual methods, we find that, like the original dynamical system, the resulting adjoint system is also holonomically constrained. We propose an augmented-Lagrangian method to numerically solve the coupled set of differential-algebraic equations within the solution of the two-point boundary value problem.

Introduction

A significant class of problems in analytical mechanics fall under the heading of *natural* systems.[1,2] These include robotic and satellite systems wherein the joint angles between substructures may undergo large rotations. Many times, the governing differential equations of these systems are subject to holonomic constraints. That is, the equations of motion are formulated such that the generalized coordinates are not independent, but rather they are related thru algebraic equations.

Traditionally, vis-a-vis optimal control formulations, natural systems are treated no differently: the equations of motion are cast into first order form,

---

*Graduate Student, Department of Aerospace Engineering, Student Member AIAA.

†George J. Eppright Chair Professor, Department of Aerospace Engineering, Fellow AIAA.

and following the usual variational calculus techniques, one arrives at the adjoint system of first order differential equations which must be satisfied to meet the necessary conditions of optimality.[3]

When the dynamical system is subject to holonomic constraints, the optimal control formulation often begins with manipulating the governing equations by one of three methods before the usual procedures for arriving at the necessary conditions for optimal control are applied. In the first method, the holonomic constraints are used to eliminate redundant coordinates algebraically and the equations of motion are formulated using a minimal coordinate description of the system. Because these formulations rely upon a minimal set of coordinates, the resulting system is no longer explicitly constrained. In a second method, locally equivalent to the first, the generalized coordinates undergo a judicious nonlinear coordinate transformation. In these new coordinates, the constraints are trivially satisfied leaving a subset of differential equations which are not subjected to constraint forces.[4] A third approach begins by differentiating the holonomic constraint equations; the result is arranged as a linear operation on the generalized coordinate acceleration vector. This allows the elimination of the Lagrange multipliers appearing in the differential equations of motion in favor of nonlinear functions of the generalized coordinates, velocities and controls. This approach is known as either a *range space* or *null space* formulation depending on the particular method of elimination used.[5]

All three of the above methods result in a "constraint free" form of the system differential equations of motion wherein the generalized coordinates may be considered independent. As mentioned, subsequent to these manipulations, the usual procedures for deriving expressions for the optimal control may be applied. For all but trivial examples, however, these methods lead to almost intractable governing equations.

Below, we formulate the optimal control problem for natural systems in second order form. As a consequence, because the resulting coupled differential equations are in second order form, in solving

them we may use one of the many implicit integration schemes available.[6,7] These schemes were especially designed for mechanical systems. For systems subject to holonomic constraints, we pursue a different avenue towards the optimal control than those methods outlined above. Our approach is driven by the desire to avoid nonlinear transformations of the generalized coordinates or the elimination of the Lagrange multipliers from the differential equations of motion.

Governing Equations

Natural systems are identified as those for which the kinetic energy is expressed as a quadratic function of the generalized velocities. Specifically,

$$T = \tfrac{1}{2} m_{ij}(q)\,\dot{q}_i\,\dot{q}_j.$$

Here, m_{ij} is the symmetric, positive definite mass matrix and is seen to be a function of the generalized coordinates q—we adopt the convention that repetition of an index in a term will denote a summation with respect to that index over its range. Using Lagrangian mechanics to develop the equations of motion begins with forming the system Lagrangian as the difference between the kinetic and potential energies,

$$\mathcal{L}(q,\dot{q}) = T(q,\dot{q}) - \mathcal{V}(q),$$

where the potential energy $\mathcal{V}$ is generally a nonlinear function of the generalized coordinates. Upon identifying any generalized forces which do nonconservative work, the form of Lagrange's equations become

$$\frac{d}{dt}\left(\frac{\partial \mathcal{L}}{\partial \dot{q}_k}\right) - \frac{\partial \mathcal{L}}{\partial q_k} = Q_k. \qquad (1)$$

The Q_k are nonconservative generalized forces acting on the system and they are often generated by a linear operation on a vector of control inputs via $Q_k = B_{km}\,u_m$. The matrix B_{km} is often called the control influence matrix.

Performing the implied differentiation above, the differential equations of motion are

$$m_{kj}(q)\,\ddot{q}_j + \Pi_{kij}(q)\,\dot{q}_i\,\dot{q}_j + \frac{\partial \mathcal{V}}{\partial q_k} = B_{km}\,u_m, \quad (2)$$

where the third order tensor Π_{kij} is commonly referred to as the *Christoffel operator of the first kind* and is defined as

$$\Pi_{kij} \stackrel{\text{def}}{=} \frac{1}{2}\left(\frac{\partial m_{ki}}{\partial q_j} + \frac{\partial m_{kj}}{\partial q_i} - \frac{\partial m_{ij}}{\partial q_k}\right).$$

It is convenient to denote $\bar{m}_{ij}(q)$ as elements of the inverse of the mass matrix (i.e. $\bar{m}_{ik}\,m_{kj} = \delta_{ij}$), which allows us to write the governing set of equations as

$$\ddot{q}_i + h_i(q,\dot{q}) + g_i(q) = b_{im}(q)\,u_m, \qquad (3)$$

where

$$h_i(q,\dot{q}) \stackrel{\text{def}}{=} \bar{m}_{ik}(q)\,\Pi_{klj}(q)\,\dot{q}_l\,\dot{q}_j,$$

$$g_i(q) \stackrel{\text{def}}{=} \bar{m}_{ik}(q)\,\frac{\partial \mathcal{V}}{\partial q_k}, \quad \text{and}$$

$$b_{im}(q) \stackrel{\text{def}}{=} \bar{m}_{ik}(q)\,B_{km}.$$

As mentioned earlier, in many system representations the generalized coordinates q are not independent, but rather they are related thru a set of nonlinear holonomic constraint equations given by

$$\varphi_o(q) = 0.$$

Now, because the coordinates are not independent, one must account for the constraint forces which restrict the time/space evolution of the system. This is done by representing the constraint forces by

$$\frac{\partial \varphi_o}{\partial q_k}\,\lambda_o,$$

where λ_o are elements of a time varying vector of Lagrange multipliers which, when determined correctly, enforce the holonomic constraints of the system. Physically, the normal component of the constraint force is proportional to the gradient of the constraint function. These constraint forces are added to the right-hand side of eq.(1), and so, in the present context the constrained dynamical system is described by the set of equations

$$\frac{d}{dt}\left(\frac{\partial \mathcal{L}}{\partial \dot{q}_k}\right) - \frac{\partial \mathcal{L}}{\partial q_k} = Q_k + \frac{\partial \varphi_o}{\partial q_k}\,\lambda_o \qquad (4)$$

$$\text{subject to} \quad \varphi_o(q) = 0, \qquad (5)$$

or, performing the implied differentiation,

$$\ddot{q}_i + h_i(q,\dot{q}) + g_i(q) = $$
$$b_{im}(q)\,u_m + d_{io}(q)\,\lambda_o \qquad (6)$$

$$\text{subject to} \quad \varphi_o(q) = 0, \qquad (7)$$

where

$$d_{io}(q) \stackrel{\text{def}}{=} \bar{m}_{ik}(q)\,\frac{\partial \varphi_o}{\partial q_k}.$$

We emphasize that this set of differential-algebraic equations given by eqs.(4) and (5) must be solved

simultaneously for the unknown vectors $q(t)$ and $\lambda(t)$.

We next pose the optimal control statement for the natural systems described above.

Necessary Conditions for Optimal Control

The necessary conditions for optimal control are almost universally derived with the equations of motion in first order form. Below, we use the techniques of variational calculus to obtain the necessary conditions for the natural second order systems introduced in the previous section. We begin with the system governed by eq.(3) and then focus on the holonomically constrained system given by eqs.(6) and (7).

The problem statement is the minimization of a given performance index subject to the dynamical equation constraints. We consider a performance index which contains terms that are quadratic in the generalized positions, generalized velocities, controls and control rates: including the control rate term allows one to specify the value of control at the beginning and end of the manuever. Appending the dynamical equations to the performance index results in

$$
\mathcal{J} = \int_{t_0}^{t_f} \left[\tfrac{1}{2} Q_{ij}^p q_i q_j + \tfrac{1}{2} Q_{ij}^v \dot{q}_i \dot{q}_j \right.
$$
$$
+ \tfrac{1}{2} R_{lm} u_l u_m + \tfrac{1}{2} P_{lm} \dot{u}_l \dot{u}_m + v_i \left(-\ddot{q}_i \right.
$$
$$
\left. - h_i(q, \dot{q}) - g_i(q) + b_{im}(q) u_m \right) \Big] dt,
$$

where v_i is a time-varying vector of Lagrange multipliers, while Q_{ij}^p, Q_{ij}^v, R_{lm} and P_{lm} represent elements of the weight matrices which are defined in the usual way. Limiting ourselves to smooth, unbounded controls while taking the first variation yields

$$
\delta \mathcal{J} = \left[Q_{ij}^v \dot{q}_i + \dot{v}_j - v_i \frac{\partial h_i}{\partial \dot{q}_j} \right] \delta q_j \Big|_0^{t_f} - v_i \delta \dot{q}_i \Big|_0^{t_f}
$$
$$
+ P_{lm} \dot{u}_l \delta u_m \Big|_0^{t_f} + \int_{t_0}^{t_f} \left[(Q_{ij}^p q_i - Q_{ij}^v \ddot{q}_i \right.
$$
$$
- \ddot{v}_j + \frac{d}{dt} \left(v_i \frac{\partial h_i}{\partial \dot{q}_j} \right) - v_i \frac{\partial h_i}{\partial q_j} - v_i \frac{\partial g_i}{\partial q_j}
$$
$$
+ v_i \frac{\partial b_{im}}{\partial q_j} u_m) \delta q_j + (-P_{lm} \ddot{u}_l + R_{lm} u_l
$$
$$
+ v_i b_{im}) \delta u_m + (-\ddot{q}_i - h_i(q, \dot{q}) - g_i(q)
$$
$$
+ b_{im}(q) u_m) \delta v_i \right] dt = 0, \tag{8}
$$

where we have performed an integration by parts to eliminate $\delta \dot{q}_j$, $\delta \ddot{q}_i$, and $\delta \dot{u}_m$ from the integrand. Investigating eq.(8), we first comment that the second

order state equations must be satisfied. Next, because the variations of q_j are independent and arbitrary throughout the integration interval while their respective multipliers are continuous, these multipliers must be indentically zero.[8] Similar reasoning applies in regarding the variations of u_m. These arguments provide us with the second order costate (or adjoint) differential equations, and a differential optimality condition.

Original system:

$$
\ddot{q}_i + h_i(q, \dot{q}) + g_i(q) = b_{il}(q) u_l . \tag{9}
$$

Adjoint system:

$$
\ddot{v}_j - \frac{d}{dt} \left(v_i \frac{\partial h_i}{\partial \dot{q}_j} \right) + v_i \left(\frac{\partial h_i}{\partial q_j} + \frac{\partial g_i}{\partial q_j} \right.
$$
$$
\left. - \frac{\partial b_{im}}{\partial q_j} u_m \right) = Q_{ij}^p q_i - Q_{ij}^v \ddot{q}_i . \tag{10}
$$

Optimality condition:

$$
P_{lm} \ddot{u}_l + R_{lm} u_l = v_i b_{im} \tag{11}
$$

All that is remaining is the satisfaction of the boundary terms (transversality conditions) which require

$$
\left[Q_{ij}^v \dot{q}_i + \dot{v}_j - v_i \frac{\partial h_i}{\partial \dot{q}_j} \right] \delta q_j \Big|_0^{t_f} = 0; \qquad v_i \delta \dot{q}_i \Big|_0^{t_f} = 0
$$

$$
\text{and} \quad P_{lm} \dot{u}_l \delta u_m \Big|_0^{t_f} = 0. \tag{12a-c}
$$

In considering natural systems subject to holonomic constraints, we closely follow the developments above. We begin by appending eqs.(6) and (7) to the performance index which results in

$$
\mathcal{J} = \int_{t_0}^{t_f} \left[\tfrac{1}{2} Q_{ij}^p q_i q_j + \tfrac{1}{2} Q_{ij}^v \dot{q}_i \dot{q}_j \right.
$$
$$
+ \tfrac{1}{2} R_{lm} u_l u_m + \tfrac{1}{2} P_{lm} \dot{u}_l \dot{u}_m
$$
$$
+ v_i \left(-\ddot{q}_i - h_i(q, \dot{q}) - g_i(q) + b_{im}(q) u_m \right.
$$
$$
\left. + d_{io}(q) \lambda_o) + \gamma_o \varphi_o(q) \right] dt.
$$

Here v_i and γ_o are time-varying vectors of Lagrange multipliers. Taking the first variation of this equation while performing an integration by parts to eliminate $\delta \dot{q}_j$, $\delta \ddot{q}_i$, and $\delta \dot{u}_m$ from the integrand leads to

$$
0 = \left[Q_{ij}^v \dot{q}_i + \dot{v}_j - v_i \frac{\partial h_i}{\partial \dot{q}_j} \right] \delta q_j \Big|_{t_0}^{t_f} - v_i \delta \dot{q}_i \Big|_{t_0}^{t_f}
$$

$$
+ P_{lm} \dot{u}_l \delta u_m \Big|_0^{t_f}
$$

$$+ \int_{t_0}^{t_f} [\,(\, Q_{ij}^p \, q_i - Q_{ij}^v \, \ddot{q}_i - \ddot{v}_j$$

$$+ \frac{d}{dt}(v_i \frac{\partial h_i}{\partial \dot{q}_j}) - v_i \frac{\partial h_i}{\partial q_j} - v_i \frac{\partial g_i}{\partial q_j}$$

$$+ v_i \frac{\partial b_{im}}{\partial q_j} u_m + v_i \frac{\partial d_{io}}{\partial q_j} \lambda_o + \gamma_o \frac{\partial \varphi_o}{\partial q_j} \,) \, \delta q_j$$

$$+ v_i \, d_{io}(q) \, \delta \lambda_o \,] \, dt$$

$$+ \int_{t_0}^{t_f} [\,(\, P_{lm} \, \ddot{u}_l + R_{lm} \, u_l + v_i \, b_{im} \,) \, \delta u_m \, dt.$$

Note that in the above statement we have already imposed the requirement that the differential-algebraic equations which govern the original dynamical system must be satisfied throughout the integration interval. Now, arguments similar to those mentioned in the previous discussion lead us to a set of second order costate (adjoint) differential-algebraic equations and a differential optimality condition.

Original system:

$$\ddot{q}_i + h_i(q, \dot{q}) + g_i(q) = $$
$$b_{im}(q) \, u_m + d_{io}(q) \, \lambda_o \qquad (13a)$$

$$\text{subject to} \quad \varphi_o(q) = 0. \qquad (13b)$$

Adjoint system:

$$\ddot{v}_j - \frac{d}{dt}(v_i \frac{\partial h_i}{\partial \dot{q}_j}) + v_i \,(\, \frac{\partial h_i}{\partial q_j} + \frac{\partial g_i}{\partial q_j}$$

$$- \frac{\partial b_{im}}{\partial q_j} u_m - \frac{\partial d_{io}}{\partial q_j} \lambda_o \,)$$

$$= Q_{ij}^p \, q_i - Q_{ij}^v \, \ddot{q}_i + \frac{\partial \varphi_o}{\partial q_j} \gamma_o \qquad (14a)$$

$$\text{subject to} \quad v_i \, d_{io}(q) = 0. \qquad (14b)$$

Optimality condition:

$$P_{lm} \, \ddot{u}_l + R_{lm} \, u_l = v_i \, b_{im} \qquad (15)$$

The corresponding boundary terms are identical to those given earlier except that now, like the differential equations, these boundary conditions must be satisfied subject to eqs.(13b) and (14b).

Numerical Solution of the TPBVP

The set of equations defining the necessary conditions for optimal control represent a two-point boundary value problem. In most nonlinear problems of practical interest, this system of equations must be solved numerically. While there are many different numerical methods which may be applied[9] (the method of particular solutions, polynomial approximation methods, quasi-linearization methods, etc.), we use the shooting method in the examples that follow. But rather than focus on the numerical technique used to attack the two-point boundary value problem, we look to the necessary conditions in their second order form to see if any advantages are offered within the solution of the two-point boundary value problem.

Beginning with a natural system whose motion is governed by eq.(3), we recall that the necessary conditions for optimal control are given by eqs.(9) thru (11) and the boundary conditions eq.(12). One possible advantage to the second order development may be that because the differential equations are in second order form, one may take advantage of some particular implicit integration schemes.[6,7] These schemes were especially designed with natural systems in mind.

Concerning a natural system subject to holonomic constraints, we recall that the necessary conditions for optimal control are given by eqs.(13) thru (15) and the boundary conditions—recall that the equations came about by electing not to perform a nonlinear transformation of the generalized coordinates or eliminate the Lagrange multipliers which enforce the constraint forces. These equations are indentified as differential-algebraic equations and their solution requires careful attention. While numerical solutions strategies for differential-algebraic equations have been the focus of research for some years, a penalty solution method has recently shown considerable promise.

Historically, the primary use of augmented Lagrangian methods has been in obtaining solutions to time independent problems that are subject to constraints.[10] Recently however, these methods have been extended to address the differential-algebraic equations which arise in multi-body dynamic formulations.[11,12] Moreover, analysis for very general nonlinear dynamical systems has been conducted which not only proves convergence, but establishes bounds on the rate of convergence of the method.[13]

The general strategy of augmented Lagrangian methods is iterative and involves approximating the constraint forces and the Lagrange multipliers which enforce them. The approximate multipliers are updated based upon a measure of constraint violation. When applied to constrained dynamical systems, the solution process can be viewed as quasi-static

in nature. Specifically, an iteration process is triggered at each time step wherein the postions and velocities are treated as constant while the accelerations are considered a static quantity. As applied to our coupled state/adjoint differential-algebraic equations our strategy involves investigating the dynamics of the state and adjoint systems separately: the key lies in looking at the dynamics of the original system first. The iteration process is outlined below and closely parallels that given in Ref. (13).

Before we continue, we remark that with suitable defintions, we may express the state/adjoint differential-algebraic equation as

$$\ddot{q}_i = \eta_i\,(q,\dot{q},u) + d_{io}\,\lambda_o$$
$$\text{subject to} \quad \varphi_o(q) = 0,$$

$$\ddot{v}_i = \rho_i\,(q,\dot{q},v,\dot{v},u,\lambda) + \frac{\partial \varphi_o}{\partial q_i}\,\gamma_o$$
$$\text{subject to} \quad v_j\,d_{jo}(q) = 0.$$

Now then, the iterative scheme triggered at each time step is based upon the following approximation to the original system:

$$\ddot{q}_i^n = \eta_i\,(q,\dot{q},v) + d_{io}\,\lambda_o^n$$
$$\quad - \frac{1}{\epsilon}\,d_{io}\,[\,\frac{\partial \varphi_o}{\partial q_j}\,\ddot{q}_j^n + \frac{d}{dt}(\frac{\partial \varphi_o}{\partial q_j})\,\dot{q}_j$$
$$\quad + 2\zeta\omega\dot{\varphi}_o + \omega^2\varphi_o\,], \quad\quad (16)$$

$$\lambda_o^{n+1} = \lambda_o^n$$
$$\quad - \frac{1}{\epsilon}\,[\,\frac{\partial \varphi_o}{\partial q_j}\,\ddot{q}_j^n + \frac{d}{dt}(\frac{\partial \varphi_o}{\partial q_j})\,\dot{q}_j$$
$$\quad + 2\zeta\omega\dot{\varphi}_o + \omega^2\varphi_o\,], \quad\quad (17)$$
$$\text{with} \quad \lambda_o^0 = 0.$$

In the above, $\ddot{q}_i^n$ and λ_o^n represent current approximations to the true accelerations and Lagrange multipliers respectively, while the bracketed term represents a measure of constraint violation. Further, n is the iteration number, $\epsilon > 0$ is a small penalty factor, and $\zeta,\omega \geq 0$ represent a damping factor and frequency associated with the constraint violation.

The iterative procedure at time t begins by solving eq.(16) for the approximate acceleration $\ddot{q}_i^n$. This is then substituted into eq.(17) where an update to the approximate Lagrange multipliers λ_o^{n+1} is obtained. This is then substituted back into eq.(16) and the iterative process continues until convergence is recognized. For the sake of brevity, we only mention here that, convergence of the method may be shown ($\ddot{q}_j^n \to \ddot{q}_j$ and $\lambda_o^n \to \lambda_o$). That is, the

approximate accelerations and Lagrange multipliers approach the true values in the limit. The proof relies on the fact that the mass matrix is positive definite, $\epsilon > 0$, and by requiring that the constraint jacobian maintain full rank.

Now then, having converged to the true accelerations and Lagrange multipliers of the original system, we next introduce an approximation to the adjoint system as was done for the original system.

$$\ddot{v}_i^n = \rho_i\,(q,\dot{q},v,\dot{v},\lambda) + \frac{\partial \varphi_o}{\partial q_i}\,\gamma_o^n$$
$$\quad - \frac{1}{\epsilon}\,\frac{\partial \varphi_o}{\partial q_i}\,[\,d_{jo}\,\ddot{v}_j^n$$
$$\quad + 2\zeta\omega\dot{\psi}_o + \omega^2\psi_o\,], \quad\quad (18)$$

$$\gamma_o^{n+1} = \gamma_o^n$$
$$\quad - \frac{1}{\epsilon}\,[\,d_{jo}\,\ddot{v}_j^n$$
$$\quad + 2\zeta\omega\dot{\psi}_o + \omega^2\psi_o\,], \quad\quad (19)$$
$$\text{with} \quad \gamma_o^0 = 0.$$

Here, $\ddot{v}_i^n$ and γ_o^n represent current approximations to the true accelerations and Lagrange multipliers of the adjoint system, respectively, while the bracketed term represents a measure of constraint violation. Again, n is the iteration number, $\epsilon > 0$ is a small penalty factor, and $\zeta,\omega \geq 0$ represent a damping factor and frequency associated with the constraint violation.

The iterative procedure at time t is performed on eqs.(18) and (19) just like it was for the original system. This iterative scheme is also convergent ($\ddot{v}_j^n \to \ddot{v}_j$ and $\gamma_o^n \to \gamma_o$): that is the approximate adjoint accelerations and associated Lagrange multipliers approach their true values in the limit.

Thus, careful application of the augmented Lagrangian method to the numerical solution of the coupled differential-algebraic equations, which define the necessary conditions to optimal control, is seen to be a suitable and attractive solution process.

Illustrative Examples

We now focus on illustrative examples. The previous section outlined numerical techniques which may be employed within the solution process of a chosen numerical method to solving the two-point boundary value problem. For all the examples below, we use a shooting method of solution. The results are obtained through using the codes DNEQNF available in the IMSL[14] library.

The first example is a two-link rigid manipulator shown in Fig. 1. The system properties are listed in Table 1. In the simulation, we slew both links through angles of 90° in a prescribed time. We enforce that the controls begin and end at zero. Results are shown Figs. 1(a-c).

The second example, shown in Figure 2 represents a free floating satellite. Table 2 contains the system properties. A similar system was presented in Ref. 15. The system begins in a folded up fashion and the optimal control is found to rotate the main body through 90° while extending the arms in the outreached postion of 90° in a prescribed final time. In Ref. 15, the relative angles between the bodies are chosen as the generalized coordinates. This description results in the main body angle α being an ignorable coordinate (a statement of the conservation of angular momentum for the system). The equations of motion are put into a normal form via a feedback transformation, and pseudo control functions are sought rather than the acuator control torques. Here, we select the absolute angles, (as measured from a reference) as the generalized coordinates. In this description, α is no longer an ignorable coordinate. We do use a simple stabilization procedure[16] to acurately enforce the rigorous integral of motion (angular momentum) while numerically integrating the system equations. Results are shown in Figs. 2(a-d).

The last example represents a holonomically constrained system. A two-link rigid manipulator system is constrained to remain in contact with a surface (cf. Fig. 3). The constraint function for this example is

$$\varphi = l_1 \cos \theta_1 + l_2 \cos \theta_2 - L = 0.$$

The system properties are listed in Table 3. The end effector is moved a distance along the surface in a prescribed time. The augmented Lagrangian method presented earlier is used to enforce the constraint and the results are shown in Figs. 3(a-d).

Conclusions

We have investigated the necessary conditions related to the optimal control of natural second order systems. These systems represent a significant class of problems in analytical mechanics; most notably, robotic and satellite systems wherein the joint angles between substructures may undergo large rotations. We have presented a new approach to optimal control of natural systems subject to holonomic constraints. In this approach, the differential-algebraic equations are augmented to a performance index and variational calculus techniques are used to obtain the necessary conditions. Like the original dynamical system, the resulting adjoint system is also constrained. A careful application of an augmented Lagrangian method is proposed to enforce the constraints relationships of the original and adjoint systems during the numerical solution of the two-point boundary value problem. Also, the differential equations, as presented, are readily suitable to numerical integration by implicit integration schemes recently developed.

References

[1] Junkins, J.L., Kim, Y., *Introduction to Dynamics and Control of Flexible Structures*, AIAA, Inc., Washington, DC, 1993.

[2] Meirovitch, L., *Methods of Analytical Dynamics*, McGraw-Hill, New York, NY, 1970.

[3] Bryson, A.E., Ho, Y-C., *Applied Optimal Control*, Hemisphere Publishing Corporation, Washington, DC, 1975.

[4] Krishnan, H., and McClamroch, H.N., "On Control Systems Described by a Class of Linear Differential-Algebraic Equations: State Realizations and Linear Quadratic Optimal Control," *Proceedings of Automatic Control Conference*, San Diego, CA, 1990, pp.818-823.

[5] Kurdila, A.J., and Kamat, M.P., "Concurrent Multiprocessing Methods for Calculating Null Space and Range Space Bases for Multi-body Simulation," *AIAA Journal*, vol.28, No.7, 1990.

[6] Hecht, N.K., Browder, A.M., and Junkins, J.L., "Extremals of Second Order Dynamical Systems: An Implicit Integration Process with Energy Rate Matching" *Proceedings of the Eighth VPI&SU Symposium on Dynamics and Control of Large Structures*, Virginia Polytechnic Institution and State University, Blacksburg, VA, May 1991.

[7] Dean, E.J., Glowinski R., et. al., "On the Discretization of Some Second Order in Time Differential Equations: Applications to Nonlinear Wave Problems," Department of Mathematics, University of Houstion, Houston, TX, February, 1990.

[8] Luenberger, D.G., *Optimization by Vector Space Methods*, John Wiley & Sons, Inc., New York, NY, 1969.

[9] Junkins, J.L., and Turner, J.D., *Optimal Spacecraft Rotational Maneuvers*, Studies in Astronautics, vol.3, Elsevier Scientific Publishing Company, New York, NY, 1986.

[10] Glowinski, R., and Le Tallec, P., *Augmented Lagrangian and Operator-Splitting Methods in Nonlinear Mechanics*, Studies in Applied mathematics, Society for Industrial and Applied Mathematics, Philadelphia, PA, 1989.

[11] Bayo, E., *et al*, "A Modified Lagrangian Formulation for the Dynamic Analysis of Constrained Mechanical Systems," *Computer Methods in Applied Mechanics and Engineering*, vol.71, 1988, pp.183-195.
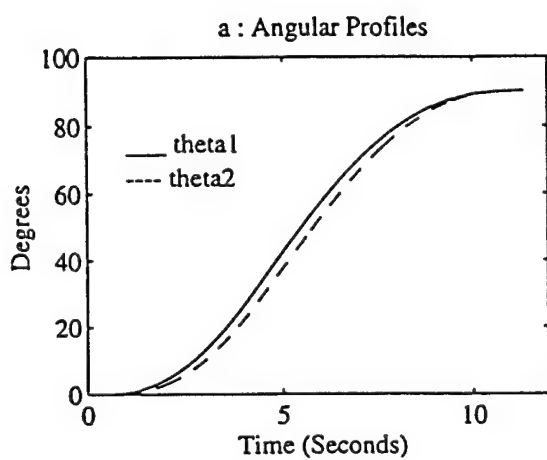
[12] Bayo, E., and Avello, A., "Singularity-Free Augmented Lagrangian Algorithms for Constrained Multibody Dynamics," preprint, to be published in *Nonlinear Dynamics*.

[13] Menon, R.G., *Concurrent Simulation and Constraint Stabilization for Flexible Multibody Systems*, Ph.D. Dissertation, Texas A&M Uneriversity, December 1992.

[14] "IMSL Math/Library," Edition 1.1, IMSL Inc., Houston, TX, Dec. 1989.

[15] Reyhanoglu, M., and McClamroch, N.H., "Planar Reorientation Maneuvers of Space Multibody Systems Using Internal Controls," *Journal of Guidance, Control, and Dynamics*, Vol. 15, No. 6, 1992, pp. 1475-1480.

[16] Baumgarte, J., "Stabilization of Constraints and Integrals of Motion in Dynamical Systems," *Computer Methods in Applied Mechanics and Engineering*, Vol. 1, 1972, pp. 1-16.
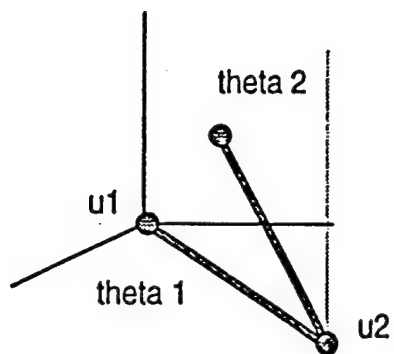
Figure 1

Table 1. System parameters

Link No.	1	2
length, m	1	1
mass, kg	12	12
I, $kg - m^2$	1	1

a : Angular Profiles

b : Angular Velocity Profiles

c : Control Profiles
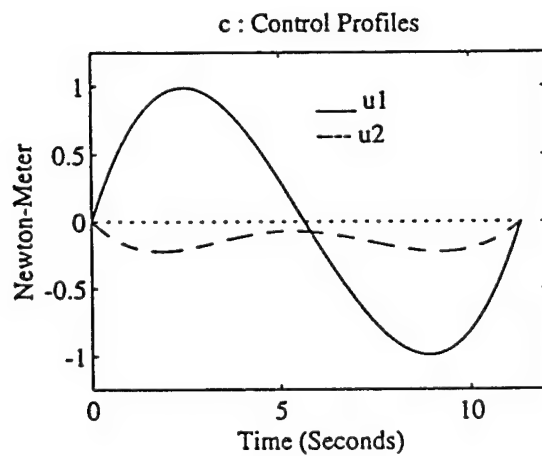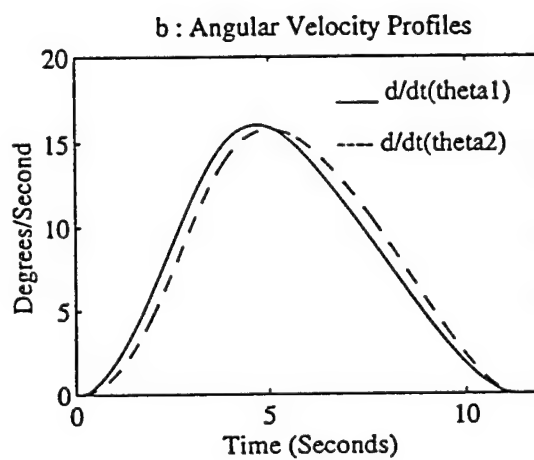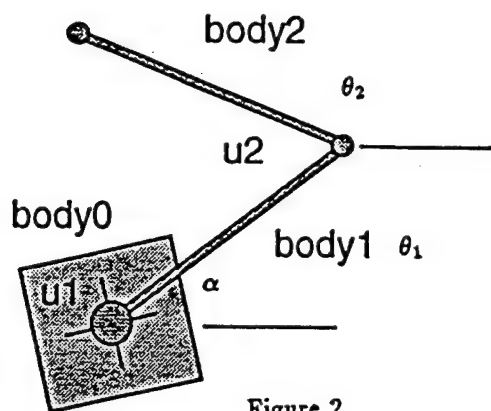
Figure 2

Table 2. System parameters

Body No.	0	1	2
length, m	—	1	1
mass, kg	—	12	12
I, kg – m²	10	1	1

a : Attitude Profile

b : Angular Profiles

c : Control Profiles

d : Angular Momentum History
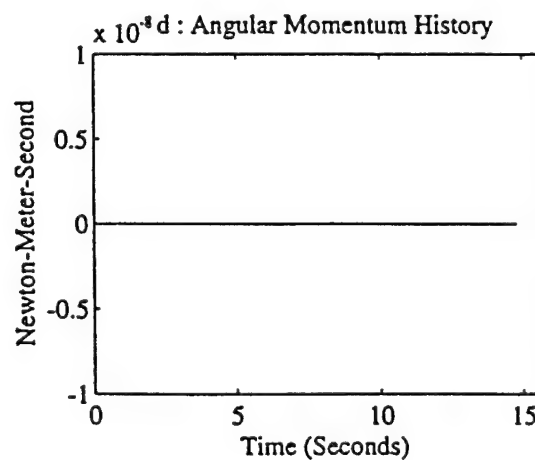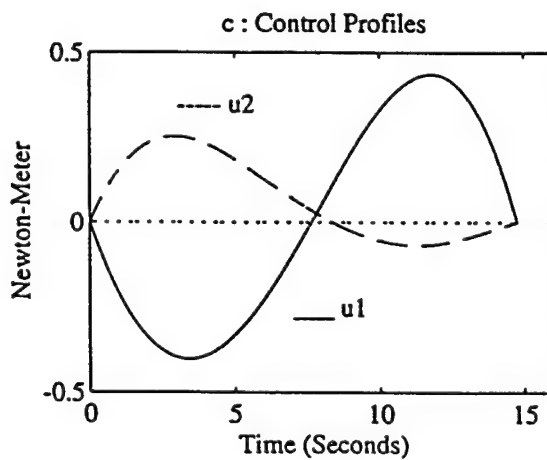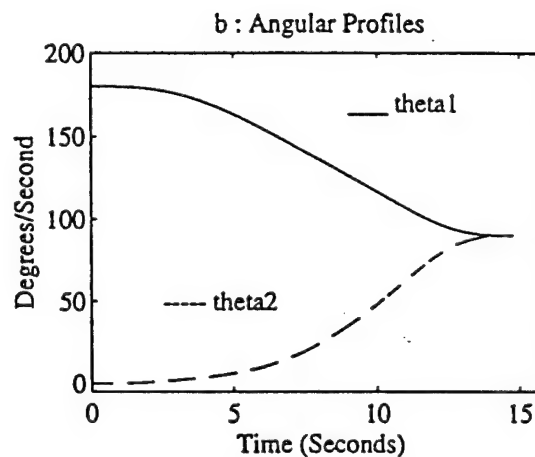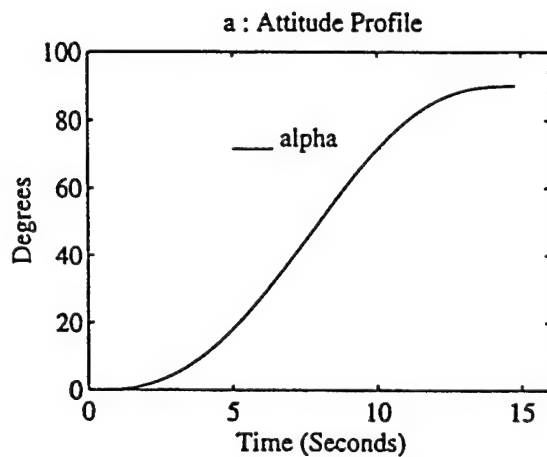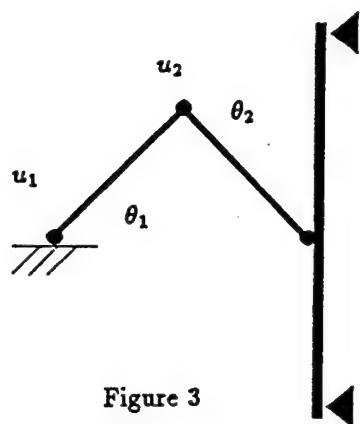
Figure 3

Table 3. System parameters

Link No.	1	2
length, m	1	1
mass, kg	12	12
I, kg $-$ m^2	1	1

a : Angular Profile

b : Angular Profile

c : Control Profiles

d : Constraint Violation
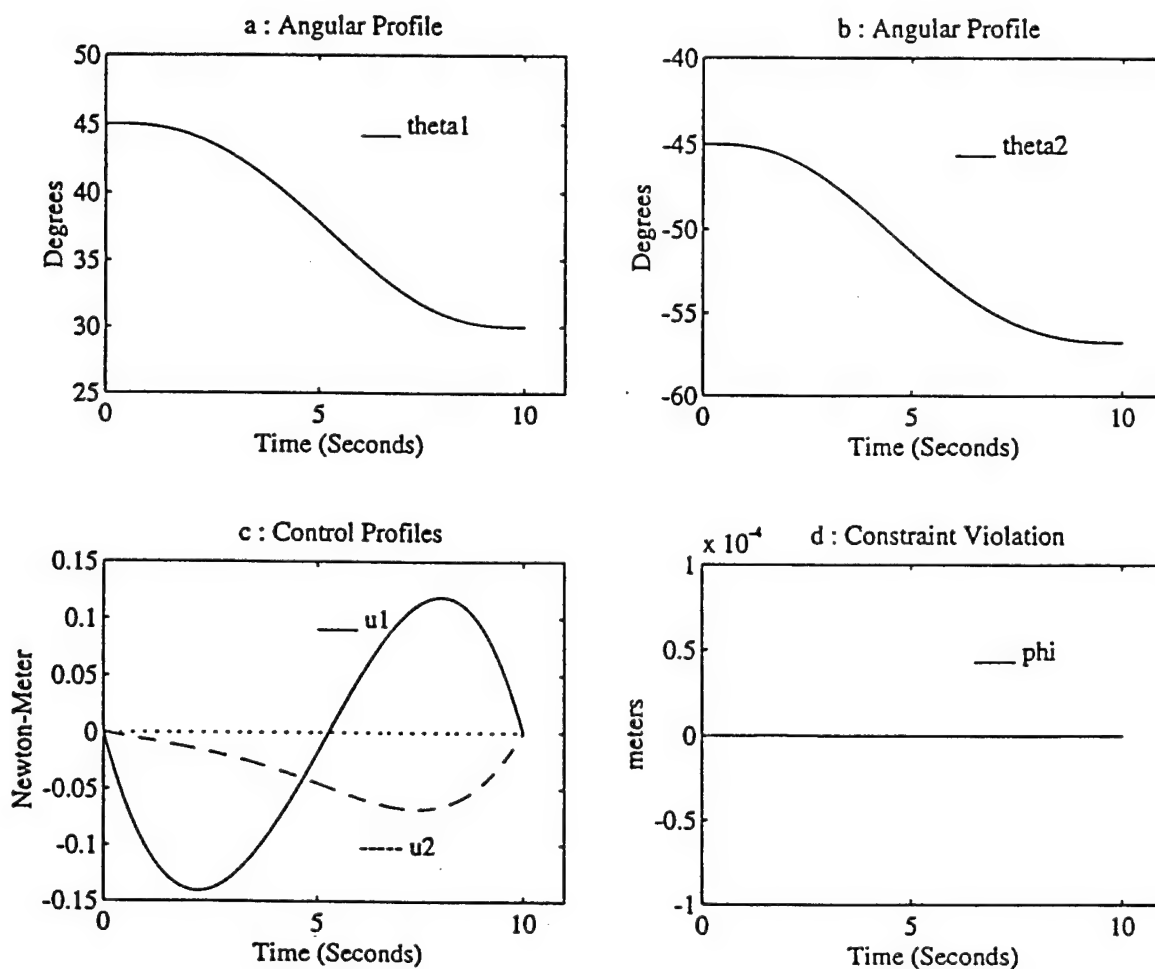
Chapter 3

Stability and Control of Nonlinear Mechanical Systems

John L. Junkins

Texas A&M University
College Station, Texas USA
77843-3141

and

Youdan Kim

Seoul National University
Seoul, Korea 151-742

Abstract—We present some elegant concepts from stability theory, and consider their applicability to the problem of designing control laws for many degree of freedom nonlinear dynamical systems. While the spirit of our presentation is classical, we include some novel stability results and methodology for designing globally stable control laws for nonlinear dynamical systems. The Lyapunov approach is attractive because it provides the most broadly applicable approach to stability analysis and guaranteed stable controller design for nonlinear, time varying, and distributed parameter systems. Especially significant is the fact that the Lyapunov approach leads to a unified stability and control perspective for both linear and nonlinear systems, as well as systems described by ordinary, partial, and hybrid differential equations. The first half of this chapter is an efficient summary of the main features of Lyapunov stability theory; however, a few examples are considered to help illustrate this material. The second half of the chapter is addressed to studies wherein we formulate stabilizing feedback control laws for multibody distributed parameter systems undergoing large, generally nonlinear motions. Analytical, numerical, and experimental results are discussed.

108

3.1 BASIC DEFINITIONS

Consider a continuous, finite-dimensional dynamical system which can be described by a first-order nonlinear vector differential equation of the form

$$\dot{x} = f(x, t), \qquad x \in R^n \tag{3.1}$$

where $x(t)$ is the state vector at time t, and the dot denotes time differentiation.

Definition 3.1: Equilibrium State

A vector $x_e \in R^n$ is said to be an *equilibrium state* of the system described by Eq. (3.1) at time t_0 if

$$f(x_e, t) = 0 \qquad \forall\, t \geq t_0 \tag{3.2}$$

If x_e is an equilibrium state of Eq. (3.1) at time t_0, then x_e is also an equilibrium state of Eq. (3.1) at all times $t_1 \geq t_0$. In other words, a motion initiating exactly at x_e at some time, remains there for all time.

Definition 3.2: Stability of an Equilibrium State

The equilibrium state x_e, or the equilibrium solution $x(t) = x_e$, is said to be *stable*, if for any given t_0 and positive ϵ, there exists a positive $\delta(\epsilon, t_0)$ such that *every* time varying trajectory (or solution) $x(t)$ initiating (time t_0) at a point x_0 which lies within in a δ-neighborhood of x_e $\{\|x_0 - x_e\| < \delta, \quad x_0 \equiv x(t_0)\}$ remains for all time within an ϵ-neighborhood of x_e $\{\|x(t) - x_e\| < \epsilon \quad \forall\, t \geq t_0\}$. The equilibrium state is said to be *unstable* if it is not stable. ∎

Definition 3.3: Asymptotic Stability of an Equilibrium State

The equilibrium state x_e is said to be *asymptotically stable*, if

(a) it is stable (Definition 3.2), and if in addition

(b) for any t_0, there exist a $\delta_1(t_0)$, such that

$$\|x_0 - x_e\| < \delta_1 \quad \text{implies that} \quad \lim_{t \to \infty} x(t) \to x_e \tag{3.3}$$

∎

If δ and δ_1 are not functions of t_0, then the equilibrium state is said to be *uniformly stable* and *uniformly asymptotically stable*, respectively. Definitions 3.2 and 3.3 constitute the two basic definitions of stability of an equilibrium state (a fixed point in the state space) for an unforced continuous time system. More generally, we need to consider the stability of a *trajectory* or a *motion*. Qualitatively, *stability of a trajectory* is concerned with whether or not a perturbed motion remains near the unperturbed trajectory, or diverges from it. Stability of a motion is of

central interest in many practical feedback control situations whereby a system is designed to execute a large nominal motion, and control inputs must be developed not only to generate the nominal motion, but also closed loop feedback is required to stabilize neighboring motions, with respect to the nominal motion, so that the actual system will behave in a near-nominal fashion.

Definition 3.4: Stability of a Motion

The *motion* $x(t)$ is said to be stable if, for all initial times t_0 and prescribed positive ϵ, there exists a positive $\delta(\epsilon, t_0)$, such that

$$\|x(t) - \bar{x}(t)\| < \epsilon \quad \forall \, t \geq t_0 \quad \text{if} \quad \|x_0 - \bar{x}_0\| < \delta$$

where $x(t)$ and $\bar{x}(t)$ are neighboring trajectories with the given initial conditions x_0 and $\bar{x}_0$, respectively, at time t_0.

∎

This *bounded motion stability property* is sometimes referred to as "path stability." Qualitatively, path stability means that "if the perturbed initial state $\bar{x}(t_0)$ is near $x(t_0)$, then the ensuing perturbed trajectory $\bar{x}(t)$ will remain near $x(t)$ for all time t."

Definition 3.5: Asymptotic Stability of a Motion

The motion $x(t)$ is said to be *asymptotically stable* if

(a) it is stable (Definition 3.4), and if in addition

(b) for any t_0, there exist a positive $\delta_1(t_0)$, such that

$$\|x_0 - \bar{x}_0\| < \delta_1 \quad \text{implies that} \quad \lim_{t \to \infty} \|x(t) - \bar{x}(t)\| = 0 \qquad (3.4)$$

Note that $\bar{x}(t)$ is *any* member of the set of neighboring (perturbed) trajectories satisfying Eq. (3.4), and *all* members of this set asymptotically approach $x(t)$.

∎

The above definitions are not directly concerned with the *global* properties of systems, but of the *local* motion in a finite local neighborhood of an equilibrium state or a motion of the system of differenital equations. If a system has a globally asymptotically stable equilibrium state, then it is obviously the *only* equilibrium state, and every motion converges to that unique equilibrium. An analogous global stability property can be defined for the stability of a motion.

The simplest class of Lyapunov stability analysis methods arises in the context of systems described by linear unforced differential equations. We summarize some of the central ideas and results below.

Consider the linear system

$$\dot{x}(t) = A(t)x(t)$$

which obviously has an equilibrium state at the origin. This linear system can be classified as stable, asymptotically stable, or unstable, depending on the stability of the origin [Vidyasagar 1978], [Willems 1970].

Now, we introduce two definitions associated with the concept of positive definite functions, these are of central importance when applying Lyapunov stability theory.

Definition 3.6: Positive Definite Function

A singled-valued function $U(x)$, which is continuous and has continuous partial derivatives with respect to the components of the vector x, is said to be *positive definite* in some region Ω about the origin if it vanishes at the origin and is positive elsewhere, *i.e.*,

(i) $U(0) = 0$

(ii) $U(x) > 0$ for all nonzero $x \in \Omega$

If the positivity condition (ii) is relaxed to simply the non-negative condition $U(x) \geq 0$ for all $x \in \Omega$, then $U(x)$ is said to be *positive semidefinite*. If the inequality sign in (ii) is reversed, then the condition for a *negative definite* function is obtained. If a function is neither positive nor negative definite, then it is *indefinite*.

Definition 3.7: Positive Definite Quadratic Forms

In the analysis of linear dynamical systems, quadratic functions of the state vector arise often in the context of energy, stability and control analyses. Especially important are *symmetric quadratic forms*. The quadratic form $U(x) = x^T Q x$ said to be *positive definite* if

$$U(x) = x^T Q x > 0 \quad \text{for all nonzero } x \in \mathbb{R}^n$$

where Q is a real symmetric matrix.

Definition 3.7 is equivalent to requiring that all the eigenvalues of Q are strictly positive, such a matrix is naturally called a *positive definite matrix*.

Further discussion of these concepts is presented in [Vidyasagar 1978] and [Willems 1970].

The following example illustrates the ideas underlying the above discussion.

Example 3.1

Consider the functions:

$$U_1(x) = x_1^2 + x_2^2 + x_3^2 \quad \text{and} \quad U_2(x) = (x_1 + x_2 + x_3)^2.$$

Clearly U_1 satisfies the condition of Definition 3.7, therefore it is a positive definite function in a three-dimensional space, but U_1 is only positive semidefinite if the

underlying space has more than three dimensions. U_2 is only positive semidefinite in three space, since it is zero everywhere in the plane $x_1 + x_2 + x_3 = 0$.

■

3.2   LYAPUNOV STABILITY THEORY (LYAPUNOV'S DIRECT METHOD)

The central ideas of the Lyapunov stability theorem are now introduced. For a given general nonlinear, forced, dissipative mechanical system, it is often useful to consider a conservative idealized approximation of system without the dissipative or nonconservative external forces acting. For this idealized nonlinear system, suppose that there exists one equilibrium state x_e of the system. Also suppose that the total mechanical energy or Hamiltonian of this idealized system is a positive definite function and is an exact integral of the idealized system. For a broad class of practical applications, the total energy or Hamiltonian of an idealized conservative system is a suitable *Lyapunov function* for studying the stability of the system, including dissipative internal and external forces; for many applications, it naturally occurs, or can be arranged that the equilibrium state is the target state for the system. More generally, a candidate Lyapunov function must belong to a class of admissible 'energy' functions which have as the most fundamental property that they are zero at the equilibrium state and positive everywhere else.

Now let us assume that the system is initially perturbed to a state neighboring the equilibrium point where the energy level is positive by assumption, and we consider the time evolution of the distance to the equilibrium as measured by the energy function. Depending on the nature of the selected "energy" (Lyapunov function), the stability of the motion may be described qualitatively as follows:

(i) if the system dynamics evolve such that the initial energy of the system is not increasing with time for all starting points in a finite neighborhood, we can conclude that the equilibrium state is stable,

(ii) if the system dynamics evolve such that the energy of the system is monotonically decreasing with time for all initial conditions in the neighborhood (and thus eventually approaches zero), the equilibrium state is asymptotically stable,

(iii) if the energy of the system is increasing with time, for *any* initial condition in the neighborhood, then the equilibrium state is unstable, and

(iv) if the chosen energy measure is indefinite (*i.e.*, it is neither strictly decreasing nor increasing), then no conclusion can be drawn on the stability of the system. The following theorem, which is a rigorous statement of the above remarks, is the basic stability concept underlying Lyapunov's direct (second) method.

Theorem 3.1: Stability Theorem

The equilibrium state x_e is stable if there exists a continuously differentiable function $U(x)$ such that

(i) $U(x_e) = 0$

(ii) $U(x) > 0$ for all $x \neq x_e, x \in \Omega$

(iii) $\dot{U}(x) \leq 0$ for all $x \neq x_e, x \in \Omega$

where $\dot{U}(x)$ denotes the time derivative of the function $U(x)$, and Ω is some region containing x_e. Notice that the "energy rate" $\dot{U}(x)$ is evaluated *along a typical trajectory* $x(t)$, and the conditions (ii) and (iii) must hold along *all infinity of trajectories of the dynamical system*, which ensue from initial states in Ω.

∎

A modest perturbation of Theorem 3.1 (making the final inequality strict) results in the following theorem, which provides necessary and sufficient conditions for *asymptotic stability*.

Theorem 3.2: Asymptotic Stability Theorem

The equilibrium state x_e is asymptotically stable if there exists a continuously differentiable function U such that

(i) $U(x_e) = 0$

(ii) $U(x) > 0$ for all $x \neq x_e, x \in \Omega$

(iii) $\dot{U}(x) < 0$ for all $x \neq x_e, x \in \Omega$

∎

Both of the previous theorems relate to local stability in the vicinity of the equilibrium state. A system has *global asymptotic stability* with respect to a unique equilibrium point if the following theorem is satisfied.

Theorem 3.3: Global Asymptotic Stability Theorem

The equilibrium state x_e is globally asymptotically stable if there exists a continuously differentiable function U with the following properties:

(i) $U(x_e) = 0$

(ii) $U(x) > 0$ for all $x \neq x_e$

(iii) $\dot{U}(x) < 0$ for all $x \neq x_e$

(iv) $U(x) \longrightarrow \infty$ as $\|x\| \longrightarrow \infty$

∎

Note that the stable region Ω extends to infinity in Theorem 3.3. The reader is referred to [Vidyasagar 1978] for further discussion, including the complete proofs

of the above theorems. Observe that there is no one unique Lyapunov function for a given system; some may be better than others. This is especially important when we seek the "least conservative" stability information when, for example, we seek to determine the size of the Ω region in which we have stability. If a poor choice of $U(x)$ results in a pessimistic conclusion that the stable region Ω is much smaller than it actually is, then this is an obvious concern. It also should be noted that if a Lyapunov function cannot be found, nothing can be concluded about the stability of the system, since the Lyapunov stability theorem provides only *sufficient* conditions for stability. Therefore, the conditions required to prove stability, based upon an arbitrary choice of Lyapunov function, may be very conservative.

Unfortunately, the above classical Lyapunov theorems are not *constructive*; these stability theorems do not reveal a process to find a candidate Lyapunov function. It is often difficult to find a suitable Lyapunov function for a given nonlinear system. The physical and mathematical insights of the analyst have historically played an important role in most successful applications of this approach; however, more systematic methods have recently emerged [Oh 1991] , [Junkins 1993, 1991, 1990] for certain classes of control design problems. *In particular, when the stability analysis and the control design analysis are merged*, one is often able to exploit the additional freedom to simultaneously design control laws and select a Lyapunov function which guarantees stability of the closed-loop (controlled) system.

Example 3.2

Consider the system described by the nonlinear ordinary differential equation

$$\ddot{x}(t) - \epsilon x^2(t)\dot{x}(t) + x(t) = 0$$

The objective is to use Lyapunov analysis to investigate the stability of motion near the origin for this system.

Introducing the state variable representation of this system with the definitions $x_1 = x$, $x_2 = \dot{x}$, we write the equivalent first-order system

$$\dot{x}_1 = x_2, \quad \dot{x}_2 = -x_1 + \epsilon x_1^2 x_2$$

It is easy to see that the above "oscillator with quadratic damping" has an equilibrium state at the origin $(x_1, x_2) = (0, 0)$. Our goal is to determine if this state is stable. For this purpose, let us choose the simplest candidate Lyapunov function is $2U(x_1, x_2) = x_1^2 + x_2^2$. We note that a physical motivation for choosing this positive definite function as a candidate Lyapunov function is that it is an exact (total mechanical energy) integral of the system, for $\epsilon = 0$. Clearly, this candidate function satisfies the two most fundamental necessary conditions that $U(0, 0) = 0$ and $U(x_1, x_2) > 0$ in any neighborhood of $(0, 0)$, and we find that

$$\dot{U}(x_1, x_2) = x_1\dot{x}_1 + x_2\dot{x}_2 = x_1 x_2 + x_2(-x_1 + \epsilon x_1^2 x_2) = \epsilon x_1^2 x_2^2$$

Thus U *is a positive definite function which is strictly decreasing along all system trajectories* if $\epsilon < 0$. Therefore, by the above theorems, the origin $(0, 0)$ is a globally

stable equilibrium point for $\epsilon = 0$, is globally asymptotically stable for $\epsilon < 0$, and is globally unstable for $\epsilon > 0$. Thus Lyapunov analysis was completely successful in establishing the global stability characteristics of this system.

∎

Example 3.3

Investigate the stability of the system of nonlinear differential equations

$$\dot{x}_1 = x_1(x_1^2 + x_2^2 - 1) - x_2, \quad \dot{x}_2 = x_1 + x_2(x_1^2 + x_2^2 - 1).$$

We try the candidate Lyapunov function $2U(x_1, x_2) = x_1^2 + x_2^2$, which is an exact integral of the simplified system $\dot{x}_1 = -x_2$, $\dot{x}_2 = x_1$. This choice for U is obviously a positive definite function having its global minimun at the origin. It is also obvious by inspection, that the origin is the only equilibrium point of the nonlinear system. Investigating the energy rate, we find

$$\dot{U}(x_1, x_2) = (x_1^2 + x_2^2)(x_1^2 + x_2^2 - 1).$$

It is evident that $\dot{U}$ is negative definite over the finite circular region $\{(x_1, x_2)|\ x_1^2 + x_2^2 < 1\}$, which includes the equilibrium point at the origin. Hence, the origin $(0,0)$ is an asymptotically stable equilibrium state of this system. Note that all points within the unit circle are asymptotically attracted to the origin. However, because $\dot{U}$ is not a negative definite function over all of R^n, we cannot conclude global asymptotic stability without more information. While we are certain we have stability within the unit circle, this conclusion results from a particular choice of $U(x_1, x_2)$, and without further analysis, we cannot conclude that the stable region is not actually larger than the unit circle. However, since $\dot{U}$ is positive *everywhere* outside the unit circle, we conclude, using the following Theorem 3.4, *that we have instability for all trajectories which initiate outside the unit circle and asymptotic stability for all trajectories initiating inside the unit circle.* Thus, we are able to use the stability and instability insights simultaneously to "establish the complete story" vis-a-vis the global stability properties of this system, *since the stable and unstable regions have a mutual boundary and together the stable and unstable regions span all of state space R^2.*

∎

The following theorem is sometimes useful in avoiding a fruitless search for Lyapunov functions for systems which are inherently unstable in certain regions of state space. This theorem is also useful in obtaining *theoretical closure of the stability analysis*, in the sense that it is sometimes possible simultaneously to apply the instability theorem with the stability theorems to establish conclusively a particular system's global stability properties. In Example 3.3, for example, we concluded that our simple choice on U gave us all of the stability information (*i.e.*, the system is stable only within the unit circle).

Theorem 3.4: Instability Theorem

The equilibrium state x_e is unstable in Ω if there exists a continuously differentiable function U such that

(i) $U(x_e) = 0$ and $\dot{U}(x_e) = 0$

(ii) $\dot{U}(x) > 0$ for all $x \neq x_e$, $x \in \Omega$

(iii) and there exists points x arbitrarily close to x_e such that $U(x_e) > 0$

∎

If one can find *any* function U satisfying the above conditions, then x_e is a completely unstable equilibrium point in Ω, and the quest for Lyapunov functions can be halted. In Example 3.3, the Ω for the instability theorem is clearly the compliment of the Ω for the asymptotically stable region, and it is apparent that *the stable and unstable regions being complimentary, (together spanning all of state space) is the key to establishing global stability/instability information.*

3.3 STABILITY OF LINEAR SYSTEMS

3.3.1 Lyapunov Theorem for Linear Systems

Lyapunov's method is easily applied to test the stability of a linear system. Consider an autonomous system described by the linear vector differential equation

$$\dot{x}(t) = Ax(t) \qquad (3.5)$$

The above system is said to be stable in the sense of Lyapunov, if the solution of Eq. (3.5) tends toward zero (which is obviously the *only* equilibrium state if A is of full rank) as $t \to \infty$ for arbitrary initial condition.

Consider the case of a constant A matrix. If all eigenvalues of A are distinct, the response of system (3.5) due to initial condition x_0 can be written as

$$x(t) = \sum_{i=1}^{n} \underline{\psi}_i^T x_0 e^{\lambda_i t} \underline{\phi}_i \qquad (3.6)$$

where λ_i are the eigenvalues of A, $\underline{\phi}_i$ and $\underline{\psi}_i$ are, respectively, the right and left eigenvectors of A associated with λ_i. For the repeated eigenvalue case, the situation is more complicated (*i.e.*, we should solve for the generalized eigenvectors of A). The generalization of Eq. (3.6) for the case of generalized eigenvectors has a similar form, but is not discussed here [Chen 1984]. From Eq. (3.6), we can see by inspection that the system is asymptotically stable if and only if all the eigenvalues of A have negative real parts, *i.e.*,

$$\Re[\lambda_i(A)] < 0 \qquad (3.7)$$

Thus, we have the well known result that the stability of a linear constant-coefficient dynamical system can be completely characterized by the signs of the real parts of the eigenvalues of the system. This approach to stability analysis yields both necessary and sufficient conditions. However, calculating all the eigenvalues of the system matrix is not always desirable, especially for high-dimensioned systems. As will be evident below, other stability viewpoints lead to important insights and generalized methods, especially vis-a-vis stability analysis for time-varying, distributed-parameter, and nonlinear systems.

For the linear dynamical system of Eq. (3.5), we choose a symmetric quadratic form as a candidate Lyapunov function

$$2U(x) = x^T P x \tag{3.8}$$

where P is a positive definite, real symmetric matrix. Thus U is positive definite with it's global minimun at the origin, which is obviously an equilibrium state. Differentiating Eq. (3.8) and substituting Eq. (3.5) into the result gives

$$\dot{U}(x) = x^T(A^T P + PA)x. \tag{3.9}$$

Using the Lyapunov stability Theorem 3.2, we require $\dot{U}(x)$ to be negative definite. We can rewrite the energy rate of Eq. (3.9) as

$$\dot{U}(x) = -x^T Q x. \tag{3.10}$$

So we see that, for asymptotic stability, P and Q must be positive definite matrices which satisfy the condition

$$A^T P + PA = -Q. \tag{3.11}$$

Equation (3.11) is commonly known as the *algebraic Lyapunov equation*.

To examine the stability of a linear system via the above Lyapunov approach we can proceed as follows: "Choose Q to be any positive definite matrix for a given A, and check the eigenvalues of the resulting P which we obtain by solving Eq. (3.11), if P is positive definite (*all* positive eigenvalues), the given system is asymptotically stable, while if P has *any* negative eigenvalues, the system is unstable." One of the potential difficulties with selecting Q and solving the Lyapunov equation (which, of course, depends on the system matrix A) is the uniqueness of the resulting solution for P. The following theorem gives the necessary and sufficient conditions for the Lyapunov Eq. (3.11) to have a unique solution.

Theorem 3.5

If $\{\lambda_1, \ldots, \lambda_n\}$ are the eigenvalues of the system matrix A, then the Lyapunov equation [Eq. (3.11)] has a unique solution P if and only if

$$\lambda_i + \lambda_j^H \neq 0, \qquad i,j = 1, \ldots, n$$

where $(\ )^H$ denotes complex conjugate.   ■

The reader is referred to [Chen 1984] for a proof of the above theorem. Thus, we cannot solve the Lyapunov equation for undamped second-order systems having pairs of eigenvalues on the imaginary axis (including rigid body modes, whose eigenvalues reside at the origin of the complex plane), and so stability analysis for systems having a neutrally stable subspace cannot be completed via solution of an algebraic Lyapunov equation.

Theorem 3.6: Lyapunov Stability Theorem for Linear Systems

A linear system is asymptotically stable or, equivalently, all the eigenvalues of A have negative real parts, if and only if for any given positive definite symmetric matrix Q there exists a positive definite (symmetric) matrix P that satisfies the Lyapunov equation

$$A^T P + P A = -Q \qquad (3.12)$$

∎

The proof of this theorem is given in [Junkins 1993]. Note that the Lyapunov equation is equivalent to a set of $n(n + 1)/2$ linear equations in $n(n + 1)/2$ unknowns for an n-th order system. The Lyapunov equation can be solved by using numerical algorithms utilizing QR factorization, Schur decomposition, or spectral decomposition; however, our experience indicates that the most efficient and robust algorithms utilize the QR factorization [Junkins 1993].

Example 3.4

Consider the system matrix

$$A = \begin{bmatrix} -2 & 1 \\ -1 & 1 \end{bmatrix} .$$

The simplest choice of Q is the identity matrix or some other diagonal matrix; we take $Q = I$ for this example, and let the three distinct elements in P be denoted

$$P = \begin{bmatrix} p_1 & p_2 \\ p_2 & p_3 \end{bmatrix} .$$

Substituting this A and P into the Lyapunov equation [Eq. (3.11)] yields the following three linear algebraic equations

$$
\begin{aligned}
-4p_1 - 2p_2 &= -1 \\
p_1 - p_2 - p_3 &= 0 \\
2p_2 + 2p_3 &= -1.
\end{aligned}
$$

The solution of these three equations is straightforward; we find

$$p_1 = -\frac{1}{2}, \qquad p_2 = \frac{3}{2}, \qquad p_3 = -2 \quad \Longrightarrow \quad P = \begin{bmatrix} -1/2 & 3/2 \\ 3/2 & -2 \end{bmatrix}$$

Even though we have a unique solution, the resulting matrix P is not positive definite. Hence, we conclude that the system is unstable, and implicitly, that not all of the eigenvalues of A have negative real parts. We would have to calculate the eigenvalues to make further assessments of eigenvalue placement.

■

In the case of a linear time-varying system $\dot{x}(t) = A(t)x(t)$, the sufficient conditions for the stability of the equilibrium state can be analyzed based on the concept of matrix measure [Vidyasagar 1978], and if the system is asymptotically stable, then a quadratic Lyapunov function exists for this system. Of course, conventional eigenvalue analysis is not applicable to the time-varying case and, therefore, the more general Lyapunov approach provides one possible avenue to characterize the stability of nonautonomous systems.

3.3.2 Linear Dynamic Systems Subject to Arbitrary Disturbances

To make the Lyapunov stability analysis in this section more complete, we briefly discuss stability in the presence of disturbances. We consider the class of systems described by the matrix differential equation

$$\dot{x}(t) = Ax(t) + f(t, x(t)) \tag{3.13}$$

where the uncertainty and/or perturbations of the system are assumed representable by arbitrary nonlinear function $f(t, x(t))$ (except we require $f(t, 0) = 0$, so that the origin of the state space remains an equilibrium state for this class of model errors or disturbances). Furthermore, we assume that exact expressions for $f(t, x(t))$ are unknown and only bounds on $f(t, x(t))$ are known. The central question we address here is the following: "Given that A is asymptotically stable, and without using specific knowledge of $f(t, x(t))$, is it possible to obtain a bound on *all* $f(t, x(t))$ such that the system maintains its stability?" Put another way, can we determine some measure of how large $f(t, x(t))$ can be without destabilizing a given stable linear system? Some insights on these issues are embodied in the following theorem:

Theorem 3.7 [Patel 1980]

Suppose that the system of Eq. (3.13) is asymptotically stable for $f(t, x(t)) = 0$, then the system remains asymptotically stable for all nonzero perturbations $f(t, x(t))$ which are sufficiently small that they satisfy the following inequality

$$\frac{\|f\|}{\|x\|} \leq \frac{\min \lambda(Q)}{\max \lambda(P)} \equiv \mu_{PT} \tag{3.14}$$

where P and Q satisfies the following Lyapunov equation

$$A^T P + PA = -2Q$$

and where the otherwise arbitrary $f(t, x(t))$ vanishes at the origin $f(t, 0) = 0$.   ■

The proof of this theorem is given in [Patel 1980], [Junkins 1993]. Since P is a positive definite matrix, the maximum eigenvalue of P is same as the largest singular value of P. It has been also shown in [Patel 1980] that when the identity matrix is chosen for Q, μ_{PT} in Eq. (3.14) is a maximum and for this choice, μ_{PT} can be expressed as

$$\mu_{PT} = \frac{1}{\max \, \lambda(P)} = \frac{1}{\sigma_{\max}(P)} \, . \tag{3.15}$$

The above bound is often very conservative, since it is only a *sufficient* condition for the stability of the system, and this stringent bound is not usually *necessary*.

An important special case is for the class of perturbations having the linear structure

$$f(t, x(t)) = Ex(t) \tag{3.16}$$

Clearly this corresponds to an additive error in the A matrix (*i.e.*, $A \rightarrow A + E$). We can apply Theorem 3.7 to arrive at the desired result; we can establish that the system remains stable if E is bounded by the following *modified stability margin*:

$$\|E\| \leq \frac{\min\left[-\Re\{\lambda_i(A)\}\right]}{\mathcal{K}(\Phi)} \tag{3.17}$$

where $\mathcal{K}(\Phi)$ is the *condition number* of Φ, and Φ is the normalized eigenvector (modal) matrix of A. The condition number definition used here is the ratio of the largest and least singular values of Φ,

$$\mathcal{K}(\Phi) = \frac{\sigma_{\max}(\Phi)}{\sigma_{\min}(\Phi)}$$

As is evident in the above discussion, the stability margin is closely related to the Patel-Toda robustness margin; the "more stable" the nominal system is, the larger the bound on the allowable perturbation E becomes. However, the important ingredient evident in Eq. (3.17) is the fact that a large condition number $\mathcal{K}(\Phi)$ degrades the effective stability margin. Qualitatively, if the eigensolution is highly sensitive (large condition number), then it is easier to introduce destabilizing perturbations, and generally, the stability margin (distance of eigenvalues from the imaginary axis) should be considered simultaneously with a measure of sensitivity. The intimate connection of the Patel-Toda robustness measure (for stability of linear dynamical systems in the presence of additive perturbations) to the Bauer-Fike Theorem (for conditioning of the algebraic eigenvalue problem [Junkins 1993]) is clear.

Note that the condition number $\mathcal{K}(\Phi)$ approaches its smallest possible value of unity if Φ is *any* unitary matrix (one for which $\Phi^H \Phi = I$), and the upper bound on the condition number is infinity which occurs if Φ is *any* singular matrix. Observe that an infinity of unitary matrices exist, some of them are "closer" to Φ than others. When one has the freedom to modify A (and therefore Φ), a natural question arises: for a given class of A-modifications, how can we make Φ as nearly unitary

as possible? Of course, one way to modify the A matrix is through design of a
feedback controller, and one avenue toward designing gains in linear robust control
laws is to maximize the right-hand side of Eq. (3.17) by minimizing $\mathcal{K}(\Phi)$. It is also
of significance that choice of actuator locations considered simultaneously with the
design of control gains can often significantly reduce the condition number $\mathcal{K}(\Phi)$.
These ideas provide some of the motivation for the *robust eigenstructure algorithms*
and actuator placement optimization approaches presented in [Junkins 1993].

3.4 NONLINEAR AND TIME VARYING DYNAMICAL SYSTEMS

In this section, we present stability analysis methods for nonlinear systems. In
section 3.4.1, we consider a method known as Lyapunov's indirect (or first) method,
whereby we can determine partial stability information for nonlinear systems by
examining the behavior of locally linearized systems. In section 3.4.2, we develop an
important result which provides easy-to-test sufficient conditions to determine if we
have asymptotic stability in spite of the common situation that the energy function's
time derivative is only a negative semidefinite function of the state variables. In
addition to the classical stability analysis for which the Lyapunov methods were
developed, these ideas can be used to motivate design methods which yield control
laws for control of large maneuvers for distributed-parameter systems.

This approach is used throughout the remainder of this chapter. In section
3.5, we consider a nonlinear multibody idealization of two robots cooperatively
manipulating a payload. Both open-loop and feedback-control designs are studied,
and Lyapunov methods are used to ensure path stability of the resulting closed-loop
dynamics, using a tracking control law.

3.4.1 Local Stability of Linearized Systems

Stability analysis of linear motion arises often in practical analysis of nonlinear
systems when we are concerned with motion near an equilibrium state. The results
presented in section 3.3.1 enable us to obtain necessary and sufficient conditions
for the stability of linear systems, but also provide us a method for determining
the local stability of a nonlinear system by linearization, which is called *Lyapunov's
indirect method*.

Consider the autonomous system

$$\dot{x}(t) = f[x(t)] \quad \text{with} \quad f(x_e) = 0 \tag{3.18}$$

Let $z(t)$ be the perturbation (departure motion) from the equilibrium state as

$$x(t) = x_e + z(t) \tag{3.19}$$

Using Taylor's series expansion of $f(\cdot)$ around the equilibrium state x_e, we can write

$$f[z(t) + x_e] = f(x_e) + \left[\frac{\partial f}{\partial x}\right]_{x=x_e} z(t) + O[z(t)]^2 \tag{3.20}$$

Using Eq. (3.20) in Eq. (3.18) gives the perturbation equation

$$\dot{z}(t) = Az(t) + O[z(t)]^2 \tag{3.21}$$

where A denotes the Jacobian matrix of f evaluated at $x = x_e$, $A = \left[\frac{\partial f}{\partial x}\right]_{x=x_e}$
and so we find the linear, constant coefficient matrix differential equation

$$\dot{z}(t) = Az(t) \tag{3.22}$$

The following theorem is given here (without proof); this is the main stability result of Lyapunov's *indirect method*.

Theorem 3.8: Lyapunov's Indirect Method

If the linearized system [Eq. (3.22)] is asymptotically stable, then the original nonlinear system [Eq. (3.18)] is also asymptotically stable if the motion initiates in a sufficiently small neighborhood containing the equilibrium state.

■

The above theorem is useful since we can analyze the local stability of an equilibrium state of a given nonlinear system by examining a linear system. However, the conclusions based on linearizations are local, and therefore to study global stability, we should rely on Lyapunov's direct method. On the other hand, if one can find *all* equilibrium points and investigate their local stability, a fairly complete picture of the overall global stability characteristics can often be derived. Note that one key shortcoming (of the indirect approach) is the absence of information on the size or boundary of the "domain of attraction" of each locally stable equilibrium point; this is precisely the information which a completely successful application of the direct approach determines. Finally, we note the most important point: *if the linear motion is critical (e.g., zero damping, some eigenvalues have zero real parts), then the stability of the locally linearized analysis should be considered inconclusive and nonlinear effects must be included to conclude local stability or instability.*

3.4.2   What to Do When $\dot{U}$ is Negative Semidefinite?

Several subtle possibilities arise if the function derived for $\dot{U}$ is not negative definite. For a significant fraction of the practical occurrences of this condition, including several applications considered subsequently in this chapter, *we can prove global asymptotic stability in spite of the fact that the function derived for $\dot{U}$ is negative semidefinite.* The main results from the traditional literature for dealing with this problem are embodied in a theorem due to [LaSalle 1961]; this theorem sometimes allows us to conclude that we have local asymptotic stability for the case that $U > 0$ and $\dot{U} \le 0$, provided we can prove that the equilibrium point is contained in a region of state space known as the *maximum invariant subspace* M.

The maximum invariant subspace is, essentially, the largest domain M containing an equilibrium point, for which all trajectories evolve such that $U > 0$ and $\dot{U} \leq 0$ for all time along the trajectories, with $\dot{U} = 0$ being approached only occasionally (at most) at isolated apogee-like states that *are not equilibrium points* (*i.e.*, $\dot{U}$ is negative almost everywhere except its asymptotic approach to zero at the equilibrium state which is a minimum of U).

It is usually easy to identify the subset Z of points in the state space for which $\dot{U} = 0$, but LaSalle's maximum invariant subspace M is, in general, a subset of Z. The main challenge of applying LaSalle's theorem then reduces to the quest to identify or approximate M; this is difficult when the differential equations are complicated nonlinear functions. While these ideas are elegant, we elect not to discuss the search for M in detail, but rather we present a recently developed result [Mukherjee 1992a, 1992b, 1993], [Junkins 1993] which is often easier to apply.

Prior to stating the theorem, we introduce some notations: Let $x = 0$ be an equilibrium state of the nonlinear system $\dot{x} = f(t, x)$, where f is a smooth, twice differentiable n-vector function of t and x. Note that the trajectories of the nonlinear differential equation $\dot{x} = f(t, x)$ generates a smooth vector field in the region Ω which includes $x = 0$. Let $U(t,x)$ be a scalar analytic function in Ω, which is locally positive definite. Suppose $\dot{U}(t, x)$ is only negative semidefinite. Let Z denote the set of points for which $\dot{U}(t, x)$ vanishes. We will be concerned with the first k derivatives $\frac{d^k U}{dt^k}$, *evaluated on the set* Z. We are now prepared to state the theorem:

Theorem 3.9

A sufficient condition for asymptotic stability, when $U > 0$ and $\dot{U} \leq 0$ for all $x \in \Omega$ is that the first (k-1) derivatives of U vanish on Z, up through some *even* order (k-1)

$$\frac{d^j U}{dt^j} = 0, \quad \forall \quad x \in Z, \quad \text{for} \quad j = 1, 2, ..., \quad k - 1 \tag{3.23}$$

and *the first* (the kth) nonzero derivative of U (evaluated on Z) is of odd order and is negative definite for all points on Z:

$$\frac{d^k U}{dt^k} < 0, \quad \forall \quad x \in Z, \quad \text{for k odd} \tag{3.24}$$

In the event that all infinity of U derivatives vanish on Z, sufficient conditions for stability are that U is positive definite and that $x = 0$ is the only equilibrium point.

∎

The proof of this theorem is given in [Mukherjee 1992a,b]. As evident below, this theorem is easy to apply to nonlinear and distributed parameter systems. In the following example, it is also shown to be useful for determining the stability of time varying systems.

Example 3.5

[Mukherjee 1992a]

Consider the damped Mathieu equation: $\dot{x}_1 = x_2$, $\dot{x}_2 = -x_2 - (2 + \sin t)x_1$. We select the candidate Lyapunov function: $U(t, x_1, x_2) = x_1{}^2 + \frac{x_2{}^2}{(2 + \sin t)}$, which we observe is positive definite and analytic for all (t, x_1, x_2). Upon differentiation of U, and substitution of the equations of motion, we find that

$$\dot{U}(x) = -x_2{}^2 g(t), \quad \text{where} \quad g(t) = \frac{4 + 2\sin t + \cos t}{(2 + \sin t)^2}$$

Even though $\dot{U}(x)$ is nonpositive, since $\dot{U}(x)$ does not depend upon x_1, it is obviously not negative-definite and without further analysis, we can only conclude mere *stability*; however, we'd like to make a stronger statement and conclude *asymptotic stability*. This can be done by considering the applicability of Theorem 3.9. Note that the set Z of points for which $\dot{U}(x)$ vanishes is the set of all real values for x_1, and zero values for x_2. Upon taking the second and third derivatives of U, and evaluating them on Z, we find that

$$\frac{d^2 U}{dt^2} = 0, \quad \text{and} \quad \frac{d^3 U}{dt^3} = -2(2 + \sin t)^2 g(t) x_1{}^2, \quad \forall \quad x \in Z$$

Since the second derivative of U vanishes on Z and the third derivative is negative on Z, except at the origin, we conclude that all of the conditions of Theorem 3.9 are satisfied; indeed this system is proven globally asymptotically stable.

3.4.3   Lyapunov Control Law Design Method

Here, we present a method for generating globally stable feedback control laws for maneuvers of nonlinear systems and distributed parameter systems. A Lyapunov function is selected which is conserved for the uncontrolled system. Then when the control $u(t) \neq 0$ is considered, $\dot{U}(x)$ depends upon $u(t)$ through the equations of motion. One strategy is to select the control function $u(t, x)$ (from a set of *admissible controls*) to make $\dot{U}(x)$ as negative as possible; this *Lyapunov Optimal* control strategy ensures that $U(x)$ will locally approach zero as fast as possible. On the other hand, any control law which makes $\dot{U}(x)$ negative is asymptotically stabilizing, and in many instances, it will be seen that very simple, yet globally stable control laws can be determined which are attractive for applications.

We will use specific dynamical systems to introduce Lyapunov control design methods for nonlinear and distributed-parameter systems. A useful viewpoint is to consider simultaneously $U(x)$ and $u(t, x)$ "available for selection" in the design process; the class of problems for which globally stable feedback laws can be obtained is surprisingly large. There is coupling between the selection of the Lyapunov function and the corresponding stabilizing control laws. We place the initial emphasis upon using work/energy methods together with stability theory to determine the structure of a stabilizing feedback law and thereby parameterize an infinite family

of stable controllers. Conventional nonlinear programming algorithms can then be invoked to optimize some specified closed loop performance criterion over the stable set. This gives rise to "Lyapunov optimal" control. Although we subsequently develop methods for controlling multi-body manipulators, and for distributed parameter systems governed by hybrid coupled sets of ordinary and partial differential equations, we first consider a system described by a *6-th* order set of nonlinear, ordinary differential equations.

Example 3.6 Large Angle Rigid-Body Maneuvers

Some key ideas are easily introduced by considering general three dimensional nonlinear maneuvers of a single rigid body. The equations governing large motion can be written as [Junkins 1986]

$$
\begin{aligned}
I_1\dot{\omega}_1 &= (I_2 - I_3)\omega_2\omega_3 + u_1 \\
I_2\dot{\omega}_2 &= (I_3 - I_1)\omega_3\omega_1 + u_2 \\
I_3\dot{\omega}_3 &= (I_1 - I_2)\omega_1\omega_2 + u_3 \\
2\dot{q}_1 &= \omega_1 - \omega_2 q_3 + \omega_3 q_2 + q_1(q_1\omega_1 + q_2\omega_2 + q_3\omega_3) \\
2\dot{q}_2 &= \omega_2 - \omega_3 q_1 + \omega_1 q_3 + q_2(q_1\omega_1 + q_2\omega_2 + q_3\omega_3) \\
2\dot{q}_3 &= \omega_3 - \omega_1 q_2 + \omega_2 q_1 + q_3(q_1\omega_1 + q_2\omega_2 + q_3\omega_3)
\end{aligned}
\tag{3.25}
$$

where $(\omega_1, \omega_2, \omega_3)$ and (q_1, q_2, q_3) are the principal axis components of angular velocity and the Euler-Rodriguez parameters ("Gibbs vector"), respectively. Note that (I_1, I_2, I_3) and (u_1, u_2, u_3) are the principal moments of inertia and the principal axis components of the external control torque, respectively.

For the case of zero control torque, it can be readily verified that total rotational kinetic energy is an exact integral of the motion described by differential Eq. (3.25), viz., $2T = (I_1\omega_1^2 + I_2\omega_2^2 + I_3\omega_3^2)$. Motivated by the this total system energy integral, we investigate the trial Lyapunov function

$$
\begin{aligned}
U &= \tfrac{1}{2}(I_1\omega_1^2 + I_2\omega_2^2 + I_3\omega_3^2) + k_0(q_1^2 + q_2^2 + q_3^2) \\
&\equiv \text{kinetic energy } + k_0 \tan^2\left(\tfrac{\phi}{2}\right)
\end{aligned}
\tag{3.26}
$$

where ϕ is the instantaneous *principal rotation angle* (about the instantaneous Eulerian principal rotation axis, from the current angular position to the desired final angular position of the body [Junkins 1986]. It is apparent that the additive term $k_0(q_1^2 + q_2^2 + q_3^2)$ can be viewed as the potential energy stored in a conservative spring, and as will be evident below, this is just the most obvious choice for a positive measure of departure from the orientation $q_1 = 0$, $q_2 = 0$, $q_3 = 0$) . We can anticipate that the system dynamics will evolve such that U is constant if the only external torque is the associated conservative moment. Of course, we are not interested in preserving U as a constant, but rather we seek to drive it to zero, because it measures the departure of the system from the desired equilibrium state at the origin. We further anticipate the necessity to determine an additional

judicious control moment to guarantee that U is a decreasing function of time. It is obvious by inspection that U is positive definite and vanishes only at the desired state $q_i = \omega_i = 0$. Differentiation of Eq. (3.26) and substitution of Eqs. (3.25) lead directly to the following ("power") expression for $\dot{U}$:

$$\dot{U} = \sum_{i=1}^{3} \omega_i \left[u_i + k_0 q_i (1 + q_1^2 + q_2^2 + q_3^2) \right] \qquad (3.27)$$

Of all of the infinity of possible control laws, we can see that *any control* u_i *that reduces the bracketed terms to a function whose sign is opposite to* ω_i *will guarantee that* $\dot{U}$ *is globally negative semi-definite.* The simplest choice consists of the following: Select u_i so that i-th bracketed term becomes $-k_i\omega_i$. This gives the control law

$$u_i = -\left[k_i \omega_i + k_0 q_i (1 + q_1^2 + q_2^2 + q_3^2) \right], \qquad i = 1, 2, 3 \qquad (3.28)$$

The closed loop equations of motion are obtained by substitution of the control law of Eq. (3.28) into the equations of motion of Eq. (3.25) to establish

$$\begin{aligned} I_1\dot{\omega}_1 &= (I_2 - I_3)\omega_2\omega_3 - \left[k_1\omega_1 + k_0 q_1 (1 + q_1^2 + q_2^2 + q_3^2) \right] \\ I_2\dot{\omega}_2 &= (I_3 - I_1)\omega_3\omega_1 - \left[k_2\omega_2 + k_0 q_2 (1 + q_1^2 + q_2^2 + q_3^2) \right] \\ I_3\dot{\omega}_3 &= (I_1 - I_2)\omega_1\omega_2 - \left[k_3\omega_3 + k_0 q_3 (1 + q_1^2 + q_2^2 + q_3^2) \right] \end{aligned} \qquad (3.29)$$

Since $\dot{U} = -(k_1\omega_1^2 + k_2\omega_2^2 + k_3\omega_3^2)$ does not depend upon the q's, it is only a negative semi-definite function, and while we have *stability*, if we choose all $k_i > 0$, we cannot immediately conclude that we have *asymptotic stability*. We can prove that we do indeed have asymptotic stability, for illumination we establish this truth by two logical paths.

Path 1: This analysis is physically motivated, we try to see if there is some equilibrium point or trajectory other than the target state (the origin) where the system can get "stuck" with $\dot{U}(x) = 0$. We directly investigate the above three closed loop equations of motion [Eqs. (3.29)] for the existence of equilibrium points in these nonlinear *closed loop equations of motion*. It can be verified that $(q_1, q_2, q_3, \omega_1, \omega_2, \omega_3) = (0,0,0,0,0,0)$ is the *only* equilibrium state where all velocity and acceleration coordinates vanish. In fact, imposing the conditions $(\dot{\omega}_1, \dot{\omega}_2, \dot{\omega}_3) = (0,0,0)$ and $(\omega_1, \omega_2, \omega_3) = (0,0,0)$ on the above closed loop equations of motion immediately gives the requirement that the q's satisfy the three equations

$$0 = -\left[k_0 q_i (1 + q_1^2 + q_2^2 + q_3^2) \right], \quad \text{for } i = 1, 2, 3$$

and it is obvious by inspection that these three nonlinear equations are simultaneously satisfied only at the origin.

Since we have shown that $(\dot{\omega}_1 \neq 0, \dot{\omega}_2 \neq 0, \dot{\omega}_3 \neq 0)$, for $(q_1 \neq 0, q_2 \neq 0, q_3 \neq 0)$, everywhere except the origin $x = (q_1, q_2, q_3, \omega_1, \omega_2, \omega_3)^T = (0,0,0,0,0,0)^T$, we conclude that $\dot{U}(x) = 0$ can only be encountered for $(q_1 \neq 0, q_2 \neq 0, q_3 \neq 0)$ at

(possibly) apogee-like points in the behavior of U ($\dot{U}$ instantaneously vanishes but these points cannot be equilibrium states because ($\dot{\omega}_1 \neq 0, \dot{\omega}_2 \neq 0, \dot{\omega}_3 \neq 0$). Therefore, we are guaranteed that $\dot{U}(x) < 0$ *almost everywhere* [thus, we have the ideal situation that the largest invariant subspace is all of state space]. We asymptotically approach the origin from all finite initial states and, therefore, have global asymptotic stability.

Path 2: This analysis is more formal and procedural (exactly analogous to Example 3.5), we simply apply Theorem 3.9. First notice the set Z where $\dot{U}(x)$ vanishes is the set of arbitrary real values for the q's and zero values for the ω's. It can be verified by direct differentiation of U that, for general motion

$$\frac{d^2U}{dt^2} = -2\sum_{i=1}^{3} k_i \omega_i \dot{\omega}_i, \quad \text{and} \quad \frac{d^3U}{dt^3} = -2\sum_{i=1}^{3} k_i (\dot{\omega_i}^2 + \omega_i \ddot{\omega}_i). \qquad (3.31)$$

Upon evaluation of these derivatives on Z where angular velocity vanishes $(\omega_1, \omega_2, \omega_3) = (0, 0, 0)$, from the closed loop equations of motion, the nonzero acceleration components are $\dot{\omega}_i = -k_0(1 + q_1^2 + q_2^2 + q_3^2)(q_i/I_i)$, we find that

$$\frac{d^2U}{dt^2} = 0, \quad \text{and} \quad \frac{d^3U}{dt^3} = -k_0^2(1 + q_1^2 + q_2^2 + q_3^2)^2 \sum_{i=1}^{3} k_i \left(\frac{q_i}{I_i}\right)^2, \quad \forall \quad x \in Z \quad (3.32)$$

Since the second derivative of U vanishes everywhere on Z, the third derivative is negative-definite everywhere on Z, the conditions of Theorem 3.9 are fully satisfied, and we again conclude that the nonlinear control law of Eq. (3.28) gives us globally asymptotically stable attitude control.

Since we have shown U to be a positive-definite, decreasing function of time along all trajectories, and since it vanishes at the origin, then the necessary and sufficient conditions are satisfied for global Lyapunov stability. We have implicitly excluded the geometric singularity ($q_i \rightarrow \infty$) associated with this parameterization of rotational motion as $\phi \rightarrow n\pi$; we can use the quaternion or Euler parameter description of motion and avoid all geometric singularities as well. This path has been successfully pursued in [Oh 1991], [Wie 1989].

The nonlinear feedback control law of Eq. (3.28) guarantees stability of the nonlinear closed-loop system under the assumption of zero model errors. In practice, of course, guaranteed stability in the presence of zero model error is not a sufficient condition to guarantee stability of the actual plant having arbitrary model errors and disturbances. On the other hand, rigorously defining a region in gain space, guaranteeing global stability for our best model of the nonlinear system is an important step; it is reasonable to restrict the optimization of gains to this stable family of designs. The determination of the particular gain values, selected from the space of globally stabilizing gains, is usually based on performance optimization criteria specified in consideration of the disturbance environment, sensitivity to model errors, desired system time constants, actuator saturation, and sensor/actuator bandwidth limitations.

Before generalizing the methodology to consider multibody and partial differential equation systems, it is important to reflect on the selection of the Lyapunov function previously given. Notice that, if a system has no inherent stiffness with respect to rigid-body displacement, it is necessary to augment the open-loop energy integral by a pseudopotential energy term [such as $k_0(q_1^2 + q_2^2 + q_3^2)$ in the preceding example]; generally speaking, the pseudoenergy term should be defined, if possible, such that the resulting candidate Lyapunov function (U) is a positive definite measure of departure motion that has its global minimum at *the desired target state*. Then the still-to-be-determined controls are usually selected as simply as possible (from an implementation point of view) to force pervasive dissipation ($\dot{U} < 0$) of the modified energy (Lyapunov) function along all trajectories of the closed-loop system, and thereby guarantee closed-loop stability.

To illustrate the relationship between the choice of the Lyapunov function and the resulting family of stabilizing control law, let us consider a slight variation on [Tsiotras 1994] the above developments. In lieu of the Lyapunov functions of Eq. (3.26), we choose a *logarithmic* measure of attitude error

$$U = \frac{1}{2}\left(I_1\omega_1^2 + I_2\omega_2^2 + I_3\omega_3^2\right) + k_0 \ln\left(1 + q_1^2 + q_2^2 + q_3^2\right) \qquad (3.33)$$

Proceeding analogously to the above developments, it is easy to verify that

$$\dot{U} = \sum_{i=1}^{3} \omega_i[u_i + k_0q_i] \qquad (3.34)$$

so that we can see that the following *linear* feedback law is globally stabilizing

$$u_i = -k_0q_i - k_i\omega_i, \qquad i = 1, 2, 3 \qquad (3.35)$$

Contrasting the two stabilizing control laws of Eqs. (3.35) and (3.28), it is clear that the simpler linear law of Eq. (3.35) is likely more attractive as regards implementation, unless the nonlinear feedback of Eq. (3.28) is found, in some circumstances, to give a desirable closed loop response.

This example points out clearly the coupling between selection of the "error energy measure" and the resulting globally stabilizing controllers; the situation is quite analogous to applications of optimal control theory, wherein there is coupling between the choice of the performance index and the resulting optimal control law. Although the above insights are useful, definitive criteria for optimal selection of the Lyapunov function do not exist. However, the above examples suggest an attractive strategy that defines the 'main part' of the Lyapunov function with relative weights on the portions of total mechanical energy associated with structural subsystems [Junkins 1993], and use of the work/energy method provides a very efficient bypass of most of the algebra and calculus leading to the power equations, analogous to Eq. (3.27), for each particular physical system [Oh 1991]. The lack of uniqueness of the Lyapunov function is not necessarily a disadvantage in practice because it

is a source of user flexibility providing needed control design freedom qualitatively comparable to the freedom one has in selecting performance indices when applying optimal control theory. Indeed, formulating the Lyapunov function as a weighted error energy to be dissipated by the controller is qualitatively attractive for both linear and nonlinear systems, since this gives intuitive and physical meaning to the Lyapunov function and the corresponding control gains.

3.5 COOPERATIVE CONTROL OF MULTIBODY MANIPULATORS

3.5.1 Mechanics

Prior to addressing the first of two studies wherein the above ideas are applied, consider the class of dynamical systems whose behavior is governed by the discrete coordinate version of Lagrange's equations

$$\frac{d}{dt}\left(\frac{\partial \mathcal{L}}{\partial \dot{q}_i}\right) - \frac{\partial \mathcal{L}}{\partial q_i} = Q_i, \qquad i = 1, 2, \ldots, N \tag{3.36}$$

or, in matrix form

$$\frac{d}{dt}\left(\frac{\partial \mathcal{L}}{\partial \dot{q}}\right) - \frac{\partial \mathcal{L}}{\partial q} = Q \tag{3.37}$$

where the *Lagrangian* $\mathcal{L}$ is defined in the classical form $\mathcal{L} = T - V$. Restrictions imposed in deriving Eqs. (3.37) are such that the coordinates q_i are independent functions of time only and that the potential and kinetic energies have the functional forms $T = T(q, \dot{q}, t)$, $V = V(q)$, and the nonconservative virtual work has the form $\delta W_{nc} = \sum_{i=1}^{N} Q_i \delta q_i = Q^T \delta q$. Thus, Eqs. (3.37) are valid for nonlinear, nonconservative systems as well as linear, conservative systems.

A modest generalization allows Eqs. (3.37) to be applied to significant classes of redundant coordinate or constrained systems (*i.e.*, the coordinates q_i are not independent). To accommodate kinematic constraints which depend on the qs and their time derivatives, Lagrange multipliers can be introduced to generate additive generalized constraint forces on the right-hand side of Eqs. (3.37) [Junkins 1986]. In particular, for m Pfaffian (linear in the generalized velocities) constraints of the matrix form

$$A\dot{q} + a_o = 0 \tag{3.38}$$

The generalized constraint force that needs to be added to the right-hand side of Eqs. (3.37) is the vector $A^T \lambda$, where q is an $N \times 1$ vector containing the generalized coordinates, $A = A(q)$ is an $m \times n$ continuous, differentiable matrix function, $a_o(q)$ is a smooth, $m \times 1$ vector function, and λ is an $m \times 1$ vector of Lagrange multipliers. One standard solution process is to differentiate the kinematic constraint of Eqs. (3.38) to obtain

$$A\ddot{q} + \dot{A}\dot{q} + \dot{a}_o = 0 \tag{3.39}$$

Equation (3.39) can be solved simultaneously with Eqs. (3.37) for $\bar{q}$ and λ, to determine the coordinate accelerations and constraint forces as a function of the qs and their time derivatives. Note that the N differential equations of Eqs. (3.37) must be solved simultaneously with the m kinematic constraint differential equations [Eqs. (3.37)] in order to determine the N+m unknowns in the vectors $\bar{q}$ and $\lambda(t)$. During recent years, significant methodlolgy has evolved for effecting numerical solutions for differential/algebraic systems of equations, see Ahmad 1991 and Krishnan 1992 for discussion of the recent literature.

For a significant class of systems, the algebra and calculus required in a straightforward application of Lagrange's equations can be dramatically reduced. For the the most common case of *natural* systems for which the kinetic energy is a symmetric quadratic form in the generalized coordinate time derivatives, one finds:

$$T = \frac{1}{2}\sum_{i=1}^{N}\sum_{j=1}^{N} m_{ij}(q)\,\dot{q}_i\dot{q}_j = \frac{1}{2}\dot{q}^T M \dot{q} \tag{3.40}$$

Note that q is an $N \times 1$ configuration vector of generalized coordinates. It is convenient (and important) to collect the mass matrix $M = M(q)$ *before* the differentiations implied by Lagrange's equations are carried out; this simple point seems to elude many individuals when symbolic codes are written to automate derivation of equations of motion. Including the possibility of Pfaffian nonholonomic constraints, the equations of motion follow from Eqs. (3.37) as the following N+m system of differential and algebraic equations:

$$M\bar{q} + G + \frac{\partial V}{\partial q} = Q + A^T\lambda, \quad A\dot{q} + a_0 = 0 \tag{3.41}$$

where $\frac{\partial V}{\partial q}$ is the $N \times 1$ vector gradient of the potential energy function, and $G = G(q,\dot{q})$ is the $N \times 1$ vector:

$$G = [\dot{q}^T C^{(1)}\dot{q} \;\; \cdots \;\; \dot{q}^T C^{(N)}\dot{q}]^T, \quad c_{jk}^{(i)} = \frac{1}{2}\left(\frac{\partial m_{ij}}{\partial q_k} + \frac{\partial m_{ik}}{\partial q_j} - \frac{\partial m_{jk}}{\partial q_i}\right) \tag{3.42}$$

and where the last equation that generates the typical element $c_{jk}^{(i)}$ of the $N \times N$ symmetric matrix $C^{(i)} = C^{(i)}(q)$ is the *Christoffel* operator.

It is apparent that deriving the equations of motion, for natural systems subject to Pfaffian nonholonomic constraints, has been reduced to formation of the kinetic energy to identify the mass matrix, then carrying out the indicated gradient operations in Eqs. (3.42), (3.43) on the mass matrix elements m_{ik} and the potential energy to form the vectors $G = G(q,\dot{q})$ and $\partial V/\partial q$.

For the case that the nonconservative forces are generated by an $m_c \times 1$ vector u of control inputs, we have $Q = Bu$ and Eqs. (3.41) assume the following form

$$\begin{aligned} M(q)\bar{q} + \frac{\partial V}{\partial q} + G(q,\dot{q}) &= Bu + A(q)^T\lambda \\ A(q)\dot{q} + a_o(q) &= 0 \end{aligned} \tag{3.43}$$

In order to appreciate some of the issues of *cooperation* associated with control design for redundantly actuated systems, we consider a specific example in the following discussion.

3.5.2 A Prototype Cooperative Control Example

Equations of Motion

Consider the pair of robot arms shown in Figure 3.1. We assume four active joints; namely, the shoulder and elbow joints on the left and right robots, for simplicity; the wrist torques are neglected. The objective is to design a feedback controller to command the four torques so as to stabilize the payload with respect to a prescribed trajectory of the payload moving from an arbitrary reachable State A to an arbitrary reachable State B. It is desired that the control law have the following attributes:

1. Accommodate an arbitrary feasible reference trajectory.

2. Be of a simple feedforward/output output error feedback form.

3. Guarantee global asymptotic stability, including nonlinear kinematics.

4. Handoff smoothly between large trajectory-tracking motion and terminal error suppression, without gain scheduling.

We present a control strategy possessing these four desirable attributes.

Under the assumption that each manipulator is composed of two rigid links, that the payload is a rigid body, and that the entire system undergoes only planar motion, but retaining all nonlinear kinematic effects, the kinetic energy of the system has the natural form

$$T = \frac{1}{2}\dot{q}^T[M(q)]\dot{q}$$
$$= \frac{1}{2}\dot{q}_L^T[M_L(q_L)]\dot{q}_L + \frac{1}{2}\dot{q}_R^T[M_R(q_R)]\dot{q}_R + \frac{1}{2}\dot{q}_P^T[M_P(q_P)]\dot{q}_P \quad (3.44)$$

where the configuration coordinate vector naturally partitions into left(L), right(R), and payload(P) configuration coordinate subsets as

$$q_L = \left\{ \begin{array}{c} \theta_1 \\ \theta_2 \end{array} \right\}, \quad q_R = \left\{ \begin{array}{c} \theta_6 \\ \theta_5 \end{array} \right\}, \quad q_P = \left\{ \begin{array}{c} \theta_3 \\ x_{c_3} \\ y_{c_3} \end{array} \right\},$$

$$q = \left\{ \begin{array}{c} q_L \\ q_R \\ q_P \end{array} \right\} = \left\{ \theta_1 \quad \theta_2 \quad \vdots \quad \theta_6 \quad \theta_5 \quad \vdots \quad \theta_3 \quad x_{c_3} \quad y_{c_3} \right\}^T$$

The 7×7 system mass matrix has the block diagonal structure

$$M(q) = \begin{bmatrix} M_L & & \\ & M_R & \\ & & M_P \end{bmatrix} \quad (3.45)$$

(a) Configuration Sketch   (b) Substructure Systems and Notation

(c) Laboratory Experiment at the Naval Postgraduate School

Figure 3.1. Cooperative control multibody manipulator experiment

where, introducing the elbow angles $\theta_{ij} = \theta_j - \theta_i$, the substructure mass matrices are compactly written as

$$M_L = \begin{bmatrix} I_1 + \frac{1}{4}m_1 l_1^2 + m_2 l_1^2 & \frac{1}{2}m_2 l_1 l_2 cos\theta_{12} \\ \frac{1}{2}m_2 l_1 l_2 cos\theta_{12} & I_2 + \frac{1}{4}m_2 l_2^2 \end{bmatrix} \tag{3.46}$$

$$M_R = \begin{bmatrix} I_5 + \frac{1}{4}m_5 l_5^2 + m_4 l_5^2 & \frac{1}{2}m_4 l_5 l_4 cos\theta_{65} \\ \frac{1}{2}m_4 l_5 l_4 cos\theta_{65} & I_4 + \frac{1}{4}m_4 l_4^2 \end{bmatrix} \tag{3.47}$$

and

$$M_P = \begin{bmatrix} I_3 & & \\ & m_3 & \\ & & m_3 \end{bmatrix} \tag{3.48}$$

The equations of motion follow in the form of Eq. (3.43), where, using Eq. (3.42), the nonlinear vector $G(q, \dot{q})$ has the following specific form

$$G(q, \dot{q}) = \left\{ \begin{matrix} G_L \\ G_R \\ 0 \end{matrix} \right\}, \quad \left\{ \begin{matrix} G_L \\ G_R \end{matrix} \right\} = \frac{1}{2} \left\{ \begin{matrix} -m_2 \dot{\theta}_2^2 l_1 l_2 sin\theta_{12} \\ m_2 \dot{\theta}_1^2 l_1 l_2 sin\theta_{12} \\ \cdots\cdots\cdots\cdots \\ -m_4 \dot{\theta}_5^2 l_4 l_5 sin\theta_{65} \\ m_4 \dot{\theta}_6^2 l_4 l_5 sin\theta_{65} \end{matrix} \right\} \tag{3.49}$$

The control vector (containing the four shoulder and elbow torques) is

$$u = \{u_1 \ u_2 \ u_6 \ u_5\}^T \tag{3.50}$$

and, using the virtual work principle, we can establish that the control influence matrices are

$$B = \begin{bmatrix} B_L & O \\ O & B_R \\ O & O \end{bmatrix}, \quad B_L = B_R = \begin{bmatrix} 1 & -1 \\ 0 & 1 \end{bmatrix} \tag{3.51}$$

Upon taking the origin for an (x,y) coordinate system as the base hinge point of the left arm, and letting the x axis pass through the base hinge point of the right arm, the geometric constraints arising from pinning of the left and right robot wrists to the payload at points Q and P are captured by the four holonomic constraints:

$$\left. \begin{matrix} l_1 cos\theta_1 + l_2 cos\theta_2 + \frac{1}{2}l_3 cos\theta_3 - x_{c_3} & = 0 \\ l_1 sin\theta_1 + l_2 sin\theta_2 + \frac{1}{2}l_3 sin\theta_3 - y_{c_3} & = 0 \\ l_5 cos\theta_6 + l_4 cos\theta_5 - \frac{1}{2}l_3 cos\theta_3 - x_{c_3} - D & = 0 \\ l_5 sin\theta_6 + l_4 sin\theta_5 - \frac{1}{2}l_3 sin\theta_3 - y_{c_3} & = 0 \end{matrix} \right\} \tag{3.52}$$

Upon differentiation with respect to time, Eqs. (3.52) yield a kinematic constraint of the Pffafian form [the second equation of Eqs. (3.43)], with $a_0 = 0$ and with

$$A(q) = \begin{bmatrix} -l_1 sin\theta_1 & l_2 sin\theta_2 & 0 & 0 & -\frac{1}{2}l_3 sin\theta_3 & -1 & 0 \\ l_1 cos\theta_1 & l_2 cos\theta_2 & 0 & 0 & \frac{1}{2}l_3 cos\theta_3 & 0 & -1 \\ 0 & 0 & -l_5 sin\theta_6 & -l_4 sin\theta_5 & \frac{1}{2}l_3 sin\theta_3 & -1 & 0 \\ 0 & 0 & l_5 cos\theta_6 & l_4 cos\theta_5 & -\frac{1}{2}l_3 cos\theta_3 & 0 & -1 \end{bmatrix} \tag{3.53}$$

and also, for subsequent use, we record the time derivative of A as

$$\dot{A}(q, \dot{q}) =$$
$$\begin{bmatrix} -l_1\dot{\theta}_1\cos\theta_1 & -l_2\dot{\theta}_2\cos\theta_2 & 0 & 0 & -\frac{1}{2}l_3\dot{\theta}_3\cos\theta_3 & 0 & 0 \\ -l_1\dot{\theta}_1\sin\theta_1 & -l_2\dot{\theta}_2\sin\theta_2 & 0 & 0 & -\frac{1}{2}l_3\dot{\theta}_3\sin\theta_3 & 0 & 0 \\ 0 & 0 & -l_5\dot{\theta}_6\cos\theta_6 & -l_4\dot{\theta}_5\cos\theta_5 & \frac{1}{2}l_3\dot{\theta}_3\cos\theta_3 & 0 & 0 \\ 0 & 0 & -l_5\dot{\theta}_6\sin\theta_6 & -l_4\dot{\theta}_5\sin\theta_5 & \frac{1}{2}l_3\dot{\theta}_3\sin\theta_3 & 0 & 0 \end{bmatrix} \quad (3.54)$$

Now, solving the first of Eqs. (3.43) and Eq. (3.39) simultaneously for the generalized constraint force $Q_C = A^T\lambda$ and $M\ddot{q}$, we obtain

$$\begin{aligned} Q_C &= A^T\lambda = F_1 + F_2 u \\ F_1 &= A^T(AM^{-1}A^T)^{-1}(G - A\dot{q}) \\ F_2 &= -A^T(AM^{-1}A^T)^{-1}AM^{-1}B \end{aligned} \quad (3.55)$$

and

$$\begin{aligned} M\ddot{q} + \bar{G} &= \bar{B}u \\ \bar{G} &= G - A^T(AM^{-1}A^T)^{-1}\left\{AM^{-1}G - A\dot{q}\right\} \\ \bar{B} &= \left[I - A^T(AM^{-1}A^T)^{-1}AM^{-1}\right]B \end{aligned} \quad (3.56)$$

It is natural to introduce the consistent partitions

$$M = \begin{bmatrix} M_L & & \\ & M_R & \\ & & M_P \end{bmatrix}, \quad \bar{G} = \left\{ \begin{array}{c} \bar{G}_L \\ \bar{G}_R \\ \bar{G}_P \end{array} \right\}, \quad \bar{B} = \begin{bmatrix} \bar{B}_L \\ \bar{B}_R \\ \bar{B}_P \end{bmatrix} \quad (3.57)$$

and rewrite the first of Eqs (3.56) as three equations

$$\begin{aligned} M_L\ddot{q}_L + \bar{G}_L(q,\dot{q}) &= \bar{B}_L(q,\dot{q})u \\ M_R\ddot{q}_R + \bar{G}_R(q,\dot{q}) &= \bar{B}_R(q,\dot{q})u \\ M_P\ddot{q}_P + \bar{G}_P(q,\dot{q}) &= \bar{B}_P(q,\dot{q})u \end{aligned} \quad (3.58)$$

This constraint-free form of the equations of motion implicitly reflects the constraints; the third of Eqs. (3.58) is sufficient to describe the dynamics of the system, since all other coordinates can be determined as a function of $(q_P, \dot{q}_P)$ through use of the constraint equations.

Prior to discussion of control law design approaches, it is useful to consider the inverse kinematics problem: Given a smooth desired (prescribed) payload motion $q_P(t)$, determine feasible/desirable corresponding control inputs. Inverse kinematics for the case of redundant coordinates involves some subtle issues which are captured in the following sections.

Inverse Kinematics

Notice that the four holonomic constraints of Eqs. (3.52) reduce the number of degrees of freedom from seven to three. Thus, in principle, we could derive all coordinates and their time derivatives history from a given trajectory of the payload

coordinates $q_P(t) = [\theta_3(t) \; x_{c_3}(t) \; y_{c_3}(t)]^T$. Obviously, if we know all of the coordinates and their first two time derivatives, then the *differential* equations of motion [Eqs. (3.56) or (3.58)] can be considered *algebraic* equations for determination of the corresponding control torques. Since there are only three degrees of freedom and four control torques, there is obviously an issue of uniqueness, and it is through the exploitation of the lack of uniqueness that we can seek an optimal control by which the robot arms may *cooperate* in carrying out the controlled maneuver. It is also important to anticipate geometric singularities on the boundary of the reachable region (the maximum feasible workspace). First let us consider some geometric issues.

With reference to Figure 3.1, observe that a given motion $q_P(t)$ of the payload dictates the motion of points P and Q though the four geometric formulas:

$$\left. \begin{aligned}
x_Q &= x_{c_3} - \left(\tfrac{l_1}{2}\right) cos\theta_3 \\
y_Q &= y_{c_3} - \left(\tfrac{l_1}{2}\right) sin\theta_3 \\
x_P &= x_{c_3} + \left(\tfrac{l_1}{2}\right) cos\theta_3 \\
y_P &= y_{c_3} + \left(\tfrac{l_1}{2}\right) sin\theta_3
\end{aligned} \right\} \qquad (3.59)$$

and obviously, the companion equations can be obtained to determine the first two time derivatives of the grapple point coordinates (x_P, y_P, x_Q, y_Q) as a function of the payload motion

$$\left(\theta_3, x_{c_3}, y_{c_3}, \dot{\theta}_3, \dot{x}_{c_3}, \dot{y}_{c_3}, \ddot{\theta}_3, \ddot{x}_{c_3}, \ddot{y}_{c_3}\right)$$

These straightforward equations are not recorded for the sake of brevity. However, given the payload motion, we can obviously determine the grapple point's velocity and acceleration coordinates

$$(\dot{x}_P, \dot{y}_P, \dot{x}_Q, \dot{y}_Q, \ddot{x}_P, \ddot{y}_P, \ddot{x}_Q, \ddot{y}_Q)$$

by differentiation of Eqs. (3.59). We consider how to determine the motion of the left and right robot arms. Considering the geometry of the left robot arm, from Figure 3.1, it is evident that the left shoulder and elbow angles θ_1 and θ_2 are related to the instantaneous position of the grapple point (x_Q, y_Q) by

$$\left. \begin{aligned}
\theta_1 &= \beta_{1L} + \beta_{2L} \\
\beta_{1L} &= tan^{-1}(y_Q/x_Q) \\
\beta_{2L} &= cos^{-1}\left(\frac{l_1^2 - l_2^2 + (x_Q^2 + y_Q^2)^{1/2}}{2l_1(x_Q^2 + y_Q^2)^{1/2}}\right), \text{two, roots, take } \beta_{2L} > 0 \\
\theta_2 &= tan^{-1}\left(\frac{y_Q - l_1 sin\theta_1}{x_Q - l_1 cos\theta_1}\right)
\end{aligned} \right\} \qquad (3.60)$$

Similarily, considering the right robot, it is evident that the right robot angles θ_6 and θ_5 are related to (x_P, y_P) by

$$
\left.
\begin{aligned}
\theta_6 &= \beta_{1R} - \beta_{2R} \\
\beta_{1R} &= tan^{-1}\left(y_P/x_P\right) \\
\beta_{2R} &= cos^{-1}\left(\frac{l_s^2 - l_4^2 + \left(x_P^2 + y_P^2\right)^{1/2}}{2 l_s\left[(D - x_P)^2 + y_P^2\right]^{1/2}}\right), \text{two roots, take } \beta_{2R} > 0 \\
\theta_5 &= tan^{-1}\left(\frac{y_P - l_s sin\theta_6}{D - (x_P - l_s cos\theta_6)}\right)
\end{aligned}
\right\} \qquad (3.61)
$$

It can be verified taking β_{2L} and β_{2R} positive corresponds to the "elbows out" configuration shown in Figure 3.1. Obviously, the "elbows in" configuration results from choosing the negative signs for β_{2L} and β_{2R}, and two other asymmetric configurations are possible if opposite signs are selected. The lack of uniqueness is a consequence of redundancy and the choice of control modes is dictated by practical configurations. Except near certain singular configurations discussed below, it is possible to manipulate smoothly through an infinite family of neighboring configurations for any one of the four choices on signs for $\beta_{2L}(t)$ and $\beta_{2R}(t)$. Straightforward differentiation yields the following kinematic equations which determine the first two time derivatives of the left and right shoulder and elbow angles:

$$
\left\{
\begin{array}{c}
\dot{\theta}_1 \\
\dot{\theta}_2
\end{array}
\right\} = A_L^{-1}
\left\{
\begin{array}{c}
\dot{x}_Q \\
\dot{y}_Q
\end{array}
\right\}, \qquad
\left\{
\begin{array}{c}
\ddot{\theta}_1 \\
\ddot{\theta}_2
\end{array}
\right\} = A_L^{-1}
\left[
\left\{
\begin{array}{c}
\ddot{x}_Q \\
\ddot{y}_Q
\end{array}
\right\} - \dot{A}_L
\left\{
\begin{array}{c}
\dot{\theta}_1 \\
\dot{\theta}_2
\end{array}
\right\}
\right]
$$

$$
\left\{
\begin{array}{c}
\dot{\theta}_6 \\
\dot{\theta}_5
\end{array}
\right\} = A_R^{-1}
\left\{
\begin{array}{c}
\dot{x}_P \\
\dot{y}_P
\end{array}
\right\}, \qquad
\left\{
\begin{array}{c}
\ddot{\theta}_6 \\
\ddot{\theta}_5
\end{array}
\right\} = A_R^{-1}
\left[
\left\{
\begin{array}{c}
\ddot{x}_P \\
\ddot{y}_P
\end{array}
\right\} - \dot{A}_R
\left\{
\begin{array}{c}
\dot{\theta}_6 \\
\dot{\theta}_5
\end{array}
\right\}
\right] \qquad (3.62)
$$

where we have introduced the matrices

$$
A_L = \begin{bmatrix} -l_1 sin\theta_1 & -l_2 sin\theta_2 \\ l_1 cos\theta_1 & l_2 cos\theta_2 \end{bmatrix}, \quad
A_R = \begin{bmatrix} -l_5 sin\theta_6 & -l_4 sin\theta_5 \\ l_5 cos\theta_6 & l_4 cos\theta_5 \end{bmatrix} \qquad (3.63)
$$

It is easy to verify that the above matrices are singular if $\theta_1 = \theta_2$, and $\theta_6 = \theta_5$, respectively. It is obvious that these singularities corresponded to the left and right arms being fully extended, and it is clear that these boundaries of the workspace are to be avoided [the reachable set of points interior to the workspace must be taken into account in the trajectory planning for the payload, leading to the nominal trajectory $q_P(t)$ of the payload].

Cooperative Actuation

Given the inverse kinematic solution for all system coordinates and time derivatives, as a function of a prescribed payload trajectory $q_P(t)$, the cooresponding control torque vector $u(t)$ is not unique, for the case of more actuators and degrees of freedom. In our particular example, since we have four actuators and three degrees of freedom, we expect an infinity of torque vectors for the nominal maneuver. As in the case of human beings jointly manipulating a heavy object, we desire to

exploit the redundancy of actuation to cooperate in the sense that large, nonworking constraint forces are avoided.

To capture these considerations as a control strategy, we introduce the following cooperation criterion to be minimized

$$J = \frac{1}{2}u^T W_u u + \frac{1}{2}Q_c^T W_c Q_c \tag{3.64}$$

subject to satisfying the third of Eqs. (3.58). Notice that the weight matrix selection permits us the flexibility of emphasizing small torques (u), or small constraint forces ($Q_c = A^T \lambda$), or a compromise between these two competing objectives. Using the Lagrange multiplier rule, we introduce the $m \times 1$ Lagrange multiplier vector γ and the augmented function $\tilde{J}$, and use Eqs. (3.55), (3.58) to write

$$\tilde{J} = \frac{1}{2}u^T W_u u + \frac{1}{2}(F_1 + F_2 u)^T W_c (F_1 + F_2 u) + \gamma^T \left(M_P \ddot{q}_P + \bar{G}_P - \bar{B}_P u \right) \tag{3.65}$$

Requiring that the gradients $\nabla_u \tilde{J}$ and $\nabla_\gamma \tilde{J}$ both vanish as a necessary condition for minimizing J leads to the solution

$$
\begin{aligned}
u &= H \left\{ \bar{B}_P \gamma - F_2^T W_c F_1 \right\} \\
\gamma &= \left(\bar{B}_P H \bar{B}_P^T \right)^{-1} \left\{ M_P \ddot{q}_P + \bar{G}_P + \bar{B}_P H F_2^T W_c F_1 \right\} \\
H &= \left(W_u + F_2^T W_c F_2 \right)^{-1}
\end{aligned}
\tag{3.66}
$$

Some simple calculations with example payload motions reveal the utility of this formulation of the inverse kinematics and cooperative actuation strategy.

An Example Nominal Payload Trajectory

Perhaps the simplest and easiest-to-motivate scheme for prescribing a nominal motion $q_P(t)$ for the payload is to adopt a smooth polynomial spline from the initial state $q_P(t_0)$ to the target final state $q_P(t_f)$ of the form

$$
\begin{aligned}
q_P(t) &= f(\tau)\{q_P(t_f) - q_P(t_0)\} + q_P(t_0), \quad \tau = \frac{(t-t_0)}{(t_f-t_0)} \\
\dot{q}_P(t) &= \dot{f}(\tau)\{q_P(t_f) - q_P(t_0)\}, \quad \dot{f}(\tau) = \frac{1}{(t_f-t_0)}\frac{df}{d\tau} \\
\ddot{q}_P(t) &= \ddot{f}(\tau)\{q_P(t_f) - q_P(t_0)\}, \quad \ddot{f}(\tau) = \frac{1}{(t_f-t_0)^2}\frac{d^2f}{d\tau^2}
\end{aligned}
\tag{3.67}
$$

where we choose the particular shape function

$$
\begin{aligned}
f(\tau) &= \tau^3(10 - 15\tau + 6\tau^2) \\
\frac{df}{d\tau} &= \tau^2(30 - 60\tau + 30\tau^2) \\
\frac{d^2f}{d\tau^2} &= \tau(60 - 180\tau + 120\tau^2)
\end{aligned}
\tag{3.68}
$$

This trajectory can be shown to be optimal for the idealized case where we consider only the payload trajectory and the vector sums (F, M) of the forces

and moments applied to the payload, without regard to how these are generated; Eqs. (3.67), (3.68) can be shown [Junkins and Turner 1986] to simultaneously minimize the translational and rotational *jerk integrals*

$$J_1 = \int_{t_0}^{t_f} \dot{F}^T \dot{F} dt, \quad \text{and} \quad J_2 = \int_{t_0}^{t_f} \dot{M}^T \dot{M} dt$$

subject to satisfaction of the third of Eqs. (3.58), and the boundary conditions:

$$\begin{aligned}
q_P(t_0) &= specified\,initial\,position \\
\dot{q}_P(t_0) &= 0 \\
\ddot{q}_P(t_0) &= 0 \\
q_P(t_f) &= specified\,final\,position \\
\dot{q}_P(t_f) &= 0 \\
\ddot{q}_P(t_f) &= 0
\end{aligned} \qquad (3.69)$$

Since the idealized optimal trajectory [Eqs. (3.67), (3.68)] does not explicitly consider workspace constraints, this nominal motion must be checked to make sure it remains feasible throughout the motion, and of course, optimality with respect to the entire systems dynamics and minimization of other performance measures cannot be claimed. These smooth, easy-to-compute, motions usually represent excellent starting solutions, however, and we elect to use this family of solutions to generate the nominal trajectories throughout the remainder of this chapter. A typical example motion of the system is shown in Figure 3.2.

A Lyapunov Stable Tracking Control Law

A smooth nominal (reference) trajectory for the entire system can be computed using Eqs. (3.67), (3.68), and via inverse kinematics, the left and right robot joint coordinates are determined from Eqs. (3.59)–(3.62), while the nominal (cooperative) shoulder and elbow torques are determined from Eqs. (3.66). This is a for-example way to determine the reference trajectory, and can be replaced by a more appropriate path-planning method in particular applications. However the reference trajectory satisfying the boundary conditions of Eqs. (3.69) is determined, we denote all state and control variables along the reference trajectory with a subscript ref. Of course, in actual applications, we can expect that the system will not follow the reference trajectory $q_{ref}(t)$ exactly when we command the control $u_{ref}(t)$, due to model errors, external disturbances, and nonideal actuation. We seek a perturbation $\delta u = \text{function}(\delta q(t), \delta \dot{q}(t))$ which will guarantee that an intitally disturbed motion will asymptotically return to the reference trajectory in the absence of model or implementation errors. Actually, it is preferable that the control perturbation δu is in *output feedback form* where it depends only upon a measurable subset of the coordinates and their time derivatives.

In view of the four kinematic constraints, we know that a minimal coordinate description requires only three generalized coordinates. By considering
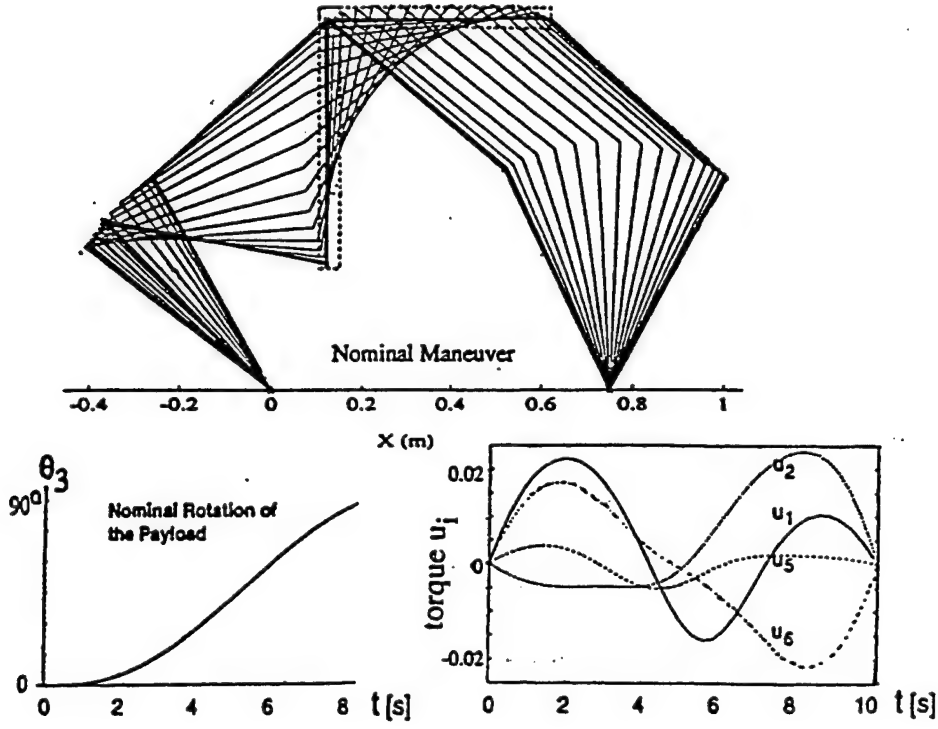
Figure 3.2. Nominal maneuver, payload rotation, and actuator torque trajectories

$(q, \dot{q})$ to be functions of $(q_P, \dot{q}_P)$, in the third of Eqs. (3.58), we are motivated to investigate the kinetic energy

$$T_P = \frac{1}{2} \dot{q}_P^T M_P \dot{q}_P \tag{3.70}$$

and observe that

$$\dot{T}_P = \dot{q}_P^T \tilde{B}_P u \tag{3.71}$$

This motivates the Lyapunov function

$$U = \frac{1}{2} \delta \dot{q}_P^T M_P \delta \dot{q}_P + \frac{1}{2} \delta q_P^T K_1 \delta q_P \tag{3.72}$$

where $\delta q_P = q_P - q_{P_{ref}}(t)$. For the simplest case that $q_{P_{ref}}(t) = $ constant, then it is easy to verify that the Lyapunov function derivative is

$$\dot{U} = \delta \dot{q}_P^T \left[\tilde{B}_P u + K_1 \delta q_P \right] \tag{3.73}$$

and selecting the bracketed term to equal $-K_2\delta\dot{q}_P$ (so that $\dot{U}$ is never positive), we are led to the global stability condition

$$\bar{B}_P u = -[K_1\delta q_P + K_2\delta\dot{q}_P] \qquad (3.74)$$

Since $\bar{B}_P$ is a 3×4 matrix, it is evident that u is underdetermined and we are free to introduce an optimization criterion to select a particular control satisfying Eq. (3.74). One attractive possibility is to minimize $u^T u$; this gives the minimum actuator torque controller

$$u = -\bar{B}_P^T\left(\bar{B}_P\bar{B}_P^T\right)^{-1}[K_1\delta q_P + K_2\delta\dot{q}_P] \qquad (3.75)$$

For the trajectory tracking case, in which we desire to stabilize the motion with respect to a prescribed reference motion, the situation is more complicated. Suppose that the reference trajectory $q_{P_{ref}}(t)$ and an associated control $u_{ref}(t)$ are determined consistent with the system dynamics [for example, using Eqs. (3.59)–(3.69)]. Then it follows that the payload dynamics at every instant on the actual and reference trajectories satisfy

$$\begin{aligned} M_P\bar{q}_P + \bar{G}_P &= \bar{B}_P u \\ M_{P_{ref}}\bar{q}_{P_{ref}} + \bar{G}_{P_{ref}} &= \bar{B}_{P_{ref}}u_{ref} \end{aligned} \qquad (3.76)$$

and it also follows that the Lyapunov function [Eq. (3.72)] has the time derivative

$$\dot{U} = \delta\dot{q}_P^T\left[\bar{B}_P u - \bar{B}_{P_{ref}}u_{ref} + K_1\delta q_P - \delta\bar{G}_P - \delta M_{P_{ref}}\bar{q}_{P_{ref}} + \dot{M}_P\delta\dot{q}_P\right] \qquad (3.77)$$

Setting the bracketed term to $-K_2\delta\dot{q}_P$ gives the stabilizing control condition

$$\bar{B}_P u = \bar{B}_{P_{ref}}u_{ref} - [K_1\delta q_P + K_2\delta\dot{q}_P] + \left[\delta\bar{G}_P + \delta M_{P_{ref}}\bar{q}_{P_{ref}} - \dot{M}_P\delta\dot{q}_P\right] \qquad (3.78)$$

and for the case of minimum control torque, a particular solution of Eq. (3.78) gives the nonlinear feedback law

$$\begin{aligned} u = \bar{B}_P^T\left(\bar{B}_P\bar{B}_P^T\right)^{-1} \Big\{ &\bar{B}_{P_{ref}}u_{ref} - [K_1\delta q_P + K_2\delta\dot{q}_P] \\ &+ \left[\delta\bar{G}_P + \delta M_{P_{ref}}\bar{q}_{P_{ref}} - \dot{M}_P\delta\dot{q}_P\right]\Big\} \end{aligned} \qquad (3.79)$$

This law, while guaranteeing stability (neglecting model errors), is cumbersome to implement due to the detailed computation required to produce all of the nonlinear terms. Note that the payload coordinates $q_P = [\theta_3 \ x_{c3} \ y_{c3}]^T$ may not be directly measurable. For example, assume that the measurable quantities are $q_L = [\theta_1 \ \theta_2]^T$ and $q_R = [\theta_6 \ \theta_5]^T$, and the time derivaties thereof; then it is easy to verify from geometry that the payload coordinates are computable as follows

$$\begin{aligned} \theta_3 &= tan^{-1}\left[\frac{y_Q - y_P}{x_Q - x_P}\right] = tan^{-1}\left[\frac{(l_5 sin\theta_6 + l_4 sin\theta_5) - (l_1 sin\theta_1 + l_2 sin\theta_2)}{(D + l_5 cos\theta_6 + l_4 cos\theta_5) - (l_1 cos\theta_1 + l_2 cos\theta_2)}\right] \\ x_{c_3} &= \tfrac{1}{2}(x_Q + x_P) = \tfrac{1}{2}[(D + l_5 cos\theta_6 + l_4 cos\theta_5) + (l_1 cos\theta_1 + l_2 cos\theta_2)] \\ y_{c_3} &= \tfrac{1}{2}(y_Q + y_P) = \tfrac{1}{2}[(l_5 sin\theta_6 + l_4 sin\theta_5) + (l_1 sin\theta_1 + l_2 sin\theta_2)] \end{aligned} \qquad (3.80)$$

and the time derivative $\dot{q}_P = [\dot{\theta}_3 \ \dot{x}_{c_3} \ \dot{y}_{c_3}]^T$ follows from differentiation of Eq. (3.80).

As an alternative to the above developments, and to obtain a direct output error feedback form for the control law, we can observe the following kinematic form for the work rate of the control torques

$$\dot{T} = u_1 \dot{\theta}_1 + u_2 \dot{\theta}_2 + u_6 \dot{\theta}_6 + u_5 \dot{\theta}_5 = \left\{ \begin{array}{c} \dot{q}_L \\ \dot{q}_R \end{array} \right\}^T u = \dot{q}_L^T u_L + \dot{q}_R^T u_R \qquad (3.81)$$

and it is obvious by inspection that setting $u_L = -K_{2L}\dot{q}_L$, $u_R = -K_{2R}\dot{q}_R$ will decrease T for all nonzero motion of the system. This energy dissipative control suggests the following output error feedback law for controlling the departure motion relative to the reference trajectory

$$u = u_{ref}(t) - \left\{ K_1 \left(\begin{array}{c} \delta q_L \\ \delta q_R \end{array} \right) + K_2 \left(\begin{array}{c} \delta \dot{q}_L \\ \delta \dot{q}_R \end{array} \right) \right\} \qquad (3.82)$$

where the 4×4 positive definite gain matrices have the structure $K_i = \begin{bmatrix} K_{iL} & 0 \\ 0 & K_{iR} \end{bmatrix}$.

It can be verified that the control law of Eq. (3.82) is guaranteed to be globally stabilizing only for the case that $q_{ref} = $ constant. While global asymptitic stability is not guaranteed during the time interval $\{t_0 < t < t_f\}$, it is guaranteed during the interval $\{t > t_f\}$, for all reference maneuvers satisfying the boundary conditions of Eq. (3.69). These developments can be better appreciated in the light of some illustrative numerical examples, as provided in the next section.

Cooperative Control: A Numerical Example

To illustrate the above discussion, we consider each link of the robots to be 1 m long and to have a mass of 1 kg. The distance D between the shoulder joints is taken as 0.75 m, and the nominal initial and desired target values of five angles are listed in Table 3.1. The inverse kinematic process of Eqs. (3.59)–(3.69) was used to compute the solution shown in Figure 3.2. All the intial conditions were then perturbed by moderately large angles (order of 10°), and the feedback control law of Eq. (3.82) was used.

A typical controlled response from large inital disturbances is shown in Figure 3.3. Notice that the order of 10° initial errors are less than 0.5° by the nominal final time of 10 s; however, a few more seconds of terminal control are required to effectively null the errors. The weight matrices [in Eq. (3.64)] were $W_u = I$, $W_c = 0$, and the control gains [in Eq. (3.82)] were $K_1 = 0.5I$, $K_2 = 0.2I$; these affect the controlled response, however we found a large family of feasible values. From evaluating the response using several other intitial conditions and variations in the selections of the control gains and weight matrices, we confirmed that a wide range of choices give excellent tracking stability over a large domain of intital conditon errors. Thus the control law of Eq. (3.82) seems to be an attractive candidate for practical applications.

Table 3.1. Initial and final angles for the nominal maneuver

	$\theta_1[deg]$	$\theta_2[deg]$	$\theta_3[deg]$	$\theta_6[deg]$	$\theta_5[deg]$	time[s]
initial:	121.0430	40.0323	00.0000	58.9570	139.9677	0
target:	137.2041	-10.3342	90.0000	117.3017	142.3095	10

The above results have been extended to more general multilink configurations, including base motion, and they have beeen successfully validated in an experimental study [Yale 1993], including consideration of the case of the robot arms mounted on a movable base.
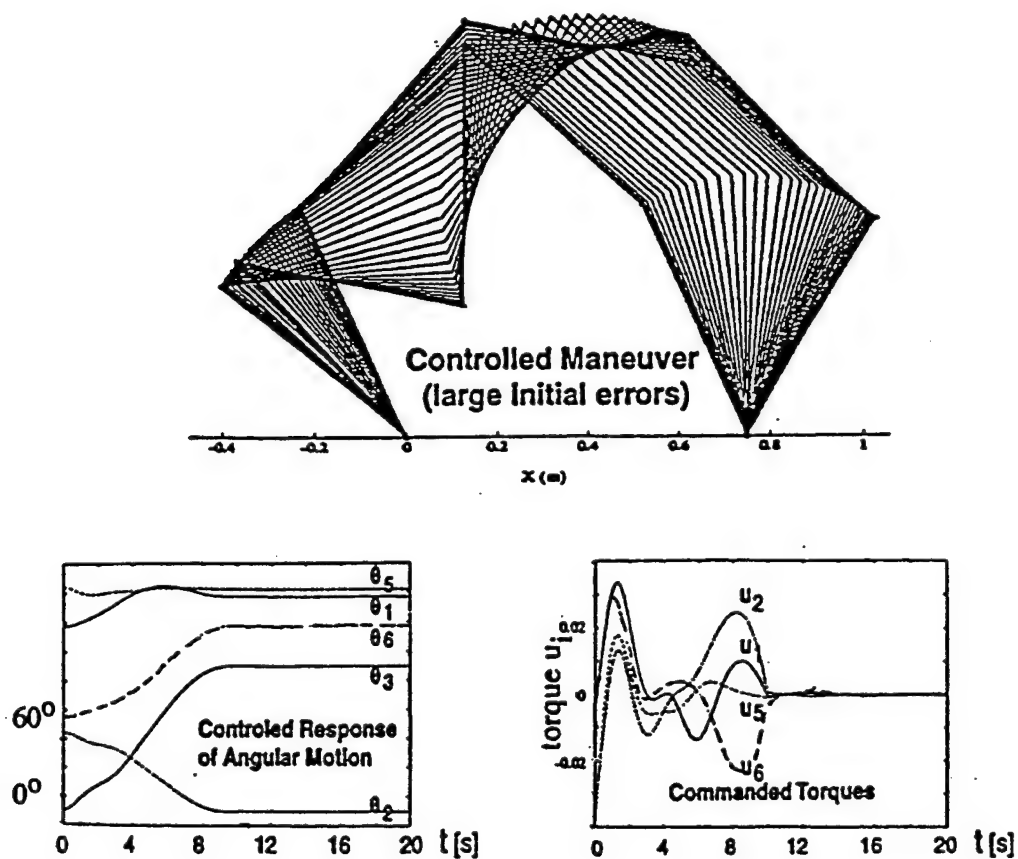
Figure 3.3. Controlled response from disturbed initial conditions

3.6 DYNAMICS, STABILITY, AND CONTROL OF A DISTRIBUTED PARAMETER SYSTEM

In Figure 3.4 we consider control of a rigid hub with four cantilevered flexible appendages. We consider the appendages to be identical uniform flexible beams and make the Euler-Bernoulli assumptions of negligible shear deformation and distributed rotary inertia. Each beam is cantilevered rigidly to the hub and has a finite tip mass. Motion is restricted to the horizontal plane and, control torque $u(t)$ acting on the hub is the only external effect considered.

We are interested in a class of rest-to-rest maneuvers, and under the previously mentioned assumptions, we can show that the beams will deform in the antisymmetric fashion (Figure 3.4), with the configuration's instantaneous mass center remaining at the hub's geometric center. Also, because of the assumed antisymmetric deformation of the beams, in this section we need to concern ourselves only with the deformation $y(x, t)$ of a single beam. We subsequently relax this restriction, to permit more general kinematic assumptions and the analysis that flows form it. We adopt the continuum viewpoint and avoid introducing spatial approximations in the application of Lyapunov stability concepts; the resulting control law and stability arguments will therefore apply rigorously to the distributed parameter system. The hybrid system of ordinary and partial differential equations governing the dynamics of this system is readily obtained from Hamilton's principle to be [Junkins 1993]

$$
\begin{aligned}
I_{hub}\frac{d^2\theta}{dt^2} &= u + 4(M_0 - S_0 L_0) \\
-(M_0 - S_0 L_0) &= \int_{L_0}^{L} \rho x \left(\frac{\partial^2 y}{\partial t^2} + x\frac{d^2\theta}{dt^2}\right)dx + m_t\left(L\frac{d^2\theta}{dt^2} + \frac{\partial^2 y}{\partial t^2}\Big|_{L}\right) + \text{HOT} \\
\rho\left(\frac{\partial^2 y}{\partial t^2} + x\frac{d^2\theta}{dt^2}\right) &+ EI\frac{\partial^4 y}{\partial x^4} = 0 + \text{HOT}
\end{aligned}
$$

$$(3.83)$$

where

$$
\begin{aligned}
\rho &= \text{assumed constant mass/unit length of the beams} \\
EI &= \text{assumed constant bending stiffness of the beams} \\
(M_0, S_0) &= \text{bending moment and shear force at the root of the beam} \\
\theta &= \text{hub inertial rotation} \\
m_t &= \text{mass of the tip mass} \\
(L, L_0) &= \text{distance from the hub center to the beam tip and the hub radius}
\end{aligned}
$$

In Eq. (3.83), we denote higher-order terms by HOT to indicate other *known* linear and nonlinear effects (such as rotational stiffening, and shear deformation). The most fundamental developments do not consider these higher-order effects; however, we selectively discuss the generalizations that accommodate these effects as well. Of course, in general, there are *unknown* model errors and disturbances as well, and a practical control scheme must be stable in the presence of reasonable model errors. The boundary conditions on Eqs. (3.83) are:
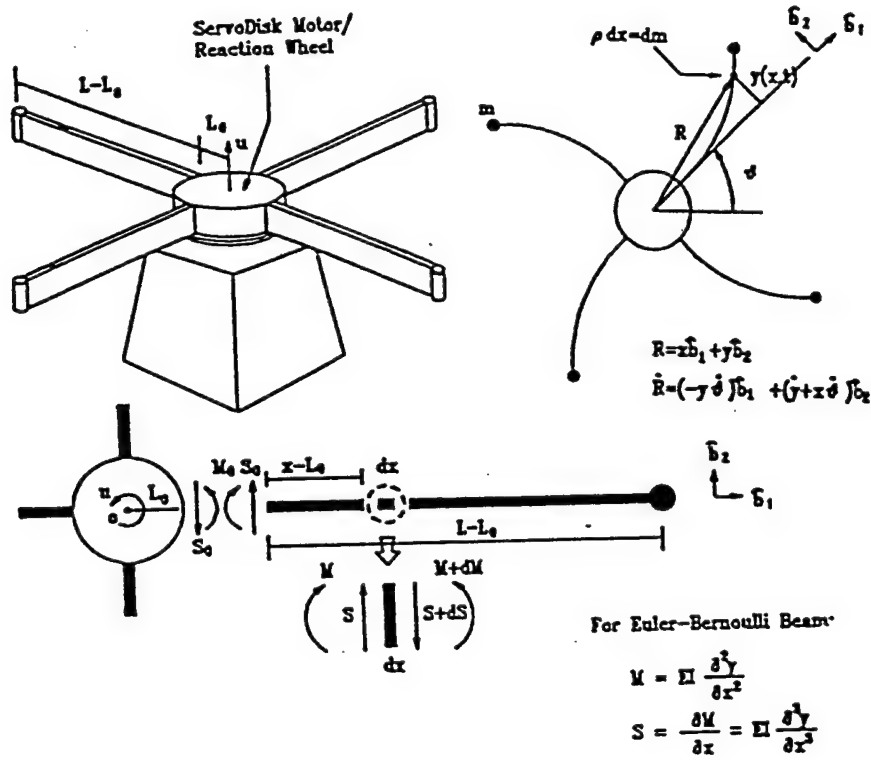
Figure 3.4. Texas A&M flexible structure maneuver experiment

at $x = L_0$: $y(t, L_0) = \frac{\partial y}{\partial x}\big|_{L_0} = 0$ (clamped beam geometric B.C.s)

at $x = L$: $\frac{\partial^2 y}{\partial x^2}\big|_L = 0$ (moment)   (3.84)

$$\frac{\partial^3 y}{\partial x^3}\Big|_L = \frac{m_t}{EI}\left(L\frac{d^2\theta}{dt^2} + \frac{\partial^2 y}{\partial t^2}\Big|_L \right) \quad \text{(shear)}$$

The total energy of the system (constant in the absence of control or disturbances) is

$$2E = I_{hub}\left(\frac{d\theta}{dt}\right)^2 + 4\left[\int_{L_0}^{L} \rho\left(\frac{\partial y}{\partial t} + x\frac{d\theta}{dt}\right)^2 dx \right.$$
$$\left. + \int_{L_0}^{L} EI\left(\frac{\partial^2 y}{\partial x^2}\right)^2 dx + m_t\left(L\frac{d\theta}{dt} + \frac{\partial y}{\partial t}\Big|_L \right)^2 \right] \quad (3.85)$$

Motivated by results published in the recent literature (Refs. 3–5,19,21,22), we investigate the following weighted energy function as a candidate Lyapunov function:

$$2U = a_1 I_{hub}\dot{\theta}^2 + a_2(\theta - \theta_f)^2$$
$$+ 4a_3\left[\int_{L_0}^{L} \rho\left(\frac{\partial y}{\partial t} + x\dot{\theta}\right)^2 dx + \int_{L_0}^{L} EI\left(\frac{\partial^2 y}{\partial x^2}\right)^2 dx + m_t\left(L\dot{\theta} + \frac{\partial y}{\partial t}\Big|_L\right)^2\right] \quad (3.86)$$

where the positive weighting coefficients a_i are included to allow relative emphasis on the three contributors to the "error energy" of the system. Note that this is one of many possible ways to weight the mechanical system error energy, and merely provides one illustration of an approach. It is physically reasonable to consider placing relative emphasis upon dissipating subsets of mechanical energy as a control strategy, because some energy subsets are obviously more degrading of system performance objectives than others in practical applications. Since θ does not appear in the total mechanical energy of Eq. (3.85), the total energy of Eq. (3.85) is only positive semidefinite. We have added the positive "torsional spring energy" term $a_2(\theta - \theta_f)^2$ in Eq.(3.86) as a pseudoenergy to make the target final state

$$\left(\theta, \dot{\theta}, y(x, t), \frac{\partial y(x, t)}{\partial t}\right)_{desired} = (\theta_f, 0, 0, 0)$$

be the global minimum of U. It is obvious by inspection that imposing $a_i > 0$ in Eq. (3.86) guarantees that $U \geq 0$ and that indeed the global minimum of $U = 0$ occurs only at the desired state (we wish to begin at rest and rotate to a new angular position $\theta = \theta_f$, suppressing vibration enroute and returning to zero flexural deformation in the final position). Differentiation of Eq. (3.86), substitution of the equations of motion [Eqs. (3.83) and (3.84)], and considerable calculus leads to the weighted power

$$\dot{U} = \frac{dU}{dt} = \dot{\theta}\left[a_1 u + a_2(\theta - \theta_f) + 4(a_3 - a_1)(L_0 S_0 - M_0)\right] \quad (3.87)$$

Since we require that $\dot{U} \leq 0$ to guarantee stability, we set the term in brackets to $-a_4\dot{\theta}$, and this leads to the control law

$$u = -\frac{1}{a_1}\left[a_2(\theta - \theta_f) + a_4\dot{\theta} + 4(a_3 - a_1)(L_0 S_0 - M_0)\right] \quad (3.88)$$

In [Oh 1992], we developed a shortcut based upon the work/energy rate method that avoids most of the algebra and calculus required to establish the weighted power expressions like Eq. (3.87), we could make use of this idea here to arrive more efficiently at Eq. (3.87).

From Eqs. (3.87) and (3.88), and considering all possible values for the a_i, we see that the following *linear, spatially discrete* output feedback law globally stabilizes this distributed-parameter system:

$$u = -\left[g_1(\theta - \theta_f) + g_2\dot{\theta} + g_3(L_0S_0 - M_0)\right]; \qquad (3.89)$$
$$g_1 \geq 0, \quad g_2 \geq 0, \quad g_3 > -4 \qquad \text{for stability}$$

This control law is elegant. Notice that the rigorous stability proof does not depend on introducing spatial discretization methods such as the finite element method. Furthermore, we have verified from root locus calculations that the gain stability boundaries are apparently exact in this case (to 10 digits for the first 10 eigenvalues). Of important practical consequence, notice that controllers based on this law of Eq. (3.89) are easy to implement since no state estimation is required. The root shear and bending moment can be measured by using conventional strain gauges. The value and sign of the shear/moment feedback gain $g_3 = 4(a_3 - a_1)/a_1$ depends on whether we wish to emphasize dissipation of the beam vibration energy (for $a_3 > a_1$) or the energy of hub motion (for $a_3 < a_1$), as is evident from Eq. (3.86).

Since $\dot{U} = -a_4\dot{\theta}^2$ is not an explicit, negative definite function of the subset of state variables

$$\left[\theta, y(x,t), \frac{\partial y(x,t)}{\partial t}\right]$$

the stability arguments implicitly depend on the truth *that all infinity of the antisymmetric modes of motion of this structure*, have generally nonzero hub angular velocity ($\dot{\theta}$). Note under the kinematic assumptions leading to Eqs. (3.83), only antisymmetric modes are present, and no nontrivial motion can exist while the hub angular velocity vanishes identically for finite time intervals. A more elegant proof of global asymptotic stability using the feedback law of Eq. (3.89) can be done by applying Theorem 3.9. This has been carried to completion in [Mukherjee 1992], including consideration of the cases in which we relax the antisymmetric deformation assumption applied in deriving Eqs. (3.83), thereby admitting a richer and more general set of motions (the four beams are described by four distinct functions of space and time, and there are now four PDEs and one hybrid differential/integral equation). For this more general configuration, it can be shown that a single hub actuator cannot provide rigorous asymptotic stability, because only an antisymmetric subset of the modes are controllable by a hub actuator (physically/qualitatively, the uncontrollable modes have identical adjacent beams moving in opposition, which results in equal and opposite root moments and, because of this cancellation, zero hub motion). For rest-to-rest maneuvers, however, only the antisymmetric modes considered here are disturbable (by a hub torque actuator), and they are also controllable. Thus, for the assumptions/constraints imposed in deriving the differential equation model developed above, the control law of Eq. (3.89) is globally stabilizing.

It is significant that this same linear feedback law of Eq. (3.89) maintains its globally stabilizing character even when the Euler-Bernoulli assumptions are relaxed to include the most common additional linear and nonlinear effects. In particular, we have verified that closed-loop stability is maintained when we include the following: rotational stiffening, Coriolis kinematic coupling terms, aerodynamic

drag, shear deformation, beam rotary inertia, and finite inertia of the tip mass. The verification of these truths requires appropriate modifications of the kinetic and potential energy functions and, of course, the differential equations of motion must be generalized consistently. In particular, $\dot{U} = -a_4\dot{\theta}^2$ can vanish only if the conditions $\dot{\theta} = 0$, $\ddot{\theta} = 0$ can be encountered at some point other than U=0 (the target state), so the nonlinear proof proceeds directly from the closed-loop system differential equations by showing that the condition $\dot{\theta} = \ddot{\theta} = 0$ occurs only at the desired equilibrium:

$$\left(\theta, \dot{\theta}, y(x,t), \frac{\partial y(x,t)}{\partial t}\right)_{desired} = (\theta_f, 0, 0, 0)$$

In short, global stability of the system using the simple linear output feedback control law of Eq. (3.89) has been found to be very forgiving of the usual variations in modeling assumptions and, therefore, modeling errors. In this section, an indirect method of Lyapunov for analyzing the motion of a nonlinear system near the equilibrium state has been presented, and also a method for generating globally stabilizing feedback control law for distributed-parameter structural systems has been discussed as an important application of Lyapunov direct method.

We have discussed the vibration suppression problem of the hub-appendage configuration in the previous sections. As discussed above, the constant gain linear feedback control law works poorly if we try to use the same constant gains for both large angular motions and for small terminal motions. This is because the large gains required for effective vibration suppression and disturbance rejection to accurately isolate the target state are typically several orders of magnitude too large for the en-route portion of the maneuver (*i.e.*, the large gains appropriate for vibration suppression, when used during a large-angle maneuver, typically result in significant θ overshoots and, often, actuator saturation). Also, the large initial torque command typically introduces a large vibratory transient into highly flexible structures. From a qualitative point of view, if we wish to maneuver a highly flexible structure while suppressing vibration, then it is unlikely that we should initiate this process by hitting the structure with a large hammer! To obtain a control law more appropriate for near-minimum-time large-angle maneuvers with vibration suppression, stable tracking-type feedback control laws discussed in this section can be applied.

Consider briefly the near-minimum-time maneuver of a rigid body. We know that the strict minimum-time control is a bang-bang law which, for the rest-to-rest maneuver-to-the origin case, saturates negatively during the first half of the maneuver and positively during the last half of the maneuver [Junkins 1986, 1991, 1993], [Meirovitch 1987], [Singh 1989], [Breakwell 1981], [Slotine 1991], [VanderVelde 1983]. From an implementation point of view, the instantaneous switches of the bang-bang law are sometimes troublesome because (1) no torque-generating device exists that can switch instantaneously; (2) when generalized and applied to a flexible structure, the bang-bang class of controls excite poorly modeled

higher modes; and (3) the switch times (and, therefore, the dynamics of the actual system) are usually very sensitive to modeling errors.

An attractive family of *parameterized sharpness* approximations of the switch function has been introduced to modify the admissible controls in near-minimum-time control formulations. The approximation presented in [Thompson 1989] and [Byers 1990], involves transcendental functions, but recent analytical/experimental work [Junkins 1991, 1993] indicates that a much simpler piecewise continuous spline approximation of the switching function is attractive from an implementation point of view. Using this approach, a typical near-minimum-time control law (for single axis, rest-to-rest maneuver of a rigid body) has the form

$$I\ddot{\theta} = u = \pm u_{max} f(\Delta t, t_f, t) \tag{3.90}$$

where t_f is the maneuver time and $\alpha = \Delta t / t_f$. We choose the (+) sign if $\theta_f > \theta_o$. As a torque shaping function, we adopt the smooth sign function approximation $f(\Delta t, t_f, t)$:

$$f(\Delta t, t_f, t) = \begin{cases} \left(\frac{t}{\Delta t}\right)^2 \left[3 - 2\left(\frac{t}{\Delta t}\right)\right], & \text{for } 0 \leq t \leq \Delta t \\ 1, & \text{for } \Delta t \leq t \leq \frac{t_f}{2} - \Delta t \equiv t_1 \\ 1 - 2\left(\frac{t - t_1}{2\Delta t}\right)^2 \left[3 - 2\left(\frac{t - t_1}{2\Delta t}\right)\right], & \text{for } t_1 \leq t \leq \frac{t_f}{2} + \Delta t \equiv t_2 \\ -1, & \text{for } t_2 \leq t \leq t_f - \Delta t \equiv t_3 \\ -1 + \left(\frac{t - t_3}{\Delta t}\right)^2 \left[3 - 2\left(\frac{t - t_3}{\Delta t}\right)\right], & \text{for } t_3 \leq t \leq t_f \end{cases}$$

Adopting the positive sign, Eq. (3.90) integrates to yield

$$\dot{\theta}(t) = \dot{\theta}_0 + \frac{u_{max}}{I} \int_{t_0}^{t} f(\Delta t, t_f, \tau) d\tau \tag{3.91a}$$

$$\theta(t) = \theta_0 + (t - t_0)\dot{\theta}_0 + \frac{u_{max}}{I} \int_{t_0}^{t} \int_{t_0}^{\tau_1} f(\Delta t, t_f, \tau_2) d\tau_2 d\tau_1 \tag{3.91b}$$

The integrations in Eqs. (3.91) can be carried out in terms of elementary functions, which are not presented here for the sake of brevity; the results of these integrations give Eqs. (3.93), (3.94) below. Figure 3.5 shows a maneuver resulting from these integrations for a typical selection of parameters ($\alpha = 0.25$, $u_{max} = 400$ oz-in.), and a $40°$ rest-to-rest maneuver of a rigid approximation of the structure in Figure 3.4 and Table 3.2. For rest-to-rest maneuvers, we impose the boundary conditions:

$$\begin{aligned} \text{at } t_0 = 0: \quad & \theta(0) = \theta_0, \quad \dot{\theta}(0) = 0 \\ \text{at time } t_f: \quad & \theta(t_f) = \theta_f, \quad \dot{\theta}(t_f) = 0 \end{aligned} \tag{3.92}$$

and upon carrying out the integrations implied in Eq. (3.91), we obtain the useful relationship

Table 3.2. Texas A&M maneuverable flexible structure: configuration parameters

Total undeformed system inertia, I	2128, oz-s^2-in.
Hub radius, L_0	5.5470, in.
Hub center to tip mass, L	51.07, in.
Tip mass, m_t	0.15627, oz-s^2/in.
Appendage modules of elasticity, E	161.6×10^6, oz/in.^{2}
Inertia of bending section, I	0.000813, in.^{4}
Mass density of appendage/length, ρ	0.003007, oz-s^2/in.^{2}
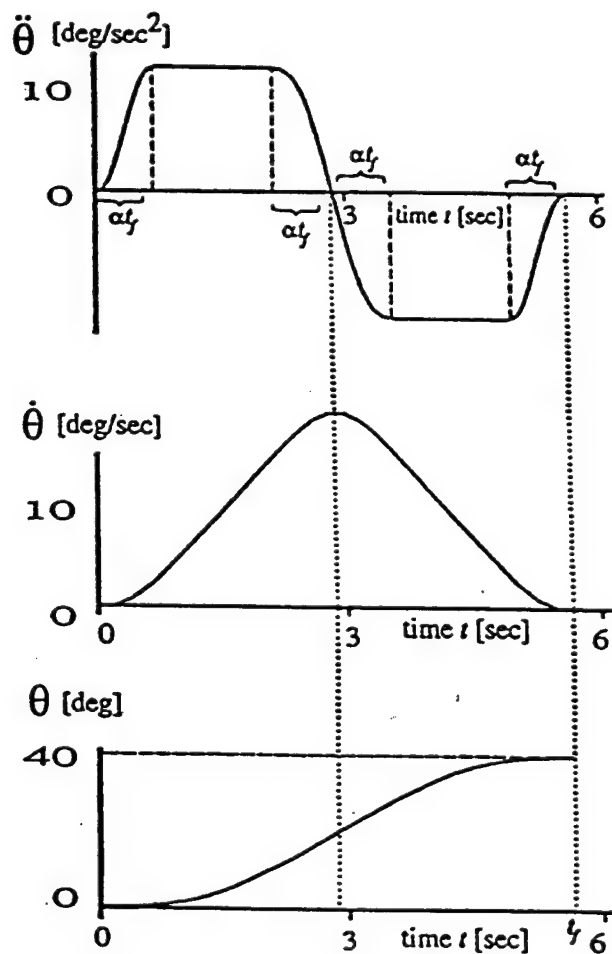
Figure 3.5. Torque-shaped rigid body maneuver

$$\theta_f - \theta_0 = \left(\frac{u_{max}}{I}\right)\left[\frac{1}{4} - \frac{1}{2}\alpha - \frac{1}{10}\alpha^2\right]t_f{}^2, \qquad \Delta t = \alpha t_f, \qquad 0 < \alpha < \frac{1}{4} \qquad (3.93)$$

or

$$t_f = \left\{\frac{I(\theta_f - \theta_0)}{u_{max}[(1/4) - (1/2)\alpha + (1/10)\alpha^2]}\right\}^{\frac{1}{2}} \qquad (3.94)$$

In Eq. (3.94), we see the explicit tradeoff between torque shaping α, target maneuver time t_f, maneuver angle $\theta_f - \theta_0$, and maximum angular acceleration u_{max}/I. Obviously, Eq. (3.93) can be inverted for any of these as a function of the remaining parameters. If we set $\alpha = \Delta t/t_f = 0$, of course, we obtain the well known special case result expressing the relationship between the minimum time, maneuver angle, inertia, and saturation torque for bang-bang control. It is obvious that selection of α controls the sharpness of the switches, with $\alpha = 0$ corresponding to bang-bang control (instantaneous switches) and $\alpha = 0.25$ being the smoothest member of this family of torque-shaped maneuvers. Figure 3.6 shows the rigid body maneuver time t_f vs α, from Eq. (3.94), whereas Figure 3.7 shows the residual total energy (at time t_f) when the torque-command $u_{ref} = u_{max}f(\alpha t_f, t_f, t)$ is applied to simulate the flexible body response [first six modes from a discrete assumed mode model (Chapter 4 of [Junkins 1993] of order 20). Notice (Figure 3.7) that open-loop torque shaping reduces residual vibration at time t_f by three orders of magnitude ($\alpha = 0.1$) with only a modest ten percent increase over the theoretical minimum time rigid body maneuver ($\alpha = 0$). The preceding results and [Junkins 1991, 1993], [Thompson 1989], [Vadali 1990], and [VanderVelde 1990], support the intuitively obvious truth that applying judiciously smoothed bang-bang controls such as Eq. (3.90) to generate an open-loop maneuver of a flexible body can result in near negligible structural vibration for sufficiently slow maneuvers (small u_{max} and large α) and neglecting disturbance torques. Of course, unmodeled disturbances, control implementation errors, and model errors can be expected to negate some of these apparent gains. However, sharper control switches obviously increase the probability that higher frequency, less well modeled modes will be excited and, therefore, robustness with respect to model errors is generally more of an issue for bang-bang control than for smoother torque profiles. Even for relatively small departures (slightly smoothed switches) from bang-bang control, torque-shaped maneuvers of highly flexible structures typically enjoy a reduction of several orders of magnitude in residual vibration. Thus, the overall maneuver time (including terminal vibration suppression) can be reduced significantly by torque shaping.

These observations suggest the following strategy: Use an optimized shaped-input profile to establish a "trackable" a priori reference rigid (or reduced-order flexible) body maneuver; then, based on real-time measurements of the actual flexible body's departure from this smooth reference motion, superimpose a perturbation feedback control on the reference shaped-torque history that stabilizes the departure motion from the reference motion. Also of significance, it is usually desirable
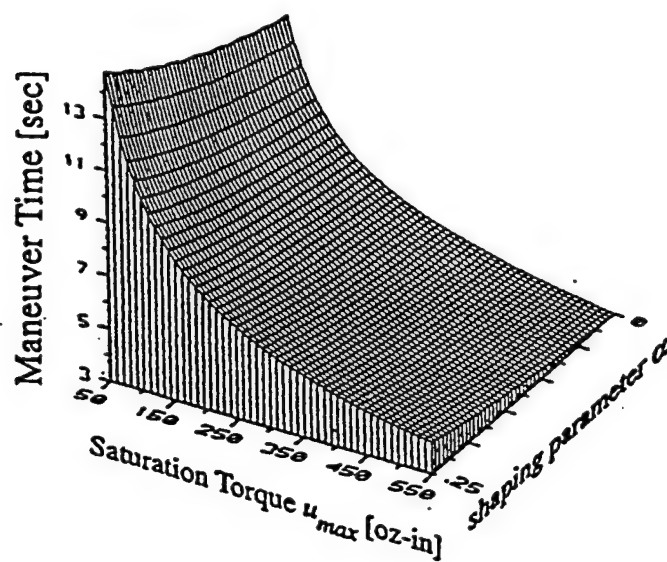
Figure 3.6. Rigid body maneuver time vs saturation torque and torque-shaped parameter
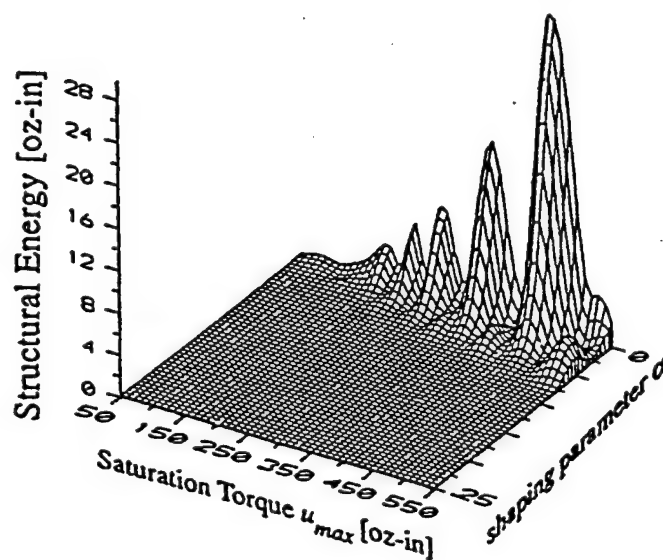

Figure 3.7. Flexible body open-loop residual vibration energy vs saturation torque and torque-shaped parameter

to select the reference torque profile parameters (*e.g.*, u_{max}, α, etc.) to consider the available sensor and actuator dynamics and thereby make the commanded torque history more nearly achievable physically.

Pursuing this logic judiciously, attractive tracking-type feedback control laws can be established for near-minimum-time, large angle maneuvers. Since bang-bang flexible body controllers are sensitive to modeling and control implementation errors, we seek control laws that are a smooth torque-shaped compromise between the competing objectives of minimizing: (1) maneuver time, (2) residual vibration, and (3) sensitivity of closed-loop performance measures with respect to model and control implementation errors.

We adopt a reference rigid body maneuver $\{\theta_{ref}(t), \dot{\theta}_{ref}(t), \ddot{\theta}_{ref}(t) = u_{ref}/I\}$ satisfying Eqs. (3.90)–(3.94), where I is the undeformed moment of inertia of the structure, and we have implicitly selected α, u_{max} and computed the corresponding t_f from Eq. (3.94) for specified initial and final angles. For designing a globally stable tracking controller, the candidate error energy Lyapunov function can be established by considering Eq. (3.86) as

$$
\begin{aligned}
2U \;=\; & a_1 I_{hub}\delta\dot{\theta}^2 + a_2\delta\theta^2 + 4a_3\left\{ \int_{L_0}^{L} \rho\left[\delta\frac{\partial y}{\partial t} + x\delta\dot{\theta}\right]^2 dx \right. \\
& \left. + \int_{L_0}^{L} EI\left(\delta\frac{\partial^2 y}{\partial x^2}\right)^2 dx + m_t\left[L\delta\dot{\theta} + \delta\frac{\partial y}{\partial t}\Big|_{L}\right]^2 \right\}
\end{aligned}
\tag{3.95}
$$

where $\delta(\;) \equiv (\;) - (\;)_r$ and the $(\;)_r$ quantities are evaluated along the open-loop flexible body solution of Eqs. (3.83) with $u(t) = u_{ref}(t)$. Considering Eqs. (3.87) and, the time derivative of U is given by

$$
\dot{U} = (\dot{\theta} - \dot{\theta}_r)\left\{ \begin{array}{l} a_1 u - a_1 u_{ref} + a_2(\theta - \theta_r) \\ + 4(a_3 - a_1)[(L_0 S_0 - M_0) - (L_0 S_0 - M_0)_r] \end{array} \right\}
\tag{3.96}
$$

Pursuing the objective of globally stable control, it is clear that setting the [ ] term equal to $-a_4(\dot{\theta} - \dot{\theta}_r)$ leads to the following globally stabilizing [with $\dot{U} = -a_4(\dot{\theta} - \dot{\theta}_r)^2$] control law:

$$
u = u_{ref}(t) - \left\{ g_1(\theta - \theta_r) + g_2(\dot{\theta} - \dot{\theta}_r) + g_3[(L_0 S_0 - M_0) - (L_0 S_0 - M_0)_r] \right\}
\tag{3.97}
$$

To enable easy implementations, the following structure for a tracking control law can be hypothesized:

$$
u = u_{ref}(t) - \left\{ g_1(\theta - \theta_{ref}) + g_2(\dot{\theta} - \dot{\theta}_{ref}) + g_3[(L_0 S_0 - M_0) - (L_0 S_0 - M_0)_{ref}] \right\}
\tag{3.98}
$$

where it is easy to show that the root moment for the special case of a reference (rigid body) motion is proportional to the angular acceleration:

$$
(L_0 S_0 - M_0)_{ref} = [\rho(L^3 - L_0^3)/3 + m_t L^2]\ddot{\theta}_{ref}(t)
\tag{3.99}
$$

Obviously, the globally stabilizing control law of Eq. (3.97) is similar to the conjectured law (for practical implementation) of Eq. (3.98), the difference being that Eq. (3.98) requires presolution for the open-loop rigid body ( )$_{ref}$ quantities, whereas, the globally stabilizing control law of Eq. (3.97) requires solution for the open-loop flexible body ( )$_r$ quantities from the partial differential equations. Since near-minimum-time control implies a certain urgency(!), it is obvious that the negligible computational overhead of Eq. (3.98) is more attractive than Eq. (3.97) from the point of view of real-time implementations. For the purpose of finding the region possessing Lyapunov stability, substitute Eq. (3.98) into Eq. (3.96)

$$\dot{U} = -a_1(\dot{\theta} - \dot{\theta}_r)\Big\{g_2(\dot{\theta} - \dot{\theta}_r) + \big[g_1\Delta\theta + g_2\Delta\dot{\theta} + g_3\Delta(L_0S_0 - M_0)\big]\Big\} \qquad (3.100)$$

The Lyapunov stability condition comes from requiring $\dot{U}$ of Eq. (3.100) to be negative; a sufficient condition is

$$|\dot{\theta} - \dot{\theta}_r| > \mu \equiv \frac{1}{g_2}\big|g_1\Delta\theta + g_2\Delta\dot{\theta} + g_3\Delta(L_0S_0 - M_0)\big| \qquad (3.101)$$

If the angular velocity tracking error $|\dot{\theta} - \dot{\theta}_r|$ exceeds μ, then $\dot{U}$ is negative and apparently U decreases until encountering the region bounded by Eq. (3.101). It is further apparent that the Δ quantities on the right side of Eq. (3.101) are finite and (pre-)computable differences between open-loop flexible ( )$_r$ and rigid body ( )$_{ref}$ motions. Thus, an upper bound μ can be established directly by precomputation of a family of two open-loop motions and the use of a particular set of feedback gains. Equation (3.101) thus determines an angular velocity variable boundary defining a region Γ near the ( )$_{ref}$ motion. Note that large motions are globally attracted to Γ because $\dot{U} \leq 0$ everywhere outside of this region. Thus, the control law of Eq. (3.98) is almost globally stabilizing, and the only region where asymptotic stability is not guaranteed is the small Γ boundary layer region near the target trajectory. Furthermore, the right side of Eq. (3.101) is essentially a measure of how nearly the reference target trajectory satisfies the flexible body equations of motion; a judicious choice of the shaping parameters defining the target trajectory and the associated reference control input can usually be made to result in μ (and therefore Γ) being sufficiently small.

A bounded-input/bounded-output (BIBO) viewpoint of stability can be used to establish some insight into the motion in the Γ region. Departure motion differential equations for $\delta(\ ) = (\ ) - (\ )_r$ quantities can be obtained by differencing Eqs. (3.83), driven by the control law of Eq. (3.98), from the rigid body equations of motion, driven by u_{ref}. Upon formulating these equations, one can verify that the departure motion is governed by a linear, otherwise asymptotically stable, system of differential equations, forced by the known Δ terms that appear in Eq. (3.101). The $\delta(\ )$ motion in the Γ region is thus bounded because the Δ forcing terms are bounded; the finite maxima of these terms can be found by direct calculation. The resulting departure motion is therefore bounded everywhere in the Γ region,

which was already known to have a (typically small) finite dimension μ. Since the actual numerical bounds on the Δ and μ quantities can be made arbitrarily small (depending on how nearly the user-defined reference trajectory is made to satisfy the open-loop equations of motion), we have a very elegant theoretical and practical situation vis-à-vis stability of the closed-loop tracking motion. We see that the closed-loop motion is globally attracted to the controllably small Γ region near the target trajectory and, considering the motions within Γ, we have BIBO stability.

In this application, we use a torque-shaped rigid body reference trajectory, which is very attractive since the reference maneuver can be calculated in closed form [such as the family of Eqs. (3.90)-(3.96)] and since the ensuing tracking law performs extremely well. Note that Eqs. (3.90)-(3.96) have a C^1 continuous transition to the final fixed state:

$$\left\{ u_{ref}(t), \theta_{ref}(t), \dot{\theta}_{ref}(t), [M_0(t)]_{ref}, [S_0(t)]_{ref} \right\} = \left\{ 0, \theta_f, 0, 0, 0 \right\}, \qquad \text{as } t \to t_f$$

so that, for $t > t_f$, only the three feedback terms of Eqs. (3.98) are contributing to the terminal fine-pointing/vibration arrest control. Thus, the controls blend continuously from the large-angle tracking law of Eq. (3.98) into a constant gain controller (for $t > t_f$) identical to the globally stable fixed point output feedback case of Eq. (3.88). Thus we have unqualified global stability for $t > t_f$.

Simulated Results for Large Angle Maneuvers

Returning to the family of 40° open-loop maneuvers used to generate the energy surface of Figure 3.7, we computed the velocity tracking bound μ for Lyapunov stability [as given by Eq. (3.101)] and found the maximum value (μ_{max}) of $\mu(t)$ along each trajectory. Figure 3.8 displays this worst-case tracking bound (maximum value of μ) surface $\mu_{max}(\alpha, u_{max})$ region used to generate Figures 3.6 and 3.7. The closed-loop tracking error bound has a roughly analogous behavior to the open-loop residual vibration energy surface of Figure 3.7. Recall that, outside the region bounded by the inequality of Eq. (3.81), we have guaranteed Lyapunov stability, using the control law of Eq. (3.98) and the reference rigid-body torque given by Eqs. (3.90)–(3.94). From Figure 3.7, it is clear that sufficiently small μ_{max} and large α result in arbitrarily small tracking errors, but the (small α, large u_{max}) near-bang reference maneuvers cannot be tracked as precisely. It is easy to see how a subset of the candidate (α, u_{max}) designs can be found that satisfy specified inequalities on maneuver times, tracking errors, and residual vibration energy by direct examination of the surfaces of Figures 3.6–3.9.

The results obtained from the simulations (and in the actual hardware implementations discussed later and in [Junkins 1991,1993]) support the conclusion that these surfaces can be used to establish a large region of feasible designs for near-minimum-time controls in the space of torque-shaped parameters and control gains. Optimization over the set of feasible designs should, in general, include consideration of the nature of expected disturbances to be rejected. One detailed simulation
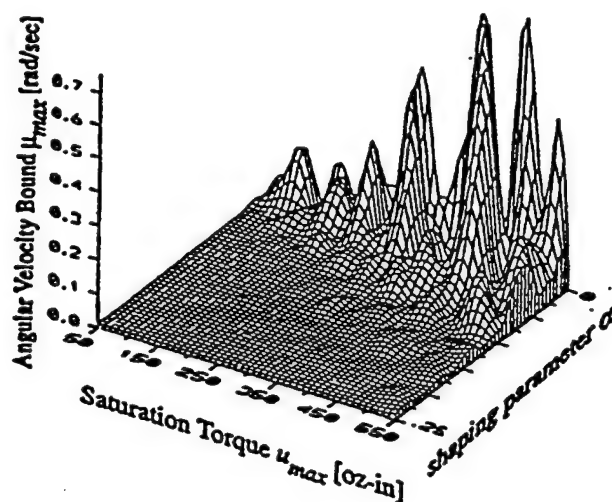
Figure 3.8. Boundary of the Lyapunov-stable tracking region vs saturation torque and torque-shaped parameter
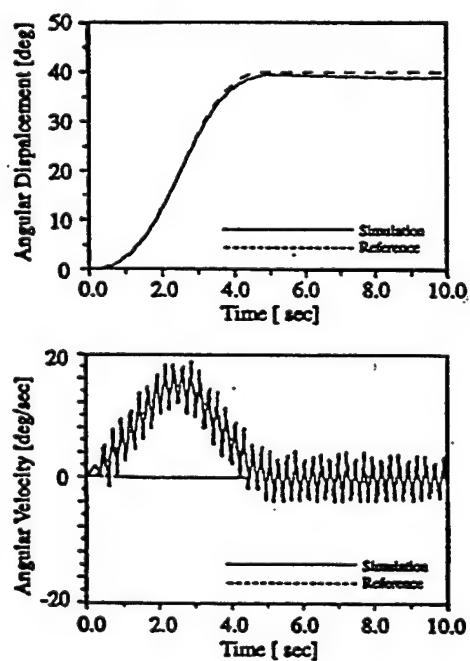

Figure 3.9. Open-loop 40° maneuver with random disturbances

is now considered to show state and control variable histories along a typical trajectory of the family of trajectories underlying the above surfaces. In these simulations the effects of worst-case disturbance torques are included in order to illustrate the effectiveness of controls in the presence of unmodeled effects. For simplicity, only the case of 40° rest-to-rest maneuver is considered here, along with setting $u_{max}=$ 400 oz-in. for all cases.

For the computational studies, two control laws are considered: namely, the output feedback law (control law I) of Eq. (3.88), and the tracking-type feedback control law (control law II) of Eq. (3.98). Although control law II could be used with an arbitrary reference trajectory, the torque-shaped rigid body trajectories of Eqs. (3.90)–(3.94) are specifically selected for investigation. The torque-shaped open-loop control history u_{ref} can be precomputed (in a fraction of a second!) from Eqs. (3.90)–(3.94) and stored, whereas the instantaneous trajectory variables $\{\theta_{ref}, \dot{\theta}_{ref}, [L_0S_0(t) - M_0(t)]_{ref}\}$ are integrated easily in real time. Note that the boundary conditions of Eqs. (3.92) are enforced by using Eq. (3.94) to compute the trajectory maneuver time as a function of the maneuver angle, saturation torque, and torque-shaped parameter.

We now discuss the simulation results using control law II, which obviously blends into control law I in the end game (for $t \geq t_f$). In the experimental results in the subsequent discussion, maneuvers carried out by both control laws are reported. Both open-loop (all $g_i = 0$) and closed-loop time histories of selected state variables are shown in Figures 3.9 and 3.10.

Figures 3.9(a) and (b) show the hub angle and angular velocity for the case of an open-loop control and in the presence of substantial impulsive and quasirandom (5 oz-in., 1σ) disturbance torques. It is evident that the disturbance torque history is very significant vis-à-vis disturbing flexible dynamics in our experimental hardware; however, certain nonrandom, nonlinear effects associated with the bearing friction cause disturbances that are highly correlated in time and are not well represented by the present white-noise model of the disturbance torques. In spite of the substantial disturbance torques (Figure 3.9), however, it is evident that the simulations indicate that the closed-loop flexible body dynamics, in fact, follow the near-minimum-time rigid-body motion closely while effectively suppressing vibration, as shown Figure 3.10. In addition to the variables graphed in Figures 3.9 and 3.10, we confirmed that the energy of the first 10 modes was effectively suppressed. These simulated results are very consistent with the experimental results discussed in the following section and those presented in [Junkins 1991,1993].

Experimental Results

In all of the experiments in the following discussion, the target final angle is set to 40° and $u_{max} = 400$ oz-in. A detailed description of the hardware is given in Appendix I. We overview the system as follows: the configuration (Figure 3.4, Table 3.2) has a span of approximately 9 ft and has six natural frequencies below 20 Hz. The system is accurately balanced, and the four aluminum appendages'
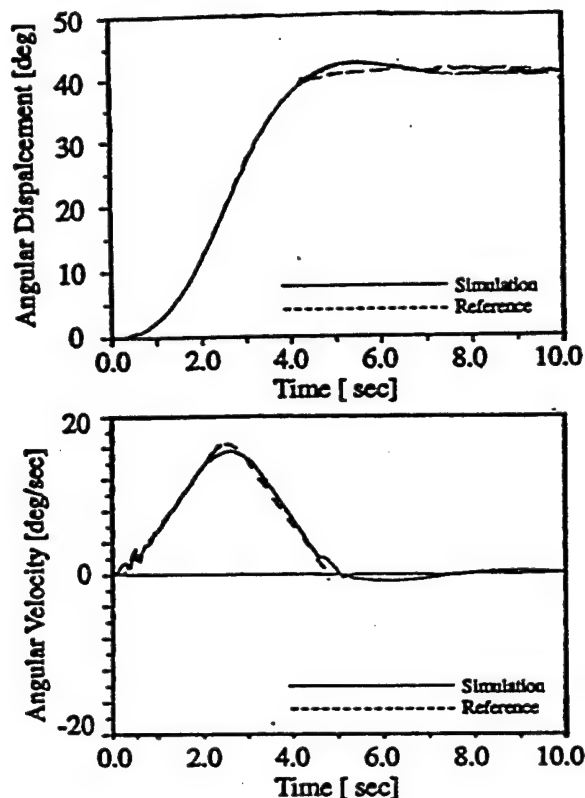
Figure 3.10. Closed-loop 40° maneuver with random disturbances

geometric, mass, and stiffness parameters are matched to high precision; the first three measured cantilevered natural frequencies of the four individual beams were found to be identical tō within 0.05 Hz.

With this design, the appendages vibrate almost exclusively in the horizontal plane; the hub is balanced on a custom-designed needle-jewel bearing that constrains the hub to rotate about the vertical axis. Our measurements confirm that negligible out-of-plane motion occurs in our experiments, although there is occasional evidence of small beam torsional vibrations. Also, to very high accuracy, we can state that our experimental results confirmed that only the antisymmetric in-plane modes [implicit in the derivation of Eqs. (3.83)] were excited during rest-to-rest maneuvers using the hub torque actuator. The bearing stiction/friction torque is significant ($\sim$ 20 oz-in.), but is sufficiently small and predictable to permit meaningful experiments. Aerodynamic damping is important only during the most rapid slew maneuvers; in most cases, it represents a small perturbation as compared to the larger active vibration damping introduced by the feedback controller. The control torque is

achieved by means of a reaction wheel mounted to the shaft of a DC motor [Figure 3.4(c)], which is, in turn, mounted to the hub. The commanded motor torque is achieved by precision current control using power amplifiers, as described in Appendix I of [Junkins 1993]. The angular rotation of the hub is measured using a Teledyne-Gurley angle encoder, accurate to about $0.01°$, whereas the root bending moment and shear force estimates are derived from conventional full-bridge strain-gauge measurements. The derived estimates of the angular velocity history have a variance of approximately $1°/s$ and a time lag of 0.01 s. The noise and phase lag in the angular velocity estimates and the strain-gauge-derived root shear force and bending moment estimates limit the bandwidth of the closed-loop system to the range from approximately 0 to 10 Hz. The errors (noise and phase lag) in the derived hub angular velocity estimates represent the main source of the precision and bandwidth constraints of the experimental implementations. The control loops were closed, for all experiments discussed later, at 75 Hz; the angle encoder was also sampled at 75 Hz, whereas the strain gauges were sampled an order of magnitude faster, and filtered to reduce the effects of sensor noise and higher-frequency modes outside the bandwidth of our controller.

Figure 3.11 shows the experimental system response for a maneuver using control law I [the constant gain control law of Eq. (3.88)] with $g_1 = 600$ oz-in./rad, $g_2 = 800$ oz-in./rad/s, and $g_3 = 0$. Even though control law I [Eq. (3.88)] is anticipated to be poorly suited for large-angle maneuvers, we nonetheless apply this law to carry out $40°$ maneuvers to provide a reference for the subsequent discussion. Since the initial position error is large, the maneuvers start from zero with a large initial discontinuity to a large torque. For this gain selection, we see a large hub angle overshoot ($\sim 10°$) and significant structural vibration that was effectively suppressed by around 12 s; the control was terminated at 16 s. These results were repeatable; however, the residual angle was typically $\sim 0.25°$ because the constant gain g_1 could not be set sufficiently large to overcome terminal bearing stiction without causing initial actuator saturation and large overshoots, and a compromise value was adopted for the sake of illustration. As is demonstrated in Ref. 5, the overall maneuver shape and settling time is sensitive to the gains selected; however, less than 10% reductions in the 12 s settling time can be achieved without initially saturating the actuator.

Control law II, on the other hand, leads to very attractive near-minimum-time maneuvers. One feasible set of gain settings and torque shaped parameters leads to the experimental results shown in Figure 3.12. The effect of using a smooth, judiciously shaped reference torque history is evident if one compares the output and control variable histories in Figure 3.12 with those of Figure 3.11. This implementation of control law II produced much smaller overshoot ($\approx 1.5°$ *vs* $\sim 10°$) and shorter maneuver time (6 s *vs* 12 s), and greatly reduced the severity of peak vibration, compared to control law I. These results, especially when considered in conjunction with numerous other cases, are reported in [Junkins 1990] and [Thompson 1989], provide convincing evidence that control law II is a versatile and highly effective way to incorporate open-loop torque-shaped optimization with
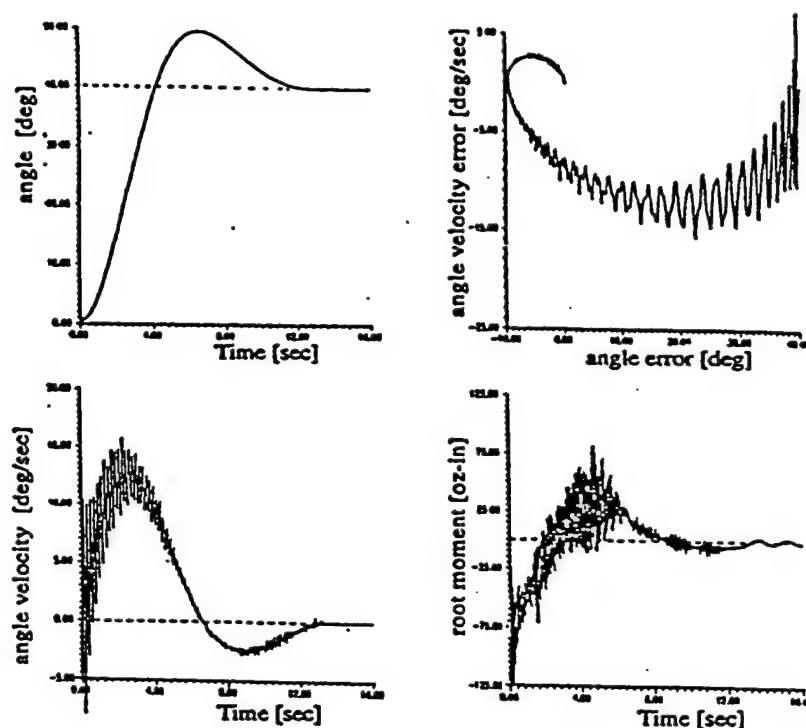
Figure 3.11. Experimental results: a 40° maneuver using control law I ($g_1 = 600$, $g_2 = 800$, $g_3 = 0.0$).

en route and terminal vibration suppression. The fact that a globally continuous control structure is implicit in this approach leads to minimal difficulties in realizing robust control laws.

We encountered several practical difficulties in our experimental work, but these difficulties are not central to our control-law design approach. First, the root shear force and bending moment approximations obtained using strain-gauge measurements resulted in sufficiently noisy and nonlinear measurements that, using this feedback ($g_3 \neq 0$), only marginally improved the controlled response over, for example, the results in Figure 3.11. These anomalies resulted, we hypothesize, from the nonideal beam-clamp effects near the station where the strain measurements were being made. Any slight play in the clamp due to large root moment variations would manifest itself in spurious strain measurements. Also, deriving the angular velocity estimate from the noisy angle-encoder readout was difficult to accomplish with high precision and, as a consequence, we constructed a digital filter to process the angle encoder data and roll off the frequency content in the rate estimates
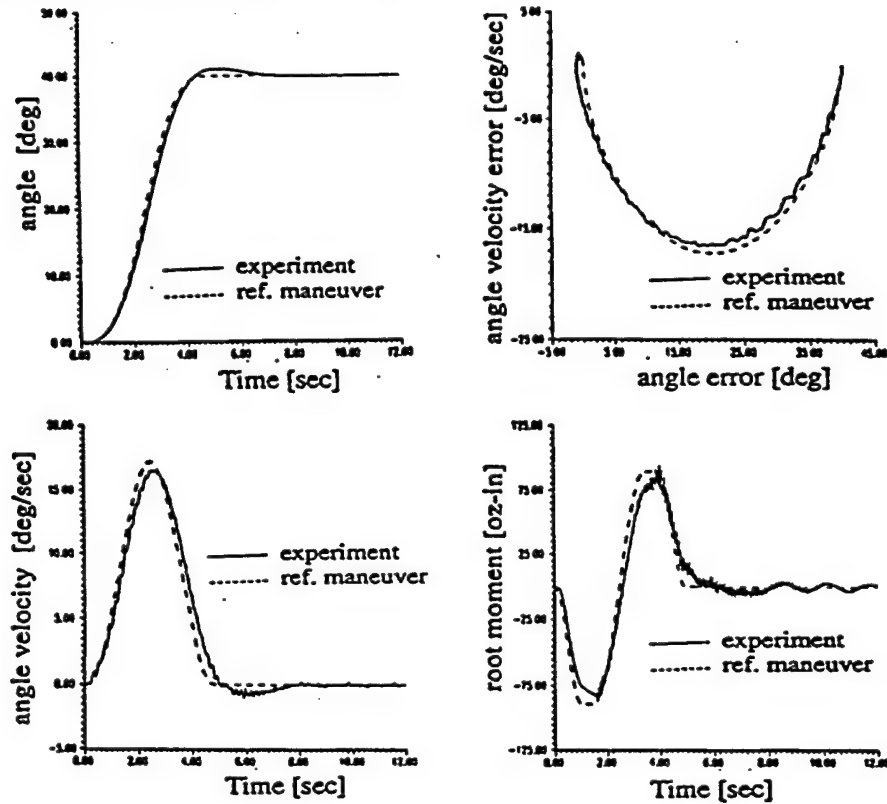
Figure 3.12. Experimental results: a 40° maneuver using control law II ($g_1 = 3000$, $g_2 = 800$, $g_3 = 0.0$, $\alpha = 0.2$, $u_{max} = 400$).

above 10 Hz. We found this was useful to avoid erroneous, phase-lagged high-frequency components of the feedback that disturbed the higher-frequency modes. These problems can be essentially eliminated, of course, by investing in a more precise sensor to measure angular displacement and/or angular velocity, as well as a load cell to measure the root shear and bending moments. Finally, our bearing presented us with another set of practical difficulties. Based on analysis of our bearing hardware, it became evident that interaction of the structure with the bearing accounts for the overwhelming source of disturbance torques. The bearing friction/stiction model developed from our analysis [Junkins 1990] has the form

$$\tau_{bearing} = -c_1 \text{sign}(\dot{\theta}) - c_2 \dot{\theta} + \text{HOT} \qquad (3.102)$$

where we find $c_1 \sim 20$ oz-in. and $c_2 \sim 0.001$ oz-in./rad/s.

Thus, the first (stiction) term of Eq. (3.102) dominates the bearing torque for moderate $\dot{\theta}$ and is about 5% of the peak commanded torque of 400 oz-in. Although we believe that Eq. (3.102) models the bearing friction well, we found that it is difficult to use this model to compensate for bearing friction in real time

because angle-encoder noise results in uncertainty in the estimated instants that $\dot{\theta}$ switches sign. This difficulty has significant practical consequences. If we modify our control to compensate for bearing-disturbance torques (essentially, attempt to cancel it) using Eq. (3.102), the commanded discontinuity (at the estimated time that $\dot{\theta}$ changes sign) will not coincide exactly with the actual stiction discontinuity; even slightly mistimed compensation torque discontinuities can actually worsen the disturbance! Although we experimented with several bearing-torque compensation schemes, we ultimately decided simply to consider bearing torque an anticipated and well modeled disturbance. Our simulations (such as the results shown in Figure 3.10) indicated that our control approach could easily tolerate disturbances of this magnitude, and our successful experiments in Figures 3.11 and 3.12 and [Junkins 1990] certainly confirm that our implemented control laws are robust in the presence of the actual disturbances from all sources.

This case study provides a good illustration of the mix of theoretical analysis, numerical computation, and engineering judgment required to carry out successful applications. The ultimate objective, of course, is to obtain perfect closure between theory and experiment. However, it is not realistic to expect the high degree of closure obtained above, when faced with more complicated dynamical systems. Note that excellent results were obtained, in spite of modest investments in sensors and actuators; however, for systems requiring high precision and wide control bandwith, it would be necessary to have corresponding improvements in the precision and bandwith of the sensors. In the context of the above numerical and experimental results, however, we observe that a large degree of model-error robustness implicit in our approach stems from our theoretical verification that the control of Eq. (3.88) remains stabilizing for most of the usual variations in modeling assumptions, and we used judicious sensor filtering to roll off the effects of the system dynamics outside the sensors' bandwidth. In conclusion, the excellent agreement between theory and experiment evident in Figures 3.10 and 3.12 represents prototypical (rather than usual) results.

3.7 CONCLUDING REMARKS

In this chapter, we have summarized the central aspects of Lyapunov stability theory with particular emphasis upon the role that it can play in designing stable controllers for nonlinear multibody systems. Several elementary analytical and numerical examples are provided to illustrate the ideas and to provide some basis for extrapolating the practical implications of the methods presented. A more extensive example is offered to introduce some ideas on cooperative control, in which two or more manipulators are manipulating a payload while cooperating with each other to minimize a measure of the associated control and constraint forces and moments. The chapter concludes with an example wherein maneuvers are designed for a multibody flexible structure and good closure is obtained between the analytical, computational, and hardware experimental results. These results support the theoretical and practical value of these developments.

Acknowledgements

3.8   REFERENCES

AHMAD, S., AND ZRIBI M., "Lyapunov based control design for multiple robots handling a common object", In *Lecture Notes in Control and Information Sciences, Vol 170*, J.M. SKOWRONSKI, H. FLASHNER, AND R.S. GUTTALU (eds), Springer-Verlag, New York, 1991.

BREAKWELL, J.A., "Optimal feedback control for flexible spacecraft", *Journal of Guidance, Control, and Dynamics*, 4 (5) (1981), 427-479.

BYERS, R.M., VADALI, S.R., AND JUNKINS, J. L., "Near-minimum-time closed-loop slewing of flexible spacecraft", *Journal of Guidance, Control, and Dynamics*, 13 (1) (1990), 57-65.

CANAVIN, J.R., "The control of spacecraft vibrations using multivariable output feedback", *AIAA/AAS Astrodynamics Conference*, Palo Alto, CA, Aug. 7-9, 1978.

CHEN, C.T., *Linear System Theory and Design*, Holt, Rinehart and Winston, New York, NY, 1984.

CREAMER, N.G. AND JUNKINS, J.L., "A pole placement technique for vibration suppression of flexible structures", *AIAA/AAS Astrodynamics Conference*, Mpls., MN, Aug. 15-17, 1988.

FUJII, H., OHTSUKA, T., AND UDOU, S., "Mission function control for slew maneuver experiment", *Journal of Guidance, Control, and Dynamics*, 12 (6) (Nov.-Dec. 1989), 858-865.

GOH, C.J. AND CAUGHEY, T.K., "On the stability problem caused by finite actuator dynamics in the collocated control of large space structures", *International Journal of Control* 41 (3) (1985), 787-802.

INMAN, D.J., *Vibration with Control, Measurement, and Stability*, Prentice Hall, Englewood Cliffs, NJ, 1989.

JOSHI, S.M., *Control of Large Flexible Space Structures*, Lecture Notes in Control and Information Sciences, Vol. 131, Springer-Verlag, New York, NY, 1989.

JUANG, J.N., HORTA, L.G., AND ROBERTSHAW, N.H., "A slewing control experiment for flexible structures", *Proceedings of the 5th VPI & SU Symposium on Dynamics and Control of Large Structures*, Virginia Polytechnic Institute and State University, Blacksburg, VA, 1985, 547-551.

JUNKINS, J.L. AND TURNER, J.D., *Optimal Spacecraft Rotational Maneuvers*, Elsevier, Amsterdam, 1986.

JUNKINS, J.L. AND KIM, Y., "A minimum sensitivity design method for output feedback controllers", In *Mechanics and Control of Large Flexible Structures*, Progress in Astronautics and Aeronautics, Vol. 129, J.L. JUNKINS (ed), AIAA, 1990.

JUNKINS, J.L., RAHMAN, Z.H., AND BANG, H., "Near-minimum-time control of distributed parameter systems: Analytical and experimental results", *Journal of Guidance, Control, and Dynamics* 14 (2) (Mar-Apr 1991), 406-43.

Y.,

JUNKINS, J. L., AND KIM, Y., *An Introduction to Dynamics and Control of Flexible Structures*, AIAA Education Series, American Institute of Aeronautics and Astronautics, Washington, D.C., 1993.

JUNKINS, J.L. AND KIM, Y., "Stability and control of robotic manipulators", *AIAA Progress in Aeronautics Series* 161, S.B. SKAAR (ed), AIAA, 1994.

KALMAN, R.E. AND BERTRAM, J.E., "Control system analysis and design via the second method of Lyapunov", *Trans. ASME, Journal of Basic Engineering* 82 (1960), 371-392.

KALMAN, R.E., "Lyapunov function for the problems of Lure in automatic control", *Proc. Nal. Acad. Sci.* 49 (Feb. 1963), 201-205.

KRISHNAN, H., "Control of nonlinear systems with appliocations to constrained robots and spacecraft attitude stabilization", doctoral dissertation, Aerospace Engineering, University of Michigan, Ann Arbor, MI, 1992.

LASALLE, J., AND LEFSCHETZ, S., *Stability by Lyapunov's Direct Method with Applications*, Academic Press, New York, NY, 1961.

MEIROVITCH, L. AND QUINN, R., "Maneuvering and vibration control of flexible spacecraft", *Journal of Astronautical Sciences* 35 (3) (1987), 301-328.

MUKHERJEE, R., AND CHEN, D., "Stabilization of free-flying under-actuated mechanisms in space", *Proceedings of the 1992 American Control Conference*.

MUKHERJEE, R., AND CHEN, D., "An asymptotic stability theorem for nonautonomous systems", *Journal of Guidance, Control, and Dynamics* (1992) (to appear).

MUKHERJEE, R., AND JUNKINS, J.L., "An invariant set analysis of the hub-appendage problem", *AIAA Journal of Guidance, Control, and Dynamics*, 16 (6) (Nov-Dec 1993), 1191-1193.

OH, H.S., VADALI, S.R., AND JUNKINS, J.L., "On the use of the work-energy rate principle for designing feedback control laws", *AIAA Journal of Guidance, Control, and Dynamics* 15 (1) (Jan-Feb 1992), 275-277.

PATEL, R.V. AND TODA, "Quantitative measures of robustness for multivariable systems", *Proceedings of JACC*, TP-8A, San Francisco, CA, 1980.

POPOV, V.M., "Hyperstability and optimality of automatic systems with several control functions", *Rev. Roum. Sci. Tech.* 9 (1964), 629-690.

SINGH, G., KABAMBA, P., AND MCCLAMROCH, N., "Planar time optimal slewing maneuvers of flexible spacecraft", *Journal of Guidance, Control, and Dynamics* 12 (1) (Jan-Feb 1989), 71-81.

SLOTINE, J.E., AND WEIPING, L., *Applied Nonlinear Control*, Prentice Hall, New York, NY, 1991.

THOMPSON, R.C., JUNKINS, J.L., AND VADALI, S.R., "Near-minimum time open-loop slewing of flexible vehicles", *Journal of Guidance, Control, and Dynamics* 12 (1) (Jan-Feb 1989), 82-88.

TSIOTRAS, P., "A new class of globally asymptotically stabilizing controllers for the attitude motion of a rigid body", *International Federation of Automatic Control Conference*, 1994.

VADALI, S.R., "Feedback control of space structures: A Lyapunov approach", In *Mechanics and Control of Large Flexible Structures* Progress in Astronautics and Aeronautics, Vol. 129, J.L. JUNKINS (ed), AIAA, 1990.

VANDERVELDE, W. AND HE, J., "Design of space structure control systems using on-off thrusters", *Journal of Guidance, Control, and Dynamics* 6 (1) (1983), 759-775.

VIDYASAGAR, M., *Nonlinear System Analysis*, Prentice Hall, Englewood Cliffs, NJ, 1978.

WIE, B., WEISS, H., AND ARAPOSTHATHIS, A., "Quaternion feedback for spacecraft eigenaxis rotations", *Journal of Guidance, Control, and Dynamics* 12 (3), (May-June 1989), 375-380.

WILLEMS, J.L., *Stability Theory of Dynamical Systems*, John Wiley and Sons, New York, NY, 1970.

YALE, G., "Cooperative control of multiple space manipulators", doctoral dissertation, Aeronautical and Astronautical Engineering, Naval Postgraduate School, 1993, Monterey, CA.

Nonlinear Dynamics, Control and Identification of Structural Systems

John L. Junkins and Andrew J. Kurdila

Center for Mechanics and Control

Texas A&M University

AFOSR Contract No. F49620-92-J-0496

Macroscopic Motivations & Directions

Based Upon Historical/Ongoing Laboratory Interactions

GI at Phillips Lab <=> Structural Mechanics, Dynamics, Control
(ASTREX, PACE)

Wright Aeronautical Labs <=> Nonlinear Mechanics, Optimization, Fluid/Structure Interaction, Aeroelasticity

And our Reading of the "Tea Leaves" ... The principal focii for our research program have been established as:

=> High fidelity modeling, structural analysis, computational methods, and structural model/solution validation methods.

=> Prototype problems from A/C flight mechanics, sensing/actuation, aeroelasticity, & associated dynamics/control/stability issues.

OUTLINE

Introduction/Overview/Macroscopic Motivation

A New Approach to Nonlinear Structural Response

Dynamical Model Validation for Distributed Parameter Systems

Nonlinear Structural Mechanics & Nonlinear Control in Aeroelasticity

For Each of the Above, We Address:

Motivation/Relevance/Approach

Key Results/Examples

Status and "Where to From Here?"

A New Approach to Nonlinear Structural Response

Motivation:

A large class of geometrically nonlinear structural dynamic response problems involve the solution of differential/algebraic systems:

$$[M(x)]\ddot{x} = f(x, \dot{x}) - A^T \lambda, \quad (\dot{}) \equiv \frac{d()}{dt}, \quad x \in R^n$$

$$[A(x)]\dot{x} + a(x) = 0$$

Problem: The configuration dependence of the mass matrix introduces numerical difficulties that limit the dimensionality, precision, and speed of many DOF nonlinear response simulations.

Question: Without approximation, is it possible to avoid inversion of $[M(x)]$ on every time step?

Answer: Yes, we have found an elegant/general solution to this fundamental problem =>> Improves the basic accuracy/ speed/numerical stability tradeoffs by over an order of magnitude.

An Orthogonal Quasi-Coordinate Formulation of Dynamical Models for Nonlinear Structural Systems

Classical Approach

$$L = T - V = \frac{1}{2}\dot{x}^T M(x,t)\dot{x} + G^T(x,t)\dot{x} + T_o(x,t) - V(x), \quad A(x,t)\dot{x} + b(x,t) = 0$$

$$\frac{d}{dt}\left(\frac{\partial L}{\partial \dot{x}}\right) - \frac{\partial L}{\partial x} = Q - A^T\lambda$$

$$M(x,t)\ddot{x} = RHS \equiv -\left(\frac{dM}{dt} - \frac{\partial G^T}{\partial x}\right)\dot{x} - \frac{1}{2}col\left\{\dot{x}^T\frac{\partial M}{\partial x_i}\dot{x}\right\} - \dot{G} + \frac{\partial T_o}{\partial x} + \frac{\partial V}{\partial x} + Q - A^T\lambda$$

$$A(x,t)\dot{x} + b(x,t) = 0$$

Orthogonal Quasi-Coordinate Approach: Unconstrained Case

$$v = \left[\begin{smallmatrix}\ddots & & \\ & \sigma_i & \\ & & \ddots\end{smallmatrix}\right]C\dot{x} \iff \dot{x} = C^T\left[\begin{smallmatrix}\ddots & & \\ & 1/\sigma_i & \\ & & \ddots\end{smallmatrix}\right]v$$

$$M(x,t) = C^T\left[\begin{smallmatrix}\ddots & & \\ & \sigma_i^2 & \\ & & \ddots\end{smallmatrix}\right]C \iff [M(x,t)]^{-1} = C^T\left[\begin{smallmatrix}\ddots & & \\ & 1/\sigma_i^2 & \\ & & \ddots\end{smallmatrix}\right]C, \quad C^T C = I$$

$$L = \frac{1}{2}v^T v + G^T C^T\left[\begin{smallmatrix}\ddots & & \\ & 1/\sigma_i & \\ & & \ddots\end{smallmatrix}\right]v + T_o - V$$

$$\dot{v} = -\left(\left[\begin{smallmatrix}\ddots & & \\ & \sigma_i & \\ & & \ddots\end{smallmatrix}\right]\Omega\left[\begin{smallmatrix}\ddots & & \\ & 1/\sigma_i & \\ & & \ddots\end{smallmatrix}\right] - \frac{1}{2}\left[\begin{smallmatrix}\ddots & & \\ & \mu_{ii}/\sigma_i^2 & \\ & & \ddots\end{smallmatrix}\right]\right)v + \left[\begin{smallmatrix}\ddots & & \\ & 1/\sigma_i & \\ & & \ddots\end{smallmatrix}\right]C\{RHS\}, \quad \dot{C} = -\Omega C, \quad \dot{\sigma}_i = \frac{1}{2}\frac{\mu_{ii}}{\sigma_i}$$

where:

$$\Omega_{ij} = -\Omega_{ji} = \begin{cases} \dfrac{\mu_{ij}}{\sigma_j^2 - \sigma_i^2} & , \left|\dfrac{\mu_{ij}}{\sigma_j^2 - \sigma_i^2}\right| < \Omega_{max} \\ 0 & , \sigma_j = \sigma_i \\ \Omega_{max}\,sign\left(\dfrac{\mu_{ij}}{\sigma_j^2 - \sigma_i^2}\right), & \left|\dfrac{\mu_{ij}}{\sigma_j^2 - \sigma_i^2}\right| \geq \Omega_{max} \end{cases}, \quad \mu_{ij} = c_j\left[\frac{dM}{dt}\right]c_i^T, \quad C = \begin{bmatrix} c_1 \\ \cdots \\ \vdots \\ \cdots \\ c_n \end{bmatrix}$$

⇨ So what is the significance of these developments?

A Low-Dimensioned Example

Nonlinear Mechanism
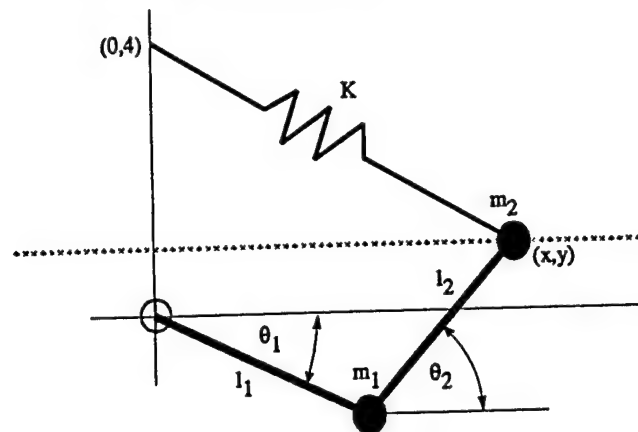
Unconstrained Free Response

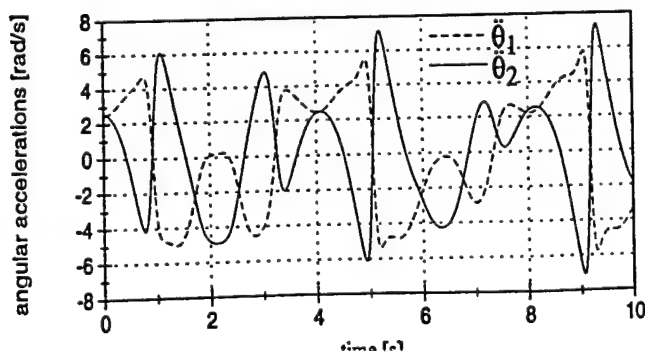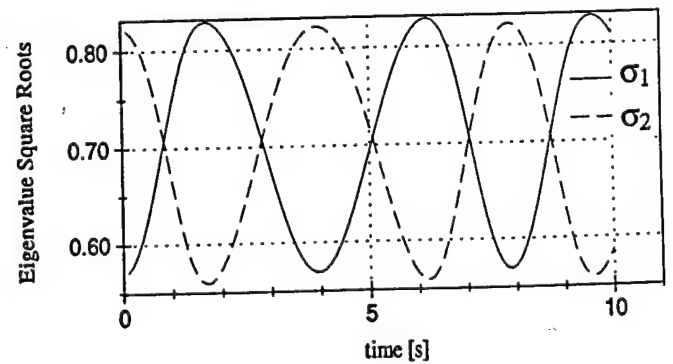t= 1.0 sec   = 0 sec
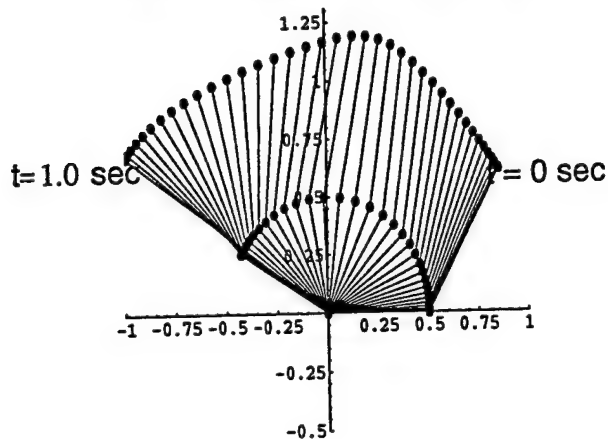
Constrained Free Response
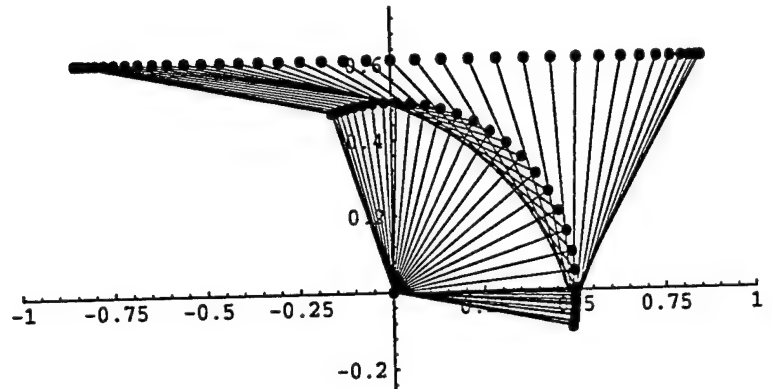
Angular Response
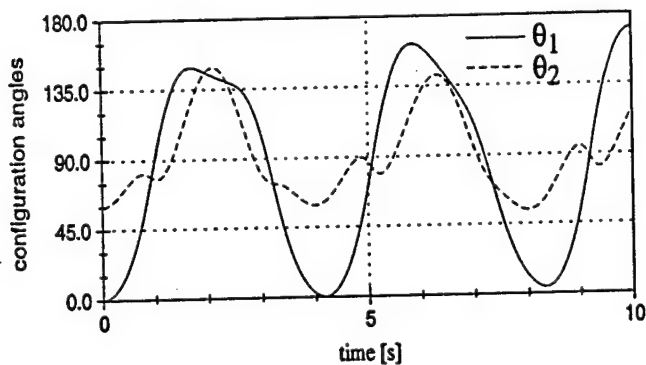
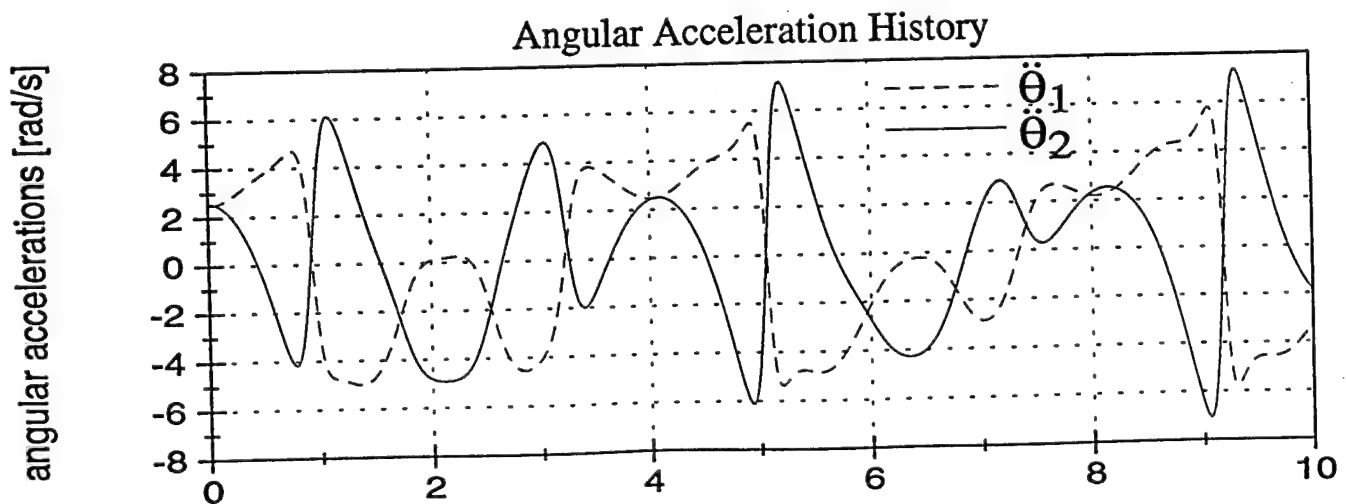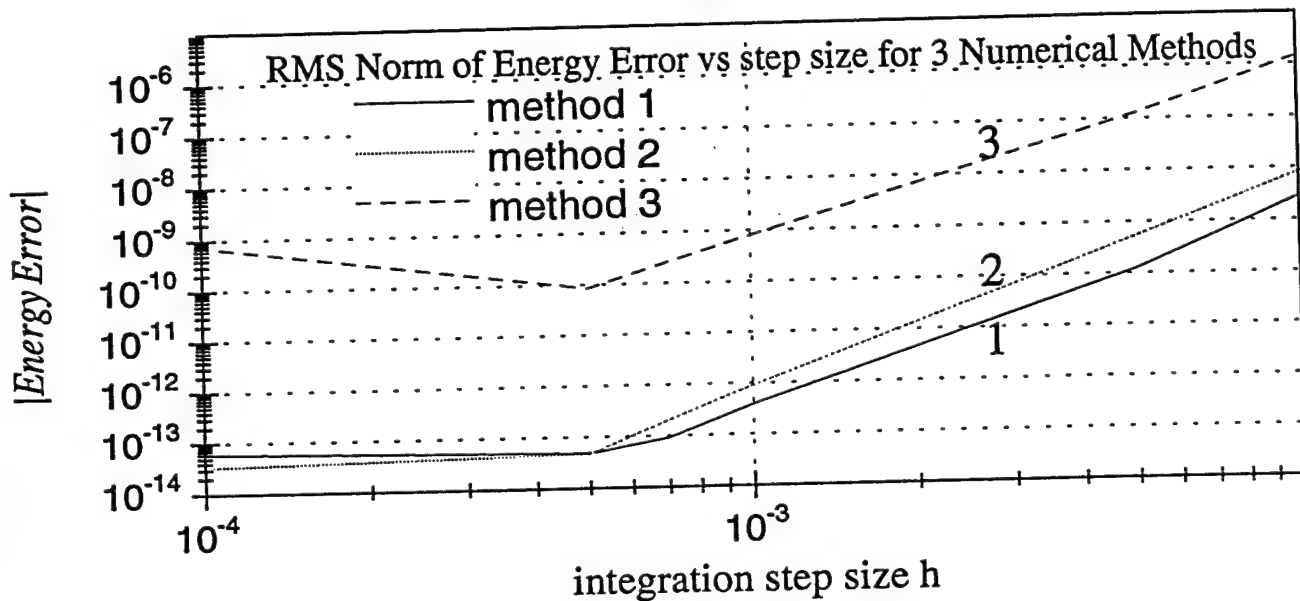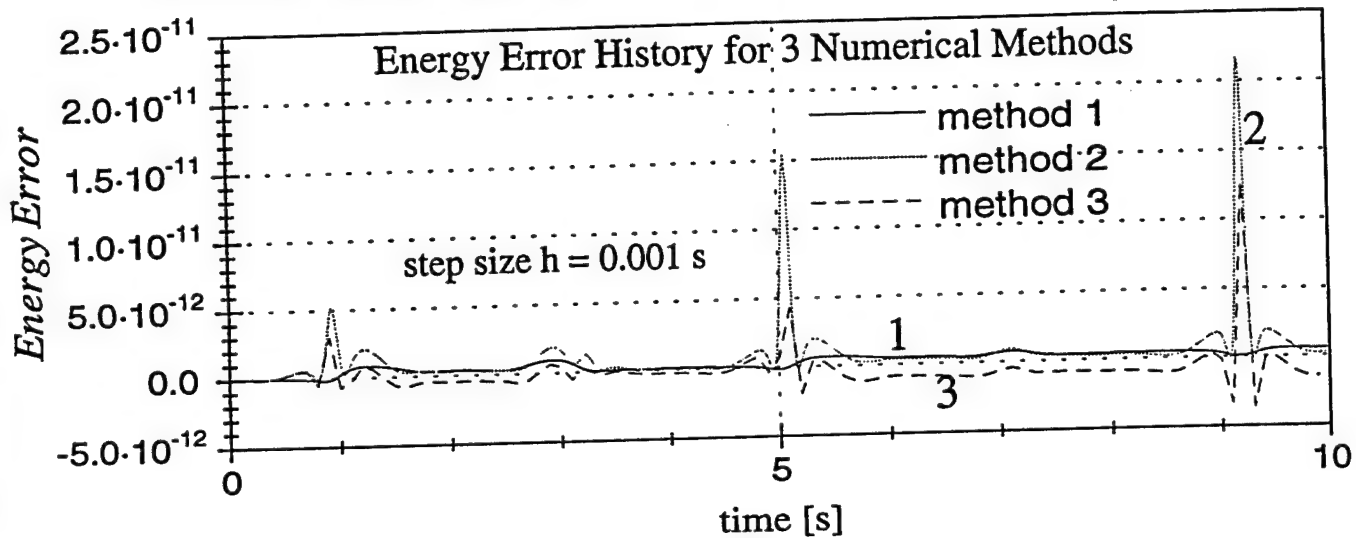## Instantaneous Mass Matrix Eigenvalues
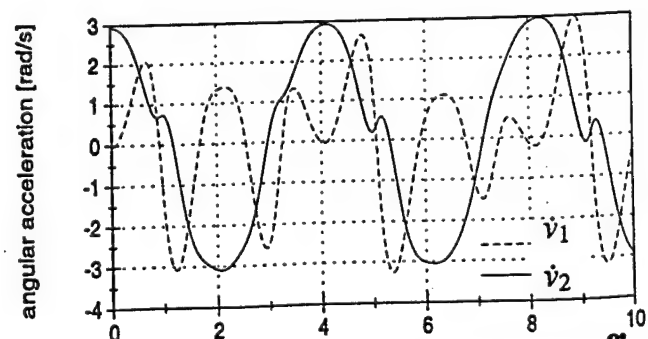
Some Simulations

Method 1: *state vector is* $\{v, x\}$, *using orthogonal quasi* − *coordinate approach*

*Method* 2: *state vec tor is* $\{\dot{x}, x\}$, *using* $M^{-1}(x) = C^T S^{-2} C$ *to solve for* $\ddot{x}$

Method 3: *state vec tor is* $\{\dot{x}, x\}$, *using LDU decomp. of* $M(x)$ *to solve for* $\ddot{x}$

Energy Error History for 3 Numerical Methods

RMS Norm of Energy Error vs step size for 3 Numerical Methods

Angular Acceleration History

A Stable Transition Between Flight Modes:

Accomplished via a Novel Compromise Between Fixed and Rotary Wing Configurations

The *Freewing Tilt-Body UAV Vehicle*

High Speed Flight Mode   Intermediate Mode   Takeoff / Land / Loiter Mode
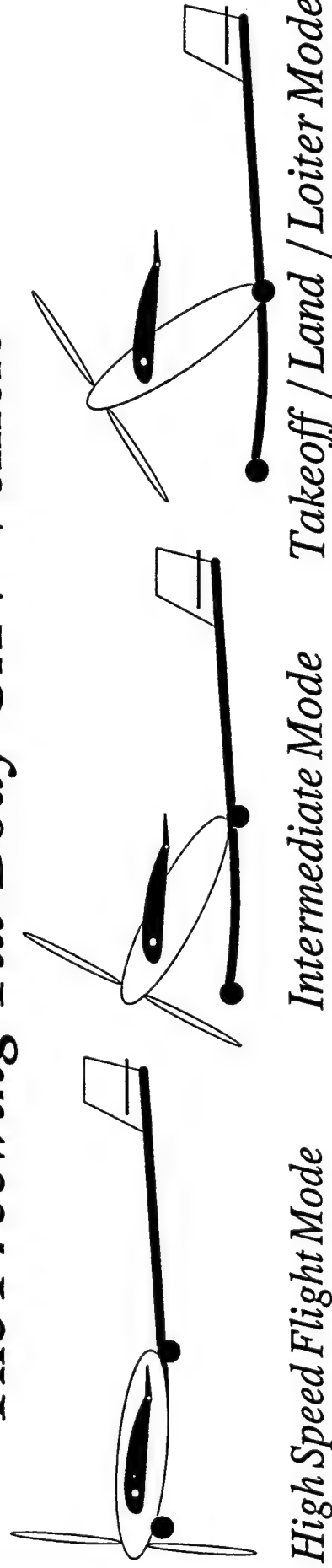
Throughout the flight mode transitions, the free wing angle of attack is independently *auto-stable at a specific angle of attack for each* flight regime, depending only on the elevon setting. Also note:

Wing stabilization is *passive and inherent* in the design.

Gust response is greatly reduced (~ one order of magnitude).

Unusual Near-VTOL, Loiter, and Endurance capabilities ...

Auto-Stable Free Wing: Essential Idea

Consider a Free Wing in trim:

=> The Free Wing can be thought of as a *'variable geometry lifting weathervane'*

=> Due to the free pivot, for trimmed flight, *both the wing and the aircraft must be in trim with zero moment about the pivot point.* => *The free wing is 'stall-proof'.*

For fixed velocity, we can consider the wing trim forces/moments, and angle of attack to be functions of only the elevon deflection angle δ.   There are *an infinity of trim states for the wing.*

Conditions for Wing to Trim:

$$\sum Moments\,(\alpha_w, \delta) = 0 \Rightarrow \alpha_w(\delta)$$

$$\sum Forces\,(\delta) = 0 \Rightarrow F_w(\delta)$$
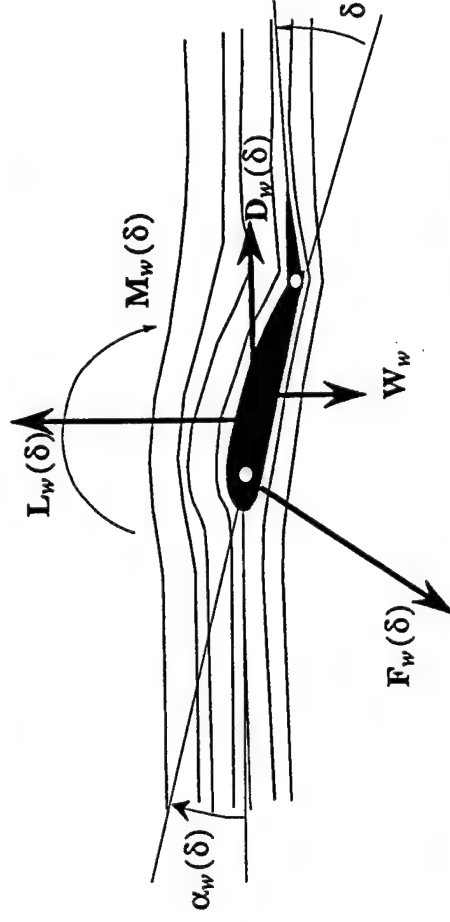
The bearing reaction force on the A/C fuselage obviously must be $-\mathbf{F_w}$, the req'd $\mathbf{F_w}$ to trim the A/C implicitly dictates the req'd wing trim δ. Notice further that

=> *The variable geometry Tilt-Body design allows us to alter the direction/magnitude of the thrust* $\mathbf{T}$ => *gain access to an infinite set of trimmed flight modes for the A/C.*

Satisfying trim conditions obviously does not guarantee stable flight of the aircraft.

=> The aerodynamics are coupled to the tilt angle and thrust, and *dynamic stability analysis of variable geometry aircraft is inherently non-linear and non-trivial!*

=> Research Issues: fluid/structure interaction, stability/control, aeroelastic effects.

Nonlinear Gust Response for The Freewing Scorpion Vehicle in Loiter Mode

$U_\infty = 52 ft/s \ (\sim 36mph))$
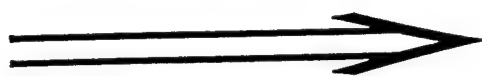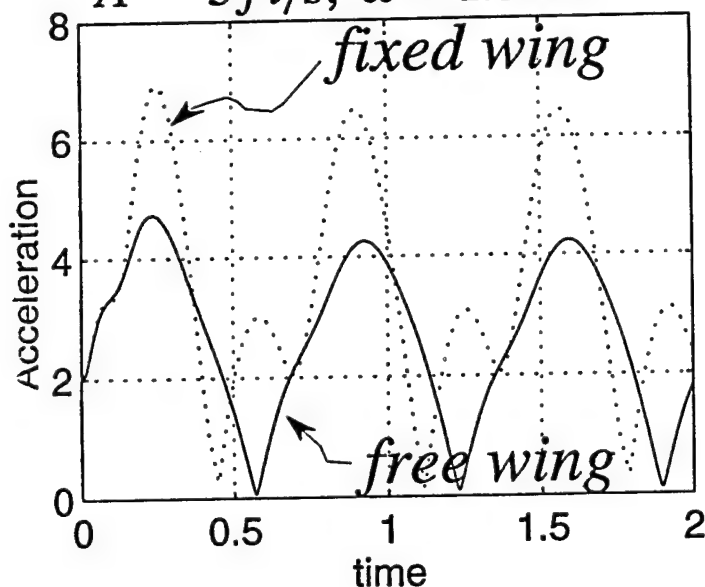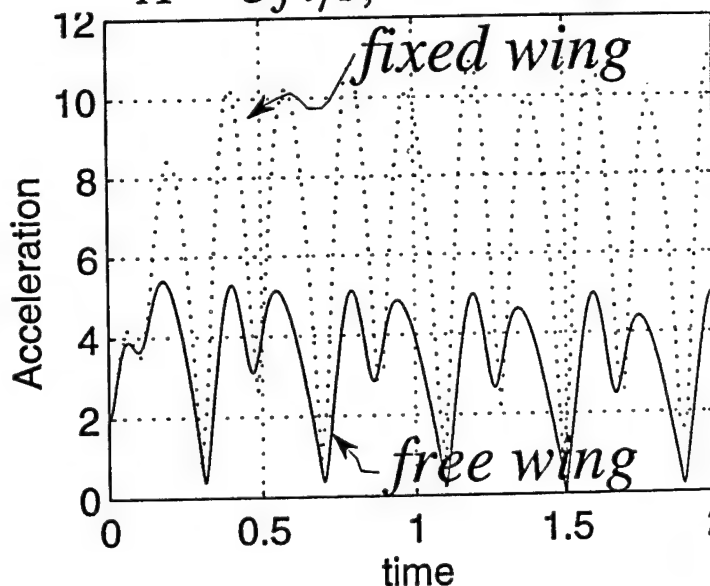
Vertical Harmonic Gust:

$A \sin\omega t$
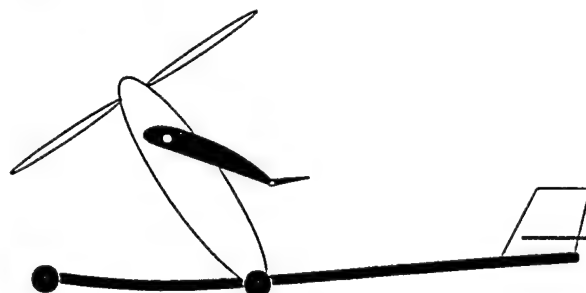
Landing/Takoff/Loiter Mode

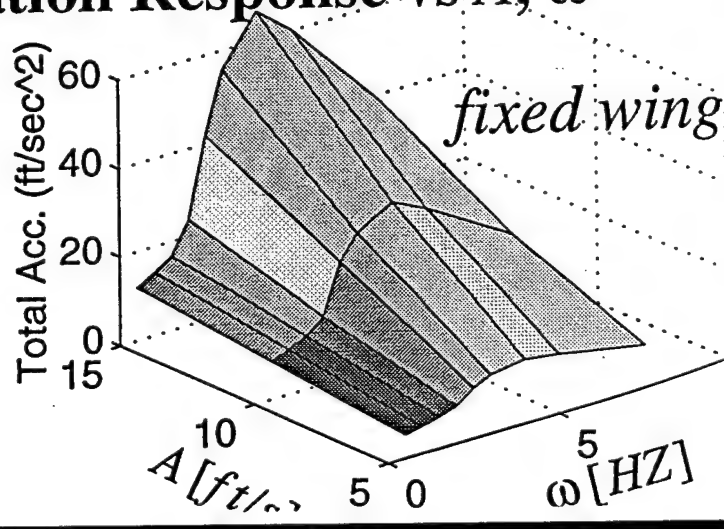---

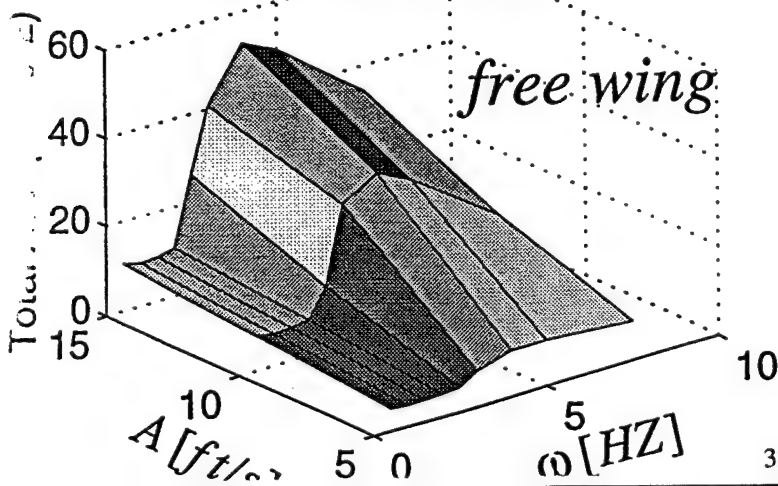# Typical Nonlinear ||Acceleration|| Responses vs *time*

$A = 5ft/s, \ \omega = 1.5HZ$

$A = 5ft/s, \ \omega = 2.5HZ$

Peak Nonlinear Acceleration Response vs A, ω

free wing

fixed wing

A New Approach to Nonlinear Structural Response: Summary

Status:

An orthogonal quasi-coordinate formulation has been developed:

Broadly applicable to nonlinear structural dynamics.

Motivated by and builds upon *Square Root* Ricatti Eq Soln.

Has been programmed and validated carefully.

Order of magnitude improvement vis-a-vis fundamental accuracy/stability/efficiency tradeoffs.

Where to From Here?

Devevlop a Recursive form of the formulation.

Investigate the integration of this approach with Augmented Lagrangian Methods for more efficicient constrained dynamics.

Study prototype applications

Dynamical Model Validation for DPS

Problem: Dynamic response simulations for DPS, especially for nonlinear constitutitive & geometric deformations of multi-body systems remain very difficult to validate.

There are at least two meanings of validation:

Mathematical/Numerical Validation: The issues associated with *convergence of spatial and temporal discretization*, for a given set of constitutitive, kinematic, and modeling assumptions.

=>> Error estimation for time discretization is most painful.

System Identification: The issues of validation/refinement of the model to *resolve the theory versus experiment discrepancies through simultaneous refinement of the experiments and the model.*

Question: Can we routinely generate *exact solutions* for a problem which is a *near neighbor* of the problem we seek to solve?

Answer: A qualified yes =>> Attractive solution validation tool.

329

Flow Chart for Construction of Exactly Solved Benchmark Problems Near an Approximate Solution

---

GIVEN A DYNAMICAL SYSTEM

$$\ddot{x}(t) = f(t, x, \dot{x}, p),$$

where p is the model parameter vector

$$x(t_O) = x_O, \quad \dot{x}(t_O) = \dot{x}_O, \quad t_O \le t \le t_f$$

⬇

GIVEN A NUMERICAL SOLUTION PROCESS

$$\{\bar{x}_1, \bar{x}_2, \cdots, \bar{x}_n\}, \quad where \quad \bar{x}_i = \bar{x}(t_i)$$

⬇

ORTHOGONAL CHEBYSHEV APPROXIMATION

$$x_b(t) = \ smooth\ interpolation\ of$$

$$\{\bar{x}_1, \bar{x}_2, \cdots, \bar{x}_n\}$$

⬇

INVERSE DYNAMICS

$$e(t) = \ddot{x}_b(t) - f(t, x_b(t), \dot{x}_b(t), p)$$

⬇

BENCHMARK PROBLEM

The known interpolated solution: $x_b(t)$
exactly satisfies the differential eqns

$$\ddot{x}(t) = f(t, x, \dot{x}, p) + e(t),$$

with the boundary conditions:

$$x(t_O) = x_b(t_O), \quad \dot{x}(t_O) = \dot{x}_b(t_O), \quad t_O \le t \le t_f$$
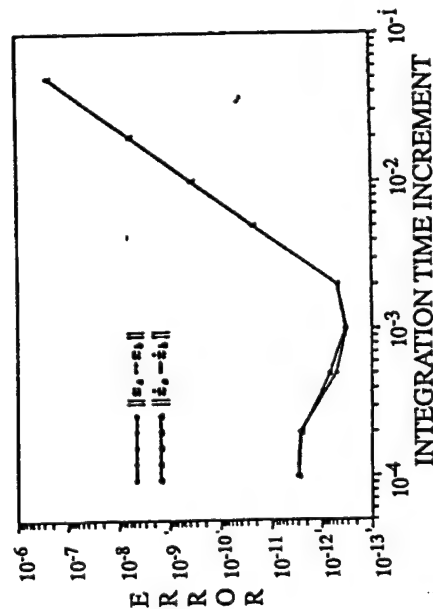
Example ODE System

$$\ddot{x}(t) = f(t, x, \dot{x}, p) + e(t) \equiv -x - \frac{1}{10}(1 + x^2)\dot{x} + \frac{1}{10}x^3 + sin(t) + e(t)$$
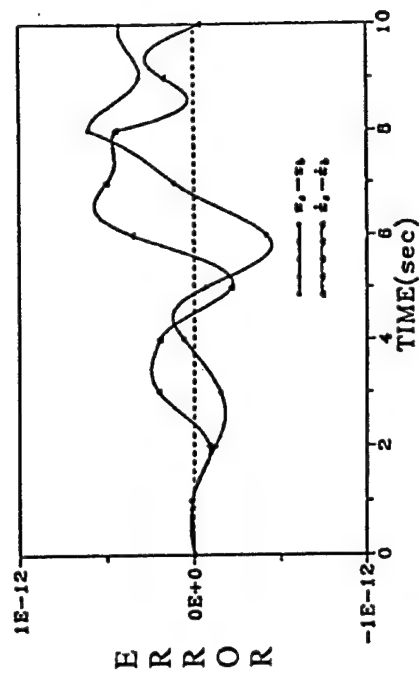

Benchmark Solution vs Integration Time
(NOMINAL PROBLEM)

Exact Residual Errors vs Integration Time
(NOMINAL PROBLEM)
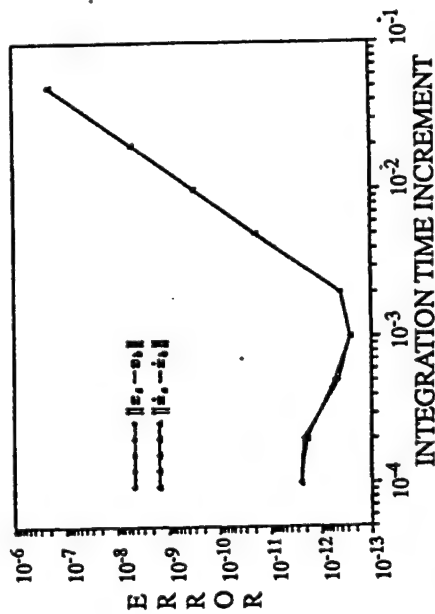
Error Measure vs Integration Step Size
(NOMINAL PROBLEM)

Error Measure vs Integration Step Size
(20% PERTURBED PROBLEM)

A Three Body Distributed Parameter System

Tip Mass m_{tip}
Tip Inertia I_{tip}

u_{tip}
f_{tip}

$y(x, t)$

Euler Beam EI, ρ, L

$f(x, t)$

$\theta(t)$

Hub Inertia I_{hub}
Hub Radius r

u_{hub}
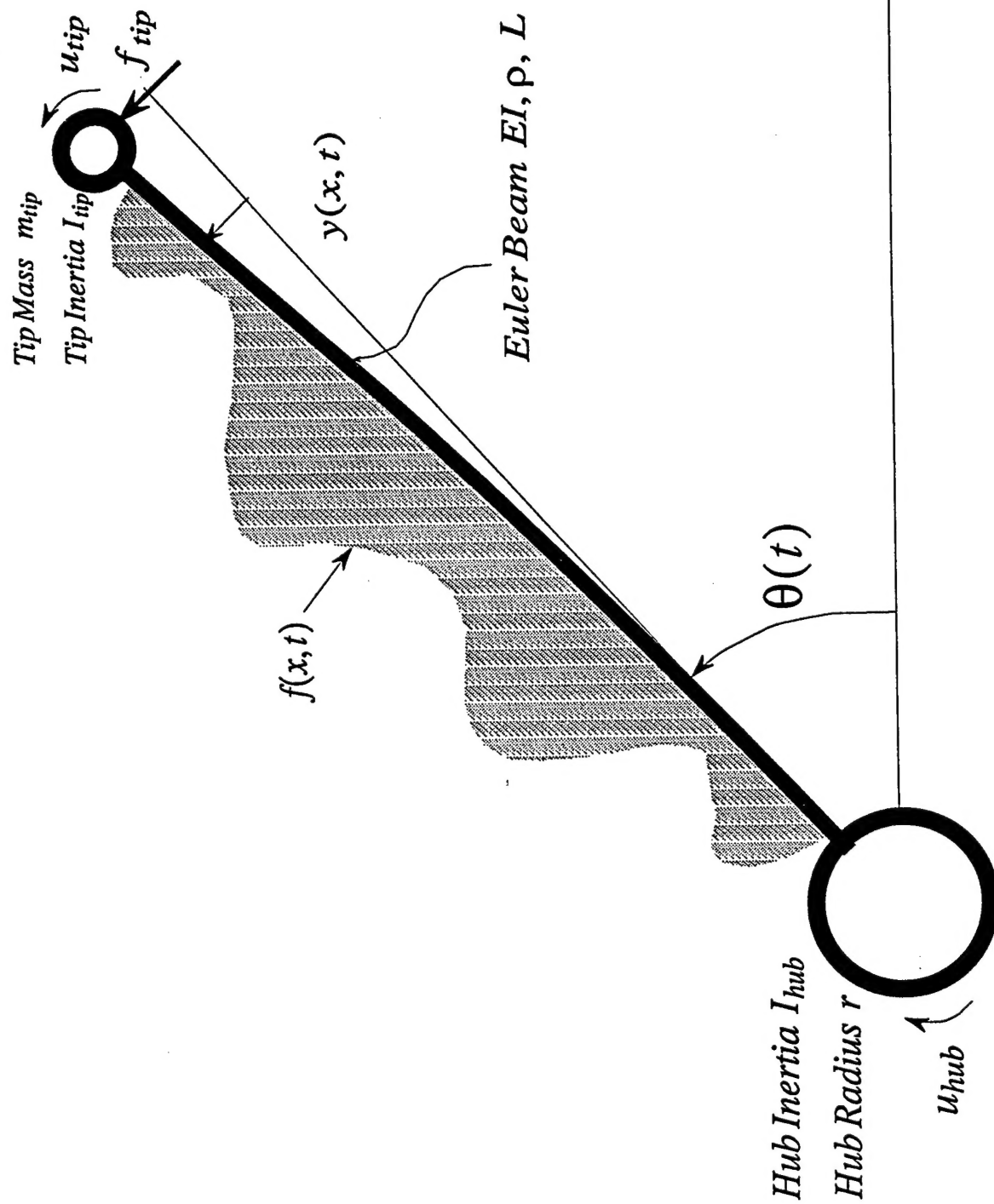
Example ODE/PDE Hybrid System

Exact Hybrid System Model:

$$J\ddot{\theta} + \int_0^L \rho(x+r)[\ddot{y} + (x+r)\ddot{\theta}]dx + m(L+r)[(L+r)\ddot{\theta} + \ddot{y}]$$

$$+ J[\ddot{\theta} + \ddot{y}'] - \int_0^L f(x)(x+r)dx + (L+r)f_{tip} + u_{tip} + u(t) = 0$$

$$\rho[\ddot{y} + (x+r)\ddot{\theta}] + EI y'''' - f(t,x) = 0$$

with the boundary conditions:

$$EI y'''(t,L) - m[(L+r)\ddot{\theta} + \ddot{y}(t,L)] + f_{tip}(t) = 0$$

$$EI y''(t,L) + J[\ddot{\theta} + \ddot{y}'(t,L)] - u_{tip}(t) = 0$$

Approximate FEM System Model:

$$\begin{bmatrix} J+M_{\theta\theta} & M_{\theta\upsilon} \\ M_{\upsilon\theta} & M_{\upsilon\upsilon} \end{bmatrix}\begin{Bmatrix} \ddot{\theta} \\ \ddot{\upsilon} \end{Bmatrix} + \begin{bmatrix} 0 & 0 \\ 0 & K_{\upsilon\upsilon} \end{bmatrix}\begin{Bmatrix} \theta \\ \upsilon \end{Bmatrix} - \begin{bmatrix} 1 & r+L & 1 \\ 0 & 0 & 0 \\ \vdots & \vdots & \vdots \\ 0 & 1 & 0 \\ 0 & 0 & 0 \end{bmatrix}\begin{Bmatrix} u \\ f_{tip} \\ u_{tip} \end{Bmatrix}$$

$$-\begin{Bmatrix} \int_0^L f(t,x)(x+r)dx \\ \int_0^h f(t,x)\psi_3^{(1)}(x)dx + \int_h^{2h} f(t,x)\psi_1^{(2)}(x)dx \\ \int_0^h f(t,x)\psi_4^{(1)}(x)dx + \int_h^{2h} f(t,x)\psi_2^{(2)}(x)dx \\ \vdots \\ \int_{(n-2)h}^{(n-1)h} f(t,x)\psi_4^{(n-1)}(x)dx + \int_{(n-1)h}^{nh} f(t,x)\psi_2^{(n)}(x)dx \\ \int_{(n-1)h}^{nh} f(t,x)\psi_3^{(n)}(x)dx \\ \int_{(n-1)h}^{nh} f(t,x)\psi_4^{(n)}(x)dx \end{Bmatrix} = 0$$

Benchmark System Model: Given interpolated $\{y(t,x),\ \theta(t)\}$, find $\{\delta f(t,x),\ \delta u(t),\ \delta f_{tip}(t),\ \delta u_{tip}\}$ to exactly satisfy the hybrid system of odes/pdes:

$$J\ddot{\theta} + \int_0^L \rho(x+r)[\ddot{y} + (x+r)\ddot{\theta}]dx + m(L+r)[(L+r)\ddot{\theta} + \ddot{y}] - \int_0^L \{f(t,x) + \delta f(t,x)\}(x+r)dx$$

$$+ J[\ddot{\theta} + \ddot{y}'] + (L+r)\{f_{tip} + \delta f_{tip}\} + \{u_{tip} + \delta u_{tip}\} + \{u + \delta u\} = 0 \qquad \Rightarrow step\,4:\ \delta u(t)$$

$$\rho[\ddot{y} + (x+r)\ddot{\theta}] + EI y'''' - \{f(t,x) + \delta f(t,x)\} = 0 \qquad \Rightarrow step\,1:\ \delta f(t,x)$$

with the boundary conditions:

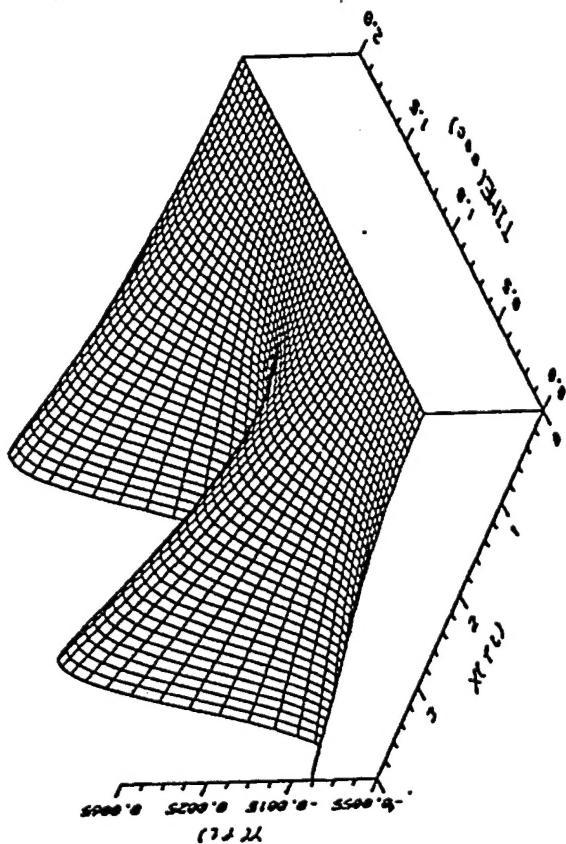$$EI y'''(t,L) - m[(L+r)\ddot{\theta} + \ddot{y}(t,L)] + \{f_{tip}(t) + \delta f_{tip}(t)\} = 0 \qquad \Rightarrow step\,2:\ \delta f_{tip}(t)$$

$$EI y''(t,L) + J[\ddot{\theta} + \ddot{y}'(t,L)] - \{u_{tip}(t) + \delta u_{tip}(t)\} = 0 \qquad \Rightarrow step\,3:\ \delta u_{tip}(t)$$
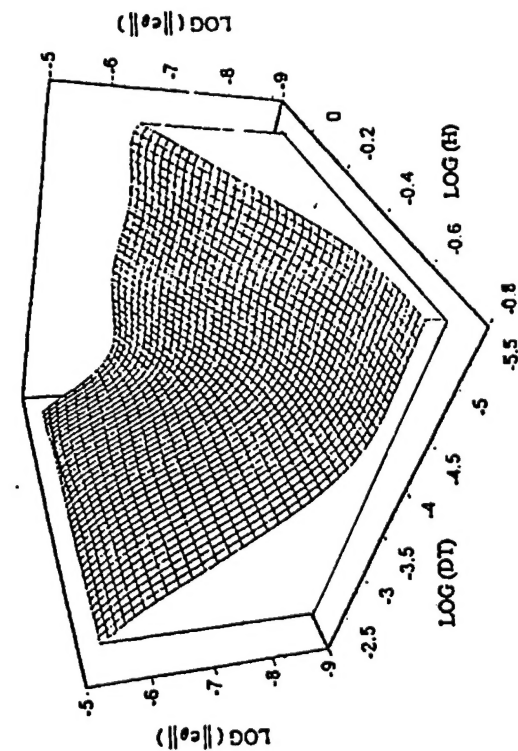
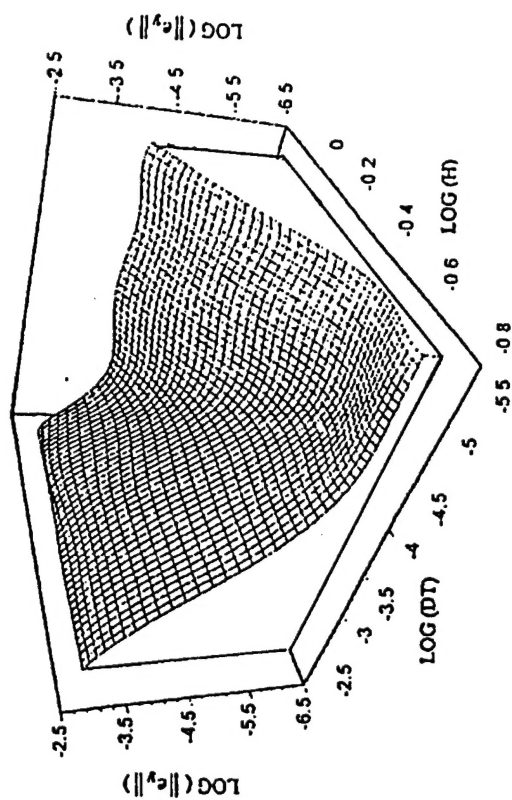# Convergence Study on a Distributed Parameter System

ERROR(x,t)

residual error $\delta y_b(t,x)$

Elastic displacement $y_b(t,x)$

log of rms error in $y(t,x)$

log of rms error in $\theta(t)$
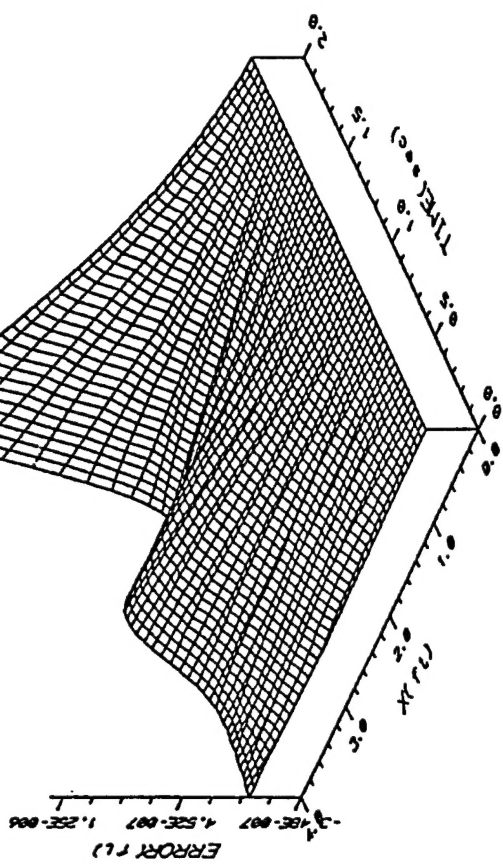
Dynamical Model Validation for DPS: Summary

Status:

A method akin to inverse dynamics for constructing solutions exactly satisfying perturbed nonlinear ode/pde models, near a given approximate solution. the method is useful for studying convergence of space/time discretization methods.

For the case of a general system of nonlinear odes, we have developed a general software package that has been recently published in *Shock and Vibration Computer Programs*.

For the case of DPS described by hybrid ode/pde/integral eqns, only a limited class of applications have been done. While nice results were obtained for the cases studed, no general code can apparently be developed.

Where to from here?

Study more applications.